JUSTUS-LIEBIG-UNIVERSITÄT GIEßEN

Influence of dye characteristics on the photoelectrochemical kinetics in dye-sensitized solar cells

Einfluss von Farbstoffeigenschaften auf die photoelektrochemische Kinetik in farbstoff-sensibilisierten Solarzellen

Dissertation

zur Erlangung des Doktorgrades der Naturwissenschaften
(Dr. rer. nat.)

vorgelegt von
Jane Caroline Falgenhauer

dem Fachbereich 07
der Justus-Liebig-Universität Gießen

Institut für Angewandte Physik

Gießen – 2017

Supervisor and first referee:	Prof. Dr. Derck Schlettwein
Second referee:	Prof. Dr. Bernd Smarsly

Abstract

In this work, the properties of dye sensitized solar cells after the application of different preparation parameters were characterized. The focus lies on solar cells based on electrodeposited ZnO, sensitized with four different indoline dyes and for three different sensitization times. The four indoline sensitizers included the established dye D149 with one carboxylic anchor group, and three less investigated indoline dyes containing a second anchor group with an increasing length of the alkyl spacer, DN91, DN216 and DN285. Additionally to current voltage curves the solar cells were characterized by different photoelectrochemical methods like impedance spectroscopy, which allowed the assignment of the observed changes in cell parameters e.g. to increased recombination due to molecular aggregates, or to a shift of the conduction band edge. For a given sensitization time and at a given density of states, indoline dyes with a longer alkyl spacer showed a slightly decreased recombination due to a better shielding of the ZnO surface against the electrolyte. For the variation of the adsorption time, intermediate sensitization times of 15 min led to the best cell parameters, as more dye was adsorbed compared to a sensitization for 1 min, and yet recombination was not increased by a higher extent as observed for a sensitization for 1 h. A sensitization of the indoline dyes without coadsorbate resulted in cells with an increased recombination due to an increase in aggregation, on the other hand the short circuit current increased because of the larger amount of adsorbed dye. The observed increase in the short circuit current density during a storage of cells in the dark was traced to a shift of the conduction band edge to lower energies, and thus an enhanced injection. For all cells, very different recombination was observed for measurements at different illumination intensities, which was explained by a decreased regeneration efficiency at high illumination intensities, leading then to increased recombination via oxidized dye molecules. ZnO-based cells sensitized by phthalocyanine, perylene and triphenylamine dyes, and TiO_2-based cells sensitized by different indoline dyes served for a comparison, where e.g. perylene dyes showed very low power conversion efficiency due to high aggregation and a reduced injection because of low dye states. For cells based on TiO_2 the power conversion efficiency and the short circuit current density I_{SC} was low after preparation, however the cell values increased upon illumination with AM1.5 because of a considerable shift of the conduction band edge to lower energies as observed by impedance measurements. The decrease of the conduction band edge proved beneficial for the TiO_2-based cells, as I_{SC} increased by a factor of 2, and V_{OC} decreased only slightly because of a decreased recombination. For the cells in this work, with the complete set of methods each change in cell parameters could be assigned to a specific cause. A simulation of the chemical capacitance C_μ of the cells by a combination of different capacitance contributions corresponded well with measured values, and helped to elucidate different influences on C_μ.

Zusammenfassung

Im Rahmen dieser Arbeit wurden Farbstoffsolarzellen und der Einfluss unterschiedlicher Herstellungsparameter auf deren Eigenschaften untersucht. Insbesondere wurden Solarzellen basierend auf elektrochemisch abgeschiedenen ZnO-Filmen untersucht, die sich in der Sensibilisierung mit vier unterschiedlichen Indolinfarbstoffen bei drei verschiedenen Sensibilisierungszeiten unterschieden. Die untersuchten Indoline umfassen den bekannten Farbstoff D149, mit einer Carboxyl-Ankergruppe, und die weniger untersuchten Farbstoffe DN91, DN216 und DN285, die sich in der Länge der Alkylkette an einer zweiten Ankergruppe unterscheiden. Außer den Messungen der Strom-Spannungs-Kennlinien wurden die Solarzellen mittels photoelektrochemischer Methoden wie Impedanzspektroskopie charakterisiert, wodurch die beobachteten Veränderungen in Zellparametern beispielsweise auf stärkere Rekombination durch Molekül-Aggregate oder eine Verschiebung der Leitungsbandkante zurückgeführt werden konnten. Indoline mit längerer Alkylgruppe führten bei gleicher Adsorptionszeit und bei der Betrachtung bei gleicher Zustandsdichte zu einer leicht erniedrigten Rekombination durch eine bessere Abschirmung der ZnO-Oberfläche gegenüber dem Elektrolyten. Eine Variation der Adsorptionszeit führte für mittlere Zeiten von 15 min zu den besten Zellparametern, da mehr Farbstoff als bei einer Sensibilisierung für 1 min adsorbiert wurde, jedoch die Rekombination durch Farbstoffaggregate noch nicht so stark erhöht war wie für die Sensibilisierung für 1 h. Eine Sensibilisierung mit Indolinen ohne Coadsorbat führte zu einer erhöhten Rekombination durch mehr Aggregation, andererseits aber auch zu höheren Kurzschlussströmen, da die Menge an adsorbiertem Farbstoff stieg. Für die Beobachtung eines erhöhten Stromes während der Lagerung von Solarzellen im Dunkeln konnte ein Absinken der Leitungsbandkante und eine dadurch erhöhte Injektion verantwortlich gemacht werden. Für alle Zellen lieferten Messungen bei unterschiedlichen Lichtintensitäten sehr unterschiedliche Ergebnisse für die Rekombination, was auf eine erniedrigte Regenerationseffizienz bei hohen Lichtintensitäten zurückgeführt wurde, die eine erhöhte Rekombination über oxidierte Farbstoffmoleküle bewirkte. ZnO-basierte Zellen, die mit anderen Farbstoffen wie Phthalocyaninen, Perylenimiden und Triphenylaminen sensibilisiert wurden, und TiO_2-basierte Zellen, die mit unterschiedlichen Indolinfarbstoffen sensibilisiert wurden, dienten zum Vergleich, wobei für Perylenimide eine sehr geringe Effizienz auf Grund von Aggregation und erschwerter Injektion durch tiefliegende Farbstoffzustände gefunden wurde. TiO_2-basierte Zellen zeigten zunächst eine niedrige Effizienz und geringe Kurzschlussströme I_{SC}, die Werte stiegen jedoch unter AM1.5 Belichtung durch eine deutliche Absenkung der Leitungsbandkante an, wie durch Impedanzmessungen bestätigt wurde. Diese Verschiebung der Leitungsbandkante zu geringeren Energien führte zu einer deutlich verbesserten Effizienz durch eine Erhöhung von I_{SC} um den Faktor 2. Dabei sank V_{OC} nur wenig, da sich die Rekombination verringerte. Das breite Methodenspektrum erlaubte es, für die beobachteten Änderungen der Zellparameter jeweils eine spezifische Ursache zu finden. Eine Simulation der chemischen Kapazität C_μ der Zellen durch eine Kombination aus unterschiedlichen Kapazitäten gab die gemessenen Werte gut wieder, und erklärte unterschiedliche Einflüsse auf C_μ.

TABLE OF CONTENTS

Abbreviations and formula symbols

Throughout this work, different abbreviations and formula symbols are used. For a better understanding of the text, these are denoted here. The formula symbols are explained in more detail in the context.

AM1.5	Air mass 1.5
C_μ	Chemical capacitance
DOS	Density of states
DSC	Dye-sensitized solar cell
EIS	Electrochemical impedance spectroscopy
FTO	Fluorine-doped tin oxide
HOMO	Highest occupied molecular orbital
IMPS	Intensity-modulated photocurrent spectroscopy
IMVS	Intensity-modulated photovoltage spectroscopy
IPCE	Incident photon-to-current conversion efficiency
I_{SC}	Short-circuit current density
IV-curve	Current-voltage curve
LUMO	Lowest unoccupied molecular orbital
n_{SC}	Charge density at short circuit
N_t	Total trap density of the semiconductor
OCVD	Open-circuit voltage decay
PEC	Photoelectrochemical/Photoelectrochemistry
R_{rec}	Recombination resistance
R_s	Series resistance of the substrate (TCO)
R_{series}	Series resistance of the cell
RT	Room temperature
TCO	Transparent conductive oxide
TPAI	Tetrapropylammonium iodide
V_f	Fermi-level voltage or internal voltage
V_{OC}	Open-circuit voltage
λ	Wavelength
λ_{re}	Reorganization energy in Gerischer model
τ_n	Effective electron lifetime (optional superscript gives the method with which the value is determined)
τ_{tr}	Transport time of electrons in the porous semiconductor film

Introduction

Dye-sensitized solar cells (DSCs) are an interesting alternative to silicon-based solar cells. Even though the efficiencies are still lower for DSCs, a short energy payback time [1], a possible application on flexible substrates [1,2] and various design possibilities [3] lead to a continuous interest in the field of DSCs [4]. Some products (e.g. solar cells for mobile usage [5]) and prototypes (e.g. building-integrated colorful solar-cells [6]) show possible applications of DSCs. Highest efficiencies of 13% can be reached e.g. with a material combination of TiO_2 nanoparticulate film sensitized with a porphyrin dye SM315, and a Co(II/III) redox shuttle [7].

Even though TiO_2-based DSCs reach the highest efficiency compared to other semiconductor materials, also other semiconductors can be of interest because of their specific properties. Crystalline nanoporous ZnO can for example be synthesized via electrodeposition at low temperatures [8,9], which allows the use of flexible substrates, usually sensitive to the high-temperature treatment needed for the sintering of TiO_2 nanoparticles. Additionally, the energy payback time will be even lower for such production route without an energy-consuming sintering step, different from the standard TiO_2 cells.

However the Ruthenium dyes which are standardly used for TiO_2-based DSCs have to be applied with care to a less stable ZnO surface because of their high acidity [10]. Almost from the emergence of electrodeposited ZnO as a porous material in DSCs, indoline dyes were found to reach comparatively high power conversion efficiencies without notable etching of the ZnO surface. The indoline dye D149 reached 4.56% efficiency on electrodeposited ZnO [3], and this dye and similar indoline dyes lead also to high efficiencies for TiO_2-based (9.52% [11]) solar cells. However, D149 is easily desorbed from the semiconductor surface by more demanding electrolytes [12], thus causing problems in the course of measurements or for cell stability [13]. The addition of a second anchor group to the dye structure of D149 enhances the binding stability of the adsorbed dyes, yet leads to similar efficiencies [13,14,15]. Until now, these double-anchor dyes were used only under not yet optimized conditions [15] or under special conditions required by the experiments [13], which did not yet allow an interpretation of the performance under optimized conditions and thus a comparison with state-of-the-art D149-sensitized DSCs based on electrodeposited ZnO. To obtain such a comparison was one of the aims of this work.

For the characterization of DSCs, different methods were developed, each focusing on different aspect of the solar cell. One of the most powerful methods is electrochemical impedance spectroscopy (EIS), described in detail in [60]. By itself or in combination with other methods, different values can be determined which give insight into the functioning of the solar cells, also under real working conditions when choosing the appropriate experimental conditions. For D149 and some other dyes adsorbed on electrodeposited ZnO, this method was used before with success [16,17,18,19]. In this work, a comparative study by dynamic photoelectrochemical methods with a focus on EIS was performed for

cells sensitized with different indoline dyes. The differences in performance of the cells, induced by a change of the dye or other adsorption conditions, should with these methods be associated to a change of the electrical properties, and where possible be traced to their physical origin. The comparison of measurements performed under different conditions aimed at a better understanding of the limiting factors of the cells.

1 Concepts, materials and methods

1.1 Dye-sensitized solar cells

1.1.1 Invention and development

The sensitization of a photoelectrode was first recorded in 1887 [20,21]. The sensitization of semiconductors with dyes that inject an electron into the conduction band was investigated since about 1968, first with the electrolyte contained the sensitizing dye [22-27]. It was stated later that the current generation takes place only on the semiconductor surface by adsorbed dyes [26,28,29], leading then to the concept of a higher surface area by sintered ZnO [29] and TiO_2 [30,31] particles (see also [32] for different materials and concepts). The power conversion efficiency already exceeded 1% in [29] and [31]. Further development led to a cell with a power conversion efficiency of more than 7% in 1991 [33]. This type of solar cell, later also termed Grätzel cell, consisted of sintered nanoparticulate TiO_2 sensitized by a Ruthenium complex with a platinized counter electrode and a liquid iodide-containing electrolyte [34]. A great many variations, improvements and methodical investigations of DSCs were since then applied [4,35]. The variations include the semiconductor or the semiconductor structure [36], the electrolyte [37,38,39] or hole-transporting material [40], the sensitizer [41] and the counter electrode [42], as well as different substrates for flexible [43] or wire-like solar cells [44,45,46] (and other references). Recently, a new type of DSC-like solar cells with organic-inorganic hybrid perovskites by replacing the dye in the concept has been developed. Cells from this concept are now by far exceeding the efficiencies reached by traditional DSCs [47-50].

1.1.2 ZnO-based dye-sensitized solar cells

From the beginning of sensitization experiments, ZnO was used as a semiconductor material [29]. As bulk intrinsic material, ZnO has several advantageous properties over TiO_2 [51]. These are in the first place the high conductivity of the bulk ZnO compared to bulk TiO_2. Another very interesting property is also the vide variety of structures and production routes [51,52,53]. This wider variety is partly caused by the lower chemical stability of ZnO compared to TiO_2, which even allows the deposition of crystalline porous ZnO at low temperature via electrodeposition [9]. One of these electrodeposition methods, also compatible with flexible and wire-like substrates, led to DSCs with maximum efficiencies of 5.56 % with the indoline sensitizer D149 [3], as mentioned in the introduction. Electrodeposition of ZnO is the method employed for the fabrication of most of the films characterized in this work.

Further work was conducted on the field of ZnO-based DSCs, either with different dyes, or new structures found, and efficiencies of about up to 7.5 % were reached [54]. Other work focusses on the combination of the high-stability semiconductor material TiO_2 with the versatile material ZnO [53,55-58].

1.1.3 Working principles

A dye-sensitized solar cell (DSC) has a comparably simple working principle, but as all physical problems, can get very intricate when details are considered. In this section, first a brief overview is given, then some of the processes of interest will be discussed in more detail. Some of the principles will be dealt with also in the context of the measurement methods which are used to probe different parameters of a DSC, see section **1.3**. A more detailed description of dyes and associated principles can be found in section **1.2**. (For more detailed information, the reader is referred to several works about DSCs [4,59-62].) A schematic representation of the different components of a DSC is shown in Figure 1.

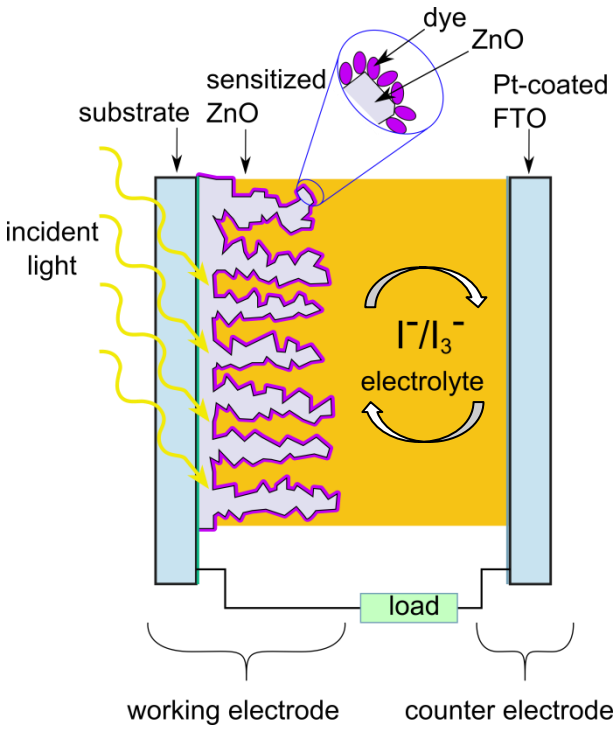

Figure 1 – Schematic representation of a dye-sensitized solar cell showing the different components. Thicknesses are not to scale.

For the working of a DSC, first the incident light excites the active component of a dye-sensitized solar cell, a dye molecule (see also Figure 2, path **1**). The excited dye molecule injects an electron into the conduction band of the semiconductor, typically TiO_2 or ZnO (path **2a**). The electron diffuses through the semiconductor matrix and is collected at the transparent conductive oxide (TCO) coated

glass at the working electrode side (path **3a**). Through the external circuit the current then reaches the Pt-coated counter electrode. At this catalytically active electrode triiodide is reduced to iodide which diffuses through the electrolyte to the oxidized dye (path **4**). By oxidizing the iodide in the electrolyte (path **5**), the dye is regenerated and can again be excited by incoming light. With this, the steps that lead to a working DSC are summarized.

However, in a real device, also loss mechanisms occur. The main loss mechanisms are indicated by red arrows in the schematic energy diagram in Figure 2. A possible path where electrons can be lost to the current that is obtained at the outer contacts is path **2b**, radiative recombination of excited electrons. Another loss path is indicated by path **3b**, which indicates the recombination of conduction band electrons of the semiconductor directly to the reduced species of the electrolyte. Electrons in the semiconductor can also recombine via path **3c**, where electrons are transferred from the semiconductor to the oxidized dye molecule.

For a more detailed consideration of the different processes in a DSC, some of the "theory behind it" is needed. A model which describes the combination of the three different components semiconductor, dye and electrolyte, is the Gerischer model, derived from Marcus theory. This model describes the electrolyte as a (Gaussian) distribution of filled and empty states, which are centered at the Redox energy E_{redox} and whose maxima are separated from this energy by the reorganization energy λ_{re} [i]. The dye can also be described as a distribution of states, centered around the energies $E^0(S^+/S)$ and $E^0(S^+/S^*)$. The energy transfer (both desired and not desired transfer) occurs only isoenergetically, and the transfer probability depends on the overlap of filled and empty states. The distribution of states however is not fixed, but will change with for example dye loading, the energy levels of the different components, and also on experimental conditions like light intensity [4].

It is also important to be aware of the fact that the porous semiconductor which serves as a binding site for the dye and as an electron conductor for the light-induced electrons, cannot be considered as a perfect semiconductor. The production processes and the porous structure with a high surface area induces a large number of traps, that are generally distributed with exponentially decreasing density of states below the conduction band edge. This large number of trap states enables conduction of electrons even below the energy of the conduction band edge. The energy down to which electrons can still be conducted in the semiconducting material is referred to as mobility edge. In many works about DSCs, the term conduction band edge E_c is used synonymously for mobility edge, even if it these values are not identical or cannot be determined. In accordance to this, also throughout this work these terms are used as synonyms.

[i] The index "re" is used here to differentiate the symbol from the wavelength λ.

The distribution or filling of the trap states in the semiconductor material is not fixed for each material, but can be changed for example by adsorption of different molecules or ions. Dipolar molecules or a change in the charge can increase or decrease the density of states, leading to an upward or downward shift (energetically) of the conduction band edge E_c.

It is also important for the consideration of DSCs that the Fermi-level occupies different positions depending on the state of the cell. The Fermi-level E_f in general gives the probability of population of electronic states in a semiconductor by

$$E_f = E_c + k_B T \, ln\left(\frac{n_c}{N_c}\right) \quad \textbf{(1)}$$

with E_c the energy of the conduction band edge, k_B Boltzmann's constant, T the temperature, n_c the density of conduction band electrons and N_c the effective density of conduction band states. In a DSC, where illumination or applied voltage change n_c, another term is defined additionally to this equilibrium state in the dark, the quasi-Fermi-level $E_{f,n}$ (under illumination, under non-equilibrium conditions). $E_{f,n}$ has a constant value over the complete thickness of the semiconductor film under open-circuit conditions, while under short-circuit conditions it is lower in energy, and bended downward near the substrate as charge is extracted there. In the dark, the Fermi-level E_f equals the redox potential of the electrolyte, E_{redox}. On the following pages, the different processes indicated in Figure 2 are explained in more detail.

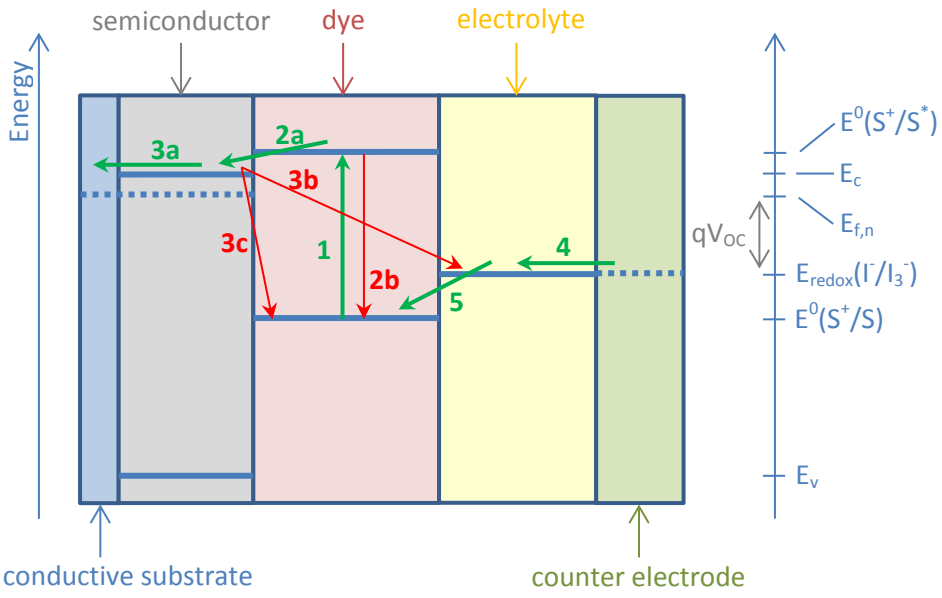

Figure 2 – Schematic representation of different energy levels in a DSC. Electron movement proceeds in the direction of the arrows. The respective electron transfer paths that lead to a working solar cell are indicated by green arrows, while loss pathways are indicated by red arrows. The outer connection of the cell was left out for clarity. The numbers of the different paths relate to the respective numbers in the text. The different energies of the energy levels are indicated on the right side of the diagram, E_v being the energy of the valence band of the semiconductor. The starting and end points of the arrows indicating electron transfer paths give the approximate energy difference and do not indicate the exact path of transfer, as electron transfer will occur isoenergetically.

Path **1** – Excitation of dye molecules

This path automatically takes place in a light-absorbing dye, when light of an energy exceeding the HOMO-LUMO difference (HOMO/LUMO – highest occupied/lowest unoccupied molecular orbital) of this dye is illuminated into the dye-sensitized solar cell. The light harvesting efficiency (LHE) gives a measure of how much of the illuminated light is absorbed and can eventually be used for current generation. This wavelength-dependent value increases with increasing amount of dye molecules attached to the semiconductor surface. For most solar cells, the highest-possible current is desirable, which leads to the use of dyes that absorb over a wide range of the visible spectrum. However for some applications where design is important, colorful dyes or even transparent sensitizers (utilizing the infrared portion of the spectrum) are used for the sensitization of the semiconductor material.

Path **2** – Injection of electrons (**a**) and radiative recombination or relaxation (**b**)

Directly after excitation of an electron of the dye to the LUMO, the electron can be injected into empty states of the semiconductor. This step is only possible, if the LUMO level of the sensitizer lies energetically above E_c of the semiconductor, or rather at an energy of many empty states of the semiconductor. The higher the LUMO level lies above E_c, the higher is the driving force for injection as more empty states are available – but on the other hand an efficient solar cell can only be maintained if also the relative position of the HOMO level still allows regeneration of the dye. For solar cells with a sufficiently high LUMO level, the injection takes place within femtoseconds to picoseconds, which is much faster than the excited state lifetime of the dye (nanosecond range). This ratio of the different times ensures that excited electrons are injected into the semiconductor instead of recombining radiatively to the HOMO level. Only for inefficient injection, which can occur for a bad level alignment of dye or semiconductor, or when a voltage is applied (increasing the density of occupied states in the semiconductor, or decreasing the density of free states to which electrons from the dye can be transferred, thus also decreasing injection efficiency [63]), the relaxation to the ground state becomes more important. This also leads to the observation that luminescence increases with increasing applied voltage in complete DSCs [63,64].

Another factor that influences the injection efficiency η_{inj} in the solar cell is the distance of the dye molecule (or rather its donor part) to the semiconductor surface. A large overlap of the electronic states of the dye with the states of the semiconductor increases the transfer probability of electrons, while for example a longer spacer at the molecule increases the tunneling distance for excited electrons, and thus decreases the injection efficiency. To achieve a large electronic coupling of the electronic states of dye and semiconductor, a covalent binding of the dye to the semiconductor surface is preferable. Some of the requirements to the sensitizing dye are discussed in more detail in section **1.2**.

Path **3** – Electron conduction (**a**) and electron recombination via the oxidized dye (**b**) or the electrolyte (**c**)

After injection, the electron in the semiconductor has then to be conducted to the working electrode contact to ensure a high efficiency of the cell. The transport of electrons through the semiconductor is greatly influenced by the abovementioned trap states in the semiconductor, leading to a considerably slower electron conduction than what would be expected from values obtained from bulk semiconductors. On its way to the electrode, the electron is trapped and then thermally released for several times, which slows down the conduction of the electron. The diffusion coefficient connected with these trapping-detrapping events is also called the effective diffusion coefficient D_n. This coefficient leads to another important value, the electron diffusion length L. When this value is larger than the length that the electron has to travel in order to reach the electrode, the collection efficiency η_{col} for collecting the injected electrons at the electrode approaches unity [4].

Recombination of the photogenerated electrons can in principle occur via three routes. However, the recombination route from the substrate to the electrolyte is not shown in Figure 2, because the use of a compact blocking-layer (of the same material as the nanoporous matrix) between the substrate and the electrolyte usually efficiently prevents recombination via this route. If this path is available, for example due to cracks in the blocking-layer or due to uncovered parts of the substrate, a transfer of electrons via this route can occur from the high density of donor states in the degenerated semiconductor of the substrate to the electrolyte.

The recombination route that is studied in most detail by many work groups is path **3b**, the recombination of electrons in the semiconductor with electrolyte states. The most intuitive path for this recombination is the recombination of conduction band electrons to the electrolyte. However, for the trap-dominated semiconductors which are used in DSC, the traps also influence the recombination. The recombination via surface trap states, which usually occurs for DSCs, introduces a nonideality into the solar cell behavior, which is quantified by the exponent β in the recombination term (see also section **1.3.3.5)**. This prevalent model used for the description of recombination in DSCs is therefore often called β-recombination model. The recombination from the semiconductor can either be mediated by the exponential part of the trap states (shallow traps – in thermal equilibrium with the conduction band states) or by monoenergetic trap states deep inside the energetic gap of the semiconductor (deep traps – not in equilibrium with the conduction band) [65].

Another recombination route is given by path **3c** in Figure 2, which indicates the recombination via oxidized dye molecules. During the normal operation of an efficiently working solar cell, this route can be neglected, as the regeneration of the oxidized dye (path **5**) takes place at a faster time scale, and thus leaves no holes for recombination with the electrons in the semiconductor. If for some reason (see explanation for path **5**) the regeneration is slowed down or not sufficiently efficient, the oxidized dye

molecules can act as efficient recombination centers and significantly reduce the efficiency of the solar cell [66].

The recombination is usually quantified by different parameters like the effective electron lifetime τ_n, which include trap effects. As recombination via path **3c** usually does not occur (as regeneration is supposed to be fast enough), this lifetime mostly represents the recombination of electrons via the conduction band and via surface states to the electrolyte. If the regeneration is not sufficiently efficient, τ_n reflects a combination of the recombination routes **3b** and **3c**. For lower absolute voltages, recombination via path **3b** becomes less import, as the DOS in the semiconductor decreases at lower voltages, and thus the overlap between filled semiconductor states and empty electrolyte states decreases due to an increase in the recombination resistance of the semiconductor electrode.

Path **4** – Reduction of the electrolyte at the counter electrode

Through the outer circuit and over a load, the substrate of the working electrode and the counter electrode are connected. At the catalytically active surface of the counter electrode (for example Pt clusters on a conductive substrate), which is in contact with the electrolyte, the redox couple of the electrolyte is reduced, which means that in an iodide electrolyte I_3^- is reduced to I^-. The reduced electrolyte species diffuses to the dye-semiconductor interface (and the oxidized species diffuses in the other direction) [67]. For electrolytes based on ionic liquids, a Grotthus mechanism was observed, which leads lead to a faster transport of electrons and holes through the electrolyte [68].

Path **5** – Transport of holes in the electrolyte and regeneration of the oxidized dye

When the reduced electrolyte species comes near the dye-semiconductor surface, the oxidized dye molecules (after path **2a**) can be regenerated to the neutral dye by an electron from the reduced electrolyte species, for example I^- in an iodide electrolyte. I^- is thus oxidized to I_3^-, which can diffuse back to the counter electrode. Thus the electrical circuit is closed. Regeneration of the oxidized dye can however only take place, when the energy of the vacant state in the dye ($E^0(S^+/S)$) lies below the redox level E_{redox} of the electrolyte, or in terms of the Gerischer model, a sufficient probability of electron transfer will be given only when the overlap of filled electrolyte states and empty dye states is large enough. This overlap will depend mainly on the concentration of states (that is the concentration of the species) and also on the reorganization energy λ_{re} for the dye and the electrolyte. For TiO_2 films sensitized with Ruthenium sensitizers, a difference of the dye and electrolyte levels of more than about 0.55 eV was found to be sufficient for efficient DSCs [4].

1.2 Sensitizers used in this work

There is a very wide variety of dyes that were tested as to their working in dye-sensitized solar cells. Not only that one class of dye was varied and investigated, there are also numerous classes of sensitizer dyes [4,41,69-75]. To work efficiently as sensitizers in dye-sensitized solar cells, dyes have to meet some general requirements. Some of these requirements are listed below [4,76]:

1. The dyes have to contain a light-absorbing part. The larger the wavelength region of the absorbance of the dye, the more current can be harvested if all other dye and cell parameters are well-adjusted.
2. The dye has to contain a molecular anchor so that the dye is attached directly to the semiconductor surface. A good anchor thus provides a good orbital overlap for dye and semiconductor which is essential for fast injection of electrons into the semiconductor. Commonly used anchor groups are –COOH (or anhydride group), $–SO_3H$ and $–H_2PO_3$ [77,78]. On the other hand, for less stable semiconductors like ZnO, the anchor group(s) should not be too acidic to avoid etching of the semiconductor surface [10,79].
3. Level alignment between dye and semiconductor and dye and redox pair of the electrolyte (or hole-conductor) is essential. Only if the LUMO level of the dye is energetically higher than E_c of the semiconductor, the injection rate is sufficiently high for an efficient solar cell. Analogically, the HOMO level of the dye has to be lower in energy than the redox level of the hole-conducting phase, so that regeneration of the dye can take place. In the more detailed description of the Gerischer model, the overlap of the excited dye DOS and the semiconductor DOS has to be maximized. On the regeneration side, the overlap between filled electrolyte states and empty dye states has to be maximized, so that the transfer probability of electrons via path **2** and **5** is favored over possible recombination paths.
4. To achieve a good injection, a directionality of charge transfer and a separation of donor and acceptor are helpful. A D-π-A (donor, π conjugated bridge, acceptor) dye structure is often discussed as beneficial, and even better performances can sometimes be found by introducing a second internal electron-withdrawing unit, leading to a D-A-π-A structure of the dye [80].
5. As many organic sensitizer molecules are π-conjugated to ensure light absorption and good electron transfer, the conjugated dye structures are often planar. Without additional changes in the dye structure, such planar structures lead to enhanced van-der-Waals interaction (aggregation) and often to radiationless deactivation of the excited state of a dye molecule. Means to overcome this problem are bulky side groups that separate the sensitizer molecules and thus reduce aggregation, molecular centers that reduce the symmetry of the molecule or co-adsorbates that also lead to a separation of the individual dye molecules. However the bulky side-groups should still allow efficient regeneration of the dye by the electrolyte [81].

6. Another important requirement of the sensitizer dye is that it should be stable against light, electrochemical and chemical influences and thermal impact, meaning stability against possible interactions during the operation of a DSC.

Four different dye classes are discussed more in detail below, of which one or more dyes were applied as sensitizers for DSCs in this work.

1.2.1 Indoline dyes

Since 2003, a new class of organic dyes, indoline dyes, were introduced as a sensitizers in DSCs [82-85], initially used as photographic sensitizers [82]. These indoline dyes fascinated from the beginning by a high absorption coefficient (about 4 times higher than for standard Ruthenium dyes [82]), a relatively easy route of synthesis [84] and a wide structural variety. The variation of groups attached to the name-giving part of the molecules, the indoline group, leads to a large number of different indoline dyes which were investigated in DSCs with different cell components [11,86-104], on semiconductor films [91,105-108], in solution [91,105,109,110], or theoretically with the aspect of further use in DSCs [91,95,111-118]. The group of indoline dyes is now one of the most efficient organic sensitizers in DSCs [11].

The perhaps best known and most studied indoline dye is D149, see Figure 3, which is also used as a reference dye in this work. The first publication of D149 [83] (termed indoline dye 1 in that reference) was in 2004, where it was adsorbed to TiO_2 films, reaching power conversion efficiencies of 6.51%. In later years, this efficiency of D149 on TiO_2 was extended to 9.03% [119], while for a similar indoline sensitizer, D205, a power conversion efficiency of up to 9.40% was achieved on TiO_2 [11]. The efficiency of D149 on electrodeposited ZnO reached 5.56% [3]. Mostly, the indoline dyes were adsorbed to the semiconductor together with a chemical compound that does not adsorb light in the visible wavelength range, but reduces the aggregation, which is called coadsorbate (see also**1.2.2**).

One of the major problems of D149 and related structures which leads to an efficiency degradation after some time [82], is the desorption of molecules from the surface [12,16]. Typically, electrolytes less demanding towards the binding stability have to be used for indoline-sensitized DSCs, so that electrolytes cannot be optimized with the same variability as for Ruthenium-based dyes [12,82]. The application range of D149 and similar compounds was widened after several years by the introduction of indoline dyes with two anchor groups (compared to one anchor group in D149), for example dye D358 [14,87,120]. Infrared spectroscopy measurements showed that for D358 the features of both carboxylic groups disappeared upon adsorption to ZnO, indicating that the dye binds covalently via both groups to the ZnO surface [87].

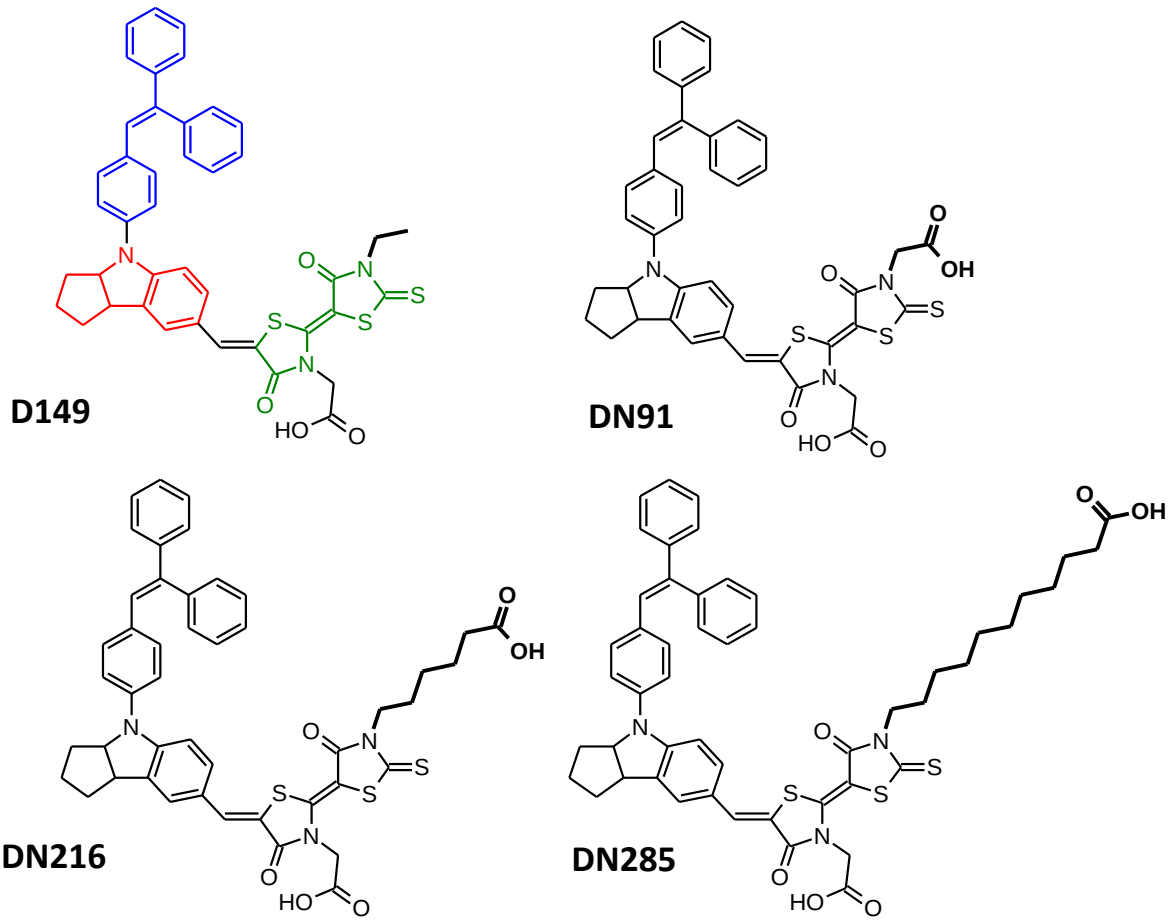

Figure 3 – Molecular structure of the indoline dyes used as sensitizers in this work, D149, DN91, DN216 and DN285. Different parts are marked with different colors in the structure of D149. Red – indoline unit; blue – phenylethenyl unit; green –rhodanine rings. The groups on the outer rhodanine ring, by which the dyes differ, are accentuated by bold characters and thick lines.

The double anchoring also leads to a higher binding stability in contact with different solvents or electrolyte additives, as it was shown for similar dyes DN216 and DN285 [15,121]. The double-anchor indoline dyes can then be used as sensitizers even for femtosecond laser spectroscopy on whole cells without desorption, in opposition to D149 [13]. The higher binding stability also opens up the possibility of the use of indoline dyes in contact with solid hole-conductors, which was not possible for the standard dye D149 because of desorption [122,123].

D149 and its double-anchor derivatives used in this work (DN91, DN216, DN285) all consist of an indoline unit, which acts as a weak donor upon light absorption [70], see also Figure 3. Two rhodanine rings with one or two anchoring groups act as the acceptor part of the indoline dyes [70], enabling a charge flow upon excitation from the donor in the direction of the semiconductor, when the dye is adsorbed to a semiconductor. The non-planar phenylethenyl unit should (together with the cyclopentane in the indoline moiety [124]) hinder aggregation of the otherwise planar molecules and increase the polarity for a good contact with the electrolyte, which is also important for dye regeneration. On the other hand the large phenylethenyl unit increases the distance of the electrolyte to

the semiconductor surface and thus decreases the recombination of electrons from occupied states in the semiconductor to holes in the electrolyte.

The difference of the four indoline dyes investigated in this work is basically only in the optional second binding group at the outer rhodanine ring (see Figure 3). For D149, there is only one binding group at the inner rhodanine ring, bound at a distance of two carbon atoms from the five-atom rhodanine ring. The nitrogen in the outer rhodanine ring binds an ethyl group (for D149), and a second binding group in the case of the three derivatives. The length of the spacer for this second carboxylic acid group increases from one to ten carbon atoms, with DN91 containing the shortest spacer, DN216 with an intermediate length of five carbon atoms and DN285 with the longest spacer group. This change outside the chromophore of the dye thus leads to very similar extinction coefficients [15]. E. Rohwer et al [13,125] found that the length of this alkyl group has an influence on the injection time measured by ultrafast transient absorption measurements, with increasing injection times and decreasing short-circuit photocurrents with increasing length of the alkyl spacer at the second anchor group. This observed effect was ascribed to the closer proximity of the chromophore to the ZnO for the shorter spacers of the second anchor groups, which facilitates electron injection. S. Ito et al. [11] found that for TiO_2 films the introduction of a long alkyl group (at the position of the ethyl group in D149 in Figure 3) lead to a more efficient blocking of recombination than for D149.

For the standard indoline dye D149, the dependence of cell performance on dye adsorption time and on the presence or absence of coadsorbate has already been studied [16,17,108,126,127]. The optical absorbance of D149 adsorbed on ZnO shows a maximum at about 510 nm and a shoulder at about 540 nm for very short adsorption times [16], slightly shifted and broadened compared to solution spectra [15,126]. An increase in the absorbance and a broadening of the spectra of the sensitized films with increasing sensitization time was found, with a saturation for longer adsorption times. This increase however did not always lead to an increase in the power conversion efficiency, especially for longer adsorption times, which was accounted to aggregation of dye molecules. An adsorption isotherm for D149 on ZnO powder suggested even the absorption of a second dye layer on an initial monolayer for an excess of dye molecules [126], and thus a high aggregation. In particular, the aggregation lead mostly to a decrease in the fill factor of the solar cells which then counteracted an increase in current, or an increase in current was not observed due to increased recombination via dye aggregates. The addition a coadsorbate to the sensitization solution led to a reduced aggregation of dye molecules at the semiconductor surface, and for the cells an increase of the fill factor was observed.

For indoline dyes with two carboxylic anchor groups like DN91 and DN216, the dependence of cell parameters on the absorption time or on the presence or absence of a coadsorbate is relatively unknown. Even though similar measurements to those for D149 [126] were performed for such stronger binding dyes in the workgroup of Prof. T. Yoshida [128], these results were not all published. A second

anchor group could effect an adsorption behavior different from D149, which to study was one of the main aims of this work.

1.2.2 Coadsorbates for indoline dyes

Often a chemical compound (not absorbing in the visible wavelength range) is adsorbed to the semiconductor surface together with the sensitizer to reduce aggregation of dye molecules, the coadsorbate. The effect of reducing the aggregation is simply achieved with a binding group attached to the coadsorbate. Thus the coadsorbate also adsorbs to the semiconductor surface, decreases the number of available binding sites and increases the average distance of the dye molecules. Regarding the coadsorbate for indoline sensitized solar cells, different molecules have already been investigated. A standard molecule used often (and also for different dyes) is cholic acid or its derivatives like chenodeoxycholic acid or deoxycholic acid [90,96,102,126,129]. The molecular structures of cholic acid and deoxycholic acid are shown in Figure 4, together with the structure of another cholic acid derivative, lithocholic acid, which was used for the cosensitization of indoline dyes in this and related work [19,130,131]. It was shown that cholic acid and similar molecules not only prevent aggregation by coadsorption, but also shift the conduction band edge to higher energies by the introduction of an additional surface dipole [132].

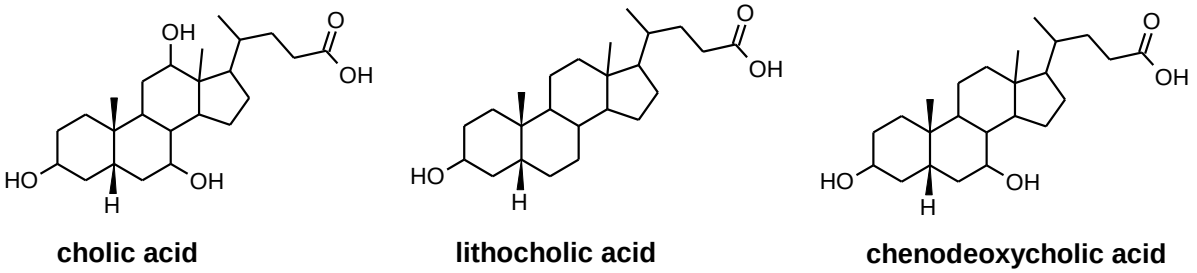

Figure 4 – Molecular structure of different coadsorbates used in this work.

1.2.3 Perylene dyes

Perylene dyes, especially perylene diimides, are widely known as an active material in organic solar cells. The planar organic molecule can be functionalized at 12 different positions, which makes it possible to prepare molecules with different properties to adjust them to specific applications [133]. Perylene imides can also be easily synthesized with an anchoring group like a carboxylic acid or anhydride group, which opens up the use in dye-sensitized solar cells. Bulky groups that prevent the intense aggregation can also be added to the molecules, so that dissipation of energy through otherwise very strong intermolecular coupling is reduced. Power conversion efficiency of peryleneimide

sensitizers was enhanced to 2.6% with additional donor groups at the perylene core to increase the electron concentration at the perylene core [134]. In that work, the authors also found that for their specific perylene molecules, the binding moiety had a very large influence on the DSC efficiency. Diimides with a carboxyphenyl anchoring group produced almost no current, whereas corresponding perylene dyes with an anhydride binding group showed significant current, which was ascribed to the different coupling of the dye to the TiO_2. Even larger efficiencies of up to 12.0% could be obtained with specially designed perylene dyes with an N-annulated perylene core with donor and spacer groups and bulky side groups [135]. As for many perylene diimide dyes the LUMO levels lie at comparably low energies, another possible application of perylene diimides is the use as sensitizers in p-type DSCs, which apply a p-type semiconductor (mostly NiO) for the semiconductor matrix [133]. In this special case of a dye-sensitized solar cell, after dye excitation by incident light an electron is transferred from the conduction band of the p-type semiconductor to the dye, which equals a hole injection from the dye to the semiconductor. The hole is then extracted at the substrate of the photoanode, while the dye is regenerated by a hole injection from the electrolyte into the LUMO level of the dye [136].

The dyes used as sensitizers in this work are perylene diimide dyes from the group of Prof. Dr. H. Langhals and were first described regarding their synthesis in 1998 [137]. The dye structures of the two dyes investigated in this work are shown in Figure 5. Similar dyes (without dedicated anchoring group) were also investigated on monocrystalline TiO_2 surfaces with an atomic force microscope (AFM) [138,139]. It was found in the second work that the adsorbed molecules can be switched in their position from being tilted on one side of a bridging oxygen row to the other side by a slow scan of the AFM.

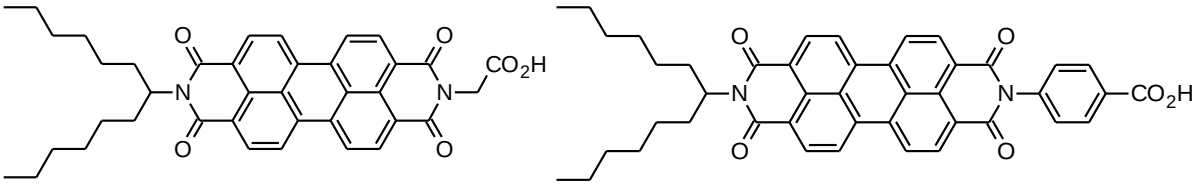

Figure 5 – Molecular structures of the two perylene diimide dyes used as sensitizers in this work, J102 and J109.

1.2.4 Triphenylamines

Regarding the molecular design of organic sensitizer molecules, many D-π-A (donor – π-conjugated bridge – acceptor) dyes have a rather planar structure, which supports aggregation of the dye molecules and thus radiationless deactivation of the excited state, as well as recombination of electrons with the hole-conducting phase [140]. A donor group that can overcome these issues is the

triphenylamine (or triarylamine) group. This group introduces an additional asymmetric center to the dye molecule and gives the possibility to form a D-D-π-A structure with two donor groups. The possibility of adding two bulky groups to the structure (which can be the donor groups) decreases the dye-dye interaction and the interaction of excited electrons with the electrolyte [141,142,143]. The variation of the donor, acceptor and bridging parts of triphenylamine dyes led to many different dyes [144-150]. One of the triphenylamine dyes, Y123, was also cosensitized with a porphyrin, giving a record efficiency of 12% for a porphyrin-based DSC [151]. A variation of Y123, the molecule JF419, reached the highest power conversion efficiency for triphenylamine dyes in DSCs, 10.3% [152]. DSCs sensitized with another triphenylamine dye C219 also led to power conversion efficiencies of up to 10.3% [153].

Three triphenylamine dyes were used as sensitizers for electrodeposited ZnO in this work, synthesized by Dr. Chunyang Jia (University of Electronic Science and Technology of China, Chengdu, China). The synthesis is described in the literature [154,155], the structures of the dyes is depicted in Figure 5. The adsorption of these dyes on TiO_2 for dye-sensitized solar cells has also been described in the abovementioned literature, together with cyclic voltammetry (CV) experiments, theoretical calculations and UV-vis spectroscopy experiments. The yellow dye TPA-B1 reached an efficiency of 2.4% on TiO_2, while the two orange dyes WD-2 and WD-3 reached 3.1% and 2.1% power conversion efficiency, respectively.

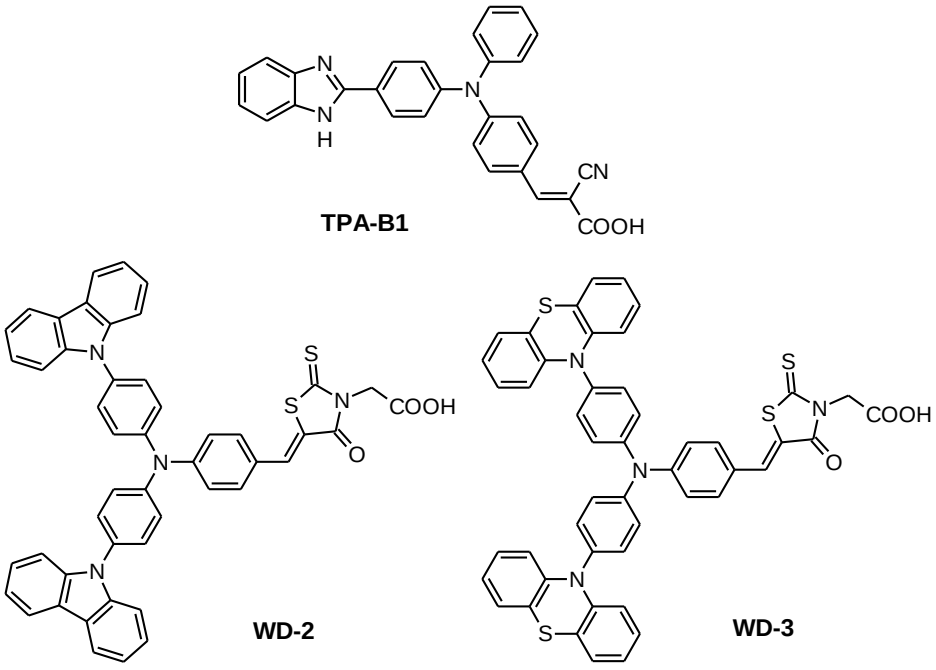

Figure 6 – Molecular structure of three triphenylamine dyes used as sensitizers in this work, TPA-B1, WD-2 and WD-3.

1.2.5 Phthalocyanines

Phthalocyanine dyes are widely-studied artificial dyes [156-159]. A large π-electronic system in a conjugated ring is responsible for a very high extinction coefficient of phthalocyanines (mostly in the longer-wavelength region of the visible light spectrum). In the center of this ring either two hydrogen atoms are located or a central metal atom. The phthalocyanine ring can be substituted at all outer carbon atoms, leading to a wide variety of different phthalocyanine molecules. Due to this variety of phthalocyanine dyes, many promising applications were investigated since their first introduction [156]. Possible applications include the use of phthalocyanines as semiconductors in organic solar cells, as electrocatalysts, photocatalysts (also in their polymeric form, see for example [160-163]) and also for electrochromic displays [156]. Phthalocyanines are also often used as sensitizers for dye-sensitized solar cells. A wide variety of different phthalocyanines has already been reported [75,164,165,166]. It has been found that phthalocyanines for the use in dye-sensitized solar cells need a special design to work efficiently, and the designed properties are different from those needed for organic solar cells. One important property of a sensitizer phthalocyanine molecule is (at least) one binding group, that ensures the binding of the molecules to the semiconductor surface and thus an efficient transfer of electrons from the excited dye molecules to the semiconductor. Another helpful addition to the phthalocyanine core are bulky side groups for the prevention of aggregation. Such groups should efficiently prevent radiationless deactivation of the excited states, which is a large problem in the otherwise strongly aggregating planar phthalocyanine molecules. To further enhance the injection efficiency of the phthalocyanine molecules, a push-pull or donor-acceptor structure of the molecules can be designed.

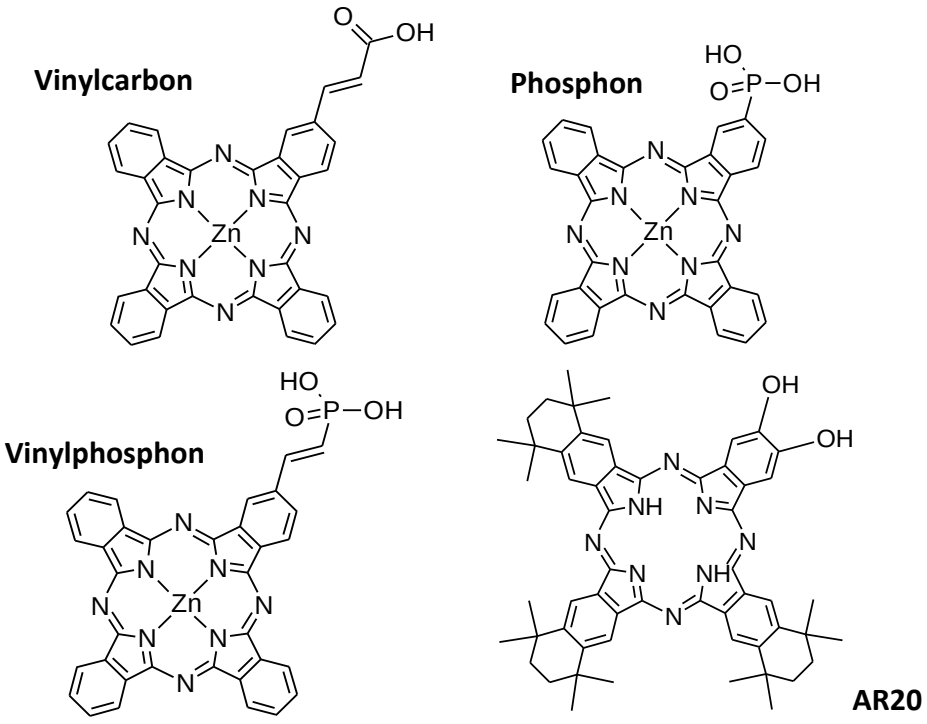

Figure 7 – Chemical structures of the phthalocyanine dyes used in this work. The phthalocyanines are coded Vinylcarbon, Phosphon, Vinylphosphon and AR20.

The realization of an asymmetric molecular structure which results from these optimum molecular properties is synthetically highly demanding, but power conversion efficiencies of up to 6.4% were obtained [167]. A dye with four symmetric substituents with an efficiency of 6.81% was reported recently [168].

In a previous work of the author, relatively simple phthalocyanines (Zn phthalocyanines with different degree of sulfonation) were adsorbed to electrodeposited ZnO [169,170]. Only low power conversion efficiencies were achieved despite a wide variation of the adsorption conditions, mainly caused by a low short-circuit photocurrent. One problem that supposedly led to such low photocurrents could be a mismatch of the energy levels of the phthalocyanine dyes and the conduction band edge of ZnO and/or the redox level of the electrolyte. A too small difference of the respective dye and electrolyte/ZnO levels could result in a too small regeneration/injection efficiency. The mismatch of energy level was also found to be a problem for different phthalocyanines in the literature [166]. Another problem of those dyes which could be defined was the low amount of dye that was adsorbed and the rather high aggregation of the dyes on the electrode surface in spite of many variations of the adsorption conditions. It was found that for a Ruthenium-based dye a single phosphonate binding group leads to an approximately 80 times stronger adsorption than four carboxylic anchor groups [77,171]. That led to the development of several phthalocyanine dyes that differ in their binding group, synthesized by Martin Liebold (work group of Prof. Dr. J. Sundermeyer, Phillips-University Marburg). The phthalocyanine dyes that were used as sensitizers in this work contain either a vinylcarbonyl, a phoshonate or a vinylphosphonate anchor group. One of the dyes can interact with the ZnO surface via two carbonyl groups. The structure of the dyes is shown in Figure 7.

1.3 Measurements and Methods

1.3.1 Absorbance measurements

Absorbance of a compound in solution is a well-defined process described by Beer-Lambert law [172]. After this law, the initial intensity I_0 of a wave is damped exponentially in an absorbing medium according to the path length L. This gives the equation

$$I(\lambda) = I_0(\lambda) \cdot e^{-\epsilon(\lambda) \cdot c \cdot L} \quad \textbf{(2)}$$

where I is the intensity after passing the optical medium, ϵ is the wavelength dependent molar extinction coefficient (or molar attenuation coefficient) of the optical medium, and c is the concentration of the absorbing compound. The theoretical derivation contains several approximations or conditions that need to be fulfilled for the exact validity of the equation. This is especially the homogeneity of the absorption in space and time, and also the condition that the absorbing centers do not influence each other. Both conditions are usually fulfilled in a dilute solution of a dye.

1.3.1.1 Absorbance in transmission setup for solid samples

Most of the absorbance measurements in this work were performed in a transmission setup. By transmitting light through a solid sample, several processes take place for the photons. First, there is absorption in the material, which mostly represents the property of interest. Major loss mechanisms of the absorbance are especially reflection at the substrate and other interfaces, and scattering of the incoming light (especially at the semiconductor film). Scattering is described by Mie theory, and for many films containing very small structures (smaller than about 1/10 of the wavelength λ), the special case of Rayleigh scattering occurs [173]. The scattering cross-section σ_s for round particles averaged over all angles is

$$\sigma_s = \frac{2\pi^5}{3} \frac{d^6}{\lambda^4} \left(\frac{n^2-1}{n^2+2} \right)^2 \quad \textbf{(3)}$$

where d is the diameter of the particles, λ is the wavelength of the light and n is the refractive index of the material (of the particle). With the density of particles (per volume) N_p, the ratio of scattered to incoming light intensity can be calculated

$$\frac{I}{I_0} = N_p * \sigma_s \quad \textbf{(4)}$$

As this light is scattered in all directions, it leads to a wavelength dependent background in absorbance spectra. For dyed substrates, the absorbance of the not-dyed film can be subtracted from the absorbance of the dyed film to achieve the absorbance of the dye without background. However, if the scattering is too strong, the loss of transmitted light is too high, and the absorbance can no longer be evaluated on the large background.

A method to overcome this problem is to gather stray light from strongly scattering samples (as are most of the solid-state samples measured in this work) in an absorption setup including an integrating sphere (*Ulbricht-Kugel*). The basic principle of the integrating sphere is to integrate the scattered light, which is then scattered at a diffuse-reflecting surface of a sphere and collected with a light sensor. The sample is mounted in a way to reflect or transmit most of the light while also capturing light inside the sphere that is scattered at the sample, see also Figure 8(a). The incoming light is scattered at the sample and collected approximately from a hemisphere above the sample. This light is then reflected and re-reflected at the diffuse-reflecting inner surface of the integrating sphere, until the light finally enters the measurement port. A baffle hinders the incidence of direct scattered light into the measurement port. Even though the reflecting material of the inner sphere surface has a very high reflectivity in most cases, the intensity at the measurement port is very low, and has to be compensated by increasing the integration time of the spectrometer.

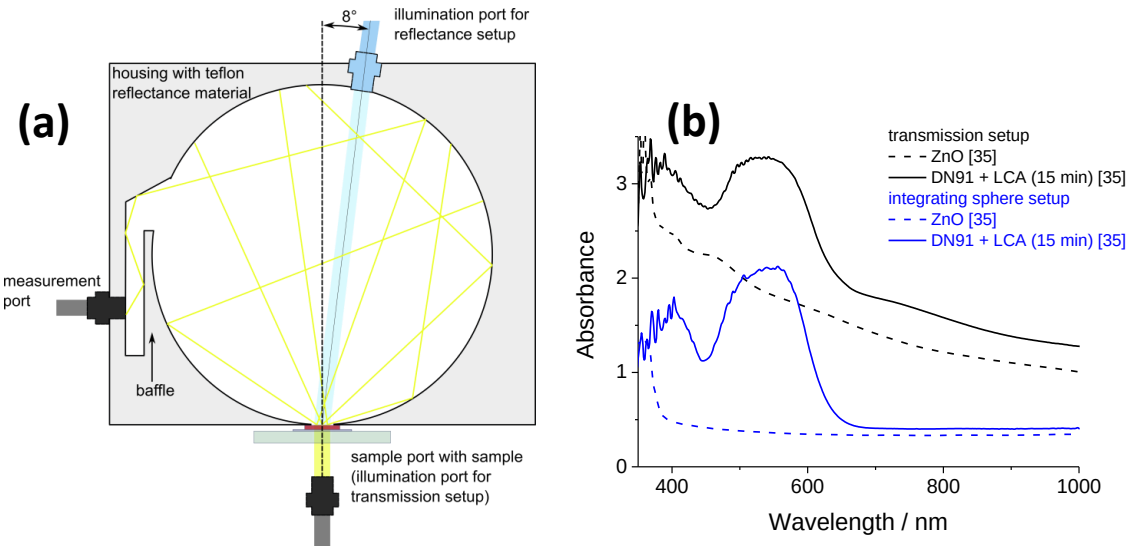

Figure 8 – (a) Illustration of an integrating sphere setup with incoming and scattered light in the transmission setup (yellow), after [174]. The incoming light for the reflectance setup is shown in blue. (b) Absorbance of a scattering ZnO film with or without adsorbed dye, measured either in a standard transmission setup or with an integrating sphere (transmission setup).

Figure 8(b) shows the absorption of a strongly scattering ZnO film with and without dye, which was measured in a standard transmission setup (without collecting scattered light) and in a transmission setup with integrating sphere, where light scattered in the direction of the incoming light is collected (Measurement conditions are described in section **2.4.3**). For the pure transmission setup, a high background absorbance coming from light scattering on the porous film can be clearly seen the

measurement curves. On the other hand, the measurement from the integrating sphere setup shows almost no scattering background down to the wavelengths where ZnO begins to absorb.

1.3.2 ZnO electrodeposition

ZnO thin films can be synthesized by various methods including sputter deposition, doctor blading of nanoparticle suspensions. Many of these methods however require high-temperature annealing to achieve an interconnection of particles, so that conductive pathways and thus good conductivity is obtained. This is only compatible with either cost-intensive glass substrates or Titanium sheets, which can be illuminated only from the counter-electrode side. A method which is compatible with low-temperature, flexible and low-weight plastic conductive substrates is the electrodeposition of ZnO at low temperatures (usually below 100°C). Two different methods for the electrodeposition of ZnO were independently discovered in 1996. One method applies the reduction of dissolved oxygen [175,176] for the deposition of ZnO, and was first described by S. Peulon and D. Lincot. Since the first introduction, much research was done as to different reaction conditions and applications [177,178,179]. The other method (first described by M. Izaki and T. Omi) requires nitrate ions for the deposition of ZnO [180,181]. Another method, applying hydrogen peroxide for ZnO electrodeposition was developed further on [182,183].

The basic principle of the electrodeposition of ZnO is to build up an excess of hydroxide ions at the electrode surface. For the two methods used in this work (oxygen- and nitrate-based electrodeposition) the reactions for the formation of OH^- ions are respectively [3]:

$$O_2 + 2\ H_2O + 4\ e^- \rightarrow 4\ OH^-$$

$$NO_3^- + H_2O + e^- \rightarrow NO_2^- + 2\ OH^-$$

While the reaction of oxygen is strongly dependent on the oxygen concentration and reaction is enhanced for example at a rotating-disc electrode, the reaction of nitrate is kinetically slow. It was found out that Zn^{2+} acts like a catalyst to the reaction with nitrate so that an increase of the Zn salt concentration also increases the reaction rate [184].

The hydroxide ions formed in one of the previous reactions then react with Zn ions from a zinc salt in the solution, precipitate (preferentially) on the substrate as $Zn(OH)_2$ which dehydrates to ZnO:

$$Zn^{2+} + 2\ OH^- \rightarrow Zn(OH)_2 \rightarrow ZnO + H_2O$$

The separate reactions can also be summed up to overall reactions for the oxygen- and nitrate-based electrodeposition of ZnO, respectively:

$$Zn^{2+} + \frac{1}{2} O_2 + 2\ e^- \rightarrow ZnO$$

$$Zn^{2+} + NO_3^- + 2\ e^- \rightarrow ZnO + NO_2^-$$

Even though also other nanocrystalline oxides can be electrodeposited from aqueous solutions, ZnO outperforms these materials by an unusually high crystallinity. This high crystallinity is ascribed to dissolution and recrystallization of ZnO during the electrodeposition [3]. The ZnO films also show very good conductivity, which is partially ascribed to a chloride doping of the ZnO, if the films are deposited from a chloride-containing solution [185].

A very interesting variation of the electrodeposition of pure ZnO is the deposition of ZnO/organic hybrid structures with a structure-directing agent added to the deposition solution [3], as the pure ZnO is crystalline but has a very low surface, which is ineffective for DSCs. First experiments on the electrodeposition of a ZnO/dye hybrid film were made with a water-soluble tetrasulfonated phthalocyanine dye [186]. The xanthene dye EosinY was then introduced as a structure-directing agent (SDA) [187] and is now one of the most often used SDAs for the electrodeposition of nanostructured ZnO (see Figure 9). Even though the SDA influences the structure of the ZnO film, the crystallinity remains high. The crystal orientation can even be changed by variation of the SDA properties [188].

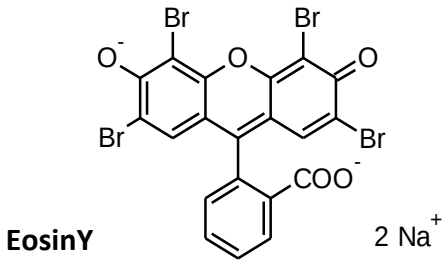

Figure 9 – Molecular structure of the sodium salt of a structure-directing agent for electrodeposition of ZnO, EosinY.

It was found early during the research of electrodeposition with dye structure-directing agents that the hybrid film with the incorporated dye could not be used as-prepared for an efficient electrode for dye-sensitized solar cells [3]. The resulting photocurrents were very low (even when a high light harvesting efficiency was reached) because the dye molecules in the ZnO matrix were either inaccessible to the electrolyte for regeneration, or were highly aggregated and excited electrons recombined within these aggregates. A method to overcome this problem is the desorption of the SDA (possible for example in KOH for EosinY) and the re-adsorption of the same or another sensitizer [3,9].

An interesting feature of the electrodeposition of ZnO was observed when the substrate was changed to aluminum or zinc by Stephanie Künze [189,190]. It was found that when the substrate (or a part of it, for example a thin film deposited from solution) consisted of zinc, a deposition of ZnO takes place even without applied voltage. This electroless deposition can, similar as discussed above for the

electrochemical deposition, be also performed with EosinY as a structure-directing agent. The electroless deposition on zinc in the presence of EosinY leads to porous ZnO films with a thickness self-limited to around 8 µm.

A variation of the nitrate-based electrodeposition is a pulsed electrodeposition. It was found that if the current or the voltage were pulsated in galvanostatic or potentiostatic deposition mode, the film quality and deposition rate could be enhanced, with or without the application of an SDA [191-197]. Especially the pulsed nitrate-based electrodeposition in galvanostatic mode, which was analyzed in detail by Martina Stumpp, was found to cover wire substrates in a favorable manner [198,199]. With this method, the complete coverage of the substrate can be directly monitored via the shape of the deposition curve, as the reduction reaction of the nitrate at different surface materials leads to different overpotentials. Such a monitoring of complete coverage of a substrate is vital for the possible application of solid hole-conductors as recombination gets more important there.

1.3.3 Photoelectrochemical characterization methods

In this chapter, the photoelectrochemical methods used for the characterization of DSCs in this work will be described briefly. The main aspect is to give the important relations of the measured values and the related equations, and thus point to how the respective method can be used for evaluation. More detailed information about the measurement methods, their principles and the derivation from theoretical models are found for example in [59,60,127].

1.3.3.1 Current-voltage curves

The current-voltage curve (IV-curve) gives much information about the characterized solar cell. The measurement consists in principle of a simple voltage sweep, where the current is measured. The resulting curve shows a diode characteristic, with the equation [59]

$$I = I_{ph} - I_{rec} = I_{ph} - I_0 \left(\exp\left(\frac{qV_f}{mk_BT} - 1\right)\right) \quad \textbf{(5)}$$

where I is the measured current density, I_{ph} is the photo-current density, I_{rec} is the recombination current density, I_0 is a constant determining the dark current of the solar cell, q is the elementary charge, V_f is the Fermi-level voltage (or internal voltage), see also section **1.1.3**, m is the diode quality factor, k_B is Boltzmann's constant, and T is the temperature. Some of the values will be explained in more detail further below. In principle, this equation is derived from the following conservation equation at steady state [200]

$$D_0 \frac{\partial^2 n}{\partial x^2} - U_n + G = 0 \qquad \textbf{(6)}$$

with D_0 the electron diffusion coefficient, n the free electron concentration, x the distance, U_n the recombination rate per unit volume, and G the generation rate.

Two IV-curves, one measured under illumination (typically "1 sun" – 100 mW cm^{-2} with an AM1.5 spectrum) and one measured in the dark, are shown in Figure 10. In the graph, important values of a solar cell are indicated. For most applications, the most interesting value is the power conversion efficiency η given by the equation [4]

$$\eta = \frac{P_{max}}{P_{in}} = \frac{I_{SC} V_{OC} FF}{P_{in}} \quad \text{and thus} \quad FF = \frac{P_{max}}{(I_{SC} V_{OC})} \qquad \textbf{(7)}$$

where P_{max} is the maximum attainable power of the solar cell, P_{in} is the power of the incident illumination, I_{SC} is the short-circuit current density, V_{OC} is the open-circuit voltage and FF is the so-called fill factor of the cell. Values like η, I_{SC}, V_{OC} and FF are already a good measure to compare solar cells with different preparation parameters, and so IV-curves give a good overview of the performance of the characterized solar cells.

Another value that can be determined from current-voltage curves is an estimation of the recombination current in the dark and under illumination [17,127]. The IV-curve measured in the dark already gives the recombination current in the dark, as in principle only recombination occurs there (no generation term). With the assumption that no recombination occurs at short-circuit conditions, an estimate of the recombination current under illumination, I_{rec}^{light} can be determined by subtracting the short-circuit current from the IV-curve measured under AM1.5 illumination.

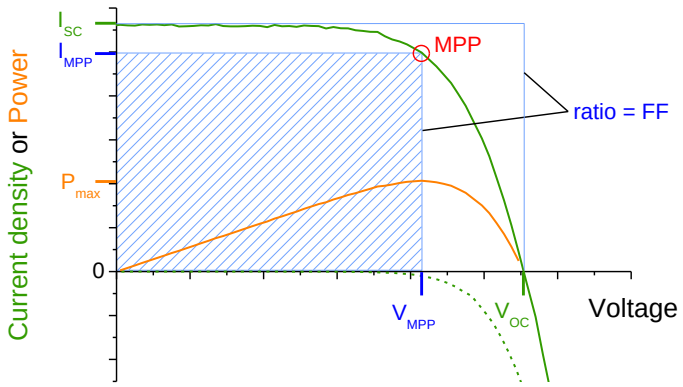

Figure 10 – Current-voltage curve and related values. The IV-curve measured in the dark is indicated by a green dashed line, the IV-curve under 100 mW cm^{-2} illumination is indicated by a continuous green line. The voltage with no current flow, V_{OC}, and the current at short circuit, I_{SC}, are indicated in the graph for the illuminated curve, as well as the maximum power point (MPP) and the respective current density and voltage. The power of the cell with respect to the voltage, calculated from the product of the current and the voltage, is also shown (orange line).

1.3.3.2 Incident photon-to-current conversion efficiency

The efficiency of current generation at different wavelengths is probed by the incident photon-to-current conversion efficiency (IPCE), also often termed external quantum efficiency (EQE). The resulting spectrum can give valuable information about the wavelengths at which the current in the cell is generated, especially when different dyes or different dyeing procedures are used. There are several methods to determine the current generation [4], from which two were used in this work. One method uses a monochromatic illumination at relatively low but modulated intensities, scanning through the available wavelength range. The comparison of the cell current to a reference photodiode measuring the photon flux Φ_{ph} allows the calculation of the IPCE. Another method of IPCE determination used in this work also utilizes a monochromatic illumination at relatively low illumination intensities, only excluding the modulation of the monochromatic light source. The IPCE can be calculated after following equation [4]

$$IPCE(\lambda) = \frac{(I_{SC}(\lambda))}{(q\Phi_{\mathrm{ph}}(\lambda))} \quad \textbf{(8)}$$

where $I_{SC}(\lambda)$ is the wavelength-dependent short-circuit current density, and $\Phi(\lambda)$ is the wavelength-dependent photon flux of the illumination source. From its physical origin, the IPCE consists of several values that all influence the IPCE, after [4]

$$IPCE(\lambda) = LHE(\lambda) \cdot \eta_{inj}(\lambda) \cdot \eta_{reg} \cdot \eta_{col}(\lambda) \quad \textbf{(9)}$$

where LHE is the light-harvesting efficiency or absorptance, calculated from the absorbance A of the cell with $LHE = 1 - 10^{-A}$, η_{inj} is the injection efficiency, η_{reg} is the regeneration efficiency (in some references included in η_{inj}), and η_{col} is the charge collection efficiency (most of the values depend on the wavelength).

The short-circuit current density I_{SC} of the cell can be calculated with an integral of the IPCE over the wavelength [4]

$$I_{SC,theor} = \int IPCE(\lambda)\, q\, \Phi_{ph}(\lambda)\, d\lambda \quad \textbf{(10)}$$

If the IPCE is determined at a low-intensity illumination (like for most measurements in this work), the photocurrent has to increase linearly with the intensity to render this relation valid also for a high photon flux, for example at AM1.5 illumination. By dividing the IPCE value with the LHE, the absorbed photon to current conversion efficiency (APCE, also called internal quantum efficiency) can be determined. This value gives the efficiency by which an absorbed photon is converted into an electron, allowing a better comparison of cells that absorb light by a different amount. Practically, the

value of the IPCE is limited to about 85% (if measured correctly) due to losses in the light-harvesting efficiency through reflectance and scattering of light at the substrate.

1.3.3.3 Photovoltage and photocurrent transients

From the variety of tools that can be applied for the characterization of DSCs, also photovoltage and photocurrent transients were used in this work. For the photovoltage transient, also called open-circuit voltage decay (OCVD) [201,202], the cell is first illuminated under open-circuit conditions until it reaches a steady value of the photovoltage. Then the light source is switched off, and the voltage (still at open-circuit) is measured against the decay time, see also Figure 11. The photovoltage shows an approximately exponential decrease for longer decay times, if recombination involves electrons from the conduction band [203]. From the inverse slope of the OCVD, the effective electron lifetime τ_n can be calculated after the equation [203]

$$\tau_n^{OCVD} = \frac{k_B T}{q}\left(\frac{dV_{OC}}{dt}\right)^{-1} \quad \textbf{(11)}$$

with t being the decay time in the dark. At voltages approaching short circuit, also possible recombination via the substrate influences τ_n^{OCVD} by decreasing this value, if this recombination path is not sufficiently blocked by integrating a blocking layer into the cell design [204,205]. Thus the OCVD measurement can be used as a sensitive monitor of the effectiveness of the blocking layer.

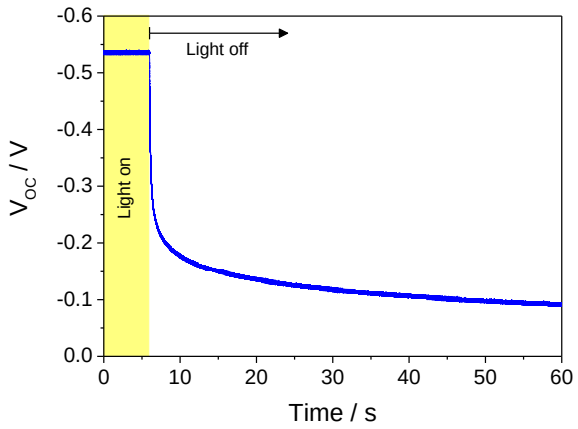

Figure 11 – Photovoltage transient of a DSC, where a yellow background color indicates the period of time where the cell is illuminated.

Photocurrent transients (also called charge extraction under short circuit) are performed analogously to the photovoltage transients [206,207]. After a time of illumination, with the cell under short circuit, the light is switched off while the cell is still under short-circuit conditions. From an integration of the decaying photocurrent, the charge stored in the semiconductor film (under short circuit, Q_{SC}) can be

determined. Using geometrical parameters of the film, the charge density under short circuit n_{SC} can be determined after the equation [206,207]

$$n_{SC} = \frac{Q_{SC}}{qAd[1-p]} \quad \textbf{(12)}$$

where A is the geometrical area of the porous semiconductor film, d is the thickness of the film and p the porosity of the film. Measurements at different illumination intensities allow a determination of n_{SC} for different short-circuit currents I_{SC}. Normalizing these curves for different cells to one reference cell, a relative value of the total trap density N_t with respect to the reference cell can be obtained after [17,127]

$$\frac{n_{SC}}{n_{SC,ref}} = \frac{N_t}{N_{t,ref}} \quad \textbf{(13)}$$

where the subscript "ref" denotes the values of the reference cell. The ratio $N_t/N_{t,ref}$ can be used for the normalization of the chemical capacitance from electrical impedance spectroscopy and of the electron transport time from intensity-modulated photocurrent spectroscopy [17,127] to exclude influences from different total trap densities.

1.3.3.4 Intensity modulated photocurrent/photovoltage spectroscopy

Two analogous methods that use modulated illumination to determine cell parameters are the intensity-modulated photovoltage and photocurrent spectroscopy (IMVS and IMPS). For both methods, the illumination intensity is modulated in a sine wave superimposed to a non-modulated intensity. The resulting photovoltage or photocurrent for different frequencies are measured, giving a semicircle in the Nyquist plot. IMVS is often used for the determination of the effective electron lifetime τ_n [208], which can be determined by fitting the imaginary part of the resulting data to the following equation [209]

$$im(\Delta V_{OC}) = -\frac{X_{OC}\omega\tau_n^{IMVS}}{\left(1+\omega\tau_n^{IMVS}\right)^2} \quad \textbf{(14)}$$

where X_{OC} is a scaling factor for the IMVS measurement and ω is the angular frequency of the light modulation. If the function cannot be fitted with a sufficient quality to measurement data, the electron lifetime can also be estimated from the frequency at the maximum of the semicircle ω_{min} [203], with $\tau_n^{IMVS} = 1/\omega_{min}^{IMPS}$. In a semi-logarithmic plot of the resulting lifetimes τ_n against the open-circuit

voltage, an approximately linear relationship is observed, with increasing lifetime for decreasing absolute values of V_{OC}.

Analogously, for the IMPS measurements the time constant for charge collection at short circuit can be determined from the response to the light modulation for the cell at short circuit [210]. This time constant is often referred to as effective electron transport time τ_{tr} (also transit time) This time can (analogously to τ_n) either be determined by a fit to

$$im(\Delta I_{SC}) = -\frac{X_{SC}\omega\tau_{tr}^{IMPS}}{\left(1+\omega\tau_{tr}^{IMPS}\right)^2} \quad \textbf{(15)}$$

where X_{SC} is a scaling factor for the IMPS measurement, or from the frequency at the maximum of the semicircle ω_{min} [211], with $\tau_{tr}^{IMPS} = 1/\omega_{min}^{IMPS}$. In principle, the time constant determined from IMPS measurements also contains contributions from recombination (or the electron lifetime τ_n). For the usual measurement condition, short circuit, τ_n is large enough to ensure that influences from recombination do not influence the time constant determined from IMPS by a too large extent, so that this time constant equals the electron transport time τ_{tr}. To exclude influences of the total trap density N_t on τ_{tr}, the values can be normalized relative to a reference cell with the ratio given in equation (13) [17,127]. In a semi-logarithmic plot of τ_{tr} vs. I_{SC}, τ_{tr} usually shows a linear decrease with increasing I_{SC}. The slope of the curves is also influenced by the trap-distribution parameter α (see section **1.3.3.5**

Combining the values determined from IMVS and IMPS, the charge collection efficiency η_{col} is often calculated after the equation [4]

$$\eta_{col} = \frac{1}{1+\left(\frac{\tau_{tr}}{\tau_n}\right)} \quad \textbf{(16)}$$

For the values from IMVS and IMPS at open and short circuit, respectively, this calculation gives only a rough estimate of η_{col}, as both values are determined at a different state of the cell which in turn leads to a different Fermi level [203]. To overcome this difference, the difference of the Fermi level can be determined under short and open circuit via charge extraction at open-circuit [203,212], or the charge collection values can be estimated with the help of electron lifetime values from for example impedance spectroscopy at approximately the same Fermi-level as the transport times [17].

A method for the calculation of a more exact value of η_{col} was described by Schlichthörl et al. [209]. There the nonlinearity of the recombination rate on the electron concentration in the semiconductor (which was described as a main cause for the inaccuracy of η_{col} as determined by the simple combination of IMVS and IMPS time constants) is accounted for by the introduction of a factor m_1 (or the inverse of the trap distribution parameter α [213]). IMVS and IMPS measurement are performed and

evaluated as described before. The parameter m_1 is determined from the slope of a plot of $\ln(I_{SC})$ over $\ln(I_{SC} \cdot \tau_n)$.

The collection efficiency can then be calculated from the characteristic time constants τ_n and τ_{tr} from IMVS and IMPS measurements and the slope m_1 with the following relationship

$$\eta_{col} \approx 1 - \left(\frac{\tau_n}{\tau_{tr} \cdot 1.2}\right)^{-\frac{m_1}{0.9}} \quad \textbf{(17)}$$

1.3.3.5 Electrochemical impedance spectroscopy

A very versatile method for the study of dye-sensitized solar cells is the electrochemical impedance spectroscopy (EIS). This method is described in detail in many works [60,214,215,216]. The basic concept of the EIS measurement is similar to IMPS and IMVS measurements, with a periodic perturbation of the voltage that is applied to the solar cell, and the cell response is then measured for different frequencies of the modulation. Conveniently, some of the DSC elements lead to characteristic features of the solar cell, allowing the distinction and determination of different cell values via a fit of the impedance spectrum to an established model (see also Figure 12). The different values include the series resistance of the substrate, the wires and contacts R_s, the chemical capacitance of the porous sensitized film C_μ, the recombination resistance at the semiconductor+dye/electrolyte interface R_{rec}, the electrolyte resistance Z_d and the resistance and capacitance of the platinized counter electrode (R_{Pt} and C_{Pt}). For TiO_2-based solar cells at low absolute voltages, another element can be determined, the transport resistance R_{tr}. For high voltages (more charge accumulated) and for ZnO-based cells (higher conductivity of ZnO compared to TiO_2), this resistance is not observed as a feature in the impedance spectra, as the high conductivity leads to a small transport resistance [203]. The most informative measurement of the EIS is a consecutive measurement of different spectra over a range of applied voltages.

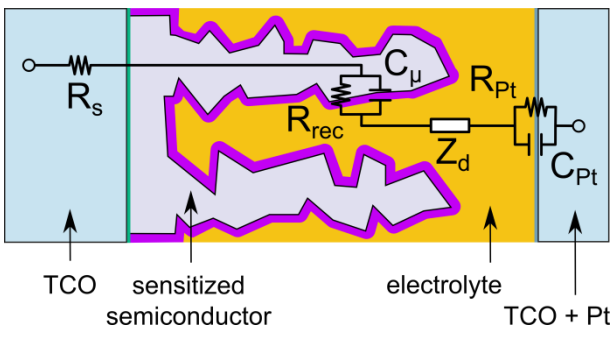

Figure 12 – Illustration of a DSC and the respective (simplified) equivalent circuit model for a TiO_2-based cell at high voltages, after [60]. See also Table 2, p. 60 for the designation of the respective circuit elements.

This representation allows the determination and comparison of different influences on the chemical capacitance and the recombination resistance, for example the relative conduction band edge position of different cells. When currents flow through the cell, the applied voltage V_{app} has to be corrected for voltage losses at the cell series resistance, resulting in the Fermi-level voltage V_f

$$V_f = V_{app} - V_{series} \quad \textbf{(18)}$$

with V_{series} being the voltage drop at the overall series resistance R_{series}. V_{series} is obtained out of the following integration [17,60,215]

$$V_{series} = \int_0^i R_{series} di \quad \text{with} \quad R_{series} = R_s + Z_d + R_{Pt} \quad \textbf{(19)}$$

where i is the current flowing through the cell. With this method and under the assumption that the series resistance stays constant over the measurement range, also the IV-curves can be corrected for series resistance influences, and so-called internal IV-curves can be calculated.

Another method can be used for the determination of the corrected voltage V_f, the determination via the resistance of the nanoporous film [17,60]. If $R_{rec} > R_{tr}$, V_f can be determined from the following equation

$$V_f = V_{OC} + \int_0^i \frac{1}{3} R_{tr} + R_{rec} di \quad \textbf{(20)}$$

When R_{tr} is small, it can be assumed that it does not influence the overall resistance, and the integration can be performed only over R_{rec}.

The chemical capacitance C_μ, also called thermodynamic density of states [59,217], has a dependence on the voltage which can be described by the following relationship [60,127,215]

$$C_{\mu,theor} = \alpha N_t \frac{q^2}{k_B T} \exp\left(\alpha \frac{qV_f - E_c}{k_B T}\right) \quad \textbf{(21)}$$

where "theor" indicates that the values are calculated based on the theory. E_c is the energy of the conduction band edge. α is the trap distribution parameter, often given also as the ratio of the characteristic temperature of the distribution of the traps T_0 to the temperature during the measurement [203]

$$\alpha = \frac{T}{T_0} \quad \textbf{(22)}$$

Typically, C_μ shows an exponential variation with the Fermi-level voltage V_f after equation **(21)**. However, for high (absolute) voltages, the accumulated charge leads to an additional capacitance that eventually dominates the overall capacitance and leads to a saturation of the capacitance. This capacitance has its physical origin either in a thin dielectric layer at the electrode-electrolyte interface, or in the double-layer capacitance at this interface, and a part of the voltage drops at this capacitor. This capacitance is often simplified as a constant Helmholtz capacitance C_H, which is in series to C_μ [218]. For voltages approaching 0 V, another capacitance dominates the overall capacitance, the space-charge capacitance C_{SC}. This dielectric capacitance has its origin in a Schottky-barrier at the semiconductor-substrate interface or the semiconductor-electrolyte interface [219]. For increasing forward voltage, the space-charge region decreases and C_{SC} increases, while for increasing reverse bias, the space-charge region increases and C_{SC} decreases, after [220]

$$C_{SC} = A\left(\frac{\epsilon_r \epsilon_0 q N_{SC}}{2(V_f - V_{bi})}\right)^{\frac{1}{2}} \quad \textbf{(23)}$$

with ϵ_r the relative permittivity of the semiconductor material, ϵ_r the vacuum permittivity, N_{SC} the doping concentration in the semiconductor material and V_{bi} the built-in voltage of the Schottky-barrier. This relationship is also known as Mott-Schottky relationship, with a linear dependence of ${C_{SC}}^{-2}$ on the voltage [220].

Additionally to the mentioned capacitances, another capacitance can appear in the capacitance-voltage plot, the capacitance of deep monoenergetic trap states C_{mono} that are not in thermal equilibrium with the exponential trap distribution [65]. If this capacitance is present, it appears as a peak or shoulder between the regions where C_{SC} and C_μ dominate the overall capacitance. These monoenergetic trap states contribute to the total capacitance with the following relationship derived from a Fermi-Dirac distribution [218]

$$C_{mono} = \frac{N_{mono} q}{k_B T} f(1-f) \text{ with } f\left(V_f - V_{mono}\right) = \frac{1}{1+\exp[q(V_f - V_{mono})/(k_B T)]} \quad \textbf{(24)}$$

with N_{mono} the density of monoenergetic trap states and qV_{mono} the energetic position of the monoenergetic trap states in eV. The combination of the different contributions of the overall capacitance will be discussed in section **3.3.1**.

From the chemical capacitance, the density of states (DOS) can be calculated via the equation [221]

$$DOS = C_\mu/(qAd[1-p]) \quad \textbf{(25)}$$

When the trap distribution parameter α of the chemical capacitance plot has a comparable value for different cells, the relative position of the conduction band edges of these cells can be determined from

the horizontal shift of the capacitance curves in the C_μ-voltage plot. The value determined is mostly the conduction band edge shift ΔE_c relative to a reference cell. However, also the total trap density N_t, which often has different values for different cells, affects the chemical capacitance by a vertical shift. To exclude influences of N_t on conduction band edge shifts, C_μ is normalized relative to a reference cell, using the ratio from equation **(13)** [17,127].

Another important value for the comparison of different DSCs is the recombination. Based on the finding that recombination generally occurs non-linearly in DSCs, the recombination rate U_n in equation **(6)** is given with the empirical equation [127,200]

$$U_n = k_r n^\beta \tag{26}$$

where n is the free electron concentration, k_r is the recombination rate constant and β is the recombination parameter, or according to this equation an empirical estimation of the reaction order in sublinear recombination kinetics. High values of β (β ≈ 1) were reported especially for DSCs where recombination takes place predominantly via the conduction band edge, while for typical DSCs with recombination via semiconductor surface states and conduction band edge states, β values around 0.5 to 0.7 were reported [222]. If recombination via surface states within the energy gap of the semiconductor is the only source of nonideality, then β relates to the ideality factor m of the cell with the inverse [203]

$$\beta = 1/m \tag{27}$$

The recombination can also be compared via the recombination resistance R_{rec}. This resistance can be determined for example from the fitting of the electrochemical impedance spectra, and it gives a measure of how efficiently recombination is blocked. With increasing accumulated charge for increasing voltages, R_{rec} decreases after the relationship [60,127]

$$R_{rec} = R_{rec,0} \exp\left(-\beta \frac{qV_f}{k_B T}\right) = \frac{k_B T}{q\beta j_{0k}} \exp\left(-\beta \frac{qV_f}{k_B T}\right) \tag{28}$$

with R_{rec} the exponential prefactor, and j_{0k} the recombination rate independent of the conduction band position. Comparable to the chemical capacitance, R_{rec} is found especially in an intermediate voltage range and for higher voltages. For voltages approaching 0 V, the approximately constant back layer resistance R_{BL} dominates the overall resistance and leads to a flattening of the resistance curve vs. voltage [60].

Another parameter that describes recombination is the constant determining the dark current of the solar cell, I_0, which can also be seen as an exchange current density. I_0 is given by several other parameters after the following equation [127]

$$I_0 = I_{0k} \cdot \exp\left(-\frac{\beta E_c}{k_B T}\right) = q k_r d\, {N_c}^{\beta} \cdot \exp\left(\frac{\beta E_{redox}}{k_B T}\right) \cdot \exp\left(-\frac{\beta E_c}{k_B T}\right) \quad \textbf{(29)}$$

with I_{0k} describing the dependence of the current on the recombination rate constant k_r (independent of the position of the conduction band edge), and N_c being the effective density of states at the position of the conduction band edge. When R_{rec} is plotted against the Fermi-level voltage corrected for conduction band edge shifts, V_c, and when cells have similar β values, in this context differences in R_{rec} directly correlate to the reciprocal of the differences in the kinetic parameter I_{0k}. (See also below for the dependence of V_{OC} on I_{0k}.)

From C_μ and R_{rec}, the effective electron lifetime τ_n can also be determined by [203]

$$\tau_n^{EIS} = R_{rec} C_\mu \quad \textbf{(30)}$$

As for lower voltages R_{rec} and C_μ are affected by influences from the back layer (i.e. electrode and blocking-layer), the product of these values reflects the electron lifetime for intermediate voltages only [205]. A very small to no difference should be observed for lifetimes obtained from EIS or from IMVS measurements, as the semicircle from which the lifetime is determined in IMVS measurements corresponds to the semicircle from which R_{rec} and C_μ are determined in EIS measurements [223].
Additionally to the usual plot of R_{rec} and τ_n against the voltage V_f, another representation can give useful information about the characterized cells. Both values, R_{rec} and τ_n, represent recombination in the cell, and thus depend on the density of states in the semiconductor. A plot against the DOS (calculated from C_μ) excludes the effects of the DOS (and thus also of different α and N_t) on R_{rec} and τ_n, thus giving a method to compare even cells with different trap distribution and total trap density [16,18,127].
With the values determined from EIS and other measurements, different influences on the open-circuit voltage are given. The following equation sums up these different influences in a mathematical expression based on the diode equation (equation **(5)**) [60]

$$V_{OC} = \frac{E_c}{q} + \frac{k_B T}{q\beta} \ln\left(\frac{I_{SC}}{I_{0k}}\right) \quad \textbf{(31)}$$

A difference in V_{OC} can be determined for differences in I_{SC} and the recombination rate I_{0k}, relative to a reference cell [17,127]. When the trap distribution parameter α is of a comparable value for the cells (for the determination of ΔE_c), and when the recombination parameter β is also similar for all compared cells (for the validity of the following two equations), a difference in V_{OC}, ΔV_{OC}, can be calculated for the different influences. The following equation gives $\Delta V_{OC}(I_{SC})$, the voltage difference caused by a difference in the short-circuit current [17]:

$$\Delta V_{OC}(I_{SC}) = \frac{k_B T}{q\beta} \ln\left(\frac{I_{SC}}{I_{SC,ref}}\right)$$

(32)

The subscript "ref" indicated the current of the reference cell. As difference of the recombination rates I_{0k} for two different cells cannot be directly determined, the difference of the recombination current under illumination I_{rec}^{light} can be calculated instead, provided that the recombination parameter β is of a comparable value, and that the value of I_{rec}^{light} is determined at the same density of states (for example by a correction of the voltage by the difference in the conduction band edge). This leads to [17]

$$\Delta V_{OC}\left(I_{rec}^{light}\right) = \frac{k_B T}{q\beta} \ln\left(\frac{I_{rec,ref}^{light}}{I_{rec}^{light}}\right)$$

(33)

Again, the subscript "ref" indicates the current of the reference cell. In this equation, the current of the reference cell is in the numerator, as a higher recombination current leads to a lower V_{OC}. In contrast to this, in equation **(32)** the current of the reference cell is in the denominator, as a higher short-circuit current leads to a higher V_{OC}.

With the value of ΔE_c and the shifts of the open-circuit voltage determined from differences in I_{SC} and I_{rec}^{light}, the overall theoretical change in V_{OC}, $\Delta V_{OC,calc}$, due to these three influences (relative to a reference cell) can be calculated by the following equation [17]

$$\Delta V_{OC,calc} = \Delta E_c/q + \Delta V_{OC}(\Delta I_{SC}) + \Delta V_{OC}\left(I_{rec}^{light}\right)$$

(34)

Also the fill factor shows a defined dependence on different factors, especially β and V_{OC} [60]

$$FF = \frac{\beta\frac{qV_{OC}}{k_B T} - \ln\left(\beta\frac{qV_{OC}}{k_B T} + 0.72\right)}{\beta\frac{qV_{OC}}{k_B T} + 1}$$

(35)

With this equation, the different influences on FF can be discussed.

1.3.3.6 Measurement of the current or voltage vs. light intensity

Recombination parameters can also be determined from the measurement of the photocurrent or photovoltage against a varied illumination intensity. The cell is set to short-circuit conditions (photocurrent measurement) or to open-circuit conditions (photovoltage measurement), and the illumination intensity is gradually increased, with a certain time between the measurement points which allows the cell to adapt to the new illumination conditions.

The curve shape obtained from the measurement of the photovoltage vs. intensity gives mainly information about the recombination in the cell [65]. An approximately linear shape of the curve in a semi-logarithmic plot (especially at high voltages or intensities) indicates a well-functioning solar cell [203,204], with the slope at high intensities following the relationship [203]

$$V_{OC} \propto \frac{mk_BT}{q} \ln(I_0) \quad \textbf{(36)}$$

with I_0 the intensity of the illumination. In the absence of other nonidealities than recombination via surface states, the ideality factor m can be directly transformed to the recombination parameter β via equation **(27)**. This is assumed to be the case for the calculations in this work, even though other nonidealities may arise, for example the recombination via oxidized dye molecules [17]. A more detailed analysis of this measurement [65] revealed that for higher intensities, the recombination is dominated by recombination via the conduction band (with an ideal slope of 59 mV for m = 1), for intermediate voltages shallow surface traps (within the exponential trap distribution) dominate the slope of the V_{OC} vs. intensity plot, and for very low intensities the recombination occurs via deep monoenergetic trap states. For a high exchange current via the substrate-electrolyte interface, which means an inefficiently working blocking layer between substrate and nanoporous film, the voltage decreases earlier for low illumination intensities.

The measurement of J_{SC} dependent on the illumination intensity ideally results in a line in a logarithmic plot. However, when the regeneration of the oxidized dye by the reduced electrolyte species (I^- for iodide-based electrolytes) is not sufficiently efficient, recombination can also take place via the oxidized dye. This can be the case for a lower concentration of the redox species in the electrolyte, which leads to a depletion of the reduced electrolyte species at high light intensities. As this recombination also takes place at short circuit (in contrast to the assumption for the recombination via surface trap states and the conduction band edge), the current at high light intensities is diminished when the regeneration efficiency η_{reg} is too low due to such a depletion of the redox species in the electrolyte. This means that the measurement of I_{SC} vs. intensity, especially at varied concentration of the electrolyte, can give information about the regeneration of the studied dye-sensitized solar cells.

1.3.4 Microscopy

1.3.4.1 Scanning electron microscopy

Scanning electron microscopy is a widely used method to characterize the structure of diverse samples. This method uses electrons as the "illumination" source, which allows a higher spatial

resolution of the resulting image than the use of visible light in an optical microscope, simply due to a lower de-Broglie wavelength of electrons. The main element of a scanning electron microscope (SEM) is the electron beam, which is generated and then focused on the sample. Because of the low travelling distance of electrons in air, the whole system has to work under vacuum. The electron beam used for the imaging process is often generated at a heated filament, where electrons are extracted by an applied high voltage of several kV. The extracted electrons are then accelerated by an applied voltage at an anode, and by electromagnetic lenses the beam can be focused, tuned and directed to the surface of the sample. Electrons that thus hit the sample surface (primary electrons) interact with the sample atoms in various ways resulting for example in backscattering of a primary electron, emission of a secondary electron accompanied by emission of X-rays, and emission of a secondary electron accompanied by the emission of an Auger electron. By scanning the surface of the sample with the electron beam and detecting secondary electrons emitted from the sample, the surface topology can be reconstructed. However it is important to remember that the emission of the secondary electrons from the sample is not only dependent on the energy of the electron beam, but also on the properties of the sample (i.e. high or low atomic mass, ionization potential or work function, conductivity), which requires a careful consideration of the obtained image, or a comparison with results from other measurement techniques. Some of these techniques, like EDX (energy-dispersive X-ray spectroscopy) for the analysis of the elemental composition can be used directly at the SEM signals with an appropriate sensor [224,225,226].

1.3.4.2 Confocal Microscope

Confocal microscopy works with the resolution of a standard optical microscope, but allows additionally a tree-dimensional analysis of the surface. A confocal microscope works on the principle that the measured point on the sample is on the same focal plane as (or confocal with) the light source and the detector. This is usually realized by first emitting the light (often UV light to obtain a higher resolution) from the light source through a small hole. The light is then pointed on the sample with a mirror (and beam splitter), which can be moved to successively scan the complete imaging area. Light reflected from the sample can pass though the beam splitter to the detector. Before reaching the detector, the light has again to pass through a small hole, the confocal aperture. The exact position of this hole ensures that only the point located directly on the focal plane passes through the hole and contributes to the signal. When the scan of one plane is completed, the sample or the focusing unit is moved in z-direction, and another plane is scanned, thus gradually giving a three-dimensional picture of the sample [227].

2 Experimental Procedures

2.1 Electrodeposition of hybrid ZnO-EosinY-films on planar substrates

The majority of the characterized ZnO films were deposited with the following deposition routine, very similar to the deposition routine established in our laboratory by Max Beu [123] and Christoph Richter [130].

2.1.1 Preparation of the substrate

FTO-coated glass sheets (thickness 2 mm, resistivity ~7 Ω/sq., Aldrich) were cut in pieces of 2.5 cm x 3 cm. The FTO glass was then cleaned subsequently with a detergent (20 mL RBS®25 for 1 L H_2O, Roth), acetone (Roth, ≥ 99.8%) and 2-propanol (Roth, ≥ 99.8%), each for 15 min in an ultrasonic bath. The substrates were rinsed thoroughly after each cleaning step and then stored in 2-propanol until use.

For deposition, a cleaned substrate is inserted into a stainless steel substrate holder (insulated against the electrolyte with the polymer Polyoxymethylene (POM) on the outer edge). The FTO film is contacted with a conductive tape (Parker Chomerics), and afterwards covered with a mask of typically 1 cm x 1 cm opening for the deposition of the ZnO blocking layer (green FN914, Polyester, FN Klebeprodukte; alternatively a clear tape from 3M for larger areas to ensure adhesion during the complete time of electrodeposition). This mask also serves to isolate the contacts against the deposition solution (see also Figure 13). The resistance of the mounted substrate is measured and should not exceed 20 Ω to ensure a successful deposition of ZnO. The complete substrate holder can then be mounted onto the rotating unit of a rotating disc electrode setup (CTV101 speed control unit with BM-EDI101 rotating disc electrode, Radiometer analytics).

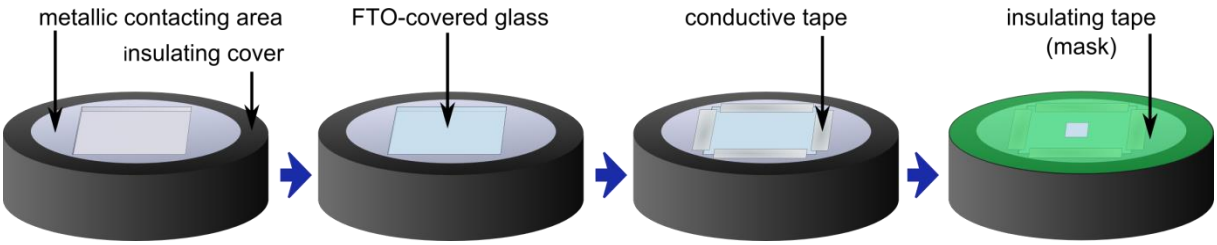

Figure 13 – Preparation of sample holder and FTO-covered glass for electrodeposition.

2.1.2 Deposition of porous ZnO films

150 mL of a 0.1 M KCl (Roth, ≥99.5%) solution are added into a thoroughly cleaned double-walled deposition cell that is kept 70°C. The substrate holder including the masked substrate is then mounted onto the rotating disc electrode (head down) and included into the cell cover. This setup then covers the tempered cell. A reference electrode (RedRod, Ref201, Ø 7.5 mm, Radiometer) in a salt bridge, a counter electrode (Pt-wire, min. 10 cm long) and an O_2-frit are added into different holes of the cover. The O_2 flow is set to 400 cm^3 min^{-1}. A different frit is used for the activation and the deposition of the blocking layer (without EosinY) and for the deposition of the porous layer (with EosinY) to avoid a contamination of the blocking layer with EosinY. A reflux cooler at the gas outlet of the cell minimizes the evaporation loss of water from the deposition solution. After these preparations, the solution is allowed to be saturated with O_2 for about 10 min, while the substrate is already rotated at the final rotating speed of 500 rpm.

The deposition itself is carried out in three phases, activation of the substrate, deposition of ZnO blocking layer and deposition of the hybrid ZnO-EosinY film.

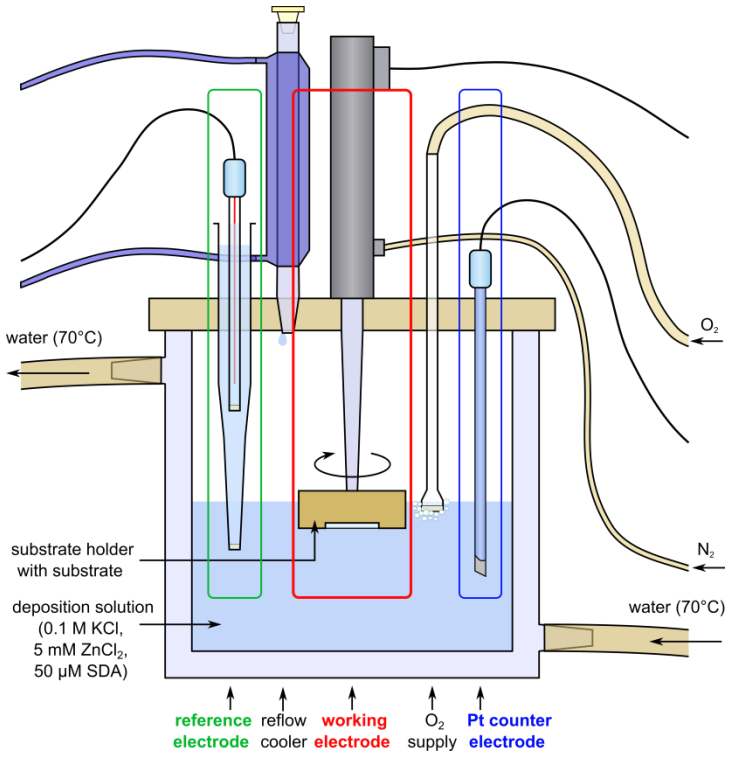

Figure 14 – Schematic representation of the setup for electrochemical deposition on conductively coated glass substrates.

Phase I: Activation of the substrate

A voltage of -1.16 V vs. Ag|AgCl is applied to the substrate for at least 300 s or until a steady value of -2.9 mA/cm² (as an optimum) is achieved. During this phase the solution consists only of 0.1 M KCl. The voltage is maintained with a Wenking LPG 03 potentiostat (Bank Elektronik) controlled via the associated software CPC.

Phase II: Deposition of ZnO blocking layer

This phase is performed directly following Phase I, as the CPC software allows a programming of different voltages. The voltage is first changed to -1.06 V and directly afterwards 1 mL of a stock solution of $ZnCl_2$ (from $ZnCl_2 \cdot 6\ H_2O$; Merck, ≥ 98.0%) is added to the deposition solution. This leads to a final concentration of $ZnCl_2$ in the deposition bath of 5 mM. The voltage is maintained for 10 min.

For standard films (for use in DSCs), the blocking layer has a larger area than the hybrid ZnO-EosinY film. Therefore after the deposition of the blocking layer, the mask has to be changed. In this case the following steps have to be performed:

- Removing of the substrate holder from the deposition cell and rinsing of the ZnO film with warm water and water at RT, subsequently, to avoid quick drying and thus mechanical stress of the blocking layer.
- Drying of the film with dry N_2 and replacement of the mask by a mask with a smaller opening (generally a round hole with 7 mm diameter, see Appendix **9.4** for the respective diameter of each cell).
- Mounting of the substrate holder to the rotating disc electrode setup, closing of the electrodeposition cell.

Phase III: Deposition of hybrid ZnO-EosinY film

Before the deposition of the hybrid ZnO-EosinY film can be started, there are still steps to be taken. First, the counter electrode is changed to a Zn wire (Ø 1mm, Goodfellow, 99.9%), cleaned by sandpapering and rinsed with deionized water before introducing it into the deposition bath. Secondly, the O_2 frit is changed for the one used during deposition with EosinY. Thirdly, a certain amount of EosinY stock solution (Kanto Chemical, ≥ 85 %) is added to the deposition solution, so that a concentration of 75 µM is achieved in the deposition bath (for a variation an EosinY concentration of 50 µM was used).

After that, a voltage of -0.96 V vs. Ag|AgCl is applied for a period of 20 minutes. At the end of the deposition, the substrate holder is put into warm water (heated to 70°C beforehand) and is allowed to cool to RT. This slow cooling should enhance the quality of the ZnO film by avoiding cracks.

After the films are prepared with this three-phase procedure, they are put into a KOH solution (from solid KOH; Merck, > 85%) with pH 10.5. The pH value is set using pH-paper with a range from pH10.1 to pH11.3 (L683, Lyphan, Dr. Gerhard Kloz). The films are left in this desorption solution overnight, and are then thoroughly rinsed with deionized water. Remnants of the conductive tape on the edges of the FTO used for contacting are removed with a tissue or with 2-propanol (no acetone, as the ZnO film is more brittle after treatment with acetone). The porous ZnO films are dried with a flow of dry N_2 and kept dry in a petri dish (wrapped with Parafilm®, Bemis Flexible Packaging) until use.

2.2 Electrodeposition of ZnO-EosinY hybrid films on metal wires and threads

Aluminum wires (Goodfellow, 99.95+ %, degree of hardness: as-drawn, Ø 250 µm or 50 µm), tantalum wires (Alfa Aesar, 99.9+ %, Ø 250 µm, annealed, temper: soft) and metal-coated polyamide threads (from project partners, TITV Textilforschungsinstitut Thüringen Vogtland e.V., Dr. A. Neudeck and TU Clausthal, Institute of Electrochemistry, Prof. Dr. F. Endres) are used as different substrates for the electrodeposition of hybrid ZnO-EosinY films. Nitrate- and oxygen-based electrodeposition is performed on these substrates. Prior to the electrodeposition, the substrates are cleaned and a part of the samples is pretreated with the pretreatment methods mentioned below.

2.2.1 Treatment of wires and threads

2.2.1.1 Preparation for electrodeposition

Laminating of samples: All wire- or threadlike substrates were masked for an easy realization of the deposition. For this purpose, the wires are laminated between the two layers of a laminating foil (Laminierfolie, Karstadt) with a precut window of a defined length. A silver-coated contact thread (Elitex®, from project partner TITV) is inserted into the laminating foil and led to the outside of the laminating foil for contacting during deposition. The contact between the deposition wire/thread and the Elitex® contact thread is enhanced by adding conductive silver paste (G3692 Acheson Silver DAG 1415, Plano), see Figure 15.

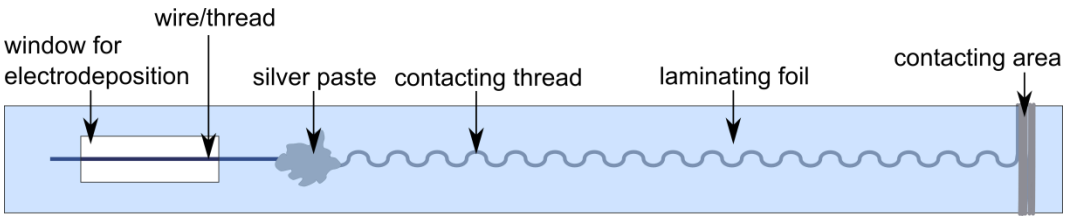

Figure 15 – Schematic representation of a laminated wire/thread with contacting, used for the electrodeposition of ZnO on wires/threads.

Cleaning: Metal wires are sonicated subsequently for 10 min in acetone and 2-propanol. Metal-coated threads are left in 2-propanol for 10 min to prevent damages in the metal coatings.

2.2.1.2 Pretreatment of samples

For most of the used wires/threads, the deposition takes place on a passivated metal like Al or Ta. As the deposition on untreated Al gave no good results (see also [228]), the Al substrates have to be pretreated for a successful deposition. Different pretreatments were tested (also by Stephanie Künze [190]) and are further discussed in the results part.

Pickling routine: The aluminum oxide layer is dissolved in 20 wt% NaOH solution (from solid NaOH, Merck, ≥ 99%), remnants from the etching are removed in a 32% HNO_3 (Roth, "reinst") and a Zn layer is formed in a zincate solution. The zincate solution consists of 35 wt% NaOH with added 7.5 wt% of ZnO (Sigma-Aldrich, 99+ %) [189,190].

For Al wires, especially the dipping times in each solution had to be adjusted, and the following procedure was used for most Al wire samples, with rinsing in deionized water and careful drying in a nitrogen flow repeated after every step:

- 20 s dipping in NaOH solution
- 20 s dipping in HNO_3
- 20 s dipping in zincate solution
- 20 s dipping in HNO_3
- 1 min dipping in zincate solution

For Al-coated threads, only the last step (including rinsing and drying) was performed after some initial experiments.

Electrochemical etching: The oxide layer of some Al wires was also etched in the electrochemical bath before oxygen-based electrodeposition of ZnO. Before $ZnCl_2$ is added to the solution (deposition solution only containing KCl) and before the deposition starts (step 1 in section **2.2.2.1)**, a more negative voltage of -1.65 V vs. Ag|AgCl is applied to the substrate wire. The voltage is applied over a time of 300 s.

H_2O_2-based deposition of blocking layer: For some samples (coded H2O2), the deposition of the blocking layer, see step 2 in section **2.2.2.1**, was performed with a H_2O_2-based electrodeposition. The electrolyte for the deposition consisted of an aqueous solution of 0.1 M KCl and 50 mM H_2O_2. The blocking layer was deposited with or without stirring the solution, in a different bath than the oxygen-based electrodeposition and not directly before the oxygen-based electrodeposition. For most samples that were pretreated with this method, a voltage of -1.06 V vs. Ag|AgCl was applied for 100 or 200 s. The exact conditions are given in the text.

2.2.2 Electrodeposition methods for wires or threads

Two methods were used to deposit ZnO films on metal wires or metal-coated threads, first the potentiostatic electrodeposition in an oxygen-saturated deposition solution (deposition also used by Thomas Loewenstein [229], Kerstin Strauch [230], Alexander Geiger [231] and in a project cooperation [46,232]), and second the deposition with zinc nitrate with pulsating current applied to the substrate (developed by Martina Stumpp [193,198], based on the deposition of ZnO with pulsating voltage, developed by Melanie Rudolph and others [191,233]). Both deposition methods were performed using an IVIUMstat potentiostat (IVIUM technologies). Further details are described below.

2.2.2.1 Oxygen-based electrodeposition of ZnO

In principle, the oxygen-based deposition is very similar to the deposition on planar substrates (see also section **2.1**). The deposition solution contains 0.1 M KCl in the beginning, and is warmed to 70°C. At the beginning of the different phases of electrodeposition, $ZnCl_2$ as zinc salt and EosinY as structure directing agent are added. A RedRod reference electrode is used, together with a Pt sheet counter electrode (M241PT, Radiometer analytics). Prior to deposition, the solution is purged with oxygen for at least 10 min, to ensure oxygen saturation. During deposition, an oxygen flow of 400 cm^3 min^{-1} is established. Then, the cleaned substrate is inserted through one of the holes in the cover, and the deposition can start. In detail, the deposition was carried out as follows:

1. If an electrochemical etching or activation of the substrate is used for the substrate, this phase is carried out first, preferentially in the same deposition bath and directly followed by the second phase (see above).
2. For the deposition of a ZnO blocking layer, 1 mL of a $ZnCl_2 \cdot 6\ H_2O$ solution is added to give a final Zinc concentration of 5 mM. A voltage of -1.06 V vs. Ag/AgCl is applied for typically 100 s.
3. The deposition of a porous layer is achieved by adding EosinY stock solution (final concentration 50 or 75 µM (both concentrations showing very similar results in [234]). The voltage is again -1.06 V vs. Ag/AgCl, the deposition time is typically 1000 s.

After deposition, the ZnO-coated samples are directly transferred into warm deionized water (70°C) and the water is then allowed to slowly cool to room temperature. This slow cooling leads to less stress to the ZnO layer and reduces the occurrence of cracks in the ZnO film.

2.2.2.2 Nitrate-based electrodeposition of ZnO

The nitrate-based electrodeposition as described here was used by Martina Stumpp[192,198], also some of the samples used in this work were deposited by her.

The deposition solution consists of a 0.1 M zinc nitrate hexahydrate solution ($Zn(NO_3)_2 \cdot 6\ H_2O$, Sigma-Aldrich, ≥ 99.0%). To achieve a porous layer, EosinY is added to the solution to give a concentration of 75 µM. The solution is saturated with N_2 for at least 10 min prior to deposition. During the deposition a nitrogen flow of 400 $cm^3\ min^{-1}$ is maintained above the solution to avoid solution movement. The reference and counter electrode are the same as in **2.2.2.1**.

For the deposition, a pulsating current is applied to the substrate. During the on-time, a current density of -100 mA cm^{-2} is applied, while during the off-time a current of 0 mA cm^{-2} is applied. The on- and off-time both last 0.01 s and are repeated 5000 times. The complete deposition time is 100 s (IVIUM settings: Interval time 0.002 s, voltage range 4 V). For an optional blocking layer, the EosinY solution is added during the deposition instead of before. The deposition time remains 100 s. After deposition, the sample is transferred into warm water and allowed to cool slowly to room temperature (see also **2.2.2.1**).

2.3 Preparation of porous TiO_2 films

2.3.1 Preparation of TiO_2 blocking layer

For the preparation of a TiO_2 blocking layer, a solution for spin-coating has to be prepared. First, a solution of 370 µL of Titanium(IV) isopropoxide (Aldrich, 97%) in 2.53 mL ethanol (ethanol denaturated, Roth, purity ≥ 99.8% – including ca. 1% methyl ethyl ketone) is prepared. While stirring this solution, a solution of 35 µL of a 2 M HCl (Roth, 2 M ± 0.2%) in 2.53 mL ethanol is added dropwise, until a clear solution for spin-coating is obtained. A cleaned FTO glass substrate (2.5 cm x 3 cm, cleaning see also **2.1.1**) is treated in a UV-ozone cleaner for 15 min to obtain a hydrophilic FTO surface. After filtering the solution through a syringe filter (Roth, 0.20 µm pore size), 100 µL of the spin-coating solution are spread on the FTO surface. Then, the rotation of the spin-coater is set immediately to 2000 rpm, and held for 45 s. The spin-coated substrate is heated for 15 min at 150°C on a hotplate at air and then stored until the porous TiO_2 film is applied. In this case, the sintering of the TiO_2 takes place with the sintering of the porous layer (see next preparation step).

2.3.2 Preparation of TiO_2 porous layer

A nanoparticle paste prepared by Iulia Minda (after [235]) with TiO_2 nanoparticles (P25, Degussa) was used for doctorblading the porous TiO_2 films. Cleaned FTO glass substrates (2.5 cm x 3 cm) are masked by a tape (4124, Tesa®) with a round hole (⌀ 7 mm) in the center. A drop of the nanoparticle paste is placed on the tape near the hole. The paste is doctorbladed with a clean glass rod over the hole with a continuous dragging movement (no rolling movement of the glass rod). Then the tape is removed from the substrate and the film is placed in an oven at 100°C for 30 min. The TiO_2 films are sintered in a tube oven, for 15 min at 350°C, for 15 min at 375°C, for 15 min at 450°C and for 30 min at 500°C. After that, the films are slowly cooled to RT and can now be used for sensitization with a dye.

2.4 Preparation of dye-sensitized solar cells

2.4.1 Pretreatment of porous films

To optimize the adsorption of dyes, the porous ZnO- and TiO_2-films have to be pre-treated first. The following procedure was established by Max Beu [123] and Christoph Richter [130,236] for ZnO.

First, the porous films are heated at 150°C on a hotplate for 1 h. After a short cooling, the films are put under a UV lamp (Eurolite, UV-tube 15 W) for 30 min to increase the number of hydroxyl groups at the surface through water adsorption [237,238], which enhances the dye adsorption as the acidic group of the dye can form an ester binding group with the hydroxyl surface groups [4].

2.4.2 Adsorption procedure

The pretreated films are directly transferred into the adsorption solution. They are left inside the solution (laying on the ground of the vial with the porous film facing the bulk of the solution) for a specified time of for example 1 min, 15 min, 1 h or overnight (given in the sample name). After this time, the films are removed from the solution, rinsed thoroughly with ethanol and afterwards dried with a flow of dry N_2.

Types of sensitization solutions used for adsorption of dyes (numbered for exact designation, see also Appendix **9.4**, for the use of the respective sensitization solution in the cells):

1. 0.5 mM of D149 (Chemicrea) in a 1:1 mixture of acetonitrile (Roth, ≥ 99.9%, ≤ 10 ppm H_2O) and *tert*-butanol (Sigma-Aldrich, ≥ 99.5%, anhydrous)
2. 0.5 mM of D149 + 1 mM of cholic acid (Sigma, ≥ 98%) in a 1:1 mixture of acetonitrile and *tert*-butanol
3. 0.5 mM of DN91 (Chemicrea) in a 1:1 mixture of acetonitrile and *tert*-butanol
4. 0.5 mM of DN91 + 1 mM of lithocholic acid (Sigma Aldrich, ≥ 97%) in a 1:1 mixture of acetonitrile and *tert*-butanol
5. 0.5 mM of DN216 (Chemicrea) in a 1:1 mixture of acetonitrile and *tert*-butanol
6. 0.5 mM of DN216 + 1 mM of lithocholic acid in a 1:1 mixture of acetonitrile and *tert*-butanol; (b) variation: cholic acid instead of lithocholic acid
7. 0.5 mM of DN285 (Chemicrea) in a 1:1 mixture of acetonitrile and *tert*-butanol
8. 0.5 mM of DN285 + 1 mM of lithocholic acid in a 1:1 mixture of acetonitrile and *tert*-butanol

9. 0.2 mM of J102 (see also section **1.2.3**) in absolute ethanol (VWR, 99.9%)
10. 0.2 mM of J102 + 2 mM Triton® X-100 (TritonX, Sigma Aldrich)
11. 0.2 mM of J102 in ethyl acetate (Fluka, anhydrous)
12. 0.2 mM of J109 in ethyl acetate
13. 0.2 mM of J109 + 0.4 mM of cholic acid in ethyl acetate
14. 0.2 mM of WD-2 in acetonitrile
15. 0.2 mM of WD-3 in acetonitrile
16. 0.2 mM of TPA-B1 in absolute ethanol
17. 0.5 mM of the phthalocyanines (a) Vinylcarbon, (b) Phosphon, (c) Vinylphosphon or (d) AR20 in N,N-dimethylformamide (DMF, Alfa Aesar, 99.8+%)

2.4.3 UV-vis characterization of sensitized films

The sensitized films are characterized by UV-vis absorbance measurements, either in a simple transmission setup or for more scattering samples with an integrating sphere (getProbe 5393 SET) to collect all light scattered by the nanoporous films. The reflectance material is Teflon with over 95% reflectance over the visible wavelength range [174]. A Tec5 diode array spectrometer (LS-C H lamp with LOE-USB MMS 1 spectrometer, Tec5) is used for both setups. For the integrating sphere setup, the light is pointed with fiber optics directly onto the back side of the FTO glass substrate, and the scattered light is collected with a collimated fiber optics at the integrating sphere output at an angle of 90° with respect to the incoming light. Maximum integration time (6500 ms) is used within the software MultiSpec Pro, and 15-20 scans are averaged for the final spectrum. Even though often a reflecting setup is used with an integrating sphere, in this work a transmission setup was chosen as the transmission or absorbance values are essential for different evaluations. In this case, the backscattered light is not captured and adds to the error of the measurement. Absorbance is then calculated from transmission assuming zero reflection.

For the long measurements in the integrating setup, an upward shift of the sample rate is observed for the whole spectrum (even after long equilibration times of lamp and sensor). Therefore the spectra (sample data) and the references are corrected by a downward shift (minimum value set to 0) and the absorbance is then calculated from these corrected data sets.

For each film, the absorbance of the non-sensitized and the sensitized film is measured, and the absorbance of the non-sensitized film is then subtracted from the absorbance of the sensitized film. So the spectra shown in the results contain only the absorbance of the dye. Additionally, the absorbance above 650 nm, where no more absorbance of the dye is expected (from solution spectra), is set to 0.

2.4.4 Preparation of a platinized counter electrode

First, a piece of cleaned FTO glass with two predrilled holes (2.5 cm x 3 cm, hole diameter 1 mm; cleaning see above) is treated in a UV-ozone box for 15 min. To achieve a platinized counter electrode, 20 µL of a ~5 mM chloroplatinic acid solution (H_2PtCl_6 • 6 H_2O, Sigma-Aldrich, ≥ 37.50% Pt basis) are spread on the substrate. The solution is allowed to dry in the fume hood, and then heated at 450°C in a tube oven for 30 min (= 45 min including heating to the final temperature). The substrates are allowed to cool to RT or at least below 150°C (else cracks in the substrates are possible). This platinized FTO film can now be used as a counter electrode in the assembly of a DSC.

In some cases, the counter electrode consists of a sputtered Pt layer on a cleaned FTO glass sheet. The sputtering conditions are: DC sputtering with argon gas (Z400 setup, 50 sccm argon flow) at 400 mA for 14 s, yielding a Pt layer of 25 nm thickness. For better reproducibility of the Pt films, the heating current can be reduced to 30 mA while increasing the sputter time to 3.5 min.

2.4.5 Dye-sensitized solar cell assembly

Sealed DSCs are prepared following the description below.

The sensitized nanoparticulate film (working electrode) and a platinized counter electrode are sandwiched together with a cleaned hot-melt foil mask (Jurasol-PV-encapsulation-film Type B, Juraplast; thickness: 0.025 mm) in between the conductive sides of the electrodes facing each other. Prior to use, the foil is sonicated first for 10 min in acetone and then for 10 min in 2-propanol. The sandwiched assembly is placed on a hotplate at 130°C, and pressed together with a hot soldering iron until the sealing foil melts and connects the two electrodes without leaving any holes (see also Figure 16). The cell is allowed to cool to room temperature.

After cooling, an electrolyte is filled into the cell by placing a drop of it onto one of the holes. The electrolyte (different electrolytes used are listed in Appendix, **9.4**), consisting of 0.05 M I_2 (VWR, resublimed) and 0.5 M PMII in acetonitrile (Roth, ≥ 99.9%, ≤ 10 ppm H_2O) enters the cell by capillary forces and also fills up the other hole. The remnant of the electrolyte is wiped with a tissue wetted with 2-propanol. A square piece of the Jurasol foil covering both holes is added on top, and covered by a cover glass (Roth, 18 x 18 mm). A hot soldering iron is placed for a short time directly above the holes to melt the foil and seal the cell, and the complete foil is melted to ensure a more efficient sealing.

The procedure above describes the latest cell setup, which was used for most cells sensitized with indoline dyes (from cell 34 upwards). Some differences are listed below, and mentioned in the text if valid for the specified cell:

- Only one hole used for the filling of the electrolyte. In this case, a drop of the electrolyte solution is placed on top of the hole. Then the cell is placed within a vacuum lock chamber and rough vacuum is applied for some seconds. After applying atmospheric pressure again, the space within the two electrodes should be filled with electrolyte. If not, the process is repeated. The sealing process is the same as described above.
- A different electrolyte is used for some of the cells. It contains 1 M tetrapropylammonium iodide (TPAI, Aldrich, ≥ 98%) and 0.1 M I_2 (Scharlau, ≥ 99.9%) in a 4:1 solvent mixture of ethylene carbonate (Aldrich, 98%) and acetonitrile (Roth, ≥ 99.5%)
- To this electrolyte, for some cells also a lithium salt is added, with 0.1 M concentration of $LiClO_4$ (Sigma Aldrich, ≥ 98.0%)

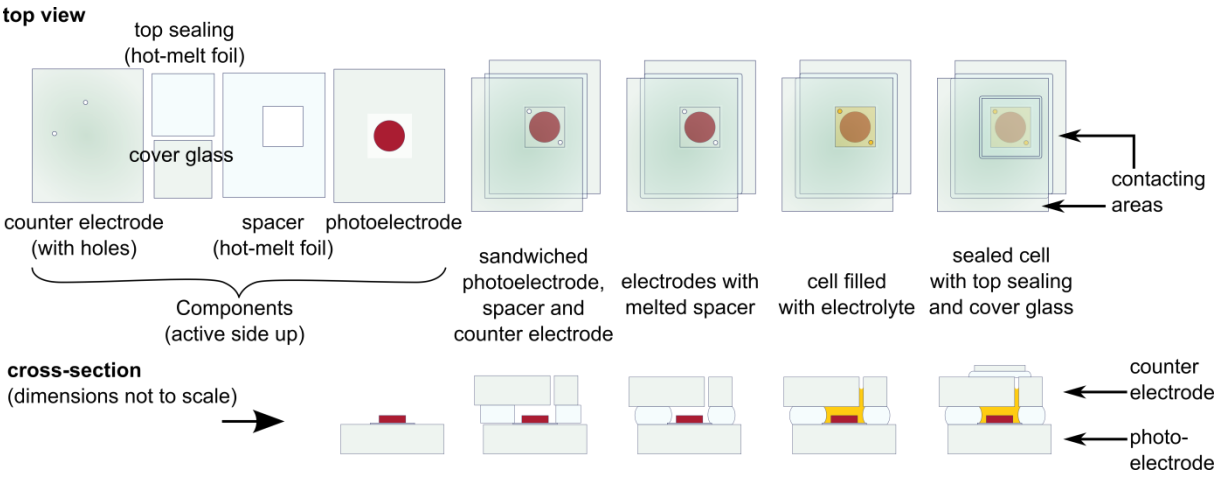

Figure 16 – Schematic representation of the assembly of a sealed DSC, viewed from the top and in cross-section.

2.4.6 Preparation of wire solar cells

For electrochemical measurements of sensitized ZnO layers on metal wires, cells have to be prepared out of the deposited wires. The ZnO-coated wires are treated similarly to the ZnO films, with slight variations to make the procedure compatible to textile substrates. That leads (in short) to the following procedure:

1. Heating of laminated samples to 100°C in an oven, afterwards ensuring that the lamination is still intact.
2. Inserting of the laminated ZnO-coated wire into the sensitization solution (see **2.4.2**) for 1 h or 15 min (specified in the text or in the sample name), and rinsing with ethanol or acetonitrile.

The sensitized substrates can now be used for the solar cell assembly. In the case of the wire substrates, the solar cell consists of a compartment made of a platinized FTO glass and a clean glass object slide (Roth) connected with glue (hot melt glue, Pattex). The compartment leaves enough space for the sensitized sample including the lamination and a spacer to avoid a contact of the sample and the Pt counter electrode. For long-term electrochemical analysis like EIS, the compartment is sealed with glue at the top to avoid electrolyte evaporation. The cell setup is depicted in Figure 17.

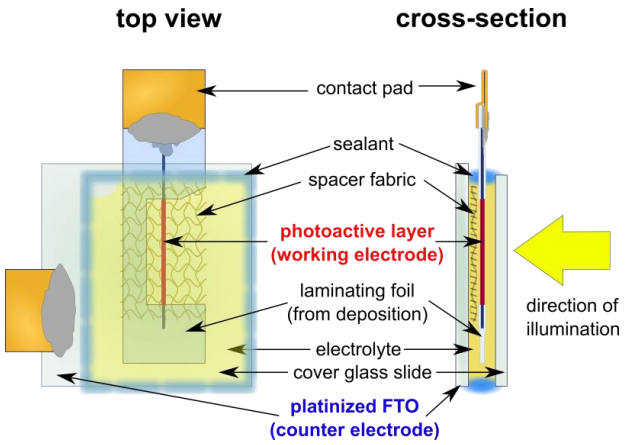

Figure 17 – Schematic cell setup for wire cells, shown from the top and in cross-section. The cell is illuminated from the back, also including absorption of light by the electrolyte.

2.5 Photoelectrochemical characterization of solar cells and evaluation

For the photoelectrochemical characterization of the solar cells, a Zahner IM6 potentiostat is used. Additional modules and diodes allow the measurement of transients with high temporal resolution, IPCE and IMVS and IMPS and other dynamic methods. All photoelectrochemical measurements are performed in a metallic, grounded box to avoid influences from outer electrical fields or from ambient light.

2.5.1 IV-curves at simulated AM1.5 illumination

The most important characterization of the solar cells, giving cell factors like efficiency, fill factor, open-circuit voltage and short-circuit current, is the current-voltage curve (IV-curve).

To achieve an approximate AM1.5 G spectrum, a solar simulator (LS0106, LOT) consisting of a 100 W halogen lamp as light source and an appropriate AM1.5 G filter is used. The intensity is measured with a pyranometer (EKO-ML-020VM, Eko instruments, extended spectral sensitivity from 300 to 1100 nm). A final intensity of 100 mW cm^{-2} is obtained by changing the distance of the sample holder to the lamp (giving 7.11 mV voltage due to the area of the pyranometer which is illuminated). The cell is then placed in the center of the light spot. The IV-curves are recorded from 0.1 V to a value higher than the open-circuit voltage on the day of preparation (if not stated otherwise). In most cases, the IV-curve is measured in a voltage range of 0.1 to -0.8 V, with a scan rate of 100 mV s^{-1} [ii] and 10 mV voltage steps. If different scan parameters are used, it is stated within the text. The IV-curves are plotted in the 1. quadrant.

To have a measure of the influence of increased light intensity at the film (through scattered light at the glass edges) on the cell efficiency, some IV-curves are measured with a mask slightly larger in the diameter than the active film (8 mm mask diameter for the commonly used film diameter of 7 mm), according to the literature [239]. The current is about 10% higher without mask for all cells measured with mask. As the solar simulator used for the majority of the measurements has a lower intensity than other solar simulators and thus leads to an about 10% lower current (see Appendix, **9.1**), the currents were not normalized to the values measured with a mask. Additionally, measurements measured without mask from [131] are directly compared with the results from the present work, making the presentation of similar conditions imperative at least for that comparison (chapter **5**, p. 124).

[ii] An increase or decrease of the scan rate leads to almost no changes in the IV-curves for the type of cells which was characterized in this work.

Current densities are calculated with help of the exact area of the film (even with mask during deposition, the area of the film varies slightly). To obtain this area, a picture of the film is taken on graph paper. The number of pixels of the film can now be compared (for example with the software GIMP) with the number of pixels of a given area, resulting in the exact area of the film.

The measurement of the IV-curves can also be performed as a steady-state measurement. In this case, the applied voltage is held until either the current change (ΔI) drops by less than 0.5% s^{-1} of the actual current or the absolute current drops slower than 1 nA s^{-1}. Especially for voltages around 0 V in IV-curves without illumination the values are more significant when measured with this method.

Evaluation: IV-curves are evaluated with the help of a LabView program IV_SolarCellAnalysis (written by André Dragässer), giving the solar cell conversion efficiency, the open-circuit photovoltage, the short circuit photocurrent density and the fill factor.

Internal IV-curves are calculated by correcting the applied voltage by the voltage drop at the series resistance of the cell. The voltage drop is calculated from the integral of the series resistance vs. the current after equation **(19).** As series resistance, a mean value is taken from the overall series resistance (determined from EIS measurements), assuming that the series resistance is constant over the complete measurement range. The voltage drop is then subtracted from the applied voltage to give the Fermi-level voltage V_f. The same procedure is also used to obtain the corrected voltage V_f for a plot of the recombination currents in the dark and under illumination.

To calculate the recombination current under illumination, the short-circuit current is subtracted from the current of an IV-curve at AM1.5 after [17]. The recombination current in the dark is equal to the current of the IV-curves measured in the dark.

2.5.2 IPCE measurements

Most IPCE measurements were performed using the Zahner setup. The light source is a halogen lamp TLS02 with a monochromator unit placed before the lamp (for further information see [240]). The lamp current is set to 300 mA with an amplitude of 100 mA (according to the recommended settings). The resulting monochromatic light intensity is relatively low, and depends on the spectrum of the light source. The frequency of the light source variation used for the measurement of cells is 10 Hz unless otherwise stated. The wavelength range is from 430 to 730 nm with a resolution of 5 nm or less. 10 sine waves are measured and then the mean values are recorded. The final spectra are normalized to the exact cell area. The APCE is calculated from the light harvesting efficiency LHE from the photoelectrode side , that is the transmittance without correction of contributions from substrate or from the porous film [241].

2.5.3 Electrochemical impedance spectroscopy

The electrochemical impedance spectroscopy (EIS) can be measured with or without illumination. In this work, three different illumination conditions were used, either red LED illumination (also coded RTR) of up to 250 mW cm^{-2} was used, or EIS was measured in the dark, or AM1.5 G illumination with 100 mW cm^{-2} (setting of light source and intensity see above) was applied. The sequence of these measurements was as it is written here, the exact settings follow below.

AM1.5 G illumination: The EIS measurements are carried out in a potentiostatic setup with the "EIS series measurement" method within the Thales software (integrated into the Zahner setup). A voltage more negative than the open-circuit photovoltage V_{OC} (to allow changes due to the illumination or heating of the cell to take place before passing V_{OC}) is applied and changed according to the program inputs. The most often used settings are a voltage varied from ca. -0.75 V to 0 V in steps of 10 mV. At each voltage, an EIS spectrum is recorded with the parameters listed in Table 1. To avoid a too long illumination with the intense AM1.5 light, only for voltages of ca. -0.75 V to about -0.4 V the spectra were measured to a lower frequency of 0.2 Hz. For lower absolute voltages (scattered data for lower frequencies, no distinct feature visible), the frequency was varied down to about 20 Hz, only.

Table 1 – Setting parameters used for the EIS measurements at AM1.5 G illumination

Parameter 1	**Value**		**Parameter 2**	**At low frequencies (below 66 Hz)**	**At high frequencies (above 66 Hz)**
Starting frequency	500 kHz		**Steps per decade**	4	10
End frequency	0.2 Hz		**Measure periods**	4	20
Amplitude	10 mV				

EIS in the dark: For EIS measurement in the dark, the measurements are performed similar to measurements at AM1.5, however, without a change of the lower frequency range, without any illumination.

Red LED illumination: The Zahner setup used in this work contained a red LED with a maximum at 632 nm (RTR01). The Zahner setup also includes a photodetector to measure the intensity of the incoming light, referenced with a light-source-specific data file. The correct position of the photodetector and the correct distance of the solar cell to the lamp are essential to ensure that the correct intensity is recorded by the Zahner workstation. The intensity of the red LED is usually varied from 0.1 to 25 mW cm^{-2} for the measurements in this work.

The EIS measurements at red LED illumination are performed after recording an IV-curve at the same intensity. The open-circuit voltage, determined by the Zahner software from this IV-curve, is then

applied to the illuminated cell (same illumination). At this voltage, an EIS spectrum is then recorded. The EIS settings can be the same as for the EIS measurement at AM1.5 G (see Table 1). If the EIS measurements with red LED are performed overnight using a SciTE4 AutoHotKey script (kindly supplied by André Dragässer and also used for the following measurements with the red diode RTR01 and the Zahner potentiostat), the number of steps per decade and the number of periods measured can be increased, and the frequency can be scanned from mid-frequency range to higher frequencies and then back to low frequencies. This leads to longer measurements at each applied voltage, but at the same time increases the quality of the EIS spectra.

Evaluation of electrochemical impedance spectroscopy measurements: First, the impedance spectra are fitted with the program ZView. After deleting strongly scattering points (for example points at 50 Hz for AM1.5 illumination, where the frequency of the power supply influences the lamp) and choosing the reproducible part of the spectrum (i.e. leaving out the scattered lower frequency part for low absolute voltages), the spectrum is fitted with applied starting values. The measured spectra are fitted to the often described [60,203,127] equivalent circuit model for dye-sensitized solar cells, containing a transmission line (active layer of the solar cell), an RC element (Pt counter electrode), a Warburg element (electrolyte) and a series resistance of the substrate (FTO).

In this work, the equivalent circuit was extended by an inductor in series to the series resistance, reflecting the inductance of contact wires. The capacitor of the Pt counter electrode was changed to a constant phase element, which accounts for a real non-planar surface structure of the counter electrode. Figure 18 shows the final equivalent circuit used for fitting of the impedance spectra of planar solar cells, while for wire-based cells a capacitor was used for the Pt counter electrode.

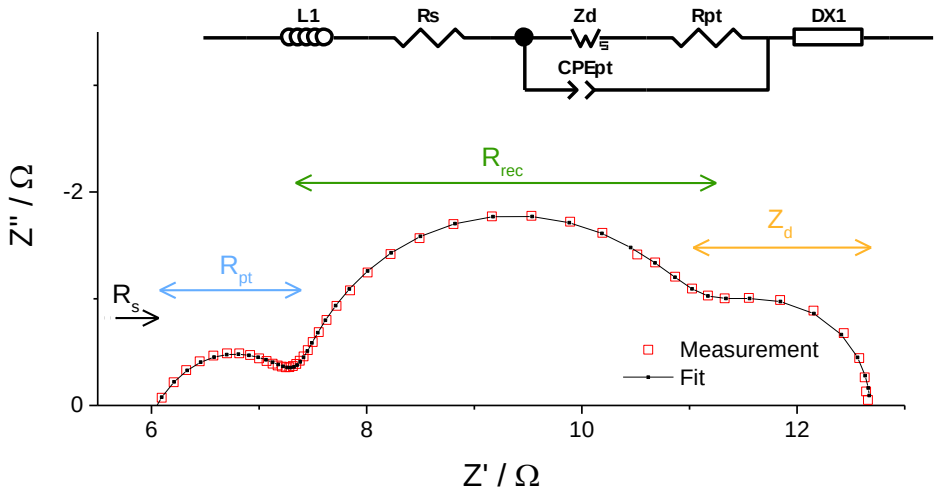

Figure 18 – Measured and simulated EIS spectrum at -0.75 V applied voltage and with AM1.5 illumination. Red points: measured EIS spectrum; black points and line: fitted EIS spectrum. Cell parameters determined from the fit are listed in Table 2. The inset shows the equivalent circuit model used for fitting impedance spectra of dye-sensitized solar cells, with the following circuit elements (physical meaning in parentheses, see also Table 2): L1 – inductor (contacts), Rs – series resistance (substrate), Zd – Warburg element (electrolyte), Rpt – resistor (counter electrode), CPEpt – constant phase element (Pt counter electrode) and DX1 – transmission line (solar cell active layer).

Applying suitable values, the new equivalent circuit gave fits of improved quality, even though the extracted values used for further evaluation (e.g. R_{rec}, C_{μ}) were similar for the traditional and the adapted equivalent circuit. However when constant phase elements are used, the values may have to be corrected depending on the equations that are used by the fitting software (see for example the extended help menu in ZView).

Table 2 – Parameters in ZView from equivalent circuit fitting of the impedance spectra of dye-sensitized solar cells. Some values were fixed during fitting or left out from fitting, according to the EIS spectrum, to give best fits. These EIS measurements were performed under AM1.5 illumination.

[Cell], measurement Value	[71], -0.75 V	[71], -0.60 V	[71], -0.45 V	[71], -0.30 V	[TiO2-03] -0.6 V	Designation of the values in **1.3.3** and in following chapters
Chi squared	$2.75 \cdot 10^{-3}$	$2.85 \cdot 10^{-3}$	$1.44 \cdot 10^{-2}$	$1.52 \cdot 10^{-2}$	$7.41 \cdot 10^{-3}$	
Weighed sum of squares	$2.81 \cdot 10^{-5}$	$2.97 \cdot 10^{-5}$	$1.67 \cdot 10^{-4}$	$2.42 \cdot 10^{-4}$	0.24464	
Wire/contact inductance						
L1	$8.62 \cdot 10^{-7}$	$8.76 \cdot 10^{-7}$	$8.31 \cdot 10^{-7}$	$7.86 \cdot 10^{-7}$	-	
Series resistance of the substrate						
Rs	5.45	5.37	5.61	5.87	12.75	$\mathbf{R_s}$
Electrolyte (Warburg element – short circuit type)						
Zd-R	1.85	1.42	-	-	-	$\mathbf{Z_d}$
Zd-T	0.0691	0.0662	-	-	-	
Zd-P	0.5 (fixed)	0.5 (fixed)	-	-	-	
Platinized counter electrode (constant phase element with parallel resistance)						
Rpt	1.91	2.21	12.6	64.1		$\mathbf{R_{Pt}}$
CPEpt-T	$2.79 \cdot 10^{-5}$	$4.88 \cdot 10^{-5}$	$5.43 \cdot 10^{-5}$	$1.68 \cdot 10^{-5}$		$\mathbf{C_{Pt}}$
CPEpt-T	0.772	0.704	0.711	0.831		
Solar cells active layer (transmission line)						
DX1						
DX1-R	0.01 (fixed)	0.01 (fixed)	0.01 (fixed)	0.01 (fixed)		$\mathbf{R_t}$
DX1-T,-P,-U,-A,-B	-	-	-	-		
DX1-C	3.45	9.30	115	1890	9.721	$\mathbf{R_{rec}}$
DX1-D	$5.49 \cdot 10^{-4}$	$2.46 \cdot 10^{-4}$	$2.26 \cdot 10^{-5}$	$2.97 \cdot 10^{-6}$	$4.46 \cdot 10^{-4}$	$\mathbf{C_{\mu}}$ [iii]
DX1-E	0.943	0.949	0.972	0.98 (fixed)	0.95 (fixed)	
DX1-F	1 (fixed)	1 (fixed)	1 (fixed)	1 (fixed)	1 (fixed)	

[iii] For the values of C_{μ} which are used below, the DX1-D value has to be corrected by the exponent DX1-E via the equation $C_{\mu} = (DX1\text{-}D)^{1/DX1\text{-}E}$.

As the shape of the EIS spectrum changes with decreasing applied voltage, the fitting has to be adapted by leaving out certain elements or by setting some parameters as fixed (see also Table 2 for fit parameters from different cells or different voltages applied to the cells). First, the Warburg impedance has to be omitted for the fitting, as the corresponding feature no longer appears in the EIS spectrum. With further decreasing voltage, the semicircle belonging to the active layer is no longer complete, and the constant phase parameter DX1-E has to be fixed if it deviates from the values obtained for more negative voltages. The transport resistance R_t (DX1-R in ZView) is fixed to a low value, as is reasonable for ZnO films and more negative voltages.

The error of fitting R_t is very high for all voltages (even for high voltages, where the exponentially increasing transport resistance should be high enough), so this parameter stays fixed during all voltages. It seems, that for low voltages R_{pt} is fitting the increasing R_t, as R_{pt} becomes too small in comparison to the other resistances. For TiO_2, the transport resistance is large enough to change the center semicircle from the shape of an ideal constant phase element, but the impedance spectra could not be fitted without a large error. This led for TiO_2-cells to the method of fitting only the second half of the center semicircle and (at more negative voltages) the Warburg impedance of the electrolyte (fitting of only one semicircle used also in [203]). The series resistance R_s determined from the fit then consists of the series resistance of the substrate, the resistance of the platinized counter electrode and a part of the transport resistance.

For the impedance spectra of EIS measured at the open-circuit voltage (illumination with red LED), the voltage directly corresponds to the internal or Fermi-level voltage V_f, as no current flows through the cell. For other measurements, where the current is different from zero (illumination with AM1.5 light or measurement in the dark), the applied voltage V_{appl} has to be corrected for the voltage drop at the series resistance. There are two methods to correct the applied voltages, as shown in the theory section, the determination of V_f with the recombination resistance R_{rec} and the determination via the series resistance R_{series}. The procedure for both methods is further explained in section **1.3.3.5**, p. 35. Both methods result in slightly different values of V_f. For reasons discussed in section **9.1.2**, the data shown in this work were all corrected with R_{series}.

The chemical capacitance obtained from the fits is normalized with the exact area of the films. The trap distribution parameter α is calculated after equation **(21)**, and the DOS is calculated from C_μ after equation **(25)** with a porosity assumed to be 0.6 for ZnO [17,242,243], and 0.7 for TiO_2 [244]. The recombination resistance obtained from fits of EIS spectra I also normalized with the exact area of the active layer. β is calculated from equation **(28)** and the lifetime from EIS after equation **(30)**.

2.5.4 IMPS/IMVS measurements

IMPS and IMVS measurements are performed using the red LED (RTR01) included in the Zahner setup. As the intensity of the LED is continually monitored by a photosensor, it can be easily modulated and serves as the modulated light source essential for the IMPS and IMVS measurements. As IMPS and IMVS measurements differ only in the state of the measured cell (IMPS: 0 A applied; IMVS at open circuit), the general method is described below.

The illumination for the IMPS and IMVS measurements is set to a certain intensity ranging from 25 to 0.1 mW cm^{-2} when using the red LED RTR01. Additionally, a small perturbation is superimposed to the light signal (~5% of the voltage applied to the diode). For this modulated illumination, the impedance of the measured cell is determined (settings see Table 1). The abovementioned script from André Dragässer varies the intensities and the amplitudes automatically and thus records a series of EIS spectra at different illumination intensities.

Evaluation: The measured spectra in their optimum shape resemble a semicircle in the complex plane or a peak in a Bode plot. The curves can be fitted with a nonlinear fit in OriginPro, which gives the respective frequency constant after equation **(14)** and **(15)**. The reciprocal of this frequency value (given as an angular frequency) yields the specific time constant of the IMPS (τ_{tr}) or IMVS (τ_n) measurement. Fitting of curves and plotting has been implemented in an OriginPro script by André Dragässer. The fitted curves are then examined regarding the quality and potential fitting errors, and corrected in case of errors. The IMPS or IMVS time constants are then plotted versus the current density or the open-circuit voltage, respectively.

2.5.5 Voltage/current transients

Voltage and current transients are also recorded at red LED (RTR01) illumination. Both measurements are very similar, only the state of the cell and some settings differ (measurement of voltage transient: open circuit; measurement of current transient: 0 A; different settings see Table 3). First, the red LED is set to a certain intensity, and the cell is illuminated during the settling time before the measurement starts. Then the measurement starts, and the Zahner potentiostat records the intensity of the LED and the cell voltage/current (with light still on). A certain time after starting the measurement the LED is set to OFF. After the switching of the diode, the measurement of the cell voltage/current continues for a certain time in the dark.

Table 3 – Settings used for the measurements of the voltage and current transients at red LED illumination.

Parameter	Light intensity (RTR01)	Settling time	Measurement time	Trigger (light off at x% of measurement time	Time resolution
Voltage transient	25 mW cm^{-2}	5 s	60 s	10%	100 µs
Current transient	Variation from 25 to 0.1 mW cm^{-2}	5 s	5 s	20%	100 µs

Evaluation of current transients: The measured current transients are evaluated to give the short-circuit charge Q_{SC} of the respective cells at a certain (red LED) illumination intensity. To obtain the charge from the current transients, the current is integrated over the time. This is achieved with the help of an Origin script, made available by André Dragässer. Some adaptations for optimized evaluation of dye-sensitized solar cells were added by Melanie Rudolph. This leads to the following procedure: For the evaluation of the charge, first, a mean value of the current is determined from the constant part at the end of the measurement (except scattering of data). This mean value is then subtracted from all data points, as even a slight deviation of this value from zero leads to a continuous increase or decrease of the determined charge, and thus a wrong result. Then the charge is integrated from the point of turning the light off to the end of the measurement. The maximum charge then is taken to be the short circuit charge Q_{SC}, from which the electron density n_{SC} can be determined using equation **(12)**. The values of n_{SC} can be additionally normalized with the ratio $N_t/N_{t,ref}$ after equation **(13)**.

Evaluation of voltage transients: From the open-circuit voltage decay (OCVD), the effective electron lifetime τ_n can be determined after equation **(11)**. For the calculation of τ_n, the derivative of the open circuit voltage against time has to be determined. However, the long measurement time (needed for an almost complete decay of the voltage) and the high time resolution (an increase of the time increment in the measurement settings is not possible, only to much larger times) leads to a large number of points with a small distance to each other. Due to digitalization the direct derivative of the measurement data yields in principle only the values 0, 1 and -1. A simple reduction of the data (for example by averaging) is not possible, as the voltage decay is fast in the beginning (larger distance of points) and slow in the end of the measurement (small distance of points). Thus the evaluation was technically performed in Origin by a data reduction in five steps, using averaging of the data over an increasing number of data points with increasing decay time. The raw data are reduced in the following five steps: averaging over 10 data points in the beginning of the voltage decay, then over 25 points, over 100 points, over 250 points and in the end over 1000 data points. This leads to a good reproduction of the original curve shape for all decay times and a reduced number of data points

especially for long decay times. From the reduced data set, the derivative is calculated and equation **(11)** can be applied to calculate τ_n.

2.5.6 Photocurrent/photovoltage vs. intensity

To measure static transfer functions of current and voltage vs. intensity, the Zahner software and the red LED RTR01 can be used. Again, the measurements of current and voltage versus intensity differ only in the applied voltage or current (short circuit or open circuit). The intensity of the red LED is increased stepwise by the Zahner potentiostat while the photocurrent or photovoltage is measured. The settings are: Starting intensity 0 mW cm^{-2}, intensity steps 0.5 mW cm^{-2} (or 0.1 mW cm^{-2} for higher resolution measurement), end intensity 25 mW cm^{-2} for RTR01 (or 5 mW cm^{-2} for higher resolution measurement) and settling time at each intensity at least 2 s.

Evaluation: The photovoltage vs. intensity plot can be further analyzed to give the ideality factor m (reciprocal of the reaction order β). A linear fit is applied to the linear part of the plot at high voltages, giving the m after equation **(36)**.

2.5.7 Charge extraction measurement

With the red LED RTR01 and the script by André Dragässer, charge extraction measurements at different intensities were measured for the different DSCs. The charge extraction measurement is implemented in the Zahner software (after [245], see also [246]). In this work, the charge extraction measurements were mainly used for the determination of the charge stored in the dye-sensitized film. This leads to following settings of the Zahner potentiostat: Target voltage 0 V, discharge current 400 µA, light on time 10 s, light off time 0 s (leading to only two stages of measurement), discharge time 20 s and sample time 100 ms.

Evaluation: The resulting charge is already given in the Zahner output files and has only to be checked for correctness. This can be done by plotting the charge extraction curves versus time. In this plot, the charge should be almost constant to the end of the measurement time.

3 Indoline sensitizers on ZnO

In this chapter, a detailed analysis of DSCs prepared from indoline-sensitized ZnO films will be presented. The sensitization of the films is varied by the adsorption of four different indoline dyes and three different adsorption times. The effect of the indoline sensitizer and the adsorption time on the absorbance, on cell parameters and on different photoelectrochemical properties are discussed, and conclusions are drawn for the different sensitization procedures. The effects of the presence or absence of a coadsorbate on the cells are discussed in the following chapter **4**, while the change of the substrate material to TiO_2 is the content of chapter **6**. The effect of storage in the dark on ZnO-based cells is dealt with in chapter **5**, and in chapter **7** sensitizers different from indoline dyes are discussed.

Nomenclature of films/cells

Quite a variety of samples will be discussed in the following chapters, and are either characterized as films or as cells. Films mean the electrodeposited and sensitized semiconductor films on a substrate (for absorbance measurements), while cells mean the complete DSCs with counter electrode and electrolyte. Each sample is specified by the dye used as sensitizer, the optional use of a coadsorbate, the adsorption time, and the sample identification number (sample ID). To have an unambiguous naming of each film, all these characteristics are included in the film or cell name [iv]. For example the sample $DN216_{1h}^{LCA}$ [70] is an electrodeposited ZnO film sensitized for 1 h with the dye DN216 and the coadsorbate lithocholic acid (LCA), with the sample ID 70. For electrochemical measurements, this film is then used to assemble a solar cell. The sample $D149_{15min}$ [47] is a film with the sample ID 47, which was sensitized for 15 min with D149, without the use of a coadsorbate. All samples with the respective conditions of preparation are listed in Appendix **9.4** (p. 239).

Outline of the comparison in this chapter

In this work, four different indoline dyes are compared as sensitizers for ZnO and TiO_2. The standard D149 dye with one carboxylic anchor group is compared to the dyes DN91, DN216 and DN285 with two anchor groups and an alkyl spacer of increasing length (**1.2.1**). These dyes are already known to be suited as sensitizers for porous ZnO, but until now the efficiencies of the prepared cells did not yet reach the efficiencies obtained with the sensitizer D149. Thus similar preparation conditions of the sensitized films were used as before for D149-based cells, and variations of these conditions should reveal differences and similarities to D149, or even advantages of the double-anchor dyes over D149.

[iv] Cells usually have the same name as the films, as mostly the electrolyte is not varied. If a direct comparison of similar cells with different electrolytes is performed, the type of the varied electrolyte is added to the cell name.

It was shown before that the dye D149 should be combined with a coadsorbate for optimal performance [16,126,247], thus for the main comparison of the dyes in this chapter, the very similar coadsorbates cholic acid (CA) or lithocholic acid (LCA) (see also **1.2.2**) are used [v]. The variation of the sensitization in this chapter thus includes the sensitization with one of the dyes D149, DN91, DN216 or DN285 (each with a coadsorbate), and the sensitization for 1 min, 15 min or 1 h. The following subchapters discuss the influence of these variations on absorbance and the performance of the DSC, measured by different electrochemical methods.

3.1 Absorbance of ZnO films sensitized with indoline dyes

The sensitization of electrodeposited ZnO with the indoline dyes D149, DN91, DN216 and DN285 and a coadsorbate led to intense-colored films, especially for sensitization times of 15 min and 1 h. Similar observations were made for D149 on the highly porous electrodeposited ZnO films before [16-19]. The sensitization for 1 min was too short to achieve a complete dyeing of the film for some of the samples (films [45] and [46]), which was visible by a more whitish appearance of the film from the substrate side. Looking from the film side of the samples, the intensity of the coloring observed by eye increased with increasing sensitization time.

To characterize the adsorbed dye in more detail, the absorbance of the sensitized films was measured before the semiconductor films were assembled to solar cells. As described in detail in **2.4.3**, the films were measured with an integrating sphere in transmission setup to gather also scattered light from the strongly-scattering ZnO films, and the absorbance of the non-sensitized substrate is subtracted from the absorbance of the sensitized films. As the scattering of the films also influences the absorbance values, the different scattering of films is briefly discussed prior to the absorbance of the sensitized films [vi].

[v] Similar but slightly different coadsorbates were chosen to ensure a better comparability to the D149-sensitized films of Melanie Rudolph [16,17,127] or the cells sensitized with double anchor dyes in the work of Felix Fiehler [131].

[vi] Note that "absorbance" in this work includes also backward scattered and reflected light. Usually the absorbance spectra contain only the absorbance of the dye, as the absorbance of the substrate and of the ZnO film is subtracted from the overall absorbance.

3.1.1 Scattering of the semiconductor substrate

Using a simple transmission setup, the absorbance (including scattering and reflection) of different porous films was determined, see Figure 19. For a nanoparticulate TiO_2 film, the absorbance or scattering of the film can be simulated assuming Rayleigh scattering, which speaks for a uniform particle size. For an electrodeposited ZnO film, the addition of a linear contribution to the Rayleigh scattering is needed to achieve a good match of simulated and measured data especially at longer wavelengths [vii]. For a nanoparticulate ZnO film, also an additional linear contribution is observed for the scattering, even though this contribution is smaller than for the electrodeposited film. This deviation from a pure Rayleigh scattering indicates that also other contributions to scattering are present especially for the electrodeposited ZnO films. As seen from SEM cross-sectional images (see for example [3]), the oxygen-based electrodeposition of ZnO with EosinY leads to cauliflower-like structures with more dense "stems" and very fine "branches". Larger structures within the film can lead to additional Mie scattering, which occurs at larger particles, which would then explain the observed deviation from Rayleigh scattering. As the nanoparticulate ZnO film also shows additional Mie scattering, it will also contain larger structures, probably aggregated particles [viii]. The very good match of the fit with pure Rayleigh scattering of the absorbance of the nanoparticulate TiO_2 film indicates a good film quality without larger aggregates of particles, as expected from the preparation procedure. The different structure of the films is not only important for the absorbance or scattering, but it also influences the electrochemical behavior discussed in the following sections, especially due to a different diffusion in differently sized pores.

Even though the strong light scattering of the electrodeposited ZnO films complicates the measurement and evaluation of the absorbance (see also **9.1.1**, p. 187), it has advantages for the application of such films in a solar cell. Light will travel a longer way through a highly scattering film than for less scattering films, and thus the probability of absorption by a dye molecule is increased. That means that for the already strongly scattering electrodeposited ZnO films no additional layer with larger particles is needed, in contrast to more transparent TiO_2 films, where often a second layer of larger particles is added to the main layer to increase light scattering [119].

[vii] The undulation of the graph between 450 and 700 nm can probably be ascribed to the uniform film thickness and thus to interference of light, and not to remnants of EosinY, as the desorption procedure leads to completely discolored films. For lower wavelengths, the deviation of the simulation is most likely caused by the use of a constant value of the refractive index n.

[viii] The less stable material ZnO gives more probability to differently sized structures than TiO_2.

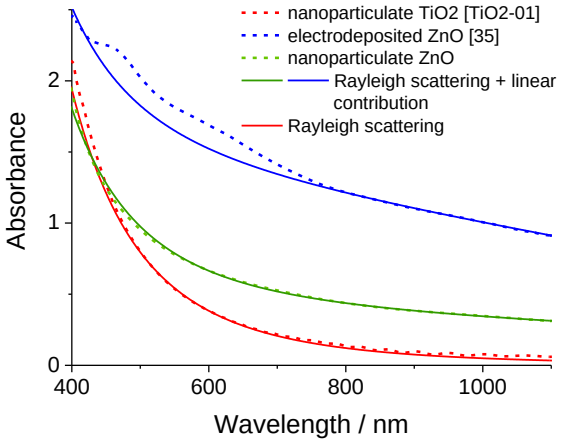

Figure 19 – Absorbance of different non-sensitized films (see legend for exact designation) measured in a simple transmission setup (without integrating sphere) to obtain scattering. Measurement data are shown as thick dashed lines, while simulations of the scattering are shown as thin solid lines. The absorbance of the substrate was subtracted from the measured absorbance, leaving only the absorbance of the porous films. [TiO2-1] and [35] are the sample IDs of the non-sensitized films. The values for the refractive index for TiO_2 and ZnO were used from [248] and [249], respectively.

3.1.2 Influence of the adsorption time and the sensitizer on the absorbance

The absorbance of differently sensitized electrodeposited ZnO films is shown in Figure 20. Due to the problems in measurement and evaluation which arose from the strong scattering of the electrodeposited ZnO films (see detailed discussion in **9.1.1**, p. 187), only films sensitized for 1 min and absorbances in the wavelength region between ca. 600 and 650 nm are considered for the following discussion. The absorbance at longer wavelengths can be taken as a rough measure of the amount and aggregation of dye molecules within the films, and values of the absorbance at 635 nm are given in Table 4.

The direct comparison of the absorbance of films sensitized for 1 min with the different indoline dyes, Figure 20(a), shows a very similar curve shape and a comparable height of the absorbance maximum, especially for the dyes containing two anchor groups. For all four sensitizers, the maximum of the spectra is located between 525 nm and 540 nm. The spectrum of the film $D149_{1min}^{CA}$ [45], which is sensitized with the single-anchored dye D149, differs slightly in shape and position, as it is shifted to lower wavelengths, and the absorbance around 500 nm is slightly increased compared to other dyes. Such a shape where the left side of the absorbance maximum is slightly higher than the left side, is commonly found for D149 adsorbed on ZnO [16,121,127]. For the double-anchor dyes, the absorption maxima are more symmetric, or the right side is slightly higher compared to D149. The spectra resemble more the solution spectra of D149 and DN216, which are also included in Figure 20(a).

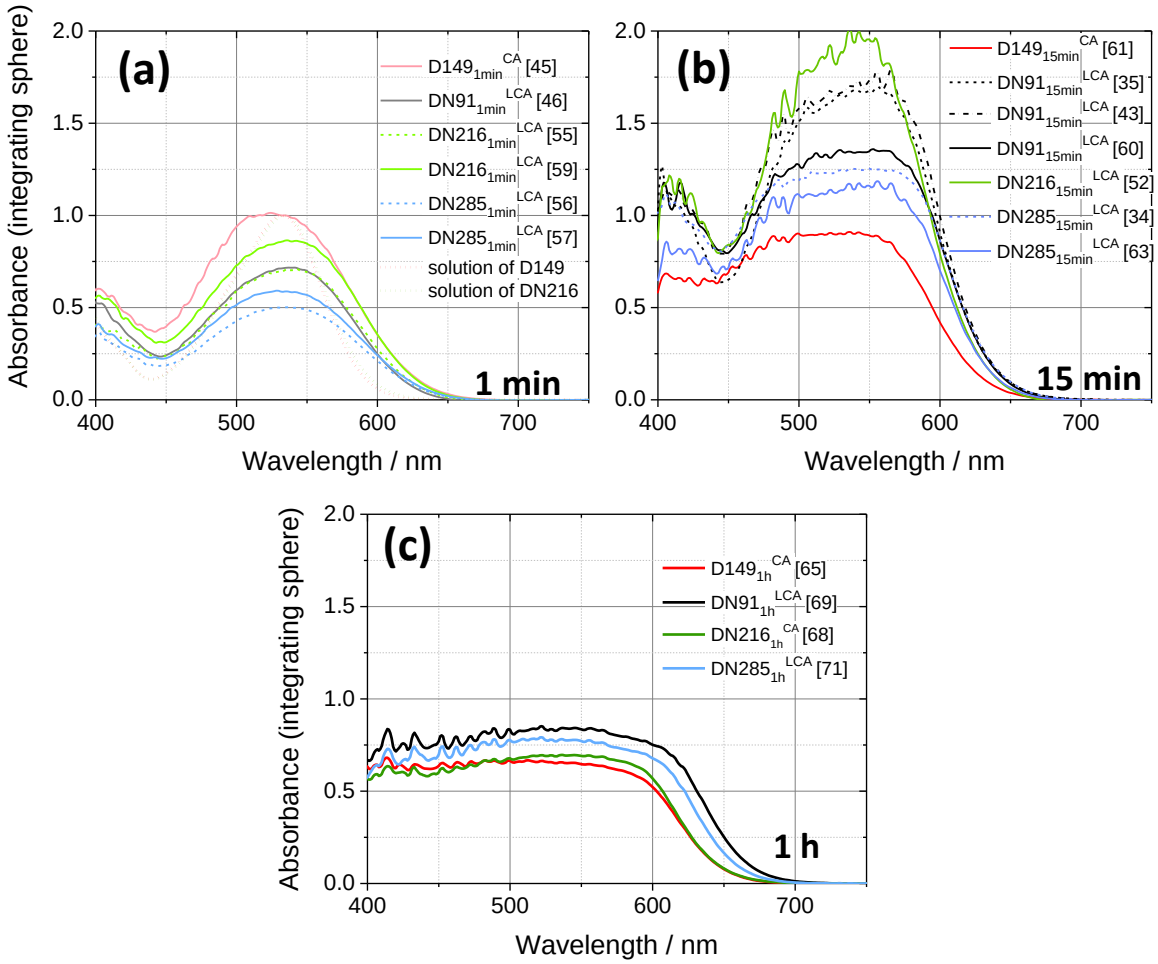

Figure 20 – Absorbance of dyes adsorbed to porous ZnO films, grouped after the sensitization time of (a) 1 min, (b) 15 min and (c) 1 h. The absorbance was measured using an integrating sphere, and the absorbance of the non-sensitized ZnO films was subtracted from the absorbance of the sensitized films. Different colors indicate the different sensitizers, while dashed lines of the same color indicate different films with the same adsorption procedure, according to the legends. Dotted lines in (a) give the absorbance (measured in transmitting setup) of D149 and DN216 in dimethyl formamide.

This means that even though the orbitals of D149 and the double-anchor dyes are very similar, as they show an almost identical absorbance in solution and similar extinction coefficients, the electronic system of the adsorbed dyes on ZnO is different depending on the absence or presence of a second carboxylic anchor group. The closer resemblance of solution spectra by double-anchor dyes speaks of more separated dye molecules, and thus less aggregated molecules for the double-anchor dyes. This difference can be caused either by a different arrangement of the dyes on the ZnO surface because of the second anchor group, or by a different dye-coadsorbate interaction due to the stronger binding [15].

The amount of dye adsorbed after 1 min is higher for D149 and lowest for the dye with the longest alkyl spacer at the second anchor group, which for such a short sensitization time will be caused by a hindered diffusion inside the porous film for the sterically more demanding double-anchor dye [ix].

[ix] Even though the different coadsorbate for D149 and the double-anchor dyes might imply that the different shape of the respective spectra is caused by this difference, this is not the case. In [108], deoxycholic acid was used as coadsorbate for both D149 and double-anchor dyes, and the shape of the spectra was comparable to those seen here, that means more different for D149.

When an adsorption time of 15 min is applied, the amount of adsorbed dyes increases for all four sensitizers, as can be seen from the higher absorbance values at 635 nm, see Table 4. For 15 min adsorption time, D149 shows lower absorbance values than the other double-anchor dyes, which is the opposite of what is observed for 1 min adsorption. Even though it is probable that the spectrum of D149 is shifted to lower wavelengths, as it was observed for 1 min adsorption, still the amount of adsorbed D149 dye molecules is probably lower than for the double-anchor dyes. For the longest adsorption time of 1 h, again the absorbance and thus the amount of adsorbed dye molecules increases for all sensitizers, yet remains lower for D149 than for the double-anchor dyes. For longer adsorption times, the amount of adsorbed dye will probably no longer be defined by diffusion, but by adsorption and desorption equilibria (also in competition to the coadsorbate or other possible adsorbates from the electrolyte). These equilibria will certainly depend on the presence of a second anchor group, so that D149 will be driven from adsorption sites more frequently than for example DN216, which might cause the lower amount of adsorbed D149. It was shown before that for double-anchor indoline dyes the adsorption is slower than for indoline dyes with a single anchor group [128], but on the other hand the double-anchor dyes bind stronger to the ZnO surface [15]. This supports well the above explanation of the observed differences in the amount of adsorbed dyes.

The D149 molecules will be aggregated for longer adsorption times, as D149 shows a strong tendency of aggregation on the ZnO surface [126], see also section **1.2.1**. The double-anchor dyes are expected to show a lower aggregation tendency, as the second anchor group and the spacer will prevent such close packing of dye molecules as it is possible for D149. In itself the graphs in Figure 20 do not allow an estimation of the aggregation, as the full maximum of the absorbance is beyond the detection limit, and a broadening of the spectrum can be caused by more adsorbed dye and/or increased aggregation. From the slope of the absorbance at higher wavelength it can be surmised that aggregation also is important for DN91, DN216 and DN285, mostly for the longest adsorption time of 1 h, not so much for shorter sensitization. These trends are even more clearly observed when the absorbance spectra are normalized to the values at 635 nm, where the absorbance is least affected by the depression of the maximum and yet high enough to be significant (Figure 21).

Table 4 – Absorbance values of differently sensitized electrodeposited ZnO films at 635 nm as a measure of dye amount and aggregation, see Figure 20 for the absorbance curves. Numbers in brackets give the cell IDs, while grey values indicate values for cells that are not mainly discussed in this chapter.

Time	1 min	15 min	1 h
$D149^{CA}$	0.079 [45]	0.091 [61]	0.173 [65]
$DN91^{LCA}$	0.034 [46]	0.206 [60]; 0.206 [35]; 0.219 [43]	0.451 [69]
$DN216^{LCA/CA}$	0.071 [59]; 0.052 [55]	0.160 [52]	0.178 [70]
$DN285^{LCA}$	0.055 [57]; 0.046 [56]	0.160 [63]; 0.217 [34]	0.330 [71]

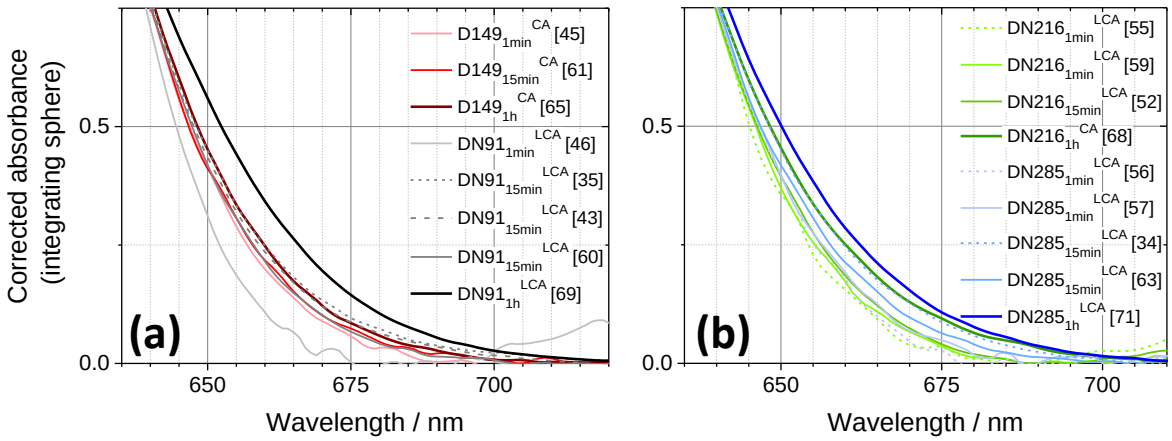

Figure 21 – Normalized absorbance of indoline-sensitized ZnO films (absorbance of the non-sensitized film subtracted). The graphs from Figure 20 were normalized to the absorbance at 635 nm and only the more relevant absorbance at lower wavelengths is displayed to show the aggregation at the right downward slope more clearly. Films sensitized with (a) D149, DN91, (b) DN216 and DN285 are shown. Increasing color depth indicates increasing sensitization time; dashed lines of the same color indicate different films of the same sensitization procedure, according to the legends.

An increase of adsorbed amount of dye (and aggregation) with increasing time of adsorption was also found before for D149 [16,126], and from the results shown here, this observation can now be extended also to the double-anchor dyes DN91, DN216 and DN285. The addition of a second anchor group thus changes the absorbance behavior especially because of additional steric hindrance and stronger binding of the molecules, but the observed trends with different adsorption conditions for the double-anchor dyes are similar to the well-established single-anchor dye D149.

3.2 Current-voltage characteristics of ZnO films sensitized with indoline dyes

Dye-sensitized cells were prepared from all films, for which the absorbance is shown in Figure 20 on p. 69. Only one of these cells, $DN285_{1h}^{LCA}$ [69] showed a short circuit, all other cells could be characterized by the usual set of photoelectrochemical experiments. Some of the cells will however be discussed in another context, as either the electrolyte was varied (cells $DN216_{1min}^{LCA}$ [55] and $DN285_{1min}^{LCA}$ [56] – see section **9.4**), or the films were prepared especially for comparison with cells from [131] and thus with a smaller diameter (cells $DN91_{15min}^{LCA}$ [35], $DN91_{15min}^{LCA}$ [43] and $DN285_{15min}^{LCA}$ [34], see chapter **5**). The current-voltage curves (IV-curves) give a first insight into the functioning of the differently sensitized dye-sensitized solar cells, see Figure 22 and Figure 23, where the IV-curves of the differently sensitized cells are grouped after the sensitizer and the sensitization time, respectively, to ensure an easy comparison of the influence of these two parameters. For each cell the first IV-curve measured under AM1.5 illumination after assembly of the cell is shown, together with an IV-curve measured in the dark directly before the illuminated curve. This should ensure the least possible influence on the IV-curves due to warming of the cells by intense

illumination. The IV-curves shown in Figure 22 and Figure 23 were measured without mask to achieve comparability to measurements in chapter **5**. Comparative measurements with a mask slightly larger than the diameter of the film [239] showed a decrease of about 10% in the photocurrent due to the exclusion of reflected light at glass edges and surfaces.

Short-circuit current

Influence of different adsorption times: The comparison of the IV-characteristics for the different indoline dyes in Figure 22 shows that for all dyes the sensitization for 1 min shows mostly the lowest short-circuit current density I_{SC}. As the absorbance spectra of the 1 min films also show the lowest absorbance (Figure 20), this lower current is explained by the lower light harvesting efficiency. The increase of I_{SC} upon a longer sensitization of 15 min, which is observed for all four sensitizers, is caused by the higher amount of dye adsorbed onto the ZnO film, compare again Figure 20. Cell $DN216_{15min}^{LCA}$ [52] reaches the highest values of I_{SC} in this set of cells, 10.81 mA cm^{-2}. When the adsorption time is extended to 1 h, the cells show lower I_{SC} values than for 15 min, sometimes even lower than for the adsorption time of 1 min [x], even though in all cells more dye is adsorbed for the time of 1 h than for both 1 min and 15 min sensitization time. Several reasons can lead to a current that is lower than expected, which will be discussed further in the following sections. However the normalized absorbance in Figure 21 suggests a higher aggregation of dye molecules for the adsorption time of 1 h, and thus more recombination via dye aggregates and current loss. With differently deposited ZnO films, an increase in I_{SC} with increasing sensitization time was observed [16], which is different from the behavior observed here probably because of the different deposition (see also Table 5 for cell values of cells discussed in this chapter and for a comparison with values obtained for similar cells in the literature. See [8,243,250] for detailed analyses of the porosity and other parameters of differently deposited ZnO films). In [126], where reducing conditions are used in the electrodeposition of porous ZnO as it is here, the tendency of I_{SC} with increasing sensitization time is similar as in Figure 22, with increasing I_{SC} for comparatively short adsorption times, and a decrease of I_{SC} for longer adsorption times. Thus, I_{SC} of cells sensitized with double-anchor indoline dyes shows approximately the same tendency with increasing sensitization time as D149. Cell $D149_{15min}^{CA}$ [61], for which several comparable cells are found in the literature, shows comparable but lower I_{SC} (see Table 5). In the case of reference [18], this difference is probably caused by the larger thickness of the porous films, whereas in reference [19] a smaller deposition area was used (see discussion in section **9.1.4**).

[x] Even though the cell sensitized with DN91 for 1 h could not be characterized more in detail due to a short circuit, I_{SC} can be determined from an IV-curve at AM1.5, and values for V_{OC}, FF and η can be roughly estimated from the photocurrent, calculated by the subtraction of the current measured in the dark from the current measured under AM1.5 illumination.

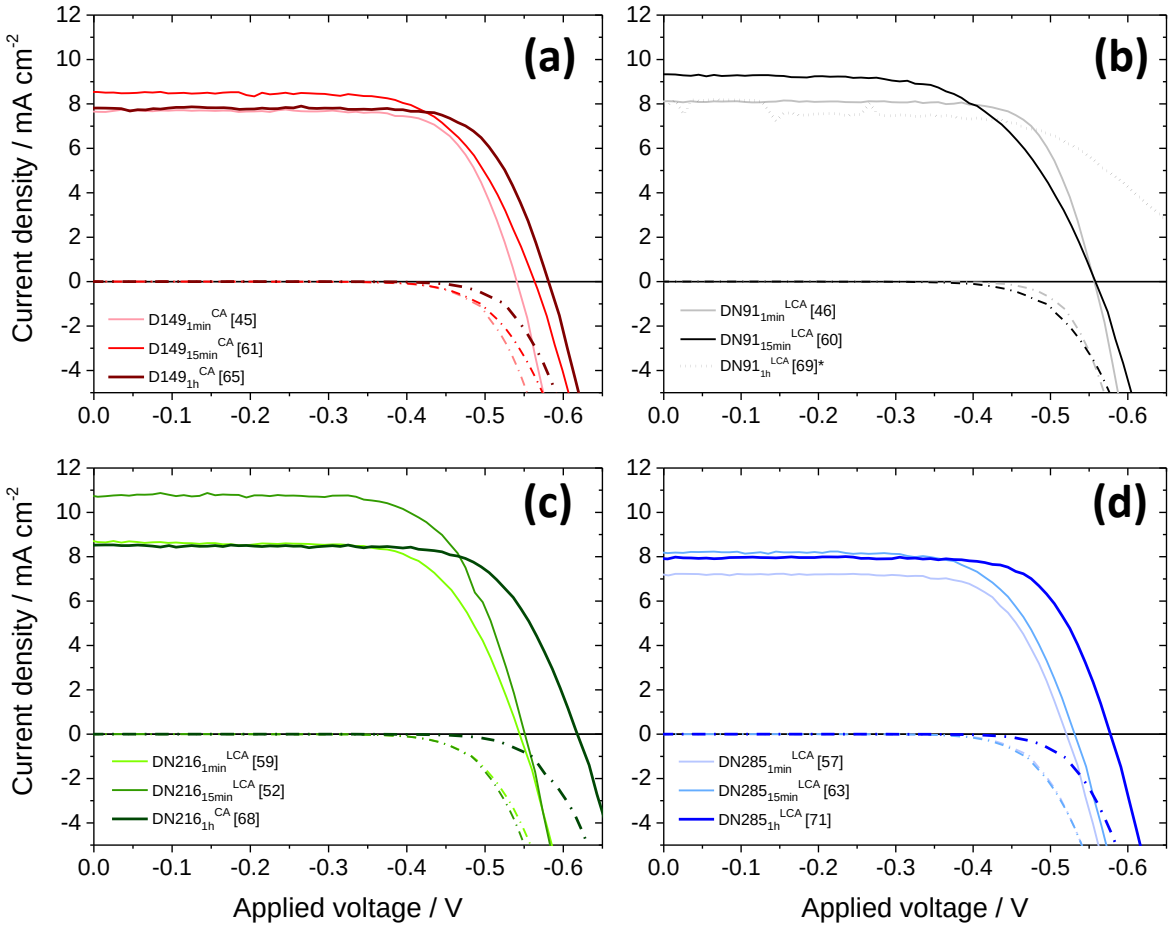

Figure 22 – IV-curves of differently sensitized ZnO-based DSCs, grouped after the sensitizing indoline dye, (a) D149, (b) DN91, (c) DN216 and (d) DN285. Dash-dotted lines indicate dark currents, while increasing color depth indicates an increasing sensitization time. Solid lines indicate measurement under AM1.5 simulated sunlight illumination, and illuminated curves of additional cells sensitized with the same dye for the same time are indicated by dashed or dotted lines of the same color. For DN91 the photocurrent of cell [69] is shown, see also [x].

Comparison of sensitizers: For a direct comparison of the different influences of the dye, the IV-curves are also shown in Figure 23, grouped there after the sensitization time. The sensitizer DN216 leads to the highest values of I_{SC} for all three adsorption times, and for 1 min and 15 min adsorption time I_{SC} for the different sensitizers decreases after the sequence I_{SC}(DN216) > I_{SC}(DN91) > I_{SC}(D149) > I_{SC}(DN285). Also for 1 h adsorption time the sequence is similar, however the values are overall more similar and almost overlap for all dyes except for DN216. This sequence is not caused by the amount of dye adsorbed on the ZnO film, as the sequence seen in the absorbance spectra in Figure 20 is different. Lower I_{SC} for DN285 was also observed in all references, where this dye was compared with similar dyes [13,15,121,131]. The lowest currents seen for DN285 can be explained by the longer injection times compared to the other double-anchor indoline dyes [13]. Even though for an adsorption time of 1 min also the absorbance is the lowest for DN285, for longer times the absorbance is similar, and yet I_{SC} is lower. For DN216 and DN91, according to the faster injection times[13] DN91 should show higher I_{SC}, however other influences like aggregation (i.e. recombination) probably decrease I_{SC} so that I_{SC} for DN216 is clearly superior to the other sensitizers, even to the reference dye D149.

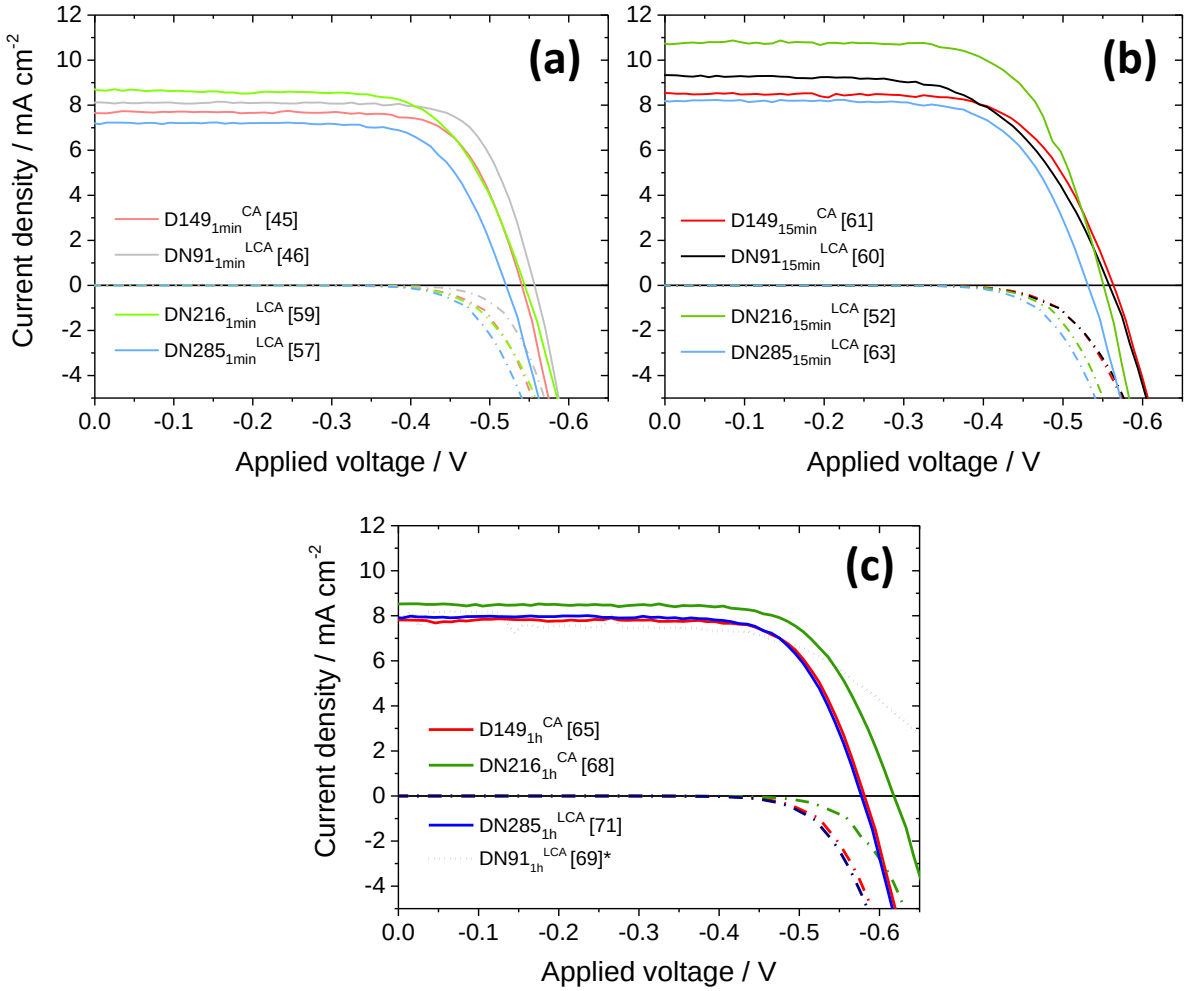

Figure 23 – IV-curves as in Figure 22, grouped after the sensitization time of (a) 1 min, (b) 15 min and (c) 1 h.

Open-circuit voltage

With increasing sensitization time, the open-circuit voltage V_{OC} increases in absolute value for almost all sensitizers. Especially for the increase from 15 min to 1 h sensitization time, the increase is very marked, even up to about 70 mV for DN216. For the comparison of V_{OC} for the different sensitizers, no clear trend is observed, only DN285 shows the lowest V_{OC} of all sensitizers for all sensitization times.

The higher V_{OC} for 15 min sensitization time compared to 1 min sensitization is probably by a larger part caused by the observed higher I_{SC}. For other sensitization times, however, V_{OC} shows no dependence on I_{SC}, as other factors outweigh the influence of I_{SC} on V_{OC}. Different factors influence V_{OC}, especially the position of the conduction band edge E_c, the recombination parameter β, I_{SC} and the recombination current (equation **(31)**). These other factors can mostly be accessed via different photoelectrochemical methods, and will be discussed in the context of these measurements in section **3.3** below.

Table 5 - Cell parameters for DSCs sensitized with different indoline dyes and a coadsorbate, from IV-curves shown in Figure 22 and Figure 23. Below are added cell parameters of cells from the literature, which are based on electrodeposited ZnO and sensitized with D149 and a coadsorbate. ~ marks approximate values, and values in parentheses give the ratio of $I_{SC,theor}$ to I_{SC}.

Sample		**I_{sc}**	**$I_{sc,theor}$**	**V_{oc}**	**FF**	**Effici-ency**	**Reference**
Sensitizer$_{time}^{coadsorbate}$ [ID] (deposition, electrolyte, film thickness) [xi]		**[mA cm^{-2}]**	**[mA cm^{-2}]** from IPCE	**[V]**		**[%]**	
D149$_{1min}^{CA}$ [45]	1min	7.57		-0.541	0.75	**3.04**	this work
D149$_{15min}^{CA}$ [61]	15min	8.54		-0.563	0.68	**3.24**	this work
D149$_{1h}^{CA}$ [65]	1 h	7.82		-0.581	0.74	**3.34**	this work
DN91$_{1min}^{LCA}$ [46]	1min	7.90		-0.557	0.76	**3.32**	this work
DN91$_{15min}^{LCA}$ [60]	15min	9.33		-0.558	0.62	**3.20**	this work
DN91$_{1h}^{LCA}$ [69] (!)	1 h	~8.2		<-0.79	>0.53	**~3.5**	
DN216$_{1min}^{LCA}$ [59]	1min	8.66	8.28(0.96)	-0.544	0.70	**3.24**	this work
DN216$_{15min}^{LCA}$ [52]	15min	10.81	9.89(0.91)	-0.551	0.69	**4.08**	this work
DN216$_{1h}^{CA}$ [68]	1 h	8.53	8.07(0.95)	0.618	0.72	**3.76**	this work
DN285$_{1min}^{LCA}$ [57]	1min	7.85		-0.521	0.73	**2.94**	this work
DN285$_{15min}^{LCA}$ [63]	15min	8.17		-0.531	0.69	**2.97**	this work
DN285$_{1h}^{LCA}$ [71] (75µM EY, IL, ~5 µm) (for all above)	1 h	7.90		-0.577	0.74	**3.36**	this work
D149$_{1min}^{CA}$ (300 µM EY, TPAI, ~4.2 µm)	1min	~6.1		~0.55	0.66	**~2.3**	ref. 16
D149$_{10min}^{CA}$ (300 µM EY, TPAI, ~4.2 µm)	10min	~9.8		~0.60	0.59	**~3.4**	ref. 16
D149$_{120min}^{CA}$ (300 µM EY, TPAI, ~4.2 µm)	2 h	~11.0		~0.63	0.57	**~4.0**	ref. 16
D149$_{2h}^{CA}$ (300 µM EY, TPAI, ~4.3 µm)	2 h	5.8		0.557	0.64	**2.06**	ref. 17
D149$_{1min}^{CA}$ (50 µM EY, TPAI, ~4 µm)	1min	~7.2		~0.65	~0.70	**~3.3**	ref. 126
D149$_{10min}^{CA}$ (50 µM EY, TPAI, ~4 µm)	10min	~11.7		~0.68	~0.60	**~4.7**	ref. 126
D149$_{120min}^{CA}$ (50 µM EY, TPAI, ~4 µm),	2 h	~10.2		~0.67	~0.55	**~3.8**	ref. 126
D149$_{15min}^{CA}$ (200 µM EY, IL, 6.6 µm)	15 min	9.6		0.55	0.73	**3.8**	ref. 18
D149$_{15min}^{CA}$ (50 µM EY, IL, 7.1 µm)	15 min	10.7		0.57	0.73	**4.4**	ref. 18
D149$_{15min}^{LCA}$ (75 µM EY, IL, ~4.5 µm)	15 min	11.19		0.613	0.71	**4.83**	ref. 19

[xi] "Deposition" gives the concentration of the structure-directing agent EosinY (EY) during electrodeposition of the porous ZnO, from which are dependent also other deposition parameters. "Electrolyte" gives the information whether the electrolyte contains tetrapropylammonium iodide (TPAI) or an ionic liquid (IL), which also standardly are used with other components. "Film thickness" gives the thickness of the ZnO (porous) layer. For the films prepared in this work, all these parameters are the same as for cell [71].

Fill factor

The power conversion efficiency η is strongly influenced by the fill factor FF. The FF changes systematically with increasing sensitization time for all four sensitizers, with high values above 0.7 for 1 min sensitization time. High values are typically found for indoline-sensitized DSCs based on electrodeposited ZnO (see also Table 5), in contrast to cells based on nanoparticulate ZnO films [203]. A sensitization of the films for 15 min leads to lower FF for all sensitizers, even though the values still remain close to 0.7. Cells which were sensitized for 1 h show again a higher FF than cells which were sensitized for 15 min, with comparable values to cells sensitized for 1 min. This observation is made for all sensitizers (unknown behavior for DN91 adsorbed for 1 h). Comparing the different sensitizers, all four sensitizers show comparable values for the respective sensitization times, no dye showing only high or only low values of the FF. After equation **(35)**, the FF is influenced mainly by V_{OC} and by the recombination parameter β. As the FF shows no direct dependence on V_{OC}, the values will be influenced by a different recombination, and will be discussed in the context of recombination in section **3.3**.

Power conversion efficiency

All cells discussed in this chapter show power conversion efficiencies η near or above 3%, with cell $DN216_{15min}^{LCA}$ [52] reaching the highest value of 4.08%. These values are comparable to values of similar cells in the literature, see Table 5. Either a sensitization time of 15 min or of 1 h reaches the highest η for the respective dyes, which is caused by either a higher I_{SC} for cells sensitized for 15 min, or a higher V_{OC} for the cells sensitized for 1 h.

In conclusion, to reach high efficiencies, not for all dyes the longest sensitization time is beneficial. For most cells, a sensitization time between 15 min and 1 h would probably yield the maximum efficiency, as I_{SC} again decreases for a sensitization for 1 h. If a decrease in efficiency is observed for longer adsorption times, this decrease is not caused by a smaller amount of dye adsorbed, as was shown in comparison with the results from the absorbance in **3.1.2**. Possible reasons for the changes in cell parameters will be shown by the application of different photoelectrochemical methods in the following sections.

Conversion of photons to current, IPCE and APCE

To investigate the current generation in more detail, incident photon-to-current efficiency (IPCE) spectra were measured, see Figure 24(a,b). For short adsorption times of 1 min, the IPCE spectra still resemble the shape of the absorption of molecules in solution in Figure 20. For higher adsorption times, a maximum can no longer be observed, as the high amount of dye on the surface absorbs almost all light around the position of the maximum. The theoretical value of the short circuit current, $I_{SC,theor}$, was calculated for DN216 as the integral of the IPCE after equation **(10)**, and shows similar values as I_{SC}, see Table 5. Because the IPCE was measured only down to 430 nm, the values of $I_{SC,theor}$ are lower than I_{SC}, especially for cells with higher absorbance where the "cut-off" at lower wavelengths is larger. For the same adsorption time and the different sensitizers, the onset of the IPCE at longer wavelengths is very similar, while for an increase of the sensitization time from 1 min to 15 min a shift of the onset to longer wavelengths is observed. This is mainly caused by the broadened absorption of the dyes because of a higher dye loading and stronger aggregation of the dye molecules for longer adsorption times (see section **3.1.2**).

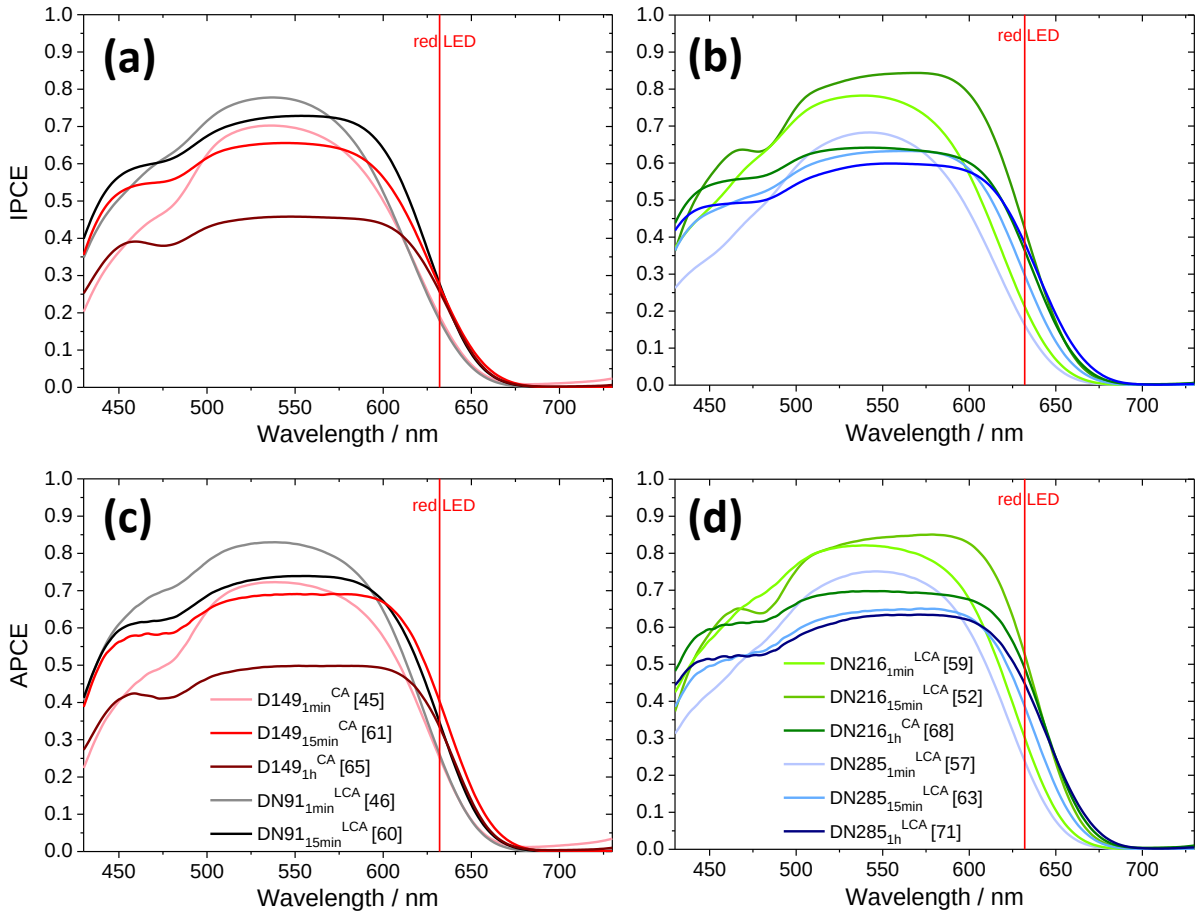

Figure 24 – Incident photon-to-current conversion efficiency (IPCE) (a,b) and absorbed photon-to-current conversion efficiency (APCE) (c,d) for differently sensitized ZnO DSCs, grouped after the indoline sensitizer (a) D149 and DN91 or (b) DN216 and DN285. Increasing color depth indicates increasing sensitization time according to the legends. Red vertical lines indicate the wavelength of the maximum of the red LED used for dynamic measurements in the following section.

APCE spectra were calculated from the light harvesting efficiency and the IPCE, see Figure 24(c,d), and show a shape and magnitude very similar to the IPCE spectra. This similarity is caused by LHE values near unity for wavelengths around the absorption maximum, which indicates that in terms of absorption the cells are well optimized. Only for very short sensitization times of 1 min the difference of IPCE and APCE is around 5% and thus an increase in LHE would effect an increase in the current, as it is also observed for the sensitization time of 15 min .

Thus increase in I_{SC} could no longer be achieved by the adsorption of more dye than is adsorbed for 15 min or 1 h, but for example by an extension of absorption to higher wavelengths (e.g. by the co-sensitization with a second dye [17]) or by an increase in the injection, collection or regeneration efficiency, which influence the IPCE in addition to the LHE (see equation **(9)**). Some of these influences will be discussed in the context of small-perturbation measurements below. As some of these measurements are performed also under red LED illumination, the maximum wavelength of the red LED used is shown in Figure 24 (vertical red line). For all cells, the wavelength is adsorbed to a smaller amount than in the maximum, which should ensure a homogeneous light absorption and thus a homogeneous charge generation over the complete film thickness.

3.3 Small-perturbation photoelectrochemical methods for ZnO-based DSCs

In the following sections, the results from different small perturbation photoelectrochemical methods are presented, together with other methods which support these measurements. Wherever direct discussion is possible, the results will be discussed in the smaller context. The broader context of the results will be discussed in section **3.4**.

3.3.1 Trap distribution in ZnO-based DSCs – chemical capacitance and related values

The chemical capacitance C_μ measured by electrochemical impedance spectroscopy gives valuable information about the distribution of states in the DSCs. C_μ for the different cells is plotted against the voltage V_f (corrected by the voltage loss at the series resistance), see for example Figure 28, p. 85. On the following pages, first the shape of the spectra will be discussed, together with a simulation of the capacitance. Then different illumination conditions during measurement of the EIS will be compared, and with this background information C_μ is compared for the different dyes and sensitization times.

Different contributions to the impedance spectra – comparison with simulated values

When plots of C_μ vs. the corrected voltage V_f are shown in the literature, often only the linear part in the semi-logarithmic plot is shown [16,18], and from this the trap distribution parameter α is calculated. When the C_μ is shown down to lower absolute voltages, the slope becomes lower [17,19], as well as for more negative voltages [60,218]. In the present work, the cells were measured and evaluated over a comparatively large voltage range, also applying a voltage correction which leads to less scattering at lower absolute voltages (see section **9.1.2**). Thus the resulting C_μ spans a voltage range from 0 V (= redox level of the electrolyte) to voltages more negative than V_{OC}. This allows the observation of the linear C_μ at intermediate voltages, as well as different contributions to the overall capacitance at more negative and more positive voltages, which are described in more detail in section **1.3.3.5** (following p. 35). It can be reasonably assumed that the different contributions will to some extent also affect the linear part in the center of the curves.

To gain more insight into the different parameters which influence the capacitance-voltage curves, simulations of such curves were performed. The different separate contributions to the total capacitance C_{all} [xii] were assumed as described in section **1.3.3.5**, which were in particular the chemical

[xii] Note that for all capacitance-voltage plots obtained from EIS measurements, the correct designation of the capacitance would be C_{all}. However, to allow a better comparison with values and plots in the literature, the designation C_μ is used throughout this work for capacitance values obtained from EIS measurements.

capacitance $C_{\mu,theor}$, a Helmholtz capacitance C_H, a capacitance with Mott-Schottky behavior from depletion of a space-charge layer C_{SC} and a capacitance arising from deep monoenergetic trap states, C_{mono}. In the literature, until now only C_H and C_μ, or C_{SC} and $C_{\mu,theor}$ were combined either in a parallel or a series arrangement [60,218]. Following these references, the overall capacitance including the four contributions is formulated for the first time:

$$C_{all} = \left(\frac{1}{C_{SC} + C_{\mu,theor} + C_{mono}} + \frac{1}{C_H} \right)^{-1}. \quad \textbf{(37)}$$

With this formula, the measured capacitance is simulated by changing the different parameters to achieve the best possible accordance to the measured capacitance values. Figure 25(a) shows the different capacitances for the measurement of cell [71] in the dark, and Table 6 lists the fit parameters and different assumptions for the parameters. C_{all} nicely reproduces the measured curves, with largest deviations at voltages more negative than -0.5 V and voltages near the contribution of the deep monoenergetic trap states (-0.35 V). These deviations could be caused by deviations of the respective capacitances from the ideal behavior, for example a not constant C_H. For three other measurements, the simulation also fits the measured values well, compare Figure 26 [xiii]. The best overlap of the simulated capacitance with the measured capacitance was achieved for C_H around 1 mF cm^{-2}. This value is high for a Helmholtz capacitance, when compared with $3.9 \cdot 10^{-6}$ F cm^{-2}, determined for a planar TiO_2 electrode sensitized with D149 [251]. However when the roughness-factor of the porous film is considered (for example ~1000 for a TiO_2 electrode [61]), the simulation value is in a correct range.

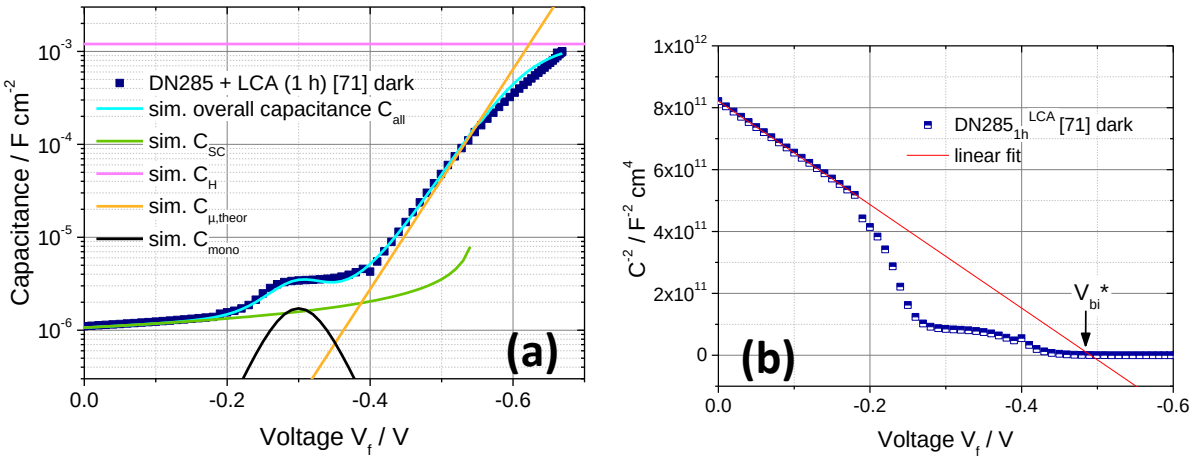

Figure 25 – (a) Simulated capacitances compared with the measured capacitance of cell [61] (measured in the dark). Contributions of the overall capacitance are shown, as well as the overall capacitance. Simulation parameters are listed in Table 6. (b) Mott-Schottky plot for the capacitance of cell [61] (measured in the dark), with a linear fit showing a Mott-Schottky behavior. V_{bi} shows the built-in voltage in this fit; it is denoted with *, as it is fitted assuming only C_{SC} without any of the capacitances shown in (a), thus it will differ from V_{bi} in Table 6, where all contributions to C_{all} are considered.

[xiii] For measurements at red LED illumination, the voltage range was not sufficient to allow a simulation of all four contributions to C_{all}. Contributions in the simulation which are based only on the theoretical description of the chemical capacitance are designated as $C_{\mu,theor}$.

The trap distribution parameter α which which led to the best simulation is high compared to literature values [16,17,18,19]. But as can also be seen in Figure 25(a), the slope of C_{all} is lower than the slope of $C_{\mu,theor}$ because of underlying contributions from other capacitances, especially C_{SC}, see also discussion in the following paragraph. A space-charge layer behavior of the measured capacitance for small absolute voltages was confirmed by the linear behavior in a Mott-Schottky representation, see Figure 25(b). Also here, the combination of capacitances influences values like the built-in voltage V_{bi} , see the difference in Figure 25(b) (only C_{SC}) and in Table 6 (C_{all}, including C_{SC}). Good simulations were found for V_{bi} around -0.6 V, comparable to simulation values in [60]. The doping concentration N_{SC} is around 10^{19} cm^{-3}, which is similar to N_{SC} found via Mott-Schottky analysis for (non-porous) ZnO thin films electrodeposited in the presence of Cl^- [252].

Table 6 – Simulation parameters for the simulations of the overall capacitance for four different measurements of DSCs. The symbols are according to the equations of the respective capacitance contributions.

Cell →	**[61]**			**[71]**		**unit**
Value ↓ \ illumination →	**AM1.5**	**AM1.5 (variation)**	**dark**	**AM1.5**	**dark**	
trap distribution parameter α	0.82	0.65	0.50	0.80	0.70	-
characteristic temperature T_0 [a]	396	500	596	406	426	K
total trap density N_t [b]	$1 \cdot 10^{19}$	$1 \cdot 10^{19}$	$1 \cdot 10^{19}$	$1 \cdot 10^{19}$	$1 \cdot 10^{19}$	cm^{-3}
position of the conduction band edge E_c/q [c]	-0.853 (-0.905)	-0.980 (-1.040)	-1.090 (-1.115)	-0.965 (-1.010)	-1.005 (-1.010)	V
$\Delta E_c/q$ [d]	-227	-110		-40		mV
Helmholtz capacitance C_H [e]	0.0010	0.0010	0.0010	0.0010	0.0012	$F\ cm^{-2}$
absolute temperature T [f]	325	325	298	325	298	K
position of the monoenergetic trap states (in volt) V_{mono} [g]	-0.3	-0.47	-0.23	-0.32	-0.30	V
density of monoenergetic trap states N_{mono} [g]	1	$5 \cdot 10^{13}$	$6 \cdot 10^{11}$	1	$1.1 \cdot 10^{12}$	cm^{-3}
relative permittivity ϵ_r [h]	8.0	8.0	8.0	8.0	8.0	-
density of states in the space-charge region N_{SC}	$4.5 \cdot 10^{19}$	$4.3 \cdot 10^{19}$	$1.6 \cdot 10^{19}$	$4.0 \cdot 10^{19}$	$1.1 \cdot 10^{19}$	cm^{-3}
built-in voltage V_{bi}	-0.57	-0.57	-0.6	-0.75	-0.55 [i]	V

[a] Value of T_0 calculated by from $\alpha = T/T_0$.
[b] Assumed values of around 10^{19} cm^{-3}, also assuming that the total density of trap states remains approximately constant under different illumination conditions. For TiO_2, values around 10^{19}-10^{20} are often used for simulations, see text. A higher N_t shifts the curve to lower absolute voltages, as well as a lower absolute value of qE_c. As these two parameters are not independent, the assumptions for one value will affect also the other value.
[c] Values in parentheses denote values when for N_t the same density is assumed as for N_{SC}.
[d] Calculated as $E_c/q(dark) - E_c/q(AM1.5)$.
[e] As described in the text, this value also depends on the roughness of the substrate or the inner surface. As these values were not determined for the films, the value for C_H gives only the observed value.
[f] The temperature for AM1.5 measurements was assumed to be around 50°C due to the warming of the cells [127].
[g] Monoenergetic traps simulated only if a clear feature was observed in the measurement curve.
[h] A constant value of the relative permittivity ϵ_r of 8.0 [252] was assumed for these ZnO-based cells, at all illumination conditions and all voltages.
[i] The value is more negative than in Figure 25(b), as here other underlying capacitances influence the overall capacitance in this voltage range.

Variations of N_{SC} from film to film are comparatively small for the four simulations, whereas the variation for EIS in the dark and under AM1.5 illumination is larger, and probably coming from additional traps released under the intense AM1.5 illumination. The feature of deep monoenergetic trap states was simulated with a value of N_{mono} around 10^{12} cm^{-3}, which is lower than values found for (the rather different) nanoparticulate TiO_2, 10^{15} - 10^{16} cm^{-3} [65]. The total density of states N_t was arbitrarily set to 10^{19} cm^{-3} [65], which means that the simulated position of the conduction band edge is comparable only if N_t is similar for all four measurements. If, however, the traps described by N_t and N_{SC} are the same (for example if the distribution of traps is more or less homogeneous over the film thickness, and the influence of the transparent conductive oxide is small), the values of E_c/q become comparable and relevant also as absolute values. Values of E_c/q in parentheses (see Table 6) were calculated with this assumption of $N_{SC} = N_t$, which leads to less differences for E_c/q for the different cells and measurements.

For cell [71] the simulated C_{all} overlays the measured data both for measurements in the dark and under AM1.5 illumination. However for cell [61], the agreement of simulated and measured curves is smaller, especially for the measurement at AM1.5, and the parameters α and E_c/q are quite different from the measurement in the dark. A better agreement of simulation and measurement and more comparable parameters to the measurement in the dark was achieved, when a less steep $C_{\mu,theor}$ and monoenergetic trap states with higher density and at higher voltage are applied for the simulation, see variation in Figure 26(a) and Table 6. Such additional trap states could for example be caused by the intense illumination at AM1.5, either by a change in the trap distribution or rather trap filling in the ZnO film [253,254], and/or by oxidized dye molecules when dye regeneration is not sufficient at high illumination intensities [17]. The simulation is not yet perfect also for the variation, adding other deep trap state densities or assuming a second overlaying $C_{\mu,theor}$ could enhance the quality of the simulation, and yet be physically relevant.

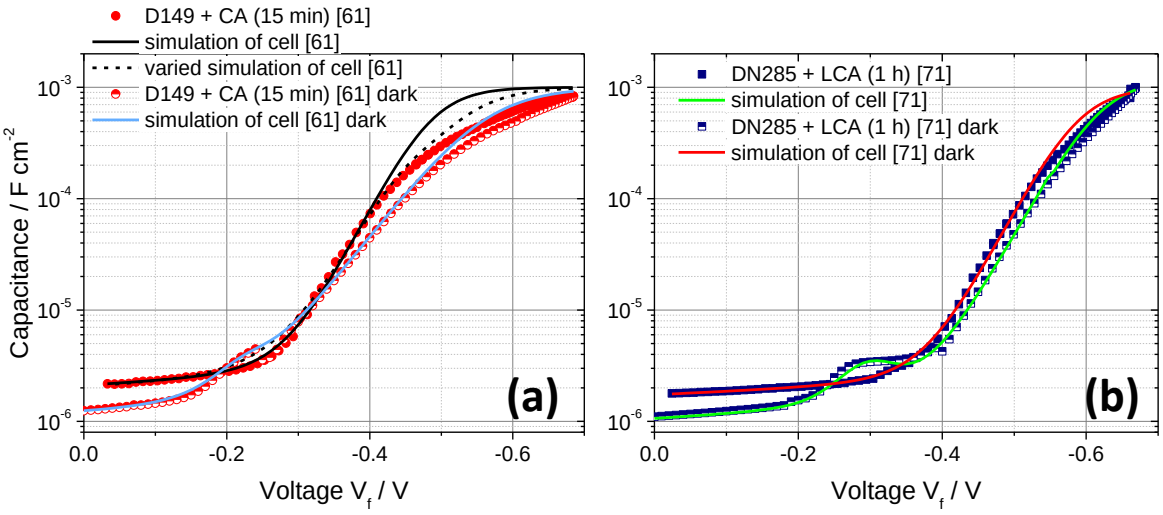

Figure 26 – Measured and simulated capacitance curves for (a) cell [61] and (b) cell [71]. Measured data are indicated by filled (measured at AM1.5) and half-filled (measured in the dark) symbols, simulated capacitance-voltage curves are indicated by a line, see legends for the color designation. The simulation parameters are listed in Table 6.

Consequences for the trap distribution parameter

As mentioned before, the different contributions of C_{all} overlap for some voltages, which means that the slope of C_{all} in the linear part is influenced especially by C_H (more negative voltages) or C_{SC} (voltages near 0 V). Thus the apparent slope of the measured and simulated curve will be lower than the slope of $C_{\mu,theor}$, see e.g. the difference of the slope for C_{all} and $C_{\mu,theor}$ at -0.45 V in Figure 25(a). This influence is also seen in Figure 27, where the trap distribution parameter α is calculated for the measured data and for the simulated curve via the slope at each point (relevant values of α are thus values at intermediate voltages). The differential α values for simulation and measurement are of a similar height, but even the maximum values are smaller than the respective α which was used for the simulations (indicated at the right axes). This means that the apparent slope of the measured chemical capacitance and of C_{all} is lower than for $C_{\mu,theor}$, of which the latter should represent the real chemical capacitance. The usual method for the determination of α, a linear fit of the linear part in the capacitance-voltage curve, thus can lead to inaccurate (mostly lower) α values, if other contributions to the measured capacitance overlap with C_μ, as it is observed here. To obtain the most accurate value for α, the capacitance-voltage curve should thus be simulated or fitted with all capacitance contributions.

However, when deviation from ideal behavior occurs (for example as discussed above for the measurement of cell [61] at AM1.5), or values are achieved over a smaller voltage range (as for measurements at red LED light), even a simulation of C_{all} may not lead to accurate values of α. Thus in this work α was determined from the maximum of the differential α values (slope determined at each point of a smoothed curve) as the best possible approximation of a simulated α (see Figure 27, and see Table 7, p. 87 for the resulting values of α for the different measurements).

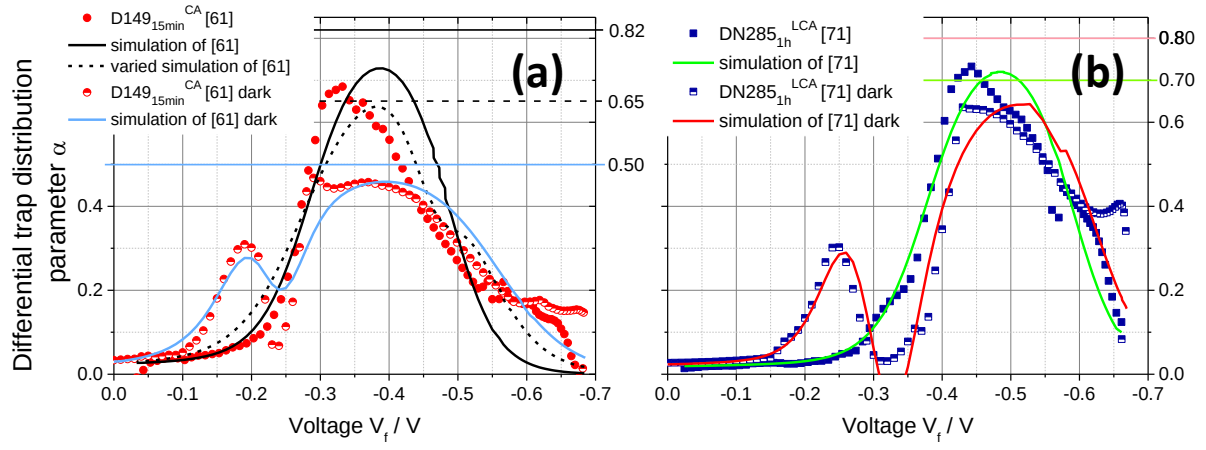

Figure 27 – Differential trap distribution parameter α determined from the slope of measured (symbols) and simulated (lines) capacitance curves shown in Figure 26(a) after $\boldsymbol{\alpha = (slope\ of \ln(C_{all}))k_BT/q}$ (from equation **(21)**). Filled symbols indicate a measurement at AM1.5 illumination, while half-filled symbols indicate a measurement in the dark. The color coding of the lines is indicated in the legend. The α values obtained from the simulation of the measurement curves are indicated at the right axis and by horizontal lines.

For low illumination intensity and measurements in the dark very similar or the same values of α are obtained, which indicates that this method leads to reproducible values. Also for a determination of α from open-circuit voltage decay curves [203], the maximum of α reaches similar values (not shown), even though the values scatter more for higher and lower voltages.

Influence of different illumination conditions on C_μ and α

The measurements of the EIS are mainly conducted under AM1.5 illumination at different applied voltages, which will give relevant information regarding the performance under conditions similar to possible operating conditions. For all cells discussed in this chapter, also EIS at varied illumination intensities of a red LED was measured, and for some cells, EIS in the dark completed the set of experiments. The detailed differences in experimental conditions for these three measurements are discussed in the supplemental information **9.1.2**. The main differences are a higher temperature [127] and a high illumination intensity (including also UV-light) and comparatively high currents flowing in forward direction for **AM1.5 conditions**, low illumination intensity (of a wavelength maximum not in the absorption maximum of the cell), with almost no current flowing at **red LED illumination**, and no illumination with no current flowing in forward direction for measurements **in the dark**. All C_μ curves for the differently sensitized cells at different illumination conditions are shown in Figure 28 and Figure 29, where the cells are grouped after the dye or the sensitization time, respectively. On the left, C_μ is shown, while on the right C_μ was additionally normalized with the total trap density relative to a reference cell, $N_t/N_{t,ref}$. This value was determined from plots of the charge density vs. I_{SC}, see Figure 84, p. 195 for the plots and Table 7, p. 87 for the values. This normalization allows the evaluation of shifts of the conduction band edge [17] relative to a reference cell, however the values were determined only for measurements at red LED illumination, assuming that N_t is constant for all measurements of one cell. Thus the normalization on the right side was only performed for one measurement to enhance the legibility of the plots, and the other measurements are assumed to shift accordingly.

Influence of the illumination on C_μ: C_μ at the three used illumination conditions differs by several aspects. First, C_μ at red LED illumination always is shifted towards more negative voltages, when compared with measurements at AM1.5 illumination. Wherever measurements in the dark are available, the shift is even larger than for measurements at red LED illumination. Or discussed in the order of measurement, the illumination with AM1.5 light shifts the conduction band edge to lower energies compared to a cell in the dark, as it was also observed before for TiO_2-based DSCs, and attributed there to band pinning. The decrease in E_c of some mV in the present work could either be ascribed to a warming of the cell and thus a decreased chemical capacitance, or to a change at the ZnO surface for example by an increase of positive charge at this interface (probably also from non-regenerated and thus oxidized dye molecules [17]).

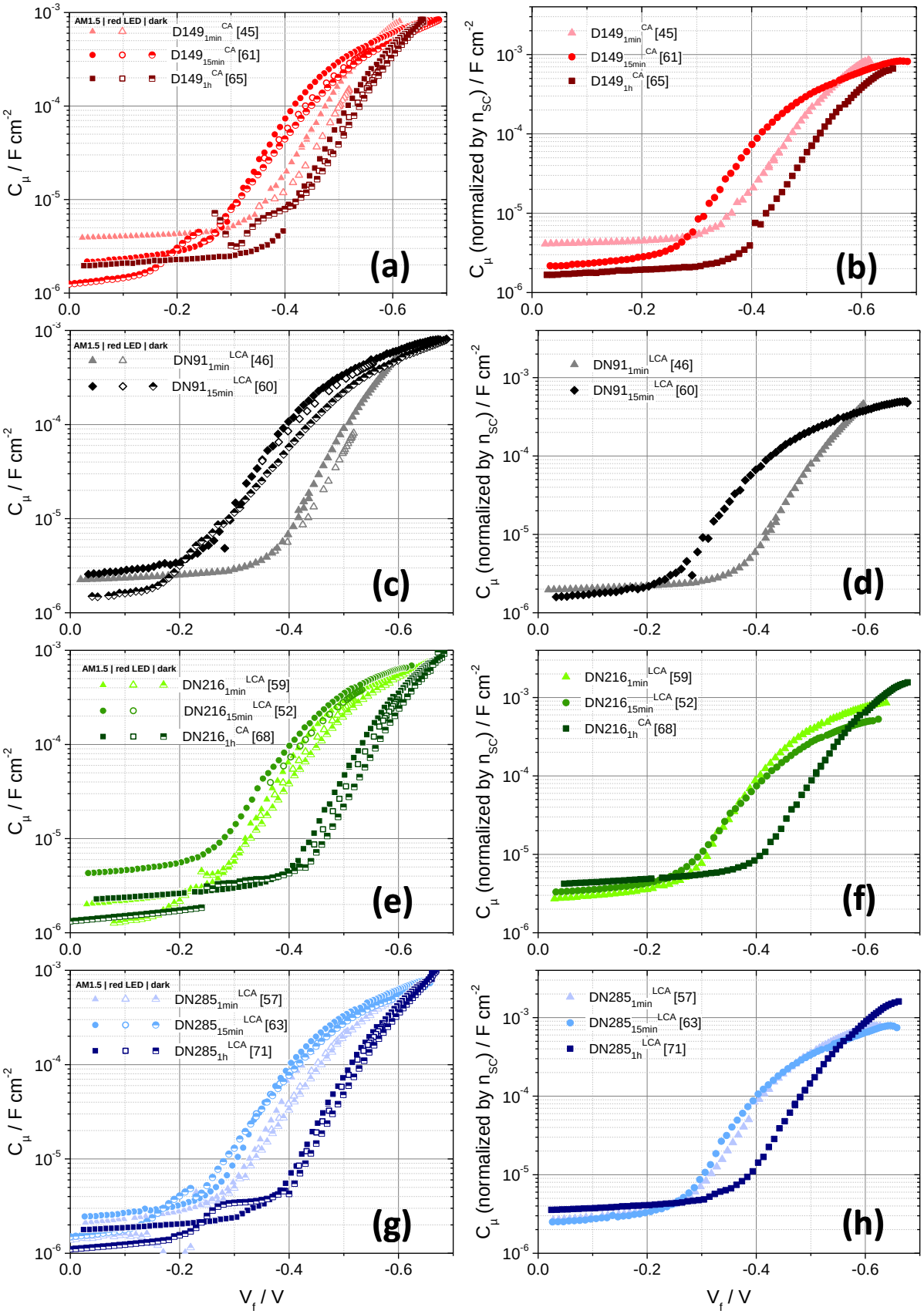

Figure 28 – Chemical capacitances of ZnO-based DSCs plotted against V_f, grouped after the sensitizing dye, (a,b) D149, (c,d) DN91, (e,f) DN216 and (g,h) DN285. The capacitance data were obtained from impedance measurements at AM1.5 illumination (indicated by filled symbols), at red LED illumination (indicated by open symbols) and in the dark (half-filled symbols). Increasing color depths indicates increasing sensitization time. The right plots (b,d,f,h) give the chemical capacitance normalized by n_{SC} determined from current transient measurements relative to cell [61].

When IV-curves are measured after the EIS measurements at the different illumination conditions, the trend in V_{OC} reproduces the change in E_c closely, with the highest V_{OC} after a measurement in the dark, and the lowest V_{OC} after EIS measurement at AM1.5 illumination, see section **9.1.3**. Thus the lower V_{OC} after longer AM1.5 illumination is caused by a downward shift of the conduction band edge, as it is observed in comparison to low-intensity illumination (or no illumination), in addition to the influence of the temperature [127]. This is confirmed also by the simulation of C_μ discussed above, where temperature effects are already included in the calculation, as for the same N_t, E_c shifts to lower energies for a measurement at AM1.5 illumination.

Changes of α at different illumination: Especially for cells sensitized for 15 min, not only the position of the C_μ curve changes for the EIS measurement at intense AM1.5 measurement, also the slope at intermediate voltages becomes steeper. This is also reflected in a higher trap distribution parameter α at AM1.5 illumination, see Table 7. For 1 min the difference in α for the different measurements of a respective cell at low and high illumination intensities is smaller than for 15 min sensitization time, and for 1 h this difference is even smaller, probably because C_μ is already changed more due to the long sensitization. As also the temperature is lower for the dark measurements, a part of this change in α can be ascribed to temperature, after equation **(22)**. To see how much of the change in α stems from the temperature, the values of T_0 were determined from the simulated values of α in Table 6. Even without temperature influence the distribution of trap states (given by the characteristic temperature T_0) is steeper for EIS measurements in the dark than for measurements at AM1.5. This is also the case for most measurements in Table 7. Where the difference of α is very small for the different illumination conditions (for example cell [45]), this difference is thus explained only by the temperature difference, whereas for some cells the trap distribution changes. Compared to literature values of electrodeposited ZnO, where α does not exceed a value of 0.5 [16,17,18,19,127], α for the cells in this work is high. This means that during operation of the solar cell, a small change in the Fermi-level voltage has a larger influence on the density of states for the cells in this work compared to cells in the literature, see also plots of the DOS in Figure 89, p. 197. As the values of α in Table 7 were determined at the part of the capacitance-voltage curve with the highest slope, a part of the difference to the values determined in the literature may be due to the method of determination of α, or due to exact film preparation, compare α for films with smaller deposition area (chapter **5**, and section **9.1.4**).

Deep monoenergetic trap states: For measurements at AM1.5 illumination, no additional capacitance stemming from deep monoenergetic trap states is visible in the C_μ curves. For most measurements in the dark however, this capacitance appears as a distinct shoulder at voltages between -0.2 and -0.3 V (see also the simulation of C_μ above). For almost all four indoline dyes, this feature becomes more distinct for longer sensitization times, indicating that the sensitization procedure influences or rather induces these deep trap states. Either these trap states are induced by the longer contact with the sensitization solution (directly on the surface of the ZnO film), or traps on the

semiconductor surface are produced by the sensitizer or some other adsorbate. It is improbable that traps are produced inside the film from the comparatively short treatment in the adsorption solution, thus it is assumed that these traps will be located at the surface. For the measurements at AM1.5, which were measured after EIS in the dark, the deep monoenergetic trap states are no longer observed.

This behavior is different from other ZnO-based DSCs (sensitized by indoline and/or squaraine dyes), where especially for a sensitization with the squaraine dye an additional capacitance was observed and attributed to deep monoenergetic trap states [17], caused by oxidized dye molecules, as the traps were observed for AM1.5 illumination. In the present work, the trap states occur especially in the dark (and are probably shifted to higher energy and increase in density, see varied simulation for cell [61] in Figure 26(a)). It is very likely that through the intense illumination including some UV, the occupancy of traps is changed, so that deep monoenergetic trap states no longer are observed, but maybe other traps are produced which change the trap distribution at more negative voltages (see different α). A change of the trap distribution upon illumination was described before for electrodeposited ZnO films [253,254], where sub-bandgap illumination (but more than around 600 nm wavelength) led to a persistent photoconductivity and a changed photoluminescence. This effect was attributed to the filling of trap states inside the bandgap, where charge carriers achieve a very long lifetime by relaxation processes producing an energy barrier for these carriers. A similar process could be responsible for the change in the trap distribution observed after longer illumination with AM1.5 light for the very similar electrode material, thus also leading to a reduced V_{OC} over a longer time span, compare section **9.1.3**.

Table 7 – Different cell values determined from EIS measurements, V_{OC} vs. intensity measurements and current transients. The measurements from which the values are determined are indicated in the table, as well as the illumination conditions. Values determined from EIS measurements at AM1.5 are highlighted as this illumination was mostly used for comparable cell characterization in the literature.

Value / **Sample**	**$N_t/N_{t,ref}$**	**α**			**β**			**β (1/m)**
measurement (from plot) →	current transient (n_{SC} vs. I_{SC})	EIS (C_μ vs. V_f)	EIS (C_μ vs. V_f)	EIS (C_μ vs. V_f)	EIS (R_{rec} vs. V_f)	EIS (R_{rec} vs. V_f)	EIS (R_{rec} vs. V_f)	V_{OC} vs. intensity
illumination conditions →	red LED	**AM1.5**	red LED	dark	**AM1.5**	red LED	dark	red LED
reference cell or temperature →	cell [61]	**~325 K**	~298 K	~298 K	**~325 K**	~298 K	~298 K	~298 K
$D149_{1min}^{CA}$ [45]	0.95	**0.65**	0.62	-	**0.75**	0.76	-	1.03
$D149_{15min}^{CA}$ [61]	1 (Ref.)	**0.67**	0.45	0.46	**0.42**	0.67	0.60	0.77
$D149_{1h}^{CA}$ [65]	1.18	**0.70**	0.62	0.62	**0.80**	0.82	0.78	0.90
$DN91_{1min}^{LCA}$ [46]	0.45	**0.70**	0.66	-	**0.80**	1.04		1.19
$DN91_{15min}^{LCA}$ [60]	1.61	**0.66**	0.40	0.41	**0.38**	0.69	0.61	0.78
$DN216_{1min}^{LCA}$ [59]	0.74	**0.69**	0.49	0.49	**0.47**	0.82	0.70	0.96
$DN216_{15min}^{LCA}$ [52]	1.30	**0.58**	0.42	-	**0.63**	0.83	-	0.90
$DN216_{1h}^{CA}$ [68]	0.54	**0.68**	0.65	0.64	**0.64**	0.82	0.75	0.86
$DN285_{1min}^{LCA}$ [57]	0.80	**0.69**	0.52	0.50	**0.55**	0.87	0.77	1.00
$DN285_{15min}^{LCA}$ [63]	0.98	**0.70**	0.44*	0.48	**0.48**	0.71	0.63	0.79
$DN285_{1h}^{LCA}$ [71]	0.50	**0.72**	0.65	0.63	**0.65**	0.78	0.74	0.83

* For this curve no maximum of the distributed values of α was observed, that means the correct value is probably larger.

Influence of the adsorption time on C_μ

As discussed for the simulation of the C_μ curves above, for the evaluation and discussion of trap states, especially C_μ at intermediate voltages is important. The position of the capacitance-voltage curves shows a similar behavior with increasing sensitization time for the four different indoline dyes, see Figure 28(a,c,e,g), first a shift to lower energies (lower absolute voltages) for an increase of adsorption time from 1 to 15 min, and for a further increase of the sensitization time to 1 h a shift to higher energies or more negative voltages. Even if C_μ is normalized to the total trap density of cell [61], which is important for a correct interpretation of the shift of E_c [17], this behavior is still observed for a sensitization with D149 and DN285, while for DN216 the cell sensitized for 1 min has the lowest conduction band edge. However a sensitization for 1 h leads to the highest E_c, regardless of the dye (unknown for DN91). Very similar shifts are also observed from the relative position of charge density curves determined from charge extraction at open circuit, see Figure 85, p.195. The effect of the upward shift of E_c is probably caused by the prolonged adsorption and the long contact with the sensitizing solution, partly by the coadsorbate, as cholic acid and its derivatives are known to cause as upward shift due to the additional surface dipole [132], but also the dye probably introduces an additional dipole moment. It is not directly conceivable why thus a shift of E_c to higher energies is not already observed for the increase of the sensitization time from 1 min to 15 min, but probably firstly, more molecules are adsorbed for longer adsorption times (see section **3.1.2**), and secondly both the coadsorbate and the dye can arrange and bind in a more ordered way on the ZnO surface when more time is given for equilibration. A more ordered packing of molecules could then lead to a stronger dipole on the surface, and thus an increased effect of the adsorbates on the conduction band edge. For the sensitization for 1 h, the upward shift of the conduction band edge (compared to for example 15 min sensitization) affects also the IV-curves by leading to a higher V_{OC} (Figure 22, p. 73). Especially for 1 and 15 min sensitization time, other effects like dye loading and recombination overlay the effect of the position of E_c on V_{OC}, so that the trends observed in C_μ are not directly reflected on V_{OC} for all cells, and also for a 1 h sensitization time the shift in V_{OC} is smaller than the shift in E_c. The large upward shift of E_c for a sensitization of 1 h compared to shorter sensitization times is also one reasons for the lower I_{SC} values compared to cells sensitized for 15 min (see also Table 5, p. 75), as injection is impaired for a higher E_c.

For the trap distribution parameter α determined at AM1.5 illumination, a slight increase with increasing sensitization time is observed for D149 and DN285, while for DN216 α is lowest for 15 min sensitization time. For similar films sensitized with D149 and a coadsorbate, α showed the opposite behavior with a slight decrease with increasing sensitization time [16] (with overall much lower values of α of around 0.2). This difference can be caused on the one hand by the difference in ZnO film deposition (reducing vs. non-reducing conditions), but also because α was determined at more negative voltages in [16], where for the films in the present work, C_μ was already influenced by C_H. α

determined at red LED illumination or in the dark shows the same tendency with increasing sensitization time, first a slight decrease and then a slight increase to similar α values. As EIS in the dark leads to very similar α values for red LED measurements, this trend is not an artifact due to the narrower voltage range for measurements at red LED illumination. Thus it seems that the trap distribution is less steep for 15 min adsorption times for all four sensitizers for measurements where the trap distribution is almost unchanged by illumination, whereas for intense illumination the trap distribution is overall steeper and the lowest steepness is for some dyes observed for 1 min adsorption time. It can be concluded that the change in α by the different sensitization procedure is smaller than the change which is introduced by the illumination with high-intensity AM1.5 light, probably because the sensitization takes place only at the surface whereas the illumination penetrates also the bulk of the film. However, when the very similar trap distribution is combined with a very different dipole introduced by the differently arranged molecules at the ZnO surface for the different sensitization times, the sensitization has a marked influence on the density of states and thus the performance of the cells.

Influence of the sensitizer on C_μ

The influence of the different sensitizers on C_μ is smaller than the influence of the sensitization time, see Figure 29 compared to Figure 28. For a sensitization time of 1 min, a large difference in C_μ is observed for films sensitized with D149 and DN91 (compared to films sensitized with DN216 and DN285). This difference is surely not directly caused by the influence of a shorter alkyl group at the outer rhodanine ring of the dye molecules, even though it is probable that dyes with a shorter or longer alkyl spacer will arrange differently on the ZnO surface.

A different arrangement on the ZnO surface is also supposed for D149 from the different shape of the absorption spectrum (Figure 20, p. 69), but the spectrum of DN91 was similar to the other double-anchored dyes. Exactly for the films sensitized with D149 and DN91 it was observed that a sensitization for 1 min did not lead to a complete dyeing of the film (compare **3.1**, p. 66). It is possible that free ZnO surface and thus less traps due to the binding of the dyes are present for these two films, but it also cannot be excluded that unavoidable fluctuations in the film preparation based on self-assembly of dye molecules [127] could lead to a change in the trap distribution. For sensitization times of 15 min or 1 h C_μ is very similar for all dyes, which is an indication that mostly these possible fluctuations are not large, or that they are less important when the surface is more completely covered with adsorbates. For 15 min adsorption time, E_c is similar for the four dyes, see the overlap of C_μ at intermediate voltages in Figure 29(d).

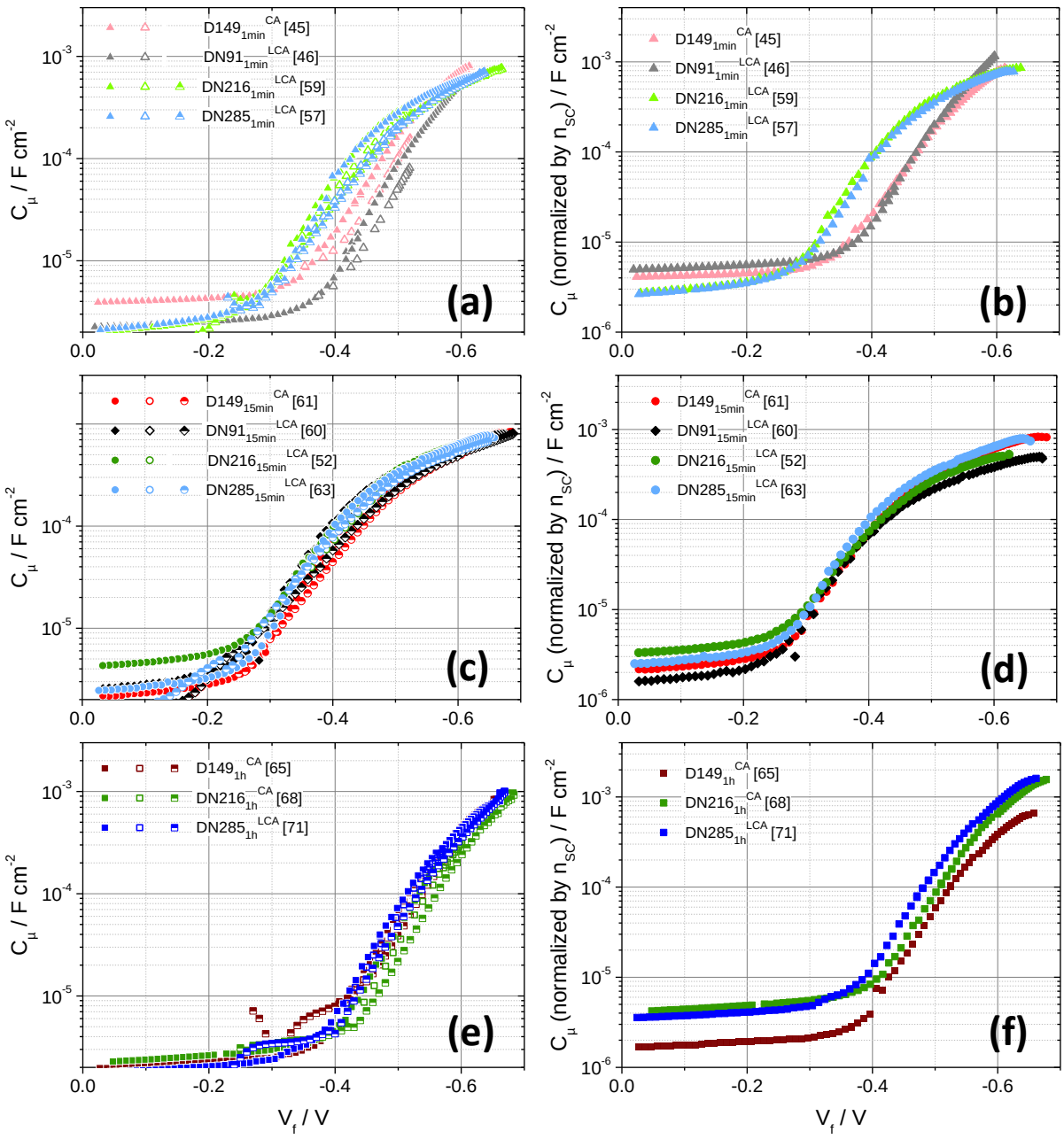

Figure 29 – Same as Figure 28, grouped after the sensitization time of (a,b) 1 min, (c,d) 15 min and (e,f) 1 h. The plots on the right (b,d,f) give the chemical capacitance normalized with the ratio $N_t/N_{t,ref}$ determined from current transient measurements.

For 1 h, when the dye molecules have more time to form aggregates, E_c is higher for D149, lower for DN216 and lowest for DN285. This difference can be caused by the difference in adsorption behavior, either by a different tendency of aggregation for the different dyes, or by a different competition for adsorption sites between the dye and the coadsorbate. As also observed for the comparison of C_μ for the different sensitization times above, the relative shifts of E_c do not directly correlate with the observed in V_{OC}, and thus also other factors like recombination influence V_{OC}.

3.3.2 Recombination and its change for different experimental conditions

Recombination was determined from EIS measurements, which were performed under different illumination conditions, see section **3.3.1**, p. 79 and section **9.1.3** for a detailed discussion of these conditions. Also other measurements were performed at different illumination conditions, resulting all in very different recombination behavior. This difference will influence the discussion of results for the different sensitization procedures. Thus, first the influence of the illumination conditions on recombination will be discussed, followed by a discussion of the changes in recombination by the different sensitization times and the different sensitizers.

Influence of the illumination conditions on recombination

For all measurements which give information about recombination and which were performed at different illumination conditions, a difference in recombination is seen especially for intense AM1.5 illumination compared to no illumination or red LED illumination (compare the recombination resistance R_{rec} in Figure 93, p. 200 and Figure 31, p. 95, the electron lifetime τ_n in Figure 96, p. 203 and Figure 32, p. 96 and the recombination currents in Figure 98, p. 205). For measurements performed at AM1.5 illumination, usually the recombination is higher than for measurements at red LED light or in the dark, see for example the decreased recombination resistance R_{rec} for AM1.5 conditions in Figure 93. For many cells, the difference in R_{rec} even exceeds one order of magnitude. Not only the absolute values of the τ_n or R_{rec} are changed for the intense AM1.5 illumination compared to red LED illumination or measurements in the dark, also the curve shape is different. A change of the recombination resistance with illumination (considerably higher R_{rec} in the dark) was described before for electrodeposited ZnO [18], and even more often for TiO_2 nanoparticulate films. A possible reason for such differences in R_{rec} is for example an ineffective regeneration under intense illumination [17,66,127], causing iodide depletion in the electrolyte [276,255], and leading to a larger amount of oxidized dye molecules on the ZnO surface, which then can act as recombination centers. Another possible reason is for example a change of the surface trap distribution by an intense illumination, surface traps, because surface traps most strongly influence recombination. For the measurements in this work, the influence of recombination for example via surface states or via oxidized dye molecules [17] cannot be separated, as recombination values like R_{rec} and τ_n represent a sum of recombination over all recombination paths. However the use of different illumination conditions helps to associate the observed recombination with the different recombination paths or exclude some of the paths. Recombination in the dark can take place for example via surface states or via the conduction band, but only from ZnO states to the electrolyte states (or for an inefficient blocking

layer: from states in the substrate material, e.g. FTO, to the electrolyte [xiv]). For increasingly negative voltages, also radiative recombination increases, as the LUMO of the dye is filled from the semiconductor. This behavior was observed in electroluminescence measurements of some of the cells discussed in this chapter (performed by Nico Hofeditz in the course of his Bachelorthesis, Phillips-Universität Marburg). Overall, for measurements in the dark, one recombination path can be excluded, that is recombination via oxidized dye molecules. These are only present in the operating and illuminated solar cell if dye regeneration does not occur with unity efficiency. Thus the comparison of the recombination at high, low and no illumination intensity also reveals whether dye regeneration in the cell is efficient or not. The regeneration efficiency is a value which can be accessed with difficulty but is more important than often thought [66], thus the comparison of the different illumination conditions gives valuable information.

If the measurements are performed at overall similar conditions like EIS measurements in the dark or at red LED illumination in Figure 31, p. 95 or in Figure 96, p. 203, the differences in recombination will represent mainly differences in the regeneration. The observed differences for these measurement conditions are consequently very similar, with slightly higher recombination (lower R_{rec} or τ_n) for measurements at red LED illumination. This small difference is probably caused by the measurement mode, for the illumination intensity with red LED increases with increasing V_f or DOS, and thus the recombination at red LED illumination gradually differs more from measurements in the dark for higher V_f or DOS. As discussed above, this difference for the otherwise similar conditions indicates that for increasing illumination intensity with red LED light gradually more recombination via oxidized dye molecules occurs, as the regeneration efficiency becomes slightly smaller by increasing diffusion limitation in the electrolyte. For measurements at AM1.5, two other factors have to be considered, so that the effect of regeneration is not overestimated, first the higher temperature of the cell [127], and second a possible change of the trap distribution, induced by the intense illumination, as discussed for Figure 28, p.85.

For cell [71], the influence of the temperature is estimated in Figure 30, where the R_{rec} measured at AM1.5 is plotted, as well as the measurement in the dark. Additionally, the curve in the dark is multiplied by the factor $\exp\left(-\frac{T(dark)}{T(AM1.5)}\right)$ (see also equation **(28)**) and the resulting curve is with the non-modified curves. The calculation includes the effect of a rise in cell temperature of about 25 K [127] for the exponential term, disregarding possible changes due to temperature in the prefactor $R_{rec,0}$ or in the recombination parameter β [xv]. It can be seen that with just this simplified temperature influence no change in the slope (proportional to β) is observed, and R_{rec} measured in the dark and corrected by temperature does not yet reach as low values as the measurements at AM1.5.

[xiv] The recombination via the substrate can be neglected for all cells in this chapter, as indicates the linear shape of τ_n determined from OCVD for low absolute voltages, see Figure 96, p. 101.
[xv] Inclusion of a changed temperature T in the pre-factor leads to slightly higher R_{rec} values compared to values where T was not changed in the prefactor.

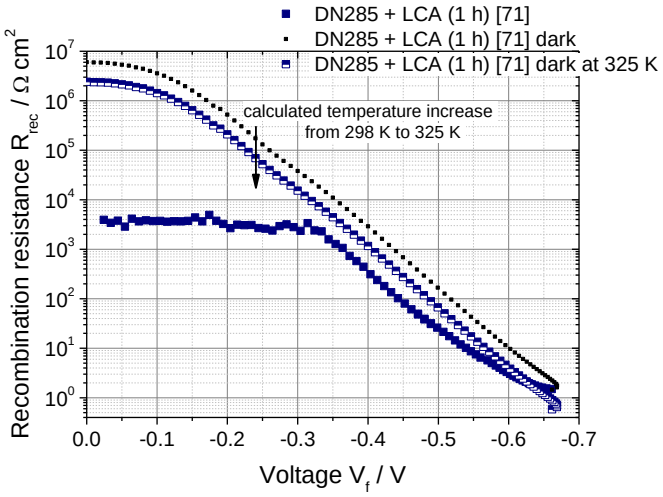

Figure 30 – Comparison of the recombination resistance R_{rec} of cell [71] obtained from EIS at AM1.5 illumination and in the dark (see legend for designation). An additional curve (half-filled symbols) was added, where the measurement in the dark (cell temperature ca. 298 K) was recalculated as if it was measured at a higher temperature which occurs at AM1.5 illumination (about 325 K; without pre-factor), see text for more details.

The difference in the slope could be caused by the abovementioned change in trap distribution, whereas the further shift of the curves is attributed mainly to an additional recombination path via oxidized dye molecules as discussed above.

The recombination parameter β [xvi] is higher at lower illumination intensities for most cells, see the higher slope in Figure 93, p. 200. This was also observed before for the measurement of D149-sensitized ZnO-based DSCs, and attributed to a change of the interface at high illumination intensity because of an increase of oxidized electrolyte species and a changed dye conformation [18]. The values of β from EIS measurements are complemented by β values from measurements of V_{OC} vs. (red LED) illumination intensity, see plots and linear fits in Figure 99, p. 206, where the values are similar to β determined from EIS measurements at red LED illumination, and Table 7, p. 87. For some measurements at red LED or in the dark, β is even ~1, which indicates that recombination occurs mainly via the conduction band edge, not via surface states. The change to lower β values for higher illumination (except for cells [45] and [65]) indicates that the trap distribution changes, as it was concluded from different C_μ in the previous section. Probably additional (or different) traps are induced by the intense illumination, but C_μ alone does not give more information whether these traps are located at the surface or in the bulk of the ZnO films. However the change in β indicates that for most cells the induced traps are at least partially surface traps, via which increased recombination can occur.

[xvi] β was determined from the differential values of beta (similar to α in the previous section), and the most constant values around V_{OC} was taken for the value of β listed in Table 7, p. 92.

Influence of the sensitization time on recombination

Information about recombination is given by the different parameters R_{rec}, τ_n and the recombination currents. To ensure a correct comparison of recombination for the different sensitization times, the influence of the density of states on recombination is removed by a plot of R_{rec} and τ_n against the DOS, whereas recombination currents are shown versus the voltage corrected by the shift of E_c relative to a reference, V_c [xvii]. For comparison, the recombination values are also shown without correction of the DOS vs. V_f in Figure 93, p. 200, which is important for the comparison of cells and the determination of β. Especially for cells sensitized for 1 h, which show a large shift of E_c compared to shorter sensitization times, a plot vs. DOS completely changes the comparison, so that recombination at the same DOS is enhanced for 1 h sensitization time compared to 15 min sensitization. For example cell $D149_{1h}^{CA}$ [65] shows a higher R_{rec} than cells with a shorter adsorption time when plotted against V_f, see Figure 93(a), p. 200, but if the recombination resistance of the same cells is compared against the DOS in Figure 31(a), $D149_{1h}^{CA}$ [65] shows a very similar R_{rec} as for a sensitization for 1 min, both being lower than for a sensitization of 15 min. For the sensitizers DN216 and DN285 Figure 31(c,d), a sensitization for 1 h even leads to a higher recombination (or lower R_{rec}) than a sensitization for 1 min when compared at the same DOS. Usually a higher dye loading at the surface would lead to less recombination, as the ZnO surface would thus be more effectively shielded against the electrolyte. This explains the increase in R_{rec} for an increase of the adsorption time from 1 min to 15 min, which is observed for all four sensitizers. However, for longer adsorption times, the higher amount of dyes also leads to an increased aggregation (see section **3.1.2**), and as aggregates are also recombination centers (for example for radiationless recombination), the beneficial effect of a better shielding by more dye molecules is counterbalanced by this increase in recombination by aggregates, leading even to R_{rec} values lower than for 1 min adsorption time. The increase in recombination in spite of a more effective shielding from the electrolyte also gives another reason why I_{SC} does not further increase for an increase of the dye loading from 15 min to 1 h (apart from the upward shift of E_c already discussed in section **3.3.1**). Very similar observations are made for the plots of τ_n vs. DOS (Figure 32, p. 96 [xviii]) and for the plot of the recombination currents vs. V_c in Figure 98, p. 205, all showing that in terms of minimized recombination it is beneficial to use an intermediate sensitization time to avoid recombination via uncovered substrate (shorter times) or via dye aggregates (longer times). In [16] however, a different behavior for the coadsorption of cholic acid was found than in the present work. Especially at high DOS, R_{rec} of the cells in [16] decreased with decreasing sensitization time, whereas for lower DOS this order was reversed. This reversion was especially owing to the different values of the recombination parameter β which introduced a different slope to curves of R_{rec}.

[xvii] Usually a plot vs. V_f is seen more often in the literature, as it can be applied for all measurements measured against a voltage. However for larger differences in α, a plot vs. DOS are preferable [16,18]. As α changes even for one cell at different illumination conditions, a plot vs. DOS was applied wherever possible, and V_c was used for all other measurements.

[xviii] The same sequence of the curves for τ_n and R_{rec} indicates also a good area normalization of R_{rec}, as τ_n is independent of the cell area.

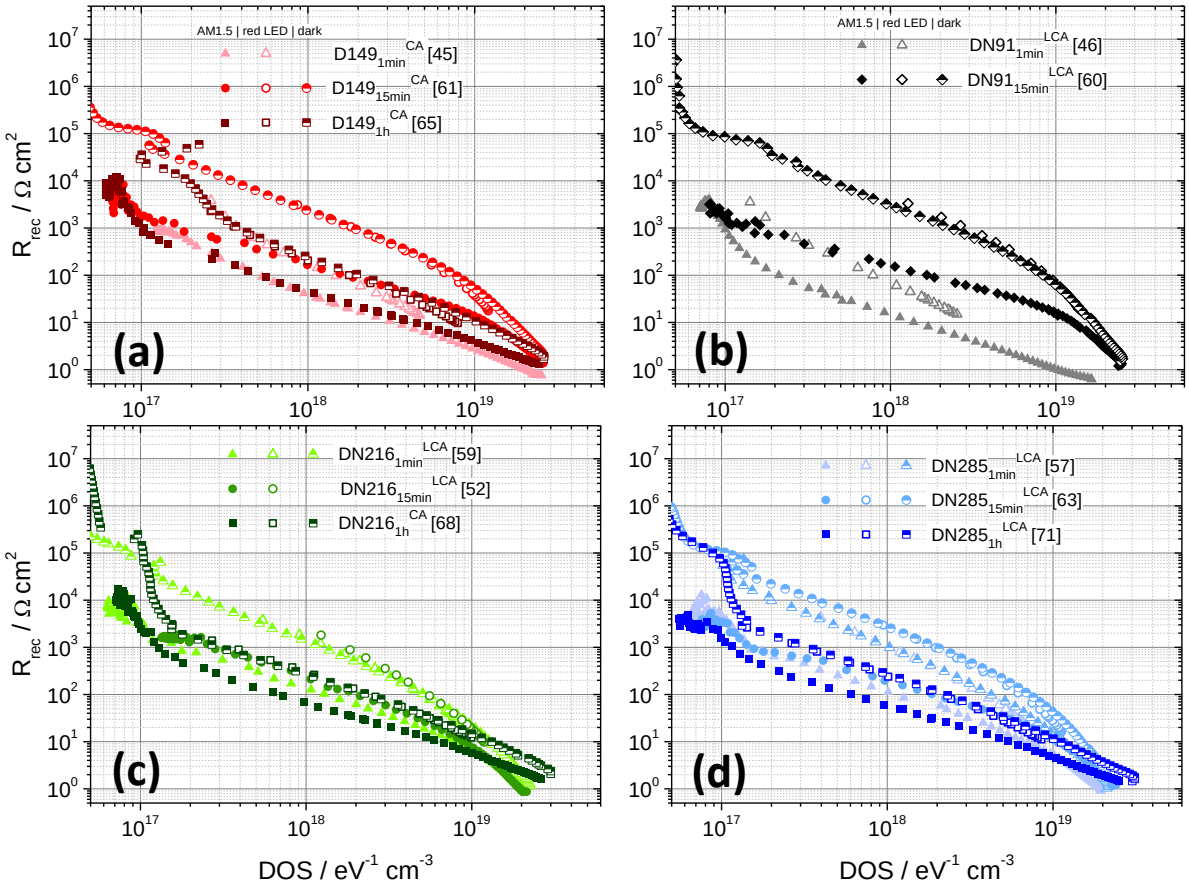

Figure 31 – Recombination resistance R_{rec} vs. the density of states for DSCs sensitized with different indoline dyes and for different times. The measurements are grouped after the sensitizer dye, (a) D149, (b) DN91, (c) DN216 and (d) DN285. Increasing color depth indicates increasing sensitization time. Filled symbols indicate measurements at simulated AM1.5 illumination, open symbols indicate measurements performed at red LED illumination, and half-filled symbols indicate measurements in the dark.

This difference compared to the results in the present work is probably caused by the different electrolyte or also the different deposition of ZnO.

To obtain more information about changes in regeneration through the different sensitization times, R_{rec} or τ_n from measurements at AM1.5 illumination are compared with the respective values determined in the dark (or at red LED illumination). If the cells are similar, it can be assumed than the larger the difference, the less effective is regeneration supposed to occur. For a comparison of more cells, it has to be noted that also the absolute value of R_{rec} (or τ_n) is important for an interpretation of the regeneration. An increased recombination via dye aggregates will decrease both R_{rec} in the dark and R_{rec} at AM1.5, however for the measurement at AM1.5 this direct recombination will decrease the amount of oxidized dye molecules compared to a sample with less aggregation and thus the difference of R_{rec} in the dark and under illumination, and thus seemingly an increase the regeneration is observed. Regardless of the dye, this difference for the different illumination conditions is highest for a sensitization time of 15 min, both for R_{rec} (Figure 32) and τ_n (Figure 33).

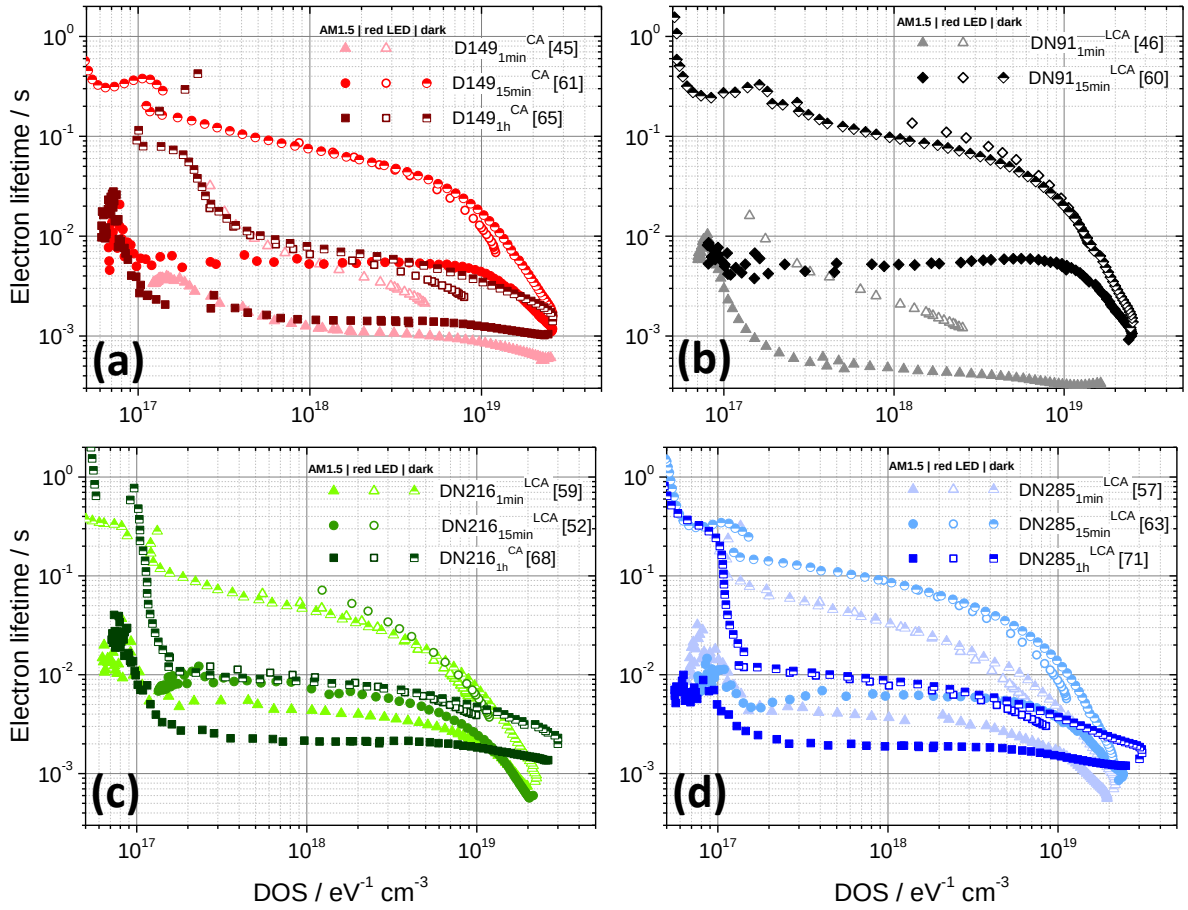

Figure 32 – Electron lifetime τ_n vs. DOS of differently sensitized DSCs, grouped after the sensitizing dye (a) D149, (b) DN91, (c) DN216 and (d) DN285. Increasing color depth indicates increasing sensitization time, while filled, open and half-filled symbols indicate measurements at AM1.5 illumination, at red LED illumination and in the dark, respectively.

This indicates that for a sensitization for 15 min, regeneration occurs with the least efficiency. This correlates with the highest values of I_{SC} for a sensitization for 15 min (compare Table 5, p. 75), and the higher current is also a reasonable explanation for a lower regeneration efficiency as transport limitation in the electrolyte becomes more important with higher current. However increase in recombination by a decreased regeneration also means that I_{SC} is limited by the lower regeneration efficiency [66].

A comparison of the recombination parameter β (see Table 7, p. 87 for β, obtained from the slope of R_{rec} vs. V_f in Figure 93, p. 200) for different sensitization times shows that at AM1.5, β is highest for a 1 h sensitization time, followed by a still high β value at 1 min sensitization time, and the lowest values for 15 min sensitization time. This is also approximately the sequence of the C_μ curves in terms of shifts of E_c, and this indicates that for the highest position of the conduction band edge, less surface states are present as recombination centers at an appropriate voltage. At red LED illumination or in the dark the values are not as consistent for all sensitizers, however mostly β is highest for 1 min sensitization time. The traps that lead to this recombination behavior are not induced by the intense light (at the absence of it), so that these traps are either intrinsically present in the ZnO film or induced

by the sensitization procedure or the electrolyte. Additional (surface) traps by the sensitization could explain a decrease in β with increasing sensitization time. However, this behavior was not observed for all dyes, so that the conclusion cannot be generalized. The observed β values are in a similar range as observed before, as typical values of β in ZnO solar cells range from 0.46 for ZnO nanowires [256] to 0.7 for nanoparticulate ZnO films [203]. For DSCs with electrodeposited ZnO, the values are in a similar range, around 0.4 [17] to about 0.6 [19] for measurements at AM1.5 illumination.

The recombination parameter β is, apart from V_{OC}, one of the main parameters influencing the FF of the cells (Table 5, p. 75), see equation **(35)**. Even with the relatively large changes in V_{OC} especially for 1 h sensitization time, the lowest β for 15 min sensitization time nicely correlates with the lowest FF for these cells. This is also seen in a plot of the differential β values (obtained by smoothing and differentiating R_{rec} vs. V_f) at voltages around -0.5 V in Figure 95, p. 202. Similar to other recombination values, β is influenced more by the different illumination conditions than by the use of different sensitization conditions.

Influence of the sensitizer on recombination

The recombination at a given sensitization time can be compared for the different sensitizers by the plots of R_{rec} vs. DOS in Figure 33. The plots of τ_n vs. DOS with the same grouping gave very similar results and are thus not shown. For a sensitization of 1 min, recombination for D149 and especially DN91 is higher than for DN216 and DN285, when compared at the same DOS. As also mentioned in section **3.1** and in the discussion of C_μ, the films sensitized with D149 and DN91 were not dyed completely after the very short sensitization time of 1 min, and the cells showed the opposite sequence for C_μ than observed here, compare Figure 29, p. 90 (the same C_μ is reached at higher energies for D149 and DN91). An incomplete dyeing usually would lead to a higher recombination, as the surface states of the ZnO are thus in direct contact to the electrolyte, which is exactly the observation for the incompletely dyed films. For D149 a higher recombination near the substrate is also corroborated by a deviation from the linear behavior near 0 V for τ_n determined from OCVD measurements, see Figure 97, p. 204. For DN91, this indication of direct recombination to the surface is not observed, and as the difference in recombination is probably not caused by the small differences in the dye structure, this difference is attributed to the unavoidable fluctuations in film preparation.
The considerably higher β values for a 1 min sensitization with D149 and DN91 compared to DN216 and DN285 (Table 7, p. 87) are caused by the higher conduction band edge for the former (Figure 29, p. 90), which leads to an increased fraction of recombination via the conduction band compared to recombination via surface states. The higher β values also lead to slightly higher FF for D149 and DN91, see Table 5, p. 75.

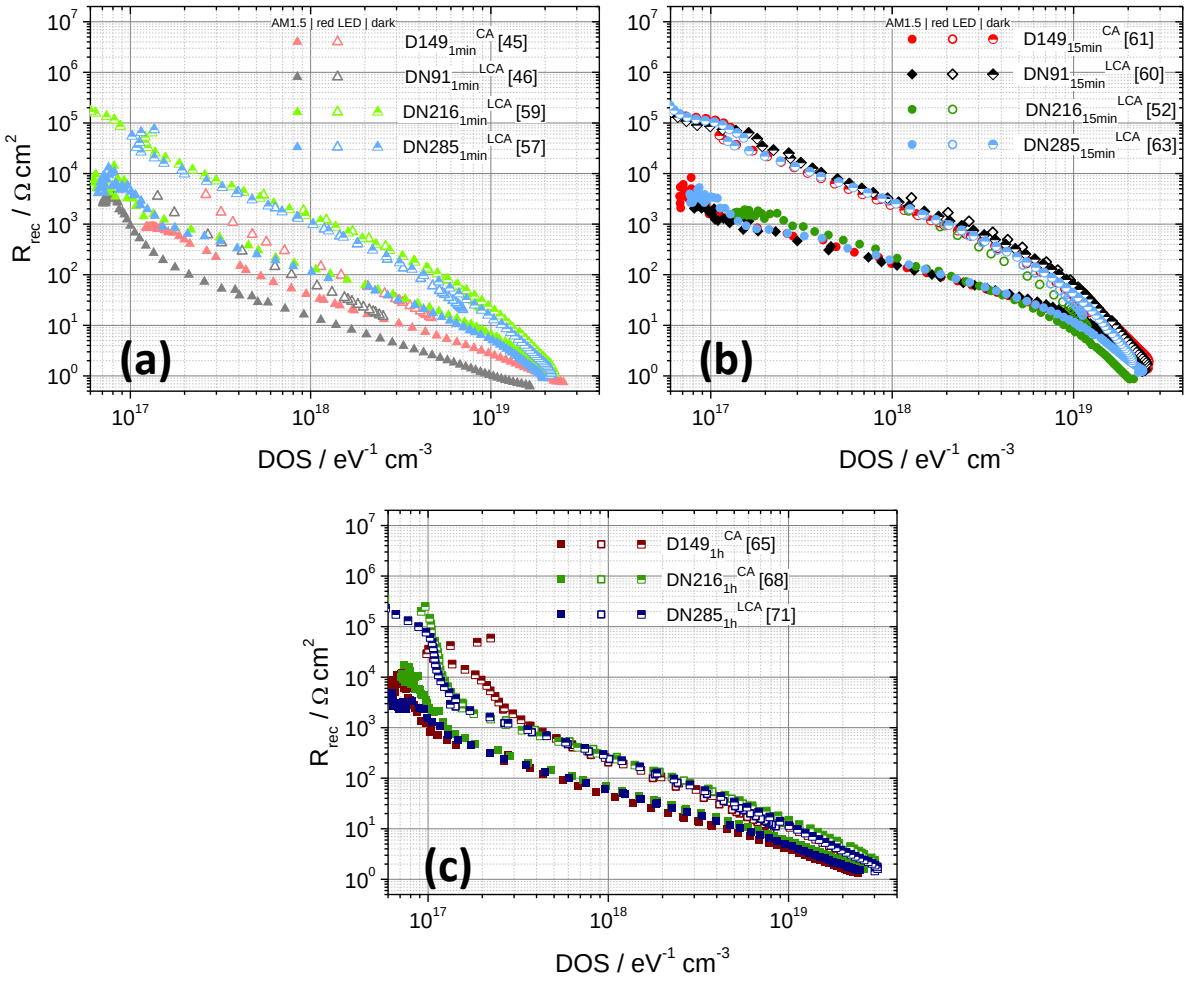

Figure 33 – Recombination resistance R_{rec} vs. the density of states for DSCs sensitized with different indoline dyes and for different times. The measurements are grouped after the sensitization time of (a) 1 min, (b) 15 min and (c) 1 h. Different colors indicate different sensitizing dyes, according to the legends. Filled symbols indicate measurements at AM1.5 illumination, open symbols indicate measurements performed at red LED illumination, and half-filled symbols indicate measurements in the dark.

For a sensitization time of 15 min, the recombination behavior is almost identical for all four sensitizers, especially at intermediate DOS. Thus the comparably small difference of the dyes does not induce a significant change in recombination. For 1 h sensitization time however, where the dye molecules have more time to arrange (and to aggregate), R_{rec} for D149 is slightly lower than for DN285 or DN216. For D149 it is known that for long adsorption times not only a monolayer of dye is formed on ZnO, but a second dye layer is adsorbed [126]. This film formation means a close proximity of the dye molecules and thus a higher probability for radiationless deactivation of photoexcited electrons, i.e. recombination. For the double-anchor dyes it is not known whether also the surface coverage for longer adsorption times exceeds 1, however it can be supposed that the distance of the dye molecules is larger due to steric hindrance from the second anchor group and the respective spacer. Thus it is supposed that the difference in recombination for single- and double-anchored dyes with 1 h sensitization time can be traced to the different dye structure. This trend can only be observed for this very specific representation, where influences like conduction band edge shifts by adsorbed

species are excluded. This does not necessarily mean that the cells sensitized with DN216 and DN285 (and a coadsorbate) have a higher efficiency or a higher V_{OC}, as other effects like the injection efficiency, a different position of E_c strongly influence the overall performance of the cell. But without these influences the indoline dyes DN216 and DN285 with a second anchor group and a longer alkyl chain would perform better as a sensitizer than D149.

3.3.3 Important findings from different measurements

Regeneration limitation

From the large difference of the recombination under AM1.5 illumination and in the dark or at low illumination intensity, it was already concluded that regeneration does not occur with unity efficiency. The largest difference was found for cells which showed higher I_{SC} values, see the discussion for Figure 31, p. 95. Measurements of I_{SC} at different illumination intensities also corroborate this finding, see Figure 34. In this figure, I_{SC} at different red LED illumination intensities is plotted and the I_{SC} values from IV-curves at 100 mW cm^{-2} are added. If a few points at low illumination intensity are fitted (as shown for cell [57] in Figure 34(b)), it can be observed that I_{SC} at 100 mW cm^{-2} AM1.5 illumination lies below the value of the fit at the same intensity, and thus I_{SC} differs from the ideal straight line [255]. This indicates that the current is limited for a high illumination intensity (however different limitations are possible, see discussion below). The same behavior is also observed for other cells, but these fits are not shown to enhance the legibility of the plot. For a correct discussion, the difference in illumination in this plot has to be regarded. Red LED illumination was standardly used for most measurements to ensure a homogeneous absorption across the film thickness, however this illumination is not optimal for measurements of I_{SC} vs. illumination intensity, as the red LED spectrum overlaps only partly with the spectrum of the cells, compare also Figure 24, p. 77. But usually a measurement of I_{SC} vs. intensity with white light would lead to even higher currents at low illumination intensities, and thus an even larger difference to the point at AM1.5 illumination. For cell [57], a cyan LED was used for illumination (see also section **9.1.8** for more measurements at cyan illumination). This measurement was added to Figure 34(b), and it can be observed that I_{SC} is indeed much higher for the cyan illumination than for the same intensity from the red LED, simply due to the better spectral match of the cyan diode and thus a more efficient absorption. When the highest I_{SC} value at cyan illumination (30 mW cm^{-2}) is compared with I_{SC} at 100 mW cm^{-2} AM1.5 illumination, for the more than three times higher intensity at AM1.5 the I_{SC} value differs only by a factor 1.1. An extrapolation of the cyan measurements to 100 mW cm^{-2} would on the other hand lead to a value of around 20 mA cm^{-2}, which is more than the double current density than is in reality achieved for the AM1.5 measurement, and indicates a value that could be obtained without current limitation.

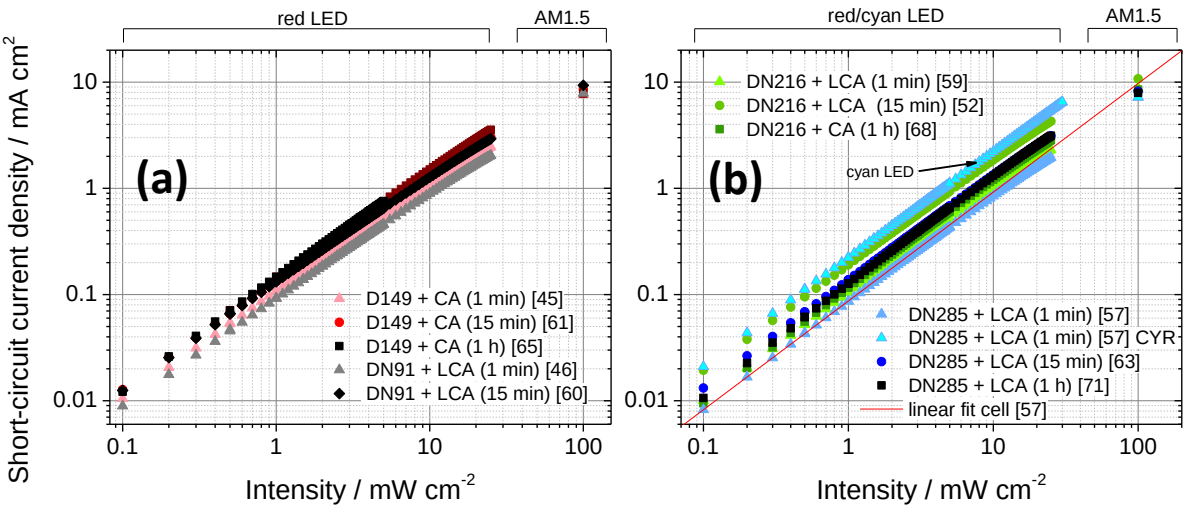

Figure 34 – Short-circuit current density I_{SC} measured vs. the illumination intensity for DSCs sensitized with different dyes, (a) D149 or DN91 and (b) DN216 or DN285. Increasing color depth indicates increasing sensitization time and different colors indicate the different dye according to the legend. The illumination was performed by a red LED for intensities up to 25 mW cm^{-2} and by a AM1.5 for an intensity of 100 mW cm^{-2} (from IV-curve). In (b), also a linear fit of four points at the lowest intensity for cell [57] is shown. For cell [57] a measurement at cyan LED illumination is shown in (b) (cyan filling) to show the influence of a different illumination.

Different reasons can lead to I_{SC} lower than possible, first the already mentioned decrease of regeneration efficiency for higher illumination intensities as the diffusion limit of the electrolyte is reached [17,66,257], second a lower injection efficiency [17] due to filled traps, third a change in the trap distribution and thus an increased recombination at AM1.5 illumination (for example due to UV light, see discussion in section **3.3.1**), and fourth a nonlinear increase of the absorbed portion of light with increasing illumination intensity. Possibly all these four reasons for a reduced current will occur for high illumination efficiencies, and from the comparison with the lifetime results above it can be concluded that reduced regeneration efficiency is one of the occurring reasons.

IMPS measurements and transport time τ_{tr}

Figure 35(a,c) shows the transport times τ_{tr} of cells sensitized for different times with the indoline dyes D149, DN91, DN216 and DN285 and a coadsorbate. As it is expected from the model (see also section **1.3.3.4**), τ_{tr} decreases approximately exponentially with the illumination intensity or I_{SC}. When τ_{tr} is compared for the differently sensitized cells, it can be seen that there are large differences in τ_{tr} spanning even one order of magnitude for the same short-circuit current density, compare for example cell [46] and cell [60]. The slope and the shape of τ_{tr} in the logarithmic plots are relatively similar for most of the cells, with a slight curvature for some cells at higher illumination intensities.

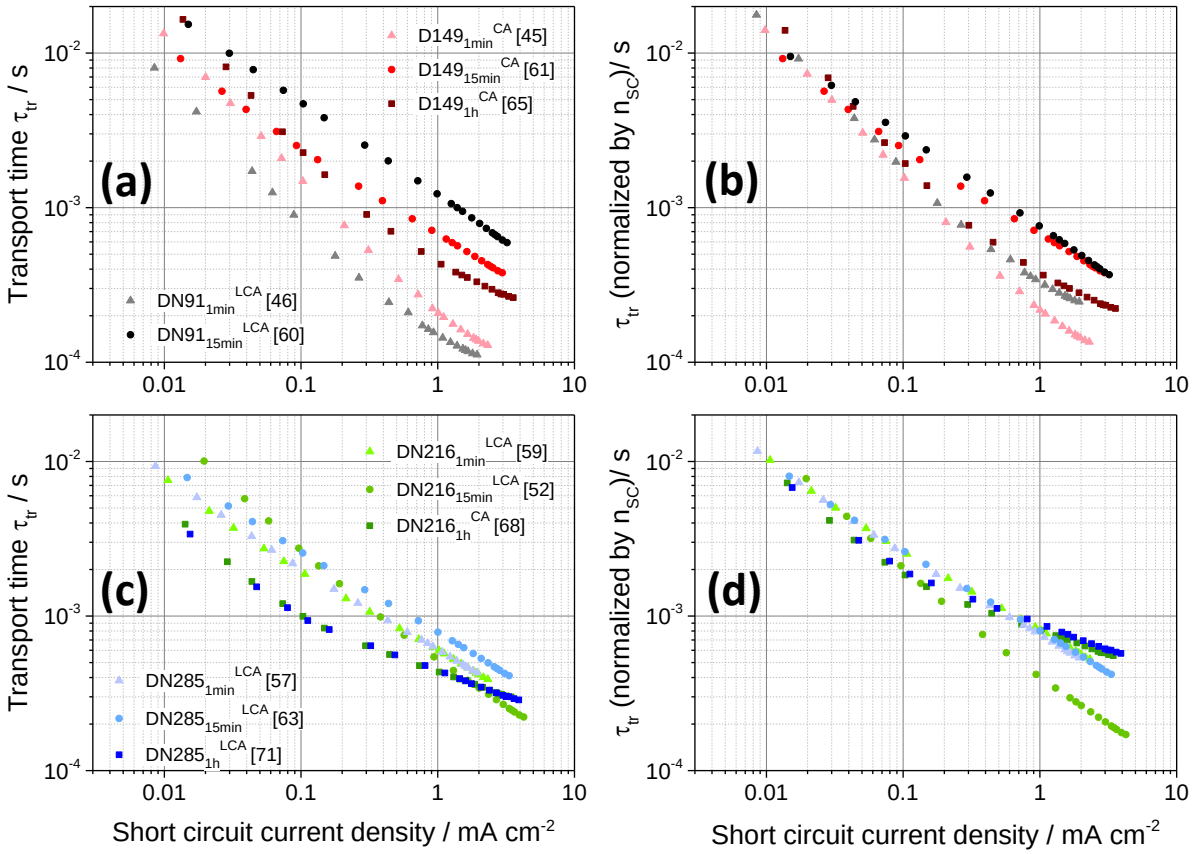

Figure 35 – Transport times τ_{tr} from IMPS measurements for DSCs fabricated from electrodeposited ZnO films. (a,c) Transport times as-measured, and (b,d) transport times normalized by the charge density n_{SC} relative to a reference cell [61]. Different colors indicate different indoline sensitizers and increasing color depth indicates increasing sensitization time, according to the legends. Different symbols of the same colors indicate different cells sensitized with the same sensitization procedure.

Melanie Rudolph emphasized in her work [127] that for many measurements the total trap density N_t in the film strongly influences the resulting values. Similar to the correction suggested for the chemical capacitance in [17], also the transport times were normalized with a relative value of the total trap density. This correction was also performed for τ_{tr} in this work, taking the ratio of the charge-density n_{SC} relative to the charge density of cell [61] as a measure for N_t (see also the values of $N_t/N_{t,ref}$ summarized in Table 7).

The values of τ_{tr} corrected by the total trap density are shown in Figure 35(b,d). The curves in Figure 35(b,d) almost overlap, especially at low light-intensities or low short-circuit currents, and thus most of the large differences found for τ_{tr} for the different cells in the uncorrected graphs stem from a different N_t. Still, the correction with N_t does not affect the different slope of the curves, which leads to differences in τ_{tr} especially at high values of I_{SC}. These differences, and also the smaller differences at lower light intensities, can be ascribed to a slightly different behavior of the films and a different α. All trap states that are taking part in the conduction process contribute to the effective value of τ_{tr}, so that these transport times consist to a large part of contributions of the bulk ZnO and its traps. It is

often concluded that adsorption of dye and coadsorbate does not affect the transport times as long as other effects are absent, which is confirmed for the measurements shown here.

Collection efficiency η_{col}

The collection efficiency η_{col} is often calculated from the effective electron lifetime τ_n and the effective transport time τ_{tr} as determined from IMVS and IMPS measurements (see equation **(16)**). As described in section **1.3.3.4**, this calculation can only serve as a rough approximation of the real collection efficiency, as the measurements are conducted under different electrical circuit conditions, leading to different positions of the Fermi-level at a given illumination condition, and mostly to lower values than expected. Thus η_{col} was also calculated via equation **(17)** after the method described in section **1.3.3.4** (also by Schlichthörl et al. [209]).

As the curves of I_{SC} over $I_{SC}\cdot\tau_n$ are not exactly linear, the slope (m_1) was determined for each point (similar to the differential trap distribution parameter α) and the collection efficiency was determined with these values of m_1. The resulting collection efficiencies η_{col} are shown in Figure 36, with some curves from the less exact determination of η_{col} after equation **(16)** for comparison. This comparison shows that the more correct determination leads to higher values of η_{col} for almost all cells, and at low light intensities the collection efficiency is higher than 95%, for most cells even reaching values near or equal to 1 at higher light intensities. The less exact determination of η_{col} on the other hand even for the best values almost does not exceed 95%, even though the trends for the different cells are similar for both determinations. Rudolph et al. [17] (supporting information) estimated the "worst-case" diffusion length in the cells based on electrodeposited ZnO films to 9.7 µm, by far exceeding even the thickest films used in the present work.

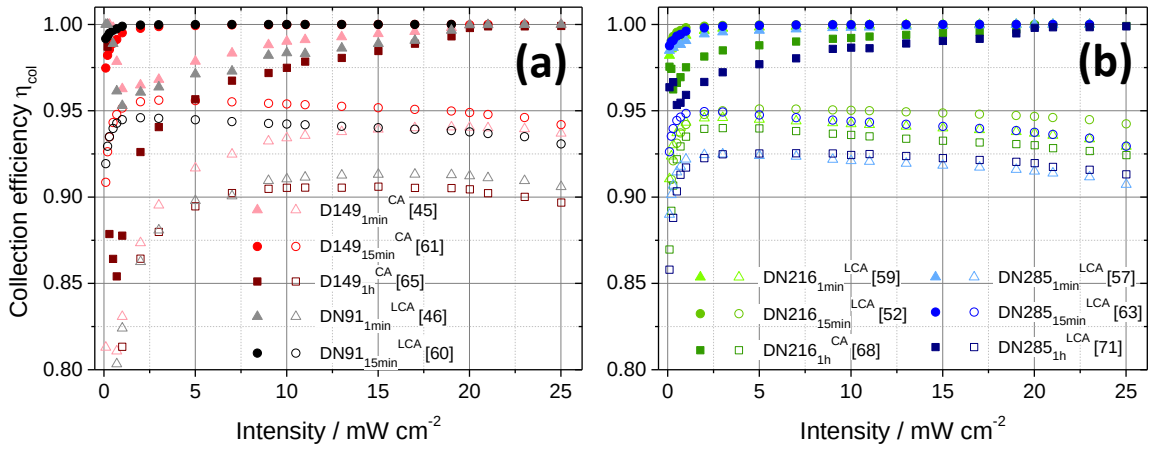

Figure 36 – Collection efficiency η_{col} of DSCs sensitized with D149, DN216 and DN285 and a coadsorbate. Filled symbols indicate the more exact determination via the factor m_1, while open symbols indicate a determination from the characteristic times from IMVS and IMPS. Increasing color depth indicates increasing sensitization time, different colors indicating sensitization with (a) D149, DN91, (b) DN216 or DN285, according to the legend.

This suggests a collection efficiency near 100% for all cells, and thus it is concluded that the higher η_{col} values are more correct. A high collection efficiency is also in line with the comparably high conductivity expected for crystalline electrodeposited ZnO films compared to e.g. nanoparticular TiO_2 films. For cells sensitized for 1 h, η_{col} decreases more at low illumination intensities, which could either be due to recombination at the more aggregated dye layer, or also due to the higher-lying conduction band edge, and thus a worse conductivity when compared at the same V_f.

3.4 Conclusions for ZnO cells sensitized with indoline dyes and coadsorbate

Dye-sensitized solar cells were prepared using the standard indoline dye D149, and three indoline dyes with a second carboxylic anchor group and varying length of the alkyl spacer. Different sensitization times were applied to study the influence on cell parameters. For an adsorption time of 1 min, the cells did not yet reach a maximum in absorption, and the absorption for such short time was fastest for the sterically less demanding indoline dye D149 with one carboxylic anchor group. Longer absorption times led to dark, fully sensitized films, where the increased number of adsorbed dye also increased the aggregation of dye molecules on the ZnO surface. In IV-measurements, the four dyes showed similar characteristics for the same sensitization time, with mostly lower I_{SC} for a sensitization with DN285, which was attributed to a slower injection due to the longer alkyl spacer [13], as the dye content estimated from optical absorbance was similar. The highest I_{SC} values for all sensitization times were achieved for a sensitization with DN216. Increasing the adsorption time from 1 min to 15 min led to higher I_{SC} values and also increased V_{OC}, which was caused by a higher dye loading. An increase in the voltage was not only effected by a higher I_{SC}, but also by a decreased recombination, probably due to a better shielding of the semiconductor against recombination with the electrolyte by the more complete dye coverage. However also a deceased regeneration efficiency was supposed from recombination measurements at different illumination conditions, and the current thus probably differs more from a possible maximum current than for a sensitization for 1 min.

Increasing the sensitization time further to 1 h led to a more pronounced increase in V_{OC}, however I_{SC} decreased approximately to values found for a 1 min sensitization time. The increase in V_{OC} was traced back to a considerable shift of E_c to higher energies, with larger shifts than the increase in V_{OC}. This upward shift of E_c is also one of the reasons for the lower I_{SC}, as fewer states are available for injection at a given DOS. Increased recombination, most probably stemming from dye aggregates (broader absorption spectra), was another factor which led to a decreased I_{SC}. The increase in recombination and the lower current are the cause why V_{OC} does not increase by the amount of the shift of E_c

For a comparison of the recombination at the same DOS the different dyes showed almost no difference. Only for a sensitization for 1 h, a higher recombination for D149 than for double-anchored dyes was found, which is attributed to a higher aggregation tendency of D149 (which does not contain a sterically more demanding longer alkyl chain at the outer rhodanine ring).

A simulation of the chemical capacitance including also the Helmholtz capacitance, the capacitance of the space-charge layer and the capacitance of deep monoenergetic trap states yielded a very good overlap with measured C_μ values and reasonable simulation parameters. A higher trap distribution parameter α from simulation than from the slope of the measured curve indicated that α is influenced

by other underlying capacitances than C_μ, and the actual trap distribution would thus be different than determined from the slope. The simulation of the capacitance was also helpful to trace the differences in C_μ found for different illumination conditions to different changed parameters. In the dark, a lower trap distribution parameter α indicated a steeper distribution than at AM1.5 illumination, and an additional capacitance contribution was observed which indicated an occurrence of deep monoenergetic trap states. The position of the conduction band edge was higher for measurements in the dark, even for the simulation where changes by the different temperature were included in the calculation. It is probable that the high illumination intensity (also with more energetic photons) leads to a change in the trap distribution, consistent with the observation of a higher conductivity under illumination with intense (UV-) light [253]. An additional trap density would also increase the recombination at high-intensity illumination, as it is observed here. The density of deep monoenergetic trap states increases with increasing sensitization time, probably because of the longer contact with the sensitization solution, and the highest density was found for a sensitization with D149 and a coadsorbate for 1 h. For measurements at AM1.5 illumination, no deep monoenergetic trap states were observed, which also indicates a change in the distribution of traps for the different illumination conditions.

From the comparison of the recombination at different illumination conditions and from I_{SC} vs. illumination intensity it was concluded that the regeneration efficiency is decreased especially at intense AM1.5 illumination. This offers an explanation for the relatively low I_{SC}, even though for most cells the light harvesting efficiency is ~1 and the cells absorb light over a comparatively wide wavelength range. As similar cells based on electrodeposited ZnO show similar I_{SC} values which do not exceed 11 mA cm^{-2} [17,18,19], it is probable that cells based on (electrodeposited) ZnO in general show a low regeneration efficiency which limits the maximum current. Probably the structure of the film with decreasing pore size limits the diffusion of electrolyte species inside the film, and thus leads to inefficient regeneration, a larger fraction of oxidized molecules at high illumination intensities and thus to an increase of recombination via oxidized molecules.

4 Influence of the coadsorbate

In the preceding chapter, all cells were prepared from films with a coadsorbate adsorbed together with the sensitizing indoline dyes. To investigate the influence of the coadsorbate on cell properties and recombination behavior, several cells discussed in this chapter were fabricated with the same indoline dyes but adsorbed without a coadsorbate. This variation was typically performed for a sensitization time of 15 min, which often had reached the highest efficiencies when coadsorbates were used, and for one cell with a longer sensitization time of 1 h. The characterization and evaluation was performed as for the cells with coadsorbate. A film adsorbed with coadsorbate from chapter **3** is used as reference for each combination of indoline dye and adsorption time [xix].

4.1 Influence of the coadsorbate on dye adsorption

Figure 37 shows the absorbance of ZnO films sensitized with different indoline dyes either with or without a coadsorbate. For more than one film sensitized by a given sensitization procedure the absorbance is shown, while not all films gave functioning solar cells and thus will no longer appear in the following sections. Similar to the films adsorbed with a coadsorbate (section **3.1**), also films without a coadsorbate show a high absorption already by an observation by eye, and usually they appear darker than films adsorbed with a coadsorbate. The measurements with an integrating sphere show the same unexpected flattening of the maximum as discussed in section **9.1.1**, p. 187, even for absorbance values near 1. This was attributed to a changed scattering background for the pure ZnO film and the film with adsorbed dye, and thus mainly the absorbance between 600 and 700 nm can be discussed. An absorbance spectrum of D149 in solution is shown in Figure 37(a) for comparison with the spectra of the dyes adsorbed to the ZnO film.

Sensitization for 15 min

For a sensitization time of 15 min, the absorbance of the films without coadsorbate in Figure 37 is higher than the absorbance of films with coadsorbate at λ between 600 and 700 nm. This increase could be caused either by the adsorption of more dye molecules, or by a stronger aggregation of the adsorbed molecules, or both. If a full maximum would have been measured, these cases could have been discerned by a comparison of the absorbance at the maximum and the full width of the peak at

[xix] Additionally, one film with a slightly different deposition procedure is compared (film/cell [70], sensitized for 1 h with DN216 and LCA), which showed a different absorption behavior and an increased power conversion efficiency.

half maximum for the different films. On the other hand, the fact that a maximum cannot be resolved in the spectrometer is an indication of a very high light harvesting efficiency for the cells, which is beneficial for current generation in the cells.

A normalization of the spectra to values at 635 nm (see Figure 38, p. 108) shows that the absorbance for higher wavelengths is higher for films without coadsorbate than with coadsorbate, which indicates a higher aggregation of dye molecules when a coadsorbate is not employed. This is observed for all four sensitizers, similar to previous results for D149 [121,126]. Similar findings were also described for another indoline dye D131 and a squaraine dye [17,127], whereas for D149 with or without coadsorbate in TiO_2-based DSCs also an increase in the amount of dye is observed, and additionally a redshift of the spectrum for lower concentration of the coadsorbate was seen [108]. However for ZnO films deposited with different parameters, the sensitization without coadsorbate unexpectedly led to a lower amount of dye molecules on the films [16].

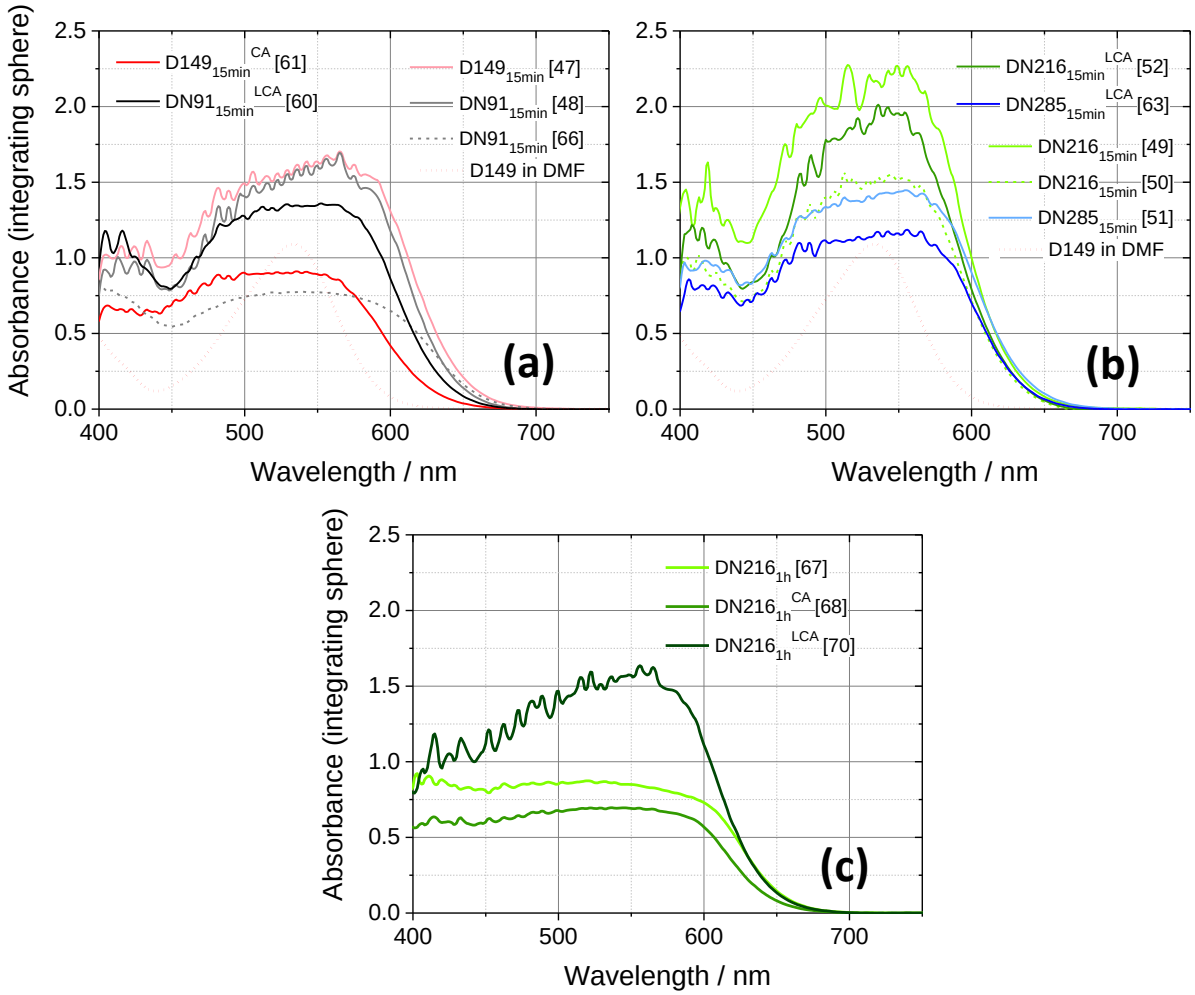

Figure 37 – Absorbance (measured with an integrating sphere) of ZnO films sensitized with different indoline dyes with and without a coadsorbate. (a,b) Films sensitized for 15 min and (c) cells sensitized for 1 h. Lighter colors indicate films sensitized without a coadsorbate, while darker colors indicate sensitization with a coadsorbate. Dashed lines of the same color in (a) indicate different films sensitized by the same sensitization procedure. A spectrum of D149 dissolved in dimethylformamide is added for comparison in (a,b).

For the films in the present work, the lower amount and lower aggregation of the sensitizer dye on the ZnO surface when adsorbed with a coadsorbate is explained by the co-adsorption of the coadsorbate and thus a steric hindering of dye aggregation, and the blocking of adsorption sites at the ZnO surface by coadsorbate molecules, thus decreasing the maximum amount of dye that can be adsorbed. For D149 a coadsorbate even leads to the suppression of an adsorption of a second monolayer, which was observed via adsorption isotherms on ZnO [126].

In contrast to the sensitization with coadsorbate, where D149 showed the narrowest "peak" and thus the least amount of dye on the ZnO surface (but similar aggregation, see Figure 20, p. 69 and Figure 21, p. 71), without coadsorbate D149 leads to a broad spectrum with higher aggregation than DN216 and DN285, whereas DN91 also shows high aggregation in one film, see Figure 38, p. 108. The higher aggregation of D149 is probably observed because of the formation of a second monolayer of dye molecules [126].

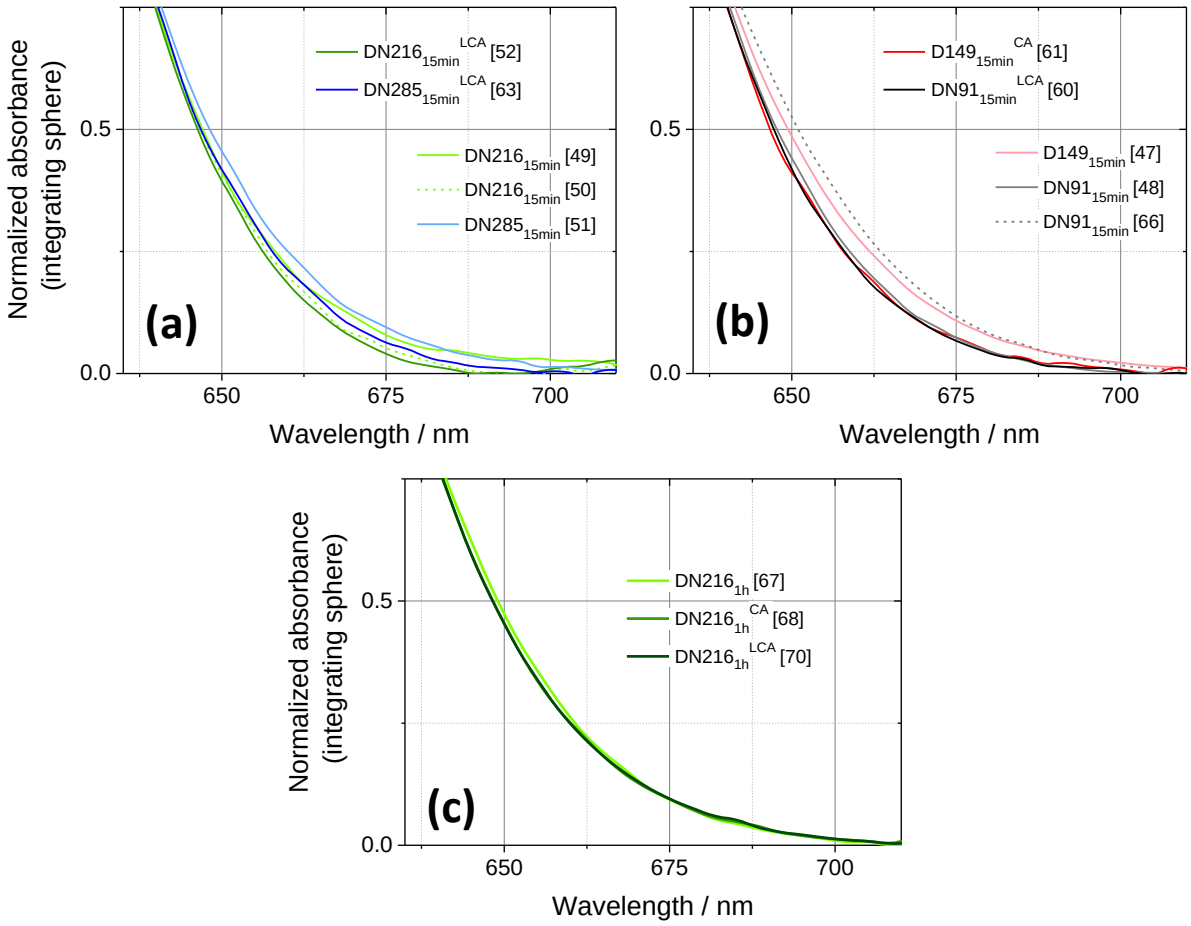

Figure 38 – Absorbance normalized to the minimum at about 450 nm for ZnO films sensitized with different indoline dyes with or without a coadsorbate. (a,b) Films sensitized for 15 min and (c) cells sensitized for 1 h. Lighter colors indicate films sensitized without a coadsorbate, while darker colors indicate sensitization with a coadsorbate. Dashed lines of the same color in (a,b) indicate different films sensitized by the same sensitization procedure.

Two causes are possible, why this behavior is not (as strongly) observed for the double-anchor dyes with longer alkyl chain: First, the steric hindrance of a longer alkyl chain and a second anchor group strong enough to either prevent such a second monolayer or at least lead to a distance of the molecules that does not lead to a much larger aggregation, and second, the weaker binding of D149 compared to for example DN216 [15] results in a higher affinity of dye molecules to each other, compared to the double-anchor dyes. For DN91 the smaller steric hindrance seems to be small enough to lead to higher aggregation, as for some films the aggregation is also enhanced more.

Sensitization for 1 h

For cells adsorbed for 1 h, the depression of the curve maximum becomes even more pronounced than for the cells adsorbed for 15 min, see in Figure 37(c). Only film [70], which showed a decreased scattering due to a change in the deposition [xx], shows a considerably higher absorbance in the maximum and also a broader spectrum, which suggests that the film contains more dye than the otherwise similarly sensitized film [68]. Comparing the dye amount of the standardly sensitized films with or without a coadsorbate, the sensitization without coadsorbate leads to a broader spectrum and thus more dye adsorbed, simply by the absence of coadsorbate molecules and thus more available binding sites. The dye molecules however do not become much stronger aggregated, compare the normalized spectra in Figure 38, p. 108. This further supports the assumption made for the sensitization for 15 min, that the steric hindrance of the longer alkyl chain and second anchor group at least partly prevents aggregation.

[xx] For film [70], a higher voltage was applied during the first few seconds of EosinY/ZnO resulting in a more transparent ZnO film. As the aggregation is similar to other films sensitized for 1 h, the different transparency is probably the cause for the somewhat different color of the film as seen by eye (more pink compared to the more brownish color impression of other films).

4.2 Influence of the coadsorbate on current-voltage characteristics

Sensitization for 15 min

The current-voltage characteristics of the cells prepared from the ZnO films sensitized with and without a coadsorbate for 15 min are shown in Figure 39(a,b), and the solar cell parameters of the DSCs are listed in Table 8. For all cells, changes in I_{SC} follow those in the absorbance, with a slight increase in current for an adsorption without coadsorbate. Thus the increase in current is probably mainly caused by a larger amount of dye molecules adsorbed to the ZnO surface. This observation was already made for D149 adsorbed with or without a coadsorbate [126]. For cells [48] and [66], which were sensitized by the same procedure, a large difference in I_{SC} is observed, indicating also a large difference in the film, which will be further discussed for results from EIS measurements [xxi].

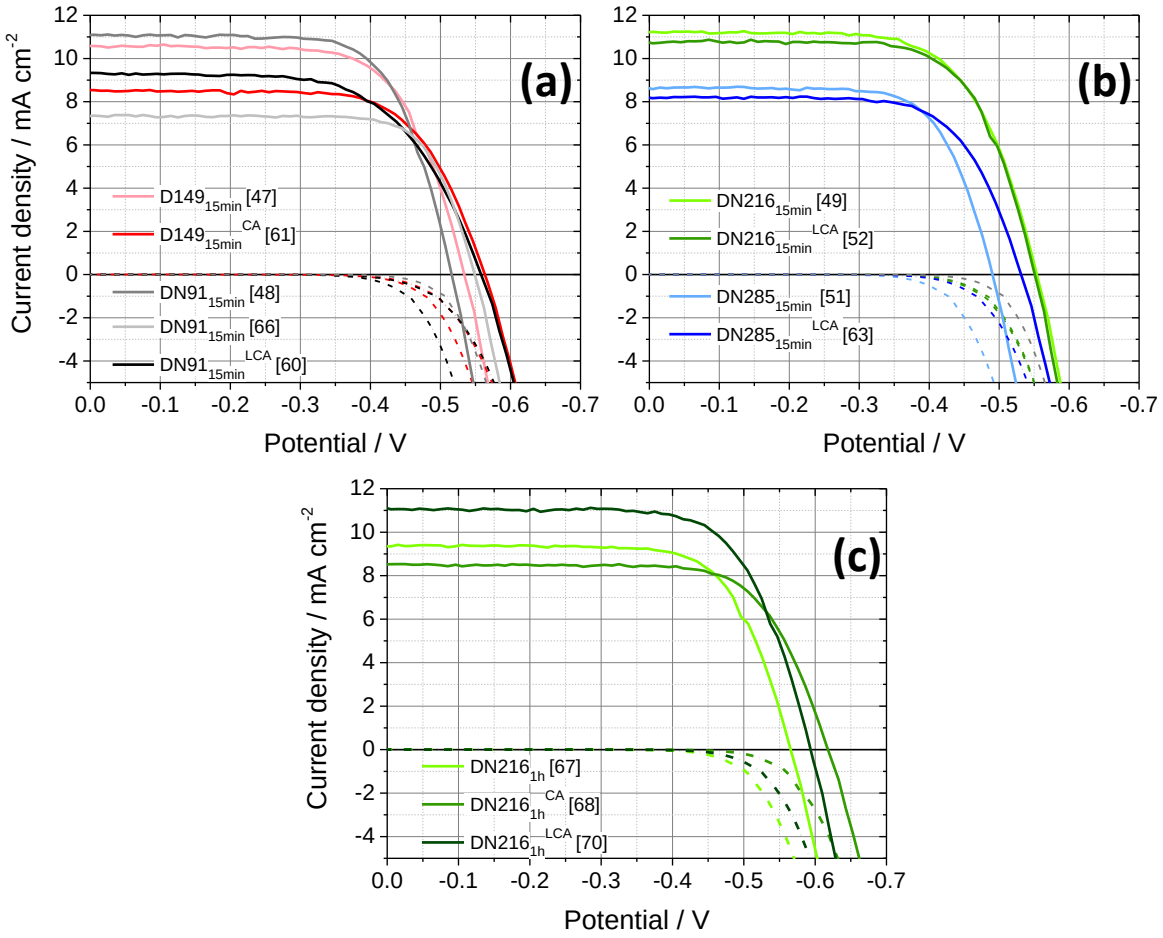

Figure 39 – IV-curves of DSCs sensitized with different indoline sensitizers (with and without a coadsorbate). (a,b) Films sensitized with D149, DN91 or DN285 (for 15 min) and (c) films sensitized with DN216 for 15 min or for 1 h. Lighter colors indicate films sensitized without a coadsorbate, while darker colors indicate sensitization with a coadsorbate. Dash-dotted lines indicate IV-curves measured in the dark.

[xxi] It can be already mentioned that for cell [66] the conduction band edge was considerably higher than for the other cells sensitized for 15 min, probably by an ineffective deposition due to contacting problems. Thus for the more relevant comparison with a sensitization with coadsorbate throughout this chapter cell [48] will be used, and cell [66] is shown to compare the effect of the large shift of the conduction band edge.

Table 8 – Solar cell parameters from IV-curves shown in Figure 39 for different cells sensitized with indoline dyes with or without a coadsorbate.

Sample	I_{sc}	V_{oc}	FF	Efficiency
	[mA cm^{-2}]	[V]		[%]
D149$_{15min}$ [47]	10.58	0.534	0.69	**3.83**
D149$_{15min}^{CA}$ [61]	8.54	0.564	0.68	**3.24**
DN91$_{15min}$ [48]	11.10	0.516	0.70	**3.94**
DN91$_{15min}$ [66]	7.36	0.549	0.75	**3.01**
DN91$_{15min}^{LCA}$ [60]	9.33	0.558	0.62	**3.20**
DN216$_{15min}$ [49]	11.23	0.554	0.67	**4.14**
DN216$_{15min}^{LCA}$ [52]	10.81	0.551	0.69	**4.08**
DN216$_{1h}$ [67]	9.34	0.566	0.72	**3.76**
DN216$_{1h}^{CA}$ [68]	8.53	0.618	0.72	**3.76**
DN216$_{1h}^{LCA}$ [70]	11.06	0.594	0.71	**4.59**
DN285$_{15min}$ [51]	8.58	0.491	0.71	**2.97**
DN285$_{15min}^{LCA}$ [63]	8.17	0.531	0.69	**2.97**

Also for an adsorption time of 1 h, I_{SC} shows the same dependence as the absorbance in Figure 37, with a higher I_{SC} for an adsorption without coadsorbate compared to the same sensitization with coadsorbate, and the highest I_{SC} for film [70] sensitized with a coadsorbate (with a slightly differently deposited ZnO film).

The open-circuit voltage V_{OC} decreases for most of the cells without coadsorbate compared to cells sensitized with the same dye with coadsorbate (for both sensitization times), similar to previous findings for ZnO-based DSCs sensitized with D149 [126]. Mostly also an increase in aggregation was observed for cells without coadsorbate, see Figure 38. As also discussed for the different sensitization times in chapter **3**, an increase in aggregation usually also leads to an increase in recombination, as charge recombines via radiativeless recombination, and thus also to a decrease in V_{OC}. Recombination and the position of E_c, which also influences V_{OC}, will be discussed in more detail below.

The fill factor FF mostly increased or stayed approximately constant for cells without a coadsorbate compared to cells with coadsorbate, see Table 8. Rudolph et al. [16] also found FF(with coads.) < FF(without coads.), while for 2 h sensitization time the reverse was found. Different from the observation in the present work, Sakuragi et al. [126] found FF(with coads.) > FF(without coads.) for all sensitization times, the difference to the present work being probably caused by a larger increase in V_{OC} compared to the increase in the present work. Also the fill factor will be discussed further in the context of recombination, which also influences the FF. The power conversion efficiency is either the same or slightly higher with and without a coadsorbate, as I_{SC} increases without a coadsorbate but V_{OC} decreases. The changed deposition conditions for film [70] led to a comparatively large increase of I_{SC} (stemming at least partly from the increased amount of adsorbed dye), which also resulted in a higher

power conversion efficiency for this film. Thus a change in the deposition where also the adsorbed dye amount and the transparency of the film was increased, is beneficial for the cell performance.

The trends for the incident photon-to-current conversion efficiency, see Figure 40, closely resemble the trends in I_{SC} for the IV-curves (after equation **(10)**). As it was already observed for the cells sensitized with a coadsorbate in the previous chapter, the maximum of the IPCE for the cells reaches high values of about 85%. Due to reflection at the substrate and scattering at different interfaces, such an IPCE is about the limit of what can be achieved for these cells. As the light harvesting efficiency calculated from the absorbance spectra is ~1 in the absorbance maximum, also the injection efficiency, the regeneration efficiency and the charge collection efficiency have to reach values near 1 to achieve such high values of the IPCE, see equation **(9)**. Such high values are found here especially because of a lower illumination intensity compared to other experiments (IV-curves, EIS at AM1.5), so that regeneration efficiency is not yet limiting the current (compare also section **3.3.2**).

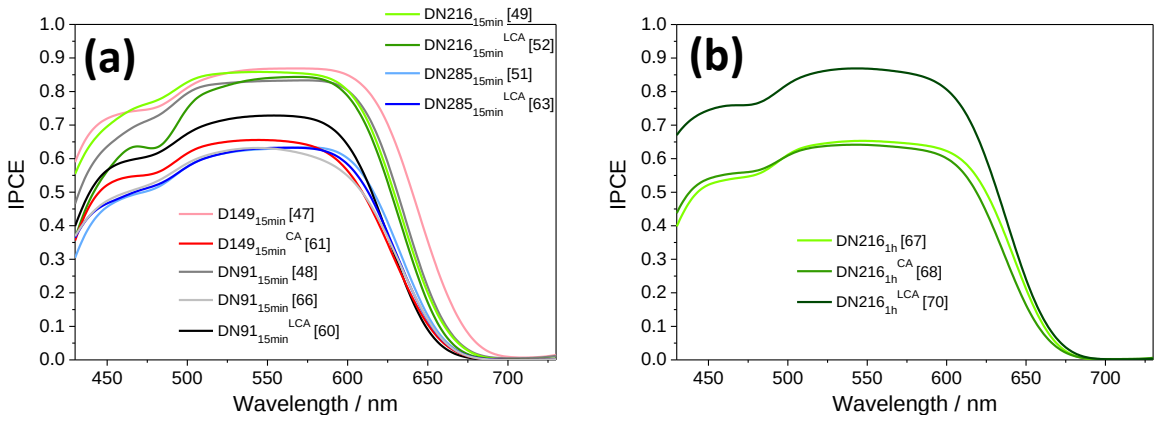

Figure 40 – Incident photon-to-current conversion efficiency IPCE for ZnO-based DSCs sensitized with indoline dyes with or without a coadsorbate. (a) Cells sensitized for 15 min and (b) cells sensitized for 1 h. Lighter colors indicate an adsorption of dye without coadsorbate, and darker colors indicate an adsorption with coadsorbate, according to the legends.

4.3 Role of the coadsorbate for transport and recombination in DSCs

Different methods were used to examine possible caused for the observations of the previous section. Most measurements were performed at red LED illumination, while EIS was additionally measured at AM1.5 illumination and in the dark, compare also section **9.1.3**. As also the absorption and the IV-curves, the results from films sensitized without coadsorbate are compared to films sensitized with a coadsorbate (found also in the comparison of different sensitization times in section **3.3**. The discussion first focusses on trap distribution in the films and transport properties, and with these results in mind recombination is discussed. The evaluation and data treatment follows closely the one discussed in the course of section **3.3** and is not re-explained in all instances, thus the reader is referred to the respective measurement or representation in section **3.3**.

4.3.1 Trap distribution and transport properties with and without coadsorbate

Trap distribution in the ZnO film

The chemical capacitance C_μ for the different films sensitized with or without a coadsorbate is shown in Figure 41, and the general shape with the contribution of different capacitances was discussed before (section **3.3.1**). For a sensitization time of 15 min, the capacitance curves have a very similar shape, see Figure 41(a,c). Even after normalization to the total trap density of a reference cell with $N_t/N_{t,ref}$ [17], the horizontal distance of the curves in Figure 41(b,d) remains small, as the change density n_{SC} is similar for the cells sensitized for 15 min, see Figure 86, p. 196 and Table 9. The similar position of the curves shows that the conduction band edge for these cells lies at similar energies. Only for film [66], where a problem occurred during electrodeposition (see note [xxi]), the C_μ curve is steeper and the conduction band edge is shifted by around 100 mV towards higher energies compared to the similarly sensitized film [48]. This finding explains the lower I_{SC} in Figure 39 for cell [66] compared to other cells sensitized for 15 min, as there are less available states in the ZnO isoenergetic to dye states, and thus the transfer is less efficient (lower injection efficiency). A plot of the DOS at the different voltages in Figure 90, p. 198, shows this difference very clearly. The trap distribution parameter α was determined from the maximum of the differential value of α, see also section **3.3.1**, and the respective α values are given in Table 9. For measurements at AM1.5 illumination, α ranges between 0.6 and 0.7 for most cells, with lower values for cells sensitized without a coadsorbate (except for a sensitization with DN216). The opposite behavior, with higher α for a sensitization without coadsorbate, was observed in [16], this difference very likely caused by the different deposition conditions (reducing vs. non-reducing).

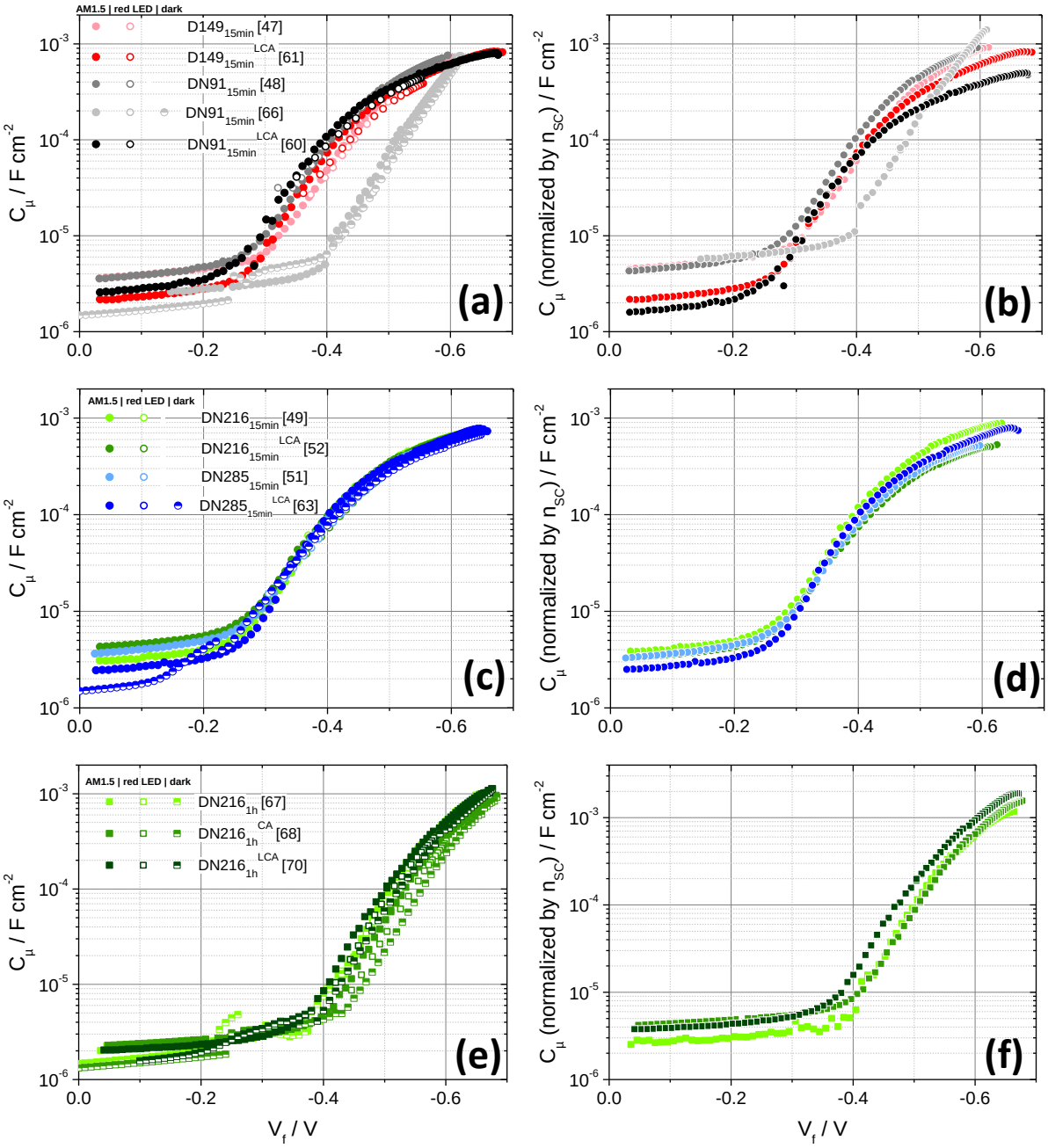

Figure 41 – Chemical capacitance C_μ of ZnO-based DSCs sensitized with different indoline dyes in the presence or in the absence of a coadsorbate. Lighter colors indicate cells with an adsorption without coadsorbate, and darker colors indicate an adsorption with coadsorbate. (a,b,c,d) Cells sensitized for 15 min and (e,f) cells sensitized for 1 h. (a,c,e) C_μ and (b,d,f) C_μ normalized by a measure of the total trap density, n_{SC}, with cell [61] as a reference. Filled symbols indicate measurements at AM1.5, open symbols indicate measurements at red LED illumination and at V_{OC}, and half-filled symbols indicate measurements in the dark.

As also observed in the previous chapter, α decreases for lower illumination intensities, which was ascribed partly to a lower temperature and partly to a changed trap distribution caused by the intense light at AM1.5 illumination, see section **3.3.1**. Even so, α is higher than usually found in the literature [16,17,18,19] (and for smaller cells in chapter **5**), which was already in the previous chapter ascribed to differences in the details of the electrodeposition. Deep monoenergetic traps states, observed only for EIS measurements in the dark in the previous chapters, are seen as a shoulder

around -0.3 V for the measurement of cell [66] in the dark, for other cells the measurement in the dark was not yet established as a part of the standard set of experiments at the time of the measurements. However, as such a shoulder is observed for all measurements in the dark and also for one cell without coadsorbate, it is probable that also for these cells deep monoenergetic trap states are present in the dark. For measurements at AM1.5, no additional capacitance from deep monoenergetic trap states around -0.3 V is observed, confirming thus that the trap distribution changes by the high-intensity at AM1.5.

For cells sensitized for 1 h with DN216 in the presence or absence of a coadsorbate, the C_μ curves also have a similar shape and a similar slope at intermediate voltages, see Figure 41(e). The trap distribution parameter α (Table 9) is higher than for cells sensitized for 15 min regardless of the presence of a coadsorbate, similar to the findings in section **3.3.1**. The relative position of the conduction band edge, see the horizontal position of the C_μ curves in Figure 41(f), for all cells with a sensitization for 1 h is higher than for a sensitization for 15 min, however it is not changed by the presence or absence of a coadsorbate. This is probably the case because for both the sensitizer and the coadsorbate the binding to the ZnO surface is supposed to occur via the carboxylic anchor group present in both, and thus the influence of the binding on the electronic structure of ZnO will be similar. A change in the deposition of ZnO, as applied for cell [70], leads to a lower position of the conduction band edge by around 30 mV, and this observed shift is also one of the causes for the higher I_{SC} found in Figure 39.

Table 9 – Different cell values for ZnO-based DSCs sensitized with different indoline dyes with or without a coadsorbate. The values were determined from EIS measurements at different measurement modes, from current transients and from measurements of V_{OC} against intensity. Values for other sensitization times for comparison are listed in Table 7. Bold values are values more relevant for the use of the solar cell (determined at AM1.5 illumination).

Value / **Sample**	$N_t/N_{t,ref}$	**α**	**α**	**α**	**β**	**β**	**β**	**β (1/m)**
Measurement (plot)	**current transient** (n_{SC} vs. I_{SC})	**EIS** (C_μ vs. V_f)	**EIS** (C_μ vs. V_f)	**EIS** (C_μ vs. V_f)	**EIS** (R_{rec} vs. V_f)	**EIS** (R_{rec} vs. V_f)	**EIS** (R_{rec} vs. V_f)	**V_oc vs. int.**
Illumination	red LED	**AM1.5**	red LED	dark	**AM1.5**	red LED	dark	**red LED**
Reference cell or temperature	cell [61]	**~325 K**	~298 K	~298 K	**~325 K**	~298 K	~298 K	~298 K
$D149_{15min}$ [47]	0.80	**0.62**	0.50	-	**0.68**	0.87	-	0.91
$D149_{15min}^{CA}$ [61]	1 (Ref.)	**0.67**	0.45	0.46	**0.42**	0.67	0.60	0.77
$DN91_{15min}$ [48]	0.83	**0.64**	0.47	-	**0.62**	0.82	-	0.92
$DN91_{15min}$ [66]	0.45	**0.65**	0.68	0.64	**0.69**	1.03	0.94	1.15
$DN91_{15min}^{LCA}$ [60]	1.61	**0.66**	0.40	0.41	**0.38**	0.69	0.61	0.78
$DN216_{15min}$ [49]	0.80	**0.66**	0.40	-	**0.58**	0.82	-	0.86
$DN216_{15min}^{LCA}$ [52]	1.30	**0.58**	0.42	-	**0.63**	0.83	-	0.90
$DN216_{1h}$ [67]	0.80	**0.76**	0.61	0.58	**0.65**	0.83	0.76	0.90
$DN216_{1h}^{CA}$ [68]	0.54	**0.68**	0.65	0.65	**0.64**	0.82	0.75	0.86
$DN216_{1h}^{LCA}$ [70]	0.54	**0.73**	0.68	0.63	**0.62**	0.81	0.77	0.89
$DN285_{15min}$ [51]	1.11	**0.60**	0.44	-	**0.63**	0.77	-	0.87
$DN285_{15\ min}^{LCA}$ [63]	0.98	**0.70**	0.44*	0.48	**0.48**	0.71	0.63	0.79

* No maximum of alpha values, thus this value could be higher.

Transport properties for films sensitized with and without coadsorbate

From IMPS measurements (measured at red LED illumination) values of the effective transport time τ_{tr} were determined, see Figure 42(a). Similar to the measurements in the previous chapter, the transport time decreases with increasing light intensity or with increasing I_{SC}, and the absolute values of τ_{tr} differ by more than a factor 5 for the different cells without apparent dependence on the sensitizer. From Figure 42(b), which shows τ_{tr} corrected by $N_t/N_{t,ref}$ (Table 9, p. 115), it becomes clear that these variations are predominately caused by the differences in total trap density, and not by differences in the transport time, as the curves almost overlap at low I_{SC}. No difference in τ_{tr} is expected for the same ZnO films, since the rate of charge transport in the ZnO network should be widely independent of the sensitizer. The different slopes for the different cells (depending on the trap distribution parameter α, see 1.3.3.4) lead to a variation of τ_{tr} at higher illumination intensities. Especially the cells sensitized for 1 h show a bending of the τ_{tr} curve with intensity, probably due to a higher α found for these cells (Table 9). The similarity of the τ_{tr} curves shows that the "bulk" (or non-surface) ZnO is not influenced by the slight, unavoidable variations in electrodeposition [127], at least not to an extent that the transfer of electrons through the ZnO matrix is affected.

Also for the film where difficulties in electrodepositions occurred and where the position of E_c is considerably higher, film [66], the transport times are similar, and even the change of the electrodeposition for film [70] does not lead to very different τ_{tr} compared to films [67] or [68]. This probably means that even when E_c is higher, and thus a lower DOS at a given energy is present, this DOS is still sufficient to maintain an efficient transport of electrons through the ZnO network. And even when the pore/grain structure is changed, as it is supposed from the lower light scattering of film [70], the transport through the film is not influenced by this change, probably because the electrodeposition is for the larger part of the time almost identical.

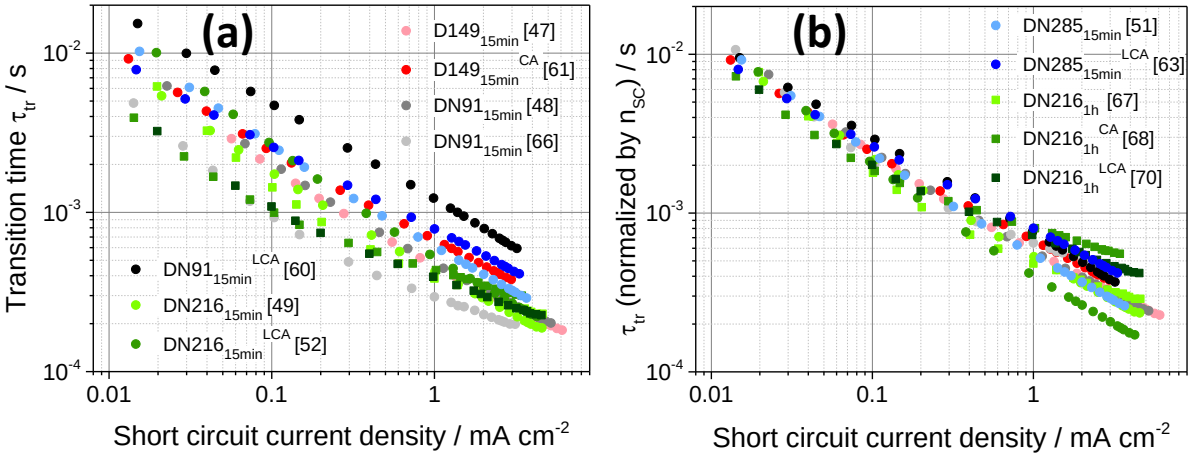

Figure 42 – Transport time τ_{tr} of ZnO-based DSCs sensitized with different indoline dyes in the presence or in the absence of a coadsorbate. (a) Transport times as determined from the measurement, and (b) transport times normalized by the relative total trap density $N_t/N_{t,ref}$ (determined from current transients with cell [61] as reference, listed in Table 9). Lighter colors indicate sensitization without coadsorbate, while darker colors indicate cells sensitized with coadsorbate. Circles indicate cells sensitized for 15 min, squares indicate a sensitization time of 1 h.

4.3.2 Recombination depending on the use of a coadsorbate

Information about recombination is given especially by recombination resistance R_{rec} or the electron lifetime τ_n. As mentioned also in section **3.3.2**, a plot of R_{rec} or τ_n vs. the voltage V_f gives recombination of the cells, see also Figure 100, p. 208 and Figure 101, p. 209. In this representation for example the higher V_{OC} of cell [66] compared to other cells sensitized for 15 min is explained, as R_{rec} or τ_n at a certain voltage is higher for this cell. However this representation contains influences like a possibly different DOS, which strongly influences the recombination. The representation of R_{rec} or τ_n vs. DOS in Figure 43 and Figure 44, respectively, allows the interpretation of the recombination without such influence, thus focusing more on the influence of the sensitization procedure.

Influence of the coadsorbate for a sensitization for 15 min

A comparison of R_{rec} at the same DOS for cells sensitized for 15 min with or without a coadsorbate in Figure 43(a,b) clearly shows a decrease in R_{rec} for a sensitization without coadsorbate for D149, DN91 and DN285, while for DN216 R_{rec} remains unchanged, resulting in the following order of R_{rec} for intermediate DOS: DN285+coads., DN91+coads., D149+coads. > DN216+coads., DN216 > DN285, D149 > DN91. The same sequence is also found for τ_n vs. DOS in Figure 44, p. 119 and in Figure 102, p. 209, where the lifetime from IMVS was plotted against n_{OC} determined from charge extraction (both at V_{OC}). An increased recombination compared to a sensitization with coadsorbate was also found before for ZnO sensitized with D149 for different times without coadsorbate for intermediate and lower DOS [16]. The increased aggregation without coadsorbate for D149 and DN285 and the approximately constant aggregation for DN216 (as observed in the normalized absorbance in Figure 38, p. 108) fits well with this observation, as dye aggregates induce additional recombination centers. However for cell $DN91_{15min}$ [48], the aggregation is only slightly higher than for $DN91_{15min}^{LCA}$ [60], but without coadsorbate the cell has a clearly lower R_{rec}. It is possible that the normalization of the absorbance does not give an exact measure of the aggregation, see discussion in section **9.1.1**, but for most cells it corresponds well with the trends in recombination. Also for cell [66], the very low R_{rec} is explained by the highest aggregation in comparison with a cell with a similar sensitization, see Figure 38, p. 108. The trends observed for the recombination are also reflected upon V_{OC} (Table 8, p. 111) especially as E_c is similar, because an increase in recombination decreases the accumulated charge in the ZnO film and thus V_{OC}. Thus mostly a higher V_{OC} is found for a sensitization with a coadsorbate, where recombination is not as much favored by dye aggregates as for a sensitization without coadsorbate. For most cells the linear curve shape near 0 V for τ_n from OCVD measurements (Figure 101, p. 209) indicates a good blockinglayer, whereas for cells [47] and [48] τ_n is decreased compared to the other cells. As this decrease in τ_n is small enough to not affect V_{OC} at low light intensities (Figure 103), it could be caused by higher aggregation rather than by a defective blocking

layer. The difference in recombination for measurements at high and low illumination intensity allows an estimation of the regeneration efficiency. The difference in R_{rec} is smallest for DN285^{15min} [51], and successively higher for DN91^{15min} [48,66], for D149^{15min} [47] and for DN216^{15min} [49]. With coadsorbate, the difference of R_{rec} is similar for all sensitizers, and comparable to the relatively high difference found for DN216 without a coadsorbate.

From Figure 100, p. 208, the differential values of β were calculated and an overall β determined (Table 9) as discussed in section **3.3.2**. The recombination parameter β determined at AM1.5 illumination is mostly higher for cells sensitized without a coadsorbate (except for DN216, where recombination is very similar), whereas differently deposited ZnO sensitized with D149 an increase of β was observed for the addition of a coadsorbate [16]. The FF (Table 8, p. 111) shows the respective trend with (slight) increase for a sensitization without coadsorbate, due to the dependence in equation **(35)**. Similar as in the previous chapter, β determined from measurements in the dark and at red LED illumination is similar even when determined from different measurements (EIS, Figure 100, p. 208 or V_{OC} vs. illumination intensity, Figure 103, p. 210). For the higher E_c for cell [66], β is ~1, which indicates that recombination occurs mainly via the conduction band.

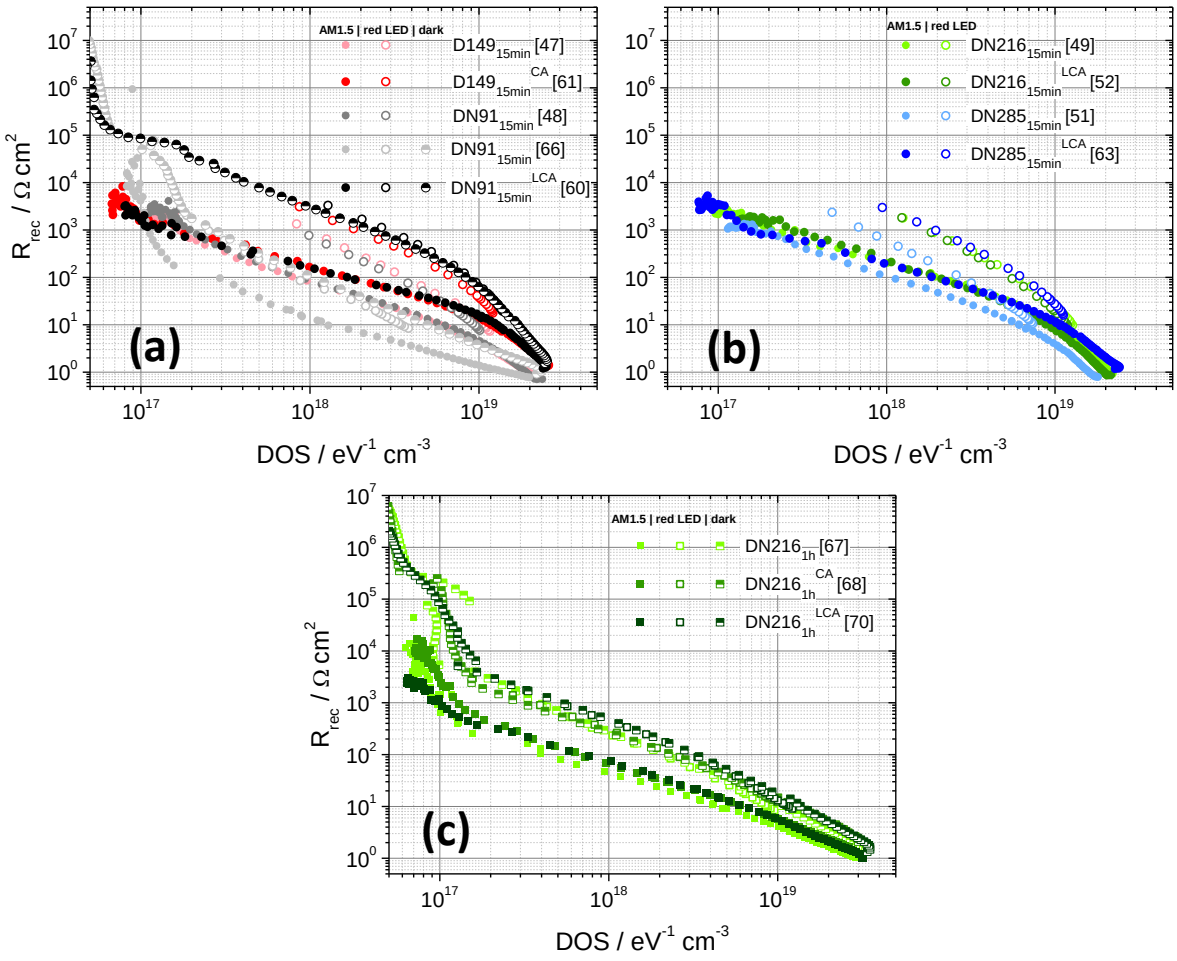

Figure 43 – Recombination resistance R_{rec} vs. the density of states DOS for different ZnO-based DSCs sensitized with different indoline dyes in the presence or absence of a coadsorbate. (a,b) Cells sensitized for 15 min and (c) cells sensitized for 1 h.

At high illumination intensity β is lower than at low illumination intensity or in the dark, which is ascribed to a different recombination due to a slightly lower conduction band edge and additional trap states generated by the high illumination intensity (oxidized dye molecules due to inefficient regeneration and light-induced trap states in the ZnO film).

From these results it is concluded that if the cells had the same position of the conduction band edge, the use of a coadsorbate would increase the performance of the cell by reducing recombination via dye aggregates, provided that other parameters are similar. However the lower amount of adsorbed dye for sensitization with coadsorbate and a probably lower regeneration efficiency lead to lower short-circuit currents, which reduces the gain from lower recombination for cells sensitized with coadsorbate, and thus a higher cell efficiency is found for most cells adsorbed without a coadsorbate.

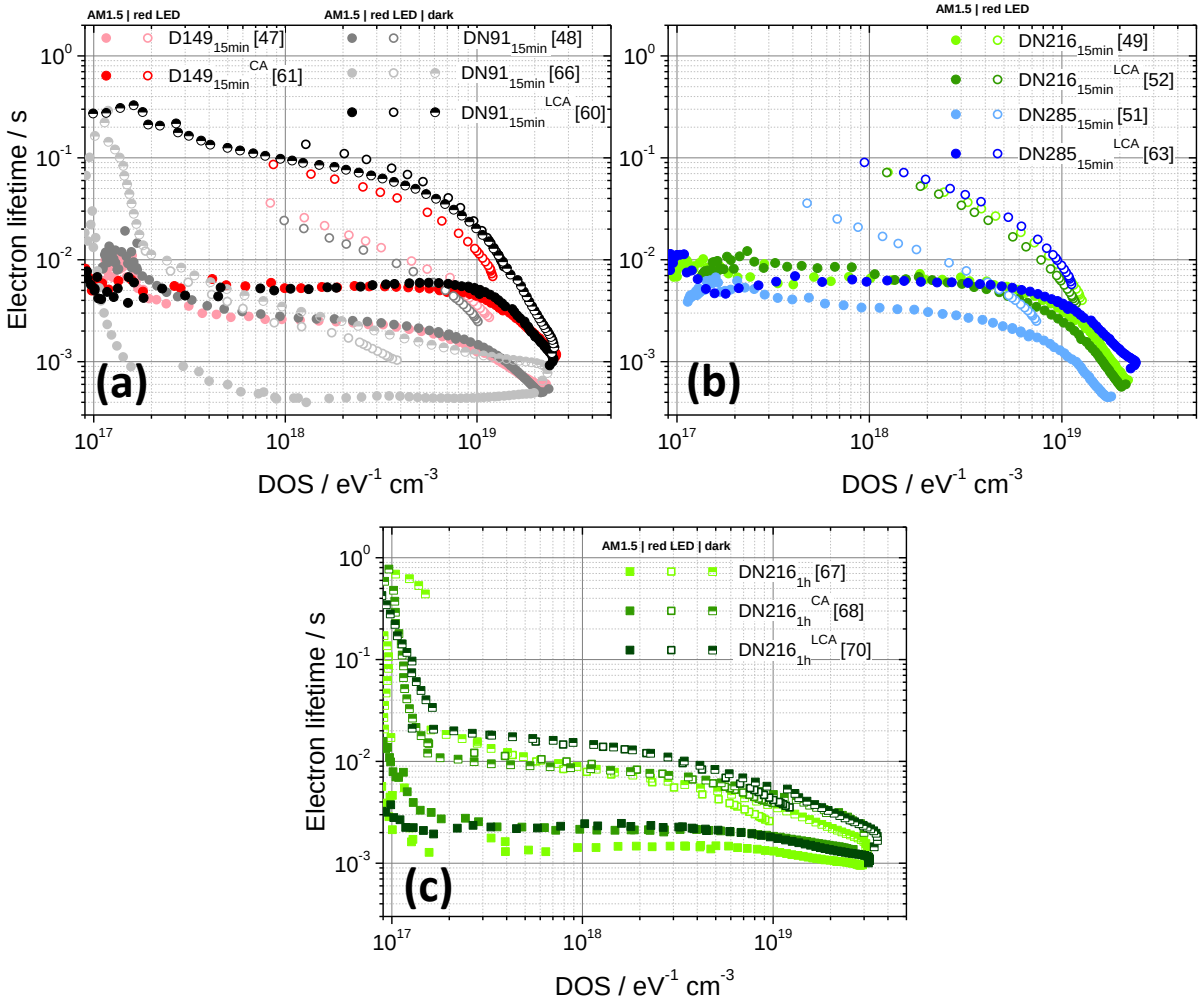

Figure 44 – Electron lifetimes vs. the DOS, determined for ZnO-based DSCs sensitized with different indoline dyes with and without a coadsorbate, for (a,b) 15 min and (c) 1 h. Measurements performed at AM1.5 illumination are designated by filled symbols, while measurements at red LED illumination are indicated by open symbols, and measurements in the dark by half-filled symbols.

Sensitization for 1 h with or without coadsorbate

For an adsorption time of 1 h, R_{rec} (Figure 100, p. 208) and τ_n (Figure 101, p. 209) vs. V_f does not directly depend on the presence of a coadsorbate. Recombination at a given DOS (R_{rec} or τ_n vs. DOS in Figure 43 and Figure 44) however is higher for the cell adsorbed without coadsorbate. This is also in line with the higher aggregation seen in the normalized absorbance, Figure 38, p. 108. For film [70], for which the ZnO deposition was altered, a very similar aggregation and recombination was observed as for the standardly deposited and similarly sensitized film [68]. Probably the change in deposition conditions has little or no effect on the final ZnO surface, as the change in deposition was an increased deposition voltage only during the first few seconds of ZnO/EosinY deposition, however the seed layer for this deposition is very likely changed by the higher voltage [258], which influences the grain density and the size of particles and thus the scattering of the films, see also section **4.1**. The difference in recombination in the dark and at AM1.5, which can give information about regeneration, is approximately the same for the cell sensitized without coadsorbate and for cell [70], but smaller for cell [68]. This indicates that the regeneration is more efficient for cell [68], at least when compared with cell [67] where recombination in the dark is very similar. This difference could be caused by the lower I_{SC} for cell [68] (Table 8, p. 111), which requires less diffusion of the electrolyte and thus might not be influenced so much by the diffusion limit of the electrolyte. The equal relative position of R_{rec} and τ_n vs. DOS shows that a correct area normalization was performed for R_{rec}.

For the very similar position of E_c , β is very similar for all cells sensitized for 1 h with or without coadsorbate, see Table 9, p. 115. This is also expected for the very similar curves of R_{rec} or τ_n, and indicates that also the recombination order is similar, not influenced by the additional recombination without coadsorbate (cell [67]) of the already aggregated samples (compare results in section **3.3.2**). The linear dependence of τ_n from OCVD measurements with voltage near 0 V (Figure 101, p. 209) indicates a good quality of the blockinglayer, which effectively hinders recombination via the substrate.

Recombination and regeneration from recombination currents

The recombination currents in the dark and under illumination for the different cells sensitized with or without coadsorbate are shown in Figure 45, with a voltage correction for voltage losses at the series resistance and for relative shifts of the conduction band edge. Similar to R_{rec} and τ_n, recombination is enhanced for the measurements under AM1.5 illumination, and mostly cells without coadsorbate show a higher recombination, also similar to earlier findings [17]. For the plot of recombination currents, a difference in dark and illuminated currents was ascribed especially to recombination with oxidized electrolyte species for intense illumination [17], and thus inefficient regeneration. Thus also these results support that inefficient regeneration occurs at higher illumination efficiency.

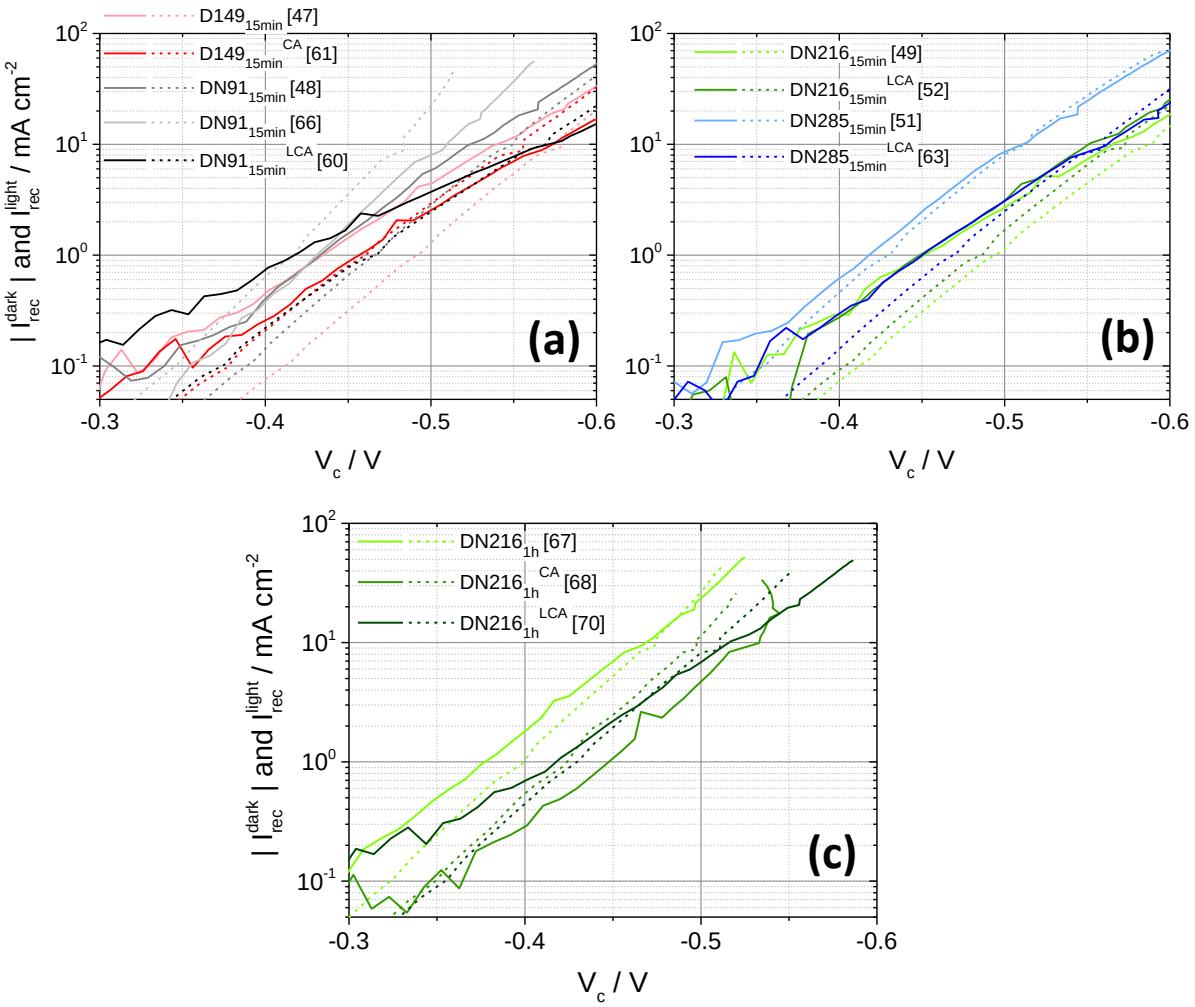

Figure 45 – Recombination current density in the dark and under AM1.5 illumination for DSCs sensitized with different indoline dyes in the presence or absence of a coadsorbate. The graphs are grouped after different dyes and adsorption times, (a) D149 and DN91 adsorbed for 15 min, (b) DN216 and DN285 adsorbed for 15 min, and (c) DN216 adsorbed for 1 h. Light colors indicate an adsorption without coadsorbate, while dark colors indicate an adsorption with coadsorbate, see also the legends. Dashed lines indicate measurements in the dark, while full lines indicate recombination currents at AM1.5 illumination.

Also the comparison of the shape of the curves in the dark and under regeneration speaks for recombination, as for a voltage range where I_{SC} is high (0 to around -0.45 V) the difference is larger, and for lower and reverse currents, where the diffusion limit of the electrolyte is probably not yet reached, this difference is smaller, and the same is observed for cells where I_{SC} (Table 8, p. 111) is smaller (cells [66], [61], [51], [63]). This finding is different from the comparison of R_{rec} or τ_n at different light intensities, where especially cells with coadsorbate show a larger difference than cells without coadsorbate. This indicates that either EIS measurements or recombination currents yet focus on different processes.

The graphs of the recombination currents show different slopes and even a crossing of the recombination current in the dark and under illumination is observed. This is very likely caused by the correction of the voltage by ΔE_c even though α and β are different. If the DOS would be available for the recombination currents, a plot vs. the DOS would probably give better results due to these different

parameters, and this is also the reason why for R_{rec} and τ_n the representation vs. DOS was preferred. Recombination at short circuit is not regarded in this approximation of recombination currents, regeneration can be even more pronounced than found in Figure 45, and is supposed to be one of the main loss mechanisms which lead to comparatively low I_{SC} values for even though the light harvesting efficiency is ~1 in the wavelength range where the sensitizers absorb light.

4.4 Conclusions for indoline-sensitized cells with and without coadsorbate

For the comparison of cells sensitized with and without coadsorbates, the amount of adsorbed dye and the aggregation tendency for most indoline dyes used in this work increased when no coadsorbate was used for both sensitization times of 15 min and 1 h, only DN216 adsorbed for 15 min showed almost no change with or without coadsorbate. This observation of a different aggregation was attributed to the coadsorbate molecules, which adsorb to the ZnO surface (as they are expected to), and thus serve to separate the individual dye molecules further from each other and decrease the overlap of molecular orbitals. The adsorption behavior was directly reflected upon cell parameters, as I_{SC} mostly increased for a sensitization without coadsorbate (due to the larger amount of dye adsorbed), and V_{OC} on the other hand decreased due to the increased aggregation of dye molecules and thus increased recombination by radiationless deactivation via molecular aggregates. This cause in the difference in V_{OC} was supported by the observation that no change in E_c was seen in C_μ (for the respective adsorption times), and a decreased recombination for a sensitization with coadsorbate was confirmed by an increase of τ_n, R_{rec} or the recombination currents. Large differences in R_{rec} and τ_n where found, when measurements at AM1.5 and red LED illumination were compared, which is attributed mainly to a more effective dye regeneration and thus less recombination via oxidized dye molecules for low illumination intensities, similar to the conclusions for chapter **3**.

A small change in the deposition, a more negative deposition voltage for a few seconds during the deposition of ZnO/EosinY, led to very different cell parameters, with an increased I_{SC} and slightly decreased V_{OC}, and the overall highest η of 4.59% compared with cells discussed in chapter **3** and **4**. This change was attributed to a different morphology of the ZnO film which less scattering, and thus an increased amount of adsorbed dye, without increased aggregation. A probable cause of the higher I_{SC} is also found in a slightly lower conduction band edge and thus increased injection. Recombination and regeneration were similar to a cell with similar sensitization even for the higher current observed.

For dyes D149, DN91 and DN216 (sensitized for 15 min), the addition of a coadsorbate decreased the power conversion efficiency, while for DN285 the efficiency remained constant, and for cells sensitized for 1 h with DN216 the efficiency either remained constant or increased. While in terms of power conversion the addition of a coadsorbate mostly proved disadvantageous, in terms of recombination and aggregation a clear improvement can be observed when a coadsorbate is included in the sensitization procedure. This is the case for the reference dye D149 as well as for two other sensitizers with a second carboxylic anchor group, DN91 and DN285. For DN216 the sensitization with or without coadsorbate showed small or no differences, which could be an indication for a more stable or reproducible sensitization process when this sensitizer is used.

5 Changes in ZnO-based DSCs after storage in the dark

Most of the work presented here was published in the following reference: Falgenhauer, J.; Fiehler, F.; Richter, C.; Rudolph, M.; Schlettwein, D. Consequences of changes in the ZnO trap distribution on the performance of dye-sensitized solar cells. *Phys. Chem. Chem. Phys.* **2017,** *19* (24), 16159–16168. DOI: 10.1039/C7CP01024A.

During the measurements of DSCs fabricated from electrodeposited ZnO an increase in the short-circuit current density I_{SC} was observed after a storage in the dark for several days. Felix Fiehler found in a systematic study in the course of his Master thesis [131] that this increase in I_{SC} was observed for cells sensitized with the different indoline dyes D149, DN216 and DN285 (all cosensitized with a coadsorbate). Extended photoelectrochemical measurements before and after a storage time of four weeks revealed a downward shift in the conduction band edge as the main cause for this increase in I_{SC}. This series measured by Felix Fiehler was completed by cells sensitized with DN91 and DN285) in this work, and the photoelectrochemical data were voltage-corrected with the method utilizing R_{series} to ensure comparability with the cells in this work (see section **9.1.2**). As no absorbance data are available for the cells of Felix Fiehler, available absorption spectra were compared to similarly sensitized cells in section **3.1** and discussed there. Additionally to the cell designation defined in the beginning of chapter **3**, in this chapter a "p" in the film name indicates a film fabricated and measured by Felix Fiehler in the course of his Master thesis [131].

All dye-sensitized solar cells discussed in this chapter were characterized directly after preparation by EIS, IMPS, IMVS and other photoelectrochemical methods. The cells were then stored in the dark for 4 weeks, with occasional measurement of IV-curves within these 4 weeks. After 4 weeks, the cells were again thoroughly characterized by the same photoelectrochemical methods. The set of cells includes at least two cells for each of the new dyes DN91, DN216 and DN285 (including two anchor groups) and one cell for the reference dye D149. [xxii]

5.1 Current-voltage curves before and after storage in the dark

Directly after preparation of the cells, IV-curves were measured at AM1.5 illumination and in the dark, and are plotted in Figure 46 (cell parameters listed in Table 10). The same figure also contains,

[xxii] All cells discussed in this chapter consist of films with a smaller mask area for electrodeposition. This leads to differences in the deposition due to a different mass transport at the edges, and thus to a lower comparability of these cells to cells in other chapters, see section **9.1.4**.

IV-curves measured after a storage of the cells in the dark for about 4 weeks. Directly after preparation, the mean values of I_{SC} for dyes with two anchor groups show a dependence on the length of the spacer of the second anchor group, similar to previous findings [15]. In a later work (for cells with larger area and shorter sensitization) [13], the increase in I_{SC} for the same indoline sensitizers with shorter spacer groups was attributed to shorter injection times measured by ultrafast transient measurements. Absorbance measurements on equivalently sensitized films (see section **3.1**) disclosed that the lower I_{SC} for DN285 and DN216 is not simply due to a lower amount of dye molecules adsorbed to the ZnO surface.

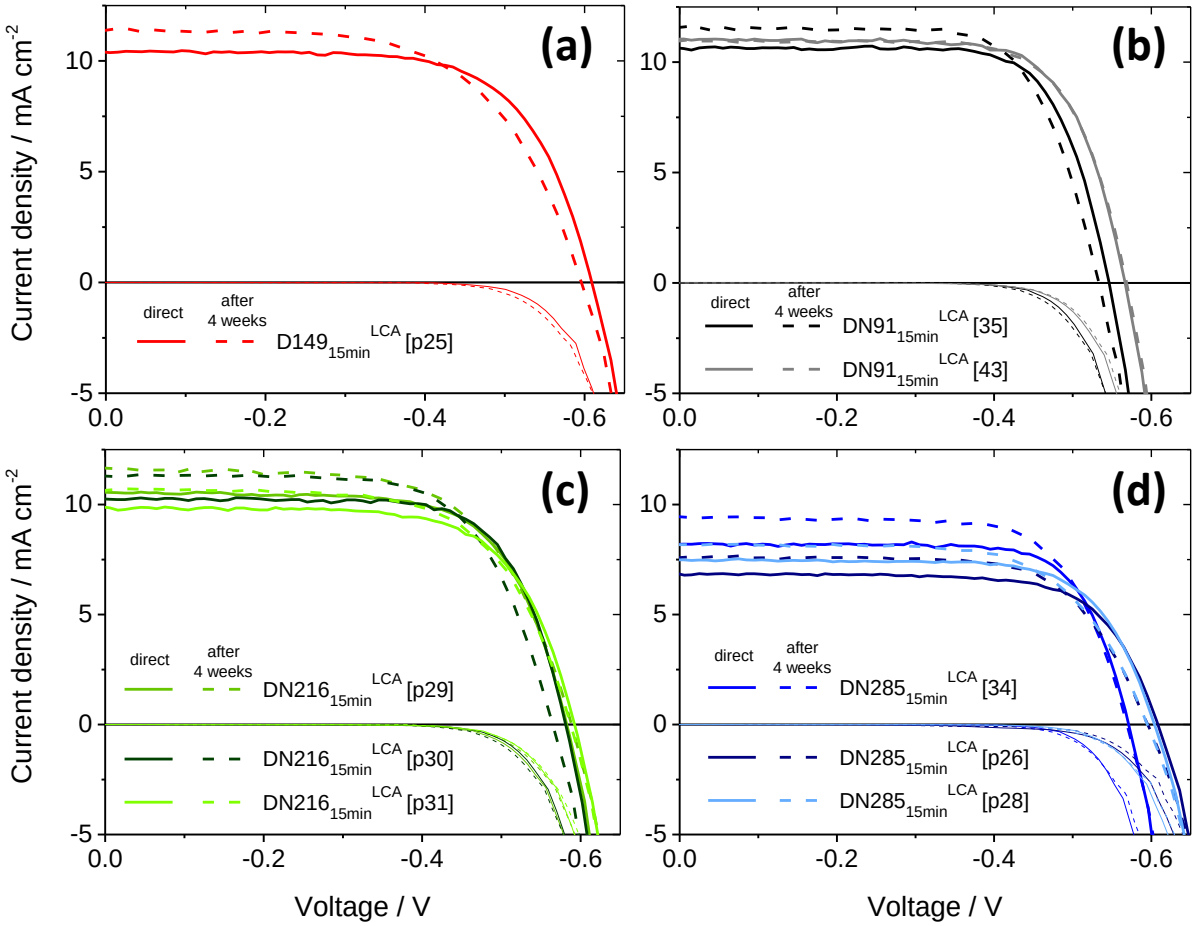

Figure 46 – Current-voltage curves of DSCs sensitized with different indoline dyes, (a) D149, (b) DN91, (c) DN216 and (d) DN285. Solid lines indicate IV-curves measured directly after cell assembly, while data measured after ca. 4 weeks are indicated by dashed lines. Curves measured at AM1.5 are indicated by thick lines, while curves measured in the dark are indicated by thin lines. Adapted from [259].

For a sensitization with D149 (only one anchor group), I_{SC} is similar to the values found for sensitizers DN216 and DN91 with a shorter anchor group, and thus the current for these dyes does not seem to be limited (as much) by the injection time as for DN285. The fill factor (FF) of the studied cells is about 70% for most cells, similar to values in the previous chapters and in the literature [18,19]. Other cell

values like the open-circuit voltage, the short-circuit current and the efficiency are also comparable to values found in those references, but do not depend systematically on the dye structure. [xxiii]

After 4 weeks, the majority of the cells show a slightly improved power conversion efficiency. As the open-circuit voltage V_{OC} and the fill factor FF slightly decrease for most of the cells, this improvement can be directly traced to the change of the short-circuit current density I_{SC}. This value increases by about 9% for the studied cells during the four weeks storage in the dark. In Figure 47, the short-circuit current densities I_{SC} determined from IV-curves for some cells are plotted against the time of storage in the dark, and most cells show a similar increase with time. I_{SC} increases especially during the first few days, while for cell [43] only a small increase in current can be observed even after 3 weeks. The decrease of the slope of the IV-curve at V_{OC} already indicates that at least one reason of this current increase could be an increase in recombination resistance. More detailed measurements were performed to enlighten the cause of this increase in current, and will be discussed below.

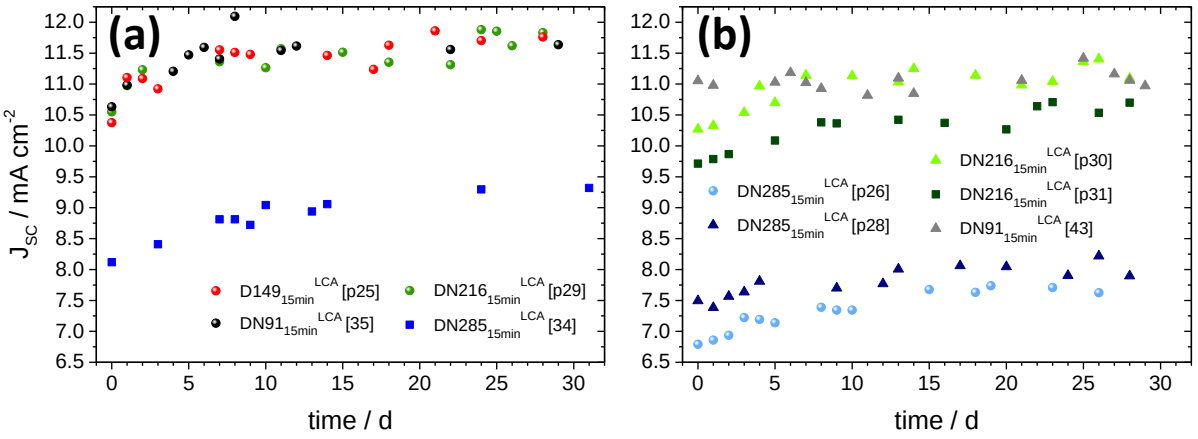

Figure 47 – Short-circuit current densities of DSCs sensitized with different indoline dyes, plotted against the time after preparation of the solar cells. Different colors indicate different sensitizers, while different symbols of the same color indicate different cells fabricated under the same conditions. Adapted from [259].

By impedance measurements, the different contributions to the overall series resistance R_{series} were analyzed, in particular the sheet resistance of the substrate R_s, the electrolyte resistance Z_d and the charge transfer resistance at the platinized counter electrode R_{Pt}. For the cells in this study, the increase of the series resistance R_{series} during the storage in the dark is due to an increase in the electrolyte resistance (see Table 11), other resistances contributing to R_{series} remain constant (not shown). This change could either be explained by a change of the electrolyte during the storage time, for example by some water still adsorbed to the semiconductor surface desorbing into the electrolyte during the storage time. Also desorption of dye into the electrolyte could lead to an increase in Z_d, it

[xxiii] The IV-curves as well as all other photoelectrochemical measurements (excluding IPCE, which was measured only for some cells, see section 3.1.2) were measured without a mask to render the determined values comparable to other measurements. When the IV-curves are measured with a mask slightly larger than the diameter of the film[239], the photocurrent and, hence, the efficiency decrease by about 10%.

was, however, shown by Melanie Rudolph [127] that addition of D149 to the electrolyte also increases the counter electrode resistance R_{pt}. A larger increase is observed only for D149 in the present cell, which indicates that only D149 is desorbed to a larger extent into the electrolyte, which is in line with the more stable binding of the double-anchor dyes[15]. This on the other hand means that the increase in Z_d observed for all dyes has some other reason than desorption of sensitizer molecules into the electrolyte. To find if adsorbed water in the cell was possibly a reason for the increase in Z_d, cell [43] was prepared with stronger avoiding of water, which included degassing of the film in the air lock of the glovebox and pre-filling of the cell with electrolyte inside the glovebox. Cell [43] shows by far the lowest increase in the electrolyte resistance R_{el}, which is a strong indication that water (either in the electrolyte or adsorbed inside the cell compartment) could be the cause for an increase in Z_d. As I_{SC} increases during the storage also for cells which show an increase in Z_d, this resistance does probably does not yet reach a value limiting current transport; for EIS results discussed below, the influence of the voltage drop at R_{series} was removed by plots vs. V_f.

Table 10 – Cell parameters for ZnO dye-sensitized solar cells sensitized with different indoline dyes. [a] Ratio of J_{SC} measured after a storage in the dark for about 4 weeks to J_{SC} measured directly on the day of preparation; [b] red LED illumination at 25 mW cm^{-2}. Table adapted from [259].

Cell	measurement	J_{SC} / mA cm^{-2} at AM1.5	V_{OC} / V	ΔV_{OC} / mV	FF	η / %
D149 + LCA (15 min) [p25]	direct after ~4 weeks	10.38 11.45	-0.609 -0.596	-13	0.68 0.62	4.29 4.15
DN91 + LCA (15 min) [35]	direct after ~4 weeks	10.63 11.64	-0.546 -0.533	-13	0.73 0.71	4.24 4.32
DN91 + LCA (15 min) [43]	direct after ~4 weeks	11.05 10.97	-0.567 -0.568	+1	0.72 0.71	4.48 4.43
DN216 + LCA (15 min) [p29]	direct after ~4 weeks	10.55 11.62	-0.582 -0.588	+6	0.70 0.64	4.22 4.36
DN216 + LCA (15 min) [p30]	direct after ~4 weeks	10.24 11.26	-0.581 -0.565	-16	0.72 0.68	4.25 4.27
DN216 + LCA (15 min) [p31]	direct after ~4 weeks	9.85 10.66	-0.592 0.587	-5	0.69 0.65	3.98 4.08
DN285 + LCA (15 min) [34]	direct after ~4 weeks	8.12 9.32	-0.571 -0.569	-2	0.74 0.70	3.43 3.72
DN91 + LCA (15 min) [p26]	direct after ~4 weeks	6.79 7.63	-0.608 -0.595	-13	0.72 0.69	2.95 3.10
DN91 + LCA (15 min) [p28]	direct after ~4 weeks	7.49 8.18	-0.604 -0.595	-9	0.72 0.67	3.22 3.20

5.2 Changes in the chemical capacitance and transport properties by a storage in the dark

C_μ vs. V_f in Figure 48 shows a similar shape as also observed in the previous chapters, with a linear increase in C_μ for intermediate voltages as expected from equation **(21)**. From this slope, α was determined (from the maximum of the differential values, compare section **3.3.1**), and the values are listed in Table 11. α is mostly smaller than the values found in chapters **3** and **4**, which is attributed to a smaller deposition area (see section **9.1.4**), however α is more comparable to values found in the literature for electrodeposited ZnO films [16-19]. For the different cells, α varies in the sequence DN91(0.48) > DN285 > DN216 > D149(0.27), without direct dependence on the length of the alkyl spacer, while α for the same cell before and after storage remains approximately constant. For D149, a decreased slope at voltages around -0.35 V (decreasing also α) could be caused by an additional capacitance from deep monoenergetic trap states as observed also in [17], but not observed for the cells in chapters **3** and **4** under AM1.5 illumination (probably because of differences in the electrodeposition, see section **9.1.4**).

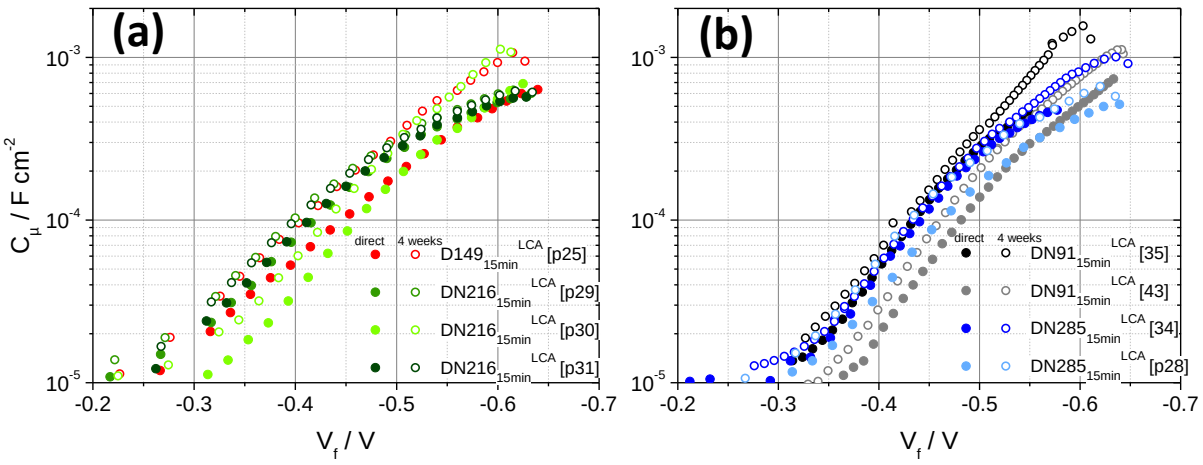

Figure 48 – Chemical capacitance C_μ of indoline-sensitized DSCs, determined from EIS measurements at 100 mW cm^{-2} simulated sunlight. (a) Sensitizers D149 and DN216; (b) sensitizers DN91 and DN285. Different colors indicate different sensitizers, while different symbols of the same color indicate different cells sensitized with the same dye. Curves with filled symbols were measured on the day of the preparation of the cells, while curves with open symbols were measured after about 4 weeks of storage in the dark. Adapted from [259].

Similar to C_μ, the total trap density $N_t/N_{t,ref}$ varies for the different cells, but remains constant for a given cell during the storage in the dark, compare Figure 87, p. 196 and Table 11. The shift of C_μ to lower absolute voltages for measurements of a respective cell after storage in the dark (compared to the same cell measured directly after preparation) indicates a shift of the conduction band edge to lower energies, which can be evaluated directly from C_μ in Figure 48 or seen directly in the DOS in Figure 87, p. 196, because of the almost unchanged values of $N_t/N_{t,ref}$. The respective shifts $\Delta E_c/q$ of each curve relative to the initial curve range from 10 to 43 mV (Table 12), with no direct dependence

of the shift on the sensitizer. For cell [43], EIS measurements performed at red LED illumination showed a very similar shift of the conduction band edge upon ageing of the cell (not shown). A downward shift of the conduction band edge as observed here during storage of the cells in the dark gives an explanation for the increase in I_{SC} which is observed during the storage.

A downward shift in E_c as observed for the storage of the cells in the dark should also decrease V_{OC} by the same amount. For most cells, however, the change in V_{OC} upon storage in the dark is either in a different direction or smaller than expected from $\Delta E_c/q$ (see Table 12). It can be concluded that the shift in the conduction band edge affects the open-circuit voltage for some of the cells, but other factors also influencing the open-circuit voltage are (over)compensating this effect [17,60]. Some possible effects influencing the open-circuit voltage are discussed below.

A possible reason for the observed $\Delta E_c/q$ could be the adsorption or desorption of polar molecules. For the oxidic semiconductor ZnO prepared from solution, a change by adsorption or desorption of water is probable; the observed downward shift would mean for example desorption of OH^- or H_2O facing with the oxygen atom to the ZnO from the ZnO surface into the electrolyte. This desorption would also be a possible reason for the observed increase in Z_d during the storage in the dark. The association with adsorbed water is further corroborated by independent measurements by Felix Fiehler [131], where deposited ZnO films (EosinY already desorbed) were stored in water for ~100 days.

Table 11 – Values determined from EIS measurements, from measurements of V_{OC} vs. intensity, from the recombination current under illumination and from IV-curves. Table adapted from [259].

Sample	**Measure-ment**	**β**	**β**	**α**	**R_s/Ω**	**Z_d/Ω**	**R_{pt}/Ω**	**$N_t/N_{t,ref}$**
		from EIS (at red LED light for one cell)	from V_{OC} vs. intensity	from EIS (at red LED light for one cell)	at -0.54 V			reference cell [61] from section **3.3.1**
$D149_{15min}^{LCA}$ [p25]	directly	0.54	0.84	0.39	5.9	1.7	3.5	3.33
	after 4 weeks	0.49	0.84	0.35	5.8	4.9	4.9	3.33
$DN91_{15min}^{LCA}$ [35]	directly	0.69	0.95	0.52	5.6	1.7	3.3	0.69
	after 4 weeks	0.67	0.96	0.48	5.8	3.9	3.7	0.69
$DN91_{15min}^{LCA}$ [43]	directly	0.64 (0.86)	0.92	0.51 (0.48)	5.8	1.4	3.6	0.45
	after 4 weeks	0.67 (0.79)	0.84	0.53 (0.46)	5.7	1.6	3.5	0.43
$DN216_{15min}^{LCA}$ [p29]	directly	0.54	0.93	0.36	5.4	1.6	3.5	1.43
	after 4 weeks	0.48	0.90	0.40	5.6	2.6	4.0	1.43
$DN216_{15min}^{LCA}$ [p30]	directly	0.60	0.95	0.40	4.8	2.4	3.6	1.67
	after 4 weeks	0.57	0.94	0.38	5.3	4.9	3.8	1.67
$DN216_{15min}^{LCA}$ [p31]	directly	0.53	0.86	0.39	5.0	1.7	3.2	0.67
	after 4 weeks	0.49	0.86	0.40	5.3	3.2	3.2	0.65
$DN285_{15min}^{LCA}$ [34]	directly	0.71	-	0.47	5.5	2.2	4.5	0.62
	after 4 weeks	0.68	0.93	0.48	5.5	3.2	5.8	0.65
$DN285_{15min}^{LCA}$ [p28]	directly	0.57	0.90	0.41	5.3	3.3	3.4	0.62
	after 4 weeks	0.51	0.86	0.42	5.5	5.6	3.2	0.65

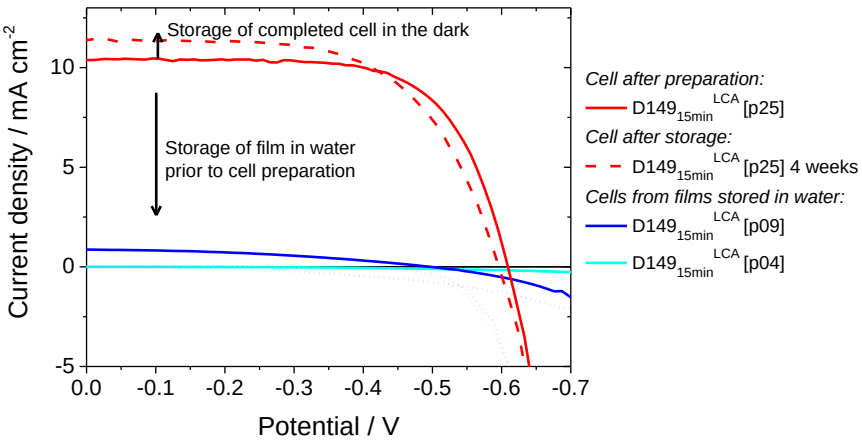

Figure 49 – Influence of water on the current-voltage characteristics at AM1.5 illumination and in the dark. Comparison the measurement of cell [p25] directly after cell preparation (red full line), the same cell after a storage in the dark for 4 weeks (red dashed line), and two cells, [p09] and [p04] prepared from films which were stored for ~100 days in water prior to cell preparation (cyan and blue line). Dotted lines indicate measurements in the dark. Adapted from [259].

After this cells were prepared as usual (see also section **2.4**) from these water-treated films. A sensitization with D149 and a coadsorbate yielded dark films with a high light harvesting efficiency, however IV-curves of these cells showed a very low I_{SC}, even though the dark current was considerably decreased compared to a reference cell [p25], see Figure 49. For one cell prepared with a water-treated ZnO film, cell [p09], EIS measurements were performed to find possible reasons for such a marked change. For the water-treated cell [p09], C_μ corrected for N_t showed a large shift of E_c of about 300 mV to higher energies, see Figure 50(a), and additionally, R_{rec} at a given DOS decreased for this cell (Figure 50(b)). The very high position of E_c slows down injection into the ZnO film, as the DOS of the film is considerably reduced at a given energy and thus also at the energy of excited state of the dye. This explains the low I_{SC} observed for cell [p09].

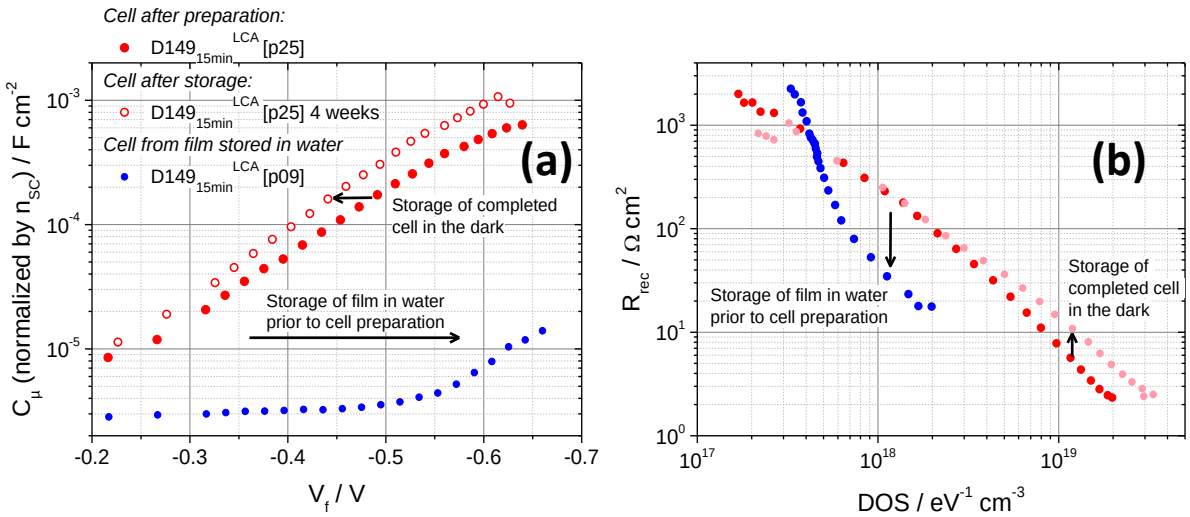

Figure 50 – Comparison of the influence of water on (a) C_μ and (b) R_{rec}. (a) for a standard cell directly after preparation and after a storage in the dark for 4 weeks, and a cell prepared from a film stored in water for ~100 days prior to film preparation. Adapted from [259].

For the long storage time in water, an adsorption of water or OH^- onto the ZnO surface is expected, and such an adsorption also thought to be the most probable explanation for the observed shift of E_c. As this change is exactly the opposite of what is observed during the storage of already prepared cells in the dark (lower E_c, higher R_{rec}, see also Figure 50), a desorption of water or OH^- from the ZnO surface might be the cause for the changes discussed in this chapter [xxiv]:

For cells sensitized with the different indoline dyes, the transport time τ_{tr} (Figure 51) was very similar after a normalization with $N_t/N_{t,ref}$ and only affected in the slope by the different α, indicating that the transport properties were similar even for the relatively different C_μ. Trap states and their occupancy have a high influence especially at low illumination intensities [210], and in this region the cells show a very good overlap. The dye molecules adsorbed to the semiconductor surface should have only a minor effect on the transport time [260], as the surface is not directly participating in the conduction of electrons. Thus no direct dependence on the sensitizer can be found for τ_{tr}. The storage of the cells in the dark slightly increased τ_{tr} probably due to the shift of E_c to lower energies, however the values were still within the range of the different cells.

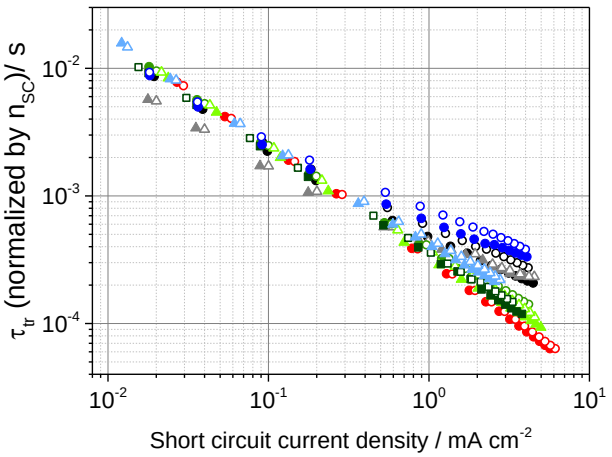

Figure 51 – Transport times of the different dye-sensitized cells determined from IMPS measurements, normalized by the relative total trap density $N_t/N_{t,ref}$, see Table 11. Measurements taken directly after the cell assembly are indicated by filled symbols while measurements taken after 4 weeks storage in the dark are indicated by open symbols. The different cells are indicated by different colors, for the exact designation see the legend in Figure 87. Adapted from [259].

[xxiv] A change of the electrolyte potential would also lead to a seeming shift of E_c, however a comparison of C_μ for a higher concentration of electrolyte species in section **9.1.8** showed that the position of the redox potential is insensitive even to relatively large changes in the electrolyte.

5.3 Changes in recombination during storage in the dark

The storage in the dark not only influences C_μ but also the recombination resistance R_{rec}, see Figure 52. R_{rec} was plotted against V_f or the voltage corrected by the shift of E_c during storage in the dark [xxv] which allows a good interpretation of the change in recombination for each cell (Figure 52(a,b)), and against the DOS in Figure 52(c,d), which makes a comparison to other cells in this work possible. For all cells, R_{rec} at a given corrected voltage or DOS increases during the storage in the dark. This increase in R_{rec} is small for some cells (DN91 [35], DN91 [43] and DN216 [p31]), while it is larger for all other cells. Also for a measurement at red LED illumination (only cell [43]), this increase in R_{rec} is observed, with a larger difference than for the measurement of the same cell at AM1.5. The observed increase in R_{rec} means that recombination is more efficiently prevented by the aged cells than by the freshly prepared cells. Such a change might be caused for example by reorganization of adsorbed species on the surface. As also the recombination under red LED illumination increases, a possible explanation could be that more loosely bound, aggregated dye molecules desorb into the electrolyte and can no longer serve as recombination centers. Also desorption of water, which is the supposed reason for the shift of E_c during the storage in the dark, could reduce surface traps and recombination centers, and thus a reduction of the recombination would be achieved. The recombination parameter β (determined from measurements at AM1.5 illumination, see Table 11, p. 129) decreases for almost all cells during the storage for 4 weeks, which means that also the recombination order changes. Lower β values indicate that recombination takes place slightly more via surface traps than for measurements after cell preparation, which is in line with the decrease of the conduction band edge, as usually high β values are found for high E_c [222]. At red LED illumination, β also decreases for most cells during the storage in the dark (see Table 11, determined from V_{OC} vs. intensity in Figure 104, p. 210), but the differences are even smaller than at AM1.5 illumination. Similar to the observations for β determined from different illumination conditions in the previous chapters, the values determined from V_{OC} vs. intensity are always higher than β determined from EIS at AM1.5 illumination, due to a reduced recombination via oxidized dye molecules or other light-induced trap states for the lower illumination intensity. Both a decreased V_{OC} and a decreased β during storage in the dark lead to the observed decrease in FF after equation **(35)**, see Table 10, p. 127.

For the electron lifetime τ_n (vs. V_f or V_f corrected for the shift of E_c from different measurements, or vs. DOS) in Figure 53 the same trends are observed as for R_{rec}, with a decrease of τ_n after the storage time of 4 weeks. From the linear increase of τ_n from OCVD for voltages near -0.3 V it can be concluded that for almost all cells the blocking layer works efficiently.

[xxv] For each cell, in the measurement after 4 weeks the voltage was corrected for the shift of E_c found in C_μ for the same cell (Table 12), so that for each measurement after 4 weeks the direct measurement is the reference. This voltage correction was not performed for all cells with one common reference, as there are considerable differences in α (and β) for the different cells, whereas α for the same cell almost remains constant.

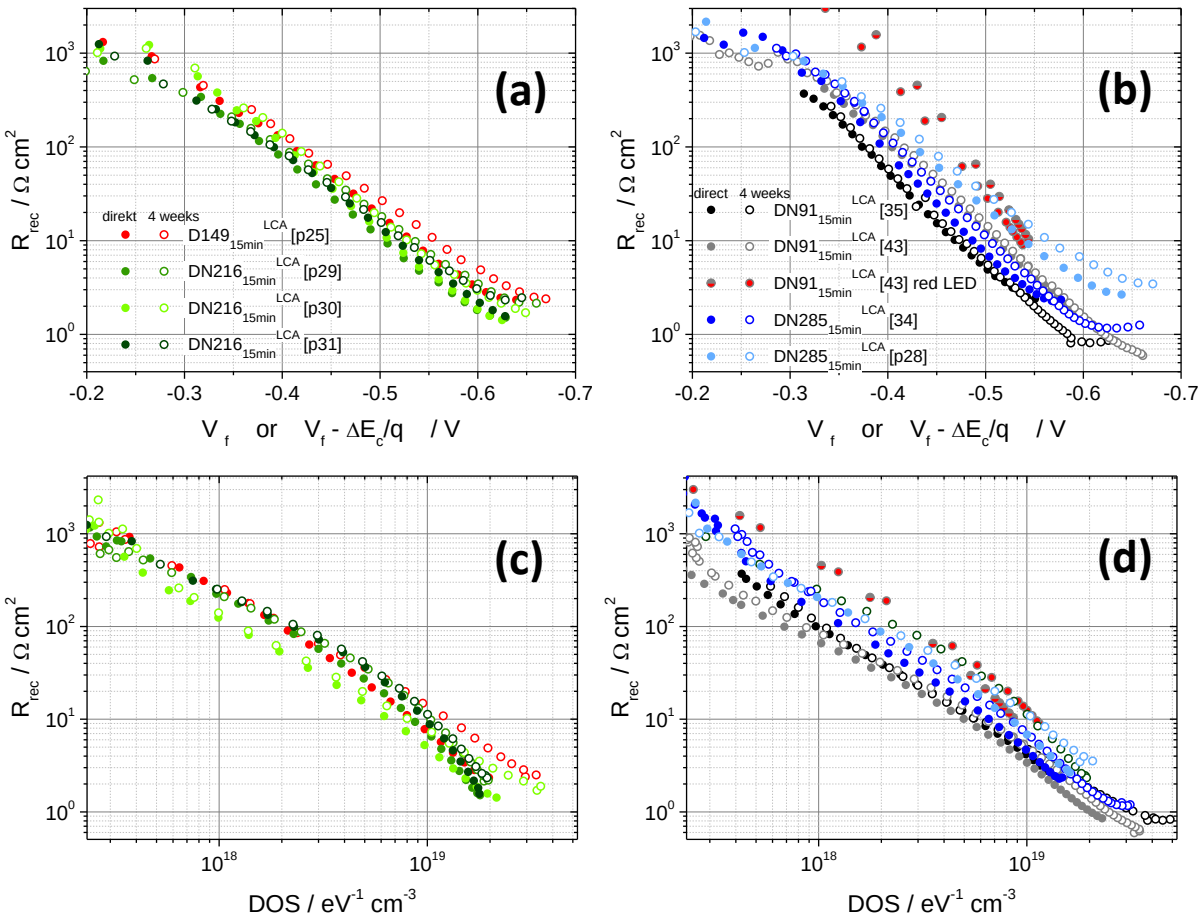

Figure 52 – Recombination resistance of dye-sensitized cells sensitized with different indoline dyes plotted (a,b) against the Fermi level voltage (for measurements directly after preparation) or the voltage corrected by the conduction band edge shift (for measurements after 4 weeks storage in the dark), and (c,d) against the DOS. Filled symbols indicate measurements performed after the preparation of the cells, open symbols of the same color indicate a measurement of the same cell after storage in the dark for 4 weeks. Grey symbols half-filled or filled with red indicate measurements of cell [43] at red LED illumination directly after preparation or after 4 weeks storage in the dark, respectively. Adapted from [259].

Only for cell [43] directly after preparation, τ_n determined from OCVD measurements is considerably decreased compared to an ideally linear slope, indicating that recombination via the substrate occurs for this cell. However the OCVD measurement of the same cell after 4 weeks results in τ_n similar to other cells (the increase is indicated by a green arrow in Figure 53(b)), which indicates that recombination via the substrate is again efficiently blocked. Probably the defect leading to a decrease of the OCVD lifetime was small, and could be "healed" even by comparatively small changes which might occur in the cell during storage in the dark, for example by a rearrangement of surface adsorbates. This instance shows the high sensitivity of OCVD lifetime at lower absolute voltages for the indication of defects in the blocking layer, superior to V_{OC} vs. illumination intensity (Figure 104, p. 210), where cell [43] measured after preparation showed no difference compared to all other cells.

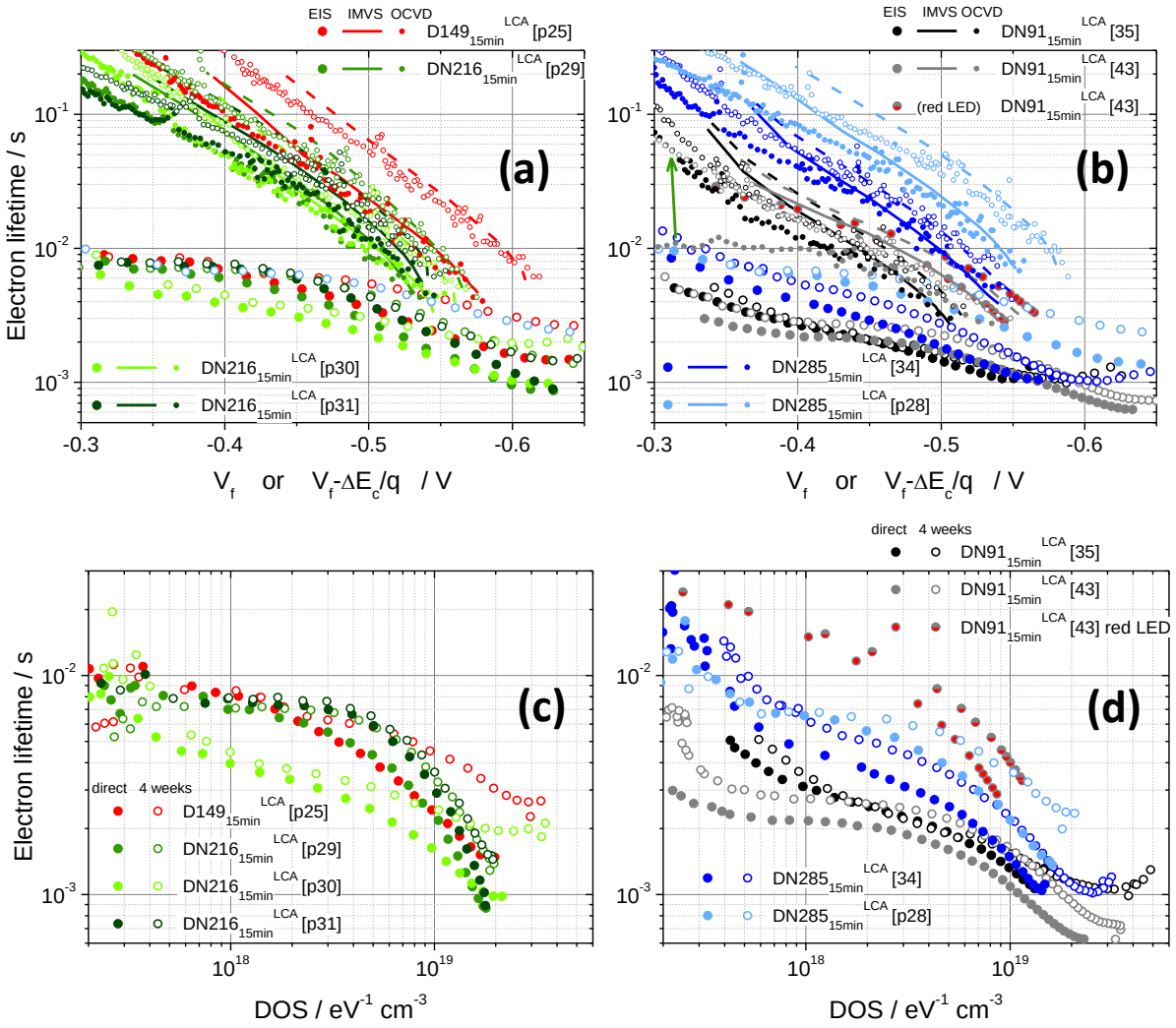

Figure 53 – Effective electron lifetimes of dye-sensitized solar cells, determined from EIS at AM1.5 illumination (symbols in (a,c,d)) and from IMVS (lines) and OCVD (symbols in (b)) measurements at red LED illumination. Filled symbols and solid lines indicate a measurement of a cell directly after preparation, while open symbols and dashed lines indicate cells measured after 4 weeks storage in the dark. (a) τ_n from EIS and IMPS vs. V_f ; (b) τ_n from OCVD vs. V_f; (c) τ_n from EIS and IMPS vs. V_f (measurements directly after preparation) or vs. V_f corrected by the conduction band edge shift (measurements after 4 weeks); (d) τ_n from EIS vs. the DOS. Grey symbols half-filled or filled with red indicate EIS measurements of cell [43] at red LED illumination measured before and after the storage in the dark, respectively. Adapted from [259].

A comparison of recombination currents in the dark and under illumination in Figure 54 gives information about regeneration, and also about the observed changes in V_{OC} after ageing of the cells. A direct comparison of the recombination current in the dark and under AM1.5 illumination for each cell shows that the recombination current at AM1.5 is always higher and has a different slope than the recombination in the dark. As also in the previous chapters, the difference in recombination for the different illumination conditions was ascribed mainly to enhanced recombination via oxidized dye molecules, and thus regeneration efficiency as one of the limiting factors of I_{SC}. This effect is larger at lower absolute voltages (as the I_{SC} is higher), which leads to the observation that for some cells the recombination current in the dark and under illumination intersect at more negative voltages.

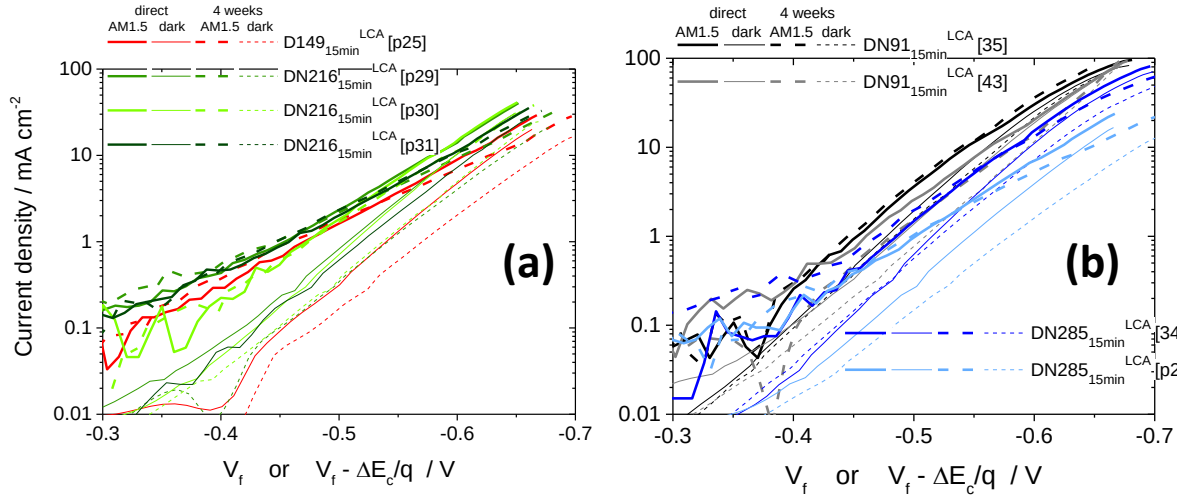

Figure 54 – Recombination currents for dye-sensitized solar cells sensitized with different dyes. The fermi-level voltage of each cell was corrected by the shift of the conduction band edge (shift after 4 weeks of storage time) to give V_C*, for cells sensitized with (a) D149, DN216, (b) DN91 or DN285. Absolute values of the dark current density vs. V_C*. Currents measured at AM1.5 illumination are indicated by thick lines, measurements in the dark are indicated by thin lines. Measurements directly after cell preparation are indicated by full lines, and measurements after storage in the dark for 4 weeks are indicated by dashed lines. Adapted from [259].

From the difference of I_{rec}^{light} at the same relative position of E_c, the change in V_{OC} by a change of the recombination current were determined after equation **(33)**, see the values $\Delta V_{OC}\left(I_{rec}^{light}\right)$ in Table 12. For most of the cells the change of V_{OC} from the recombination current under illumination is positive, indicating that a higher value of V_{OC} can be reached for aged cells due to a decrease of recombination. With the values of ΔV_{OC} from the increase in I_{SC} and the change in E_c, the theoretical change in V_{OC} due to these three influences was calculated [17] and compared to the observed change in V_{OC} after 4 weeks, see Table 12.

Table 12 – Voltage differences determined from C_μ, from the recombination current under illumination, from I_{SC}, and from IV-curves; also the calculated voltage difference is listed. The differences are determined for each measurement after 4 weeks relative to the same cell measured directly after cell preparation. Negative values indicate a shift to less negative voltages (downward in energy), and positive values indicate shifts to more negative voltages. A mean value of $\beta = 0.55$ was used for the calculations. Table adapted from [259].

Cell	$\Delta E_c/q$	$\Delta V_{OC}\left(I_{rec}^{light}\right)$	$\Delta V_{OC}(\Delta I_{SC})$	$\Delta V_{OC,calc}$	ΔV_{OC}(IV)
	determined at $C_\mu = 3 \cdot 10^{-4}$ F cm^{-2}	determined near V_{OC} after equation **(33)**	after equation **(32)**	after equation **(34)**	Shift from IV-curve
Unit	mV	mV	mV	mV	mV
$D149_{15min}^{LCA}$ [p25]	-43	17	5	**-21**	**-13**
$DN91_{15min}^{LCA}$ [35]	-15	-5	4	**-16**	**-13**
$DN91_{15min}^{LCA}$ [43]	-18	20	0	**+2**	**+1**
$DN216_{15min}^{LCA}$ [p29]	-27	25	5	**+3**	**+6**
$DN216_{15min}^{LCA}$ [p30]	-36	11	4	**-21**	**-16**
$DN216_{15min}^{LCA}$ [p31]	-11	1	4	**-6**	**-5**
$DN285_{15min}^{LCA}$ [34]	-10	0	6	**-4**	**-2**
$DN91_{15min}^{LCA}$ [p28]	-36	17	4	**-15**	**-9**

The different influences contribute to the overall change in V_{OC} by different amounts, for most cells the increase in I_{SC} leads to a relatively small change in V_{OC} by about 5 mV, while larger ΔV_{OC} is found for the influence of recombination and E_c. A good consistency is found for the measured and calculated values of ΔV_{OC} for the majority of the cells, with a deviation of not more than ±3 mV. For cells [p25], [p30] and [p28] the deviation of the calculated and measured ΔV_{OC} is larger, which is mainly attributed to a different slope of the recombination currents under illumination (before and after storage in the dark) for these cells, which complicates the exact determination of ΔV_{OC}. For cell [p25] also deep monoenergetic trap states were observed in C_μ, which in literature was mentioned as a possible reason for a deviation of $\Delta V_{OC,calc}$ from ΔV_{OC}(IV) [17]. The maximum deviation of $\Delta V_{OC,calc}$ from ΔV_{OC} determined from the IV-curves was about -7 mV, which renders this method of the determination of different influences on V_{OC} very useful.

5.4 Conclusions for cells stored in the dark

Upon storage of ZnO-based DSCs sensitized with an indoline dye and a coadsorbate in the dark for 4 weeks, an increase in the short-circuit current density I_{SC} was observed. Even though mostly a decrease of FF and V_{OC} was observed, the combined changes led to a small increase in power conversion efficiency. From dynamic measurements the cause for the increase in I_{SC} is traced back to a shift of the conduction band edge to lower energies by around 24 mV, which then increases the injection efficiency and, thus, the current. A calculation of different influences on V_{OC} showed that the shift in the conduction band edge upon storage in the dark was partially compensated by an increase of V_{OC} by an increased I_{SC} and by a decreased recombination (probably as a result from a reorganization of adsorbates at the ZnO surface). Thus, the open-circuit voltage did not decrease for all cells, but even showed a small increase for some of the DSCs. Comparison of recombination under different illumination conditions indicated that recombination increases at high-intensity illumination.

6 TiO2 films sensitized with indoline dyes

For electrodeposited ZnO films often variations in photoelectrochemical results were found, which were larger than for nanoparticulate ZnO films [127], probably owing to the rather undefined structure formation with single SDA molecules in solution. In order to obtain a more comparable semiconductor matrix for the comparison of the probably subtle differences induced by a small change in the sensitizer (DN91 vs. DN216 vs. DN285), also nanoparticulate TiO_2 films were prepared sensitized with the four indoline dyes D149, DN91, DN216 and DN285. The different semiconductor material is a further variation in the adsorption process which can lead to different solar cell parameters, for which the causes could be further defined by detailed photoelectrochemical measurements. It was observed in previous experiments (some performed by Melanie Rudolph) that nanoparticulate films mostly are dyed slower with indoline dyes than electrodeposited films, and shorter sensitization lead to an incomplete dyeing of the films. Thus a sensitization time of 1 h was chosen for the sensitization of the nanoparticulate TiO_2 films discussed in this chapter to ensure a complete dyeing of the sample. The measurements of the indoline-sensitized TiO_2 films are compared to electrodeposited ZnO films that were also sensitized for 1 h, with the assumption that for both semiconductor materials an approximate saturation of the surface occupancy is achieved after 1 h. The compared ZnO-based cells showed very similar values for most measurements and were already discussed in more detail in chapter **3**, so that for some of the graphs no direct comparison of TiO_2- and ZnO-based cells is given.

The designation of TiO_2 films and TiO_2-based cells follows the same nomenclature as defined in chapter **3**, with an additional “TiO2” in the cell name.

6.1 Absorbance of indoline-sensitized TiO_2 films

Due to the relatively uniform size of the nanoparticles inside the films, the scattering of TiO_2 films was lower than observed for ZnO films from electrodeposition, compare also the results in section **3.1.1**. This difference resulted in absorbance spectra (Figure 55) for which the absorbance maximum was not as strongly influenced as for most ZnO films sensitized for 1 h, see also the discussion about the scattering background in section **9.1.1**. This makes film [70] the most comparable ZnO film for a direct comparison with TiO_2 films, as this film showed a lower scattering than other ZnO films due to a change in electrodeposition, and thus also the maximum in absorbance was less affected by scattering, see Figure 55(b). For photoelectrochemical measurements (especially EIS), all ZnO films sensitized for 1 h are quite similar, thus any of the films can be used for comparison.

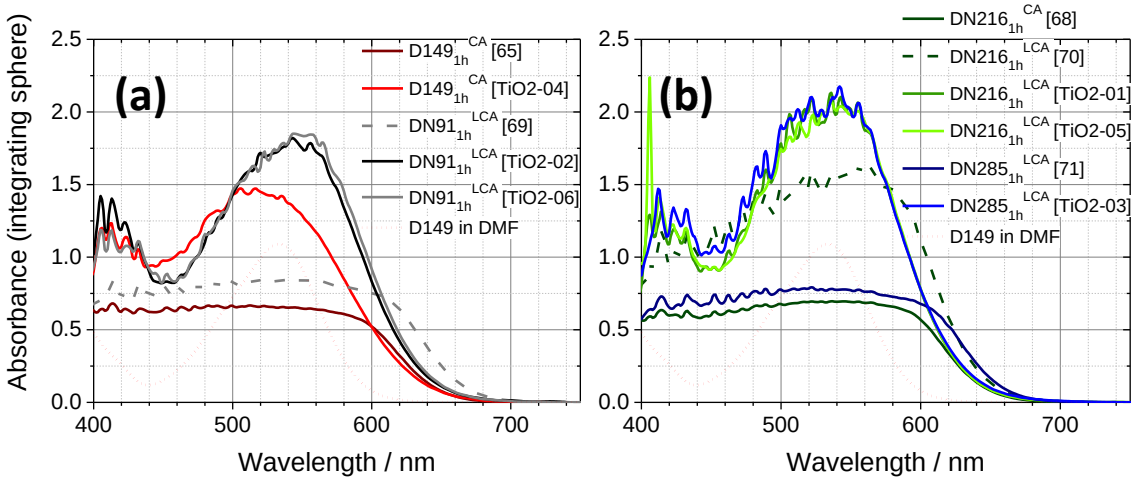

Figure 55 – Absorbance (measured with an integrating sphere) of indoline dyes (a) D149, DN91, (b) DN216 and DN285 adsorbed to TiO_2 or ZnO films, with a sensitization time of 1 h. The absorbance of non-sensitized films was subtracted from the absorbance of the sensitized films. Lighter colors indicate adsorption on TiO_2 films, while darker colors indicate adsorption on ZnO films, according to the legends. Films sensitized by the same sensitization procedure and of the same material are also differentiated by the color, see legend. A solution spectrum of D149 dissolved in dimethylformamide is indicated by a dotted line.

From the broadening of the absorbance spectra from D149 over DN216 and DN285 to DN91 it can be supposed that the least amount of sensitizer is adsorbed for D149, and the most for DN91. As the normalized spectra in Figure 56, p. 140 almost overlap for the different sensitizers, it is concluded that (different from ZnO) the four sensitizers show a similar aggregation tendency, and thus the broadening of the spectra is caused by the amount of dye molecules and not by aggregation. The larger amount of adsorbed DN91 molecules compared to DN216 and DN285 is explained by the smaller molecular size due to a shorter alkyl spacer at the second anchor group. For DN285 the increasing length compared to DN216 does not influence the absorbance. The smallest dye D149 however shows the narrowest absorption band, and thus probably the least amount of dye adsorbed. It has to be noted, however, that

the shape of the spectrum is different for D149, which can affect the interpretation of the band width. The different shape of the spectrum, which was also observed for 1 min sensitization of ZnO films (Figure 20, p. 69), could either be caused by a different arrangement of D149 molecules on the semiconductor surface due to the presence of only one anchor group, or due to a different dye-coadsorbate competition for the weaker bound D149 compared to the double-anchor dyes.

Less dye is absorbed on the TiO_2 films than on ZnO films even though the TiO_2 films are thicker than ZnO films by around 3 µm, as the spectra are narrower (absorbance around 650 nm considered, where the absorbance is least affected by a different scattering), and rather a higher than a lower aggregation is observed in the normalized spectra in Figure 56, p. 140. The cause of the lower amount of adsorbed dye is probably a lower inner surface area than for ZnO, where pores are in a range of a single molecule, compared to pores of several nanometer diameter for ~25 nm TiO_2 particles. The aggregation or arrangement of the molecules on TiO_2 is also slightly different from ZnO (see the normalized spectra in Figure 56, p. 140), possibly due to the different surface termination of a sintered TiO_2 film and a solution-processed ZnO film, and thus a slightly different binding on the different surfaces.

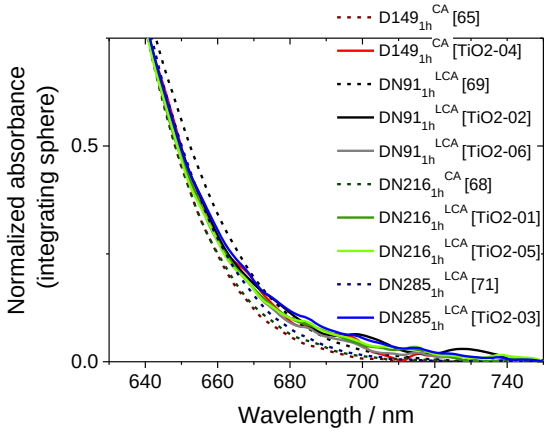

Figure 56 – Absorbance of sensitized TiO_2 and ZnO films from Figure 55, normalized to the absorbance at 630 nm. For the designation of the different films see Figure 55 and the legend.

6.2 Current-voltage characteristics of TiO_2-based DSCs

DSCs were prepared from TiO_2 films sensitized for 1 h with different indoline dyes and a coadsorbate. Two cells, cells [TiO2-01] and [TiO2-05], were sensitized with the same sensitization procedure to study reproducibility of the cell preparation. In one of the two cells sensitized with DN91 a different electrolyte was applied, which is often used as electrolyte for TiO_2 cells sensitized with a Ruthenium-based dye, coded by "iodolyte" in the cell name. As for IV-curves at AM1.5 illumination the cell parameters changed, with a very large change after a longer illumination, the changes during or after illumination and the changes observed for the different dyes will be discussed separately below.

Changes in IV characteristics of TiO_2-based cells upon intense illumination

IV-curves of differently sensitized TiO_2 films measured directly after preparation are compared with the IV-curves after an illumination for more than 1 h (mostly after EIS measurements) with AM1.5, see Figure 57. For all cells, a large increase in I_{SC} by a factor of 2 is observed after illumination (see also Table 13), while the V_{OC} decreases by ~100 mV for most cells. The FF decreases for most cell during the storage in the dark, which overall leads to a considerable increase of the power conversion efficiency by an absolute value of ca. 1%, e.g. from 2.65% to 3.88% (not from 2.65% to 2.68%). For some cells this increase is achieved already for shorter illumination times, and longer illumination again decreases η, mainly due to a further decrease in V_{OC}, as I_{SC} remained approximately constant. To a much smaller extent, a similar change upon intense illumination was observed for TiO_2 films (compare [127] and section **9.1.2**), which was attributed to an increase in cell temperature and probably also to a change in the trap distribution. For TiO_2, this behavior was reported before by several groups in the literature, for different dyes and electrolytes. The cause of such a marked change in the photoelectrochemical behavior of TiO_2-based cells was found to be a downward shift in the conduction band edge[261,262,263,264], caused probably by the ultraviolet part of the illuminated light [265,265,266]. For the cells in the present work, a change in I_{SC} and V_{OC} was even observed when the cells were illuminated only for the time of measurement of one IV-curve (several seconds), and left in the dark directly after the measurement of the illuminated IV-curve (which for ZnO-based cells leads to unchanged cell parameters due to the stable cell temperature), which indicates that the changes for TiO_2 are not (only) due to a change in the temperature. A change in E_c for the TiO_2.based cells will be discussed further below in the context of C_μ.

For the cells in this work, the change slowly reversed for longer storage times in the dark, however the initial cell values were not restored even after several days (not shown). For TiO_2 sensitized with D149 the decrease in V_{OC} upon long illumination with AM1.5 is larger than for other dyes, for which a light-induced dye desorption could be responsible, as D149 does not contain a second anchor group and

thus a desorption is more probable. By eye, a lighter color of the TiO_2 film [TiO2-04] was observed after EIS at AM1.5, which indicates a desorption of dye molecules into the electrolyte, however only aggregated dye molecules are probably desorbed, as a desorption of actively injecting dye molecules would also lead to a decrease in I_{SC} which is not observed for cell $D149_{1h}^{CA}$.

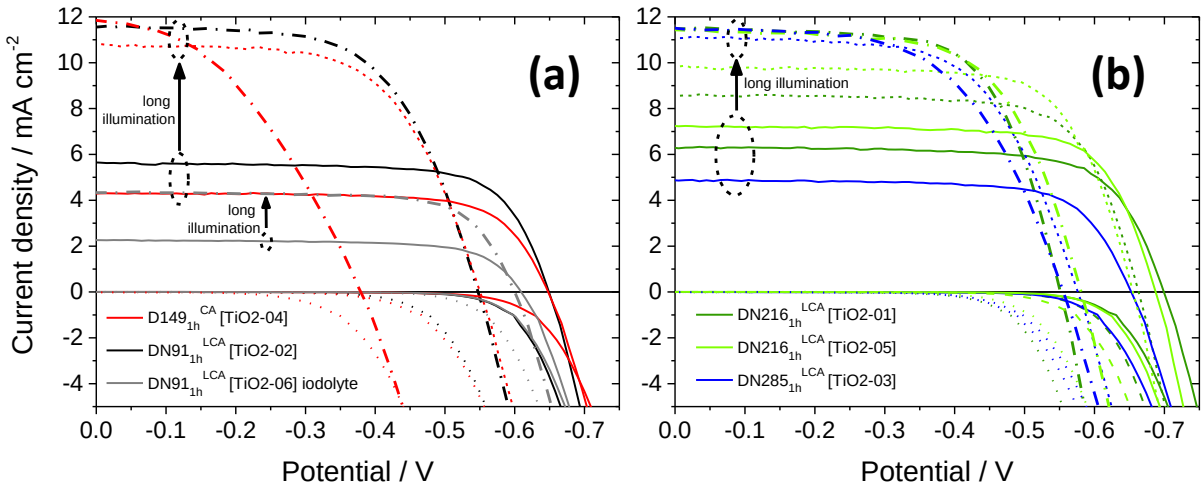

Figure 57 – Current-voltage curves of TiO_2-based DSCs sensitized with different dyes following different illumination conditions. Curves with only negative currents are dark IV-curves, while positive currents indicate measurements at simulated sunlight (AM1.5) of 100 mW cm^{-2} intensity. Full lines indicate first IV-curves after cell assembly, dashed lines indicate IV-curves after longer illumination with AM1.5 light (maximum efficiency), and dash-dotted lines indicate measurements after EIS at AM1.5, i.e. long illumination with AM1.5 light. IV-curves for ZnO films sensitized by the same sensitization procedure can be compared in Figure 23(c).

Comparison of differently sensitized TiO_2-based cells

The changes of the VI-curves gradually become slower with increasing illumination time, and thus for a comparison of the influence of the sensitizer dyes on cell values and a comparison with ZnO-based cells, measurements after a longer illumination are used. For TiO_2-based cells sensitized with different indoline dyes and filled with the same electrolyte, I_{SC} is very similar, even though the absorbance showed an increased amount of adsorbed dyes for DN91, and a decreased absorbance for D149 (compared to DN216 and DN285). It could be that the different absorbance is compensated by a respective aggregation, and the combined effects like dye amount and aggregation or a different position of E_c compensate each other and lead to similar values of I_{SC}. However the aggregation was very similar for all TiO_2 films, which makes a different explanation more probable explanation, i.e. that I_{SC} is limited by a limited transport through the electrolyte, which will be similar for the nanoparticulate TiO_2 films. Compared to literature values of indoline sensitized TiO_2-based cells, the values in the present work reach η of up to about 4.5%, which is about half the value obtained for the indoline dyes D149 (9.03% [119]) or D205 (9.40% [11]) adsorbed to TiO_2 films. Because the films in the present work were prepared with about half the film thickness used in the references, and no additional scattering layer of larger particles was applied, these values are quite comparable to literature values.

Table 13 – Cell values determined from IV-curves shown in Figure 57. As illumination with AM1.5 light changes the cell characteristics, the values for more than one IV-curve are shown for each cell, typically values from the first IV-curve, from the IV-curve with the highest efficiency (after longer illumination), and after long illumination during EIS at AM1.5 light.

Film	Comment	I_{sc}	V_{oc}	FF	Efficiency
		[mA cm^{-2}]	[V]		[%]
TiO_2 films					
$D149_{1h}^{CA}$ [TiO2-04]	first IV-curve	4.30	-0.648	0.72	**2.01**
	after longer illumination	10.82	-0.550	0.62	**3.64**
	after longer illumination *	11.79	-0.379	0.41	**1.83**
$DN91_{1h}^{LCA}$ [TiO2-02]	first IV-curve	5.64	-0.649	0.73	**2.65**
	after longer illumination *	11.56	-0.547	0.61	**3.88**
$DN91_{1h}^{LCA}$ [TiO2-06] iodolyte	first IV-curve	2.26	-0.609	0.71	**0.98**
	after longer illumination *	4.36	-0.600	0.73	**1.89**
$DN216_{1h}^{LCA}$ [TiO2-01]	first IV-curve	6.27	-0.699	0.73	**3.16**
	after longer illumination	8.56	-0.663	0.73	**4.08**
	after long illumination *	11.48	-0.551	0.67	**4.18**
$DN216_{1h}^{LCA}$ [TiO2-05]	first IV-curve	7.23	-0.688	0.74	**3.65**
	after longer illumination	9.83	-0.655	0.71	**4.54**
	after longer illumination *	11.34	-0.581	0.65	**4.22**
$DN285_{1h}^{LCA}$ [TiO2-03]	first IV-curve	4.95	-0.653	0.73	**2.32**
	after longer illumination *	11.75	-0.555	0.58	**3.73**
	after longer illumination	11.27	-0.576	0.62	**4.03**

* The marked IV-measurements were performed after EIS measurements at AM1.5 illumination.

IV-curves for ZnO-based cells, sensitized also for 1 h with a coadsorbate, can be found in Figure 23(c), p. 74, and in Figure 39, p. 110. Due to the lower scattering, film [70] is supposed to be more comparable to the (also less scattering) TiO_2 films, and will mostly be compared with the TiO_2-based cells. All cell values are quite similar for the two best cells [70] and [TiO2-05], sensitized with DN216, even though they are prepared from different semiconductor films. Other cells show either a lower I_{SC} or a higher V_{OC} for both ZnO- and TiO_2-based cells, which results in smaller η.

I_{SC} for cell [TiO2-06], which was filled by a different electrolyte, reaches only about half of I_{SC} for a cell sensitized by the same dye but with a different electrolyte applied, cell [TiO2-02]. V_{OC} directly after preparation is smaller for the cell with varied electrolyte, but with light-soaking, V_{OC} decreases by a smaller amount than any other cell. The applied electrolyte contains additives that usually cause a downward shift in the conduction band edge for TiO_2[xxvi], which would explain the low initial V_{OC}. As will be shown by more detailed analysis below, such a shift is observed for this cell, compared to cells where electrolyte without special additives is used. However a lower E_c should result in an increase in

[xxvi] For example the addition of Li^+ to the electrolyte shifts E_c to lower energies [4], also because of intercalation of lithium ions into the TiO_2 film. Intercalation would "pin" E_c to one value, which is consistent with the very small shift in E_c observed upon long illumination for cell {TiO2-06]. For ZnO, the addition of Li^+ to the electrolyte influences E_c to a much lower extent because of a lower ϵ_r.

I_{SC}, as observed for all other cells upon long illumination. As this is not observed for cell [TiO2-06], either recombination is increased by the adsorption of additional electrolyte species to the TiO_2 surface, and/or dye regeneration is less efficient for the different electrolyte (probably different redox level or reorganization energy).

The incident photon-to-current conversion efficiency (IPCE) for the TiO_2 cells (Figure 58(a)) was measured after almost no light soaking, so that the IPCE corresponds to IV-curves directly after preparation with low values of I_{SC}. Thus the maximum IPCE (~0.4) found for TiO_2-based DSCs reaches only about half of the values achieved for ZnO-based solar cells. The shape of the IPCE curves is different for TiO_2, probably due to the narrower absorption as observed in Figure 55, p. 139.

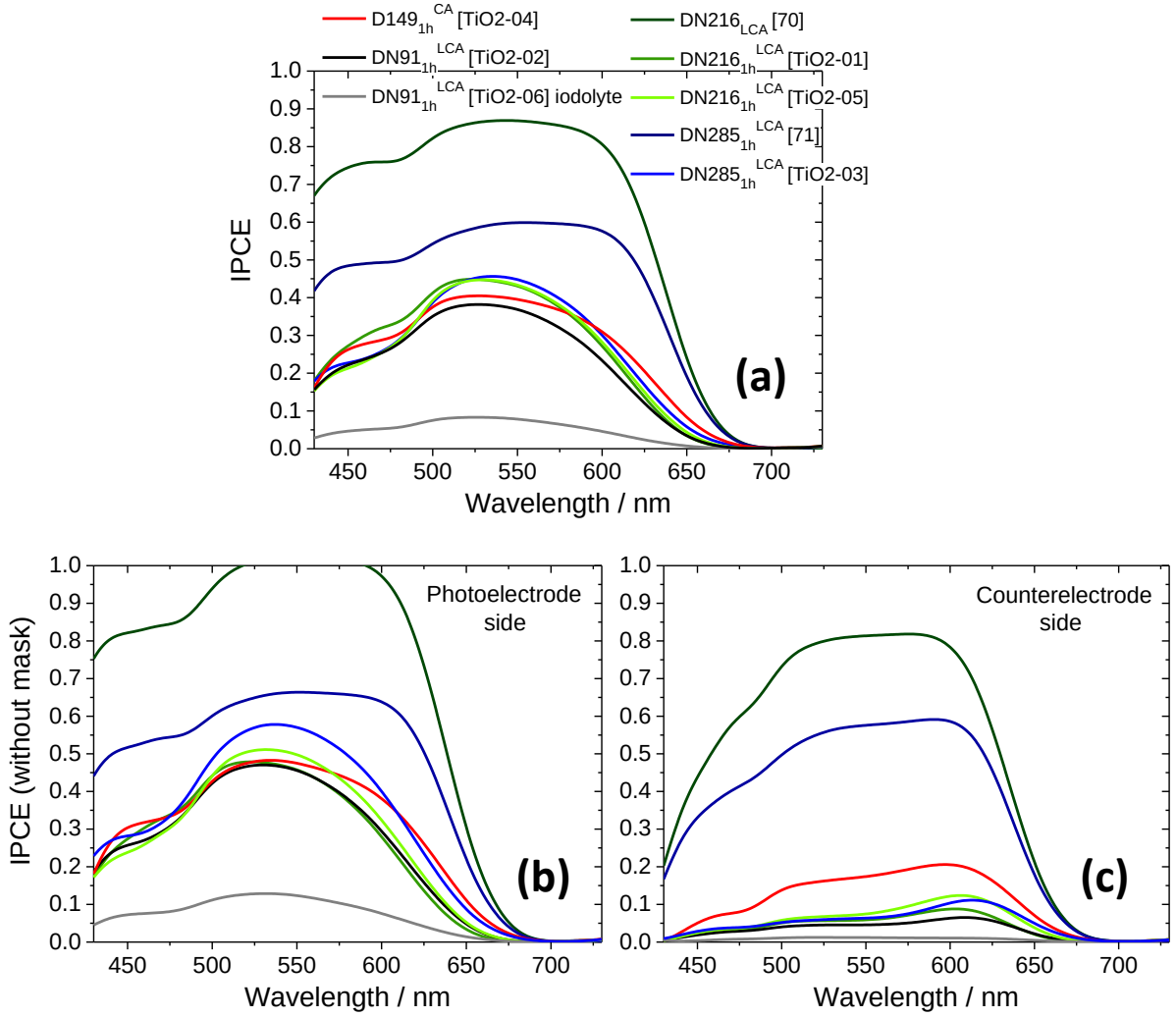

Figure 58 – (a) IPCE for TiO_2- and ZnO-based DSCs sensitized with different indoline dyes and a coadsorbate for 1 h. Lighter colors indicate TiO_2 films, while darker colors indicate ZnO films, see also the legend for exact designation of the cells. IPCE measured without mask is shown for an illumination from (b) the photoelectrode side and (c) the counterelectrode side, see text for details.

To obtain more information about the different factors influencing IPCE (equation **(9)**), measurements were performed with illumination from either the photoelectrode or the counterelectrode side, Figure 58(b,c). Both measurements were measured without mask to avoid possible influences of a different mask position. When differences are found for the comparison of IPCE from different sides, they can be attributed either to a change in injection or collection efficiency [267,268,216]. A smaller IPCE for a measurement from the counter electrode side at wavelengths around 500 nm is attributed to the absorption of the electrolyte, however quite large differences are found also at the maximum of the IPCE.

For ZnO-based cells IPCE from the counterelectrode side, decreases by about 20% compared to the measurement from the photoelectrode side, while for TiO_2 the decrease amounts to around 60% for $D149_{1h}^{CA}$ [TiO2-04], and around 80% for other TiO_2-based cells. Thus the collection efficiency and/or the injection efficiency are lower for TiO_2-based cells compared to ZnO-based cells. Because of the low illumination intensity during IPCE measurements and the findings from IV-curves, a low injection efficiency is designated as the main cause, however also a decreased collection efficiency is possible, as bulk TiO_2 has a lower conductivity than bulk ZnO [269].

6.3 Trap distribution and electron transport in TiO_2-based solar cells

The detailed photoelectrochemical characterization which was performed for ZnO-based solar cells, including illumination at different illumination (conditions see section **9.1.3**) was also performed for TiO_2-based DSCs. The change in the TiO_2 cell parameters following AM1.5 illumination is even larger than it was observed for ZnO-based cells, which adds particular value to the different measurement conditions.

The chemical capacitance C_μ of the TiO_2-based DSCs, determined from EIS is shown in Figure 59(a), together with one ZnO-based cell for comparison. To study the cells before the large change induced by the high-intensity illumination, EIS measurements at red LED light and in the dark were performed directly following cell preparation. For measurements at AM1.5, a marked change in the curvature of C_μ determined is observed at more negative voltage, where the measurement begins. This curvature is attributed to the adaptation of the TiO_2 cells to the intense illumination, which also includes a change in C_μ. Thus, the C_μ curve determined from measurements at AM1.5 begins at about the same value of C_μ as determined from EIS measurements in the dark, both measurements starting from a similar state of the cells. For C_μ ~10^{-4} F cm^{-2}, all measurements show a linear slope, indicating that in this region adaptation to the intense illumination no longer occurs, and C_{SC} does not yet influence the overall capacitance.

Changes in C_μ for intense illumination

For all TiO_2-based cells C_μ measured in the dark or at red LED illumination (Figure 59(a)) is very similar for a respective cell, however for measurements at AM1.5 C_μ is shifted by at least 300 mV to lower energies. This shift in E_c is in line with the discussion for the increase in I_{SC} and literature findings, discussed in the previous section. A part of this change in C_μ at different illumination conditions is caused by the increased temperature of the cell (similar to ZnO films discussed in section **3.3.1**). An increase of the temperature from room temperature to more than 50 °C (similar increase expected in this work) led to a downward shift of the conduction band edge by about 60 mV for DSCs sensitized with ruthenium dyes [270]. A downward shift in the conduction band edge is often observed for TiO_2 in DSCs upon high-intensity illumination [261], also for a sensitization with different indoline dyes [263], however the changes in E_c were comparatively small, probably because an electrolyte additive was used in this reference. Different from the results in the present work, the authors report an increase of V_{OC} because of decreased recombination upon high-intensity illumination.

Differences in E_c for the different cells have to be discussed with Figure 59(b), where C_μ was corrected by the relative total trap density $N_t/N_{t,ref}$ (see Table 14, determined from Figure 88, p. 196).

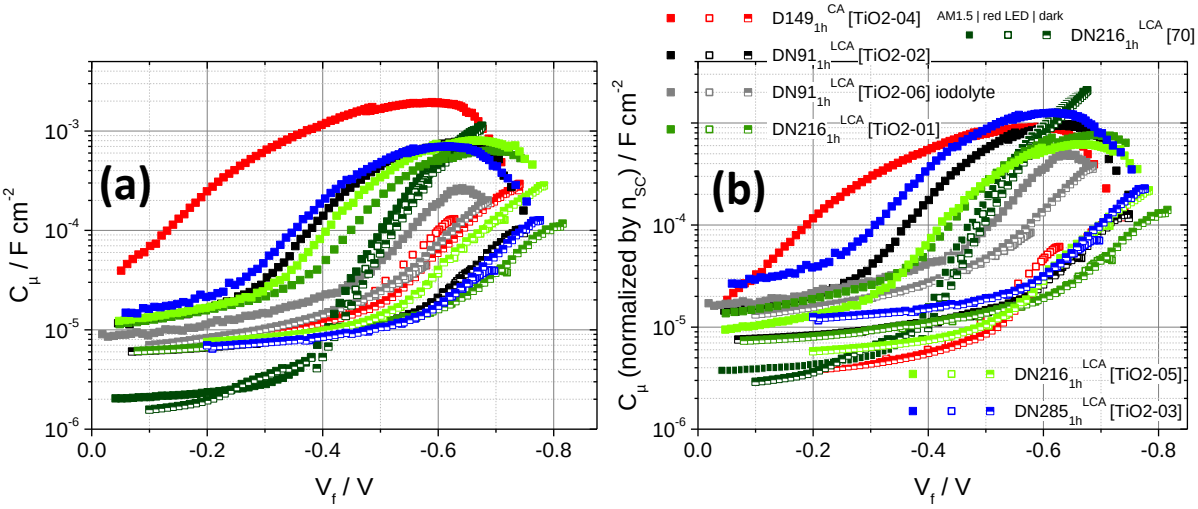

Figure 59 – Chemical capacitance C_μ of TiO_2-based DSCs, with one ZnO-based DSC for comparison (dark-blue color). (a) C_μ values as determined from EIS measurements, and (b) C_μ values normalized by the ratio of n_{SC} with respect to a reference cell [61], see also Table 14. Measurements at AM1.5 illumination are indicated by filled symbols, measurements at red LED illumination and at V_{OC} are indicated by open symbols, and measurements in the dark are indicated by half-filled symbols. The color codes the sensitizing dye, according to the legend in (b). Comparable cells based on ZnO films are plotted in Figure 29(e,f).

The different electrolyte applied in cell [TiO2-06] led to the lowest E_c for measurements during at red LED illumination, however also only a small shift to lower energies is observed for AM1.5 illumination.

Comparison of C_μ for different cells

C_μ of the TiO_2-based DSCs show a lower slope than ZnO-based DSCs, compare also values of α in Table 14, which means an faster increase of the DOS with increasing voltage, see Figure 92, p. 199. Also C_{SC} (at voltages near 0 V) is higher for the TiO_2-based cells than for ZnO-based cells, mainly due to a higher relative permittivity of TiO_2 of $\epsilon_r = 35$ [271]. A simulation of C_μ (similar to simulation in section **3.3.1**) revealed that also a higher density of states in the space-charge region N_{SC} has to be applied to achieve a good match of the curves, which is an indication that the charge density in TiO_2 is higher than in ZnO [xxvii]. As α is relatively similar for all TiO_2-based DSCs and for the different illumination conditions, $\Delta E_c/q$ was determined from Figure 59(b), see Table 15.

[xxvii] The simulation was performed for one TiO_2 cell, [TiO2-01], however the match of the simulated and measured curve was not as good as for ZnO-based cells due to technical problems with the transition of the different capacitances. Thus the simulation is not shown, and only trends from this simulation are regarded as relevant. When N_t was increased for the simulation of C_μ (as it is not clear whether N_t changes for the different illumination), the capacitance shifted to higher absolute voltages (in the wrong direction), which is a slight

The downward shift of the conduction band edge amounts to more than 200 mV for the TiO_2-based cells sensitized with DN216, and to more than 400 mV for the cell sensitized with D149, if the assumption is true that the total trap density does not change with the illumination conditions [xxviii]. In the literature, using the ruthenium dye N719 [272], a shift in the conduction band edge by 100 mV was found to change the injection half time by a factor of about 2 for the ruthenium dye N719, and the current density depended linearly on the injection quantum yield. A similar difference is observed for cells [TiO2-02] and [TiO2-06], for which the sensitization process was identical. The difference in the position of the conduction band edge for no or low intensity illumination is around 120 mV (see also Table 15), and I_{SC} for cells without previous illumination shows a difference of more than a factor 2.

Table 14 – Cell values of TiO_2-based DSCs determined from EIS measurements, V_{OC} vs. intensity measurements and from current transients.

Value	**$N_t/N_{t,ref}$**	**α**	**α**	**α**	**β**	**β**	**β**	**β**
Illumination (measurement) **Sample**	red LED (current transient)	AM1.5 (EIS)	red LED (EIS)	dark (EIS)	AM1.5 (EIS)	red LED (EIS)	dark (EIS)	red LED (V_{OC} vs. intensity)
D149 + CA (1 h) [TiO2-04]	2.13	0.35	0.32	0.33	0.42	0.81	0.76	0.75
DN91 + LCA (1 h) [TiO2-02]	0.80	0.43	0.28	0.31	0.49	0.84	0.85	0.74
DN91 + LCA (1 h) iodolyte [TiO2-06]	0.53	0.41	0.24	0.32	0.71	0.87	0.82	0.73
DN216 + LCA (1 h) [TiO2-01]	0.83	0.41	0.27	0.30	0.53	0.84	0.81	0.75
DN216 + LCA (1 h) [TiO2-05]	1.30	0.43	0.33	0.37	0.51	0.82	0.77	0.81
DN285 + LCA (1 h) [TiO2-03]	0.56	0.38	0.26	0.32	0.46	0.90	0.86	0.83

Transport properties of TiO_2 films

According to the procedure described in section **1.3.3.4**, the transport times τ_{tr} were determined from IMPS measurements and plotted against I_{SC} density in Figure 60(a). Without correction by the total trap density N_t, values of τ_{tr} for TiO_2-based cells scatter over a relatively large time range of almost one order of magnitude. With application of the correction with $N_t/N_{t,ref}$ from Table 14 (TiO_2) and Table 7 (ZnO), the curves group closer for each of the semiconductors, with lower transport times for the electrodeposited ZnO films. This is very likely caused by a higher electron conductivity inside the ZnO matrix compared to TiO_2 films, either because of a lower electron conductivity as observed already for the bulk materials [4], or because of different grain boundaries for a network of nanoparticles (TiO_2; worse particle interconnection) or nanocrystals (ZnO; better particle interconnection).

support of the supposition that N_t remains constant for a given cell. V_{bi} decreased from the dark to the AM1.5 measurement for the TiO_2-based cell, while for ZnO-based cells the opposite behavior was observed.

[xxviii] A lower total trap density would lead to a higher position of the conduction band edge, but is not expected for the measurements. A measurement of n_{SC} after long illumination of TiO_2-based cells, or the measurement of n_{SC} at varied AM1.5 intensity would answer the question whether or not N_t changes at different illumination conditions.

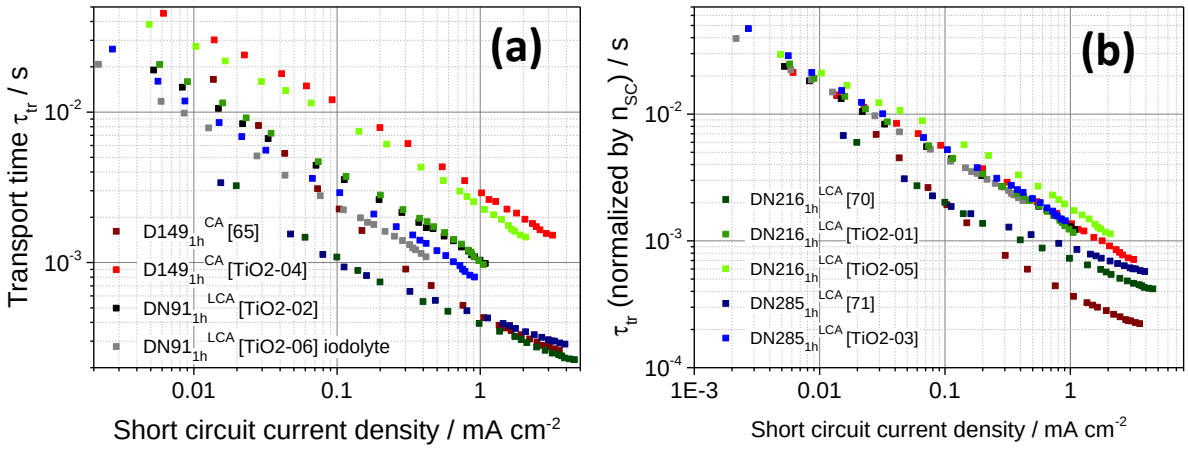

Figure 60 – Transport times for TiO_2- and ZnO-based DSCs sensitized for 1 h with different indoline dyes and a coadsorbate. (a) τ_{tr} as determined from the IMPS measurements, and (b) τ_{tr} corrected by $N_t/N_{t,ref}$ from Table 14 (TiO_2) and Table 7 (ZnO). The different symbol colors indicate different indoline sensitizers according to the legends. Darker colors indicate ZnO-based cells and lighter colors indicate TiO_2-based cells.

The collection efficiency η_{col} was calculated for the TiO_2-based cells from IMVS and IMPS measurements at red LED illumination according to the procedure described in section **1.3.3.4** and applied also in section **3.3.3**, see the comparison with ZnO-based cells in Figure 61. For most of the cells, η_{col} exceeds 95% over the complete intensity range, indicating that the collection efficiency does not limit the performance for these cells, even though the measurements are performed at red LED illumination and thus at a high E_c for TiO_2-based cells. However, for cells [TiO2-04] and [TiO2-05] the efficiency decreases to values of around 85% for intermediate intensities, indicating that loss of charge could occur during the transfer of electrons to the back contact at red LED illumination. As the power conversion efficiency of these cells does not differ from the other TiO_2-based cells, η_{col} is yet efficient enough to ensure the collection of sufficient charges.

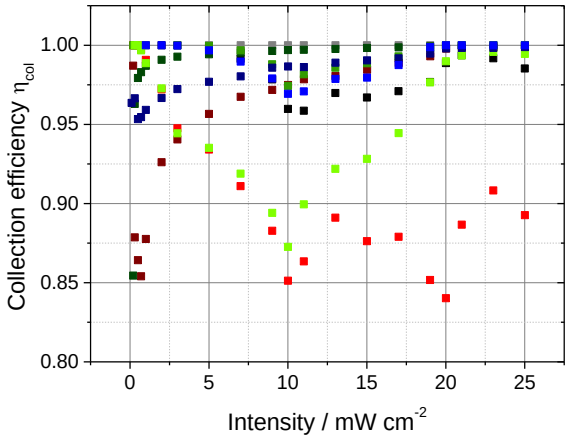

Figure 61 – Collection efficiency η_{col} of TiO_2- and ZnO-based DSCs sensitized with different indoline sensitizers and a coadsorbate for 1 h. The different symbol colors indicate the different sensitizer used, according to the legend. Lighter colors indicate TiO_2-based cells, while darker colors indicate ZnO-based cells (also according to the legends). The values of η_{col} were determined from IMVS and IMPS measurements at red LED illumination.

Another interesting point is that the collection efficiency is equal to unity over the complete illumination range for cell [TiO2-06], for which a downward shift of E_c was found due to a different electrolyte even at low illumination intensities. A high η_{col} for this cell is thus in line with the perception of the energetics inside the DSC, as a lower conduction band edge leads to a higher trap density in the semiconductor at a given energy, which increases the enhances conduction for electrons in the semiconductor. At AM1.5 illumination the other TiO_2-based cells show a lower E_c, and as suggested by the high η_{col} of cell [TiO2-06], also a higher collection efficiency after longer illumination with AM1.5 than determined here for red LED illumination.

6.4 Recombination in TiO_2-based DSCs

R_{rec} vs. V_f for TiO_2-based cells is shown in Figure 62, and one ZnO-based cell is compared in the same graph. A relatively similar R_{rec} is observed for the different semiconductors, especially at AM1.5 illumination, where the cells showed comparable performances. R_{rec} from measurements in the dark is more different for TiO_2-based cells, where a flattening of the slope is observed for low absolute voltages. Very similar observations are also made for τ_n vs. V_f in Figure 63(a). The seemingly lower R_{rec} for cell [TiO2-04] is probably affected by the very large change in E_c, which influences the slope of C_μ even to voltages around -0.2 V. From the differential slope of R_{rec} in Figure 62(a), β was determined, see Table 14. Also β from V_{OC} vs. illumination intensities, Figure 62(b), is included in the table. The higher β for low illumination intensities or for dark measurements indicates that recombination in non-illuminated ZnO occurs more via the conduction band than via surface traps. β is overall lower for TiO_2 than for similarly sensitized ZnO-based cells under identical illumination conditions. For the comparatively similar V_{OC}, the change in β is also reflected in a lower FF of the TiO_2-based cells after longer illumination, compared to the ZnO cells at AM1.5 illumination.

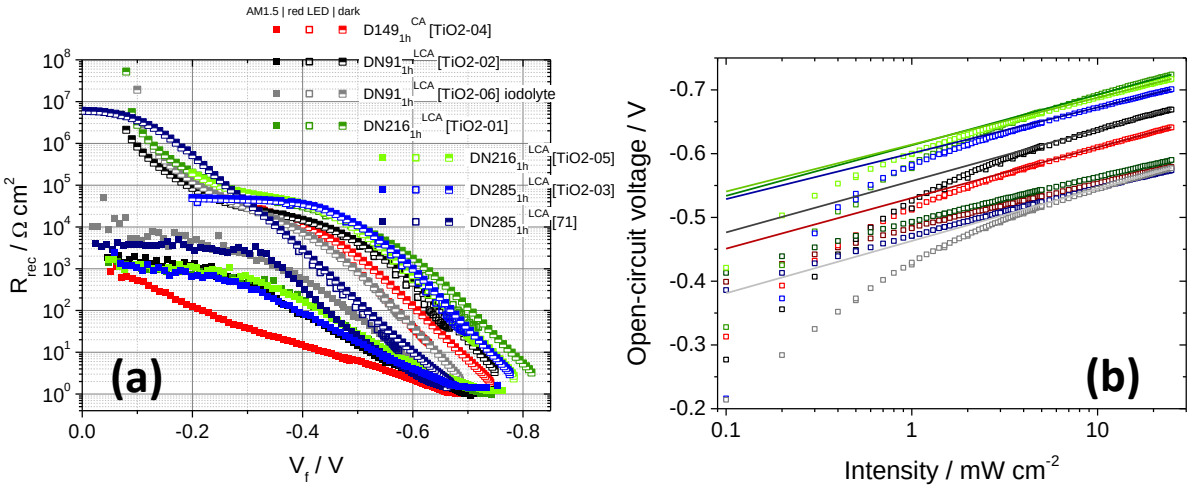

Figure 62 – (a) Recombination resistance of TiO_2-based DSCs sensitized with indoline dyes and a coadsorbate, and one ZnO-based solar cell for comparison (dark blue). Filled symbols indicate measurements at AM1.5 illumination, open symbols indicate measurements at red LED illumination and V_{OC}, and half-filled symbols indicate measurements in the dark. The sensitizing indoline dye is indicated by the symbol color, according to the legend. More curves of ZnO cells with similar sensitization are plotted in Figure 94(c). V_{OC} vs. illumination intensity (red LED) for TiO_2- and ZnO-based DSCs sensitized for 1 h with indoline dyes and a coadsorbate. The different indoline dyes are indicated by different colors, according to the legends. TiO_2 cells are indicated by lighter colors, and ZnO-based cells are indicated by darker colors, also according to the legends. The measurements were taken in two stages, leading to a transfer of the curves at intermediate light intensities.

The bending of V_{OC} at lower intensities for TiO_2-based cells as observed in Figure 62(b) has been explained for two different cases in the literature: An insufficiently blocking behavior of the compact blocking layer below the porous layer [65,203], or a bending of the curve at low intensities due to deep surface states were found as reasons [65]. The second is observed for most measurements of (TiO_2) based cells, but mostly at very low illumination intensities or at voltages between 0 V and about -0.3 V, and then an inflection point is observed in this range. The photon flux achieved in the

measurements in the present work ranges from about $3 \cdot 10^{14}$ to $8 \cdot 10^{16}$ cm^{-2} s^{-1}, the lower bound being about 4 orders of magnitude higher than the lowest values reported in [65]. This means that for the measurements in this work, it cannot be distinguished from only the V_{OC} vs. intensity measurements whether the bending at low intensities is simply coming from deep surface trap states observed often in TiO_2, or by an inefficient blocking layer. However, also the effective electron lifetime from open-circuit voltage decay (OCVD) measurements gives insight into the quality of the blocking layer, see Figure 63(b). The linear behavior of almost all TiO_2-based solar cells at low absolute voltages indicate an efficient blocking layer, even though lower τ_n are found than for ZnO-based cells. The difference between TiO_2- and ZnO-based cells could stem from a difference in the blocking layer, as electrodeposited ZnO blocking layers block recombination via the substrate very efficiently [123,130]. However for the usual working conditions of DSCs (maximum power point) the differences in the blocking layer are not relevant, as all TiO_2-based cells show very similar cell characteristics in IV-curves. Also cell [TiO2-03], for which lower lifetimes and no linear behavior for voltages near 0 V indicate that the blocking layer does not work as efficiently, shows cell parameters similar to other TiO_2-based cells [xxix].

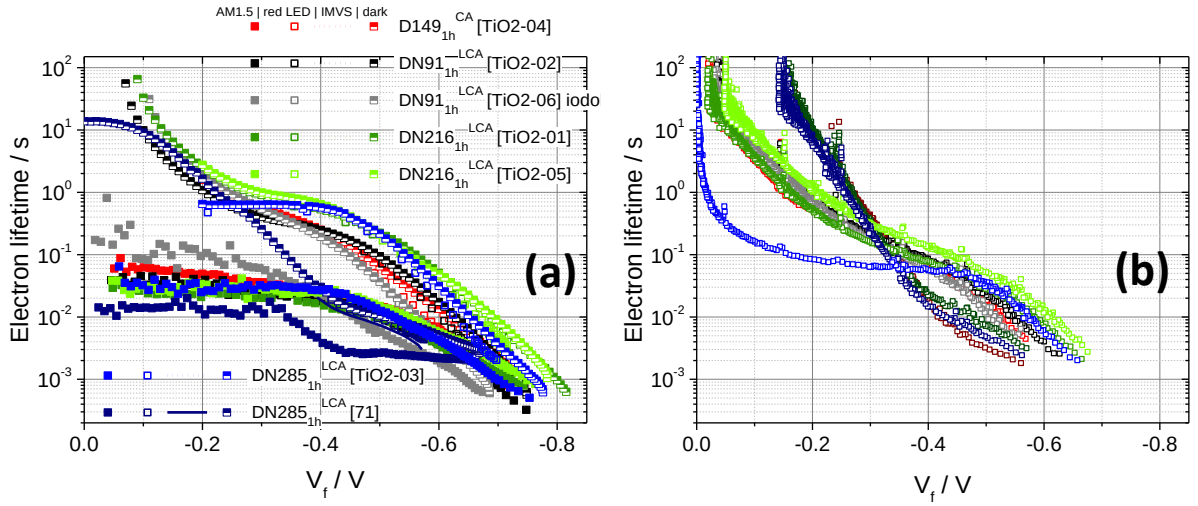

Figure 63 – Electron lifetimes τ_n for TiO_2- and ZnO-based solar cells sensitized for 1 h with different indoline dyes and a coadsorbate. The different colors of the symbols and lines indicate the different sensitizer dyes, darker colors indicating ZnO-based cells and lighter colors indicating TiO_2-based cells, according to the legends. Electron lifetimes were determined from (a) EIS and IMVS measurements and from (b) open-circuit voltage decay curves. Measurements performed at AM1.5 illumination are indicated by filled symbols, measurements performed at red LED illumination are indicated by open symbols or lines, and measurements in the dark are indicated by half-filled symbols.

[xxix] During PEC measurements of the TiO_2- and ZnO-based cells in this chapter (sensitization for 1 h) the V_{OC} decreased comparably slowly for most of the cells when the shutter was closed after the cells were illuminated with AM1.5 light. Only for cell [TiO2-03] V_{OC} reached 0 V within a few seconds, while for ZnO-based cells the decrease to 0 V took several minutes. This slow decrease of V_{OC} (partially also observed during OCVD measurements) indicates that the cells sensitized for 1 h show a very low recombination in the dark, except for a slight short-circuiting of cell [TiO2-03] by a substrate-electrolyte contact as discussed in the main text.

Comparing again the V_{OC} vs. intensity measurements in Figure 62(b) for cell [TiO2-03], a slightly steeper decrease of V_{OC} with decreasing light intensity for low intensities compared to other TiO_2-based cells can be assigned to a less blocking behavior of the blocking layer. On the other hand the deviation of V_{OC} vs. intensity from linear behavior at low intensities can be mainly ascribed to additional recombination via deep trap states, as also cells with a good blocking layer show this deviation.

To discuss the influence of the dye and coadsorbate on recombination in more detail, influences from the position of the conduction band edge have to be removed from the recombination resistance. A correction of the voltage by the conduction band edge shift $\Delta E_c/q$ (determined from the chemical capacitance C_μ) would be possible for the TiO_2-based cells, as α does not vary by a large amount. However, to enable a comparison with the ZnO-based DSCs (and to account at least partially for the changes induced by the intense illumination), the correction for the shift of the conduction band edge was performed as a plot of R_{rec} or τ_n vs. DOS, see Figure 64. At high DOS, the TiO_2-based DSCs measured at AM1.5 show an artifact (two values of R_{rec} or τ_n for the same DOS) due to the adaptation of the cells to the high-intensity illumination, see also the discussion of the chemical capacitance above. For measurements at less intense illumination, R_{rec} and τ_n shows a steeper decrease with the DOS, so that at very low DOS the curves of the different illumination conditions cross and R_{rec} and τ_n is higher for the measurement at red LED illumination or in the dark. However, over a large range of the DOS, and especially in a range of the usual working point of the solar cell, the recombination is lower for the measurements at AM1.5 illumination than for measurements in the dark or at red LED illumination (at the same DOS). Thus at the same position of the conduction band edge cells at AM1.5 illumination (or after longer illumination with AM1.5 light) block recombination more efficiently than cells without prior illumination or at low illumination intensity. The opposite behavior was found for ZnO-based cells (section **3.3.2**), where the recombination resistance at high-intensity illumination always lies below the values determined from measurements at red LED illumination or in the dark. For ZnO-based cells this difference was ascribed mainly to a lower regeneration efficiency under high-intensity illumination. The low recombination found for TiO_2-based cells under AM1.5 illumination suggests that regeneration is not limited as much as for electrodeposited ZnO, for example due to the very different pore structure (more open structure with larger pores for TiO_2). It has to be considered, however, that in principle recombination under illumination cannot be lower than recombination under illumination (all paths available for recombination in the dark are also available under illumination), and thus the increase in R_{rec} and τ_n is ascribed additionally to different trap states for the films under AM1.5 illumination, see also the discussion for recombination currents below. The measurements of TiO_2-based DSCs at red LED illumination lead to slightly lower R_{rec} values at the same DOS than measurements in the dark, similar to ZnO-based solar cells. Such lower R_{rec} is probably caused by recombination via oxidized dye molecules present under illumination, which is an indication of regeneration limitation even for low illumination intensities [255,257]. For cell [TiO2-06], for which the

electrolyte was varied, a low I_{SC} was observed compared to other cells, even though a lower E_c would suggest a high injection yield. This finding is explained by an considerably higher recombination especially at AM1.5 illumination, probably caused by a mediated recombination via adsorbed/intercalated electrolyte species, which cause the shift of E_c.

D149 shows a lower recombination than the other dyes when adsorbed to TiO_2, which is the opposite behavior from what was observed for a sensitization with ZnO, where the cell sensitized with D149 shows the lowest recombination resistance at the same DOS, compared to cells sensitized with DN216 and DN285 (see also Figure 33(c)). For TiO_2-based cells, either D149 with coadsorbate blocks the surface more effectively against recombination than the other two-anchored dyes with coadsorbate, or the changes which lead to a decreased recombination at a given DOS for AM1.5 illumination are more pronounced for cell [TiO2-04], which also showed the largest shift of E_c. For none of the illumination conditions a dependence of R_{rec} on the dye structure (or in particular the length of the alkyl spacer) is found, different from the observations for ZnO sensitized for 1 h, where a longer alkyl chain on the second anchor group lead to higher recombination resistances for the cells discussed in section **3.3.2**.

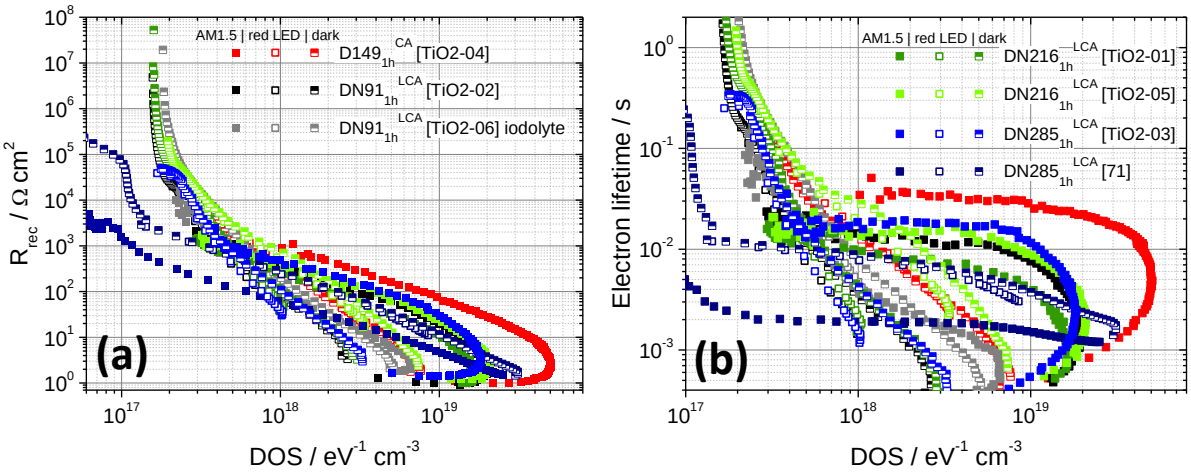

Figure 64 – (a) R_{rec} and (b) τ_n vs. the density of states for TiO_2-based DSCs sensitized with different indoline dyes and a coadsorbate; one ZnO-based cell is shown for comparison (dark blue symbols). The different indoline dyes are indicated by different colors according to the legend. Measurements at AM1.5 illumination are indicated by filled symbols, measurements at red LED illumination are indicated by open symbols, and measurements in the dark are indicated by half-filled symbols. Comparably sensitized ZnO-based solar cells are shown in Figure 33(c).

Recombination in the cells can also be discussed on the basis of recombination currents in the dark (I_{rec}^{dark}) and under illumination (I_{rec}^{light}), see Figure 65. All measurements (directly after preparation and after longer illumination) were corrected by ΔE_c relative to cell [TiO2-01] (measured in the dark) from an EIS measurement with a similar film condition, see also Table 15 for the shifts applied. I_{rec}^{dark} is always lower than I_{rec}^{light}, both for measurements without light soaking and for cells which were illuminated for a longer time with AM1.5 light before the measurements. This was also observed for the ZnO-based cells (discussed only for measurements without previous illumination, compare Figure

98, p. 205), and ascribed to additional recombination via the oxidized dye for IV-cells measured under illumination. The difference between I_{rec}^{light} and I_{rec}^{dark} is larger when the cells were subjected to longer illumination with AM1.5 light, which is an indication that more recombination via oxidized dye molecules occurs, and thus regeneration occurs less efficient, most likely because of a higher I_{SC} for measurements after light soaking. As the short-circuit current density is at least by a factor 2 higher for the cells after soaking with AM1.5 light, and thus depletion in the electrolyte is more probable. This difference is especially large for TiO_2 sensitized with D149, and the difference becomes smaller in the sequence D149 > DN285 > DN91 > DN216. The cell sensitized with D149 and a coadsorbate shows a larger difference of recombination current in the dark and under illumination also for measurements without previous illumination, indicating that regeneration is less efficient, or recombination a faster process for this dye-coadsorbate combination. For cell [TiO2-06], where a different electrolyte was applied, the difference between I_{rec}^{light} and I_{rec}^{dark} after soaking with AM1.5 light is very small, comparable to the difference in recombination current without previous illumination. This cell has a low I_{SC} (similar to I_{SC} before AM1.5 light soaking for the other TiO_2-based cells), and with the also low difference for the measurements without light soaking (also low I_{SC}) it can be concluded that below a certain short-circuit current density (about 8 mA cm^2) regeneration is comparably efficient, while for higher currents (about 10 mA cm^2) regeneration is less efficient, as observed for the measurements after light soaking, which showed high I_{SC}. For a very large change of cell parameters as observed for TiO_2-based cells in this work, the comparison above of the four different recombination currents is very important.

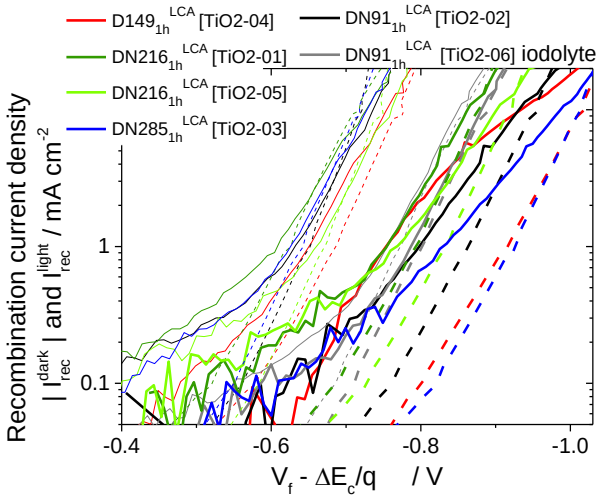

Figure 65 – Recombination current in the dark and under illumination for TiO_2-based DSCs sensitized with different indoline dyes and a coadsorbate. The different colors represent different sensitizers, according to the legends. Thin lines indicate IV-curves measured directly after solar cell preparation, while thick lines indicate measurements after longer illumination at AM1.5 light (during EIS). Dashed lines indicate recombination currents measured in the dark, while solid lines indicate measurements at AM1.5 illumination.

Table 15 – Shift of the conduction band edge and change in V_{OC} from different influences for TiO_2-based DSCs. The calculated change in V_{OC} is compared with the change in V_{OC} from IV-curves. Voltages are given in V. Negative voltage changes indicate a shift to less negative voltages (lower energy), while positive changes in the voltage indicate a shift to more negative voltages (higher energy).

		$\Delta E_c/q$ [a]	$\Delta E_c/q$ (2) [b]	$\Delta V_{OC}(\Delta I_{SC})$ [c]	$\Delta V_{OC}(I_{rec}^{light})$ [d]	$\Delta V_{OC,calc}$ [e]	$\Delta V_{OC}(IV)$ [f]
	Illumi-nation						
$D149_{1h}^{CA}$ [TiO2-04]	AM1.5	-0.575	-0.510	0.062	0.110	**-0.338**	**-0.269**
	red LED	-0.105	-0.040				
	dark	-0.065	-				
$DN91_{1h}^{LCA}$ [TiO2-02]	AM1.5	-0.393	-0.333	0.038	0.168	**-0.127**	**-0.102**
	red LED	-0.063	-0.003				
	dark	-0.060	-				
$DN91_{1h}^{LCA}$ [TiO2-06] iodolyte	AM1.5	-0.247	-0.067	0.024	0.032	**-0.011**	**-0.009**
	red LED	-0.167	+0.013				
	dark	-0.180	-				
$DN216_{1h}^{LCA}$ [TiO2-01]	AM1.5	-0.320	-0.320	0.030	0.142	**-0.148**	**-0.148**
	red LED	-0.007	-0.007				
	dark	0 (ref)	-				
$DN216_{1h}^{LCA}$ [TiO2-05]	AM1.5	-0.330	-0.275	0.023	0.124	**-0.128**	**-0.107**
	red LED	-0.055	0				
	dark	-0.055	-				
$DN285_{1h}^{LCA}$ [TiO2-03]	AM1.5	-0.445	-0.400	0.046	0.219	**-0.135**	**-0.077**
	red LED	-0.045	0				
	dark	-0.045					

[a] Shift in E_c relative to a reference measurement ([TiO-02] measured in the dark), determined at $C_\mu = 10^{-4}$ F cm^{-2}
[b] Shift in E_c relative to the respective measurement in the dark, determined at $C_\mu = 10^{-4}$ F cm^{-2}
[c] Determined after equation **(32)** relative to the respective dark measurement, with β from the AM1.5 measurement
[d] Determined at about 2 mA cm^{-2} after equation **(33)**
[e] Calculated after equation **(34)**
[f] Determined from IV-curves directly after preparation and after long illumination in Figure 57, p. 142

The different measurements further differentiate the changes observed for example in Figure 64. The direct comparison of e.g. R_{rec} at different illumination conditions would result in the conclusion that regeneration is more efficient during intense illumination, as R_{rec} is higher for this measurement. Such a comparison would however disregard possible changes in the recombination behavior by a different trap distribution (even though R_{rec} is plotted against the DOS), as for example recombination it influenced stronger by traps at the surface than by traps inside the film, however both types of traps cannot be distinguished in the DOS. The recombination current during IV-measurement at AM1.5 on the other hand is always compared to the current in the dark, and thus a reference is given [xxx]:

Similar to [17], the different influences on V_{OC} were calculated and added to a calculated difference in V_{OC}, see Table 15, where also V_{OC} as determined from IV-curves is listed. For cells [TiO2-01] and [TiO2-06] the calculated ΔV_{OC} vary from the actual ΔV_{OC} only about 2 mV, indicating that for these

[xxx] Probably such a reference would also be obtained for EIS measurements, if EIS measurements in the dark would be performed also directly following EIS at AM1.5, when the cell still shows a different E_c. EIS at AM1.5 without the influence of intense illumination however cannot be obtained, as the cell will always change during illumination with AM1.5, and thus the measurements will be changed.

cells the determination is valid in every point, and the chosen model well explains the observations. For cells [TiO2-02] and [TiO2-05], $\Delta V_{OC,calc}$ and ΔV_{OC}(IV) varies by more than 20 mV, which can be explained by a larger influence of recombination via oxidized dye molecules, as found from the recombination currents after longer illumination with AM1.5 light in Figure 65.

Cells [TiO2-03] and [TiO2-04] show an even larger influence of oxidized dye molecules on recombination, and both cells show also a larger deviation of $\Delta V_{OC,calc}$ from ΔV_{OC}(IV). Also Rudolph et al. [17] ascribed the larger difference in the calculated values of ΔV_{OC} to recombination via oxidized dye molecules. Even though recombination via oxidized dyes is in principle considered with $\Delta V_{OC}\left(I_{rec}^{light}\right)$, the difference in the slope (for curves where large influences of the oxidized dye are found compared to recombination in the dark) makes a decision where it should be determined rather arbitrary. Usually values of are determined at more negative voltages, as the slopes of the recombination currents are more similar there, but on the other hand, as seen from the comparison of theoretical and real change in V_{OC}, the influences from oxidized dye are stronger for voltages between 0 and V_{OC}, where I_{SC} is high.

Overall, the validity of the model described by Rudolph et al. [17] was also confirmed for TiO_2-based cells sensitized with indoline dyes, however a method or certain rules for a determination of $\Delta V_{OC}\left(I_{rec}^{light}\right)$ should be defined, so that also the influences of decreased regeneration efficiency for higher I_{SC} are included in the evaluation.

6.5 Conclusions for TiO_2-based DSCs

DSCs were prepared from nanoparticulate TiO_2 films and sensitized with the same indoline sensitizers which were used for the sensitization of electrodeposited ZnO films in chapters **3**, **4** and **5**. The sensitization yielded intense-colored films, however with a lower amount of dyes adsorbed than for ZnO films, probably due to a smaller inner surface area of the nanoparticulate TiO_2 films. For the more reproducible semiconductor surface of TiO_2 films (compared to electrodeposited ZnO), the amount of adsorbed dye roughly followed the size of the sensitizer molecules, as more DN91 was adsorbed compared to a sensitization with dyes with a longer alkyl spacer. The scattering of the TiO_2 films is smaller than for most ZnO films because of uniform, comparatively large TiO_2 particles.

Current-voltage characteristics of the TiO_2-based cells revealed that a light soaking with high-intensity AM1.5 illumination increased the power conversion efficiency of the cells through a large increase of the short-circuit current density. During the light soaking, the FF and the open-circuit voltage decreased. Impedance spectroscopy results revealed that these changes were effected by a shift of the conduction band edge to lower energies by more than 200 mV for most of the TiO_2-based cells. After light-soaking, the cell parameters of most of the TiO_2-based cells were comparable to the parameters determined for ZnO-based cells using the same sensitization procedure. As E_c shifted by the largest amount for D149 (containing only one carboxylic anchor group), gradually leading to a decrease in η because of a decrease in V_{OC}, it is possible that two anchor groups are not only beneficial for a higher stability, but for TiO_2 the stronger influence on the electronic structure of the film (stronger "pinning" of the conduction band edge) could also lead to a better stability against intense illumination.

The distribution of trap states was found to be steeper (lower α) for the TiO_2 cells compared to ZnO-based cells. The transport times were found to be higher for TiO_2-based cells, which was attributed to a lower conductivity due to grain boundaries and an overall lower crystallinity compared to electrodeposited ZnO films.

The recombination of the TiO_2-based solar cells at the same density of states was blocked more efficiently for the measurements at AM1.5 illumination, which can be attributed to a change of trap states, e.g. the saturation of surface traps and thus a decreased amount of recombination centers. From comparison of recombination currents under different conditions, it was concluded that also for TiO_2 the regeneration efficiency decreases at intense illumination. The decrease in regeneration efficiency and thus an increased recombination via oxidized dye molecules is higher, when the cell was illuminated with intense light before the measurement, as I_{SC} is increased by a lower E_c, and thus the diffusion limit of the electrolyte is reached. No dependence of the trap distribution or the recombination on the dye structure was observed.

7 Sensitization of ZnO by non-indoline dyes

In the previous chapters, results of cells were discussed that were sensitized with indoline dyes with or without coadsorbates. This class of dyes had proven quite appropriate for the sensitization of ZnO. However, there are many other classes of dyes available, which may be equally good or even better. Three different dye classes were chosen as a comparison for indoline dyes, 1. **triphenylamine dyes** with a comparatively narrow absorbance at shorter wavelength, which could be used for co-sensitization, and which already showed good efficiencies in TiO_2-based DSCs, 2. two dyes from a classic pigment group, the **perylene dyes**, which were synthesized with additional groups to enhance solubility and allow covalent binding to the semiconductor, and 3. **phthalocyanine dyes** which were synthesized with different anchor groups and spacers. The dye classes and the specific dyes are discussed in more detail in section **1.2**, and the chemical structure is shown in the respective context. Some of the dyes were adsorbed to ZnO that was not yet optimized it its deposition procedure, other dyes were adsorbed to films deposited with the standardized routine as ZnO-based films discussed in previous chapters. As the differences in deposition lead also to different characteristics of the films or cells, the discussion is performed separately.

7.1 Triphenylamine and perylene dyes

Cells in this chapter were prepared and characterized differently, and, thus, these cells are discussed separately. The procedure was different in the following points:

- Some of the ZnO films were deposited on a different FTO substrate, and with a 50 µM concentration of the structure directing agent EosinY (instead of the standard 75 µM), see also the appendix for exact deposition conditions. [xxxi]
- Up to 4 cells were prepared from one deposition by cutting the substrate, to reduce the differences caused by deposition.
- A different electrolyte was used (1 M TPAI and 0.1 M I_2 in a 4:1 mixture of ethylene carbonate and acetonitrile), usually giving a higher photovoltage [136].
- For films that do not scatter light by a large amount, the absorbance was measured in a transmission setup without integrating sphere.

[xxxi] Many differences in cell or film preparation are owing to a not yet standardized deposition/cell preparation procedure. The process of standardization is described in more detail in [123].

Similar to the phthalocyanine and perylene dyes discussed in the previous section, also triphenylamine dyes need a longer adsorption time than indoline dyes to achieve a sufficient coloration of the ZnO films. The absorbance of electrodeposited ZnO films sensitized with the triphenylamine dyes WD-2, WD-3 and TPA-B1, the perylene dyes J102 and J109, and (as a reference) the indoline dye D149 + cholic acid (CA) are shown in Figure 66. For comparison, also the absorbance of the respective dyes in solution are shown. For the triphenylamine dyes in Figure 66(a) it can be seen that the absorbance maxima on the ZnO film [21] are close to the maxima in solution (absorbance maximum λ_{max} in solution: λ_{max}(TPA-B1 in ethanol) = 421 nm [154]; λ_{max}(WD-2 in dichloromethane) = 473 nm and λ_{max}(WD3 in dichloromethane) = 468 nm [155] – for all three dyes a shape of absorbance in solution similar to the shape of D149 in solution was observed in these references). For TPA-B1 adsorbed on TiO_2 films, the maximum is slightly red-shifted compared to the absorbance spectrum in solution [154]. Upon first sight it seems that also for film [24] the maximum of the absorption of the dye on ZnO is red-shifted compared to the solution spectrum. When the spectra of this slightly more scattering film are measured in the integrating sphere setup (Figure 66(c)), it can be concluded that this shift is only an artifact originating in a stronger scattering of shorter-wavelength incident light. Comparing the two dyes WD-2 and WD-3, more molecules of WD-3 adsorb to the ZnO surface, in particular when the higher extinction coefficient of WD-2 compared to WD-3 is considered [155]. The even higher extinction coefficient of TPA-B1 [154] and a similar absorbance in the maximum suggests that less molecules of TPA-B1 than of the other triphenylamine dyes are adsorbed to the ZnO surface. The shape of the absorbance of D149 adsorbed for 10 min resembles the shape of D149 adsorbed for 1 min to the standard ZnO (section **3.1**) or adsorbed for 1 h to TiO_2 films (section **6.1**), indicating that the D149 molecules adsorb in a different amount but in a similar manner to the differently prepared semiconductor substrates.

The perylene dyes J102 and J109 adsorbed on ZnO show a broadened spectrum compared to the absorbance in solution. This indicates intermolecular interaction, which is not very high for film [23], but is strong for the (differently deposited) films [24] and [27]. For film [23], it is possible to distinguish the different transitions of the dye even for the dye adsorbed to the ZnO surface. A film discussed in more detail in the following, [54], is added for comparison and shows a strong aggregation similar to film [27] ([54] was also deposited with 75 µM EosinY). This indicates that a different deposition also influences the adsorption of the perylene dyes, possibly by a different preferred crystal orientation of the exposed ZnO surface or a different concentration of surface groups like –OH. The higher extinction coefficient of J109 compared to J102 [137] and a similar absorption found for [23-1] and [23-2] suggests that less molecules were adsorbed for the dye J109. The addition of a coadsorbate to the adsorption solution (film [23-3]) leads to even less adsorbed J109 because available adsorption sites are blocked by coadsorbate molecules. A slight difference in the relative peak heights could stem from less aggregated molecules due to the coadsorbate. For films [24] and [27], almost no difference can be found in the absorption spectrum for the different sensitization

procedures, as all parts of the films sensitized with perylene dyes exceed the detection limit of the spectrometer. From the absorbance onset (coming from higher wavelengths) it can be surmised that either film [27-3] has the least amount of dye adsorbed and film [27-1] the largest amount, or the aggregation is the highest for film [27-1] and lowest for film [27-3].

From the differently sensitized parts of the films, DSCs were fabricated and characterized by current voltage curves shown in Figure 67, together with the IV-curves of a perylene-sensitized cell [54], which will be discussed in more detail in the following section. The relatively low currents and fill factors even of D149-sensitized cells compared to the values in the previous chapters reflect that the cell preparation was not yet optimized.

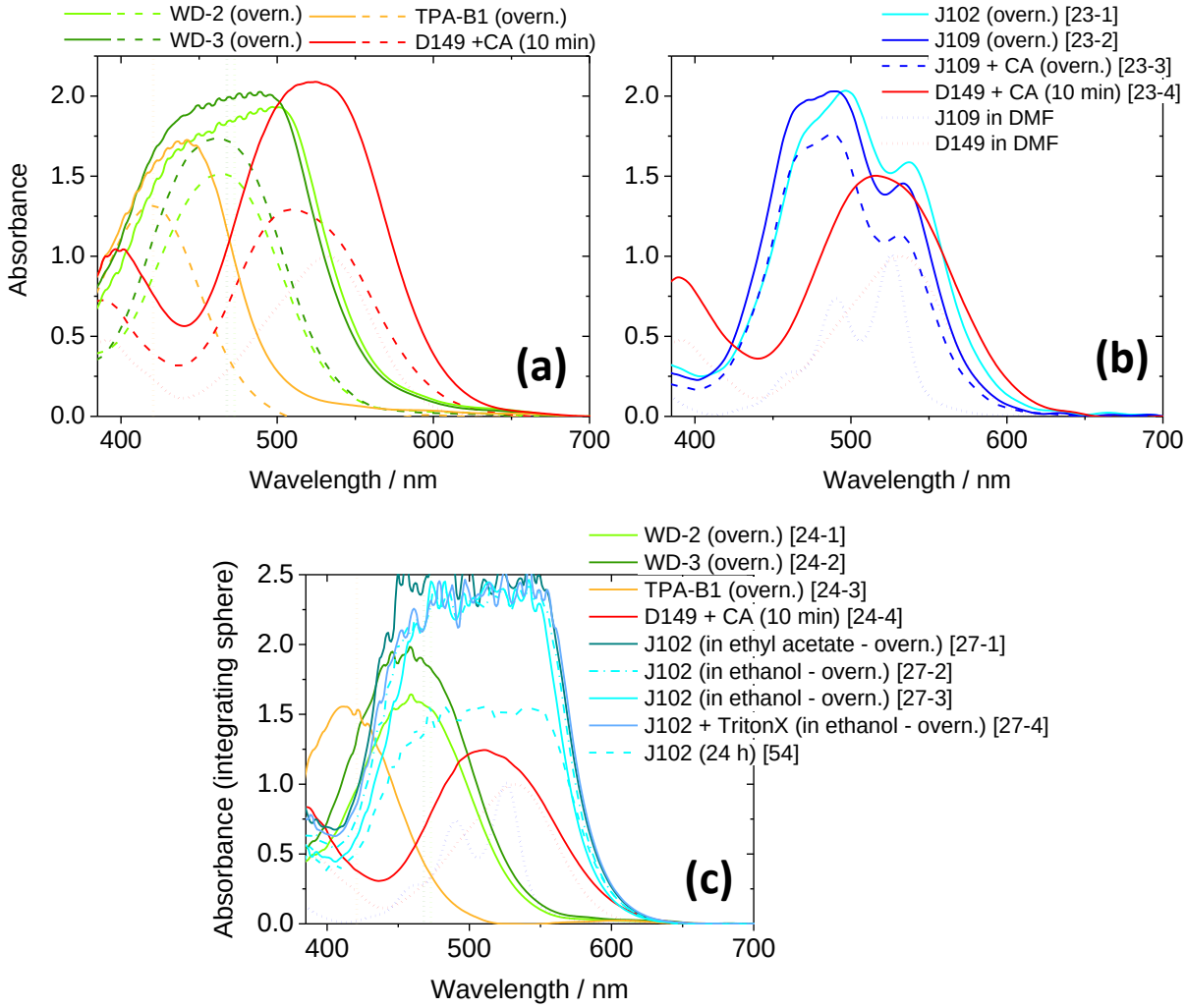

Figure 66 – Absorption spectra of dyes adsorbed on ZnO, with subtracted absorption of the ZnO films. (a) Absorbance of triphenylamine dyes and D149 + cholic acid as a reference. Cells were prepared from two different substrates, indicated by solid (film [21]) and dashed lines (film [24]; see also legend of Figure 67 for exact designation of the cells). The spectrum of D149 dissolved in DMF is indicated by a red dotted line, absorption maxima of WD-2, WD-3 and TPA-B1 are indicated by a vertical dotted line (same color as the respective dye adsorbed on ZnO). (b) Absorbance of perylene dyes and D149 + cholic acid as a reference. The spectrum of D149 and J109 dissolved in DMF is also shown and indicated by a dotted line of the respective color. (c) Absorbance (measured with an integrating sphere) of triphenylamine and perylene dyes, with D149 + cholic acid as a reference. Film [54] from the previous section is shown for comparison. Dotted lines give the absorbance or the maximum of the respective dyes in solution (see also (a) and (b)), see text for references.

Comparing the perylene and triphenylamine sensitizers with D149 for each film, it can be observed that D149 always exceeds the other dyes in terms of the short-circuit current density I_{SC} and thus also in the efficiency (see also Table 16 for a list of the cell values). For the triphenylamine dyes, this inferior I_{SC} is caused especially by the low absorbance of the dyes, as these dyes absorb less in the visible range due to a shift of the spectrum to lower wavelengths. TPA-B1, which has an absorbance most strongly shifted to higher energies, consequently should have the lowest I_{SC} for the triphenylamine sensitized DSCs (disregarding cell [21-1], where a depression at intermediate voltages indicates a larger problem of the cell). This is the case for films [21] and [24], where however the very similar values of WD-3 and TPA-B1 indicate that TPA-B1 converts light more efficiently to current than WD-3. Similar currents for WD-3 and TPA-B1 were also reached for TiO_2-based cells in the literature [154,155]. Comparing I_{SC} for WD-2 and WD-3, lower currents were found for the cell sensitized with WD-3, similar to the findings for TiO_2-based cells [155].

The open-circuit voltage V_{OC} of the cells sensitized with WD-2 and WD-3 is higher than V_{OC} of the D149-sensitized cells for each film. The lower dark current at more negative voltages for these cells indicates that the increase in V_{OC} is achieved by a decreased recombination. WD-2- and WD-3-molecules contain bulky donor groups, which can additionally shield the ZnO surface against the electrolyte, and thus decrease the recombination of electrons with oxidized electrolyte species. D149 and TPA-B1 have one or no bulky group, which leads to a more efficient tunneling of electrons from the ZnO surface to empty states in the electrolyte, and therefore to a higher recombination. Thus D149- and TPA-B1-sensitized cells show a similar shape and height of the dark current. A different trend of the V_{OC} was observed for TiO_2-based cells sensitized with these triphenylamine dyes in the literature, the differences probably being caused by the generally different cell preparation. The s-shape of the IV-curves of the [24] cells can be caused by surface states which enhance recombination in a certain voltage range [17], see also the EIS results for this film further below. It could be that the regeneration efficiency is lower for e.g. WD-3 than for TPA-B1 because of the bulky groups of the former, which would give another explanation why the currents are similar even though they are supposed to be lower for TPA-B1 from the absorbance, and the IPCE is only slightly higher in the maximum for TPA-B1.

For the perylene sensitized cells, V_{OC}, I_{SC} and the power conversion efficiency are very low, comparable to cell [54] (characterized in the previous section). From the findings there it can be concluded that this low efficiency is mainly caused by an inefficient injection due to a too low position of the LUMO of the dyes. Thus none of the perylene sensitized cells reaches efficiencies above 0.15%, and the highest I_{SC} only about 0.6 mA cm^{-2}. For cells built from film [27], the strong aggregation seen in the absorbance probably is the cause for even lower current. This effect possibly also leads to the lower I_{SC} for cell [27-1] compared to cell [23-1], which was sensitized by the same sensitization procedure, but the aggregation was considerably smaller for the differently deposited film [23].

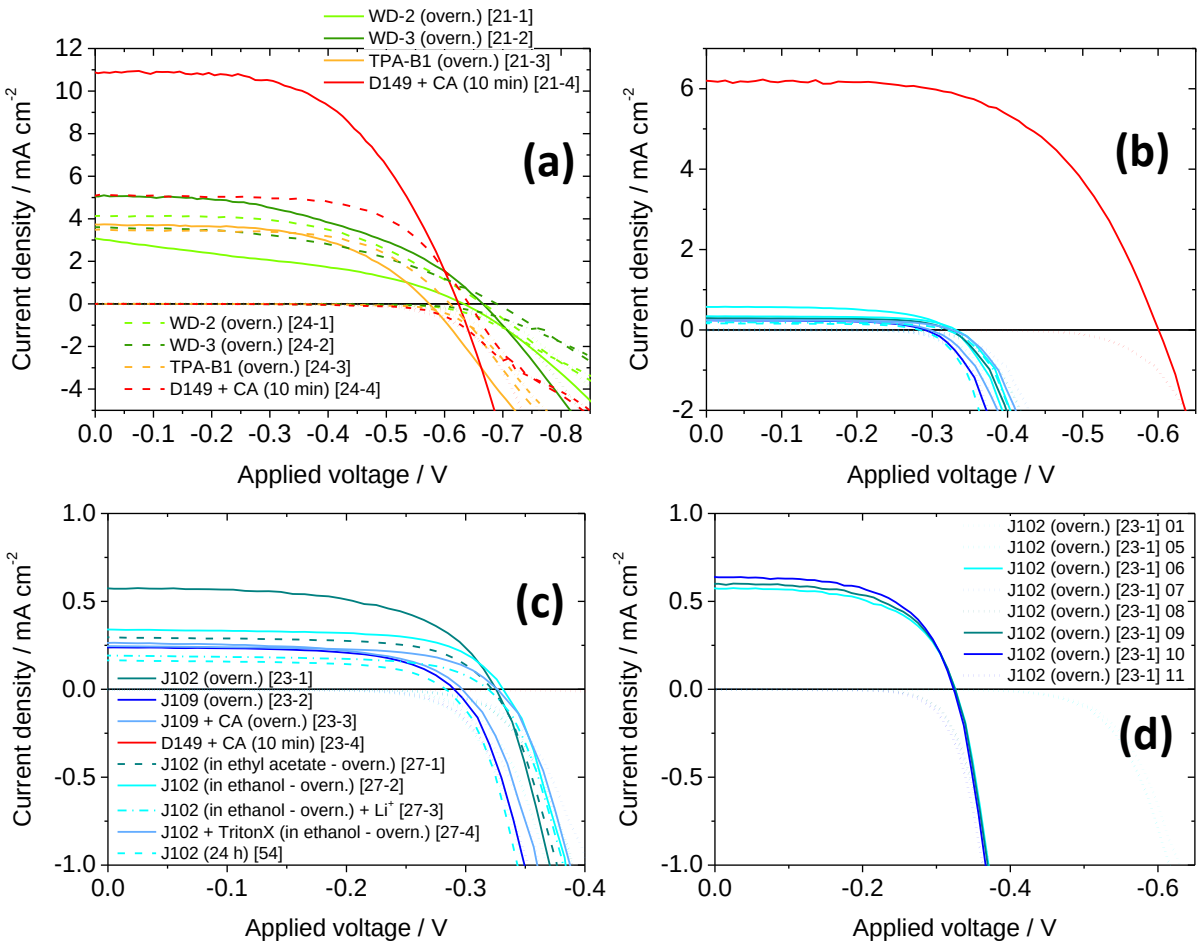

Figure 67 – Current-voltage curves of cells sensitized with triphenylamine and perylene dyes, and D149 + cholic acid as a reference. IV-curves measured in the dark are indicated by dotted curves (and dash-dotted for (a)). IV-curves measured in the dark are indicated mostly by solid lines, see also the legends for exact designation. Also note the different scaling of the axes. (a) Cells sensitized with triphenylamine dyes and D149. Two different films, [21] and [24], were used for cell preparation. (b) Cells sensitized with perylene dyes and D149. (c) Same as (b), but only perylene-sensitized cells are shown. (d) Subsequently measured IV-curves of cell [23-1], the last numbers of the legend indicating the sequence of the measured IV-curve (some IV-curves are left out for clarity).

For the cells sensitized with J109, the addition of a coadsorbate does not decrease the low current, even though less dye molecules are adsorbed. None of the variations of either the electrolyte (added Lithium salt for cell [27-3]) or the adsorption procedures induced an enhancement of the cells sensitized with perylene dyes.

An interesting effect could be observed for film [23] sensitized with perylene dyes, see Figure 67(d). When an IV-curve in the dark was measured directly after the preparation, or after a longer storage without high-intensity illumination (IV-curve 01 in Figure 67(d), measured after several days of storage in the dark), the dark current was low up to relatively high absolute voltages. Very similar IV-curves are observed even if several dark IV-curves were measured sequentially, see IV-curve 05. A subsequently measured IV-curve under AM1.5 illumination showed the typical V_{OC} around -0.3 V. The following IV-curve in the dark, IV-curve 07, shows an onset of the dark current shifted by about 200 mV to less negative voltages compared to the first IV-curve, the recombination behavior of this

curve fitting nicely to the illuminated curve. All following IV-curves show a similar shape and onset of the dark-current. I_{SC} slightly increases with the number of measured curves for the illuminated IV-curves, as the cell warms during illumination and E_c is shifted to lower energies, see also [127] and section **9.1.2**. This behavior of the dark current after storage in the dark and the change upon high-intensity illumination was observed for all perylene cells prepared from film [23], while for cells from film [23] sensitized with D149, and for cells prepared from film [27] the dark current did not change before and after illumination with 1 sun. As it was supposed from the different absorbance of the perylene dyes on the films [23] and [27], more dye molecules adsorb on film [27] probably due to a different surface structure, and less adsorbed dyes on film [23] could lead to more possibilities for movement of the dye molecules. As the recombination is suppressed for the first IV-curves in the dark for cells prepared from film [23], it can be surmised that the dye is adsorbed on the ZnO surface in a manner which allows less recombination (e.g. flat on the surface, or interlocking alkyl chains of different molecules). Upon dye excitation at AM1.5 illumination, the dye molecules could change their arrangement on the ZnO surface, thus leading to a higher recombination. A switching of the position of similar molecules adsorbed on a TiO_2 surface was observed during atomic force microscopy [138,139], providing some support for such hypothesis. The change in recombination however would have to be very large, if this would be the only cause for the lower dark currents.

Table 16 – Cell parameters of DSCs sensitized with triphenylamine and perylene dyes and D149, determined from IV-curves in Figure 67.

Value	**I_{sc}**	**V_{oc}**	**FF**	**Efficiency**
Unit	mA cm^{-2}	V		%
Sample				
WD-2 (overn.) [21-1]	3.06	0.62	0.36	**0.70**
WD-3 (overn.) [21-2]	5.05	0.67	0.46	**1.55**
TPA-B1 (overn.) [21-3]	3.73	0.56	0.56	**1.18**
D149 + CA (10 min) [21-4]	10.84	0.61	0.56	**3.75**
WD-2 (overn.) [24-1]	4.14	0.66	0.52	**1.42**
WD-3 (overn.) [24-2]	3.61	0.69	0.46	**1.14**
TPA-B1 (overn.) [24-3]	3.50	0.61	0.61	**1.30**
D149 + CA (10 min) [24-4]	5.15	0.64	0.63	**2.06**
J102 (overn.) [23-1]	0.61	0.32	0.64	**0.15**
J109 (overn.) [23-2]	0.30	0.28	0.64	**0.07**
J109 + CA (overn.) [23-3]	0.28	0.28	0.66	**0.07**
D149 + CA (10 min) [23-4]	7.19	0.62	0.64	**3.53**
J102 (in ethyl acetate – overn.) [27-1]	0.27	0.32	0.70	**0.06**
J102 (in ethanol – overn.) [27-2]	0.34	0.33	0.67	**0.07**
J102 (in ethanol – overn.) + Li^+ [27-3]	0.19	0.32	0.64	**0.04**
J102 + TritonX (in ethanol – overn.) [27-4]	0.25	0.32	0.67	**0.05**

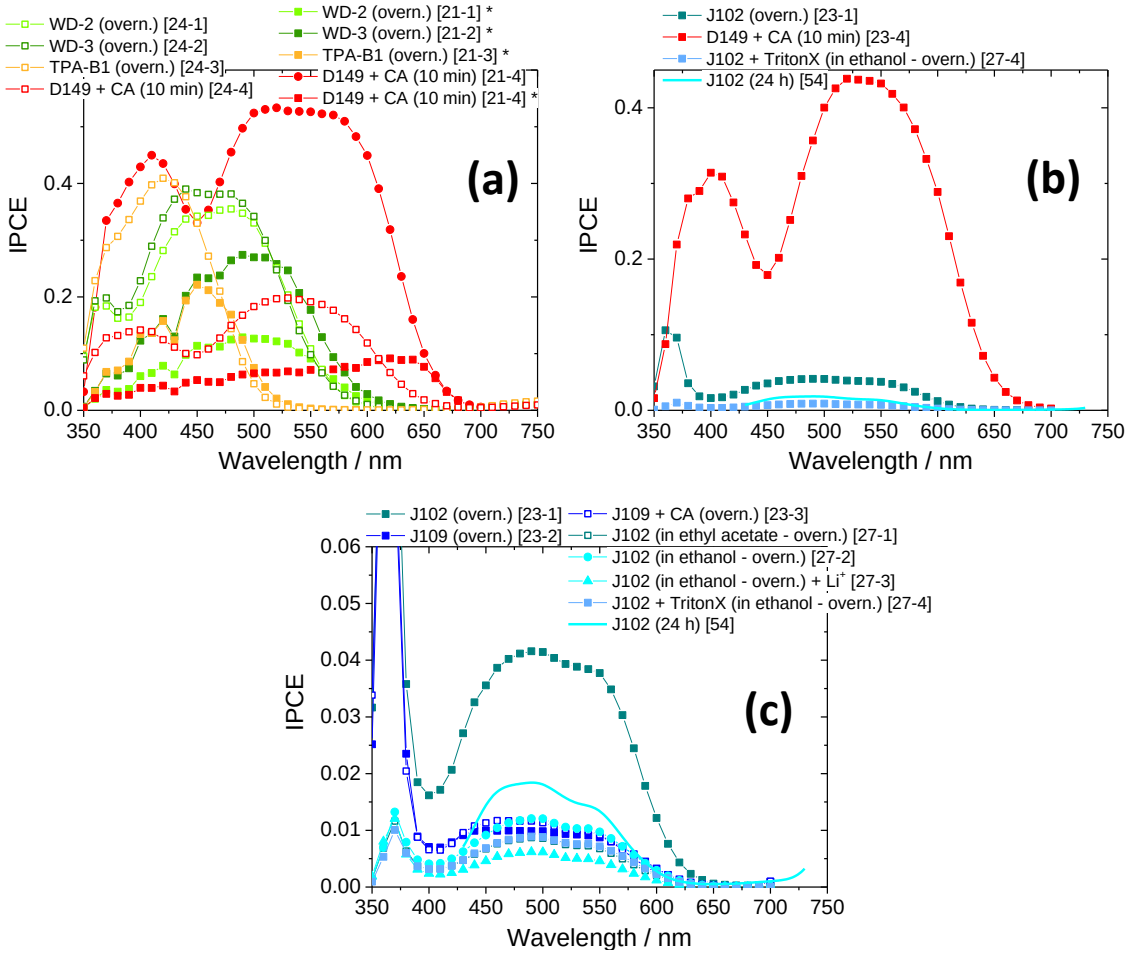

Figure 68 – IPCE spectra of different ZnO-based cells sensitized with (a) triphenylamine and (b,c) perylene dyes. Reference cell sensitized with D149 are also shown. Measurements marked with * were measured several days after cell preparation, where the cells were already partially degraded. Cell [54] is also shown for comparison. Some of the cells shown in (b) are also shown in (c). Lines are a guide to the eye.

The incident photon-to-current conversion efficiency (IPCE, see Figure 68) resembles the absorbance for most of the cells. Similar to I_{SC}, the cells sensitized with D149 and a coadsorbate reach lower values than for the optimized cells in previous chapters with similar adsorption procedure. For cell [21-4] the not yet optimized cell preparation procedure was also observed to lead to a deterioration of the IPCE during the storage of this cell in the dark for several days, comparing the different IPCE values.

Similar to the values of I_{SC}, also the IPCE of perylene-sensitized cells reach only very low values. As mentioned above (also in the previous section), from the different parameters influencing the IPCE (see equation **(9)**), the injection efficiency η_{inj} and the charge collection efficiency η_{cc} are the most probable limiting factors, as the perylene dyes show a lower position of the LUMO, and aggregate strongly on the surface. A difference in the IPCE by more than a factor 2 for the cells [23-1] and [23-2] of very similar absorbance, indicates that probably the injection efficiency is higher for J102 adsorbed to this specific film.

Only for some of the cells discussed in this section, further photoelectrochemical characterization was performed, and not all characterization methods performed in previous chapters were performed for these cells. Available data (especially for cells from film [24]) are compared with one optimized cell sensitized for 15 min with D149 (from chapter **3**), cell [61], to show different or comparable behavior. Also perylene-sensitized cells were characterized by electrochemical impedance spectroscopy (EIS), however the very different impedance spectra (for some measurements showing up to five distinct charge transfer processes instead of three observed for most DSCs) complicated an evaluation of the impedance data or a designation of the processes in the cell.

Figure 69(a) shows the chemical capacitance of cells sensitized with the triphenylamine dyes WD-2, WD-3 and TPA-B1, with a comparable cell sensitized with D149 and a coadsorbate. For voltages more negative than -0.45 V, the chemical capacitance shows the expected linear increase in the semi-logarithmic plot, with lower slopes for measurements at AM1.5 illumination (compared to measurements in the dark). This behavior is different from the behavior of the optimized cells (compare cell [61] or measurements from previous chapters), where usually the slope or the trap distribution parameter α was higher for measurements at AM1.5. The largest difference to measurements of optimized cells is an inversion of the slope for low absolute voltages. The curve shape is comparable to measurements performed by Melanie Rudolph [17,127] especially for dyes that added deep monoenergetic trap states to the cell surface, which allows the conclusion that this very large additional density of states is caused by deep monoenergetic trap states in the ZnO film.

Similar to measurements of optimized cells, the density of these trap states decreases upon illumination with AM1.5 light compared to measurements in the dark. As this feature is of a similar height for all four cells prepared from the same cell, even for very different adsorption times for D149 and triphenylamine dyes, it can be concluded that these trap states are not induced by the adsorption process, but probably by the different deposition of ZnO. As the capacitance of the deep monoenergetic trap states is comparable to the chemical capacitance of the semiconductor-electrolyte interface, also the density of states shows a large influence of these trap states, see Figure 69(b).

The recombination resistance R_{rec} determined for cells from film [24] shows differences and similarities when compared to R_{rec} of an optimized DSC, see Figure 70(a). The general curve shape is similar, with decreasing R_{rec} for increasing absolute voltages. Also the large difference in R_{rec} for measurements in the dark and under AM1.5 illumination is similar, and can most likely be ascribed to inefficient regeneration of oxidized dye molecules at high light intensities. For cells prepared from film [24], R_{rec} at lower absolute voltages shows a depression, consistently caused by the additional density of states from deep trap states at this voltage. The observation that recombination is increased by these traps allows the assumption that these deep trap states are mostly located at the surface of the ZnO, where they act as a mediator for recombination.

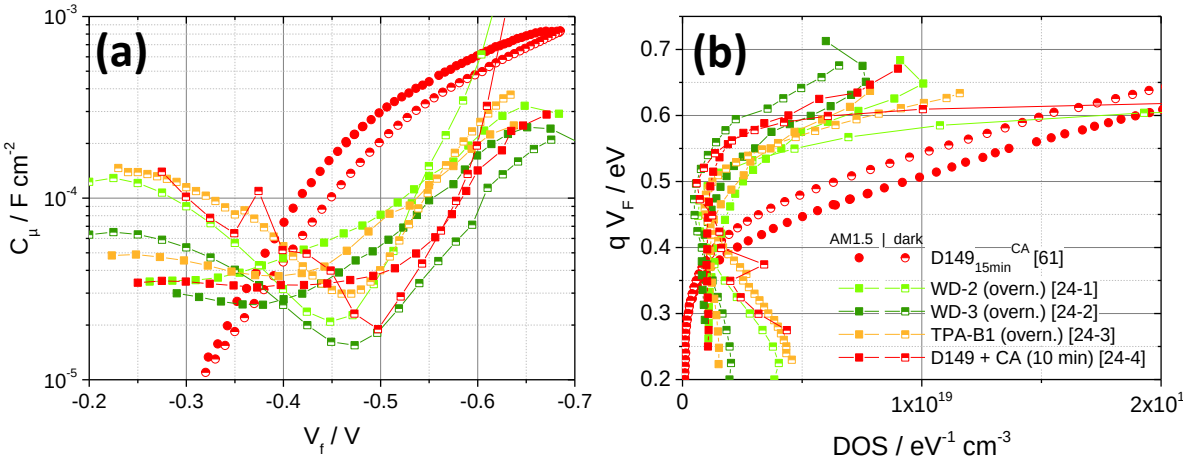

Figure 69 – Chemical capacitance C_μ and related values for cells sensitized with triphenylamine dyes and with D149. (a) C_μ vs. voltage V_f. (b) Energy of trap states vs. the DOS. Filled symbols indicate measurements at AM1.5 illumination, while half-filled symbols of the same shape and color indicate measurements in the dark. Lines are a guide to the eye.

The increased recombination also causes the depression of the current in the IV-curves. Higher values of R_{rec} are partially observed for the not yet optimized cells compared to cell [61], however a comparison with Figure 70(b) (R_{rec} vs. DOS) shows that this difference seems to be caused by a higher position of the conduction band edge (or a lower position of the redox level of the electrolyte), or a higher total trap density N_t. Compared at the same DOS, very similar values of R_{rec} (at AM1.5 illumination) are observed for a sensitization with D149 and TPA-B1, whereas a sensitization with the dyes WD-2 and WD-3 leads to lower values of R_{rec}. Either these dyes lead to an increased recombination, or regeneration is less efficient for these dyes. Recalling the dye structure with bulky side groups for WD-2 and WD-3, the possibility of retarded regeneration of the oxidized dye seems plausible.

The determination of the recombination parameter β was performed similar to measurements discussed in previous chapters. Figure 70(c) shows the distribution of values of β over the voltage. Measurement in the dark lead to relatively high β values for cells from film [24] (higher than for cell [61]), while measurements at AM1.5 illumination decreases β compared to cell [61]. As β influences the fill factor for these cells (similar V_{OC}), cells prepared from film [24] also show a lower FF than cell [61]. Values of beta were also determined from measurements of V_{OC} vs. illumination intensity (white LED light for the cells in this section), see Figure 70(d) and Table 17 for the measurements and the determined values of β. Values of β for cells prepared from film [24], determined at white LED illumination, are similar to the values of β in the dark, see Figure 70(c). For cells sensitized with perylene dyes, β shows high values around 1, similar to values found for the comparably sensitized (but optimized) cell [54]. Thus for perylene dye sensitization, recombination occurs almost exclusively via the conduction band edge, while for a sensitization with triphenylamine dyes (and especially at AM1.5 illumination) lower values of β also indicate recombination via surface trap states or oxidized dye.

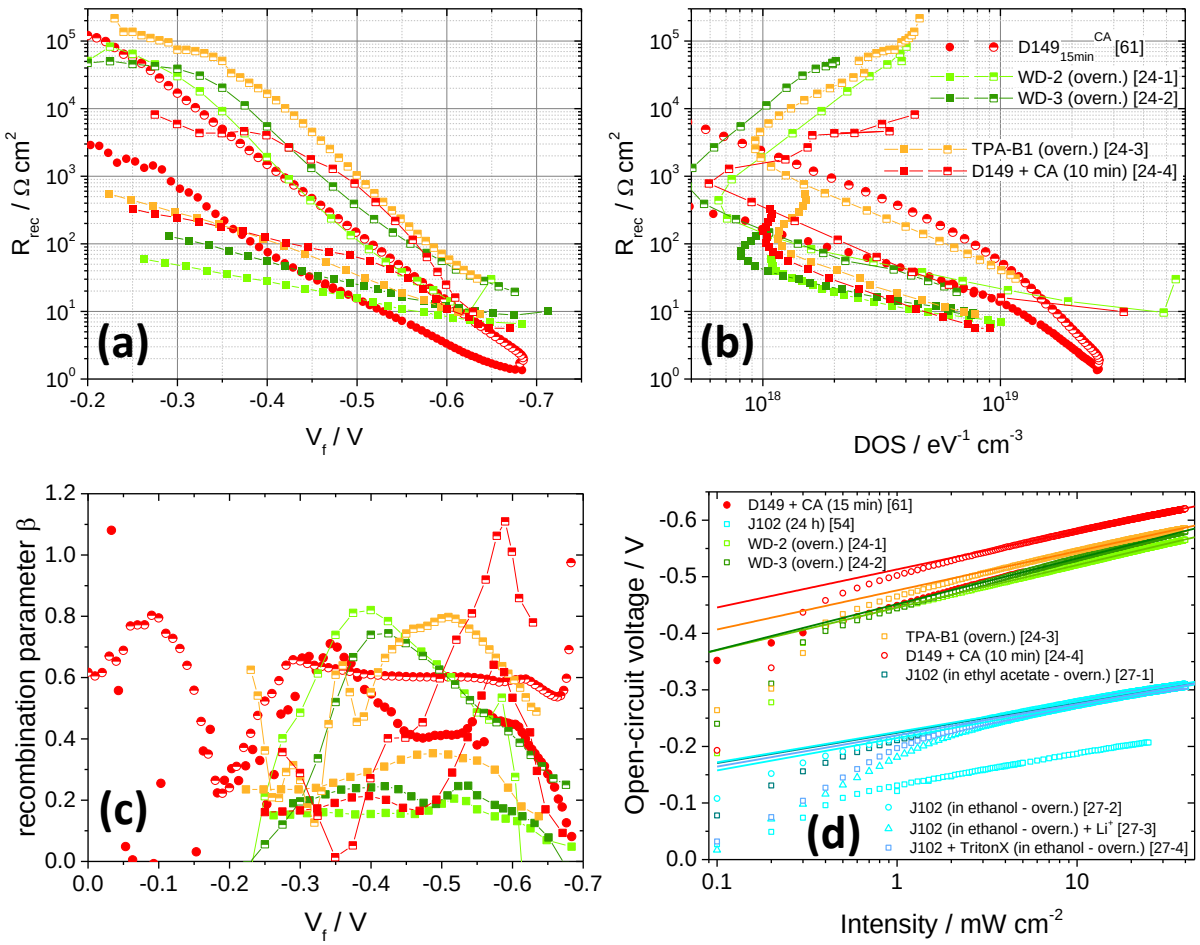

Figure 70 – Recombination resistance R_{rec} and related values for cells sensitized with triphenylamine (and perylene) dyes and with D149. (a) R_{rec} vs. voltage V_f, (b) R_{rec} vs. the DOS, (c) recombination parameter β calculated from (a), and (d) V_{OC} vs. intensity measurements. Filled symbols in (a,b,c) indicate measurements at AM1.5 illumination, while half-filled symbols indicate measurements in the dark. Measurements in (d) were performed with white LED illumination (only cells [54] and [61] were performed with a red LED).

For cells prepared from film [24], the electron lifetime τ_n was calculated from EIS results, see Figure 71(a) (vs. V_f) and (b) (vs. DOS) and from OCVD measurements (including also J102-sensitized cells), shown in Figure 71(b). The representation of τ_n vs. the voltage resembles the R_{rec} vs. V_f, however lower slopes are observed for the lifetimes.

Table 17 – Ideality factor m and recombination parameter β of cells sensitized with triphenylamine and perylene dyes (D149 for comparison), determined from measurements of V_{OC} vs. white LED illumination intensity (Figure 70(d)).

	m	**β (1/m)**
	from V_{OC} vs. intensity	from V_{OC} vs. intensity
Sample		
WD-2 (overn.) [24-1]	1.26	0.79
WD-3 (overn.) [24-2]	1.36	0.74
TPA-B1 (overn.) [24-3]	1.16	0.86
D149 + CA (10 min) [24-4]	1.13	0.88
J102 (in ethyl acetate – overn.) [27-1]	0.90	1.11
J102 (in ethanol – overn.) [27-2]	0.90	1.11
J102 (in ethanol – overn.) + Li^+ [27-3]	0.96	1.04
J102 + TritonX (in ethanol – overn.) [27-4]	0.93	1.08

Comparing the sensitization with different dyes in Figure 71(b), a considerably lower τ_n is observed for a sensitization with J102 than for triphenylamine dyes or for D149. For cell [54], the low lifetimes were especially ascribed to the high aggregation of the dye molecules, see also previous section. The different slopes at different voltages for sensitization with triphenylamine dyes and with D149 indicates that different recombination regimes are present at different voltages, with a larger dependence of τ_n on the voltage for intermediate voltages.

A linear increase of τ_n (determined from OCVD measurements) with decreasing absolute voltage indicates that the blocking layer effectively prevents recombination via the substrate. This is the case also for the not yet optimized films, as τ_n from OCVD is even higher than for the optimized films, compare for example the sensitization with D149. Comparable to the representation of R_{rec} vs. DOS, also the plot of τ_n vs. DOS indicates that recombination at a given DOS is less efficiently blocked for dyes WD-2 and WD-3 compared to TPA-B1. For the same film and a sensitization with D149, the recombination lies between TPA-B1 and WD-2/WD-3.

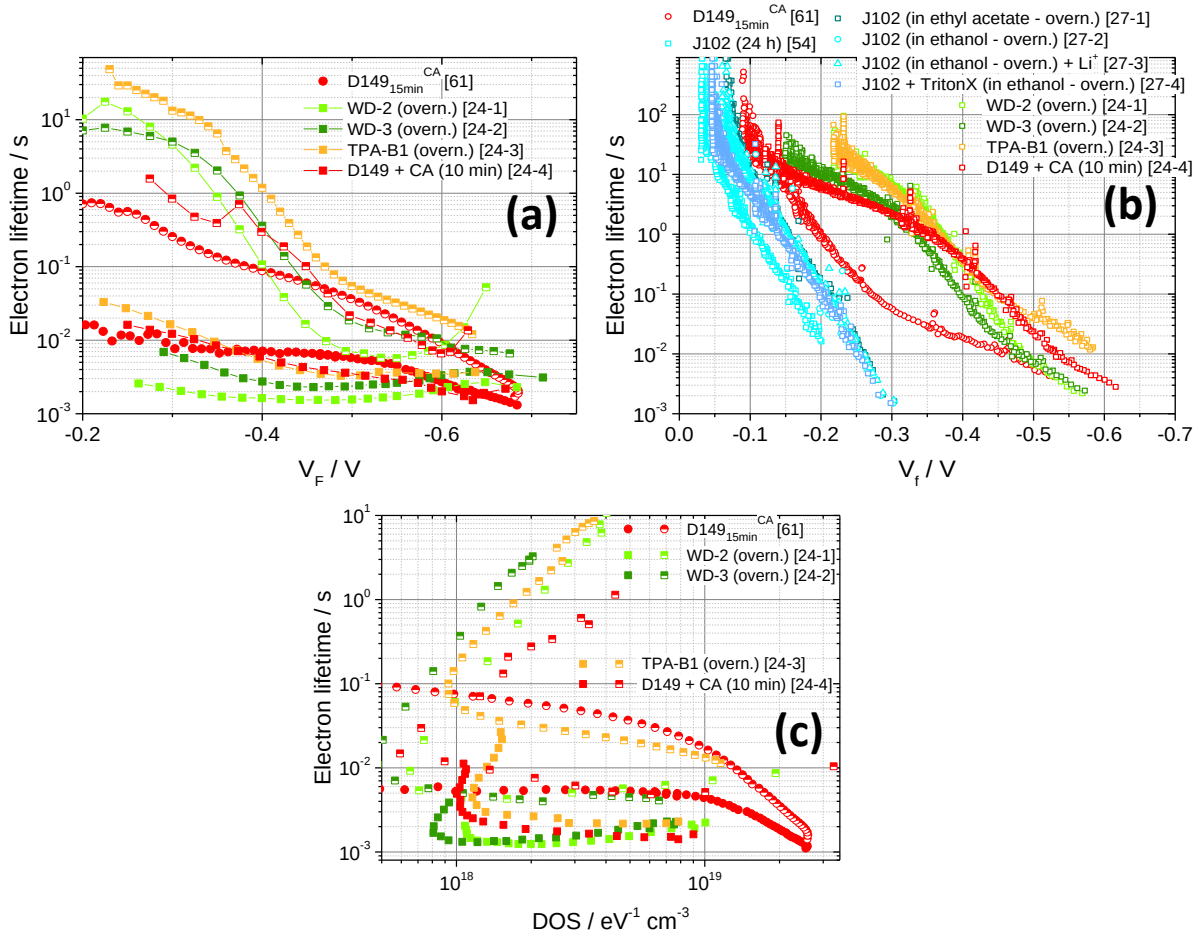

Figure 71 – Electron lifetimes τ_n of cells sensitized with triphenylamine dyes and with D149. (a) τ_n (determined from EIS measurements) vs. voltage V_f, (b) τ_n (determined from voltage transients, including data for J102) vs. V_f, and (c) τ_n from EIS vs. the DOS. Filled symbols in (a,c) indicate measurements at AM1.5 illumination, while half-filled symbols indicate measurements in the dark. Measurements in (b) were performed at white LED illumination. Note the different scaling of τ_n.

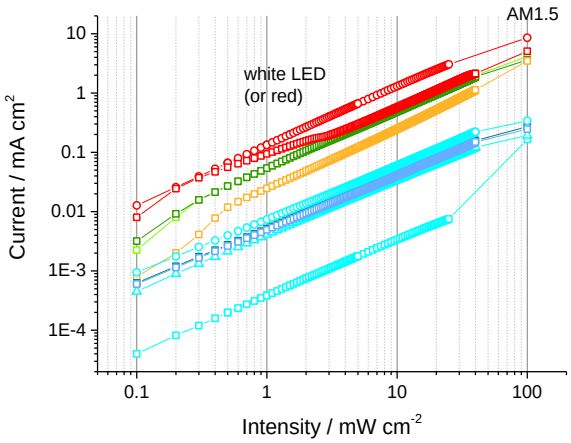

Figure 72 – Current density vs. intensity for cells sensitized with triphenylamine and perylene dyes, and with D149. The designation of the cells is the same as in Figure 70(d). Illumination intensities below 50 mW cm^{-2} were obtained by illumination with a white LED (except for cell [54], where a red LED was used).

Differences found for the measurement of I_{SC} vs. intensity (white LED) of triphenylamine-sensitized cells indicate that also the regeneration efficiency is different for these dyes, see Figure 72. The not yet optimized cell preparation caused a deviation of I_{SC} from a straight line for lower intensities for some of the cells. For measurements in previous chapters, the I_{SC} values at diode illumination (mostly red LED) and at AM1.5 illumination (100 mW cm^{-2}) cannot be directly compared, as the light from these different light sources is absorbed differently by the DSCs. However for cells prepared from film [24] and [27], a white light LED was used for this measurement, which made the measurements of the two different light sources more comparable. Thus a lower I_{SC} at 100 mW cm^{-2} than expected from a linear extrapolation of the current indicates a decreased regeneration efficiency at higher light intensities, and no deviation from the straight line at LED illumination (or higher currents, as the spectrum of AM1.5 is broader) indicates efficient regeneration even at high illumination intensities.

Thus the measurements of I_{SC} vs. intensity indicate, that regeneration for a sensitization withWD-2 or WD-3 no longer takes place with unity efficiency, while it seems that for D149 the regeneration efficiency is higher than for these two dyes, and even higher for TPA-B1. Already for the IV-curves for these dyes it was surmised from the bulkier structure of WD-2 and WD-3 that reduced regeneration might cause the observation that similar current as with TPA-B1 dye is harvested, even though more TPA-B1 molecules were adsorbed to the ZnO surface. It has to be noted that for red LED illumination the direct comparison with I_{SC} at AM1.5 is not possible due to the very different absorption for each light source in the sensitized film.

7.2 Different sensitizers on standardized ZnO films

A perylene dye, J102, and the phthalocyanine dyes Phosphon, Vinylphosphon, Vinylcarbon and AR20 (see sections **1.2.3** and **1.2.5** for the respective dye structures) were used as sensitizers on standard ZnO films. These dyes adsorb slowly to the ZnO surface, compared to the rapid adsorption of the indoline dyes. This led to adsorption times of several hours for the phthalocyanine dyes (usually overnight, coded overn. in the cell name) and an adsorption time of 24 h for the perylene dye J102. The sensitized films were analyzed by UV-vis spectroscopy using an integrating sphere setup due to the strong scattering of the ZnO films. The resulting absorption curves are plotted in Figure 73(a), with one indoline-sensitized film for comparison (sensitized without coadsorbate for 1 h, see also section **4.1**). The perylene dye J102 adsorbs by a large amount to the ZnO surface, but the broadening of the spectrum compared to the solution spectrum indicates that the dye strongly aggregates on the surface. As J102 has a planar aromatic structure without bulky anti-aggregation side-groups, aggregation has to be expected for this dye. The phthalocyanine dyes adsorb by a smaller amount to the ZnO surface than the J102 dye. Dyes with phosphonic acid binding groups adsorb to an even lower amount than the dye with carboxylic anchor group or hydroxyl groups. With increasing amount of adsorbed dye, the aggregation of the phthalocyanine dyes increases, as clearly seen by a comparison with a solution spectrum. For AR20 (hydroxyl groups), the peaks of the absorbance are strongly broadened and the relative height of the maxima changes compared to a solution spectrum, both changes indicating strong aggregation. Comparing the dyes with carboxylic and phosphonic anchor groups, it is observed that for the dyes containing an additional vinyl spacer more dye is adsorbed than for the dye Phosphon. Probably the longer binding group allows a better binding inside the porous ZnO network.

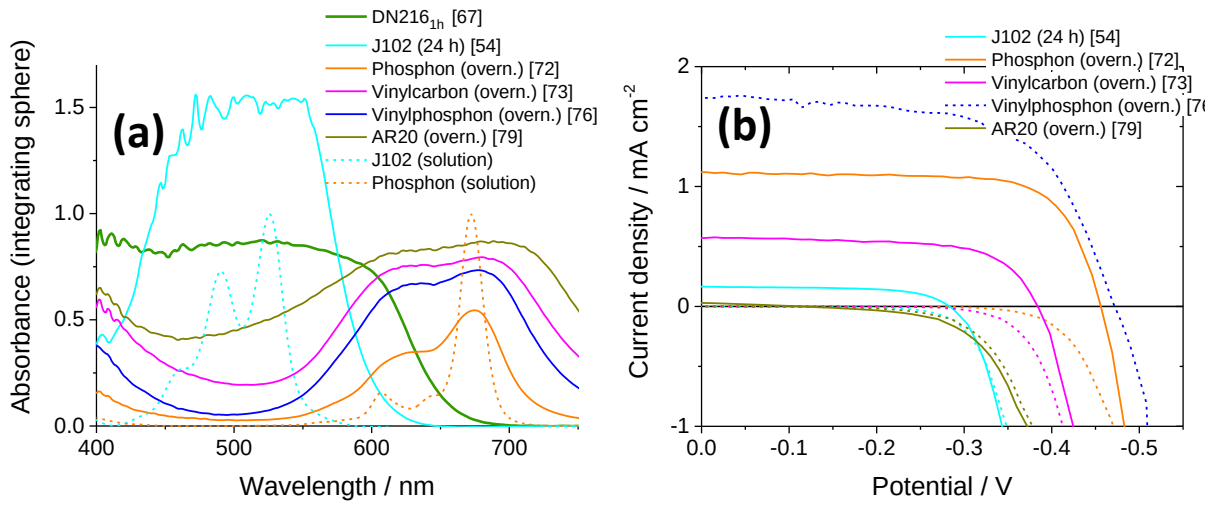

Figure 73 – (a) Absorbance of dyes on ZnO films sensitized with different sensitizers, with one indoline-sensitized cell (green) and two normalized solution spectra (dashed lines) for comparison. Solid samples were measured in an integrating sphere setup. The absorbance of the bare ZnO-films was subtracted from the absorbance of the films. (b) IV-curves of DSCs built from films in (a). Different colors indicate the different sensitizers according to the legends. Full lines in (b) indicate measurements at AM1.5 illumination, and dashed lines indicate measurements in the dark.

Table 18 – Cell values determined from IV-curves shown in Figure 73(b). Values of cell [79] were estimated from the difference of the currents under illumination and in the dark, as this cell was short-circuited.

Film	Comment	I_{sc}	V_{oc}	FF	Efficiency
		[mA cm^{-2}]	[V]		[%]
J102 (24 h) [54]		0.16	-0.283	0.65	**0.03**
Phosphon (overn.) [72]		1.12	-0.456	0.72	**0.37**
Vinylcarbon (overn.) [73]		0.57	-0.384	0.69	**0.15**
Vinylphosphon (overn.) [76] - short circuit!	$I_{illuminated}$ - I_{dark} as an estimate	~1.74	~-0.49	~0.65	**~0.55**
AR20 (overn.) [79]		0.03	-0.112	0.31	**0.001**
$DN216_{1h}$ [67]		9.34	-0.566	0.72	**3.76**

Strong aggregation and low absorbance both lead to a low short-circuit current I_{SC} for the cells sensitized with perylene or phthalocyanine dyes, see Figure 73(b) for the IV-curves of these cells, and Table 18 for the cell values. I_{SC} is especially low for the highly-aggregated dyes J102 and AR20 (for J102 however yet another effect is probably leading to the low current, see also below). Together with low open-circuit voltages, the efficiencies of these two cells are almost negligible. The phthalocyanine dyes Phosphon and Vinylcarbon reach comparably higher solar cell parameters than the dyes with highest aggregation, however the power-conversion efficiency of the best cell [72] still is about 10 times lower than for most of the indoline cells characterized in this work (compare for example values in section **4.2**). The main cause for this efficiency difference compared to indoline cells is their low I_{SC}, but also V_{OC} and FF are lower for the phthalocyanine-sensitized cells. Vinylphosphon adsorbs to a larger extent to the ZnO surface than Phosphon, which has a similar dye structure, still with lower aggregation than the dye Vinylphosphon (compare relative height of the maxima of the absorbance between 600 and 700 nm). [xxxii] The higher absorbance of the Vinylphosphon-sensitized cell compared to the Phosphon-sensitized cell leads to a higher short-circuit current [xxxiii]. The cell with a still higher absorbance, sensitized with Vinylcarbon, however shows a lower current than both of these cells. This is probably caused by a more pronounced recombination via many vibrational states, as the dyes are stronger aggregated for Vinylcarbon, see the decreased height of the Q-band at around 690 nm relative to the vibrational band at around 610 nm. Yet another possibility which could decrease the current of the carboxyl-bound dye compared to a phosphonyl-bound dye could be a lower injection efficiency, as a phosphonic group binds much stronger for example to TiO_2 surfaces [77]. Thus the electronic coupling of the dye and the semiconductor could be much higher for a phosphonic anchor group, which leads to an increased electron transfer probability from the dye to the semiconductor [273], and a higher injection efficiency.

[xxxii] As the cell prepared from the Vinylphosphon-sensitized film showed a short-circuit, the exact characteristics from current-voltage curves could not be determined. However, an estimate of these values was calculated from the difference of the current under AM1.5 illumination and the current in the dark (photocurrent)

[xxxiii] Cells sensitized with Vinylphosphon were also prepared by Jan Tinz, and showed even larger currents and power conversion efficiencies than cell [76] would have shown without short circuit.

With only the IV-curves and the absorbance of the sensitized films, it can be only surmised whether low efficiencies stem from a high recombination via dye aggregates, an energetic mismatch of the LUMO level of the dye and the conduction band edge of the semiconductor (thus lower injection efficiency) or from a worse coupling of the dye with the semiconductor (also lowering the injection efficiency). With additional measurements, the loss mechanism of recombination was addressed, and the results are discussed further below.

The difference of the absorbance spectrum and the IPCE (compare Figure 73(a) and Figure 74) gives valuable information about the current generation in the cells. It can be seen for the strongly aggregated sample [79] that only a small amount of the dyes contributes to the current, as the IPCE is below 1 % over the complete wavelength range. The shape of the curve resembles the shape of the absorbance spectrum, however the absorbance maximum at about 675 nm is higher compared to the maximum at about 625 nm, in contrast to the absorbance, where both maxima are of a similar height (Figure 73(a)). A similar observation can also be made for the aggregated dye Vinylcarbon, however with an overall higher IPCE. The IPCE spectrum of the Phosphon dye, least aggregated on the ZnO surface, most closely resembles the phthalocyanine solution spectrum (see Figure 73(a)), reaching the highest IPCE among the perylene and phthalocyanine dyes. The IPCE spectrum of the J102-sensitized DSC shows peaks as observed in solution but shifted and broadened, and at different relative height as often observed in solid perylene films.

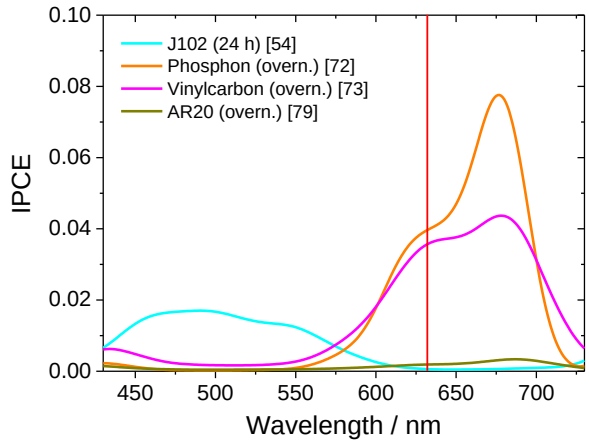

Figure 74 – IPCE for ZnO-based DSCs sensitized with perylene or phthalocyanine dyes. The different dyes are indicated by different colors, see legend. A red vertical line indicates the wavelength of the red LED, used for many photoelectrochemical characterization methods discussed further below.

More detailed information about the cells was obtained from electrochemical impedance spectroscopy (EIS) and other photoelectrochemical measurements. The EIS spectra for some of the cells differed from the spectra obtained for indoline-sensitized cells, for example no clear distinction of the semicircle belonging to the charge transfer process at the platinized counter electrode was possible for cell [54] (not shown). The charge transfer process at the sensitized semiconductor interface could be

analyzed for all EIS spectra, and thus the chemical capacitance and the recombination resistance were determined. The chemical capacitance C_μ of the semiconductor for the cells sensitized with perylene and phthalocyanine dyes is plotted in Figure 75(a), with an indoline-sensitized reference cell [67], which was adsorbed for the longest time without coadsorbate out of the indoline sensitized cells; see also chapter **4** for comparison of this cell with other indoline-sensitized cells [xxxiv]. C_μ shows the expected linear dependence on the voltage in a semi-logarithmic representation for intermediate voltages. For cell [54] sensitized with the perylene dye J102, the measured capacitance almost does not exceed the capacitance of the back layer C_{BL} at low absolute voltages, mostly because this cell reaches only a low photovoltage. For all other cells, the approximately linear region of the chemical capacitance is observed for intermediate voltages.

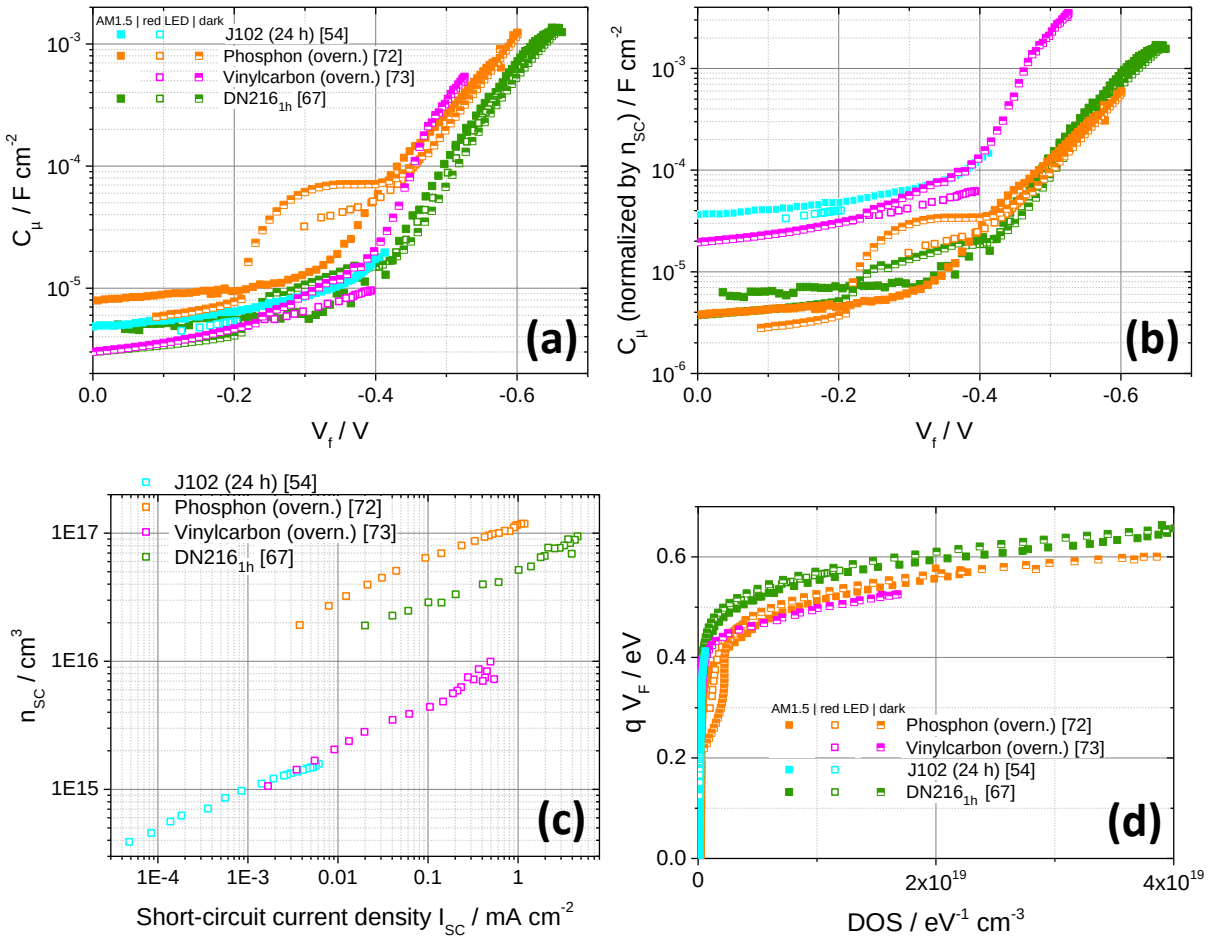

Figure 75 – Chemical capacitance C_μ and related values for ZnO-based cells sensitized with different sensitizers, and one indoline sensitized DSC, [67], for comparison. (a) C_μ as determined; (b) C_μ normalized by $N_t/N_{t,ref}$ (reference cell [61], see also Table 19); (c) charge density n_{SC} from current transients; (d) energy of trap states (in eV) vs. density of states. The different symbol colors indicate different sensitizers according to the legends. Filled symbols indicate measurements at AM1.5 illumination, open symbols indicate measurements at red LED illumination, and half-filled symbols indicate measurements in the dark.

[xxxiv] Cell [79] was not characterized by EIS or other photoelectrochemical methods due to the very low I_{SC} and V_{OC} , as even for cell [54] the low currents and voltages complicated the measurements and the evaluation.

For both phthalocyanine sensitized cells, a maximum (or shoulder) appears for measurements in the dark, similar to the feature of deep monoenergetic trap states observed for many indoline-sensitized DSCs and dark measurements, including also cell [67]. For the Vinylcarbon-sensitized cell this indication of deep monoenergetic (surface) trap states has a similar height as for the DN216-sensitized cell. However, for the cell sensitized with the phthalocyanine Phosphon [xxxv] this maximum is much larger. This difference could be caused by the anchor group, a phosphonic anchor group for cell [72] compared to a carboxylic anchor group for cell [73]. As the anchor group is (ideally) chemically attached to the ZnO surface, a difference in this group could well lead to a difference in ZnO trap states. For measurements with a red LED [xxxvi], the trap density of these deep monoenergetic trap states at the same voltage is lower, as it was also observed for the indoline-sensitized cells that showed these traps (when the measurement reached lower values of V_f). For measurements at AM1.5 illumination, no peak or shoulder is observed at the same position. However a peak arises at the linear slope of the chemical capacitance around -0.46 V, and thus the peak for the dark measurement appears to be shifted to higher energies by the intense illumination. This possibility of a shift of the energy of deep monoenergetic trap states was also discussed for the simulation of C_μ in section **3.3.1**.

The chemical capacitance C_μ is influenced by the total trap density N_t, which means that if a shift in the conduction band edge shall be evaluated, C_μ has to be corrected relative to a reference sample (cell [61] in this work) by the value $N_t/N_{t,ref}$ [17]. This value, listed in Table 19, was determined from current transient measurements, which resulted in the charge-density curves in Figure 75(c). The charge density n_{SC} is very low for the cells sensitized with the perylene dye J102 and the phthalocyanine dye Vinylcarbon. Both cells showed the lowest power conversion efficiency out of the cells characterized by EIS. The other phthalocyanine-sensitized cell, sensitized with Phosphon, shows even larger charge densities than the indoline-sensitized cell [67], even though the efficiency was considerably smaller. The correction of the chemical capacitance was performed for all capacitance curves, see Figure 75(b), assuming that the position of the charge density curves remains constant for the different illumination conditions (a strong indication that this is the case gives the cyan LED measurement in Figure 34, p. 100). The corrected C_μ curves of the DN216- and Phosphon-sensitized DSCs overlap in the relevant intermediate voltage range, indicating that these two cells have a similar position of the conduction band edge. The different slopes (or trap distribution parameters α) of these curves, however, leads to deviations at higher and lower voltages. For the two less efficient cells, the onset of the chemical capacitance (for the J102-sensitized cell) and the chemical capacitance (for the Vinylcarbon-sensitized cell) at relatively low absolute voltages lead to the assumption that the position of the conduction band

[xxxv] As the difference is large for the similarly sensitized cells [72] and [73] (same solvent, same adsorption time), it can be concluded that the large density of deep trap states for cell [72] is not induced by the long adsorption time.

[xxxvi] Red LED illumination was used for all cells to have more comparable conditions, even as this wavelength lies within the absorbance maximum for the phthalocyanine dyes. As it was shown for indoline dyes with a cyan LED (see section **9.1.8**), most of the measurement results are not affected by the illumination wavelength (largest difference for I_{SC} vs. intensity). Additionally the currents are small, so that transport limitation should not occur.

edge is lower for these cells compared to cells [72] and [67]. As the trap distribution parameter α is either unknown or not identical, this remains an assumption.

The trap distribution parameter α was determined at the point of maximum slope from C_μ. The values of α for all illumination conditions are listed in Table 19. The value of α of the Phosphon-sensitized cell appears decreased by the large feature from deep monoenergetic trap states. An extension of the measurement range for the J102-sensitized cell would probably also lead to higher α values at more negative voltages, as for this cell the inflection point is not observed. Similar to indoline-sensitized cells, α is higher for EIS measurements at AM1.5 illumination, while it is lower for measurements at red LED illumination or in the dark.

The plot of the trap energy vs. the density of states (DOS) in Figure 75(d), still including the effects of the total trap density, emphasizes the different contributions of deep monoenergetic trap states for the different cells, and also illustrates the different distribution of trap states for the different cells.

Table 19 – Different values for differently sensitized DSCs, determined from current transient measurements, from EIS measurements, and from V_{OC} vs. intensity. Values of α marked with * indicate that the determined values do not reflect C_μ but the back layer capacitance C_{BL}.

Value	**$N_t/N_{t,ref}$**	**α**	**α**	**α**	**β**	**β**	**β**	**β (1/m)**
Illumination (measurement) **Sample**	red LED (current transient) – reference cell [61]	AM1.5 (EIS)	red LED (EIS)	dark (EIS)	AM1.5 (EIS)	red LED (EIS)	dark (EIS)	red LED (V_{OC} vs. intensity)
J102 (24 h) [54]	0.13	**0.37**	0.07*	-	**0.98**	1.03	-	**1.16**
Phosphon (overn.) [72]	2.08	**0.58**	0.43	0.46	**0.66**	0.90	0.74	**1.01**
Vinylcarbon (overn.) [73]	0.15	-	0.16*	0.76	-	0.95	0.88	**0.89**
$DN216_{1h}$ [67]	0.80	**0.67**	0.57	0.59	**0.65**	0.83	0.76	**0.90**

The recombination resistance R_{rec} of the cells sensitized with different sensitizers was determined from fits of EIS measurements. The recombination resistance vs. the Fermi-level voltage V_f, shown in Figure 76(a), gives information about the recombination behavior of the cells, also at different illumination conditions. Similar to the observations made for the indoline-sensitized cells, the recombination resistance determined from measurements at red LED illumination and in the dark are very similar, overlapping over a large range of the voltage, and deviating only for more negative voltages. In the previous chapters, this deviation was ascribed to a decreased regeneration efficiency for increasing illumination intensities (increasing with more negative voltages), and thus an increased regeneration via the oxidized dye. For cell [73], R_{rec} overlaps over the complete range of the red LED measurement, as less charge is generated in this less efficient cell and thus regeneration is not a limiting factor. For the measurement at red LED illumination (the only measurement which is

available for all four cells in Figure 76(a)), R_{rec} decreases in the same sequence that is also observed for the efficiency (with highest recombination resistance for the indoline dye), even though the differences are not proportional. It indicates, however, that a part of the difference in the efficiency of these DSCs is due to differences in recombination. This recombination can for example be mediated by aggregates, as the recombination resistance decreases with increasing extent of aggregation, observed as a broadening of bands in the absorbance of the films. Also inefficient regeneration could increase recombination, as more paths are available for recombination via oxidized, non-regenerated dye molecules. This recombination becomes more important for voltages near short-circuit conditions, however it is improbable that for such low currents as for example cell [54] shows, a decrease of the regeneration efficiency by depletion of iodide in the pores would occur. Also for this cell dye aggregates are probably one cause for the poor efficiency. The recombination parameter β, calculated from the slope of R_{rec} and plotted against the voltage in Figure 76(b), gives information about the fraction of electrons recombining via the conduction band, and correlates with the fill factor of the cells, see equation **(35)**.

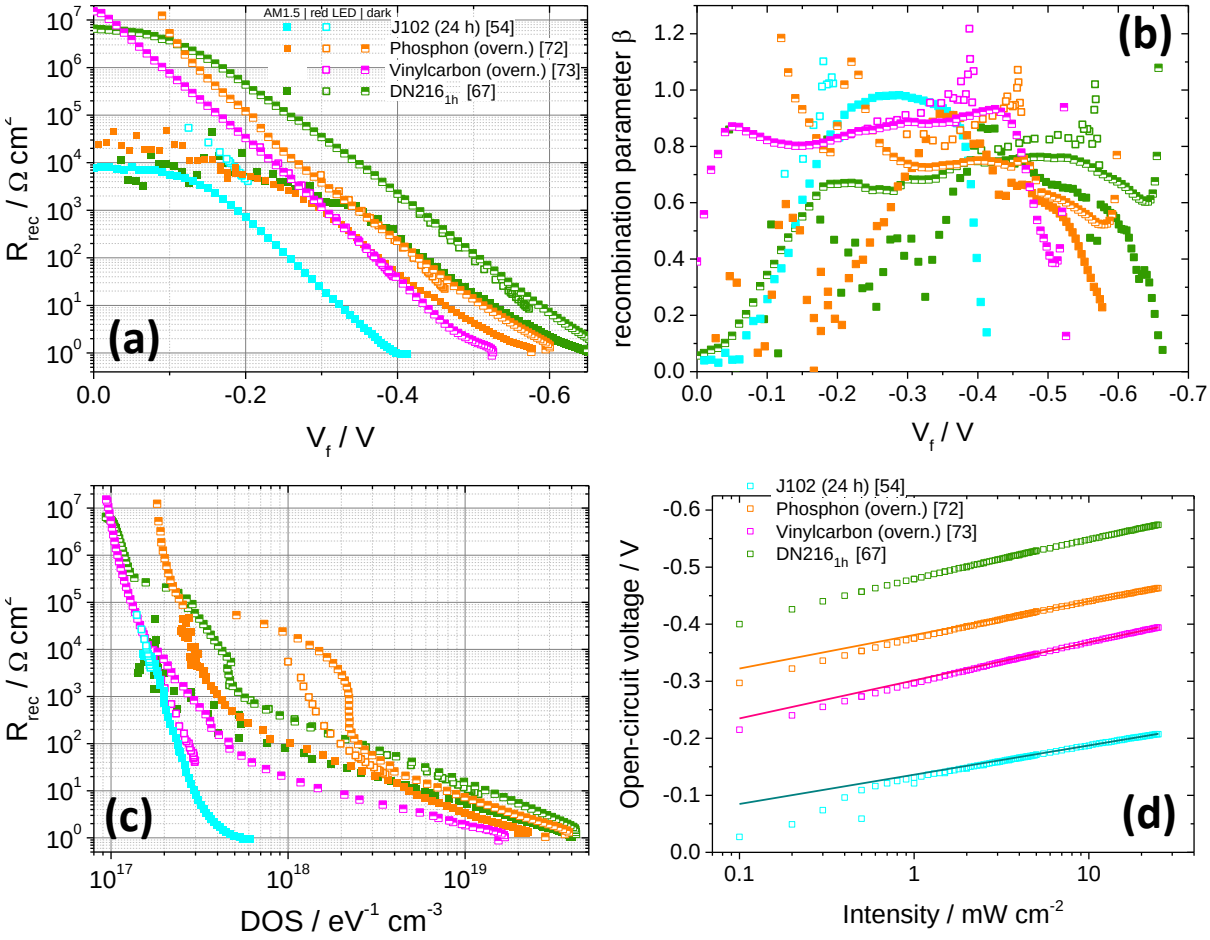

Figure 76 – Recombination resistance R_{rec} and related values for cells sensitized with perylene and phthalocyanine dyes, with an indoline-sensitized cell for comparison. (a) R_{rec} vs. voltage; (b) recombination parameter β; (c) R_{rec} vs. density of states; and (d) open-circuit voltage vs. intensity. Different colors indicate the different sensitizers according to the legends. Filled symbols indicate measurements performed at AM1.5 illumination, open symbols indicate measurements at red LED illumination, and half-filled symbols indicate measurements in the dark.

A representative value of β from a region with the most constant β is listed in Table 19. β reaches higher values for cells with a conduction band edge shifted to lower energies, as seen for cells sensitized with the perylene dye J102 or the phthalocyanine dye Vinylcarbon. This indicates that the recombination takes place to a higher extent over the (lower lying) conduction band for the J102- and Vinylcarbon-sensitized cells. Different from the cells sensitized with indoline dyes (see discussion in section **3.3.2**), the β values for voltages near the maximum power point (especially for measurements at AM1.5 illumination) of these DSCs sensitized with different dyes do not directly correlate with the FF (Table 18) because of very different values of the open-circuit-voltage, which also influence the FF after equation **(35)**. For the indoline dyes, V_{OC} was comparable even for different sensitization conditions, while for the perylene- and phthalocyanine-sensitized cells the voltage varies by hundreds of millivolts. Another measurement to determine the β value is the measurement of V_{OC} vs. the illumination intensity, see Figure 76(d) and Table 19 for values of β (determined at higher illumination intensities). The β values determined by this method are similar to β determined from EIS measurements at red LED illumination, as both methods are performed under similar conditions, speaking in favor of the validity of the model.

The representation of R_{rec} vs. the density of states in Figure 76(c) allows the evaluation of the recombination of the dyes without an influence of the total trap density N_t or differences in the position of the conduction band edge. The recombination behavior of the cells with a recombination resistance R_{rec} (J102) < R_{rec} (Vinylcarbon) < R_{rec} (Phosphon) < R_{rec} (DN216) for values that are not influenced by deep monoenergetic trap states shows the same trend as R_{rec} vs. V_f (higher DOS or more negative V_f). The differences in R_{rec} for the Phosphon dye and for DN216 are relatively small for R_{rec} vs. DOS. Also the aggregation of Phosphon on the ZnO surface was relatively low, which leads to the conclusion that recombination via aggregates is not the main efficiency-limiting factor for the phthalocyanine Phosphon. Other probable causes for the lower efficiency compared to the indoline dye could be the smaller amount of Phosphon dye adsorbed to the ZnO surface, a lower injection and/or a lower regeneration efficiency (for example caused by the position of the LUMO relative to the conduction band edge of ZnO or to the redox level of the electrolyte). Phthalocyanine dyes with sulfonate anchor groups for example showed a lower LUMO level and a higher HOMO level than the indoline dyes D149, DN216 and DN285 [121,170], which accordingly led to lower power conversion efficiencies for the phthalocyanine dyes, especially due to lower short-circuit current densities. For the two phthalocyanine dyes Vinylcarbon and Phosphon, the difference in efficiency can be ascribed especially to enhanced recombination via dye aggregates for Vinylcarbon. The recombination resistance in the dark is lower at a given DOS, indicating that recombination is increased even in the dark. For ZnO sensitized with the strongly aggregated J102, a still lower recombination resistance is observed. However, the very low efficiency for this cell is not only ascribed to recombination via dye aggregates, but also to reduced injection efficiency due to a low energy of the LUMO level (see below for a discussion of the respective energy levels).

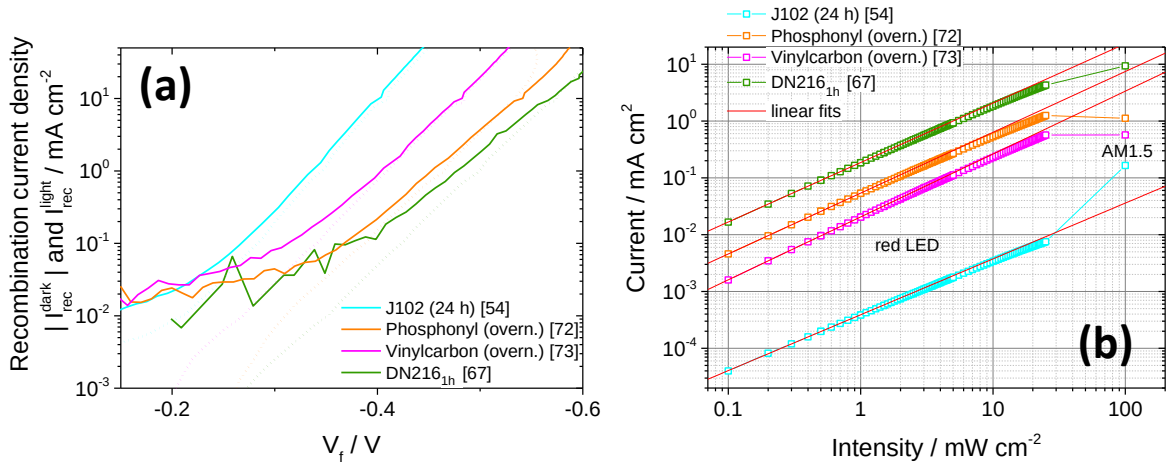

Figure 77 – (a) Recombination currents in the dark and under AM1.5 illumination for DSCs sensitized with phthalocyanine dyes, a perylene dye and an indoline dye for comparison. Solid lines indicate measurements at AM1.5 illumination, while dotted lines indicate measurements in the dark. (b) Measurements of I_{SC} vs. red LED intensity, with the point at AM1.5 illumination (100 mW cm^{-2}) for comparison. Red lines indicate linear fits of the first few points at low intensity. Different colors of the lines in (a) and of the symbols in (b) indicate different sensitizers according to the legends.

Recombination (and regeneration) can also be discussed comparing recombination currents in the dark and under illumination, I_{rec}^{dark} and I_{rec}^{light}, see Figure 77(a). The relative position of the recombination currents for different sensitizers cannot be compared, as the voltage was not corrected for the shift in the conduction band edge (too large differences in α). For cells sensitized with the phthalocyanine dyes Phosphon or Vinylcarbon or and with the perylene dye J102, I_{rec}^{dark} and I_{rec}^{light} are quite similar to each other for the linear part of the current. A larger difference I_{rec}^{light} - I_{rec}^{dark} is observed for cell [67], which was ascribed to increased recombination under AM1.5 illumination, in particular by additional recombination via oxidized dye molecules. As cells sensitized with Phosphon, Vinylcarbon or J102 show a considerably lower short-circuit current density than cell [67], this effect will be very small, and thus only a low increase of recombination is expected under illumination of these cells. For lower voltages around -0.3 V, the difference of I_{rec}^{dark} and I_{rec}^{light} becomes larger for cells [72] and [73]. As it was also concluded for similar results e.g. in section **6.4**, especially this difference indicates recombination via the oxidized dye because of inefficient regeneration. As however I_{SC} is small compared to indoline-sensitized DSCs, and thus diffusion limitation in the electrolyte should not occur, it can be that regeneration is limited by a mismatch of the energy levels important for regeneration (HOMO of the dye and electrolyte DOS).

The influence of insufficient regeneration can (partially) be also observed for the measurement of I_{SC} vs. illumination intensity, especially when values at red LED illumination (different intensities) are compared with values at AM1.5 illumination (100 mW cm^{-2}), see Figure 77(b). The slight bending of the curves at higher light intensities (deviation from linear fit) indicates that incoming photons are not harvested efficiently. Literature usually ascribes this deviation from the linear behavior to decreasing regeneration efficiency because of iodide depletion in the pores, which is probably also the cause for the phthalocyanine and the indoline dyes. For cell [54], however, the current increases for AM1.5

illumination because the spectrum of the red LED used for the I_{SC} vs. intensity measurement does not lie inside the absorbance maximum as for the phthalocyanine dyes.

Effective electron lifetimes τ_n were determined for the differently sensitized cells by IMVS, EIS and OCVD (open-circuit voltages decay) measurements. The resulting plots of τ_n against the Fermi-level voltage V_f are shown in Figure 78(a) and (b). The trend found for these cells is the same as for the recombination resistance vs. V_f, with the lowest lifetimes for the highly aggregated perylene dye J102, and the indoline cell for comparison showing the highest lifetimes for the respective illumination conditions. The electron lifetime determined from OCVD in Figure 78(b) increases linearly with decreasing absolute voltage (even to low absolute voltages), showing that the blocking layer effectively prevents direct recombination from the substrate to the electrolyte. Also for the representation of τ_n vs. the DOS in Figure 78(c) the same trend is observed, showing again that the higher aggregation of the dyes J102 and Vinylcarbon also leads to a higher recombination and thus a lower lifetime when compared at the same DOS.

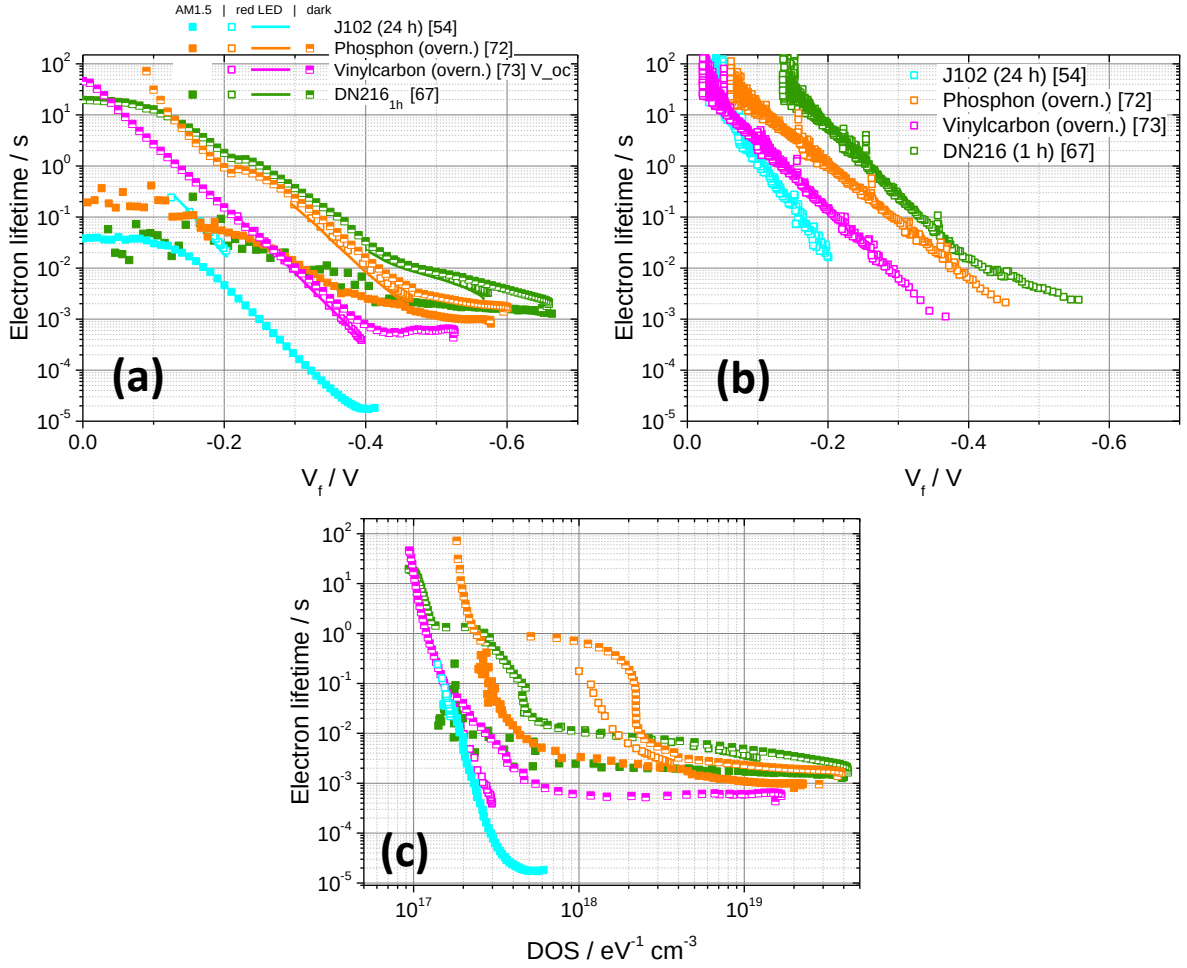

Figure 78 – Electron lifetimes τ_n for DSCs sensitized with perylene and indoline sensitizers, with one indoline-sensitized cell for comparison. (a) τ_n from IMVS (lines) and EIS (symbols) measurements plotted vs. voltage; (b) τ_n from OCVD measurements; and (c) τ_n from EIS vs. density of states. Different colors indicate different sensitizing dyes, according to the legends. Filled symbols in (a,c) indicate EIS measurements at AM1.5 illumination, open symbols indicate measurements at red LED illumination, and half-filled symbols indicate measurements in the dark.

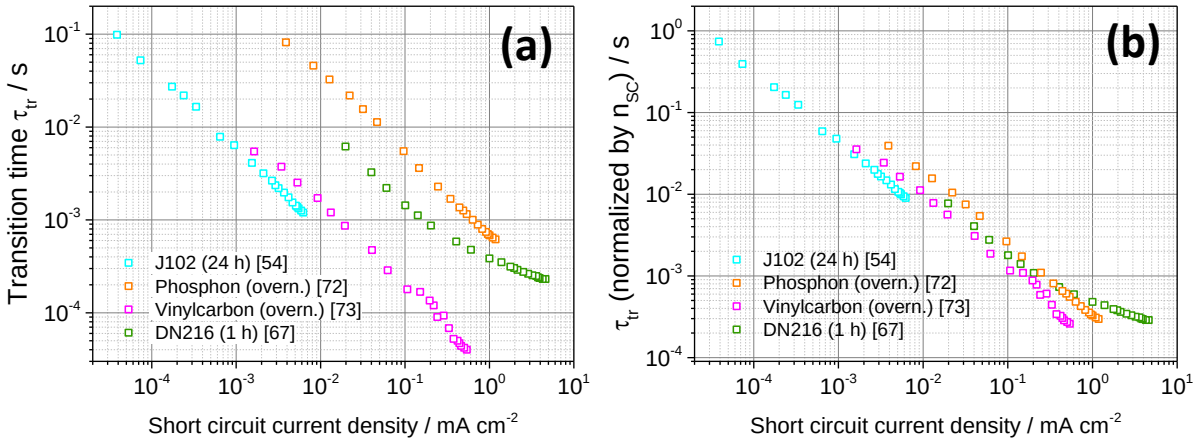

Figure 79 – Transport time τ_{tr} for DSCs sensitized with perylene and phthalocyanine dyes, with one indoline-sensitized cell for comparison. The different symbol colors indicate the different sensitizers, according to the legends. (a) τ_{tr} as measured, and (b) τ_{tr} corrected with $N_t/N_{t,ref}$ (relative to cell [61], see Table 19).

From the transport times τ_{tr} shown in Figure 79 more information about the transport properties of the ZnO films can be obtained. The as-determined values of τ_{tr} in (a) show large differences for the cells sensitized with the different dyes. A comparison with the values of τ_{tr} normalized with a measure of the total trap density ($N_t/N_{t,ref}$) in Figure 79(b) clarifies that these differences are mainly due to a different total trap density for the different cells. The normalized curves almost overlap for all cells, which indicates that the transport properties are not influenced by surface adsorption of dye molecules. Small variations can be attributed to slight differences in the electrodeposition of the ZnO films. The curve shape is more linear for the perylene and phthalocyanine dyes than for the reference indoline dye DN216.

For the perylene dye J102, apart from high recombination via dye aggregates, also a lower injection efficiency is supposed to lead to the very low cell efficiencies of cell [54]. To verify this hypothesis, cyclic voltammetry and spectroelectrochemistry were performed on a solution of J109, a dye with a very similar structure as J102 [xxxvii]. A cyclic voltammogram of dissolved J109 is shown in Figure 80, compared to a voltammogram of DN285 (see also [15] and [121] for experimental realization and the measurements of DN285). During spectroelectrochemical measurements it was observed that for both dyes, a change in absorbance did not occur for a voltage sweep from 0 V to around -0.5 V vs. Ag|AgCl. This indicates that no change in the chromophore occurs in this voltage range, and thus also no reduction. Subsequent peaks to the negative (marked by red arrows) led to changes in absorbance and were assigned to reduction processes of dye molecules. The reduction potential of -0.61 V vs. Ag|AgCl can be taken as a rough estimation of the LUMO level (disregarding possible changes in the LUMO upon dye adsorption). The HOMO level can then be calculated from the LUMO by use of absorbance data characteristic for the HOMO-LUMO gap, see also Figure 80(b). In this figure,

[xxxvii] See also section **7.1** for a comparison of the performance of J102 and J109 as sensitizers, and see section **1.2.3** for the dye structure.

different energy levels from different references are compared, to give a rough estimation of the relative position of the energy levels.

Since they were measured under slightly different conditions, the values can only be regarded as rough estimates of the real values in a cell. The references are: [274] for the iodide/triiodide redox couple in acetonitrile and for the TiO_2 conduction and valence band edge, [275] for the ZnO conduction and valence band edge (bulk ZnO, no electrodeposition), [15] and [121] for HOMO and LUMO of D149, DN216 and DN285 (identical conditions as for J109), [155] for the HOMO and LUMO levels of WD-2 and WD-3, and [154] for the HOMO and LUMO level of TPA-B1. The lower reduction potential of J109 compared to the indoline dyes used in this work indicates that the efficiency for electron injection into the conduction band of ZnO for J109 and J102 is decreased, and also the very similar dye J102 [xxxviii].

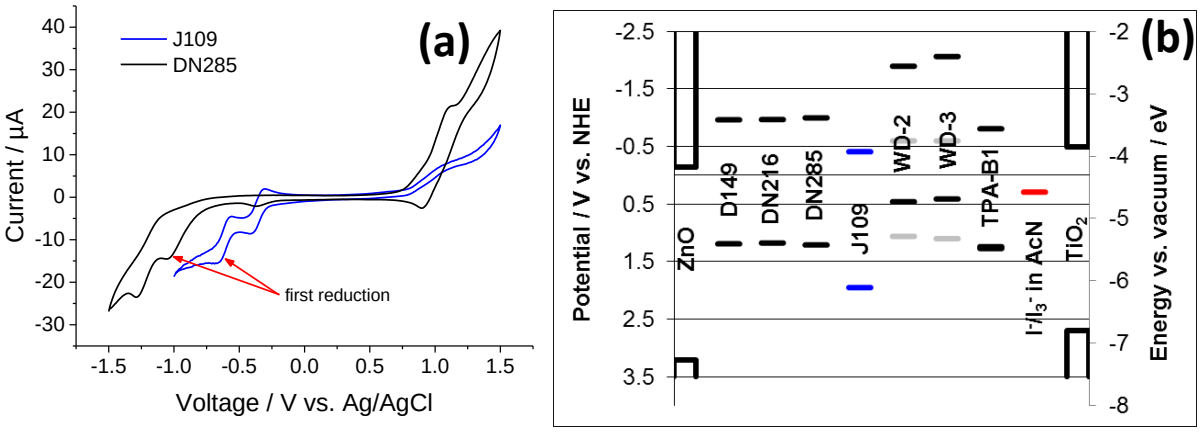

Figure 80 – (a) Cyclic voltammogram of dyes J109 and DN285 in DMF (dye DN285 also shown in [15] and [121]). Red arrows indicate the respective peak of a first reduction of the dyes, assigned by spectroelectrochemistry. (b) Schematic energy diagram of different sensitizers (higher energy – LUMO; lower energy – HOMO), of an electrolyte redox couple (redox level) and of semiconductors (higher energy – conduction band edge; lower energy – valence band edge). As the energies are taken from different references (see text), the relative energetic positions can only be regarded as an estimation. Also dyes discussed in section **7.1** were added.

[xxxviii] The fact that injection from indoline dyes like D149 is not favored into TiO_2 without soaking with AM1.5 light, and that currents (and thus injection) increase by a large amount for a downward shift in the conduction band edge indicates that injection can also be decreased by a large amount for an upward shift of the conduction band edge, or as in the case of J102, for a downward shift of the LUMO by more than 500 mV compared to indoline dyes.

7.3 Conclusions for a sensitization with different dyes

It can be concluded from this section that a sensitization with the perylene dyes J102 and J109 leads to poor efficiencies, partly owing to a low injection efficiency due to a low position of the LUMO of the dyes (see previous section), and partly because of high aggregation and thus enhanced recombination via these aggregates (also see previous section). None of the performed changes in adsorption procedure lead to an increase in efficiency, not even a cosensitization with cholic acid. Thus the changes introduced into the perylene dyes (anchor group, groups to enhance solubility) were not sufficient to lead to efficient sensitizers for ZnO-based DSCs.

The sensitization of ZnO with phthalocyanines with different anchor groups revealed comparatively high I_{SC} and efficiencies for (vinyl-)phosphonic anchor group, higher than for a vinylcarboxylic anchor group. All tested dyes yet showed strong aggregation, as the dyes were not synthesized with spacer groups which would decrease the molecule-molecule interaction. The efficiency for a vinylcarbonyl anchor group was lower than for a phthalocyanine with a phosphonyl group, which was traced back to an increased recombination due to a higher aggregation, and thus I_{SC} also was lower even though the conduction band was shifted to lower energies (probably by the different anchor group). The addition of groups preventing aggregation could render Phthalocyanines with a phosphonyl or vinylphosphonyl group quite efficient

However a sensitization with triphenylamine dyes WD-2, WD-3 and TPA-B1 lead to comparably efficient DSCs, especially when the lower range of the absorbance is taken into account. Thus these triphenylamine dyes could work especially well as cosensitizers for dyes with an absorbance at longer wavelengths because of their strong and relatively narrow absorbance at shorter wavelengths of the visible light spectrum.

8 Conclusions and outlook

In this work, several aspects of DSCs sensitized with organic dyes were addressed. It was shown that indoline dyes DN91, DN216 and DN285 which contained a second anchor group compared to the standard dye D149 reached comparable power conversion efficiencies as this reference dye. Due to the second anchor group the dyes adsorb differently, however for most measurements the differences between the comparably similar dyes were smaller than for variations of the sensitization time. For some of the results, especially for the recombination, a dependence of the values on the length of the spacer of the second binding group was observed (higher recombination resistance at the same DOS with longer alkyl spacer). A variation of the sensitization time led to an optimum between sufficient surface coverage and not too high recombination via molecular aggregates for a time of 15 min on electrodeposited ZnO. A sensitization without coadsorbate mostly led to higher short-circuit current densities, even though recombination was increased due to aggregated molecules, because more dye was adsorbed which compensated the current loss from recombination. By photoelectrochemical measurements at different illumination conditions one of the main causes of the comparably low photocurrents of indoline-sensitized electrodeposited ZnO-based DSCs was ascribed to insufficient regeneration due to a depletion of iodide in the narrow pores. A second cause is the relatively narrow absorption spectrum of the sensitized cells, limiting the current even though the light harvesting efficiency is very high over the absorbed spectral range. A co-sensitization with a dye adsorbing in the longer wavelength range could thus increase the power conversion efficiency. Overall, DSCs sensitized with a second carboxylic anchor group showed similar or better (for DN216) power conversion efficiencies, additionally giving the advantage of a higher binding stability and thus possibly a better long-term stability of cells or the use of more demanding electrolytes.

A small variation in the deposition process at the time of seed formation for the ZnO/EosinY hybrid film led to the highest power conversion efficiency of 4.59 %, thus showing an increase of about 20 % from a comparable cell without change in the electrodeposition. A higher amount of adsorbed dye without increased aggregation and a small shift of E_c to lower energies was found from the detailed analysis of this cell. The different amount of dye speaks of a changed pore structure, which was also macroscopically observed by a less light-scattering behavior of the sensitized film. An enhancement of efficiency thus can already be achieved by small changes in electrodeposition, and the study of the influence of different pore structures on cell efficiency could achieve far larger improvements. The detailed analysis and comparison of different methods as used in this work (especially EIS at different illumination intensities and recombination currents in the dark and under illumination) allows the assignment of changes in different cell parameters to a physical cause, and thus optimization can be performed in the correct direction.

For a sensitization of nanoparticulate TiO_2 a dependence of the absorbance on the dye structure was found, with a higher amount of adsorbed dye for a shorter alkyl spacer of the second anchor group. The photoelectrochemical characteristics varied largely for different illumination conditions, mainly because of a shift of the conduction band edge to lower energies upon high-intensity illumination. The shift of E_c however proved beneficial for all cells, as I_{SC} increased by a factor of 2, without on the other hand increasing recombination. Recombination rather decreased for the very changed film, only recombination via oxidized dye molecules increased as the current increased to values near the transport limit of the electrolyte and thus regeneration was less efficient. After the enhancement of cell parameters by light soaking, TiO_2-based cells reached efficiencies comparable to similarly sensitized ZnO-based DSCs.

Several novel dyes were tested as sensitizers for ZnO-based DSCs. Especially triphenylamine dyes showed the tendency of an efficient sensitizers, however the relatively narrow absorption spectrum of the dyes led to lower efficiencies than the reference dye D149. Phthalocyanine dyes with different anchor groups were not efficient sensitizers for ZnO, even though they showed higher conversion efficiencies than the perylene dyes characterized in this work. The cause for this was mainly a high aggregation of the not yet optimized dyes. A sensitization with Phthalocyanines with a (vinyl-)phosphonic anchor grouped yielded promising results, which could be improved by the addition of side-groups preventing aggregation of the dye molecules.

For all different aspects of this work, the chosen set of experiments proved a powerful tool to assign observed changes in cell parameters to different possible causes. Also a proposed combination of capacitances to an overall capacitance C_{all} and simulations of measured capacitances with C_{all} gave additional information about the trap distribution in the cells, and led to a better understanding of the effect of different parameters on C_μ. From this simulation it is suggested that a simple linear fit of C_μ mostly underestimates the real trap distribution parameter α due to the underlying space-charge capacitance of the substrate or blockinglayer.

9 Appendix

9.1 Supplemental information

This chapter includes graphs which were used for the calculation of cell parameters, additional information to different measurement conditions. Such information is collected at this point, with references within the main text pointing to the respective piece of information. For some graphs, the cell designation slightly differs, e.g. DN216 + CA (1h) [68] instead of $DN216_{1h}^{CA}$ [68].

9.1.1 Influence of the scattering background on the measured absorbance

The absorbance of the semiconductor films used for cell preparation was measured before and after sensitization in a setup including an integrating sphere to avoid major losses (of forward scattered light) due to the comparatively strong light scattering of the ZnO films. The absorbance of the adsorbed dye without ZnO background should be obtained by a subtraction of the absorbance of the film before sensitization from the absorbance after sensitization, compare Figure 81. During the evaluation of the spectra, however, it became clear that this probably is not the case. Some films with very intense coloring, for example those that were sensitized for 1 h, showed lower absorbance of the dye than films sensitized for 15 min (compare e.g. $DN285_{1h}^{DCA}$ (71) with $DN285_{15min}^{DCA}$(63) in Figure 20(d), p. 69). Bye eye, the films sensitized for a longer time were clearly more intensely colored, and also a flattening or cut-off of the absorbance curve for most sensitizations for 1 h however indicated that the lower limit of light detection of the instrument was reached even though the absorbance values did not reach a maximum, and it was obvious that the films were highly absorbing.

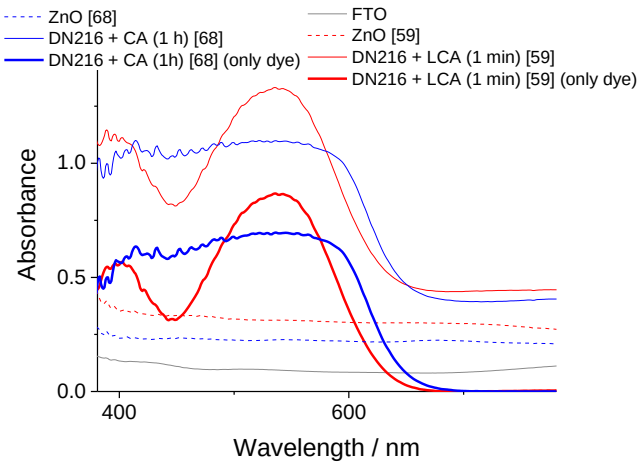

Figure 81 – Different spectra used for the calculation of the absorbance of the dye adsorbed to the semiconductor, and the resulting spectra (thick lines).

For films which showed less light scattering, e.g. film [70] discussed in chapter **4** or TiO_2 films, the maxima showed a comparable height as for a sensitization for shorter times, even though the films were sensitized for 1 h. Thus it was surmised that either the scattering or the change in scattering could be the cause for a depressed absorbance maximum especially for longer sensitization times. Possible causes for a change in the scattering background from unsensitized to sensitized films are:

- a change of the porosity by a filling of small pores by dye molecules (or other adsorbates), and thus a different Rayleigh scattering
- a change in the refractivity index ZnO/air to ZnO/dye/air (probably larger for more adsorbed dye), especially for multilayer dye adsorption [126] for longer sensitization times
- a change of the reflectivity of the ZnO film upon sensitization (macroscopic dye crystals partly show a metallic reflection), increasing the portion of backscattered (not captured) light, also especially for longer sensitization times
- a change of the ZnO film/surface during sensitization, possibly leading to a change in the scattering properties, which will become more important for longer adsorption times

Also in the literature, a similar cut-off shape of the absorbance maxima was observed for a longer sensitization with D149 [16,126], and the shape of the spectra was attributed to a change in absorbance due to molecular aggregates [16]. A different indoline dye DN-7, which is supposed to have a lower aggregation tendency at the ZnO surface than D149, did not show such a marked change in the shape of the spectrum even for an absorption time of 1 h [126].

Despite the efforts made for the measurement and the evaluation of the absorbance, the resulting spectra probably contain the varying effects of a changed scattering background or another unknown parameter. Thus the obtained spectra cannot be used for the exact determination of the dye content and a comparison of different sensitization times. Only the descending slope from 600 to 700 nm can be used for an estimation of the dye content or aggregation of dye molecules, with a broadening expected for an increased absorbance, and a change of the slope expected for different aggregation. As the light scattering property of the films is on the other hand beneficial for the cell, the films should not be produced with lower scattering. For an exact determination of the dye content, the dye could be desorbed from the surface [16], but then the films would not be exact those as in the cells, and more importantly, the very good binding of the double-anchor dyes would probably not lead to a complete desorption of the dye layer [15,121].

9.1.2 Differences in voltage corrections for EIS measurements

When current flows through the solar cell during EIS measurements, the applied voltage has to be corrected for voltage drops at a resistance to obtain a correct evaluation. As mentioned in **1.3.3.5**, p. 35, two different voltage corrections can be applied for EIS measurements at voltages different from V_{OC}, which both yield the voltage corrected by the voltage drop at the series resistance, V_f (for measurements at V_{OC}, $V_{OC} = V_f$). The first correction utilizes R_{rec}, the second method R_{series}. For the second method (which was used for the voltage correction of the EIS measurements in this work), R_{series} is determined at a voltage where still all three semicircles from the different charge-transfer processes can be observed in the EIS spectrum. R_{series} is then assumed to be constant over the complete voltage range, as some of the resistances cannot be determined at low absolute voltages, because the respective semicircle is no longer visible in the spectra. This seems to be a reasonable assumption, as for the measurement voltage range used in this work, the series resistance R_{series} was approximately constant for a similar DSC in the literature [16]. [xxxix]

Both methods of evaluation were applied for EIS data sets at AM1.5 illumination, and C_μ is plotted against both corrected voltages and against the uncorrected, applied voltage V_{appl}, in Figure 82(b). It can be observed that both corrections result in a more linear curve shape for more negative voltages, where the current flow and thus the voltage drop at the series resistance is larger. Both corrections result over a large range in very similar curves, with a shape and position very similar to the measurement at V_{OC}, which does not need a correction. However for the correction with R_{rec}, at low absolute voltages the values of V_f scatter strongly, as R_{rec} becomes very large and can be determined with less accuracy due to an incomplete semicircle in the EIS spectrum. As also R_{rec} should be evaluated with a corrected voltage, the two corrections are compared for R_{rec} in Figure 82(d). R_{rec} vs. the two differently corrected voltages has a more linear curve shape than a plot vs. V_{appl} at more negative voltages (similar to C_μ), and the measurement at V_{OC} shows a similar slope (the higher values of R_{rec} at V_{OC} are due to lower recombination at lower illumination intensity, see section **3.3.2**). Similar to C_μ, for plots of R_{rec} the correction with R_{series} yields values with a lower scattering especially at voltages near 0 V.

For EIS measurements in the dark, see Figure 82(a,c), a correction of the voltage with R_{rec} could not be achieved (performed in OriginPro), as the current ranged over several orders of magnitude where different shunt resistances were applied by the potentiostat.

[xxxix] An exponentially increasing value of R_t was estimated for a ZnO-based DSC in a voltage range between ca. -0.3 and -0.7 V, and the applied voltage was then corrected for voltage drop on the resulting increasing R_{series}. The corrected voltage showed almost no change compared to a correction with an almost constant R_{series}, as R_{rec} is still much higher for all voltages.

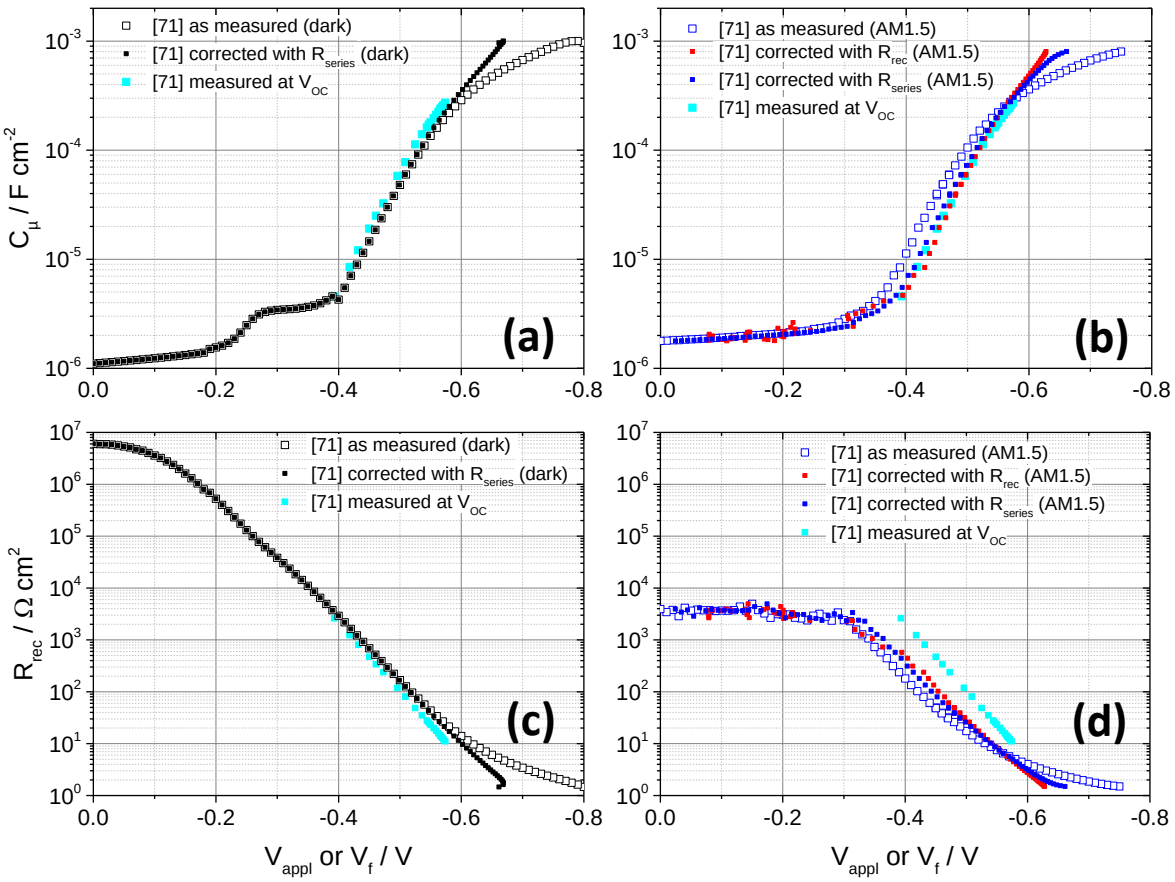

Figure 82 – Plot of C_μ (a,b) and R_{rec} (c,d) of cell [71] before and after correction of the applied voltage V_{appl} by the voltage drop at the series resistance. The uncorrected curves (open symbols) are plotted against V_{appl} while corrected curves are plotted against the corrected voltage V_f. Measurements in the dark (a,c) and under AM1.5 illumination (b,d) are shown. For measurements at AM1.5, two possible corrections are shown, and correction with R_{series} is used for the evaluation throughout this work, see text for details. The corrected curves are compared with a measurement at $V_{OC} = V_f$, see cyan curves.

The correction with R_{series} was possible, and resulted in a similar slope of C_μ as the EIS measurement at V_{OC}, and a good overlap with C_μ vs. V_{appl} is observed for voltage regions where small currents flow, the same is the case for R_{rec} in Figure 82(c).All corrections of the voltage for EIS measurements were performed with R_{series} on the basis of these experiments. Not only is the scattering of the corrected voltage considerably lower at low absolute voltages so that a simulation of C_μ is possible almost down to 0 V (Figure 26, p. 82), but also an evaluation of EIS measurements in the dark easily obtained, and valuable comparison of EIS at different light intensity can be performed. Another less technical reason for the decision for a correction with R_{series} is that the correction of the voltage with R_{rec} is based on the modelling of the voltage, and V_{OC} is treated as a constant [216]. This is approximately the case for measurements in the dark, however for AM1.5 illumination V_{OC} will change during the first few measurements (starting at more negative voltages), as the cell warms in the very intense light (see also discussion in section **9.1.3**). For TiO_2 cells, the decrease in V_{OC} is even larger, so that it cannot be assumed as constant, and the voltage correction with R_{series} is more appropriate.

9.1.3 Differences and influences of the applied EIS measurement modes

Three different measuring modes were applied for EIS measurements and are described here to indicate the differences, which will also influence the EIS values obtained. The respective EIS values like the chemical capacitance C_μ and the recombination resistance R_{rec} are determined by fitting the EIS spectra obtained from the different measurement modes with an equivalent circuit as described in section **2.5.3**.

EIS at AM1.5: For all functioning cells in this work, EIS at simulated AM1.5 illumination (100 mW cm^{-2}) with an applied voltage was measured. For all voltages except the open-circuit voltage a forward or reverse direct current is flowing additionally to the current induced by the small perturbation. The long illumination at high intensity also leads to a heating of the cell to about 50°C, which changes the cell characteristics [127]. The lowering of the V_{OC} in comparison to short measurements like IV-curves is the most significant change observed for long illumination times. Melanie Rudolph showed by heating of a DSC sample and by simulation of IV-curves at different temperatures [127], that this decrease of the V_{OC} can be explained by an increase of the temperature by the heating of the active layer, as the temperature is also included in the diode equation, equation **(5)**. When the increase in the temperature was accompanied by an increase of the short-circuit current, these changes were attributed to a lowering of the conduction band edge through the intense (partly UV) illumination, in addition to the effects of the temperature (see also [261]). If a decrease in current was observed, this change was explained by a possible desorption of dye molecules from the ZnO surface.

EIS at red LED illumination (V_{OC}): For most cells, also EIS at different intensities of red LED illumination was measured (diode RTR within the Zahner setup, intensities from 0.1 to 25 mW cm^{-2}). The measurements were performed at approximately open-circuit by determining the open-circuit voltage at each illumination intensity, and then applying the respective V_{OC} value to the cell. The respective V_{OC} can be used without correction for a plot of the respective values, as no current is flowing through the cell, except for the current induced by the small perturbation. Also no heating was observed for long illumination times due to comparably low illumination intensities.

EIS in the dark: For film numbers [57] and higher, also EIS in the dark was measured, as recombination can be different in the dark [18]. The method is otherwise identical to the measurement mode at AM1.5. Direct currents are flowing through the cell dependent on applied voltages. The currents from the small perturbation (voltage is modulated) are superimposed on these currents.

The effects of the different illumination conditions that are observed for the different EIS measurement modes, are to some extent also visible in IV-curves measured at comparable conditions. Figure 83 shows different IV-curves measured for cell $DN285_{1h}^{CA}$ [71] before and after EIS measured at different illumination conditions. The measurement sequence is the following:

- IV-curve (without preceding illumination)
- EIS at red LED illumination
- EIS in the dark, IV-curve (after EIS dark)
- EIS at AM1.5 illumination
- IV-curve (after EIS at AM1.5)
- IV-curve (6 days after EIS at AM1.5).

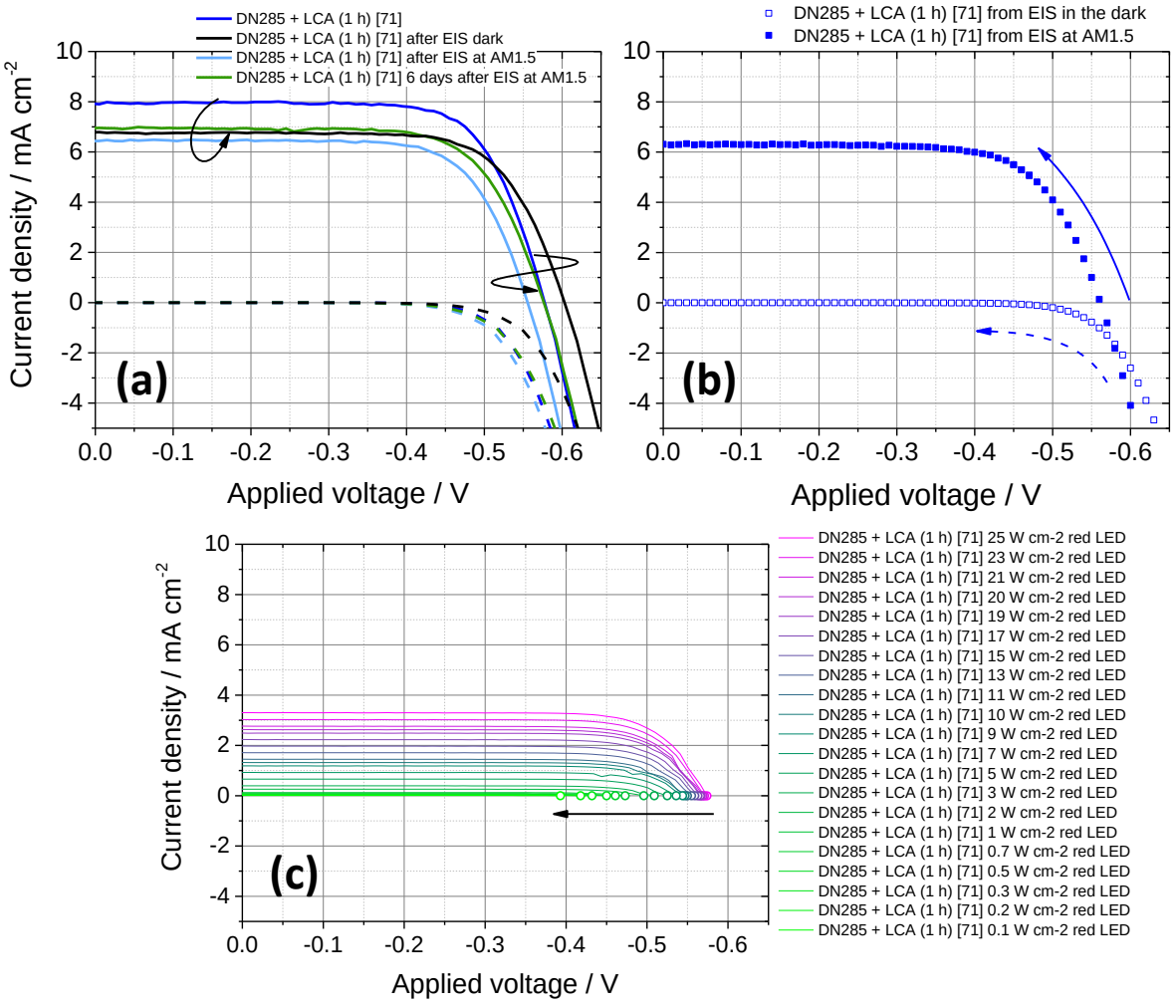

Figure 83 – IV-curves of cell [71] for different illumination conditions (without mask). (a) IV-curves in the dark and under AM1.5 simulated sunlight, each one measurement at the beginning, one after long illumination (during EIS at AM1.5) and one after regeneration in the dark for 6 days, see legend for the respective color coding. (b) IV-curve from measurement points of EIS measurements in the dark or at AM1.5 illumination. Each point represents one EIS measurement. (c) IV-curves at different red LED intensities. – Dashed lines and open symbols indicate measurements in the dark, while full lines and symbols indicate measurements at AM1.5 illumination. Arrows in (a) indicate the direction of change, arrows in (b) and (c) indicate the measurement direction of the EIS measurements. The sequence of curves in the legends is according to the sequence of the measurements.

The IV-curves measured before or after the different EIS measurements are shown in Figure 83(a). For the EIS-measurements, IV-curves can be reconstructed from the applied voltage and the measured direct current, shown in Figure 83(b). These IV-curves correspond well with the IV-measurements after the respective EIS measurement. Following the sequence of the IV-measurements, the following observations are made, together with most probable explanations (see also the following results, for example for the validation of the supposed conduction band edge shifts). The first IV-curve of cell [71] shows the highest short-circuit current density I_{SC}, and an intermediate open-circuit voltage V_{OC}. A shift of the conduction band edge to higher energy during the measurement of EIS at red LED illumination or EIS in the dark could explain the higher V_{OC} and lower I_{SC} observed for the IV-curve measured after EIS in the dark. The observed rise in V_{OC} especially during EIS at red LED illumination was observed for most cells, partly accompanied by a decrease in I_{SC}. An upward shift of the conduction band edge is usually effected by a change in the surface dipole at the semiconductor surface, for example by a decrease of positive charge at the surface [261]. In the IV-curve measured directly after the EIS measurement at AM1.5 illumination, I_{SC} and V_{OC} decrease to the lowest value for the IV-curves shown in Figure 83(a). The change in V_{OC} is mainly attributed to an increase in temperature during the long high-intensity illumination [127], and also to a downward shift of the conduction band edge upon illumination [261], see also the results of the chemical capacitance further below. Such a downward shift of E_c often leads to an increase of I_{SC}. As this is not observed here, it is probable that also a degradation of the cell takes place, for example by a change of the surface coverage of ZnO, or a change in the electrolyte. This becomes clearer when the IV-curve after a storage in the dark for 6 days is compared to this IV-curve. V_{OC} increases to the value of the first IV-curve (which supposes that the conduction band edge is on a similar position, if no other changes like a retarded or increased recombination occurred), while I_{SC} does not recover the initial value. Some of the changes discussed shortly here will also be discussed with the help of the results from EIS measurements further below, which will show that the proposed conduction band edge shifts can be proven by photoelectrochemical measurements.

The IV-curves measured before each EIS measurement at red LED illumination are shown in Figure 83(c). At the highest-intensity red LED illumination, at 25 mW cm^{-2}, I_{SC} is considerably smaller than at AM1.5 due to the lower intensity, however. When the red LED intensity decreases, also the current and the voltage decrease according to the respective dependence on illumination (see also results on intensity-dependent J_{SC} and V_{OC}).

9.1.4 Influence of a different deposition area on film and cell properties

During the preparation of DSCs from electrodeposited ZnO it was noted that a different deposition area affected cell parameters like I_{SC}. It was observed that a smaller deposition area led to higher I_{SC} values than larger cells (diameter 4 or 7 mm).This difference is for example observed for a comparison of IV-curves in chapters **3** and **5**. Even though electrodeposited films are usually subjected to smaller fluctuations of cell values [127], the change for a different deposition area was comparatively large and systematic. The change could for example be caused by a higher voltage drop at cell resistances due to the higher overall current, even though the current at the sensitized interface should be similar. Another explanation of a higher current is a changed deposition due to a different mask area. When electrodeposition is performed, only a small fraction of the substrate is exposed to the deposition solution by the application of a punched tape as mask, in order to obtain a defined area where porous ZnO grows. The tape is high compared to the final electrodeposited ZnO film, and could thus affect convection during the rotation of the substrate. For a smaller deposition area, this effect will be larger, especially if the small punched hole does not lie exactly in the center of the rotating electrode. After electrodeposition, a comparison by eye and in the microscope shows that usually films with smaller mask area are more scattering, and small grains overgrow a film with comparatively homogeneous film thickness. Such differences in ZnO could result in the observed change of cell parameters, and at least a part of the changes observed for different mask areas are attributed to such changes in the ZnO electrodeposition

9.1.5 Charge densities n_{SC} from measurements at I_{SC}

It was found by Melanie Rudolph, that a charge normalization proposed for charge extraction is also needed for capacitance measurements, so that relative shifts in the conduction band edge can be determined without influences of the total trap density N_t [17,127]. This value is obtained from graphs of n_{SC} vs. I_{SC}, which are listed here for the different chapters.

The charge densities n_{SC} determined from current transients and used for normalization in Figure 41(b,d) are shown in Figure 86. The position of the charge density curves in Figure 86(a) (without normalization) varies without a correlation to the dye or coadsorbate. When the curves are normalized to the measurement of cell [61] in Figure 86(b), a slightly different dependence of n_{SC} on the short-circuit current can be observed for cells sensitized with or without coadsorbate. At higher light intensities (and higher I_{SC}), cells sensitized without coadsorbate show a lower charge density than most cells sensitized in the presence of a coadsorbate, even though the curves show a better overlap for lower light intensities.

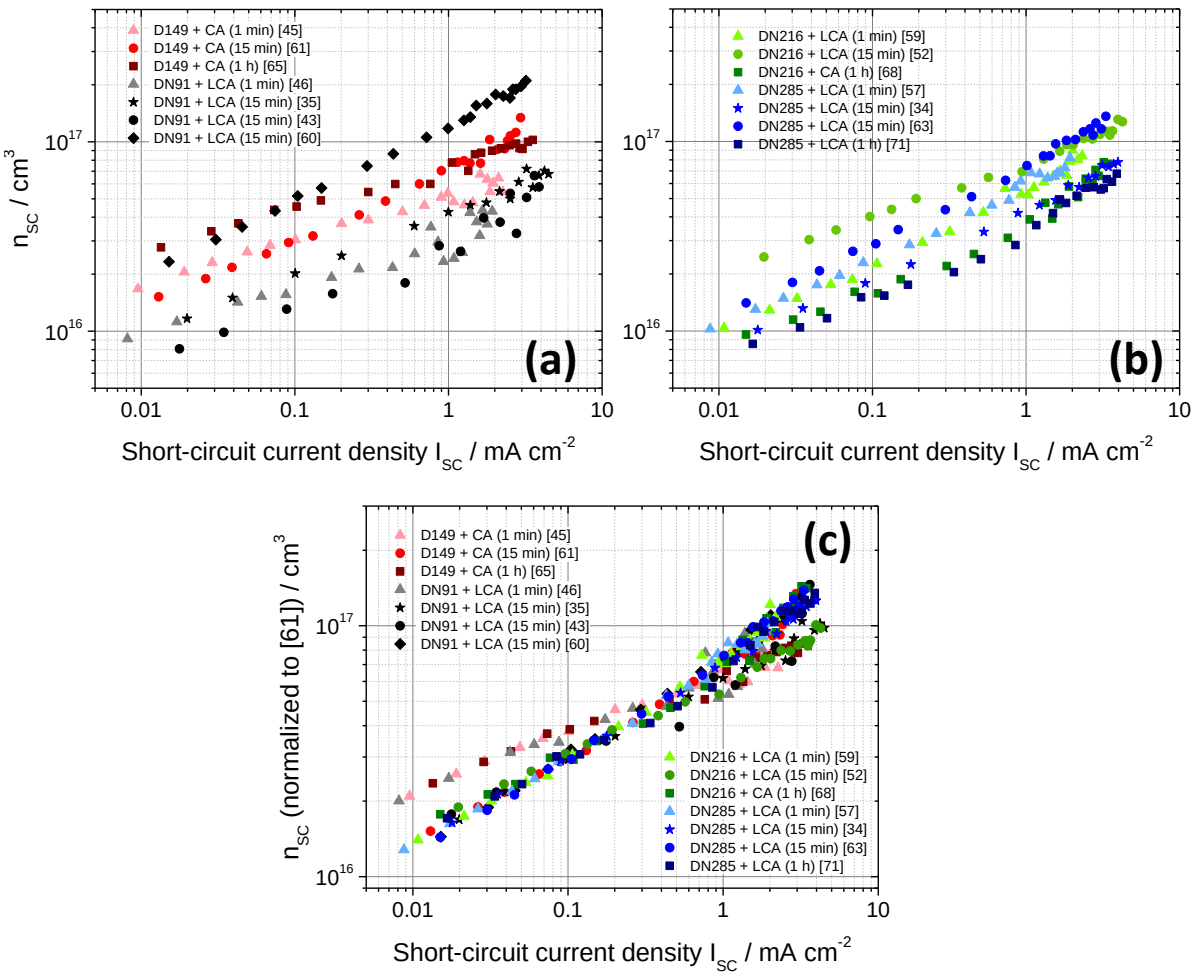

Figure 84 – Charge densities determined from current transient curves at short circuit, performed at red LED illumination. The cells were sensitized with (a) D149, DN91, (b) DN216 or DN285 and a coadsorbate for different sensitization times. (c) n_{SC} normalized to a reference cell, cell [61]. Increasing color depth indicates increasing sensitization time, and different symbol shapes of the same color indicate different cells sensitized with the same sensitization procedure.

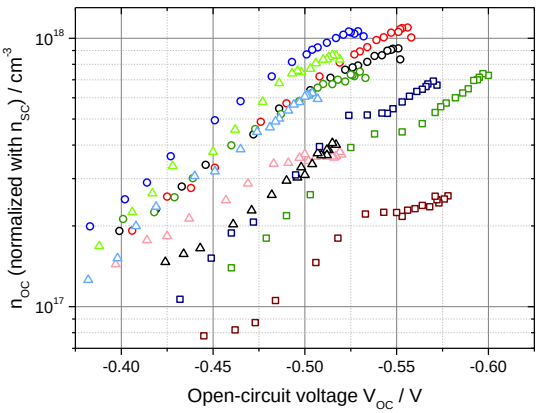

Figure 85 – n_{OC} determined from charge extraction, vs. V_{OC}. Similar to C_μ, n_{OC} was corrected for the total trap density. The different colors indicate different sensitizers, compare the legend in Figure 84 (here open instead of filled symbols are used).

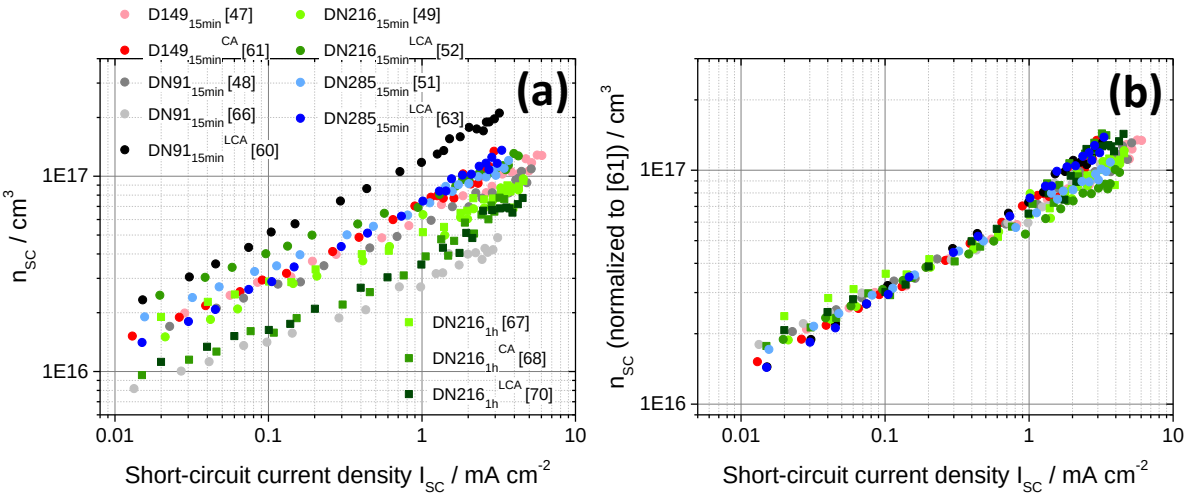

Figure 86 – Charge density n_{SC} from short-circuit current transients, determined for DSCs sensitized with different indoline dyes with or without a coadsorbate. (a) Values as determined from the measurement and (b) values normalized to a reference cell, cell [61]. Squares indicate cells sensitized for 1 h, while circles indicate cells sensitized for 15 min. Lighter colors indicate a sensitization without coadsorbate, and darker colors indicate sensitization with coadsorbate, according to the legends.

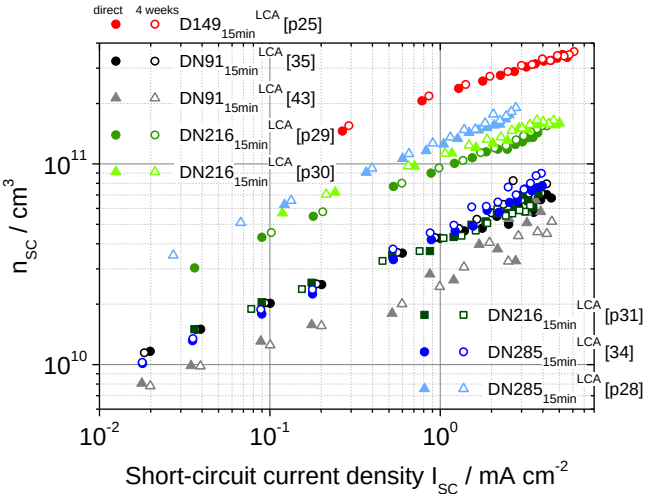

Figure 87 – Electron density at short circuit n_{SC}, determined from photocurrent decay measurements of indoline-based DSCs. Filled symbols indicate measurements after preparation, open symbols indicate measurements performed after a 4 weeks storage of the cells in the dark. Adapted from [259].

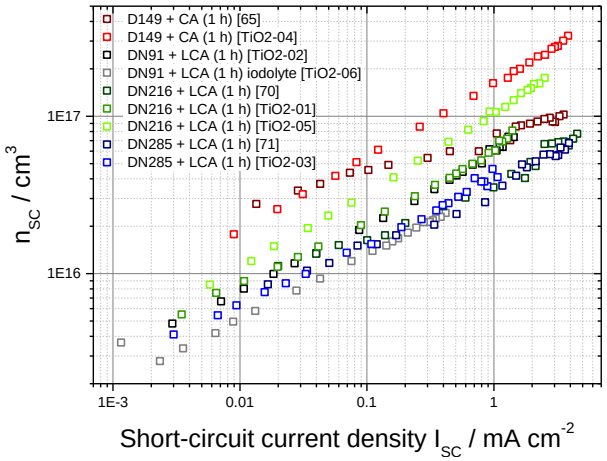

Figure 88 – Charge density n_{SC} determined from current transients, for DSCs based on TiO_2 and ZnO films. Lighter colors indicate TiO_2-based cells, while darker colors indicate ZnO-based cells, according to the legend. Relative values of $N_t/N_{t,ref}$ determined from this graph are listed in Table 14.

9.1.6 Density of states

The density of states (DOS) can be calculated directly from the chemical capacitance C_μ with equation **(25)**. Even though the information from the DOS is similar compared to C_μ (except when films with different thickness and porosity are compared), the representation of the energy qV_f vs. the DOS in the following graphs gives a more intuitive view of the density of states in the cells.

Indoline sensitizers on ZnO

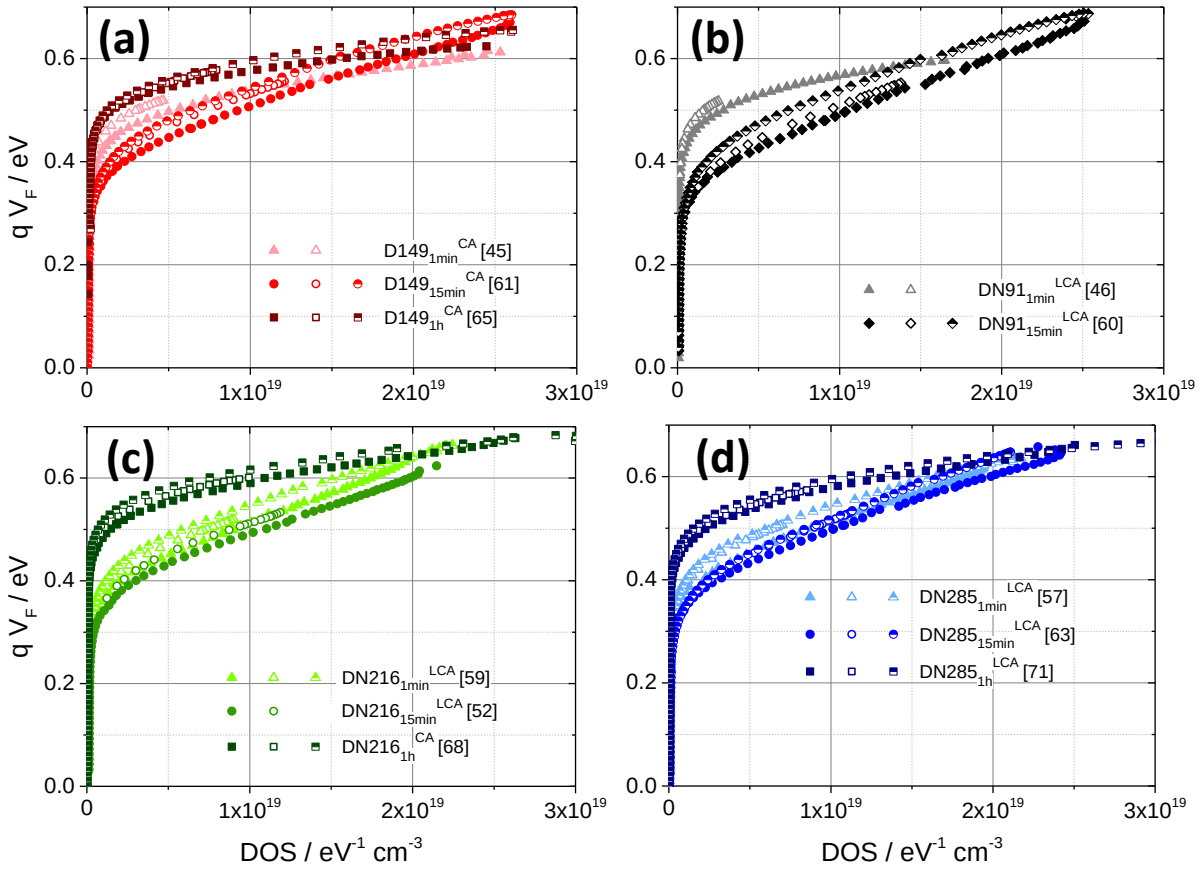

Figure 89 – Energy (in eV) vs. density of states for differently sensitized DSCs as determined from the chemical capacitance C_μ, grouped after the sensitizing dye; (a) D149, (b) DN91, (c) DN216 and (d) DN285. Increasing color depth indicates increasing sensitization time. Filled symbols indicate measurements at AM1.5 illumination, open symbols indicate measurements at red LED illumination and V_{OC}, and half-filled symbols indicate measurements in the dark. Symbols of the same color but a different shape indicate different cells sensitized with the same dye and for the same sensitization time. See also the legends for exact designation of the measurement curves.

Influence of the coadsorbate

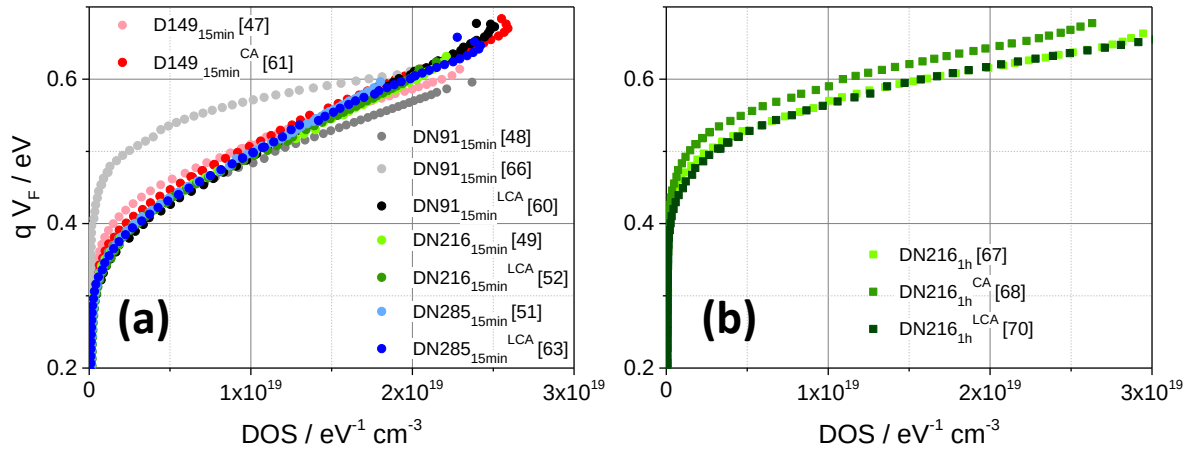

Figure 90 – Energy of the trap states vs. the density of states for ZnO-based DSCs sensitized with different indoline dyes in the presence or absence of a coadsorbate; (a) sensitization time of 15 min and (b) sensitization time of 1 h. Only measurements at AM1.5 illumination are shown.

Changes in ZnO-based DSCs after storage in the dark

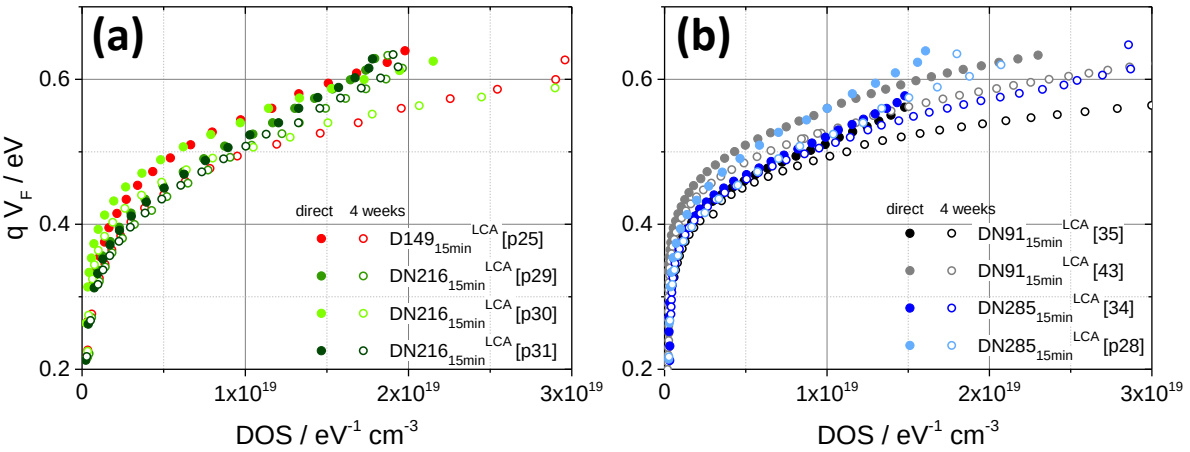

Figure 91 – Density of states of dye-sensitized cells sensitized with different indoline dyes, (a) D149 and DN216, (b) DN91 and DN285. Filled symbols indicate measurements performed after the preparation of the cells, open symbols of the same color indicate a measurement of the same cell after storage in the dark for 4 weeks. Adapted from [259].

TiO_2 films sensitized with indoline dyes

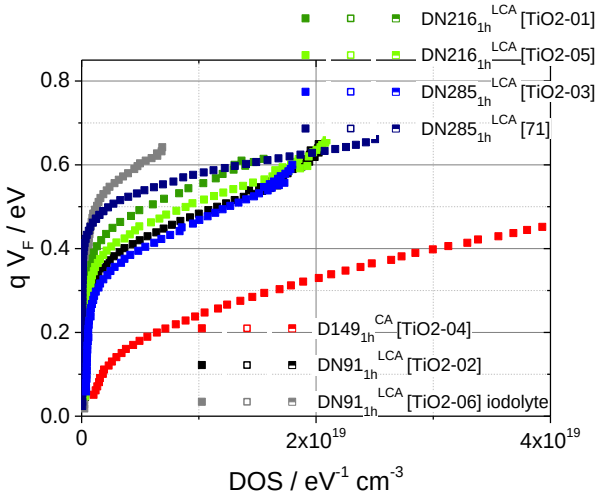

Figure 92 – Energy of the trap states (in eV) vs. density of states for TiO_2-based DSCs sensitized with different indoline dyes and a coadsorbate for 1 h, and one ZnO-based cell for comparison (dark blue). The different colors indicate different indoline sensitizers, according to the legend. Filled symbols indicate measurements at AM1.5, open symbols indicate measurements at red LED illumination, and half-filled symbols indicate measurements in the dark. Some data points for TiO_2-based cells at AM1.5 illumination at higher energies were deleted to avoid the impression of a peak in the DOS.

9.1.7 Recombination

Recombination in DSCs can be compared with different plots of R_{rec}, τ_n and V_{OC}. Some plots are shown in the context of the discussion in the respective chapters, while other graphs (used e.g. for the determination of β) are shown here. The graphs in this section include for example R_{rec} vs. V_f, β vs.V_f, τ_n vs. V_f, recombination currents vs. V_c, and V_{OC} vs. illumination intensity

Indoline sensitizers on ZnO

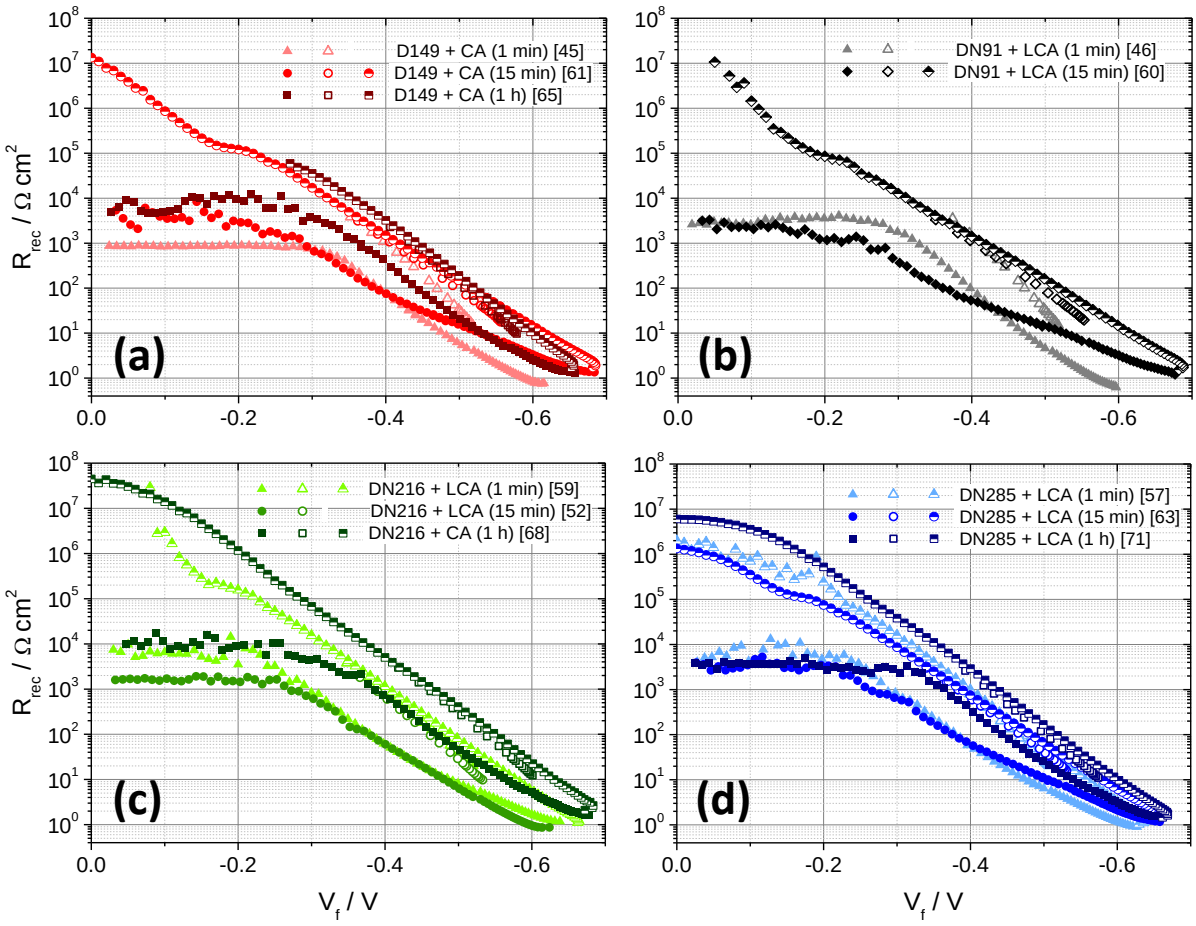

Figure 93 – Recombination resistance against V_f of ZnO-based DSCs sensitized with different indoline dyes. The measurement curves are grouped after sensitization time. Increasing color depth indicates increasing sensitization time. Filled symbols indicate measurements at AM1.5, open symbols indicate measurements at V_{OC} and red LED illumination, and half-filled symbols indicate measurements in the dark.

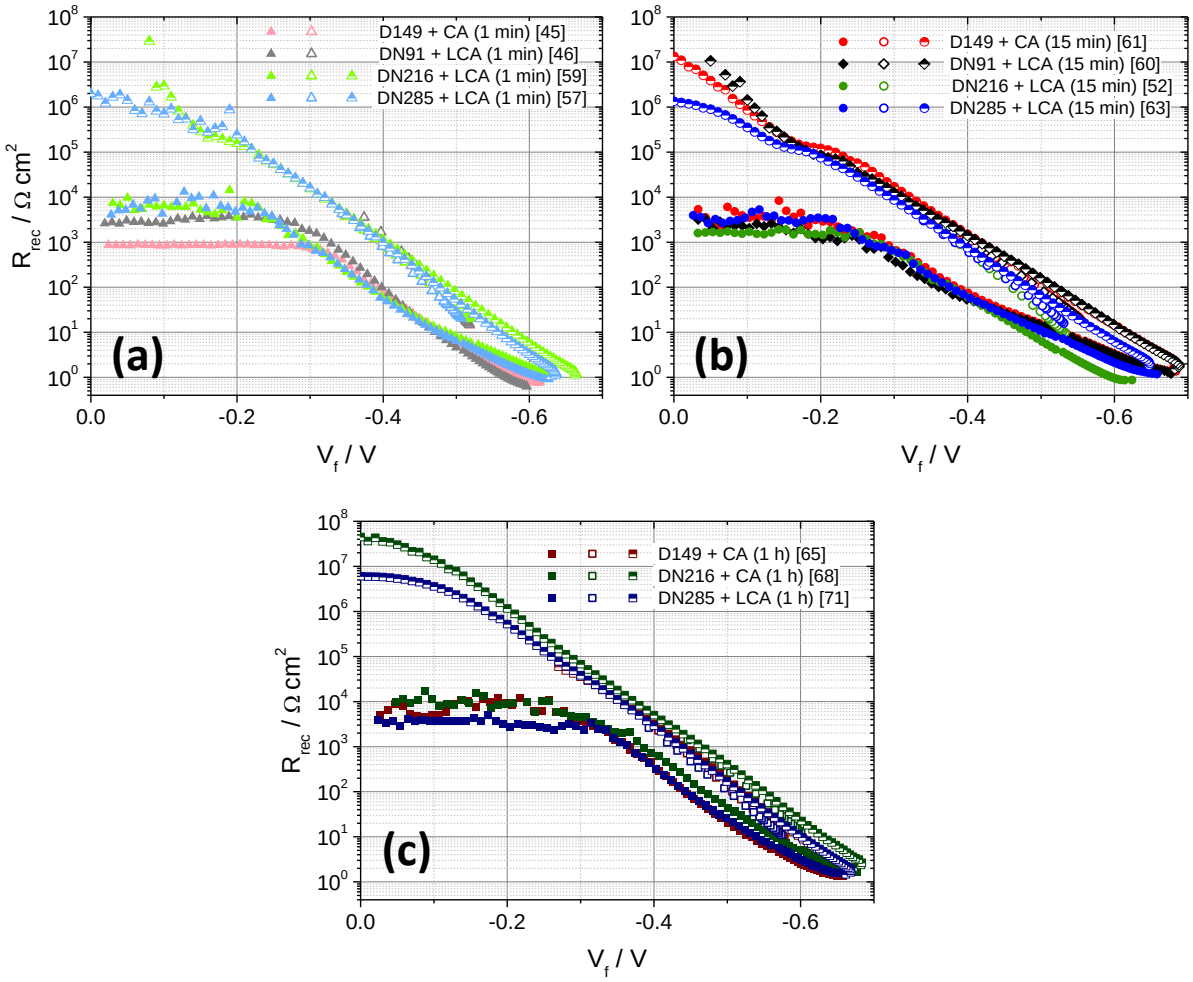

Figure 94 – Same as Figure 93, grouped after sensitization time of (a) 1 min, (b) 15 min and (c) 1 h.

Determination of β

As the recombination resistance is not linear in a logarithmic scale over the complete range of measurement (especially for measurements performed at AM1.5 illumination), for the determination of β a similar approach as for the determination of α was used, i.e. the slope of the logarithm of the recombination resistance vs. the Fermi level voltage V_f was determined, and β was calculated from that slope. The resulting distribution of the recombination parameter β vs. V_f for the different cells sensitized with indoline dyes and a coadsorbate are shown in Figure 95. The general shape of distribution of the recombination parameter β shows low β values for low absolute voltages, and for more negative voltages β increases, and often a plateau with constant β values is observed. Such a plateau indicates an exponential region of R_{rec}, thus a value of β was determined for each measurement and listed in Table 7. The β values at voltages near 0 V can be neglected, as the back layer resistance R_{BL} dominates the recombination resistance. It seems that in contrast to α values, where a similar method yielded $\alpha < \alpha$ (simulated), the method yields higher values of β at least for some cells, as

values >1 are observed for some measurements. An ideality factor close to unity was observed before in a cell with low open-circuit voltage V_{OC} [222] due to an addition of Li^+ to the electrolyte, which led to a lowering of the conduction band edge. It was concluded that recombination for a cell with high β occurs mainly via the conduction band to acceptor states in the electrolyte, and not by a larger part via surface states [205,276] as for most cells with a higher conduction band edge [59,205]. It was also found that a direct transfer of electrons via the conduction band demands a value of $\beta \approx 1$, and such a value was found for voltages close to the conduction band [65,202,277].

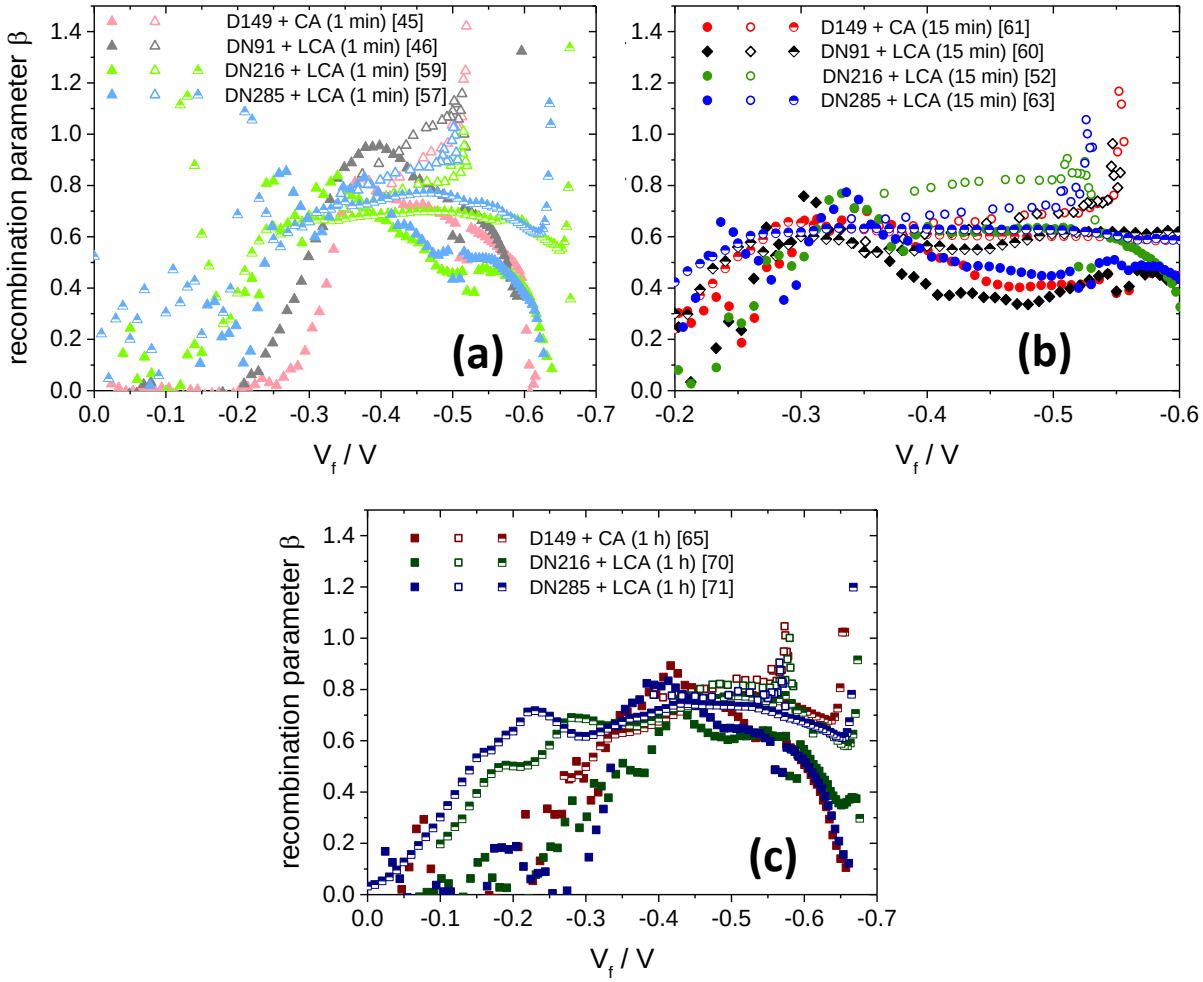

Figure 95 – Distribution of the recombination parameter β (determined from the recombination resistance in Figure 93 and Figure 94, see text for details) for DSCs sensitized with different indoline sensitizers and for different times. The graphs are grouped after the sensitizing time, (a) 1 min, (b) 15 min and (c) 1 h. Increasing color depth indicates increasing sensitization time, and different colors indicate the different sensitizers used. EIS measurements at AM1.5 illumination are indicated by filled symbols, while measurements at red LED illumination and V_{OC} are indicated by open symbols, and measurements in the dark are indicated by half-filled symbols, see legends for exact designation. At low absolute voltages, β is low due to the increasing effects of the back layer resistance.

Electron lifetime against voltage

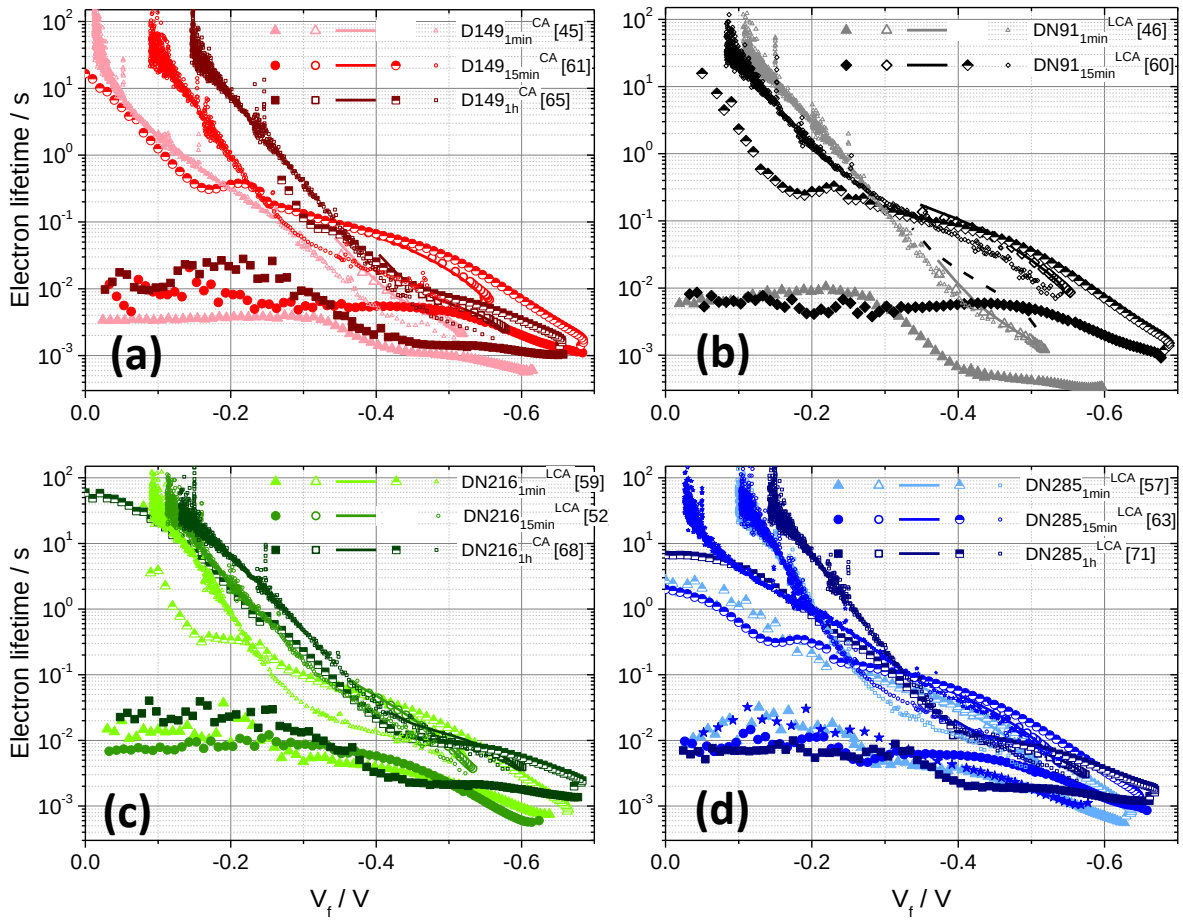

Figure 96 – Electron lifetime τ_n for DSCs sensitized with different dyes and a coadsorbate for different times. The measurements are grouped after the dye, (a) D149, (b) DN91, (c) DN216 and (d) DN285). Graphs were obtained from EIS (larger symbols), IMVS (lines) or OCVD (small symbols) measurements. Increasing color depth indicates increasing sensitization time, according to the legends. EIS measurements with filled symbols indicate measurements at AM1.5 illumination, open symbols indicate measurements at red LED illumination and V_{OC}, and half-filled symbols indicate EIS measurements in the dark.

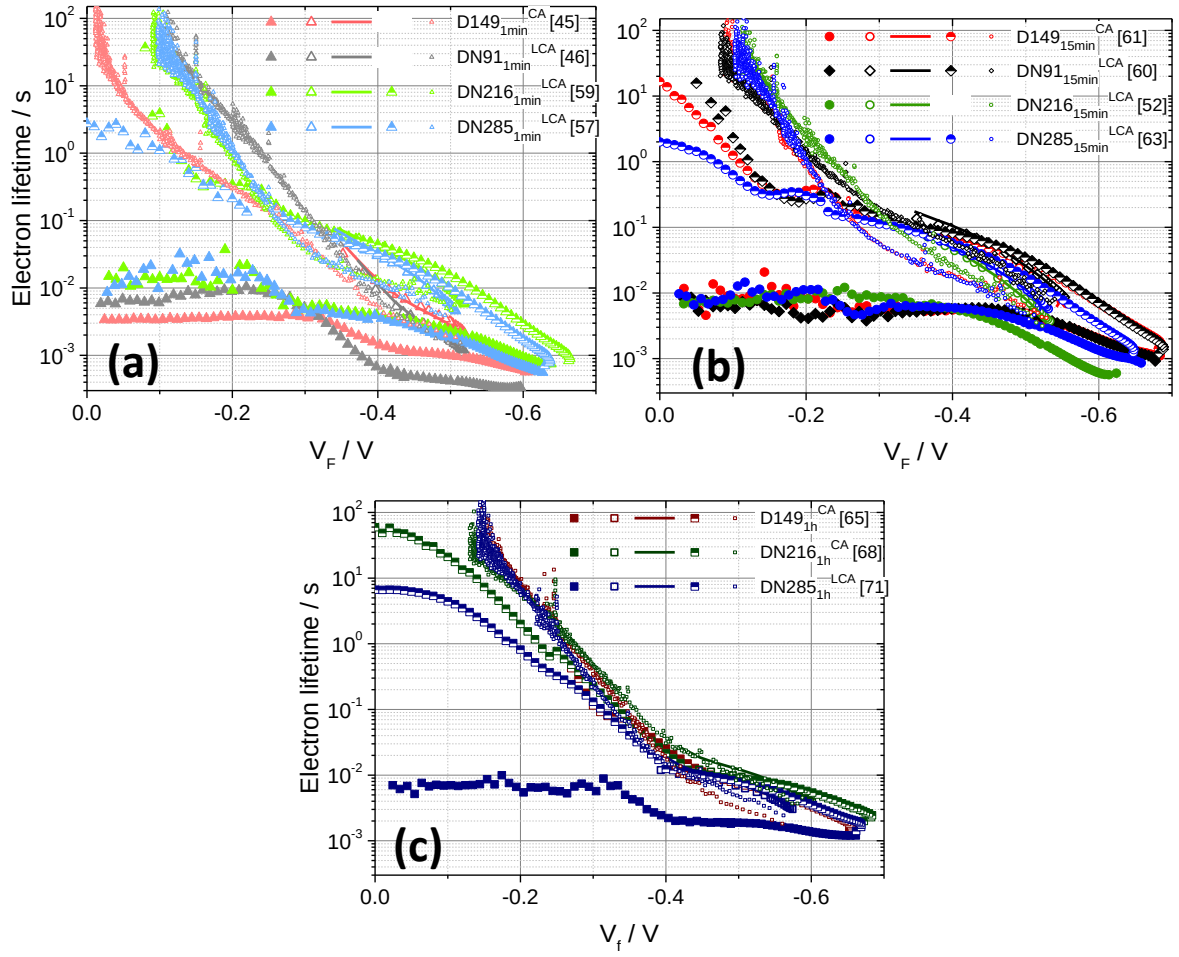

Figure 97 – Electron lifetime τ_n – same as Figure 96, grouped after the sensitization time of (a) 1 min, (b) 15 min and (c) 1 h.

Recombination current against corrected voltage

Similar to the determination in [17] (see also section **1.3.3.1**), an estimation of the recombination currents under illumination was determined and is compared with the recombination in the dark in Figure 98 (absolute values of the IV-curves in the dark taken for direct comparison). The voltage was corrected for resistance losses, and the current was plotted logarithmically to avoid an overestimation of large currents at voltages beyond the open-circuit voltage (which however together with measured higher currents and thus larger variation for the calculated recombination current under illumination leads to more scattered data at low absolute voltages). A difference in slope and in the absolute values of the recombination currents can be observed for most cells, the recombination current in the dark always being smaller than the recombination current under illumination. The difference of the two recombination currents is smaller especially for cells sensitized for 1 h, and the largest difference is found for cells sensitized for 15 min. The same trend can also be observed for the difference of the recombination current R_{rec} measured in the dark and under illumination, see also section **3.3.2**. As the IV-curves at AM1.5 (from which the recombination currents under illumination were calculated) were

measured directly after the IV-curves in the dark, no major change like heating or shift of the conduction band edge occurred in the cell. Thus the difference in the recombination current can be ascribed to recombination via oxidized dye molecules by depletion of reduced electrolyte species under illumination. Similar findings were described for very similar films in [17,127], also with the supposition that the differences could be caused by an enhanced recombination by oxidized electrolyte species accumulated under illumination [257]. The finding that almost no difference is observed for the recombination current in the dark and under illumination for cells sensitized for 1 h (cell [65] and cell [71]) could be caused by the calculation of the recombination current under illumination (i.e. subtraction of the short-circuit current density from the IV-curve under illumination). By this calculation it is assumed that no recombination occurs under short circuit conditions [16,257], which is expected to be the case for recombination via surface states of the semiconductor, but which does not hold for recombination via oxidized dye molecules. If recombination via oxidized dye molecules occurs already at short circuit for the cells, this part of the recombination will not be accounted for in the comparison of the recombination currents in the dark and under illumination.

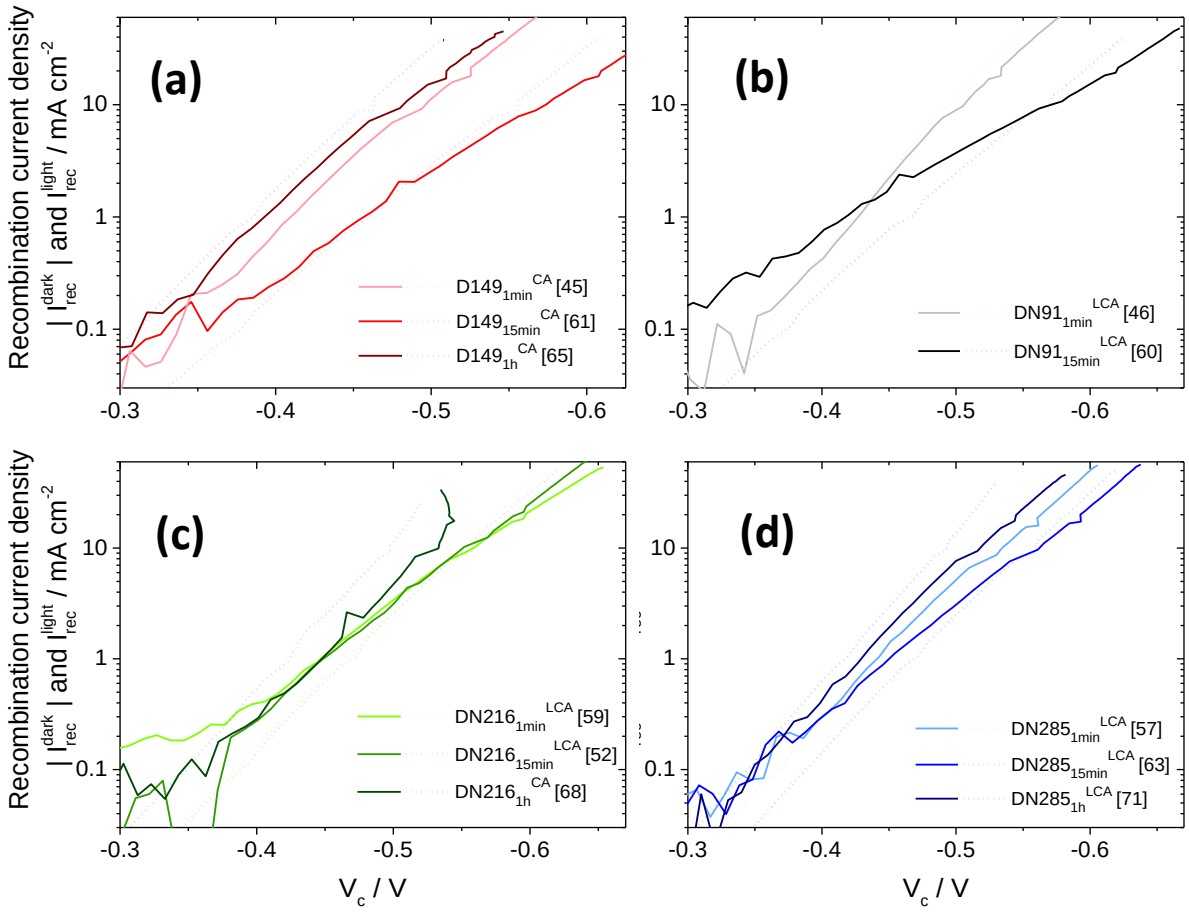

Figure 98 – Recombination current in the dark (dotted lines) or under AM1.5 illumination (full lines) of indoline-sensitized DSCs. Graphs grouped after the dye, (a) D149, (b) DN91, (c) DN216 and (d) DN285. The voltage V_c includes a correction with the conduction band edge shift determined from C_μ.

Open-circuit voltage against intensity

The curves of V_{OC} measured at different red LED intensities are shown in Figure 99 for the different cells sensitized with different indoline dyes. The graphs are grouped after the sensitizing dye, which allows a comparison of the influence of the sensitization time. Analyzing the shape of the V_{OC} vs. intensity curves, most of the graphs do not show linearity over the complete intensity range on a semi-logarithmic scale. As this observed non-linearity is not confined to low intensities, it was concluded that this behavior is not due to a less efficient blocking-layer covering the substrate, but due to the different influences of surface and bulk traps, see also section **3.3.2**. For cells which show recombination via the substrate (for example for cell [43]), the electron lifetime from OCVD measurements shows a nonlinear (and lower than expected) lifetime at voltages near 0 V, as cell [45] in Figure 97.

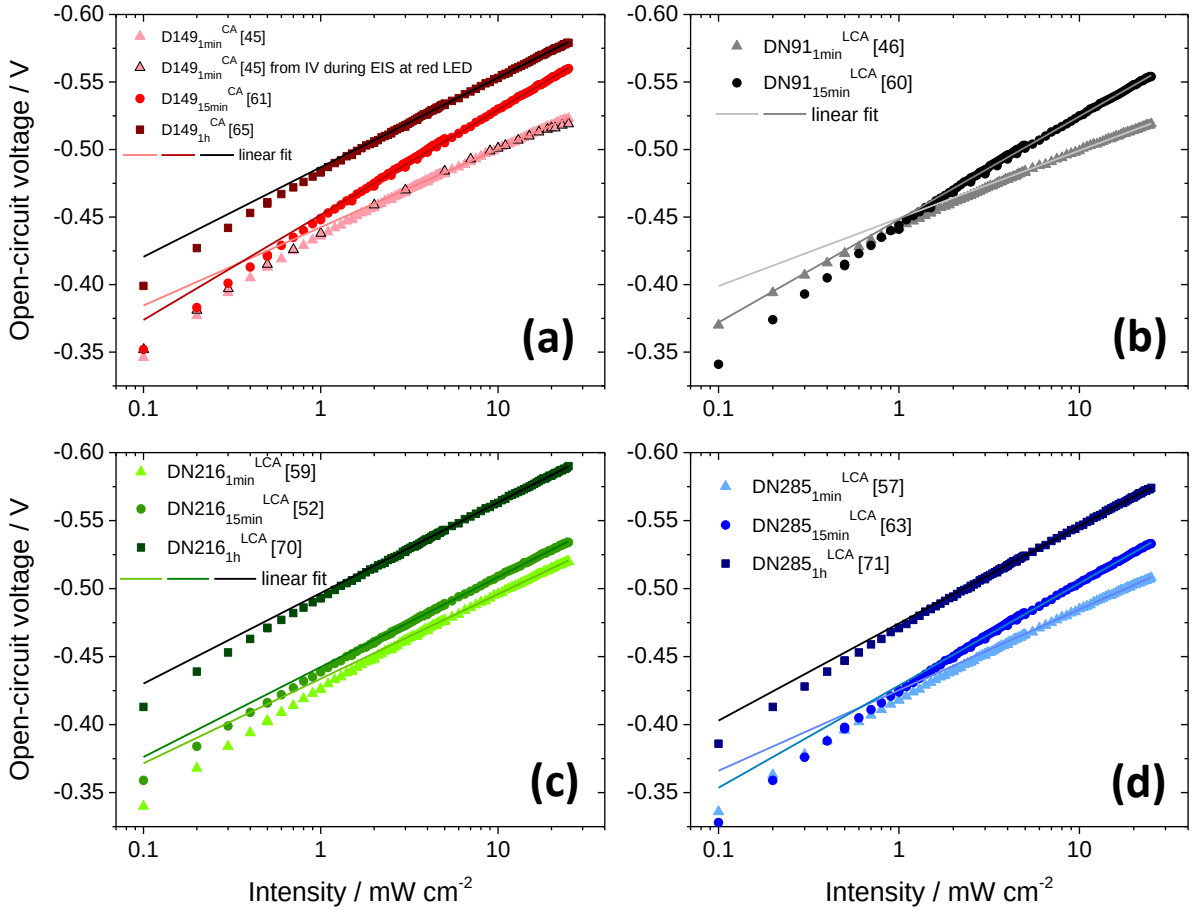

Figure 99 – Open-circuit voltage vs. intensity plots for DSCs sensitized with different indoline dyes and for different times, grouped after the sensitizer dyes, (a) D149, (b) DN91, (c) DN216 and (d) DN285, each with a coadsorbate. Increasing color depth indicates increasing adsorption time according to the legends. In (a), the V_{OC} vs. intensity curve for cell [45] was additionally determined from IV-curves at different red LED intensities, each measured before the EIS at the respective illumination intensity. In (d), no V_{OC} vs. intensity was measured directly after the preparation of cell [34], so a curve measured 4 weeks after preparation is shown. For most of the cells, the measurements were performed in two stages that overlap in the center of the graph. A lower slope indicates a lower ideality factor m and a higher recombination parameter β. Lines indicate linear fits of V_{OC} , fitted to values at higher light intensity.

To explain the high β values found from these measurements, V_{OC} vs. the illumination intensity determined from IV-curves before EIS at different red LED illumination intensity is also shown in Figure 99(a) for cell [45], giving a very similar shape of the curve, only with a lower slope at high light intensities. This difference in the slope is thus most probably explained by an enhancement of V_{OC} during the measurement of EIS at red LED illumination, as discussed in section **9.1.3**. For a comparison with EIS measurements, a value of β was also determined from V_{OC} vs. intensity measurements for each cell. The values, determined at higher light intensities (almost at maximum intensities), are listed in Table 7, and the respective linear fits are also shown in Figure 99. Compared to the β values determined from EIS at red LED illumination, the β from V_{OC} vs. illumination is higher for all cells. The β parameter for different voltages for the V_{OC} vs. intensity curves shows a similar dependence on the voltage as β determined from EIS measurements at red LED illumination, with increasing β for increasing absolute voltage. This behavior is ascribed to an increasing part of the recombination via oxidized dye molecules (because of inefficient regeneration) with increasing light intensity. Such a decrease of the slope for higher intensities was not observed for DSCs based on ZnO nanoparticles [203], probably because of a different pore structure and thus a different transport of electrolyte species in the pores (see also section **6.3**).

Influence of the coadsorbate

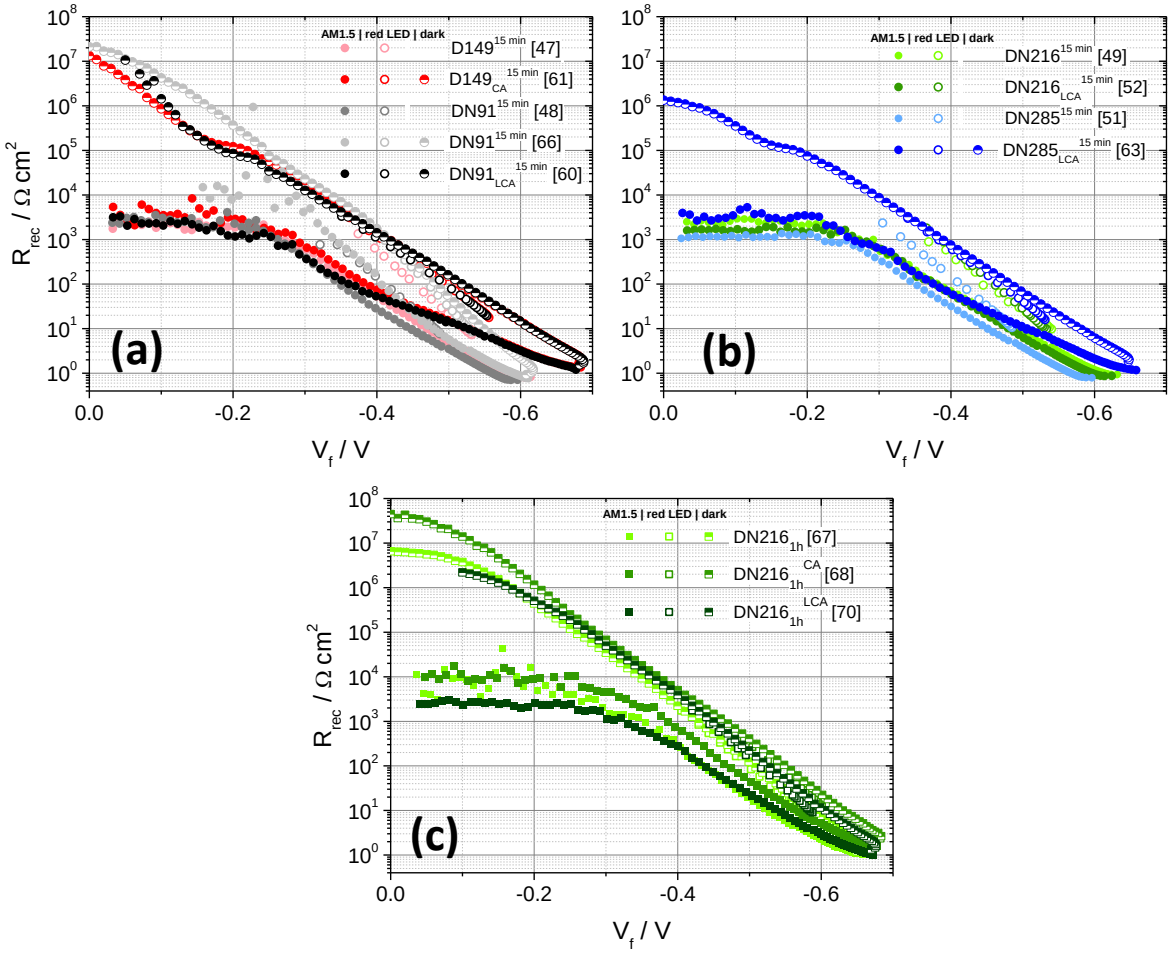

Figure 100 – Recombination resistance R_{rec} of ZnO-based DSCs sensitized with different indoline dyes in the presence or in the absence of a coadsorbate. (a,b) Cells sensitized for 15 min and (c) cells sensitized for 1 h. Lighter colors indicate an adsorption without coadsorbate, and darker colors indicate an adsorption with coadsorbate, according to the legends. Filled symbols indicate measurements at AM1.5 illumination, open symbols indicate measurements at red LED illumination and V_{OC}, and half-filled symbols indicate measurements in the dark.

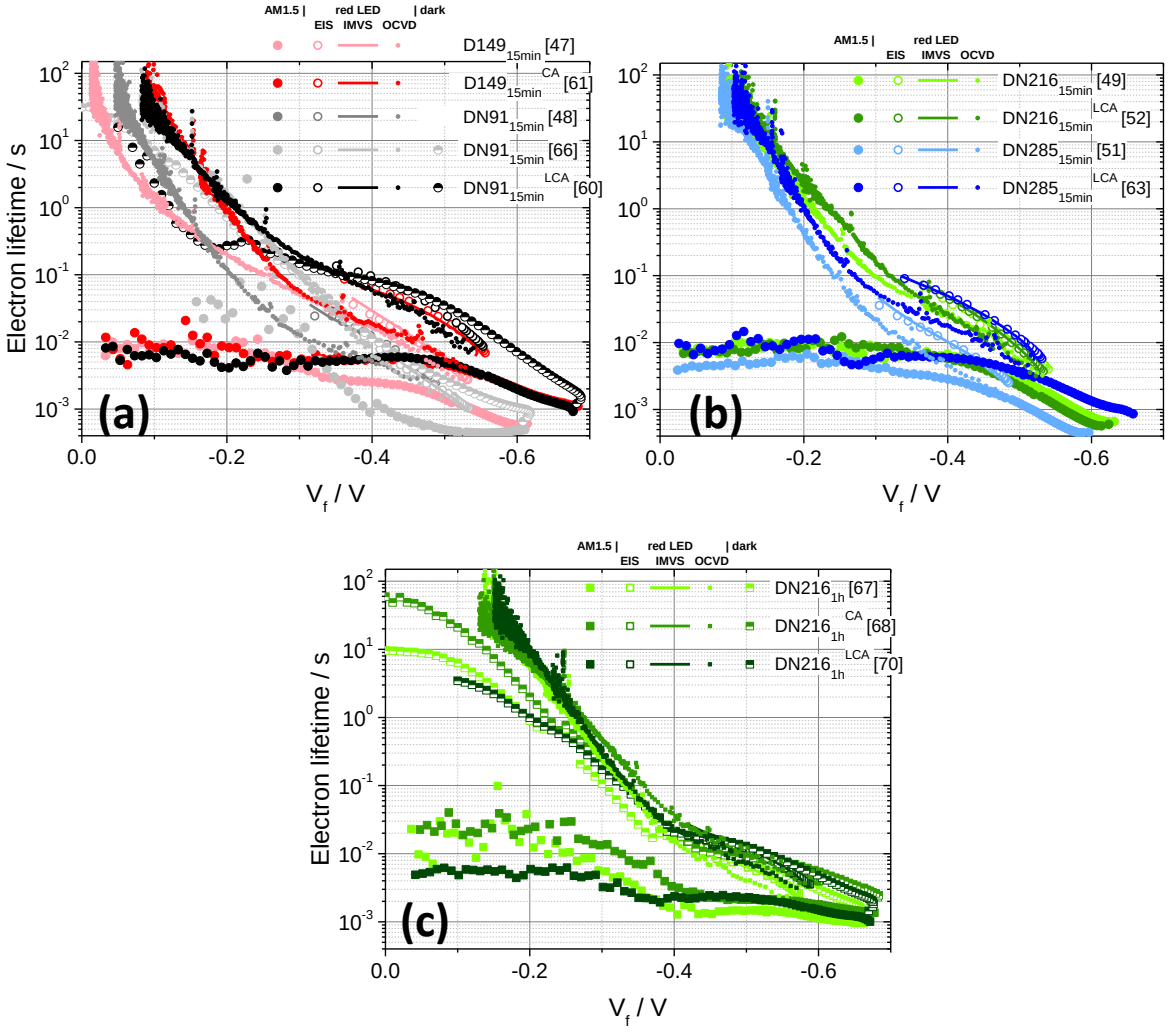

Figure 101 – Electron lifetime τ_n vs. V_f of ZnO-based DSCs sensitized with different indoline dyes with or without a coadsorbate, (a,b) adsorbed for 15 min and (c) adsorbed for 1 h. Values from EIS measurements at AM1.5 illumination are indicated by larger filled symbols, from EIS measurements at red LED by open symbols, and from EIS measurements in the dark by half-filled symbols. Values from IMVS measurements are indicated by a line, and from OCVD measurements by small symbols. Lighter colors indicate cells without coadsorbate, while darker colors indicate cells with coadsorbate.

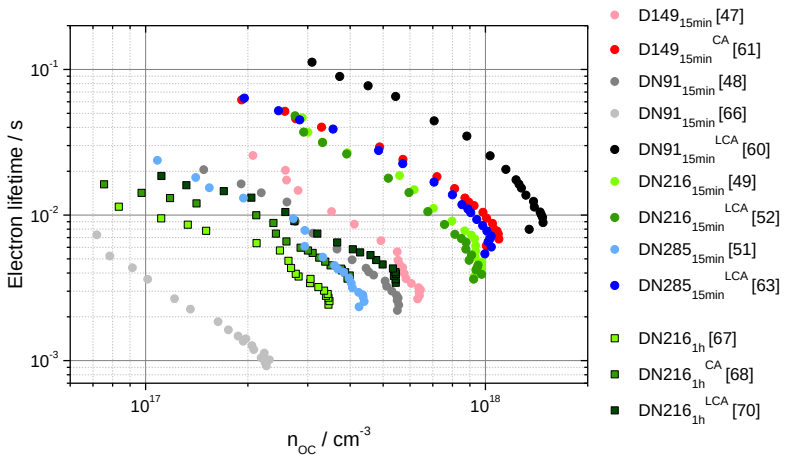

Figure 102 – τ_n from IMVS vs. the charge density n_{OC} from charge extraction (both determined at V_{OC}), for cells sensitized with and without a coadsorbate. Lighter colors indicate cells sensitized without coadsorbate, darker colors indicate a sensitization with coadsorbate. Circles indicate a sensitization for 15 min, while cells sensitized for 1 h are designated by squares.

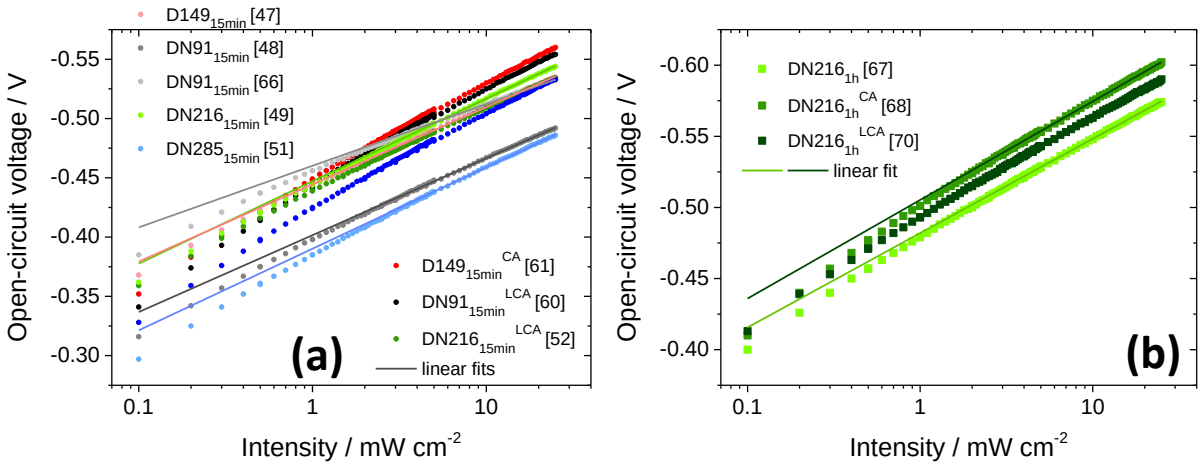

Figure 103 – Open-circuit voltage V_{OC} vs. red LED illumination intensity for ZnO-based cells sensitized with different indoline dyes in the presence or absence of a coadsorbate for (a) 15 min, and (b) 1 h. Lighter colors indicate cells sensitized without a coadsorbate, and darker colors indicate cells sensitized with a coadsorbate, according to the legends. All measurements were fitted by a linear fit (indicated by lines) to determine β (see Table 9).

Changes in ZnO-based DSCs after storage in the dark

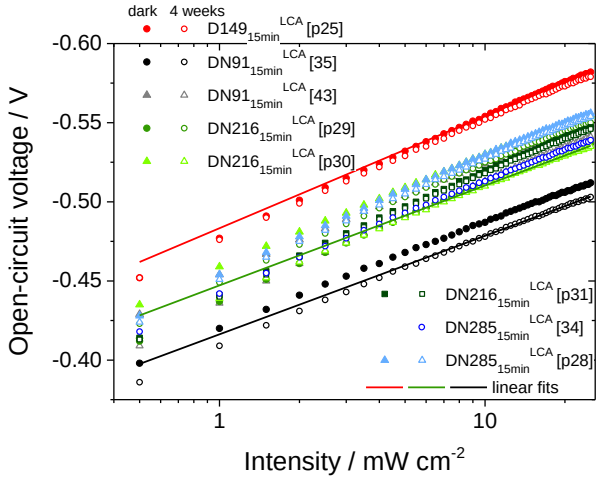

Figure 104 – Open-circuit voltage measured vs. illumination intensity (red LED illumination) for indoline-sensitized DSCs before and after storage in the dark for 4 weeks. Filled symbols indicate measurements directly after cell preparation, and open symbols indicate measurements after storage in the dark for 4 weeks (only measurement after 4 weeks for cell [34]). Different indoline dyes are indicated by different colors, see the legend for exact designation. Adapted from [259].

9.1.8 Variation of the electrolyte concentration

For a sensitization with DN216 and DN285 with a coadsorbate for 1 min, the electrolyte was varied. The variation consisted in a higher concentration of the electrolyte components (except the solvent acetonitrile), and the results are shown in this chapter. Additionally, one of the reference cells was also measured at cyan LED illumination additionally to the standardly used red LED illumination, and the results are also compared here.

Some variations were performed during the preparation and characterizations of ZnO-based solar cells which can shed more light on the working of the solar cells and how results are affected by these variations. In particular, an electrolyte was applied with a larger concentration of all electrolyte components like ionic liquid and iodide, which was achieved by evaporation of the solvent, acetonitrile. This variation of the electrolyte was used for two cells sensitized for 1 min with either DN216 or DN285 and a coadsorbate. As the cells show comparable results for all measurements, only one of these cells will be shown for measurements that lead to a larger number of graphs, like EIS measurements. The results for the varied electrolyte will also be compared to cells prepared by the same sensitization procedure, but filled with the standard electrolyte.

Another variation discussed in this section is the diode illumination during several photoelectrochemical measurements. For most of the measurements, a red LED with an intensity maximum at 632 nm is used. As this wavelength is not in the maximum absorbance of the indoline dyes (see also vertical line in Figure 105(b)), it should ensure a homogeneous absorption of light over the complete film thickness. For one cell, cell [57], an additional measurement of the same methods was performed with the use of a cyan LED (coded CYR), which has a maximum of the intensity at 513 nm. This wavelength is well within the absorbance maximum of the indoline dyes, which should lead to a higher absorbance of the light at the illuminated side (substrate side). Possible differences on the results of the different measurements will also be discussed in this chapter. The results from this variation are also important for cells sensitized with dyes with a different absorption maximum (section **7**).

The absorbance of the films used for the cells with higher-concentrated electrolyte was already discussed in the context of different sensitization times (section **3.1**). Except for small differences in the absolute absorbance due to possible variations of the amount of adsorbed dye for the short adsorption time, the absorbance is the same for the same sensitizer. The current-voltage curves of the cells with the higher concentrated electrolyte (Figure 105(a)) however reveal that even though the absorbance is very similar, the different electrolyte changes the cell behavior by a large extent. The short-circuit current I_{SC} of the cells with the higher concentrated electrolyte decreases to about half of the value found for cells containing the standard electrolyte, see also Table 20. Also the open-circuit voltage V_{OC} decreases when the concentration of electrolyte components is increased.

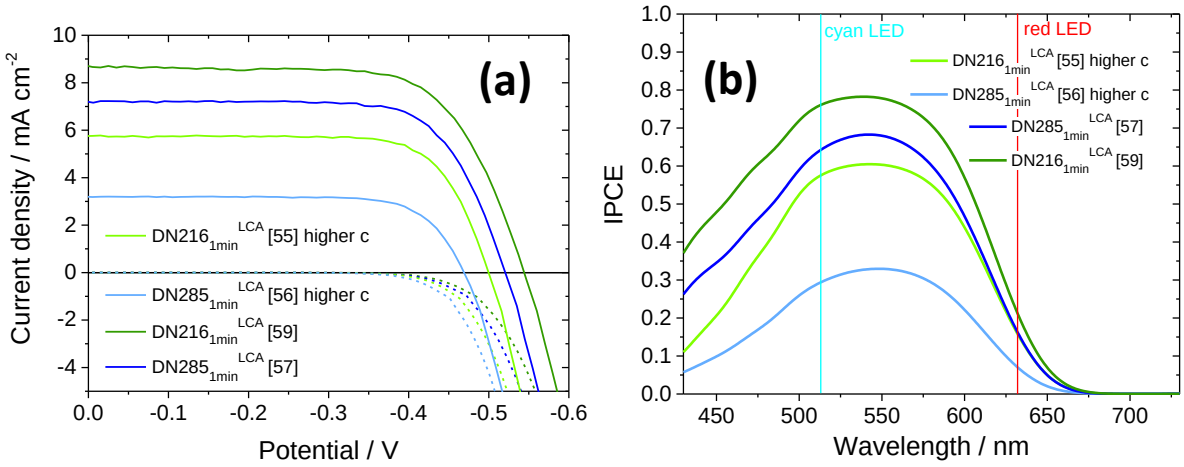

Figure 105 – (a) IV-curves for ZnO-based DSCs sensitized with indoline dyes. For two of the cells, the electrolyte was varied by increasing the concentration of the electrolyte components. (b) Incident photon-to-electron conversion efficiency for the same cells. The different colors of the curves indicate a sensitization by different sensitizers according to the legends. Darker colors indicate cells containing the standard electrolyte, while lighter colors indicate cells containing a varied, higher concentrated electrolyte. Vertical lines in (b) indicate the wavelength of the LEDs used for many photoelectrochemical measurements.

With a slightly higher FF for the varied cells, the power conversion efficiency decreases to about two thirds (DN216 as sensitizer) or one third (DN285 as sensitizer) of the value with standard electrolyte. Even though an increase of electrolyte species (especially iodide) should increase the current density, as the regeneration efficiency should increase [255], on the other hand regeneration is enhanced for a higher density of acceptor states in the electrolyte. The causes of the decrease in the different cell parameters will be discussed in the context of recombination further below.

A similar decrease as for the short-circuit current is also observed for the incident photon-to-current conversion efficiency (IPCE) in Figure 105(b), as the integrated convolution of the IPCE and the AM1.5 spectrum should amount to the short-circuit current density. As the absorbance is very similar for the same sensitizer, the shape of the IPCE spectrum also does not change significantly.

As mentioned above, because of the large number of graphs for EIS measurements and the similarity of the results, only the curves of cells [56] and [57] will be shown for most EIS measurements.

Table 20 – Cell parameters from IV-curves shown in Figure 105(a).

Film	I_{sc}	V_{oc}	FF	Efficiency
	[mA cm^{-2}]	[V]		[%]
DN216$_{1min}^{LCA}$ [55] higher c	5.76	-0.500	0.74	**2.12**
DN216$_{1min}^{LCA}$ [59]	8.66	-0.544	0.70	**3.24**
DN285$_{1min}^{LCA}$ [56] higher c	3.18	-0.469	0.75	**1.12**
DN285$_{1min}^{LCA}$ [57]	7.85	-0.521	0.73	**2.94**

Additionally, the measurements of cell [57] at cyan LED illumination are shown for a comparison of the influence of the wavelength of the illumination source during PEC measurements. Figure 106 contains several graphs of either the chemical capacitance C_μ or values related to C_μ.

The chemical capacitance (Figure 106(a)) of the two cells [56] (with higher-concentrated electrolyte) and [57] (with standard electrolyte) is very similar over the complete voltage range. For cells [55] and [59] (both sensitized with DN216; not shown), the differences due to the different electrolyte are even smaller. The small differences in the chemical capacitance are conceivable as the same sensitization is applied, and the ZnO films were also deposited on consecutive days (which mostly means a more similar deposition, and thus a more similar internal structure of the films). Also the different illumination conditions influence cells with the different electrolytes in the same manner (e.g. shift to less negative voltages for AM1.5 illumination, see also the respective discussion in the previous sections). However, illumination with a cyan LED leads to a change of the chemical capacitance compared to an illumination with a red LED. The resulting shape and position of the capacitance curve for the cyan LED illumination resembles more the curve shape under AM1.5 illumination than the dark measurement, in fact it is almost identical in the available voltage range. The measurement at red LED illumination resembles more the measurement in the dark, with slightly higher C_μ values at more negative voltages.

To estimate the shift of the conduction band edge for the different cells, the chemical capacitance was (as for the differently sensitized films in section **3.3.1**) corrected by the relative total trap density, $N_t/N_{t,ref}$ (see also Table 21 for these values). These values were determined from a plot of the charge density n_{SC} vs. the short-circuit current density, Figure 106(c), where the curves were shifted to overlap with a reference cell, cell [61]. The shifted curves are shown in Figure 106(d) (cell [61] not shown in this graph). This normalization also makes the values comparable to results discussed above and below. The shape of the charge density plots is very similar for all four cells that were compared with a different electrolyte. For the variation of the LED sources (red or cyan light) it can be observed that even without a shift, the curves of cell [57] measured at red LED light and at cyan LED light overlap. This is a strong indication that the assumption that the trap density stays constant for the same cell at different illumination conditions is true, so that the value $N_t/N_{t,ref}$ (usually determined at red LED light) can also be used for the correction of C_μ from measurements at AM1.5 illumination and from measurements in the dark (as it is done for all normalized capacitance curves in this work).

The chemical capacitance corrected by the total trap density in Figure 106(b) shows that the conduction band edge relative to the redox level of the electrolyte of cell [56] (higher concentration of the electrolyte) is shifted to slightly lower energies than the reference cell [57] with the standard electrolyte. However, this difference seems to be due to small differences in the film and not due to the electrolyte, as for cells [55] and [59] no such shift was observed (not shown). This indicates that the

position of the conduction band edge as well as the position of the redox level of the electrolyte remain unchanged for a higher concentration of the electrolyte components.

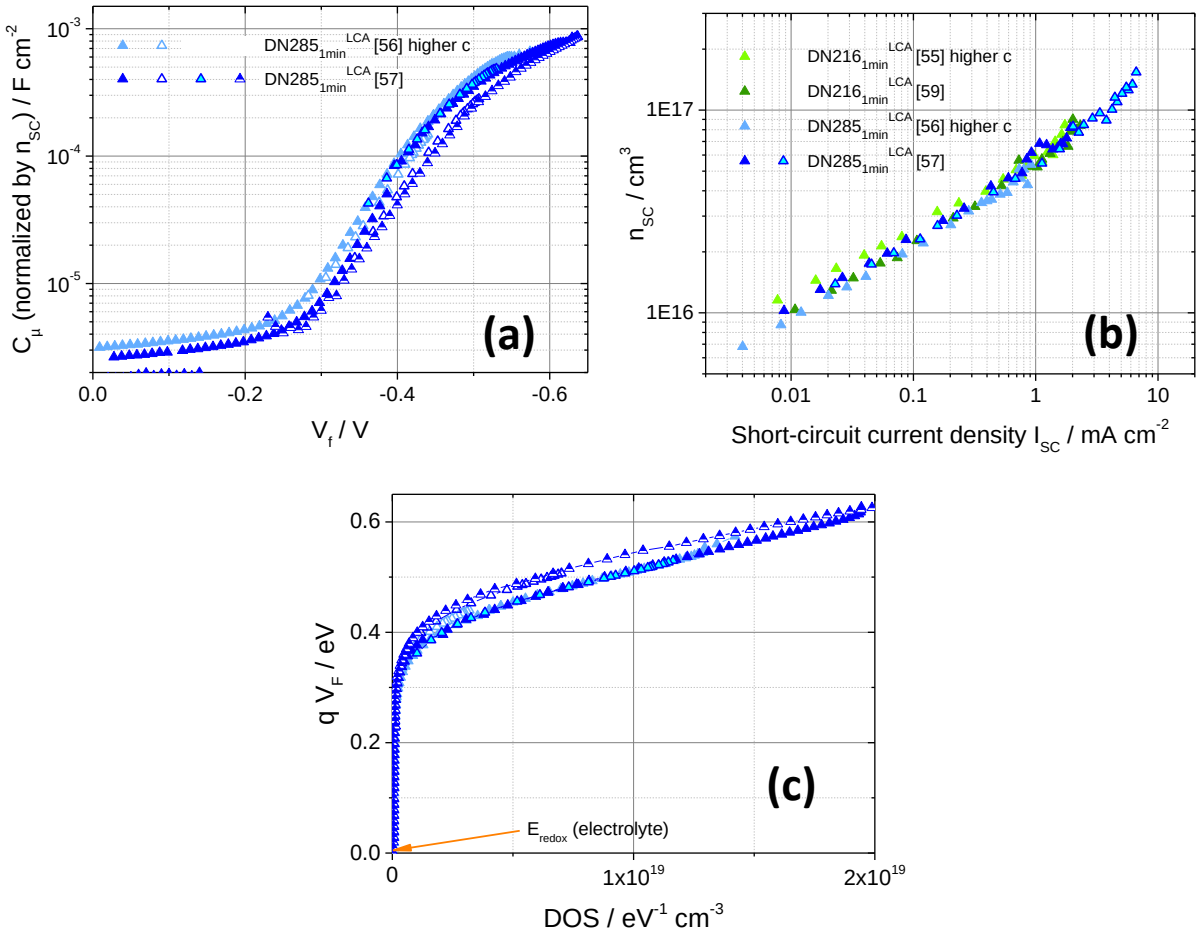

Figure 106 – Chemical capacitance and related values for two ZnO-based DSCs sensitized with DN285 for 1 min. One cell contains the standard electrolyte, and another cell contains an electrolyte with a higher concentration of the electrolyte components. (a) Chemical capacitance C_μ; (b) C_μ normalized by $N_t/N_{t,ref}$; (c) energy of the trap states vs. the DOS. A lighter color indicates a filling with electrolyte of higher concentration, while darker blue indicates the cell filled with the standard electrolyte, see also the legends. Filled symbols indicate measurements at AM1.5 illumination, open symbols measurements at red LED illumination, and half-filled symbols measurements in the dark. Symbols filled with cyan color indicate measurements at cyan LED illumination.

Another important information from C_μ is the trap distribution parameter α, which can be determined from the slope of C_μ. A distribution of α over the voltage range, similar to the results in **3.3.1**, is shown in Figure 106(e). It can be seen that for the cells with different electrolyte the alpha values are very similar for the respective illumination conditions, with higher α values for the measurements at AM1.5 illumination, see also Table 21 for the maximum values of α. This also indicates that even though the trap distribution define the functioning of the DSCs, for the same film a variation in the electrolyte can lead to efficiency differences which do not appear in a plot of C_μ. For the illumination with cyan LED, the maximum values of α reach only about the values of the measurement with red LED illumination, even though the measurement at cyan light led to a chemical capacitance more similar to the measurements at AM1.5 illumination. This could be the case because the measurements at any LED

illumination do not cover the complete voltage range (measurement performed at a value corresponding to V_{OC} at the respective illumination intensity). As no more measurement points are available for lower absolute voltages, the values of α of cyan (and red) LED measurements at these voltages are not known.

Another representation for the trap distribution is the plot of the trap energy vs. the density of states (DOS), see Figure 106(f). This plot shows even more clearly than the plot of C_μ that the trap distribution for the two different electrolytes is very similar, even though slightly shifted to lower energies for the cell with higher concentrated electrolyte. As mentioned above, this difference is probably due to a difference in the film from electrodeposition, as this difference is not observed for the electrolyte variation of DN216 sensitized cells (cells [55] and [59]). This is, as mentioned above, an indication that the electrolyte redox level (reference level, indicated by an arrow) is similar for a different concentration of the same electrolyte species.

Essential information about the recombination behavior of the cells is given by the recombination resistance R_{rec} plotted against the Fermi-level voltage V_f, shown in Figure 107(a). This plot shows that the recombination resistance of the cell with higher concentration of electrolyte components, cell [56], is lower than for a cell with the standard electrolyte, cell [57]. This behavior is observed for all illumination conditions, indicating that for all measurement conditions, recombination of electrons to the electrolyte is enhanced for an electrolyte with a higher concentration of electrolyte components. Due to the very similar chemical capacitance of comparable cells sensitized with DN216, the behavior of R_{rec} vs. V_f with a changed electrolyte is also very similar (not shown). Also the back layer resistance R_{BL} at voltages between 0 V and about -0.3 V has a similar value for the different electrolytes.

Table 21 – Different cell values determined from current transient measurements, from EIS measurements at different illumination conditions, and from measurements of V_{OC} vs. intensity. Some of the values are taken from Table 7 for comparison.

Sample	$N_t/N_{t,ref}$	**alpha**			**beta**			
measurement	current transient (n_{SC} vs. I_{SC})	**EIS**	EIS	EIS	**EIS**	EIS	EIS	**V_{oc} vs. intensity (1/m)**
illumination	red LED	**AM1.5**	red (cyan) LED	dark	**AM1.5**	red (cyan) LED	dark	**red (cyan) LED**
	Ref. cell [61]	**~325 K**	~298 K	~298 K	**~325 K**	~298 K	~298 K	~298 K
$DN216_{1min}^{LCA}$ [55] higher c	0.87	**0.68**	0.48		**0.76**	0.93		**1.04**
$DN216_{1min}^{LCA}$ [59]	0.74	**0.69**	0.49	0.49	**0.47**	0.82	0.70	**0.96**
$DN285_{1min}^{LCA}$ [56] higher c	0.69	**0.63**	0.52		**0.81**	0.96		**1.04**
$DN285_{1min}^{LCA}$ [57]	0.80	**0.69**	0.52	0.50	**0.55**	0.87	0.77	**1.00**
$DN285_{1min}^{LCA}$ [57] CYR	0.77		0.49			(0.85)		**(0.87)**

A plot of R_{rec} vs. the DOS (Figure 107(b)) removes the influence of the very small shift of the conduction band edge (and the also small difference in N_t), leading to the same conclusion that the electrolyte with a higher concentration of electrolyte components leads to an increased recombination of electrons in the conduction band. Very similar values of the electrolyte resistance Z_d for the different electrolytes excludes an influence of electrolyte diffusion or conductivity on the cell performance. As the increase in recombination is observed for a higher electrolyte concentration, it can be concluded that mostly the recombination from ZnO states to the electrolyte is enhanced because of an increase of the DOS in the electrolyte, which leads to a higher transfer probability of electrons from the sensitized film to the electrolyte.

Increasing the iodide concentration in electrolytes should lead to a higher regeneration efficiency (see also below), but the higher density of states in the electrolyte also increases the probability for recombination [255], so that an optimized electrolyte should maximize the efficiency with respect to these factors. From the IV-curves for the cells for the different electrolytes and from the result of the recombination resistance it can be concluded that the increase of the concentration of electrolyte compared to the standardly used electrolyte is disadvantageous for the cell (see also below for the discussion of the regeneration).

The recombination parameter β, calculated from the slope of R_{rec} vs. V_f and shown in Figure 107(c), is also different for the different electrolyte concentrations. Both for the measurements at AM1.5 illumination and at red LED illumination, β is higher for the cells with higher electrolyte concentration, especially in a voltage range between -0.3 and -0.5 V (also for the cells [55] and [59], which are not shown). A look at the fill factors of the cells in Table 20 supports the observation from section **3.3.2** that β in a voltage region of the maximum power point directly correlates with FF, if V_{OC} is of a comparable value. Higher β values in this region for the cells with a higher electrolyte concentration also mean higher FF for these cells. The measurement at cyan LED illumination leads to slightly lower β values than the respective measurement at red LED illumination. Comparing the fill factors from IV-measurements at the respective LED illumination (not shown), the FF is indeed higher for IV-curves measured at red LED illumination than for IV-curves measured with a cyan LED. Another method to determine the recombination parameter β is the measurement of V_{OC} vs. the illumination intensity, shown in Figure 107(d). The resulting β values determined at high light intensities, as well as β values from EIS measurements (values from regions with most constant β) are listed in Table 21. Comparing the cells with different electrolytes in Figure 107(d), the voltage at a certain illumination intensity is higher for the cells with standard electrolyte, as it was also observed in the IV-curves. The shape of the curves, ideally linear in the semi-logarithmic plot, is similar for all cells with a slight deviation from the expected linear behavior for high intensities, when the measurements are performed with illumination of a red LED. When a cyan LED is used for illumination, the curve shape at higher and intermediate intensities is linear, which leads to a lower β

value compared to the value determined from the V_{OC} vs. intensity measurement for the same cell at red LED illumination, see equation **(36)**. Probably the more efficient absorption of the cyan light leads to a more ideal behavior for this measurement, especially for the relatively narrow absorption band of the cells sensitized for 1 min. Also other cells sensitized for a longer time (with a broader absorption spectrum) mostly show a more linear behavior for higher intensities, see e.g. Figure 99.

A large difference of recombination under AM1.5 illumination and in the dark (or at red LED illumination) was ascribed especially to a low regeneration efficiency. As a higher concentrated electrolyte leads to a smaller difference of these curves, it can be concluded that a higher concentration of electrolyte components led to a higher regeneration efficiency for the cells discussed in this chapter. This is also the desired effect of an increase of the concentration of electrolyte species, see also [255]. However the loss through a large increase in recombination (not via oxidized dye molecules) overcompensates the gain through a higher regeneration efficiency, leading to an overall lower performance of the cells with higher electrolyte concentration.

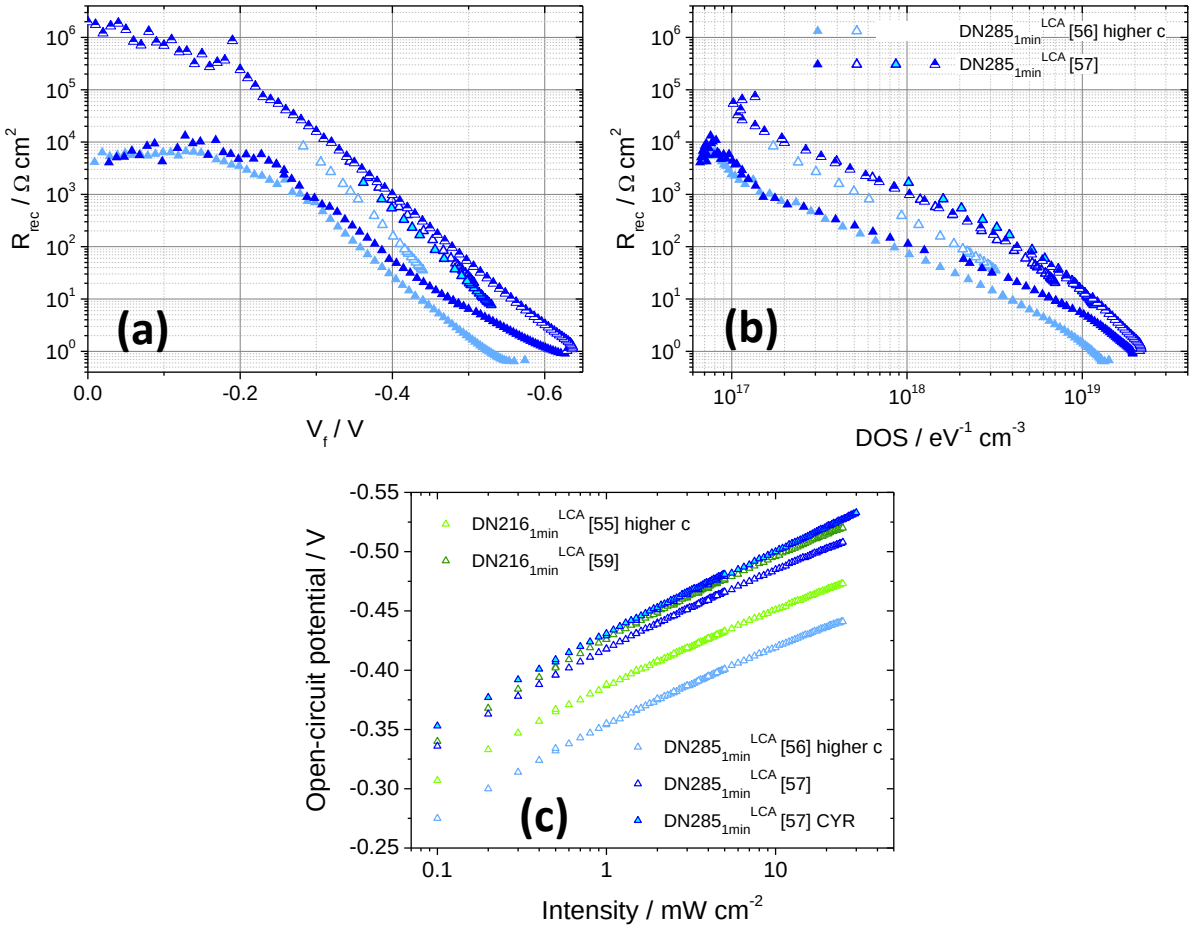

Figure 107 – Recombination resistance R_{rec} and related values for ZnO-based cells sensitized with indoline dyes, filled with different electrolytes. (a) R_{rec} vs. voltage; (b) R_{rec} vs. DOS; (c) recombination parameter β; and (d) V_{OC} vs. intensity. Blue symbols indicate a sensitization with DN285, green symbols a sensitization with DN216. Lighter symbols indicate a cell filled with an electrolyte with a higher concentration of electrolyte components. Filled symbols indicate measurements at AM1.5 illumination, open symbols measurements at red LED illumination, and half-filled symbols measurements in the dark. Symbols filled with cyan color indicate measurements at cyan LED illumination.

The effective electron lifetime τ_n in Figure 108 shows a behavior similar to the recombination resistance for the cells with varied electrolyte. This is the case for the representation of τ_n against voltage as well as for the representation of τ_n against the DOS. Also additional measurements like IMVS and open-circuit voltage decay (OCVD) lead to the same conclusions, showing higher recombination for the cell with higher-concentrated electrolyte. Also cells sensitized with DN216 and a coadsorbate for 1 min show the same change for the variation of the electrolytes (not shown). For lifetimes determined from OCVD measurements, the linear behavior of the lifetimes at voltages near 0 V indicates that the blocking layer works efficiently for all cells. Only for the OCVD measurements the lifetimes can be discussed down to small absolute voltages, where due to the different slope of the lifetimes the cells with a higher-concentrated electrolyte eventually reach even higher lifetimes than the cells with the standard electrolyte. For voltages relevant for working conditions (voltage at the maximum power point), the lifetime is decreased for a higher concentrated electrolyte, explaining the lower performance of cells filled with this electrolyte. For all plots of τ_n vs. the voltage, the lifetimes of measurements performed at cyan LED illumination overlap with the respective measurements performed at red LED illumination, indicating that no change in the recombination behavior is effected by the used illumination wavelengths, even though differences were observed in the chemical capacitance for the different electrolytes.

A measurement which indicates whether regeneration works efficiently in a DSC is the measurement of I_{SC} vs. the illumination intensity, see also sections **1.3.3.6** and **3.3.3**. To the measurement points at different red or cyan LED illumination intensities, also I_{SC} at AM1.5 (100 mW cm^{-2}) was added in Figure 109(a) for a comparison of an application-relevant illumination. For diode illumination, a deviation from a linear behavior can be observed at higher illumination intensities, see also a linear fit in the previous section. This indicates that even for relatively low illumination intensities, regeneration no longer works with unity efficiency.

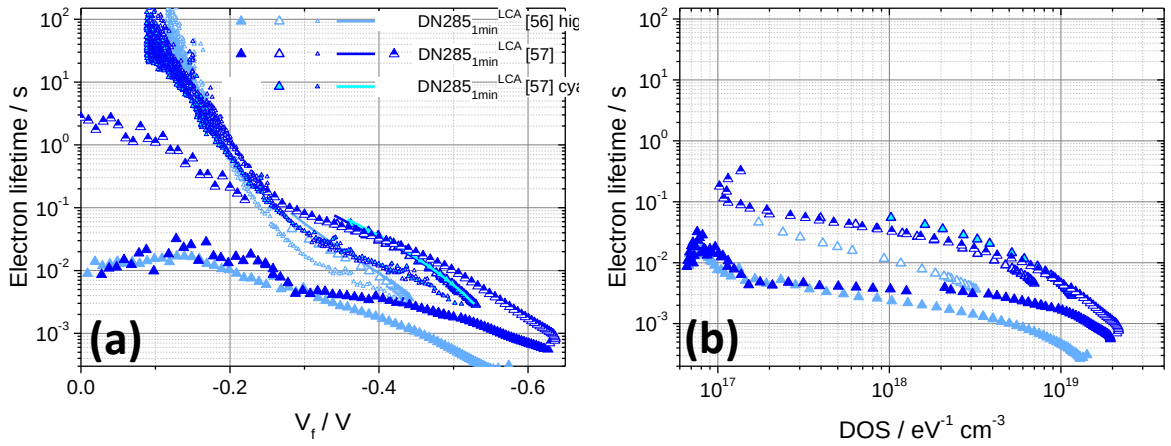

Figure 108 – Electron lifetimes τ_n of DN285-sensitized DSCs filled with different electrolytes. (a) τ_n vs. voltage determined from EIS and IMVS measurements; (b) τ_n vs. voltage determined from OCVD measurements; and (c)) τ_n vs. DOS. Dark blue color indicates a cell filled with standard electrolyte, while light blue color indicates a cell filled with electrolyte with higher concentration of electrolyte components. Filled symbols indicate measurements at AM1.5 illumination, open symbols (EIS, OCVD) and lines (IMVS) indicate measurements at red LED illumination, and half-filled symbols indicate measurements in the dark. Symbols filled with cyan color and a cyan line indicate measurements at cyan LED illumination.

It was already discussed in the previous section that the different absorption of red and AM1.5 light complicates a direct comparison of the I_{SC} values measured at the different illumination. Thus the loss of current via inefficient regeneration is underestimated by this direct comparison. A comparison with measurement at the better absorbed cyan illumination (more similar to absorption of AM1.5 light) corroborates this reflection. I_{SC} at cyan LED illumination is more than two times higher than I_{SC} at the same red LED intensity. The point measured at AM1.5 no longer lies approximately in one line with the cyan LED measurement points, but is considerably lower than a value lying in one line with the cyan measurement points. This indicates that the regeneration efficiency is considerably decreased for the measurements at AM1.5, probably because of depletion of the reduced electrolyte species, and thus an increase of recombination via oxidized dye molecules. A threefold increase in illumination intensity (however with a different spectrum) increases the current only by a small amount, comparing the cyan measurement with I_{SC} at AM1.5. Unity regeneration efficiency would increase I_{SC} for cell [57] at AM1.5 (100 mW cm^{-2}) to about 18 mA cm^{-2} (continuing the trend of the cyan LED measurement up to 100 mW cm^{-2}), provided that no other loss mechanisms change. This fits quite well to the value of about 17 mA cm^{-2} can be obtained for an absorption edge of 650 nm [278]. Even without accounting for the probably considerable regeneration at short circuit [257], by the difference of IV-curves in the dark and under illumination it was concluded by Jennings et al. [66] that the internal power conversion efficiency could be raised from ca. 8 to about 10 %.

The comparison of recombination currents in the dark and under illumination also gives information about recombination and regeneration, see Figure 109(b). As the position of the conduction band edge changes only by a small amount for all cells, the curves can be directly compared without an additional correction of the voltage. The higher recombination current and a different slope under illumination is especially ascribed to recombination via oxidized dye molecules (not present in the dark). Thus a difference indicates a depletion of reduced electrolyte species, and inefficient dye regeneration. A comparison of the curves for the electrolytes with higher concentration of electrolyte species shows a smaller difference of recombination currents in the dark and under illumination for the higher concentrated electrolyte. This leads to the conclusion that regeneration is more efficient for a higher concentration of electrolyte species [255], in line with the conclusions from the recombination resistance. However a larger recombination current in the dark for higher concentration of the electrolyte indicates (also comparable to results from R_{rec}) that the recombination is higher for a higher concentrated electrolyte due to a higher DOS in the electrolyte.

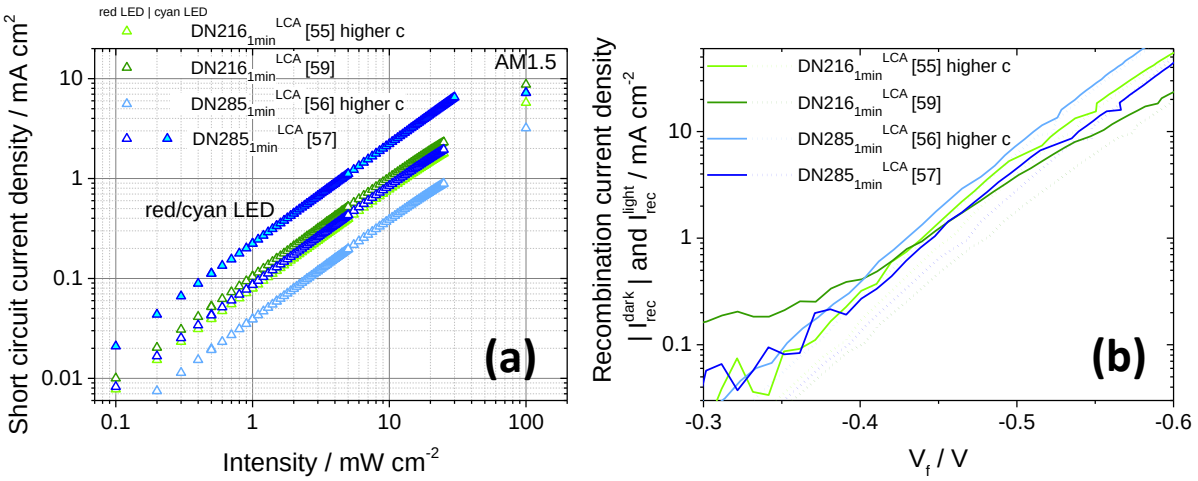

Figure 109 – (a) Measurement of the short-circuit current density I_{SC} vs. illumination intensity for cells with a standard electrolyte and an electrolyte with higher concentration of electrolyte species. The measurements were performed at red LED illumination (one measurement at cyan LED illumination indicated by cyan filled symbols). Additionally, I_{SC} at AM1.5 illumination (100 mW cm^{-2}) was added to the plot. (b) Absolute values of recombination currents in the dark (dotted lines) and under illumination (full lines). Cells filled with an electrolyte with higher concentration of electrolyte species are indicated by lighter colors.

In conclusion, the applied higher concentration of electrolyte components is not beneficial for the cell performance, even though the regeneration efficiency is slightly increased. Detailed photoelectrochemical measurements lead to the conclusion that the main reason for this is a higher recombination, likely due to an increased probability of recombination to a higher density of electrolyte states.

9.2 Sensitized ZnO on wire and thread electrodes

9.2.1 Broader context of experiments

The experiments in this section were made in cooperation with several groups from universities and technical research institutes, working within the projects TexSolar and KorTeSo. The main aim of these projects was to design a textile-based dye-sensitized solar cell with the use of electrodeposited ZnO. Within the TexSolar project, porous ZnO was successfully deposited on silver-coated polyamide threads (Elitex®, Shieldex®) [232]. Also the sensitization of thus prepared porous ZnO was successful. A problem arose when these samples were characterized by photoelectrochemistry. This characterization is usually performed in an iodide-containing electrolyte, which dissolved the silver coating of the polyamide threads. So with these samples, no working solar cells could be built. For future work it was noted that either the substrate should be passivated against corrosion, or the electrolyte should be iodide-free for silver-coated electrodes.

These conclusions lead into another project, KorTeSo (Korrosionsstabile Textile Solarzellen). It was found, that for example fine stainless steel wire bundles (Bekinox®) also work as substrates for ZnO deposition. Having a natural oxide protection layer, the coated Bekinox® bundles can be used as solar electrodes in contact with an iodide-containing electrolyte. Another set of corrosion stable metals was defined by different experiments, and Al and Ta were chosen as possible passivated surfaces for the project.

In the project KorTeSo, four main points were pursued, dealing with passivated surfaces.

1. Elitex® and Shieldex® threads were coated with Al or Ta using ionic liquids (performed by the work group of Prof. Dr. Endres, University of Clausthal). It was found out during the project that only a coating with Al worked satisfactorily, so that Al-coated threads were used for the deposition of ZnO in 2.
2. Al-coated threads and Al- and Ta-wires (as model systems) were used as substrates for electrodeposition of ZnO (electrodeposition mainly done in our group, at the Justus-Liebig-University Gießen) With specific pretreatments, homogeneous ZnO films could be achieved on the different substrates.
3. Sensitized ZnO-films on different substrates were characterized photoelectrochemically (in the group of Dr. S. Sensfuß, TITK Rudolstadt, and in our group). For Al-coated threads, no relevant solar activity was found. Also Al-wires mostly showed no photocurrent. Ta-wires coated with ZnO showed promising power conversion efficiencies exceeding 1%.
4. A method for the electrodeposition of ZnO compatible to industrial techniques on threads/wires was developed (group of Dr. A. Neudeck, TITV Rudolstadt).

Some of the results from point 2 and 3 are shown in this chapter.

9.2.2 ZnO electrodeposition

The deposition of ZnO was carried out on different wires and metal-coated threads. They can be divided into three groups, Al wires, Al-coated threads and Ta wires.

9.2.2.1 ZnO electrodeposition on Al wires

A homogeneous deposition of ZnO on untreated aluminum substrates was already found to be impossible with oxygen-based electrodeposition [228]. The native aluminum oxide layer prevented current flow from the wire to the electrolyte and thus also a deposition of ZnO. An example of the attempt to deposit ZnO on untreated Al can be seen in Figure 110. The parts where ZnO has been deposited are clearly visible because of the red structure directing agent EosinY, which is incorporated into the ZnO film. Probably a thinner or damaged aluminum oxide layer on some parts (by manipulation of the wire or the production), allowing the deposition of ZnO on these parts of the wire. To achieve homogeneous ZnO on Al surfaces, the surface has to be pretreated in order to obtain a thinner oxide layer. However if another type of deposition, a nitrate-based electrodeposition with pulsating current is applied, the pretreatment of the substrate is no longer essential, see section **2.2.2.2**.

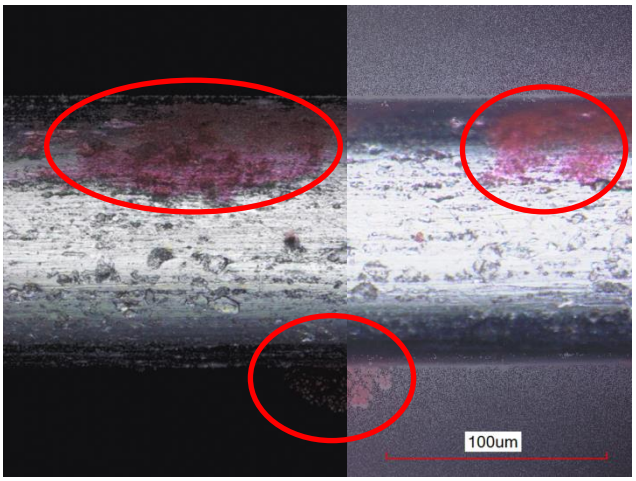

Figure 110 – Confocal laser microscopy image of an untreated Al-wire, on which it was tried to deposit ZnO/EosinY via oxygen-based electrodeposition. Left half: Laser intensity and color image, right half: color image. Parts with deposited ZnO/EosinY are marked with red ovals.

Zincate pretreatment

A pretreatment of the Al wire is essential to obtain a homogeneous ZnO film, if oxygen-based electrodeposition is going to be applied. One pretreatment method was found through the work of Stephanie Künze on planar aluminum substrates, in particular a zincate pretreatment routine (also called pickling routine [189,190,279]). This method is based on the dissolution of aluminum oxide in

concentrated NaOH. A following step of etching in HNO_3 cleans the surface from remnants of the preceding treatment. In the next step, dipping of the treated Al in a highly alkaline zincate solution leads to a deposition of zinc metal onto the Al surface, and thus a relatively stable surface for electrodeposition. Al wires used for electrodeposition are less resistant against etching than planar Al substrates used by Stephanie Künze, resulting in a too intense etching of the surface (including pitting corrosion). Thus the zincate pretreatment had to be adjusted to this specific requirement. The final treatment times can be found in the experimental section (**2.2.1.2**). An inhomogeneous coverage of the Al surface with Zn (Figure 111(a)), could be improved by an optimized zincate pretreatment, for which the coverage with Zn is higher and more homogeneous (Figure 111(b)). On these substrates, oxygen-based electrodeposition of ZnO was performed successfully, with the conductive Zn particles serving as deposition sites leading to a quite homogeneous deposition of ZnO (see Figure 112).

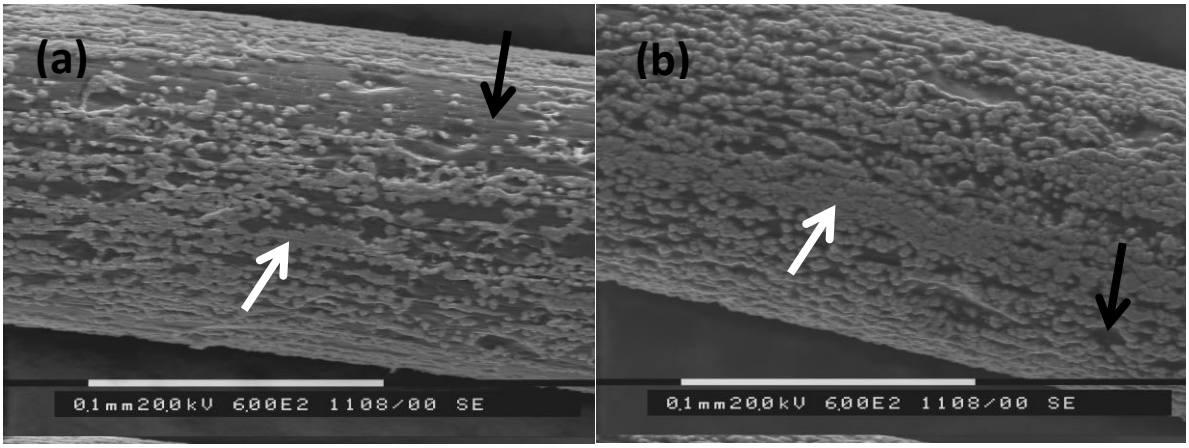

Figure 111 – SEM image of two Al wires pretreated with a zincate pretreatment, leading to a deposition of Zn to the surface. (a) An early pickling routine, (b) zincate pretreatment with adjusted times. White arrows point to Zn, black arrows indicate still uncovered Al.

Although still uncovered Al substrate is seen (strongly reflecting in the confocal microscopy image), this part of the substrate should be protected by the native oxide layer.

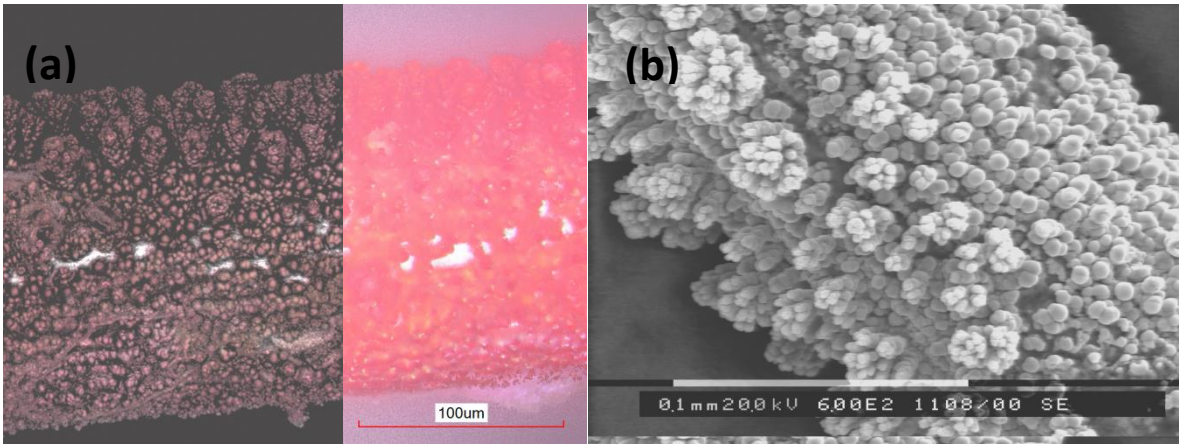

Figure 112 - (a) Confocal laser microscopy image of a ZnO/EosinY film electrodeposited (oxygen-based electrodeposition) on an Al wire pretreated with an optimized pickling routine. Left part: Laser intensity and color image, right part: color image. (b) SEM image of the same sample, with desorbed EosinY and an adsorbed sensitizer.

Electrochemical etching

Another possibility to remove the native oxide layer of the Al to allow electrodeposition of ZnO is electrochemical etching. This was performed by applying a negative voltage prior to the oxygen-based electrodeposition. The voltage was applied in pure KCl, so that no deposition of Zn or ZnO could take place, and after the etching procedure $ZnCl_2$ and EosinY are added to the deposition bath, to allow deposition of ZnO/EosinY films (at less negative voltages).

In Figure 113, the laser-microscopy images of two Al wires are shown which were polarized at different voltages. In Figure 113(a), a wire is shown where the chosen voltage was too negative, so that holes were etched into the Al wire (pitting corrosion). Only on some spots, ZnO/EosinY was deposited. A more homogeneous deposition was achieved, when the etching voltage was only slightly more negative than the standard voltage of Al/Al^{3+} (-1.6 V vs. Ag/AgCl for these experiments). The Al wires were homogeneously covered with a thin film of ZnO/EosinY (see Figure 113(b)), but the resulting ZnO film is very thin even for a comparatively long deposition time and will thus incorporate only a small amount of sensitizer for DSC characterization. Thus films prepared with this method are not relevant for the usage as working electrodes in dye-sensitized solar cells. Only for the study of corrosion current such samples are an interesting alternative to Al-wires where a zincate pretreatment was applied, as no Zinc metal is present in the film (see also section **9.2.4**).

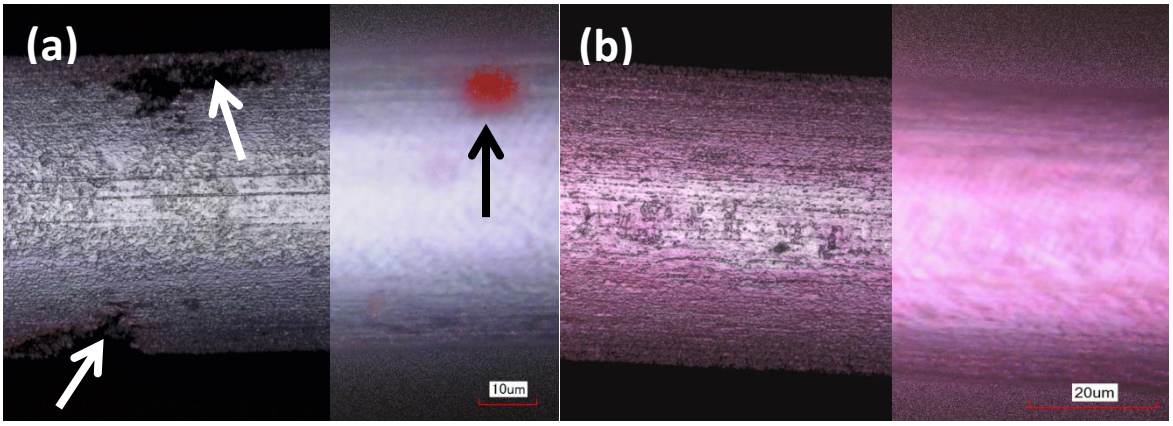

Figure 113 – Confocal laser microscopy images of two Al wires with electrochemical etching pretreatment; left image part: laser intensity and color display, right image part: color display. (a) A Al wire etched with a too negative voltage of -2 V vs. Ag/AgCl, with holes (white arrows) and a ZnO/EosinY grain (black arrow). (b) A voltage of -1.6 V vs. Ag/AgCl with a thin homogeneous ZnO/Eosin coating.

Nitrate-based electrodeposition

When the ZnO layer is deposited using a method developed by Martina Stumpp (see section **2.2.2.2**), no pretreatment is needed to obtain homogeneous films. This method employs a Zinc nitrate solution as the electrolyte, and a pulsating current applied to the substrate under galvanostatic control. The relatively negative voltage that is established at the electrode during the on-time of the pulse can lead to the partial dissolution of the aluminum oxide layer, especially in combination with the relatively aggressive zinc nitrate solution. On the sites where aluminum oxide has been dissolved, Zn or ZnO

can be deposited (Zn is then oxidized to ZnO). As the pulses are short and the aluminum is comparably thick, the wire can be coated with ZnO without getting macroscopically damaged. Thus a deposition is possible even on an initially passivated substrate [193].

Figure 114 – Confocal laser microscopy image (laser intensity and color) of an aluminum wire on which ZnO was deposited by nitrate-based pulsating current electrodeposition. The structure directing agent EosinY is already desorbed.

A ZnO film, deposited via nitrate-based electrodeposition on an aluminum wire, is shown in Figure 114. A complete coverage of the Al wire could be achieved, relatively homogeneous over the whole substrate. The desorption of the structure-directing agent was almost complete (only light red color in Figure 114).

9.2.2.2 ZnO electrodeposition on Al-coated threads

The pretreatment methods used for Al wires were also used and adapted for Al-coated threads. With chemical etching, no homogeneous ZnO/EosinY film could be achieved on the threads (example of an aluminum-coated Elitex® thread partly covered with ZnO/EosinY in Figure 115).

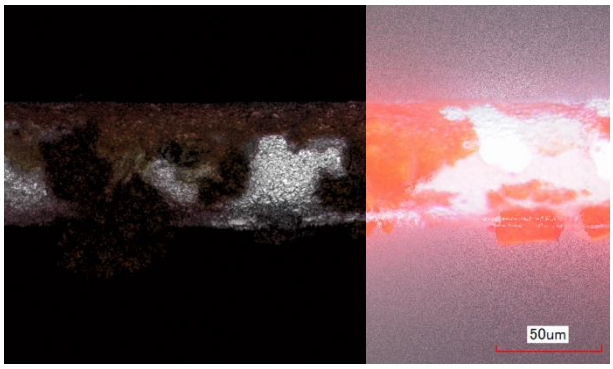

Figure 115 - Confocal laser microscopy image of an Al-coated Elitex® thread pretreated with electrochemical etching in KCl; left image part: laser intensity and color display, right image part: color display. Areas with deposited ZnO/EosinY (red areas) and uncoated Al surface (white/silver areas) are seen.

The zincate pretreatment (if used as for Al wires) first led to damaged samples because of the acidic treatment. It is known that polyamide is relatively stable in alkaline solutions, whereas the stability in acids strongly depends on the pH of the solution and on the residence time of the sample in the acid. The zincate pretreatment for threads was reduced to sole dipping in the alkaline zincate solution. This variation led to a homogeneous coverage with Zn that later served as deposition centers during oxygen-based electrodeposition of ZnO/EosinY. At the same time, the substrates remained intact.

Electrodeposition on substrates treated with the zincate solution yielded relatively homogeneous ZnO/EosinY films with relevant thickness. One example of an aluminum-coated thread, on which ZnO/EosinY was deposited, is shown in Figure 116. In picture (a), the uncoated Shieldex® substrate can be seen with the bright silvery color of the aluminum coating. Some voids from the processing of this industrial product are also indicated. In picture (b), the same substrate position is shown after the deposition of ZnO/EosinY. The substrate is completely covered with ZnO/EosinY, interestingly also the voids are covered. This could be explained by the deposition of some grains of Zn from the zincate solution also on the non-conductive parts of the substrate. These Zn grains could then be transformed into ZnO/EosinY by electroless deposition, even if they have no contact to the electrode. If they grow large enough, they can gradually connect to the electrode and thus cover the void. Another interesting point is the enhanced growth of ZnO/EosinY on the edges of the substrate (the substrate has a triangular cross-section in this case). This enhanced growth was also shown in [198] for a diffusion-controlled deposition on electrode arrays.

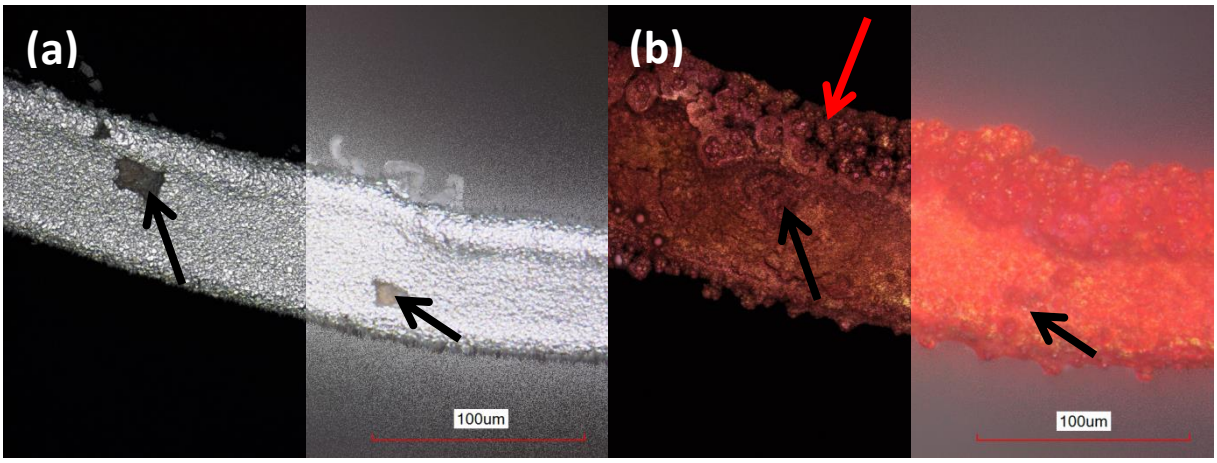

Figure 116 - Confocal laser microscopy images of an aluminum-coated Shieldex® thread; left image part: laser intensity and color display, right image part: color display. (a) Substrate before zincate treatment and (b) after the oxygen-based electrodeposition of ZnO/EosinY. Black arrows indicate voids in the conductive coating, red arrow indicates enhanced growth of ZnO on the edges of the substrate. Both images were taken at the same position of the substrate.

9.2.2.3 ZnO electrodeposition on Ta wires

Ta is also a valve metal which forms a protective oxide layer in contact with air or water. It has been shown before by Kerstin Strauch, that this native oxide layer prevents the effective deposition of ZnO.

Only a few islands of ZnO/EosinY could be found on the Ta wire used [228]. In this work, a different Ta wire was used, and a homogeneous coverage with ZnO/EosinY was observed. It is presumed that the native oxide layer of the Ta wire used in this work was thinner so that electrons could tunnel from the Ta wire and drive the electrochemical deposition. On the hand of this successful first try, all other depositions on Ta wires were performed without any etching or activating pretreatment. As also for the Al wires, two different methods were applied for the deposition of ZnO, the oxygen-based and the nitrate-based electrodeposition.

Oxygen-based electrodeposition on Ta wires

A large part of the work about the oxygen-based electrodeposition on Ta wires was performed by Alexander Geiger in the context of his Master thesis under my guidance (see also [231]).

With the standard deposition procedure, relatively homogeneous ZnO films could be achieved. Figure 117(a) shows an uncoated Ta wire with dents from the production process. The coated wire (Figure 117(b)) is covered by a relatively homogeneous ZnO/EosinY film. Cracks and peeled-off ZnO, which still appear in this sample, should be minimized by slow cooling of the coated wires. ZnO shows a large tendency to flake off the Ta substrate during manipulation of the rather inflexible Ta wire.

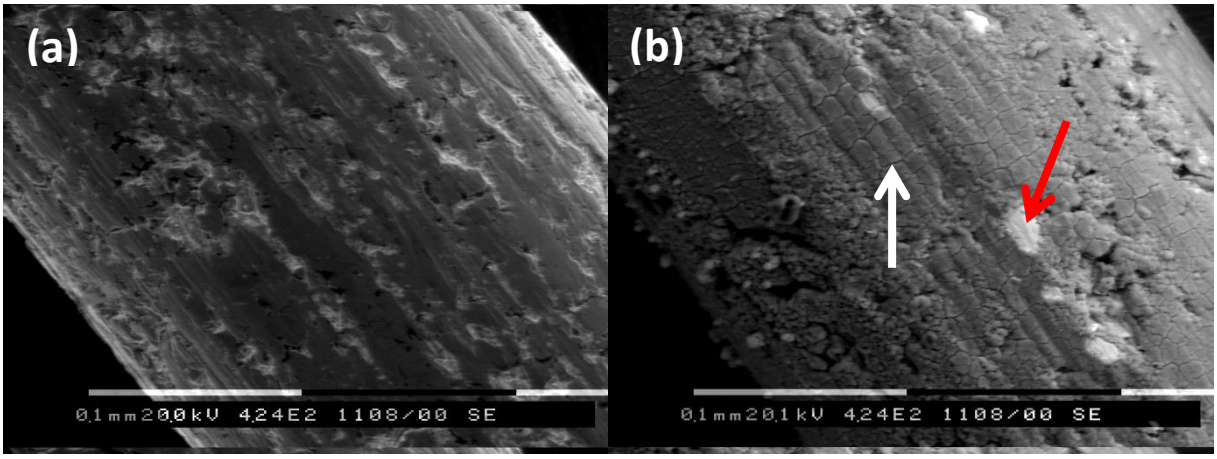

Figure 117 – SEM image of (a) an uncoated Ta wire and (b) a Ta wire with electrodeposited ZnO/EosinY (oxygen-based electrodeposition); one crack in the ZnO layer is marked by a white arrow, a possible hole in the ZnO layer is marked by a red arrow. Deposited and measured by Alexander Geiger [231].

Nitrate-based electrodeposition on Ta wires

The nitrate-based electrodeposition (developed by Martina Stumpp) has already been shown for Al-wires. The deposition on Ta wires also gives a relatively homogeneous and complete coating of the Ta surface. One example of such a film can be seen in Figure 118. Beside a homogeneous layer directly on the Ta surface, there are also some larger grains or dendrites, perhaps stemming from the high applied current. It had been shown by Martina Stumpp *et al.* [198], that a high current density during pulsed galvanostatic deposition of ZnO enhances the growth of dendrites. (Samples Ta06-09 were deposited by Martina Stumpp.)

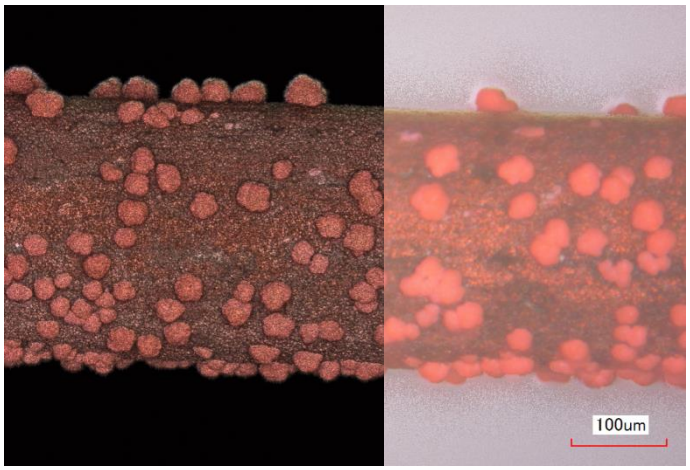

Figure 118 – Confocal laser microscopy image of a Ta wire coated via nitrate-based electrodeposition with ZnO/EosinY.

Electrodeposited ZnO has a high electrical conductivity and the structure directing agent can be desorbed also from the dendrites. Therefore, these films could also be utilized in the following photoelectrochemical measurements.

9.2.3 Photoelectrochemistry of ZnO-coated wires

DSCs were built with ZnO-coated Ta and Al wires, dye-sensitized solar cells. For tantalum, after some parameter variation, solar cells could be produced with efficiencies of up to 1.4% (Ta41). When aluminum wires were used as substrates, only few cells showed a small reproducible photovoltaic effect. This was also found to be the case for planar substrates, and possible reasons will be discussed.

The current-voltage curves of the best cells that were achieved with different deposition methods on Ta-wires as substrates are shown in Figure 126.

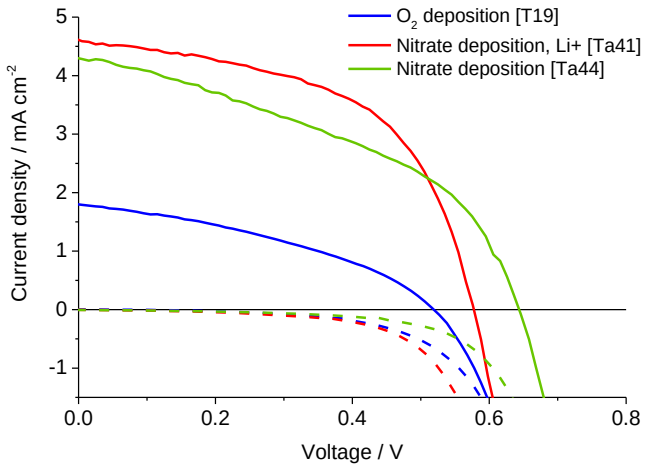

Figure 119 – Current-voltage curves of three best DSCs with ZnO deposited by different methods on Ta wires and sensitized with DN285; dashed lines: dark curves, solid lines: illuminated curves (AM1.5).

The films deposited via oxygen-based electrodeposition have a significantly lower short-circuit current and also a lower open-circuit voltage than films deposited by nitrate-based electrodeposition. The lower photocurrent is explained by a lower thickness of the oxygen-based ZnO films. Typically, ZnO film thicknesses of about 8 µm are found for films deposited by the oxygen-based electrodeposition, whereas films deposited by the nitrogen-based electrodeposition have typical thicknesses about 15 µm, and consists of larger grains or dendrites.

Another reason for both reduced current and voltage may exist in the low mechanical stability of the oxygen-based ZnO, which leads to cracks and detachment of parts of the ZnO from the Ta substrate. This exposed area can then act as a recombination site for charges that are produced, and can thus reduce the photocurrent and the photovoltage. The thin native oxide layer obviously cannot prevent charge recombination from the substrate to the electrolyte, as also the deposition is not significantly hindered by this oxide layer. An insufficient contact between ZnO and the Ta surface would also lead to a decreased current. Such a poor adhesion is probable as the mechanical contact is not as strong as for nitrate-deposited films.

Table 22 - Photoelectrochemical parameters of wire-based DSCs, determined from IV-curves in Figure 119, Figure 120 and Figure 123.

Film	**I_{SC}**	**V_{OC}**	**FF**	**Efficiency**
	[mA cm^{-2}]	**[V]**		**[%]**
Best cells on Ta wire (Figure 119)				
O_2 deposition [T19]	1.79	0.52	0.38	0.35
Nitrate deposition. Li^+ [Ta41]	4.59	0.58	0.55	1.45
Nitrate deposition [Ta44]	4.28	0.64	0.43	1.18
Oxidation pretreatment of Ta (Figure 120)				
without oxidation [Ta08]	2.30	0.60	0.40	0.55
short anodization [Ta28]	0.47	0.42	0.36	0.07
longer anodization [Ta29]	0.30	0.39	0.26	0.03
longest anodization [Ta09]	0.25	0.44	0.13	0.01
Aluminum cell (Figure 123)				
oxidized in water [Al50]	0.50	0.51	0.52	0.13

Nitrate-deposited ZnO films show mostly higher currents than oxygen-deposited films, with variations as to the exact deposition parameters or the electrolyte used. In Figure 126, the IV-curves of two films are shown that vary in the composition of the electrolyte used in the photoelectrochemical cell: the cell built with the nitrate-deposited sample Ta44 contains the standard electrolyte used for wire solar cells (4:1 mixture of ethylene carbonate and acetonitrile with TPAI and I_2), while the electrolyte in the cell of Ta41 contains a lithium salt (0.1 M $LiClO_4$). Li^+ is known to lower the flatband potential of TiO_2 (shift to lower energies) [280]. Such a downward shift of the conduction band edge would in this case

explain the slightly higher photocurrent and also the lower photovoltage of the sample containing Li^+ in the electrolyte (Ta41). Interestingly, also the fill factor was increased for the sample with Li-containing electrolyte (further discussion of fill factors see below).

Another variation performed on nitrate-based electrodeposited ZnO on Ta was the anodization of the Ta wire after electrodeposition, which should result in a thicker oxide layer of Ta. The reason for this treatment was the hypothesis that often the low fill factor of the standard cells (also seen for the cell Ta44 in Figure 126) comes from recombination through free Ta substrate in contact with the electrolyte. As the native oxide layer of the Ta wire is thin enough to allow electrodeposition, recombination through it should also be rapid. Thus on some samples gradually increasing positive voltage was applied, which is known to increase the oxide layer of uncovered Ta.

Three different anodization times were used to oxidize the Ta surface of samples on which nitrate-based ZnO had already been grown. For all samples, the voltage was increased with a rate of 5 V min^{-1}. For sample Ta28 (short anodization), the voltage was increased to 3 V and then the sample was removed from the setup. For sample Ta29 (longer anodization), the procedure was performed with an end voltage of 5 V. Sample Ta09 (longest anodization) was left inside the setup with still applied voltage of 5 V for 2 more minutes. After this, the samples were sensitized with DN285 + CA for 15 minutes (D149 desorbs from the surface, thus the more stable dye DN285 was used). It could be seen already by eye that the anodized samples adsorbed much less dye than typically treated samples. Probably also the ZnO structure or the surface changed during the application of the high positive voltage during anodization. This decreased amount of dye contributes to a decreased I_{SC} seen in the current-voltage curves of the anodized samples in Figure 120.

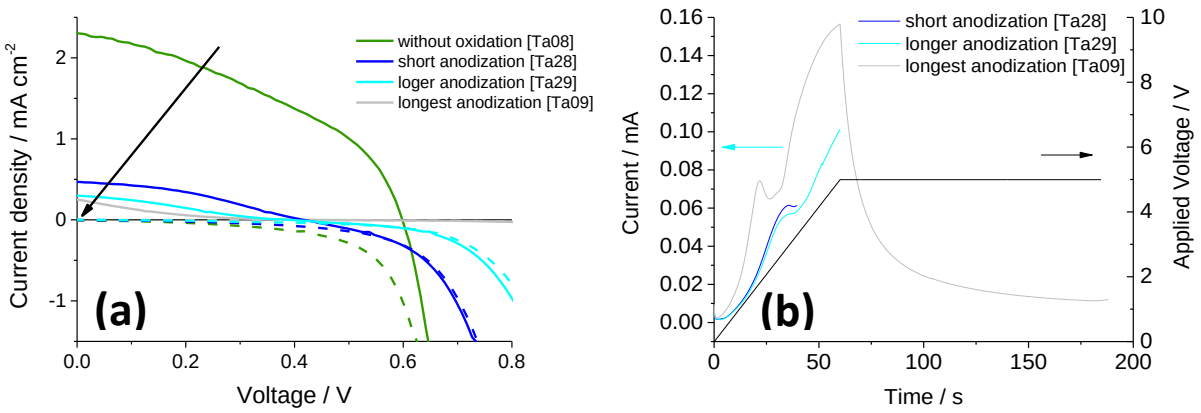

Figure 120 – (a) Current-voltage curves of differently anodized ZnO-coated Ta wires; dashed lines: dark curves, solid lines: illuminated curves (AM1.5). (b) Anodization current and applied voltage during the anodization procedure for the samples shown in (a). The arrow in (a) indicates increasing anodization time, while the arrows in (b) indicate the assignment of the curves to the different axes.

Another reason for the decreased photocurrent seems to be the evidently increased transfer resistance of the substrate. This intended increase of resistance can be seen in the decrease of the dark recombination current in the fourth quadrant. With increasing anodization length, this current decreases to almost 0 mA cm^{-2} for Ta09. However, also the charge transfer of photoexcited charge from the ZnO to the substrate seems to be partially blocked, as I_{SC} particular of Ta09 is much lower than expected from the dye loading.

R_{rec} and C_{μ} of the four cells with different anodization discussed above are shown in Figure 121. The increase of the recombination resistance with increasing anodization time in Figure 121(a) is consistent with the decreasing current in the fourth quadrant of the current-voltage curves in Figure 120(a). The back layer capacitance C_{BL}, which is ascribed to the substrate and blocking layer (see also [60]) can be observed at lower voltages in Figure 121(b). This back layer capacitance depends on the treatment of the substrate or blocking layer [60]. An increased time of oxidation of the substrate metal, Ta, increases the thickness of the tantalum oxide on the Ta surface. This increased thickness is translated into a lower capacitance after

$$C = \frac{\varepsilon_0 \varepsilon_r A}{d}$$

(Capacitance of a plate capacitor, ε_0 vacuum permittivity, ε_r relative dielectric constant, A electrode area, d distance of electrodes)

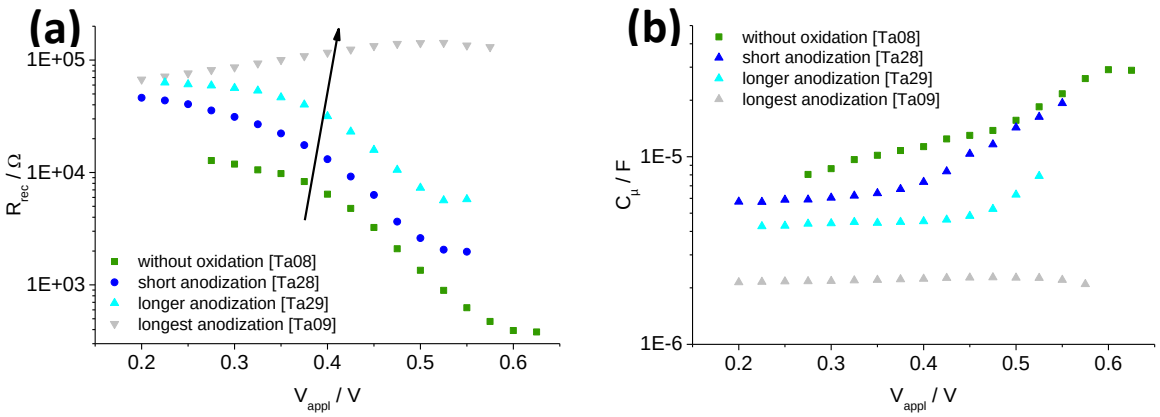

Figure 121 – (a) Recombination resistance and (b) chemical capacitance of the ZnO-covered anodized Ta samples, determined from EIS measurements.

These cells have to be illuminated through the electrolyte, as unlike standard planar cells, which can be illuminated through the transparent working electrode, there is no possibility of illumination through the (metal) working electrode. Thus also the IPCE is 0 for wavelength below ~470 nm, as incoming light is first adsorbed by the iodide electrolyte, compare Figure 122.

Cells prepared from ZnO films that were deposited on Al wires barely showed any photovoltaic activity. If some cells worked as dye-sensitized solar cells, there could be found no dependence of this fact on parameters applied for cell or film preparation.

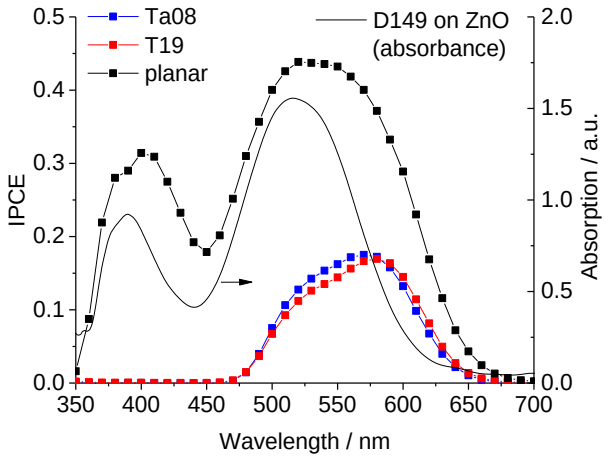

Figure 122 - Incident photon-to-current efficiencies (symbol + line) of two DSCs with Ta wires as substrates (samples Ta08 and T19) and of one planar cell with FTO as substrate for comparison. Ta08 and T19 were illuminated through the electrolyte, the planar cell was illuminated through the working electrode. Absorbance of an indoline dye adsorbed to ZnO for comparison (solid line).

In fact, only one cell (Al50) showed evident photocurrent without having at the same time significant positive dark current (see Figure 123(a)). This film was prepared via oxygen-based electrodeposition (zincate pretreatment), and the film was oxidized in boiling water to achieve a denser oxide layer of the uncovered Al surface. In the same figure, the IV-curves of a similarly treated sample (Al53, nitrate-based electrochemical deposition of ZnO, oxidation in water) are shown, together with a sample without any oxidation treatment and one anodized sample (see also above for anodization of Ta). None of these samples shows significant photocurrent, but also very low dark current.

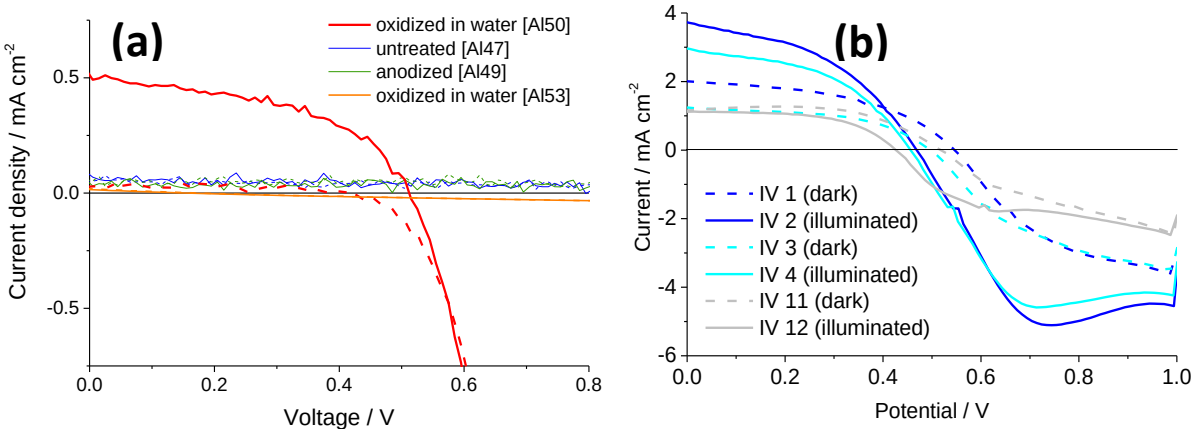

Figure 123 – (a) IV-curves of several solar cells built from ZnO-coated Al-wires. (b) A sequence of IV-curves of one cell (Al16) at AM1.5 illumination and in the dark.

An explanation for this behavior could be the formation of an oxide layer (either enhanced by oxidation treatment or natively) even below the ZnO. So no current can flow from the sensitized ZnO to the substrate. Perhaps Al50 has a slightly different coverage of the Al with ZnO, so that there are still conductive paths from the ZnO to the Al metal.

A problem often occurring in cells based on Al wires was a high positive current of the cells even without illumination. In Figure 123(b), subsequently recorded current-voltage curves of one cell (Al16) are shown, which illustrate this observation. The first dark current-voltage curve shows a short-circuit current of about 2 mA cm^{-2}, while the first illuminated IV-curve has a short-circuit current of about 4 mA cm^{-2}. Such high dark current, together with an also observed high open-circuit voltage in the dark, is a strong indication of some corrosion reaction in the cell. Very similar observations have also been made with wire DSCs based on stainless steel wires by W. Wang *et al.* [281]. This galvanic battery effect (as it was called there) was ascribed to the corrosion of the stainless steel. An oxidation procedure before the deposition of ZnO from the gas phase successfully inhibited the oxidation reaction and thus eliminated the corrosion dark current.

For cells with high dark current measured in this work, the difference between illuminated and dark IV-curves decreased with measurement time, see also Figure 123(b). This means the photovoltaic activity of the sample decreased, probably due to degradation or desorption of the dye at such unfavorable conditions. Another effect seen in the same figure is the decrease of the dark current. Mostly the short-circuit current of the cells decreased with the number of IV-curves recorded. Interestingly, a battery-like behavior could be seen for cells with high dark current – after polarizing the cell to negative voltages, the dark current increased again. To get more information about the cause of the observed corrosion current, cyclic voltammetry measurements on different samples were performed in contact with the redox electrolyte used for solar cells.

9.2.4 Cyclic voltammetry on different samples

High currents even in the dark were observed for several cells based on zincate-treated Al wires. This current was attributed to corrosion of a part of the cells by the electrolyte, which should be identified by cyclic voltammetry of different samples. As samples for the electrochemical analysis, four aluminum-based samples were prepared and are compared with two tantalum-based samples. First, a CV of a plain untreated Al wire was measured in an iodide-containing electrolyte (Figure 124(a)). A very low current flows through the Al/electrolyte interface, indicating that no corrosion of the Al wire occurs. The Al wire is sufficiently protected by the native oxide layer (also supported by the fact that electrodeposition is not possible on an untreated Al wire).

An Al wire with a zincate pretreatment shows a completely different behavior, see Figure 124(b). A high positive corrosion current is seen, which decreases more and more after each scan. Still, the lowest current after 6 scans is about 3 orders of magnitude higher than the current of the untreated wire. After CV measurements, the greyish color of the sample (from Zn metal) changed to white, a common color for highly porous ZnO. This supports the assumption that the high corrosion current stems from the oxidation of the Zn layer to ZnO. Zn is probably not dissolved by the electrolyte, at least not to a large extent, because no free Al is seen on the sample after CV. At air and without applied voltage, Zn is protected against corrosion/oxidation by a thin native ZnO layer, so the Zn film cannot be converted into ZnO. But when a voltage is applied to the Zn layer, an oxidation of Zn to ZnO is possible.

For a sample with ZnO deposited directly onto the Al surface (Al46, Figure 124(c)), the currents flowing through the film are of the same order of magnitude as for an untreated Al wire. The ca. 5 times higher current can be probably traced to a thinner aluminum oxide layer (thinned out during electrochemical etching), either below the grown ZnO or on still free Al surface.

A typical sample used also for photoelectrochemical experiments is shown schematically in the inset of Figure 124(d). It is an Al wire, pretreated with zincate solution before an oxygen-based electrodeposition. The sensitized sample was then used for either IV-curve measurements, or in this case, CV measurements. This particular sample (Al45) showed a significantly higher negative current than the sample also covered with ZnO in Figure 124(c), Al46. The reason might be the more aggressive etching with NaOH and the reactions in the zincate solution, where aluminum oxide and aluminum is etched to give electrons for the deposition of Zn. No oxide layer should be left on the Al wire, it should only develop again in contact with air, where it had not been covered with Zn. This treatment thus leads to an electrically relatively conductive structure. On the other hand, no corrosion currents are observed as for the Zn-covered Al wire in (b), although the structure of Al45 contains or contained Zn metal. Probably the Zn was oxidized to ZnO during the treatment of the Zn-covered wire, which included deposition in an oxidizing atmosphere and under oxidizing conditions and heating to 100°C at air. At least a compact layer of ZnO could protect the Zn from corrosion. A slightly different Zn layer deposited by the zincate pretreatment or a slight mechanical damage of the ZnO protective layer during sample handling could lead to the fact that sometimes corrosive currents (positive currents in IV-curves) could be observed, and sometimes no corrosion occurred.

For Ta wires, a different observation was made than for Al wires. Even an untreated, uncoated Ta wire (Figure 124(e)) showed a significantly higher negative current than an untreated Al wire. The current is of a similar order of magnitude as the reacted Al/Zn sample. This high current is in line with the fact that ZnO can be deposited on untreated Ta. It was reported that thin tantalum oxide films (up to 15 nm) were found to be n-type semiconductors, while thicker tantalum oxide films are insulators [282-286]. Supposing the oxide layer of the Ta wires used was thin (which is likely for a native oxide layer,

although nothing is known about the specific industrial production process for the Ta wire used) this could also explain the relatively high current passing through the wire during a cyclic voltammogram. For a ZnO-covered Ta wire, the result is very similar to the uncovered wire, see Figure 124(f). The current is of a similar order of magnitude, still a little higher than for the bare substrate. As such a high current can be also seen through the ZnO for Al45 and through the reacted Zn (=ZnO) in the Al/Zn structure, it is astonishing that a relatively high current can flow through ZnO. It also has to be kept in mind, that for the oxygen-based electrodeposited sample T06, free Ta can be found due to cracks and voids in the ZnO.

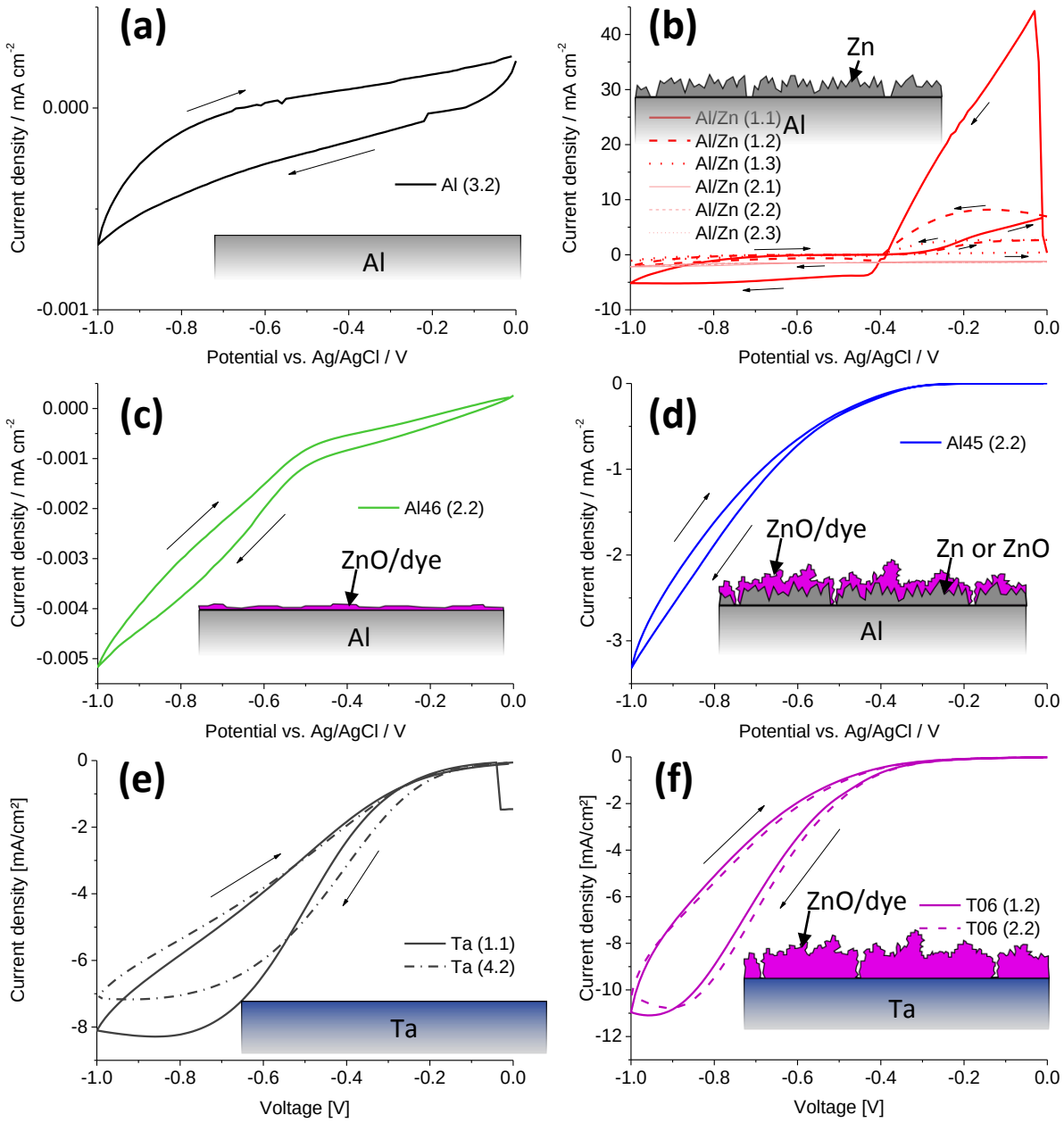

Figure 124 - Cyclic voltammograms of different samples , with shemes of the sample texture as insets. All samples containing ZnO were sensitized. Samples: (a) Al wire, (b) Al wire covered with Zn (zincate pretreatment), (c) Al wire covered with a thin sensitized ZnO layer (electrochemical etching pretreatment, Al46), (d) Al wire covered with Zn (by zincate pretreatment) and subsequent oxygen-based deposition of ZnO (Al45), (e) Ta wire and (f) Ta wire covered with oxygen-based electrodeposited ZnO (T06). Note: Currents are shown in the same direction as in IV-curves, while voltages are not inverted (CV-like)

9.2.5 Summary for electrodeposited ZnO on wires and threads

Several interesting points could be investigated for the electrodeposition of ZnO on wires and metal-coated threads. Al-coated threads and Al wires could be efficiently coated with porous ZnO either by first applying a zincate pretreatment and then depositing with the oxygen-based electrodeposition, or by nitrate-based pulsed current electrodeposition (developed by Martina Stumpp). A relatively homogeneous porous ZnO layer could be achieved, from which the structure directing agent could be desorbed and a sensitizer could be adsorbed. Dye-sensitized solar cells were prepared from ZnO-coated sensitized Al-wires, but only one cell yielded a measurable efficiency. Other cells either showed a high positive dark current probably from the corrosion of the Zn-layer from the zincate pretreatment, or showed no increase of current upon illumination.

ZnO was deposited on Ta wires with both nitrate- and oxygen-based electrodeposition. No pretreatment was needed, as the native oxide layer shows semiconducting behavior. However, oxygen-based electrodeposition yielded thinner ZnO films with relatively low mechanical stability, which led to voids in the ZnO layer. Nitrate-based electrodeposited ZnO films on Ta showed better mechanical stability. Cells could be prepared with relatively high open-circuit voltages and sufficient current densities, but with low fill factors. A thickening of the tantalum oxide layer on the surface after electrodeposition brought no improvement of the fill factor or the cell efficiencies. The best cell, prepared from a nitrate-based ZnO film on Ta, showed an efficiency of 1.45%.

9.3 Comparison of different solar simulators

In most photoelectrochemical experiments during this work measured at an intensity of 100 mW cm^{-2}, the LOT solar simulator LS0106 with appropriate AM1.5 filter was used. During the cooperation with the TITK (in the project TecSolar and KorTeSo), even very similar or the same cells showed a higher efficiency when measured by the cooperation partner. This let the question arise, if the intensity of the solar simulator setup used here matches the solar spectrum well. Another solar simulator in the work group of Dr. Roland Marschall in the Physical Chemistry Institute (Sol1A, Oriel) was used to perform a more thorough comparison under similar conditions. The same intensity sensor was used to set the intensity of the particular solar simulator, the same potentiostat (IVIUM potentiostat, IVIUM technologies) was used for IV-curves measurement, and the same cells were measured on both experimental sites on the same day. The spectra for the different solar simulators are shown in Figure 125, and it can be observed that both solar simulators differ from the ideal AM1.5 spectrum especially for wavelengths >700 nm. The spectral mismatch for LS0106 is larger than for Sol1A.

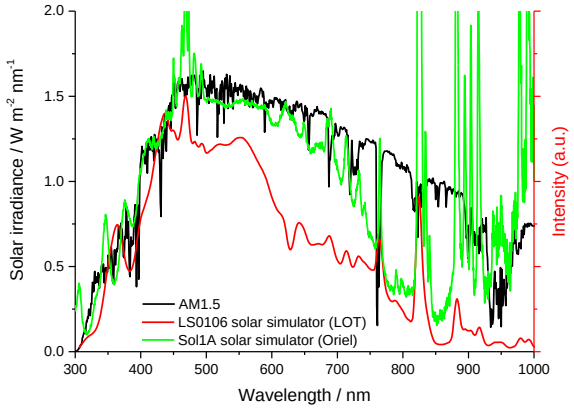

Figure 125 – AM1.5 spectrum, and spectra of two different solar simulators. AM1.5 spectrum is obtained from NREL, the Sol1A spectrum from Oriel, and the LS0106 spectrum was measured by M. Beu [123].

A first observation during the measurements of IV-curves at the different solar simulators was that the intensity of the Oriel Sol1A simulator was more stable in a short-time range. This resulted in smoother IV-curves, see also Figure 126. In the same figure, it can also be seen that the short-circuit current density of cells measured under Oriel Sol1A illumination was higher than the short-circuit current density under LOT LS0106 illumination. The increase in current amounted to 19-25% for the different cells, see Table 23. Thus also the efficiencies measured at the Oriel Sol1A solar simulator are higher than those measured at the LOT LS0106 solar simulator. The increase in efficiency ranged from 15 to 22% for the cells [68], [70] and [71].

Table 23 – Comparison of solar cell parameters from IV-curves, measured with two different solar simulators, LOT LS0106 and Oriel Sol1A (corresponding IV-curves shown in Figure 126)

	I_{SC} [mA cm^{-2}]	**V_{OC}** [V]	**FF**	**Efficiency** [%]	Ratio: Current at Oriel Sol1A/ Current at LOT LS0106	Ratio: Efficiency at Oriel Sol1A/ Efficiency at LOT LS0106
$DN216_{1h}^{CA}$ [68]						
Sol1A	8.85	0.59	0.68	3.54	**1.188**	**1.153**
	8.84	0.59	0.68	3.54	**1.195**	**1.153**
LOT LS0106	7.45	0.60	0.69	3.07		
	7.40	0.60	0.69	3.07		
(longer illumination)	7.38	0.59	0.69	2.99		
$DN216_{1h}^{LCA}$ [70]						
Sol1A	13.19	0.58	0.68	5.20	**1.212**	**1.182**
	13.20	0.58	0.68	5.18	**1.213**	**1.180**
LOT LS0106	10.89	0.59	0.68	4.40		
	10.88	0.58	0.7	4.39		
$DN285_{1h}^{LCA}$ [71]						
Sol1A	8.29	0.57	0.71	3.34	**1.248**	**1.228**
	8.26	0.57	0.71	3.34	**1.250**	**1.219**
LOT LS0106	6.64	0.57	0.72	2.72		
	6.61	0.57	0.73	2.74		

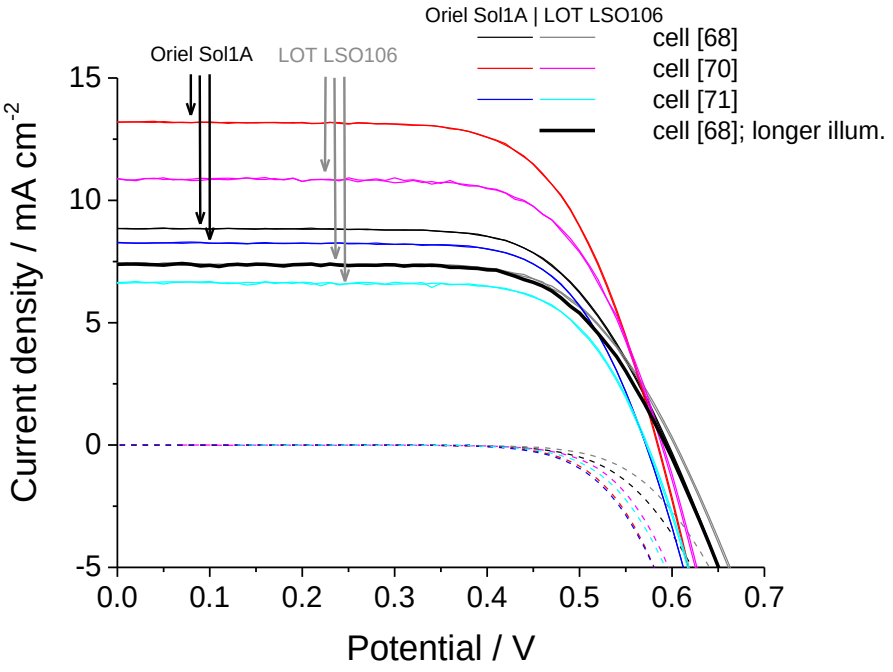

Figure 126 - IV-curves of three cells measured comparatively with the illumination of two different solar simulators, LOT LS0106 and Oriel Sol1A. Solid lines: IV-curves under 100 mW cm^{-2} illumination; dashed lines: IV-curves in the dark. Two IV-curves under illumination are shown for each cell to show the stability of the lamp illumination. The IV-curves shown are measured without mask.

9.4 Sample list

The different samples used in this work are listed in the following table. Different deposition conditions, sensitization and the electrolytes are indicated by numbers, which reflect the following conditions (exact conditions see also section **2**):

Deposition:

1. FTO-coated glass from Aldrich, mostly small circular area for deposition of porous ZnO; activation of the substrate until saturation current is reached (mostly 300 s); 75 µM EosinY used as structure-directing agent.
2. FTO-coated glass from Asahi Glass, mostly larger area for deposition of porous ZnO; activation for 1800 s; 50 µM EosinY used as structure-directing agent.

Sensitization:

- Sensitization in a dye solution (numbers and exact conditions given in section **2.4.2**) for the given time.

Electrolyte:

1. PMII and I_2 in acetonitrile
2. TPAI and I_2 in a mixture of ethylene carbonate and acetonitrile; (b) variation: addition of $LiClO_4$
3. Iodolyte from Solaronix, with Li-salt and an additive

Sample no.	**ZnO deposition**	**Sensitizer, solution no.**	**sensitization time**	**electrolyte**	**comment**
[21]	2	WD-2, 14	overnight	2	
		WD-3, 15	overnight	2	
		TPA-B1, 16	overnight	2	
		D149 + CA, 2	10 min	2	
[23]		J102, 11	overnight	2	
		J109, 12	overnight	2	
		J109 + CA, 13	overnight	2	
		D149 + CA, 2	10 min	2	
[24]	75 EY, new FTO large area, cut	WD-2, 14	overnight	2	
		WD-3, 15	overnight	2	
		TPA-B1, 16	overnight	2	
		D149 + CA, 2	10 min	2	
[27]	see 24	J102, 11	overnight	2	
		J102, 9	overnight	2	
		J102, 9	overnight	2 + $LiClO_4$	
		J102 + TritonX,	overnight	2	

		10			
[34]	4, 75 EY (also all below)	DN285 + LCA, 8	15 min	1	
[35]	4	DN91 + LCA, 4	15 min	1	
[43]	4	DN91 + LCA, 4	15 min	1	
[45]	7	D149 + CA, 2	1 min	1	
[46]	7	DN91 + LCA, 4	1 min	1	
[47]	7	D149, 1	15 min	1	
[48]	7	DN91, 3	15 min	1	
[49]	7	DN216, 5	15 min	1	
[50]	7	DN216, 5	15 min	1	short circuit
[51]	7	DN285, 7	15 min	1	
[52]	7	DN216 + LCA, 6	15 min	1	
[53]	14x20				
[54]	7	J102, 9	24 h	1	
[55]	7	DN216 + LCA, 6	1 min	1	
[56]	7	DN285 + LCA, 8	1 min	1	
[57]	7	DN285 + LCA, 8	1 min	1	
[58]	14x20				
[59]	7	DN216 + LCA, 6	1 min	1	
[60]	7	DN91 + LCA, 4	15 min	1	
[61]	7	D149 + CA, 2	15 min	1	
[62]	7				
[63]	7	DN285 + LCA, 8	15 min	1	
[64]	7				
[65]	7	D149 + CA, 2	1 h	1	
[66]	7	DN91, 3	15 min	1	
[67]	7	DN216, 5	1 h	1	
[68]	7	DN216 + CA, 6b	1 h	1	
[69]	7	DN91 + LCA, 4	1 h	1	short circuit
[70]	7	DN216 + LCA, 6	1 h	1	
[71]	7	DN285 + LCA, 8	1 h	1	
[72]	7	Vinylcarbon, 17a	overnight	1	
[73]	7	Phosphon, 17b	overnight	1	
[74]	15x20				
[75]	15x20				
[76]	7	Vinylphosphon, 17c	overnight	1	short circuit
[77]	7				
[78]	7				
[79]	7	AR20, 17d	overnight	1	
[80]	7				
[TiO2-01]	7	DN216 + LCA, 6	1 h	1	
[TiO2-02]	7	DN91 + LCA, 4	1 h	1	
[TiO2-03]	7	DN285 + LCA, 8	1 h	1	
[TiO2-04]	7	D149 + CA, 2	1 h	1	
[TiO2-05]	7	DN216 + LCA, 6	1 h	1	
[TiO2-06]	7	DN91 + LCA, 4	1 h	3	

10 List of publications

Falgenhauer, J.; Fiehler, F.; Richter, C.; Rudolph, M.; Schlettwein, D. Consequences of changes in the ZnO trap distribution on the performance of dye-sensitized solar cells. *Phys. Chem. Chem. Phys.* **2017,** *19* (24), 16159–16168. DOI: 10.1039/C7CP01024A.

Su, Y.; Falgenhauer, J.; Leichtweiß, T.; Geiß, M.; Lupó, C.; Polity, A.; Zhou, S.; Obel, J.; Schlettwein, D.; Janek, J.; Meyer, B. K. Electrochemical properties and optical transmission of high Li + conducting LiSiPON electrolyte films. *Phys. Status Solidi B* **2017,** *254* (2), 1600088. DOI: 10.1002/pssb.201600088.

Meyenburg, I.; Falgenhauer, J.; Rosemann, N. W.; Chatterjee, S.; Schlettwein, D.; Heimbrodt, W. Charge transfer at organic-inorganic interfaces—Indoline layers on semiconductor substrates. *J. Appl. Phys.* **2016,** *120* (21), 215502. DOI: 10.1063/1.4969041.

Minda, I.; Ahmed, E.; Sleziona, V.; Richter, C.; Beu, M.; Falgenhauer, J.; Miura, H.; Schlettwein, D.; Schwoerer, H. Identification of different pathways of electron injection in dye-sensitised solar cells of electrodeposited ZnO using an indoline sensitiser. *Phys. Chem. Chem. Phys.* **2016,** *18* (13), 8938–8944. DOI: 10.1039/c5cp07841e.

Pan, Q.; Freitag, L.; Kowacs, T.; Falgenhauer, J. C.; Korterik, J. P.; Schlettwein, D.; Browne, W. R.; Pryce, M. T.; Rau, S.; González, L.; Vos, J. G.; Huijser, A. Peripheral ligands as electron storage reservoirs and their role in enhancement of photocatalytic hydrogen generation. *Chem. Commun. (Camb.)* **2016,** *52* (60), 9371–9374. DOI: 10.1039/C6CC05222C.

Su, Y.; Falgenhauer, J.; Polity, A.; Leichtweiß, T.; Kronenberger, A.; Obel, J.; Zhou, S.; Schlettwein, D.; Janek, J.; Meyer, B. K. LiPON thin films with high nitrogen content for application in lithium batteries and electrochromic devices prepared by RF magnetron sputtering. *Solid State Ionics* **2015,** *282*, 63–69. DOI: 10.1016/j.ssi.2015.09.022.

George, R. C.; Falgenhauer, J.; Geis, C.; Nyokong, T.; Schlettwein, D. Characterization of porphyrin nanorods on fluorine doped tin oxide glass sheet. *J. Porphyrins Phthalocyanines* **2015,** *19* (11), 1147–1158. DOI: 10.1142/S1088424615500923.

Falgenhauer, J.; Richter, C.; Miura, H.; Schlettwein, D. Stable Sensitization of ZnO by Improved Anchoring of Indoline Dyes. *ChemPhysChem* **2012,** *13* (12), 2893–2897. DOI: 10.1002/cphc.201200085.

Acknowledgements

I would like to thank especially Prof. Derck Schlettwein for the possibility to perform by doctoral research in his group, for all discussions and mentoring and for every helpful advice. I much appreciated the time in your workgroup, the good atmosphere and every support I got.

I would like to thank Prof. Bernd Smarsly for the review of my thesis.

I would like to thank the following people from different cooperation:

- Dr. Hidetoshi Miura (Chemicrea) for the indoline dyes D149, DN91, DN216 and DN285.
- Prof. Heinz Langhals (Ludwig-Maximilians-Universität München) for the perylene dyes J102 and J109.
- Dr. Chunyang Jia (University of Electronic Science and Technology of China, Chengdu) for the triphenylamine dyes WD-2, WD-3 and TPA-B1.
- Dr. Yurong Su and Dr. Angelika Polity for the cooperation on LiPON and other solid electrolytes.
- Ingo Meyenburg (Philipps-Universität Marburg) for the cooperation on photoluminescence of indoline dyes and the characterization of cells, also Prof. Wolfram Heimbrodt for the discussions of results, and Nico Hofeditz for electroluminescence measurement of cells from this work.
- Martin Liebold (Philipps-Universität Marburg) for phthalocyanine dyes with different anchor groups.
- Dr. Reama George for the cooperation on porphyrins (and for your much appreciated friendship).
- Qing Pan for the interesting cooperation on electrochemical measurements of ruthenium dyes.
- and all other people who contributed to the work I did, or also helped to widen my scientific view.

I would like to thank all people from the AG Schlettwein for the good working atmosphere and many helpful advices. My special thanks to:

- Melanie Rudolph for everything you showed me, either experiments or evaluation, and also for many helpful discussions.
- André Dragässer for programming many measurement and evaluation routines, it eased experiments and evaluation so much…
- Martina Stumpp, Christoph Richter, Max Beu, Christian Lupó, Clemens Geis, Raffael Rueß for showing me many experiments, for all discussions and also for some samples.

- Felix Fiehler and Alexander Geiger for their contributions to this work.
- Silvia Schmand for every “technical support” and for every help with experiments, also Ursula Hermann-Lippert for every administrative work.

I would also like to thank the former “AG Eickhoff” for the use of the microbalance, and Dr. Roland Marschall for the use of the Solarsimulator Sol1A, and Tobias Weller for the respective introduction.

Funding of this work by the Bundesministerium für Bildung und Forschung (BMBF) within the project “KorTeSo” and within the Loewe Forschungsschwerpunkt “Store-E” is gratefully acknowledged.

Danke auch an meine Familie, die mich auf jede mögliche Weise unterstützt hat, mich motiviert hat, und mir auch die nötige Geduld bis zur Fertigstellung entgegenbrachte…

Erklärung

Ich erkläre: Ich habe die vorgelegte Dissertation selbstständig und ohne unerlaubte fremde Hilfe und nur mit den Hilfen angefertigt, die ich in der Dissertation angegeben habe. Alle Textstellen, die wörtlich oder sinngemäß aus veröffentlichten Schriften entnommen sind, und alle Angaben, die auf mündlichen Auskünften beruhen, sind als solche kenntlich gemacht. Ich stimme einer evtl. Überprüfung meiner Dissertation durch eine Antiplagiat-Software zu. Bei den von mir durchgeführten und in der Dissertation erwähnten Untersuchungen habe ich die Grundsätze guter wissenschaftlicher Praxis, wie sie in der „Satzung der Justus-Liebig-Universität Gießen zur Sicherung guter wissenschaftlicher Praxis“ niedergelegt sind, eingehalten.

_____ _____

Ort, Datum Unterschrift

References

[1] Wild-Scholten, M. J. de; Veltkamp, A. C. Environmental life cycle analysis of dye sensitized solar devices; status and outlook. In *Proceedings of the 22nd European Photovoltaic Solar Energy Conference*; Milan, Italy: WIP-Renewable Energies, 2007.

[2] Miettunen, K.; Halme, J.; Lund, P. Metallic and plastic dye solar cells. *WIREs Energy Environ* **2013,** *2* (1), 104–120. DOI: 10.1002/wene.46.

[3] Yoshida, T.; Zhang, J.; Komatsu, D.; Sawatani, S.; Minoura, H.; Pauporté, T.; Lincot, D.; Oekermann, T.; Schlettwein, D.; Tada, H.; Wöhrle, D.; Funabiki, K.; Matsui, M.; Miura, H.; Yanagi, H. Electrodeposition of Inorganic/Organic Hybrid Thin Films. *Adv. Funct. Mater.* **2009,** *19* (1), 17–43. DOI: 10.1002/adfm.200700188.

[4] Hagfeldt, A.; Boschloo, G.; Sun, L.; Kloo, L.; Pettersson, H. Dye-Sensitized Solar Cells. *Chem. Rev.* **2010,** *110* (11), 6595–6663. DOI: 10.1021/cr900356p.

[5] http://gcell.com/product/gratzel-solar-backpack-2, 2016-05-18

[6] https://actu.epfl.ch/news/epfl-s-campus-has-the-world-s-first-solar-window/, 2016-05-18

[7] Mathew, S.; Yella, A.; Gao, P.; Humphry-Baker, R.; Curchod, Basile F E; Ashari-Astani, N.; Tavernelli, I.; Rothlisberger, U.; Nazeeruddin, M. K.; Grätzel, M. Dye-sensitized solar cells with 13% efficiency achieved through the molecular engineering of porphyrin sensitizers. *Nat Chem* **2014,** *6* (3), 242–247. DOI: 10.1038/nchem.1861.

[8] Yoshida, T.; Pauporté, T.; Lincot, D.; Oekermann, T.; Minoura, H. Cathodic Electrodeposition of ZnO/Eosin Y Hybrid Thin Films from Oxygen-Saturated Aqueous Solution of $ZnCl_2$ and Eosin Y. *J. Electrochem. Soc.* **2003,** *150* (9), C608. DOI: 10.1149/1.1598213.

[9] Yoshida, T.; Iwaya, M.; Ando, H.; Oekermann, T.; Nonomura, K.; Schlettwein, D.; Wohrle, D.; Minoura, H. Improved photoelectrochemical performance of electrodeposited ZnO/EosinY hybrid thin films by dye re-adsorption. *Chem. Commun.* **2004,** *1* (4), 400–401. DOI: 10.1039/b312127e.

[10] Keis, K.; Magnusson, E.; Lindström, H.; Lindquist, S.-E.; Hagfeldt, A. A 5% efficient photoelectrochemical solar cell based on nanostructured ZnO electrodes. *Solar Energy Materials and Solar Cells* **2002,** *73* (1), 51–58. DOI: 10.1016/S0927-0248(01)00110-6.

[11] Ito, S.; Miura, H.; Uchida, S.; Takata, M.; Sumioka, K.; Liska, P.; Comte, P.; Pechy, P.; Gratzel, M. High-conversion-efficiency organic dye-sensitized solar cells with a novel indoline dye. *Chemical communications (Cambridge, England)* **2008,** *1* (41), 5194–5196. DOI: 10.1039/b809093a.

[12] Le Bahers, T.; Labat, F.; Pauporté, T.; Ciofini, I. Effect of solvent and additives on the open-circuit voltage of ZnO-based dye-sensitized solar cells: a combined theoretical and experimental study. *Phys. Chem. Chem. Phys.* **2010,** *12* (44), 14710. DOI: 10.1039/c004358c.

[13] Rohwer, E.; Minda, I.; Tauscher, G.; Richter, C.; Miura, H.; Schlettwein, D.; Schwoerer, H. Ultrafast Charge-Transfer Reactions of Indoline Dyes with Anchoring Alkyl Chains of Varying Length in Mesoporous ZnO Solar Cells. *Chemphyschem : a European journal of chemical physics and physical chemistry* **2015,** *16* (5), 943–948. DOI: 10.1002/cphc.201402784.

[14] Premaratne, K.; Kumara, G.; Rajapakse, R.; Karunarathne, M. L. Highly efficient, optically semi-transparent, ZnO-based dye-sensitized solar cells with Indoline D-358 as the dye. *Journal of Photochemistry and Photobiology A: Chemistry* **2012,** *229* (1), 29–32. DOI: 10.1016/j.jphotochem.2011.12.010.

[15] Falgenhauer, J.; Richter, C.; Miura, H.; Schlettwein, D. Stable Sensitization of ZnO by Improved Anchoring of Indoline Dyes. *ChemPhysChem* **2012,** *13* (12), 2893–2897. DOI: 10.1002/cphc.201200085.

[16] Rudolph, M.; Yoshida, T.; Schlettwein, D. Influence of indoline dye and coadsorbate molecules on photovoltaic performance and recombination in dye-sensitized solar cells based on electrodeposited ZnO. *J. Electroanal. Chem.* **2013,** *709*, 10–18. DOI: 10.1016/j.jelechem.2013.09.028.

[17] Rudolph, M.; Yoshida, T.; Miura, H.; Schlettwein, D. Improvement of Light Harvesting by Addition of a Long-Wavelength Absorber in Dye-Sensitized Solar Cells Based on ZnO and Indoline Dyes. *J. Phys. Chem. C* **2015,** *119* (3), 1298–1311. DOI: 10.1021/jp511122u.

[18] Magne, C.; Moehl, T.; Urien, M.; Grätzel, M.; Pauporté, T. Effects of ZnO film growth route and nanostructure on electron transport and recombination in dye-sensitized solar cells. *J. Mater. Chem. A* **2013,** *1* (6), 2079–2088. DOI: 10.1039/c2ta00674j.

[19] Richter, C.; Beu, M.; Schlettwein, D. Influence of counter-anions during electrochemical deposition of ZnO on the charge transport dynamics in dye-sensitized solar cells. *Phys. Chem. Chem. Phys.* **2015,** *17* (3), 1883–1890. DOI: 10.1039/c4cp00723a.

[20] Moser, J. Notiz über Verstärkung photoelectrischer Ströme durch optische Sensibilierung. *Monatsh. Chemie* **1887,** *8*, 373.

[21] Nazeeruddin, M. K.; Baranoff, E.; Grätzel, M. Dye-sensitized solar cells: A brief overview. *Solar Energy* **2011,** *85* (6), 1172–1178. DOI: 10.1016/j.solener.2011.01.018.

[22] Hauffe, K.; Range, J. Sensitization Mechanism of Zinc Oxide by Organic Pigments. *Zeitschrift für Naturforschung Part B* **1968,** *B 23* (5), 736-&.

[23] Gerischer, H.; Tributsch, H. Elektrochemische Untersuchunge zur spektralen Sensibilisierung von ZnO-Einkristallen. *Ber. Bunsenges. Phys. Chem* **1968,** *72* (3), 437–445. DOI: 10.1002/bbpc.196800013.

[24] Hauffe, K.; Pusch, H.; Range, J. Experimente zur spektralen Sensibilisierung der Elektroden-Eigenschaft von Zinkoxid. *Zeitschrift für Physikalische Chemie* **1969,** *64* (1_4), 122–132. DOI: 10.1524/zpch.1969.64.1_4.122.

[25] Hauffe, K.; Martinez, V.; Pusch, H.; Range, J.; Schmidt, R.; Stechemesser, R. Experiments on dye sensitization of zinc oxide. *Appl. Optics* **1969,** *8* (1), 34–41.

[26] Gerischer, H. Electrochemical Techniques for the Study of Photosensitization. *Photochem. Photobiol.* **1972,** *16* (4), 243–260. DOI: 10.1111/j.1751-1097.1972.tb06296.x.

[27] Gerischer, H.; Lübke, M. Löschung von Farbstoff-sensibilisierten Photoströmen an Halbleiter-Elektroden durch geringe Mengen elektrolytisch abgeschiedener Metalle. *Zeitschrift für Physikalische Chemie* **1975,** *98* (1-6), 317–326. DOI: 10.1524/zpch.1975.98.1-6.317.

[28] MEMMING, R. PHOTOCHEMICAL AND ELECTROCHEMICAL PROCESSES OF EXCITED DYES AT SEMICONDUCTOR AND METAL ELECTRODES*. *Photochemistry and Photobiology* **1972,** *16* (4), 325–333. DOI: 10.1111/j.1751-1097.1972.tb06302.x.

[29] TSUBOMURA, H.; MATSUMURA, M.; NOMURA, Y.; AMAMIYA, T. Dye sensitised zinc oxide: aqueous electrolyte: platinum photocell. *Nature (Nature)* **1976,** *261* (5559), 402–403. DOI: 10.1038/261402a0.

[30] Dare-Edwards, M. P.; Goodenough, J. B.; Hamnett, A.; Seddon, K. R.; Wright, R. D. Sensitisation of semiconducting electrodes with ruthenium-based dyes. *Faraday Discuss. Chem. Soc.* **1980,** *70*, 285. DOI: 10.1039/DC9807000285.

[31] Desilvestro, J.; Graetzel, M.; Kavan, L.; Moser, J.; Augustynski, J. Highly efficient sensitization of titanium dioxide. *J. Am. Chem. Soc.* **1985,** *107* (10), 2988–2990. DOI: 10.1021/ja00296a035.

[32] Heller, A. Conversion of sunlight into electrical power and photoassisted electrolysis of water in photoelectrochemical cells. *Acc. Chem. Res.* **1981,** *14* (5), 154–162. DOI: 10.1021/ar00065a004.

[33] O'Regan, B.; Grätzel, M. A low-cost, high-efficiency solar cell based on dye-sensitized colloidal TiO2 films. *Nature (Nature)* **1991,** *353* (6346), 737–740. DOI: 10.1038/353737a0.

[34] Nazeeruddin, M. K.; Kay, A.; Rodicio, I.; Humphry-Baker, R.; Mueller, E.; Liska, P.; Vlachopoulos, N.; Graetzel, M. Conversion of light to electricity by cis-X2bis(2,2'-bipyridyl-4,4'-dicarboxylate)ruthenium(II) charge-transfer sensitizers (X = Cl-, Br-, I-, CN-, and SCN-) on nanocrystalline titanium dioxide electrodes. *J. Am. Chem. Soc.* **1993,** *115* (14), 6382–6390. DOI: 10.1021/ja00067a063.

[35] Hagfeldt, A. Brief overview of dye-sensitized solar cells. *Ambio* **2012,** *41 Suppl 2*, 151–155. DOI: 10.1007/s13280-012-0272-7.

[36] Zhang, Q.; Cao, G. Nanostructured photoelectrodes for dye-sensitized solar cells. *Nano Today* **2011,** *6* (1), 91–109. DOI: 10.1016/j.nantod.2010.12.007.

[37] Wu, J.; Lan, Z.; Lin, J.; Huang, M.; Huang, Y.; Fan, L.; Luo, G. Electrolytes in Dye-Sensitized Solar Cells. *Chem. Rev.* **2015,** *115* (5), 2136–2173. DOI: 10.1021/cr400675m.

[38] Kuwajima, T.; Nakanishi, Y.; Yamamoto, A.; Nobusawa, K.; Ikeda, A.; Tomita, S.; Yanagi, H.; Ichinose, K.; Yoshida, T. Fabrication of Carbon Nanotube/Zinc Oxide Composite Films by Electrodeposition. *Jpn. J. Appl. Phys.* **2011,** *50* (8), 85504. DOI: 10.1143/JJAP.50.085504.

[39] Wang, M.; Grätzel, C.; Zakeeruddin, S. M.; Grätzel, M. Recent developments in redox electrolytes for dye-sensitized solar cells. *Energy Environ. Sci.* **2012,** *5* (11), 9394. DOI: 10.1039/c2ee23081j.

[40] Zhang, W.; Cheng, Y.; Yin, X.; Liu, B. Solid-State Dye-Sensitized Solar Cells with Conjugated Polymers as Hole-Transporting Materials. *Macromol. Chem. Phys.* **2011,** *212* (1), 15–23. DOI: 10.1002/macp.201000489.

[41] Lee, C.-P.; Lin, R. Y.-Y.; Lin, L.-Y.; Li, C.-T.; Chu, T.-C.; Sun, S.-S.; Lin, J. T.; Ho, K.-C. Recent progress in organic sensitizers for dye-sensitized solar cells. *RSC Adv* **2015,** *5* (30), 23810–23825. DOI: 10.1039/c4ra16493h.

[42] Wu, M.; Ma, T. Platinum-free catalysts as counter electrodes in dye-sensitized solar cells. *ChemSusChem* **2012,** *5* (8), 1343–1357. DOI: 10.1002/cssc.201100676.

[43] Weerasinghe, H. C.; Huang, F.; Cheng, Y.-B. Fabrication of flexible dye sensitized solar cells on plastic substrates. *Nano Energy* **2013,** *2* (2), 174–189. DOI: 10.1016/j.nanoen.2012.10.004.

[44] Chae, Y.; Kim, S. J.; Kim, J. H.; Kim, E. Metal-free organic-dye-based flexible dye-sensitized solar textiles with panchromatic effect. *Dyes and Pigments* **2015,** *113*, 378–389. DOI: 10.1016/j.dyepig.2014.09.004.

[45] Chen, T.; Qiu, L.; Yang, Z.; Peng, H. Novel solar cells in a wire format. *Chem. Soc. Rev.* **2013,** *42* (12), 5031. DOI: 10.1039/c3cs35465b.

[46] Loewenstein, T.; Rudolph, M.; Mingebach, M.; Strauch, K.; Zimmermann, Y.; Neudeck, A.; Sensfuss, S.; Schlettwein, D. Textile-Compatible Substrate Electrodes with Electrodeposited ZnO-A New Pathway to Textile-Based Photovoltaics. *ChemPhysChem* **2010,** *11* (4), 783–788. DOI: 10.1002/cphc.200900428.

[47] Gao, P.; Grätzel, M.; Nazeeruddin, M. K. Organohalide lead perovskites for photovoltaic applications. *Energy Environ. Sci.* **2014,** *7* (8), 2448. DOI: 10.1039/c4ee00942h.

[48] Boix, P. P.; Nonomura, K.; Mathews, N.; Mhaisalkar, S. G. Current progress and future perspectives for organic/inorganic perovskite solar cells. *Materials Today* **2014,** *17* (1), 16–23. DOI: 10.1016/j.mattod.2013.12.002.

[49] Song, T.-B.; Chen, Q.; Zhou, H.; Jiang, C.; Wang, H.-H.; Yang, Y.; Liu, Y.; You, J. Perovskite solar cells: film formation and properties. *J. Mater. Chem. A [Online]* **2015**.

[50] Docampo, P.; Guldin, S.; Leijtens, T.; Noel, N. K.; Steiner, U.; Snaith, H. J. Lessons learned: from dye-sensitized solar cells to all-solid-state hybrid devices. *Adv. Mater.* **2014,** *26* (24), 4013–4030. DOI: 10.1002/adma.201400486.

[51] Anta, J. A.; Guillén, E.; Tena-Zaera, R. ZnO-Based Dye-Sensitized Solar Cells. *J. Phys. Chem. C* **2012,** *116* (21), 11413–11425. DOI: 10.1021/jp3010025.

[52] Chang, W.-C.; Lin, L.-Y.; Yu, W.-C. Bifunctional Zinc Oxide Nanoburger Aggregates as the Dye-Adsorption and Light-Scattering Layer for Dye-Sensitized Solar Cells. *Electrochimica Acta* **2015,** *169*, 456–461. DOI: 10.1016/j.electacta.2015.04.056.

[53] Concina, I.; Vomiero, A. Metal oxide semiconductors for dye- and quantum-dot-sensitized solar cells. *Small* **2015,** *11* (15), 1744–1774. DOI: 10.1002/smll.201402334.

[54] Memarian, N.; Concina, I.; Braga, A.; Rozati, S. M.; Vomiero, A.; Sberveglieri, G. Hierarchically Assembled ZnO Nanocrystallites for High-Efficiency Dye-Sensitized Solar Cells. *Angew. Chem. Int. Ed.* **2011,** *50* (51), 12321–12325. DOI: 10.1002/anie.201104605.

[55] Li, F.; Jiao, Y.; Xie, S.; Li, J. Sponge-like porous TiO2/ZnO nanodonuts for high efficiency dye-sensitized solar cells. *Journal of Power Sources* **2015,** *280*, 373–378. DOI: 10.1016/j.jpowsour.2015.01.118.

[56] Lv, Y.; Li, W.; Li, J.; Yang, Y.; Li, Y.; Chen, Q. In situ formation of ZnO scattering sites within a TiO2 nanoparticles film for improved dye-sensitized solar cells performance. *Electrochimica Acta* **2015,** *174*, 438–445. DOI: 10.1016/j.electacta.2015.03.124.

[57] Manthina, V.; Agrios, A. G. Band edge engineering of composite photoanodes for dye-sensitized solar cells. *Electrochimica Acta* **2015,** *169*, 416–423. DOI: 10.1016/j.electacta.2015.04.080.

[58] Susmitha, K.; Naresh Kumar, M.; Rajkumar, G.; Giribabu, L.; Raghavender, M. Enhanced dye sensitized solar cell performance with high surface area thin ZnO film and PEDOT:PSS. *Solar Energy* **2015,** *118*, 126–133. DOI: 10.1016/j.solener.2015.03.054.

[59] *Device Modeling of Dye-Sensitized Solar Cells;* Bisquert, J., Marcus, R. A., Eds.; Springer Berlin Heidelberg: Berlin, Heidelberg, 2013.

[60] Fabregat-Santiago, F.; Garcia-Belmonte, G.; Mora-Seró, I.; Bisquert, J. Characterization of nanostructured hybrid and organic solar cells by impedance spectroscopy. *Physical chemistry chemical physics : PCCP* **2011,** *13* (20), 9083–9118. DOI: 10.1039/c0cp02249g.

[61] Bisquert, J. *Nanostructured Energy Devices. Equilibrium Concepts and Kinetics;* CRC Press: Boca Raton, FL, 2014.

[62] Kalyanasundaram, K. *Dye-sensitized solar cells;* CRC Press: Boca Raton, FL, 2010.

[63] O'Regan, B.; Moser, J.; Anderson, M.; Graetzel, M. Vectorial electron injection into transparent semiconductor membranes and electric field effects on the dynamics of light-induced charge separation: 10.1021/j100387a017. *J. Phys. Chem.* **1990,** *94* (24), 8720–8726. DOI: 10.1021/j100387a017.

[64] Tachibana, Y.; Haque, S. A.; Mercer, I. P.; Moser, J. E.; Klug, D. R.; Durrant, J. R. Modulation of the Rate of Electron Injection in Dye-Sensitized Nanocrystalline TiO 2 Films by Externally Applied Bias. *J. Phys. Chem. B* **2001,** *105* (31), 7424–7431. DOI: 10.1021/jp010173q.

[65] Salvador, P.; Hidalgo, M. G.; Zaban, A.; Bisquert, J. Illumination intensity dependence of the photovoltage in nanostructured TiO2 dye-sensitized solar cells. *The journal of physical chemistry. B* **2005,** *109* (33), 15915–15926. DOI: 10.1021/jp051515l.

[66] Jennings, J. R.; Liu, Y.; Wang, Q. Efficiency Limitations in Dye-Sensitized Solar Cells Caused by Inefficient Sensitizer Regeneration. *J. Phys. Chem. C* **2011,** *115* (30), 15109–15120. DOI: 10.1021/jp2053053.

[67] Hauch, A.; Georg, A. Diffusion in the electrolyte and charge-transfer reaction at the platinum electrode in dye-sensitized solar cells. *Electrochim. Acta* **2001,** *46* (22), 3457–3466. DOI: 10.1016/S0013-4686(01)00540-0.

[68] Zistler, M.; Wachter, P.; Wasserscheid, P.; Gerhard, D.; Hinsch, A.; Sastrawan, R.; Gores, H. J. Comparison of electrochemical methods for triiodide diffusion coefficient measurements and observation of non-Stokesian diffusion behaviour in binary mixtures of two ionic liquids. *Electrochimica Acta* **2006,** *52* (1), 161–169. DOI: 10.1016/j.electacta.2006.04.050.

[69] Li, X.; Lü, H.; Wang, S.; Guo, J.; Li, J. Sensitizers of Dye-Sensitized Solar Cells **2011,** *23* (2-3), 569–588.

[70] Ooyama, Y.; Harima, Y. Molecular Designs and Syntheses of Organic Dyes for Dye-Sensitized Solar Cells. *Eur. J. Org. Chem.* **2009,** *2009* (18), 2903–2934. DOI: 10.1002/ejoc.200900236.

[71] Delcamp, J. H.; Yella, A.; Holcombe, T. W.; Nazeeruddin, M. K.; Grätzel, M. The Molecular Engineering of Organic Sensitizers for Solar-Cell Applications. *Angew. Chem. Int. Ed.* **2013,** *52* (1), 376–380. DOI: 10.1002/anie.201205007.

[72] Kulinich, A. V.; Ishchenko, A. A. Merocyanine dyes: synthesis, structure, properties and applications. *Russ. Chem. Rev.* **2009,** *78* (2), 141–164. DOI: 10.1070/RC2009v078n02ABEH003900.

[73] Yella, A.; Mai, C.-L.; Zakeeruddin, S. M.; Chang, S.-N.; Hsieh, C.-H.; Yeh, C.-Y.; Grätzel, M. Molecular engineering of push-pull porphyrin dyes for highly efficient dye-sensitized solar cells: the role of benzene spacers. *Angewandte Chemie (International ed. in English)* **2014,** *53* (11), 2973–2977. DOI: 10.1002/anie.201309343.

[74] Zhao, J.; Yang, X.; Cheng, M.; Li, S.; Sun, L. Molecular Design and Performance of Hydroxylpyridium Sensitizers for Dye-Sensitized Solar Cells. *ACS Appl. Mater. Interfaces* **2013,** *5* (11), 5227–5231. DOI: 10.1021/am4010545.

[75] Martínez-Díaz, M. V.; de la Torre, Gema; Torres, T. Lighting porphyrins and phthalocyanines for molecular photovoltaics. *Chem. Commun.* **2010,** *46* (38), 7090. DOI: 10.1039/c0cc02213f.

[76] Robertson, N. Optimizing dyes for dye-sensitized solar cells. *Angewandte Chemie (International ed. in English)* **2006,** *45* (15), 2338–2345. DOI: 10.1002/anie.200503083.

[77] Zhang, L.; Cole, J. M. Anchoring groups for dye-sensitized solar cells. *ACS applied materials & interfaces* **2015,** *7* (6), 3427–3455. DOI: 10.1021/am507334m.

[78] Idígoras, J.; Godfroy, M.; Joly, D.; Todinova, A.; Maldivi, P.; Oskam, G.; Demadrille, R.; Anta, J. A. Organic dyes for the sensitization of nanostructured ZnO photoanodes: effect of the anchoring functions. *RSC Adv* **2015,** *5* (84), 68929–68938. DOI: 10.1039/c5ra11762c.

[79] Warnan, J.; Guerin, V.-M.; Anne, F. B.; Pellegrin, Y.; Blart, E.; Jacquemin, D.; Pauporté, T.; Odobel, F. Ruthenium Sensitizer Functionalized by Acetylacetone Anchoring Groups for Dye-Sensitized Solar Cells. *J. Phys. Chem. C* **2013,** *117* (17), 8652–8660. DOI: 10.1021/jp402608u.

[80] Wu, Y.; Zhu, W. Organic sensitizers from D–π–A to D–A–π–A: effect of the internal electron-withdrawing units on molecular absorption, energy levels and photovoltaic performances. *Chem. Soc. Rev.* **2013,** *42* (5), 2039. DOI: 10.1039/c2cs35346f.

[81] Kroeze, J. E.; Hirata, N.; Koops, S.; Nazeeruddin, M. K.; Schmidt-Mende, L.; Grätzel, M.; Durrant, J. R. Alkyl chain barriers for kinetic optimization in dye-sensitized solar cells. *Journal of the American Chemical Society* **2006,** *128* (50), 16376–16383. DOI: 10.1021/ja065653f.

[82] Horiuchi, T.; Miura, H.; Uchida, S. Highly-efficient metal-free organic dyes for dye-sensitized solar cells. *Chem. Commun.* **2003,** *1* (24), 3036. DOI: 10.1039/B307819A.

[83] Horiuchi, T.; Miura, H.; Sumioka, K.; Uchida, S. High Efficiency of Dye-Sensitized Solar Cells Based on Metal-Free Indoline Dyes. *J. Am. Chem. Soc.* **2004,** *126* (39), 12218–12219. DOI: 10.1021/ja0488277.

[84] Horiuchi, T.; Miura, H.; Uchida, S. Highly efficient metal-free organic dyes for dye-sensitized solar cells. *Journal of Photochemistry and Photobiology A: Chemistry* **2004,** *164* (1-3), 29–32. DOI: 10.1016/j.jphotochem.2003.12.018.

[85] Horiuchi, T., Miura, H. & Kodera, T. *Organic dye, photoelectric conversion material, semiconductor electrode and photoelectric conversion device* (Patent, **2008**), http://www.google.com.ar/patents/US20080087327.

[86] Dentani, T.; Kubota, Y.; Funabiki, K.; Jin, J.; Yoshida, T.; Minoura, H.; Miura, H.; Matsui, M. Novel thiophene-conjugated indoline dyes for zinc oxide solar cells. *New J. Chem.* **2009,** *33* (1), 93. DOI: 10.1039/b808959k.

[87] Gómez-Ortíz, N. M.; Idígoras, J.; Guillén, E.; Hernández, A.; Sastre-Santos, A.; Fernández-Lázaro, F.; Anta, J. A.; Oskam, G. Influence of dye chemistry and electrolyte solution on interfacial processes at nanostructured ZnO in dye-sensitized solar cells. *Journal of Photochemistry and Photobiology A: Chemistry* **2013,** *264*, 26–33. DOI: 10.1016/j.jphotochem.2013.04.020.

[88] Guillén, E.; Idígoras, J.; Berger, T.; Anta, J. A.; Fernández-Lorenzo, C.; Alcántara, R.; Navas, J.; Martín-Calleja, J. ZnO-based dye solar cell with pure ionic-liquid electrolyte and organic sensitizer: The relevance of the dye–oxide interaction in an ionic-liquid medium. *Phys. Chem. Chem. Phys.* **2011,** *13* (1), 207–213. DOI: 10.1039/c0cp00507j.

[89] Higashijima, S.; Miura, H.; Fujita, T.; Kubota, Y.; Funabiki, K.; Yoshida, T.; Matsui, M. Highly efficient new indoline dye having strong electron-withdrawing group for zinc oxide dye-sensitized solar cell. *Tetrahedron* **2011,** *67* (34), 6289–6293. DOI: 10.1016/j.tet.2011.06.016.

[90] Akhtaruzzaman, M.; Ekramul Mahmud, H.; Islam, A.; Ei Shafei, A.; Karim, M. R.; Sopian, K.; Han, L.; Yamamoto, Y. Simple indoline based donor–acceptor dye for high efficiency dye-sensitized solar cells. *Mater. Chem. Phys.* **2013,** *142* (1), 82–86. DOI: 10.1016/j.matchemphys.2013.06.044.

[91] Jose, R.; Kumar, A.; Thavasi, V.; Fujihara, K.; Uchida, S.; Ramakrishna, S. Relationship between the molecular orbital structure of the dyes and photocurrent density in the dye-sensitized solar cells. *Appl. Phys. Lett.* [Online] **2008,** No. 93, 23125.

[92] Liu, B.; Wang, B.; Wang, R.; Gao, L.; Huo, S.; Liu, Q.; Li, X.; Zhu, W. Influence of conjugated π-linker in D–D–π–A indoline dyes: towards long-term stable and efficient dye-sensitized solar cells with high photovoltage. *J. Mater. Chem. A* **2013,** *2* (3), 804. DOI: 10.1039/c3ta13993j.

[93] Howie, W. H.; Claeyssens, F.; Miura, H.; Peter, L. M. Characterization of Solid-State Dye-Sensitized Solar Cells Utilizing High Absorption Coefficient Metal-Free Organic Dyes. *J. Am. Chem. Soc.* **2008,** *130* (4), 1367–1375. DOI: 10.1021/ja076525+.

[94] Cheng, H.-M.; Hsieh, W.-F. Electron transfer properties of organic dye-sensitized solar cells based on indoline sensitizers with ZnO nanoparticles. *Nanotechnology* **2010,** *21* (48), 485202. DOI: 10.1088/0957-4484/21/48/485202.

[95] Matsui, M.; Inoue, T.; Ono, M.; Kubota, Y.; Funabiki, K.; Jin, J.; Yoshida, T.; Higashijima, S.; Miura, H. Application of novel N-(p-phenylene)-dicyanovinylidene double rhodanine indoline dye for zinc oxide dye-sensitized solar cell. *Dyes and Pigments* **2013,** *96* (2), 614–618. DOI: 10.1016/j.dyepig.2012.08.023.

[96] Matsui, M.; Shiota, T.; Kubota, Y.; Funabiki, K.; Jin, J.; Yoshida, T.; Higashijima, S.; Miura, H. N-(2-Alkoxyphenyl)-substituted double rhodanine indoline dyes for zinc oxide dye-sensitized solar cell. *Tetrahedron* **2012,** *68* (22), 4286–4291. DOI: 10.1016/j.tet.2012.03.060.

[97] Liu, B.; Li, W.; Wang, B.; Li, X.; Liu, Q.; Naruta, Y.; Zhu, W. Influence of different anchoring groups in indoline dyes for dye-sensitized solar cells: Electron injection, impedance and charge recombination. *J. Power Sources* **2013,** *234*, 139–146. DOI: 10.1016/j.jpowsour.2013.01.152.

[98] Matsui, M.; Fujita, T.; Kubota, Y.; Funabiki, K.; Jin, J.; Yoshida, T.; Miura, H. Substituent effects in a double rhodanine indoline dye on performance of zinc oxide dye-sensitized solar cell. *Dyes and Pigments* **2010,** *86* (2), 143–148. DOI: 10.1016/j.dyepig.2009.12.009.

[99] Li, G.; Liang, M.; Wang, H.; Sun, Z.; Wang, L.; Wang, Z.; Xue, S. Significant Enhancement of Open-Circuit Voltage in Indoline-Based Dye-Sensitized Solar Cells via Retarding Charge Recombination. *Chem. Mater.* **2013,** *25* (9), 1713–1722. DOI: 10.1021/cm400196w.

[100] Matsui, M.; Asamura, Y.; Kubota, Y.; Funabiki, K.; Jin, J.; Yoshida, T.; Miura, H. Highly efficient substituted triple rhodanine indoline dyes in zinc oxide dye-sensitized solar cell. *Tetrahedron* **2010,** *66* (37), 7405–7410. DOI: 10.1016/j.tet.2010.07.017.

[101] Kim, J. Y.; Kim, Y. H.; Kim, Y. S. Indoline dyes with various acceptors for dye-sensitized solar cells. *Current Applied Physics* [Online] **2011,** No. 11, S117-S121.

[102] Pei, K.; Wu, Y.; Islam, A.; Zhang, Q.; Han, L.; Tian, H.; Zhu, W. Constructing High-Efficiency D–A−π–A-Featured Solar Cell Sensitizers: a Promising Building Block of 2,3-Diphenylquinoxaline for Antiaggregation and Photostability. *ACS Appl. Mater. Interfaces* **2013,** *5* (11), 4986–4995. DOI: 10.1021/am400754d.

[103] Liu, B.; Wu, W.; Li, X.; Li, L.; Guo, S.; Wei, X.; Zhu, W.; Liu, Q. Molecular engineering and theoretical investigation of organic sensitizers based on indoline dyes for quasi-solid state dye-sensitized solar cells. *Phys. Chem. Chem. Phys.* **2011,** *13* (19), 8985. DOI: 10.1039/c1cp20484j.

[104] Wu, Y.; Marszalek, M.; Zakeeruddin, S. M.; Zhang, Q.; Tian, H.; Grätzel, M.; Zhu, W. High-conversion-efficiency organic dye-sensitized solar cells: molecular engineering on D–A–π-A featured organic indoline dyes. *Energy Environ. Sci.* **2012,** *5* (8), 8261. DOI: 10.1039/c2ee22108j.

[105] Rohwer, E.; Richter, C.; Heming, N.; Strauch, K.; Litwinski, C.; Nyokong, T.; Schlettwein, D.; Schwoerer, H. Ultrafast Photodynamics of the Indoline Dye D149 Adsorbed to Porous ZnO in Dye-Sensitized Solar Cells. *ChemPhysChem* **2013,** *14* (1), 132–139. DOI: 10.1002/cphc.201200715.

[106] Fattori, A.; Peter, L. M.; Wang, H.; Miura, H.; Marken, F. Fast Hole Surface Conduction Observed for Indoline Sensitizer Dyes Immobilized at Fluorine-Doped Tin Oxide−TiO 2 Surfaces. *J. Phys. Chem. C* **2010,** *114* (27), 11822–11828. DOI: 10.1021/jp103808u.

[107] Sobuś, J.; Burdziński, G.; Karolczak, J.; Idígoras, J.; Anta, J. A.; Ziółek, M. Comparison of TiO_2 and ZnO solar cells sensitized with an indoline dye: time-resolved laser spectroscopy studies of partial charge separation processes. *Langmuir : the ACS journal of surfaces and colloids* **2014,** *30* (9), 2505–2512. DOI: 10.1021/la404782s.

[108] Sobuś, J.; Karolczak, J.; Komar, D.; Anta, J. A.; Ziółek, M. Transient states and the role of excited state self-quenching of indoline dyes in complete dye-sensitized solar cells. *Dyes and Pigments* **2015,** *113*, 692–701. DOI: 10.1016/j.dyepig.2014.10.008.

[109] El-Zohry, A. M.; Zietz, B. Concentration and Solvent Effects on the Excited State Dynamics of the Solar Cell Dye D149: The Special Role of Protons. *J. Phys. Chem. C* **2013,** *117* (13), 6544–6553. DOI: 10.1021/jp400782g.

[110] Lohse, P. W.; Kuhnt, J.; Druzhinin, S. I.; Scholz, M.; Ekimova, M.; Oekermann, T.; Lenzer, T.; Oum, K. Ultrafast photoinduced relaxation dynamics of the indoline dye D149 in organic solvents. *Phys. Chem. Chem. Phys.* **2011,** *13* (43), 19632. DOI: 10.1039/c1cp22429h.

[111] Le Bahers, T.; Pauporté, T.; Scalmani, G.; Adamo, C.; Ciofini, I. A TD-DFT investigation of ground and excited state properties in indoline dyes used for dye-sensitized solar cells. *Phys. Chem. Chem. Phys.* **2009,** *11* (47), 11276. DOI: 10.1039/b914626a.

[112] Huang, D. M.; Snaith, H. J.; Grätzel, M.; Meerholz, K.; Moulé, A. J. Optical description of solid-state dye-sensitized solar cells. II. Device optical modeling with implications for improving efficiency. *J. Appl. Phys.* **2009,** *106* (7), 73112. DOI: 10.1063/1.3204985.

[113] Li, H.; Chen, M. Structure-property relationships for three indoline dyes used in dye-sensitized solar cells: TDDFT study of visible absorption and photoinduced charge-transfer processes. *J Mol Model* **2013,** *19* (12), 5317–5325. DOI: 10.1007/s00894-013-2024-4.

[114] Pastore, M.; Angelis, F. de. Computational Modeling of Stark Effects in Organic Dye-Sensitized TiO 2 Heterointerfaces. *J. Phys. Chem. Lett.* **2011,** *2* (11), 1261–1267. DOI: 10.1021/jz200443w.

[115] Pastore, M.; Angelis, F. de. Aggregation of Organic Dyes on TiO 2 in Dye-Sensitized Solar Cells Models: An ab Initio Investigation. *ACS Nano* **2010,** *4* (1), 556–562. DOI: 10.1021/nn901518s.

[116] Zhang, C.-R.; Liu, L.; Zhe, J.-W.; Jin, N.-Z.; Yuan, L.-H.; Chen, Y.-H.; Wei, Z.-Q.; Wu, Y.-Z.; Liu, Z.-J.; Chen, H.-S. Comparative study on electronic structures and optical properties of indoline and triphenylamine dye sensitizers for solar cells dye sensitizers for solar cells. *Journal of molecular modeling* **2013,** *19* (4), 1553–1563. DOI: 10.1007/s00894-012-1723-6.

[117] Liu, D.-S.; Ding, W.-L.; Zhu, K.-L.; Geng, Z.-Y.; Wang, D.-M.; Zhao, X.-L. The master factors influencing the efficiency of D–A–π–A configurated organic sensitizers in dye-sensitized solar cell via theoretically characterization: Design and verification. *Dyes and Pigments* **2014,** *105*, 192–201. DOI: 10.1016/j.dyepig.2014.01.030.

[118] Xu, J.; Zhang, H.; Liang, G.; Wang, L.; Weilin, X.; Cui, W.; Zengchang, L. DFT studies on the electronic structures of indoline dyes for dye-sensitized solar cells. *J. Serb. Chem. Soc.* **2010,** *75* (2), 259–269. DOI: 10.2298/JSC1002259X.

[119] Ito, S.; Zakeeruddin, S. M.; Humphry-Baker, R.; Liska, P.; Charvet, R.; Comte, P.; Nazeeruddin, M. K.; Péchy, P.; Takata, M.; Miura, H.; Uchida, S.; Grätzel, M. High-Efficiency Organic-Dye- Sensitized Solar Cells Controlled by Nanocrystalline-TiO2 Electrode Thickness. *Adv. Mater.* **2006,** *18* (9), 1202–1205. DOI: 10.1002/adma.200502540.

[120] Mitsubishi Paper Mills: http://www.k-mpm.com/k-new/solar-e/technology02.html (2015-03-24)

[121] Falgenhauer, J. Indoline Dyes as Sensitizers for ZnO. Master Thesis; Justus-Liebig-Universität, Gießen, 2012.

[122] Schäfer, M. Anpassung der Porosität einer Halbleiterelektrode an die Kontaktierung mit Lochleitern. Master Thesis; Justus-Liebig-Universität, Gießen, 2013.

[123] Beu, M. Nutzung von Zinkoxid-Schichten in farbstoffsensibilisierten Festkörpersolarzellen. Dissertation; Justus-Liebig-Universität, Gießen, 2014.

[124] Matsui, M.; Fujita, T.; Kubota, Y.; Funabiki, K.; Miura, H.; Shiro, M. X-ray Crystallography of D149 Ethyl Ester. *Bull. Chem. Soc. Jpn.* **2010,** *83* (6), 709–711. DOI: 10.1246/bcsj.20100021.

[125] Minda, I.; Ahmed, E.; Sleziona, V.; Richter, C.; Beu, M.; Falgenhauer, J.; Miura, H.; Schlettwein, D.; Schwoerer, H. Identification of different pathways of electron injection in dye-sensitised solar cells of electrodeposited ZnO using an indoline sensitiser. *Phys. Chem. Chem. Phys.* **2016,** *18* (13), 8938–8944. DOI: 10.1039/c5cp07841e.

[126] Sakuragi, Y.; Wang, X.-F.; Miura, H.; Matsui, M.; Yoshida, T. Aggregation of indoline dyes as sensitizers for ZnO solar cells. *Journal of Photochemistry and Photobiology A: Chemistry* **2010,** *216* (1), 1–7. DOI: 10.1016/j.jphotochem.2010.08.015.

[127] Rudolph, M. Photoelectrochemical characterization of dye-sensitized solar cells based on ZnO and organic dyes. Dissertation; Justus-Liebig-Universität, Gießen, 2015.

[128] Personal communication.

[129] Wang, Z.-S.; Cui, Y.; Dan-oh, Y.; Kasada, C.; Shinpo, A.; Hara, K. Thiophene-Functionalized Coumarin Dye for Efficient Dye-Sensitized Solar Cells: Electron Lifetime Improved by Coadsorption of Deoxycholic Acid. *J. Phys. Chem. C* **2007,** *111* (19), 7224–7230. DOI: 10.1021/jp067872t.

[130] Richter, C. Einfluss von Oberflächenmodifikationen auf die Ladungstransferkinetik in Hybridsolarzellen. Dissertation; Justus-Liebig-Universität, Gießen, 2015.

[131] Fiehler, F. Einfluss der chemischen Verankerung von Farbstoffen auf die Sensibiliserung von ZnO. Master Thesis; Justus-Liebig-Universität, Gießen, 2013.

[132] Pandey, S. S.; Sakaguchi, S.; Yamaguchi, Y.; Hayase, S. Influence of nature of surface dipoles on observed photovoltage in dye-sensitized solar cells as probed by surface potential measurement. *Org. Electron.* **2010,** *11* (3), 419–426. DOI: 10.1016/j.orgel.2009.11.021.

[133] Li, C.; Wonneberger, H. Perylene imides for organic photovoltaics: yesterday, today, and tomorrow. *Adv. Mater.* **2012,** *24* (5), 613–636. DOI: 10.1002/adma.201104447.

[134] Shibano, Y.; Umeyama, T.; Matano, Y.; Imahori, H. Electron-donating perylene tetracarboxylic acids for dye-sensitized solar cells. *Organic letters* **2007,** *9* (10), 1971–1974. DOI: 10.1021/ol070556s.

[135] Yao, Z.; Zhang, M.; Li, R.; Yang, L.; Qiao, Y.; Wang, P. A metal-free N-annulated thienocyclopentaperylene dye: power conversion efficiency of 12% for dye-sensitized solar cells. *Angewandte Chemie (International ed. in English)* **2015,** *54* (20), 5994–5998. DOI: 10.1002/anie.201501195.

[136] Gibson, E. A.; Le Pleux, L.; Fortage, J.; Pellegrin, Y.; Blart, E.; Odobel, F.; Hagfeldt, A.; Boschloo, G. Role of the triiodide/iodide redox couple in dye regeneration in p-type dye-sensitized solar cells. *Langmuir : the ACS journal of surfaces and colloids* **2012,** *28* (15), 6485–6493. DOI: 10.1021/la300215q.

[137] Langhals, H.; Lona, W. The Synthesis of Perylenebisimide Monocarboxylic Acids. *Eur. J. Org. Chem.* **1998,** *1998* (5), 847–851. DOI: 10.1002/(SICI)1099-0690(199805)1998:5<847:AID-EJOC847>3.0.CO;2-3.

[138] Schütte, J.; Bechstein, R.; Rahe, P.; Rohlfing, M.; Kühnle, A.; Langhals, H. Imaging perylene derivatives on rutile TiO2(110) by noncontact atomic force microscopy. *Phys. Rev. B* **2009,** *79* (4). DOI: 10.1103/PhysRevB.79.045428.

[139] Schütte, J.; Bechstein, R.; Rahe, P.; Langhals, H.; Rohlfing, M.; Kühnle, A. Single-molecule switching with non-contact atomic force microscopy. *Nanotechnology* **2011,** *22* (24), 245701. DOI: 10.1088/0957-4484/22/24/245701.

[140] Tang, J.; Wu, W.; Hua, J.; Li, J.; Li, X.; Tian, H. Starburst triphenylamine-based cyanine dye for efficient quasi-solid-state dye-sensitized solar cells. *Energy Environ. Sci.* **2009,** *2* (9), 982. DOI: 10.1039/b906596b.

[141] Liu, B.; Zhu, W.; Zhang, Q.; Wu, W.; Xu, M.; Ning, Z.; Xie, Y.; Tian, H. Conveniently synthesized isophorone dyes for high efficiency dye-sensitized solar cells: tuning photovoltaic performance by structural modification of donor group in donor–π–acceptor system. *Chem. Commun.* [Online] **2009,** No. 13, 1766.

[142] Alibabaei, L.; Kim, J.-H.; Wang, M.; Pootrakulchote, N.; Teuscher, J.; Di Censo, D.; Humphry-Baker, R.; Moser, J.-E.; Yu, Y.-J.; Kay, K.-Y.; Zakeeruddin, S. M.; Grätzel, M. Molecular design of metal-free D–π-A substituted sensitizers for dye-sensitized solar cells. *Energy Environ. Sci.* **2010,** *3* (11), 1757. DOI: 10.1039/c0ee00218f.

[143] Tang, J.; Hua, J.; Wu, W.; Li, J.; Jin, Z.; Long, Y.; Tian, H. New starburst sensitizer with carbazole antennas for efficient and stable dye-sensitized solar cells. *Energy Environ. Sci.* **2010,** *3* (11), 1736. DOI: 10.1039/c0ee00008f.

[144] Mahmood, A. Triphenylamine based dyes for dye sensitized solar cells: A review. *Solar Energy* **2016,** *123*, 127–144. DOI: 10.1016/j.solener.2015.11.015.

[145] Ning, Z.; Zhang, Q.; Wu, W.; Pei, H.; Liu, B.; Tian, H. Starburst triarylamine based dyes for efficient dye-sensitized solar cells. *The Journal of organic chemistry* **2008,** *73* (10), 3791–3797. DOI: 10.1021/jo800159t.

[146] Ning, Z.; Tian, H. Triarylamine: a promising core unit for efficient photovoltaic materials. *Chemical communications (Cambridge, England)* [Online] **2009,** No. 37, 5483–5495.

[147] Wang, Y.; Yang, L.; Zhang, J.; Li, R.; Zhang, M.; Wang, P. Altering the self-organization of dyes on titania with dyeing solvents to tune the charge-transfer dynamics of sensitized solar cells. *Chemphyschem* **2014,** *15* (6), 1037–1042. DOI: 10.1002/cphc.201301006.

[148] Wei, Y.; Wu, Z.; An, Z.; Chen, X.; Chen, P.; Liu, Q. Highly Efficient Dye-sensitized Solar Cells by Co-sensitization of Organic Dyes and Co-adsorbent Chenodeoxycholic Acid. *Chin. J. Chem.* **2014,** *32* (6), 474–478. DOI: 10.1002/cjoc.201400190.

[149] Yang, C.-H.; Chen, H.-L.; Chuang, Y.-Y.; Wu, C.-G.; Chen, C.-P.; Liao, S.-H.; Wang, T.-L. Characteristics of triphenylamine-based dyes with multiple acceptors in application of dye-sensitized solar cells. *Journal of Power Sources* **2009,** *188* (2), 627–634. DOI: 10.1016/j.jpowsour.2008.12.026.

[150] Zhu, X.; Tsuji, H.; Yella, A.; Chauvin, A.-S.; Grätzel, M.; Nakamura, E. New sensitizers for dye-sensitized solar cells featuring a carbon-bridged phenylenevinylene. *Chem. Commun.* **2012,** *49* (6), 582. DOI: 10.1039/c2cc37124c.

[151] Yella, A.; Lee, H.-W.; Tsao, H. N.; Yi, C.; Chandiran, A. K.; Nazeeruddin, M. K.; Diau, E. W.-G.; Yeh, C.-Y.; Zakeeruddin, S. M.; Gratzel, M. Porphyrin-Sensitized Solar Cells with Cobalt (II/III)-Based Redox Electrolyte Exceed 12 Percent Efficiency. *Science* **2011,** *334* (6056), 629–634. DOI: 10.1126/science.1209688.

[152] Yella, A.; Humphry-Baker, R.; Curchod, Basile F. E.; Ashari Astani, N.; Teuscher, J.; Polander, L. E.; Mathew, S.; Moser, J.-E.; Tavernelli, I.; Rothlisberger, U.; Grätzel, M.; Nazeeruddin, M. K.; Frey, J. Molecular Engineering of a Fluorene Donor for Dye-Sensitized Solar Cells. *Chem. Mater.* **2013,** *25* (13), 2733–2739. DOI: 10.1021/cm401593b.

[153] Zeng, W.; Cao, Y.; Bai, Y.; Wang, Y.; Shi, Y.; Zhang, M.; Wang, F.; Pan, C.; Wang, P. Efficient Dye-Sensitized Solar Cells with an Organic Photosensitizer Featuring Orderly Conjugated Ethylenedioxythiophene and Dithienosilole Blocks. *Chem. Mater.* **2010,** *22* (5), 1915–1925. DOI: 10.1021/cm9036988.

[154] Zhou, L.; Jia, C.; Wan, Z.; Li, Z.; Bai, J.; Zhang, L.; Zhang, J.; Yao, X. Triphenylamine-based organic dyes containing benzimidazole derivatives for dye-sensitized solar cells. *Dyes and Pigments* **2012,** *95* (3), 743–750. DOI: 10.1016/j.dyepig.2012.05.007.

[155] Wan, Z.; Jia, C.; Zhang, J.; Duan, Y.; Lin, Y.; Shi, Y. Triphenylamine-based starburst dyes with carbazole and phenothiazine antennas for dye-sensitized solar cells. *Journal of Power Sources* **2012,** *199*, 426–431. DOI: 10.1016/j.jpowsour.2011.10.062.

[156] *Phthalocyanines, Properties and Applications;* Leznoff, C. C., Lever, A. B. P., Eds. Volume 1-4; Wiley-VCH: Weinheim, 1989, 1992, 1993, 1996.

[157] *The Porphyrin Handbook;* Kadish, K. M., Smith, K. M., Guilard, R., Eds. Volume 15-20; Academic Press: Amsterdam, 2003.

[158] Claessens, C. G.; Hahn, U.; Torres, T. Phthalocyanines: From outstanding electronic properties to emerging applications. *Chem. Record* **2008,** *8* (2), 75–97. DOI: 10.1002/tcr.20139.

[159] La Torre, G. de; Claessens, C. G.; Torres, T. Phthalocyanines: Old dyes, new materials. Putting color in nanotechnology. *Chem. Commun.* [Online] **2007,** No. 20, 2000–2015.

[160] Geis, C. Electrocatalytic and Spectroelectrochemical Measurements on Polymeric Phthalocyanine Films. Master Thesis; Justus-Liebig-Universität, Gießen, 2014.

[161] Geis, C. Elektrochemische Messungen an polymeren Phthalocyaninen. Bericht zum Spezialisierungsmodul; Justus-Liebig-Universität, Gießen, 2013.

[162] Geis, C. Etablierung eines Verfahrens zur Herstellung von polymerisierten Cu-Phthalocyaninen auf Glas. Bericht zum Vertiefungsmodul I; Justus-Liebig-Universität, Gießen, 2013.

[163] Geis, C. XPS-Messungen an polymerisierten Phthalocyaninen. Bericht zum Vertiefungsmodul II; Justus-Liebig-Universität, Gießen, 2013.

[164] Clifford, J. N.; Planells, M.; Palomares, E. Advances in high efficiency dye sensitized solar cells based on Ru(ii) free sensitizers and a liquid redox electrolyte. *J. Mater. Chem.* **2012,** *22* (46), 24195. DOI: 10.1039/c2jm34289h.

[165] Ragoussi, M.-E.; Ince, M.; Torres, T. Recent Advances in Phthalocyanine-Based Sensitizers for Dye-Sensitized Solar Cells. *Eur. J. Org. Chem.* **2013,** *2013* (29), 6475–6489. DOI: 10.1002/ejoc.201301009.

[166] Ince, M.; Yum, J.-H.; Kim, Y.; Mathew, S.; Grätzel, M.; Torres, T.; Nazeeruddin, M. K. Molecular Engineering of Phthalocyanine Sensitizers for Dye-Sensitized Solar Cells. *J. Phys. Chem. C* **2014,** *118* (30), 17166–17170. DOI: 10.1021/jp502447y.

[167] Ikeuchi, T.; Nomoto, H.; Masaki, N.; Griffith, M. J.; Mori, S.; Kimura, M. Molecular engineering of zinc phthalocyanine sensitizers for efficient dye-sensitized solar cells. *Chemical communications (Cambridge, England)* **2014,** *50* (16), 1941–1943. DOI: 10.1039/c3cc47714b.

[168] Alamin Ali, H. E.; Altındal, A.; Altun, S.; Odabaş, Z. Highly efficient dye-sensitized solar cells based on metal-free and copper(II) phthalocyanine bearing 2-phenylphenoxy moiety. *Dyes and Pigments* **2016,** *124*, 180–187. DOI: 10.1016/j.dyepig.2015.09.010.

[169] Falgenhauer, J. Optimierung der Sensibilisierung von ZnO durch sulfonierte Phthalocyanine. Bachelor Thesis; Justus-Liebig-Universität, Gießen, 2009.

[170] Falgenhauer, J. Charakterisierung von sulfonierten Phthalocyaninen mittels Spektroelektrochemie, Elektrochemie und Photoelektrochemie. Bericht zum Vertiefungsmodul I und zum Spezialisierungsmodul; Justus-Liebig-Universität, Gießen, 2011.

[171] Péchy, P.; Rotzinger, F. P.; Nazeeruddin, M. K.; Kohle, O.; Zakeeruddin, S. M.; Humphry-Baker, R.; Grätzel, M. Preparation of phosphonated polypyridyl ligands to anchor transition-metal complexes on oxide surfaces: Application for the

conversion of light to electricity with nanocrystalline TiO 2 films. *J. Chem. Soc., Chem. Commun.* **1995,** *0* (1), 65–66. DOI: 10.1039/C39950000065.

[172] Stenzel, O. *The Physics of Thin Film Optical Spectra*. *An Introduction*, Second edition; Springer series in surface sciences 44; Springer: Cham, Switzerland, 2016.

[173] Demtröder, W. *Experimentalphysik. Band 2: Elektrizität und Optik*, 4., überarb. und erw. Aufl.; Springer-Lehrbuch; Springer: Berlin [u.a.], 2006.

[174] www.getamo.com/www/getspec.nsf/main.html?open&lang=EN&id=ISP-80-8-REFL_EN on 2015-03-19

[175] Peulon, S.; Lincot, D. Cathodic electrodeposition from aqueous solution of dense or open-structured zinc oxide films. *Adv. Mater.* **1996,** *8* (2), 166–170. DOI: 10.1002/adma.19960080216.

[176] Peulon, S.; Lincot, D. Mechanistic Study of Cathodic Electrodeposition of Zinc Oxide and Zinc Hydroxychloride Films from Oxygenated Aqueous Zinc Chloride Solutions. *J. Electrochem. Soc.* **1998,** *145* (3), 864–874. DOI: 10.1149/1.1838359.

[177] Pauporté, T.; Lincot, D. Heteroepitaxial electrodeposition of zinc oxide films on gallium nitride. *Appl. Phys. Lett.* **1999,** *75* (24), 3817–3819. DOI: 10.1063/1.125466.

[178] Pauporté, T.; Lincot, D. Electrodeposition of semiconductors for optoelectronic devices: results on zinc oxide. *Electrochimica Acta* **2000,** *45* (20), 3345–3353. DOI: 10.1016/S0013-4686(00)00405-9.

[179] Asdim; Ichinose, K.; Inomata, T.; Masuda, H.; Yoshida, T. Aggregation behavior of differently substituted Ru(II)-complex dyes as sensitizers for electrodeposited ZnO solar cells. *Journal of Photochemistry and Photobiology A: Chemistry* **2012,** *242*, 67–71. DOI: 10.1016/j.jphotochem.2012.04.024.

[180] Izaki, M.; Omi, T. Transparent zinc oxide films prepared by electrochemical reaction. *Appl. Phys. Lett.* **1996,** *68* (17), 2439–2440. DOI: 10.1063/1.116160.

[181] Izaki, M.; Omi, T. Electrolyte Optimization for Cathodic Growth of Zinc Oxide Films. *J. Electrochem. Soc.* **1996,** *143* (3), L53. DOI: 10.1149/1.1836529.

[182] Pauporté, T.; Lincot, D. Hydrogen Peroxide Oxygen Precursor for Zinc Oxide Electrodeposition I. Deposition in Perchlorate Medium. *J. Electrochem. Soc.* **2001,** *148* (4), C310-C314. DOI: 10.1149/1.1357175.

[183] Pauporté, T.; Lincot, D. Hydrogen peroxide oxygen precursor for zinc oxide electrodeposition II—Mechanistic aspects. *J. Electroanal. Chem.* **2001,** *517* (1-2), 54–62. DOI: 10.1016/S0022-0728(01)00674-X.

[184] Yoshida, T.; Komatsu, D.; Shimokawa, N.; Minoura, H. Mechanism of cathodic electrodeposition of zinc oxide thin films from aqueous zinc nitrate baths. *Thin Solid Films* **2004,** *451-452*, 166–169. DOI: 10.1016/j.tsf.2003.10.097.

[185] Lupan, O.; Pauporté, T.; Chow, L.; Viana, B.; Pellé, F.; Ono, L. K.; Roldan Cuenya, B.; Heinrich, H. Effects of annealing on properties of ZnO thin films prepared by electrochemical deposition in chloride medium. *Appl. Surf. Sci.* **2010,** *256* (6), 1895–1907. DOI: 10.1016/j.apsusc.2009.10.032.

[186] Yoshida, T.; Miyamoto, K.; Hibi, N.; Sugiura, T.; Minoura, H.; Schlettwein, D.; Oekermann, T.; Schneider, G.; Wöhrle, D. Self Assembled Growth of Nano Particulate Porous ZnO Thin Film Modified 2,9,16,23-Tetrasulfophthalocyanatozinc(II) by One-Step Electrodeposition. *Chem. Lett.* **1998,** *27* (7), 599–600. DOI: 10.1246/cl.1998.599.

[187] Yoshida, T.; Terada, K.; Schlettwein, D.; Oekermann, T.; Sugiura, T.; Minoura, H. Electrochemical Self-Assembly of Nanoporous ZnO/Eosin Y Thin Films and Their Sensitized Photoelectrochemical Performance. *Adv. Mater.* **2000,** *12* (16), 1214–1217. DOI: 10.1002/1521-4095(200008)12:16<1214:AID-ADMA1214>3.0.CO;2-Z.

[188] Yoshida, T.; Tochimoto, M.; Schlettwein, D.; Wöhrle, D.; Sugiura, T.; Minoura, H. Self-Assembly of Zinc Oxide Thin Films Modified with Tetrasulfonated Metallophthalocyanines by One-Step Electrodeposition. *Chem. Mater.* **1999,** *11* (10), 2657–2667. DOI: 10.1021/cm980619o.

[189] Künze, S.; Schlettwein, D. Electrochemical and electroless deposition of porous zinc oxide on aluminium. *Electrochim. Acta* **2014,** *128*, 360–367. DOI: 10.1016/j.electacta.2013.09.146.

[190] Künze, S. Stromlose Abscheidung von porösem Zinkoxid auf Aluminium. Dissertation; Justus-Liebig-Universität, Gießen, 2014.

[191] Rudolph, M.; Loewenstein, T.; Arndt, E.; Zimmermann, Y.; Neudeck, A.; Schlettwein, D. Pulsed electrodeposition of porous ZnO on Ag-coated polyamide filaments. *Phys. Chem. Chem. Phys.* **2009,** *11* (17), 3313–3319. DOI: 10.1039/b822534f.

[192] Stumpp, M. Abscheidung von ZnO auf mikrostrukturierten Messelektroden zur Charakterisierung als Feldeffekttransistor. Bachelor Thesis; Justus-Liebig-Universität, Gießen, 2010.

[193] Stumpp, M. Use of Microelectrodes to Study the Electrochemically Induced Growth of Zinc Oxide. Master Thesis; Justus-Liebig-Universität, Gießen, 2013.

[194] Khrypunov, G.; Klochko, N.; Volkova, N.; Kopach, V.; Lyubov, V.; Klepikova, K. Pulse and direct current electrodeposition of zinc oxide layers for solar cells with extra thin absorbers. *Photovoltaic Technology* [Online] **2011**, 2853–2860.

[195] Klochko, N. P.; Khrypunov, G. S.; Myagchenko, Y. O.; Melnychuk, E. E.; Kopach, V. R.; Klepikova, E. S.; Lyubov, V. M.; Kopach, A. V. Controlled Growth of one-dimensional zinc oxide nanostructures in the pulsed electrodeposition mode. *Semiconductors* **2012,** *46* (6), 825–831. DOI: 10.1134/S1063782612060127.

[196] Tolosa, M. D. Reyes; Orozco-Messana, J.; Damonte, L. C.; Hernandez-Fenollosa, M. A. ZnO Nanoestructured Layers Processing with Morphology Control by Pulsed Electrodeposition. *J. Electrochem. Soc.* **2011,** *158* (7), D452. DOI: 10.1149/1.3593004.

[197] V. Manzano, C.; Caballero-Calero, O.; Hormeño, S.; Penedo, M.; Luna, M.; Martín-González, M. S. ZnO Morphology Control by Pulsed Electrodeposition. *J. Phys. Chem. C* **2013,** *117* (3), 1502–1508. DOI: 10.1021/jp3107099.

[198] Stumpp, M.; Lupo, C.; Schlettwein, D. Preparation and Characterization of Electrodeposited ZnO on Microstructured Electrode Arrays. *J. Electrochem. Soc.* **2012,** *159* (12), D717–D723. DOI: 10.1149/2.041212jes.

[199] Stumpp, M.; Nguyen, T.; Lupo, C.; Schlettwein, D. Interplay of Different Reaction Pathways in the Pulsed Galvanostatic Deposition of Zinc Oxide. *Electrochimica Acta* **2015,** *169*, 367–375. DOI: 10.1016/j.electacta.2015.04.038.

[200] Bisquert, J.; Mora-Seró, I. Simulation of Steady-State Characteristics of Dye-Sensitized Solar Cells and the Interpretation of the Diffusion Length. *J. Phys. Chem. Lett.* **2010,** *1* (1), 450–456. DOI: 10.1021/jz900297b.

[201] Zaban, A.; Greenshtein, M.; Bisquert, J. Determination of the Electron Lifetime in Nanocrystalline Dye Solar Cells by Open-Circuit Voltage Decay Measurements. *ChemPhysChem* **2003,** *4* (8), 859–864. DOI: 10.1002/cphc.200200615.

[202] Bisquert, J.; Zaban, A.; Greenshtein, M.; Mora-Seró, I. Determination of rate constants for charge transfer and the distribution of semiconductor and electrolyte electronic energy levels in dye-sensitized solar cells by open-circuit photovoltage decay method. *Journal of the American Chemical Society* **2004,** *126* (41), 13550–13559. DOI: 10.1021/ja047311k.

[203] Guillén, E.; Peter, L. M.; Anta, J. A. Electron Transport and Recombination in ZnO-Based Dye-Sensitized Solar Cells. *J. Phys. Chem. C* **2011,** *115* (45), 22622–22632. DOI: 10.1021/jp206698t.

[204] Cameron, P. J.; Peter, L. M. How does back-reaction at the conducting glass substrate influence the dynamic photovoltage response of nanocrystalline dye-sensitized solar cells? *The journal of physical chemistry. B* **2005,** *109* (15), 7392–7398. DOI: 10.1021/jp0407270.

[205] Bisquert, J.; Fabregat-Santiago, F.; Mora-Seró, I.; Garcia-Belmonte, G.; Giménez, S. Electron Lifetime in Dye-Sensitized Solar Cells: Theory and Interpretation of Measurements. *J. Phys. Chem. C* **2009,** *113* (40), 17278–17290. DOI: 10.1021/jp9037649.

[206] O'Regan, B.; Xiaoe, L.; Ghaddar, T. Dye adsorption, desorption, and distribution in mesoporous TiO2 films, and its effects on recombination losses in dye sensitized solar cells. *Energy Environ. Sci.* **2012,** *5* (5), 7203. DOI: 10.1039/c2ee21341a.

[207] Jennings, J. R.; Ghicov, A.; Peter, L. M.; Schmuki, P.; Walker, A. B. Dye-sensitized solar cells based on oriented TiO2 nanotube arrays: transport, trapping, and transfer of electrons. *Journal of the American Chemical Society* **2008,** *130* (40), 13364–13372. DOI: 10.1021/ja804852z.

[208] Schlichthörl, G.; Huang, S. Y.; Sprague, J.; Frank, A. J. Band Edge Movement and Recombination Kinetics in Dye-Sensitized Nanocrystalline TiO 2 Solar Cells: A Study by Intensity Modulated Photovoltage Spectroscopy. *J. Phys. Chem. B* **1997,** *101* (41), 8141–8155. DOI: 10.1021/jp9714126.

[209] Schlichthörl, G.; Park, N. G.; Frank, A. J. Evaluation of the Charge-Collection Efficiency of Dye-Sensitized Nanocrystalline TiO 2 Solar Cells. *J. Phys. Chem. B* **1999,** *103* (5), 782–791. DOI: 10.1021/jp9831177.

[210] Dloczik, L.; Ileperuma, O.; Lauermann, I.; Peter, L. M.; Ponomarev, E. A.; Redmond, G.; Shaw, N. J.; Uhlendorf, I. Dynamic Response of Dye-Sensitized Nanocrystalline Solar Cells: Characterization by Intensity-Modulated Photocurrent Spectroscopy. *J. Phys. Chem. B* **1997,** *101* (49), 10281–10289. DOI: 10.1021/jp972466i.

[211] Peter, L.; Ponomarev, E.; Franco, G.; Shaw, N. Aspects of the photoelectrochemistry of nanocrystalline systems. *Electrochimica Acta* **1999,** *45* (4-5), 549–560. DOI: 10.1016/S0013-4686(99)00233-9.

[212] Wang, H.; Peter, L. M. A Comparison of Different Methods To Determine the Electron Diffusion Length in Dye-Sensitized Solar Cells. *J. Phys. Chem. C* **2009,** *113* (42), 18125–18133. DOI: 10.1021/jp906629t.

[213] van de Lagemaat, Jao; Kopidakis, N.; Neale, N. R.; Frank, A. J. Effect of nonideal statistics on electron diffusion in sensitized nanocrystalline TiO2. *Phys. Rev. B* **2005,** *71* (3). DOI: 10.1103/PhysRevB.71.035304.

[214] Bisquert, J.; Mora-Sero, I.; Fabregat-Santiago, F. Diffusion-Recombination Impedance Model for Solar Cells with Disorder and Nonlinear Recombination. *ChemElectroChem* **2014,** *1* (1), 289–296. DOI: 10.1002/celc.201300091.

[215] Bisquert, J. Chemical capacitance of nanostructured semiconductors: its origin and significance for nanocomposite solar cells. *Phys. Chem. Chem. Phys.* **2003,** *5* (24), 5360. DOI: 10.1039/b310907k.

[216] Halme, J.; Vahermaa, P.; Miettunen, K.; Lund, P. Device physics of dye solar cells. *Advanced materials (Deerfield Beach, Fla.)* **2010,** *22* (35), E210-34. DOI: 10.1002/adma.201000726.

[217] Lee, P. A. Density of states and screening near the mobility edge. *Phys. Rev. B* **1982,** *26* (10), 5882–5885. DOI: 10.1103/PhysRevB.26.5882.

[218] Bisquert, J.; Fabregat-Santiago, F.; Mora-Seró, I.; Garcia-Belmonte, G.; Barea, E. M.; Palomares, E. A review of recent results on electrochemical determination of the density of electronic states of nanostructured metal-oxide semiconductors and organic hole conductors. *Inorg. Chim. Acta* **2008,** *361* (3), 684–698. DOI: 10.1016/j.ica.2007.05.032.

[219] Fabregat-Santiago, F.; Garcia-Belmonte, G.; Bisquert, J.; Bogdanoff, P.; Zaban, A. Mott-Schottky Analysis of Nanoporous Semiconductor Electrodes in Dielectric State Deposited on SnO[sub 2](F) Conducting Substrates. *J. Electrochem. Soc.* **2003,** *150* (6), E293. DOI: 10.1149/1.1568741.

[220] Sze, S. M.; Ng, K. K. *Physics of semiconductor devices*, 3rd; Wiley-Interscience: Hoboken, N.J, 2007.

[221] O'Regan, B. C.; Durrant, J. R.; Sommeling, P. M.; Bakker, N. J. Influence of the TiCl 4 Treatment on Nanocrystalline TiO 2 Films in Dye-Sensitized Solar Cells. 2. Charge Density, Band Edge Shifts, and Quantification of Recombination Losses at Short Circuit. *J. Phys. Chem. C* **2007,** *111* (37), 14001–14010. DOI: 10.1021/jp073056p.

[222] Jennings, J. R.; Wang, Q. Influence of Lithium Ion Concentration on Electron Injection, Transport, and Recombination in Dye-Sensitized Solar Cells. *J. Phys. Chem. C* **2010,** *114* (3), 1715–1724. DOI: 10.1021/jp9104129.

[223] Kern, R.; Sastrawan, R.; Ferber, J.; Stangl, R.; Luther, J. Modeling and interpretation of electrical impedance spectra of dye solar cells operated under open-circuit conditions. *Electrochim. Acta* **2002,** *47*, 4213–4225.

[224] Egerton, R. F. *Physical Principles of Electron Microscopy*. *An Introduction to TEM, SEM, and AEM;* Springer Science+Business Media, Inc: Boston, MA, 2005.

[225] Vernon-Parry, K. D. Scanning electron microscopy: an introduction. *III-Vs Review* **2000,** *13* (4), 40–44. DOI: 10.1016/S0961-1290(00)80006-X.

[226] Dunlap, M.; Adaskaveg, J. E. *Introduction to the Scanning Electron Microscope*. *Theory, Practice, & Procedures;* Facility for Advanced Instrumentation, U. C. Davis, 1997.

[227] Guthoff, R. F.; Baudouin, C.; Stave, J. *Atlas Confocal Laser Scanning In-vivo Microscopy in Ophthalmology*, 1st ed.; Springer, 2006.

[228] Strauch, K. Potentiostatische O2 -basierte ZnO-Abscheidung auf korrosionsbeständigen Metalldrähten. Bericht zum Modul „Dünne Schichten und Oberflächen“; Justus-Liebig-Universität, Gießen, 2009.

[229] Loewenstein, T. Anpassung ZnO- basierter farbstoffsensibilisierter Photoelektroden an die Anwendung in textilbasierten Solarzellen. Dissertation; Justus-Liebig-Universität, Gießen, 2009.

[230] Strauch, K., *Unterdrückung der Korrosion an textilen Rückelektroden für farbstoffsensibilisierte Solarzellen*. *Modul "Präparation und Charakterisierung dünner Schichten"*, Justus-Liebig-Universität Gießen, **2009**.

[231] Geiger, A. Präparation und Charakterisierung von ZnO auf Tantaloberflächen für eine Nutzung in farbstoffsensibilisierten Solarzellen. Bachelor Thesis; Justus-Liebig-Universität, Gießen, **2012**.

[232] Loewenstein, T.; Hastall, A.; Mingebach, M.; Zimmermann, Y.; Neudeck, A.; Schlettwein, D. Textile electrodes as substrates for the electrodeposition of porous ZnO. *Phys. Chem. Chem. Phys.* **2008,** *10* (14), 1844–1847. DOI: 10.1039/b719691a.

[233] Rudolph, M. Nutzung nitratbasierter Abscheidebäder für die Präparation von ZnO auf textilen Elektroden. Bachelor Thesis; Justus-Liebig-Universität, Gießen, 2008.

[234] Goux, A.; Pauporté, T.; Yoshida, T.; Lincot, D. Mechanistic Study of the Electrodeposition of Nanoporous Self-Assembled ZnO/Eosin Y Hybrid Thin Films: Effect of Eosin Concentration. *Langmuir* **2006,** *22* (25), 10545–10553. DOI: 10.1021/la061199h.

[235] Ito, S.; Chen, P.; Comte, P.; Nazeeruddin, M. K.; Liska, P.; Péchy, P.; Grätzel, M. Fabrication of screen-printing pastes from TiO2 powders for dye-sensitised solar cells. *Prog. Photovolt: Res. Appl.* **2007,** *15* (7), 603–612. DOI: 10.1002/pip.768.

[236] Richter, C. Herstellung von farbstoffsensibilisierten Solarzellen im Zwei-Elektroden-Aufbausd. Bericht zum Vertiefungsmodul; Justus-Liebig-Universität, Gießen, 2011.

[237] Asakuma, N.; Fukui, T.; Toki, M.; Awazu, K.; Imai, H. Photoinduced hydroxylation at ZnO surface. *Thin Solid Films* **2003,** *445* (2), 284–287. DOI: 10.1016/S0040-6090(03)01162-3.

[238] Sun, R.-D.; Nakajima, A.; Fujishima, A.; Watanabe, T.; Hashimoto, K. Photoinduced Surface Wettability Conversion of ZnO and TiO 2 Thin Films. *J. Phys. Chem. B* **2001,** *105* (10), 1984–1990. DOI: 10.1021/jp002525j.

[239] Ito, S.; Nazeeruddin, M. K.; Liska, P.; Comte, P.; Charvet, R.; Péchy, P.; Jirousek, M.; Kay, A.; Zakeeruddin, S. M.; Grätzel, M. Photovoltaic characterization of dye-sensitized solar cells: effect of device masking on conversion efficiency. *Prog. Photovolt: Res. Appl.* **2006,** *14* (7), 589–601. DOI: 10.1002/pip.683.

[240] Zahner Electrics, Manual CIMPS-PCS (Photocurrent spectroscopy), 09/2011

[241] Halme, J.; Boschloo, G.; Hagfeldt, A.; Lund, P. Spectral Characteristics of Light Harvesting, Electron Injection, and Steady-State Charge Collection in Pressed TiO 2 Dye Solar Cells. *J. Phys. Chem. C* **2008,** *112* (14), 5623–5637. DOI: 10.1021/jp711245f.

[242] Tefashe, U. M.; Loewenstein, T.; Miura, H.; Schlettwein, D.; Wittstock, G. Scanning electrochemical microscope studies of dye regeneration in indoline (D149)-sensitized ZnO photoelectrochemical cells. *J. Electroanal. Chem.* **2010,** *650* (1), 24–30. DOI: 10.1016/j.jelechem.2010.09.014.

[243] Pauporte, T.; Rathousky, J. Electrodeposited Mesoporous ZnO Thin Films as Efficient Photocatalysts for the Degradation of Dye Pollutants. *J. Phys. Chem. C* **2007,** *111* (21), 7639–7644. DOI: 10.1021/jp071465f.

[244] Sommeling, P. M.; O'Regan, B. C.; Haswell, R. R.; Smit, H J P; Bakker, N. J.; Smits, J J T; Kroon, J. M.; van Roosmalen, J A M. Influence of a TiCl4 post-treatment on nanocrystalline TiO2 films in dye-sensitized solar cells. *The journal of physical chemistry. B* **2006,** *110* (39), 19191–19197. DOI: 10.1021/jp061346k.

[245] Duffy, N.; Peter, L.; Rajapakse, R.; Wijayantha, K. A novel charge extraction method for the study of electron transport and interfacial transfer in dye sensitised nanocrystalline solar cells. *Electrochem. Commun.* **2000,** *2* (9), 658–662. DOI: 10.1016/S1388-2481(00)00097-7.

[246] Zahner Electrics, Manual CIMPS (Controlled Intensity Modulated Photo Spectroscopy), 10/2009

[247] Magne, C.; Urien, M.; Ciofini, I.; Tugsuz, T.; Pauporté, T. Amphiphilic acids as co-adsorbents of metal-free organic dyes for the efficient sensitization of nanostructured photoelectrode. *RSC Adv.* **2012,** *2* (31), 11836. DOI: 10.1039/c2ra22121g.

[248] DeVore, J. R. Refractive Indices of Rutile and Sphalerite. *J. Opt. Soc. Am.* **1951,** *41* (6), 416. DOI: 10.1364/JOSA.41.000416.

[249] Bond, W. L. Measurement of the Refractive Indices of Several Crystals. *J. Appl. Phys.* **1965,** *36* (5), 1674. DOI: 10.1063/1.1703106.

[250] Pauporté, T.; Yoshida, T.; Cortès, R.; Froment, M.; Lincot, D. Electrochemical Growth of Epitaxial Eosin/ZnO Hybrid Films. *J. Phys. Chem. B* **2003,** *107* (37), 10077–10082. DOI: 10.1021/jp034079g.

[251] Cappel, U. B.; Feldt, S. M.; Schöneboom, J.; Hagfeldt, A.; Boschloo, G. The Influence of Local Electric Fields on Photoinduced Absorption in Dye-Sensitized Solar Cells. *J. Am. Chem. Soc.* **2010,** *132* (26), 9096–9101. DOI: 10.1021/ja102334h.

[252] Rousset, J.; Saucedo, E.; Lincot, D. Extrinsic Doping of Electrodeposited Zinc Oxide Films by Chlorine for Transparent Conductive Oxide Applications. *Chem. Mater.* **2009,** *21* (3), 534–540. DOI: 10.1021/cm802765c.

[253] Reemts, J.; Kittel, A. Persistent photoconductivity in highly porous ZnO films. *J. Appl. Phys.* **2007,** *101* (1), 13709. DOI: 10.1063/1.2407264.

[254] Reemts, J. Ladungstransport in farbstoffsensibilisierten porösen Zinkoxidfilmen. Dissertation; Carl von Ossietzky Universität, Oldenburg, 2006.

[255] Anderson, A. Y.; Barnes, Piers R. F.; Durrant, J. R.; O'Regan, B. C. Quantifying Regeneration in Dye-Sensitized Solar Cells. *J. Phys. Chem. C* **2011,** *115* (5), 2439–2447. DOI: 10.1021/jp1101048.

[256] Martinson, Alex B. F.; Góes, M. S.; Fabregat-Santiago, F.; Bisquert, J.; Pellin, M. J.; Hupp, J. T. Electron Transport in Dye-Sensitized Solar Cells Based on ZnO Nanotubes: Evidence for Highly Efficient Charge Collection and Exceptionally Rapid Dynamics †. *J. Phys. Chem. A* **2009,** *113* (16), 4015–4021. DOI: 10.1021/jp810406q.

[257] Barnes, P. R.; Anderson, A. Y.; Juozapavicius, M.; Liu, L.; Li, X.; Palomares, E.; Forneli, A.; O'Regan, B. C. Factors controlling charge recombination under dark and light conditions in dye sensitised solar cells. *Physical chemistry chemical physics : PCCP* **2011,** *13* (8), 3547–3558. DOI: 10.1039/c0cp01855d.

[258] Ichinose, K.; KIMIKADO, Y.; Yoshida, T. The Effect of Pre-treatments of F-Doped SnO2 Substrates for Cathodic Nucleation of ZnO Crystals in Aqueous ZnCl2 Solution with Dissolved O2. *Electrochem.* **2011,** *79* (3), 146–155.

[259] Falgenhauer, J.; Fiehler, F.; Richter, C.; Rudolph, M.; Schlettwein, D. Consequences of changes in the ZnO trap distribution on the performance of dye-sensitized solar cells. *Phys. Chem. Chem. Phys.* **2017,** *19* (24), 16159–16168. DOI: 10.1039/C7CP01024A.

[260] Hara, K.; Miyamoto, K.; Abe, Y.; Yanagida, M. Electron transport in coumarin-dye-sensitized nanocrystalline TiO2 electrodes. *The journal of physical chemistry. B* **2005,** *109* (50), 23776–23778. DOI: 10.1021/jp055572q.

[261] Listorti, A.; Creager, C.; Sommeling, P.; Kroon, J.; Palomares, E.; Fornelli, A.; Breen, B.; Barnes, Piers R. F.; Durrant, J. R.; Law, C.; O'Regan, B. The mechanism behind the beneficial effect of light soaking on injection efficiency and photocurrent in dye sensitized solar cells. *Energy Environ. Sci.* **2011,** *4* (9), 3494. DOI: 10.1039/c1ee01443a.

[262] Yum, J.-H.; Humphry-Baker, R.; Zakeeruddin, S. M.; Nazeeruddin, M. K.; Grätzel, M. Effect of heat and light on the performance of dye-sensitized solar cells based on organic sensitizers and nanostructured TiO2. *Nano Today* **2010,** *5* (2), 91–98. DOI: 10.1016/j.nantod.2010.02.003.

[263] Cabau, L.; Pellejà, L.; Clifford, J. N.; Kumar, C. V.; Palomares, E. Light soaking effects on charge recombination and device performance in dye sensitized solar cells based on indoline–cyclopentadithiophene chromophores. *J. Mater. Chem. A* **2013,** *1* (31), 8994. DOI: 10.1039/c3ta11242j.

[264] Gregg, B. A. Interfacial processes in the dye-sensitized solar cell. *Coord. Chem. Rev.* **2004,** *248* (13-14), 1215–1224. DOI: 10.1016/j.ccr.2004.02.009.

[265] Ferrere, S.; Gregg, B. A. Large Increases in Photocurrents and Solar Conversion Efficiencies by UV Illumination of Dye Sensitized Solar Cells. *J. Phys. Chem. B* **2001,** *105* (32), 7602–7605. DOI: 10.1021/jp011612o.

[266] Gregg, B. A.; Chen, S.-G.; Ferrere, S. Enhanced Dye-Sensitized Photoconversion Efficiency via Reversible Production of UV-Induced Surface States in Nanoporous TiO 2. *J. Phys. Chem. B* **2003,** *107* (13), 3019–3029. DOI: 10.1021/jp022000m.

[267] Barnes, Piers R. F.; Anderson, A. Y.; Koops, S. E.; Durrant, J. R.; O'Regan, B. C. Electron Injection Efficiency and Diffusion Length in Dye-Sensitized Solar Cells Derived from Incident Photon Conversion Efficiency Measurements. *J. Phys. Chem. C* **2009,** *113* (3), 1126–1136. DOI: 10.1021/jp809046j.

[268] Barnes, Piers R. F.; Miettunen, K.; Li, X.; Anderson, A. Y.; Bessho, T.; Gratzel, M.; O'Regan, B. C. Interpretation of Optoelectronic Transient and Charge Extraction Measurements in Dye-Sensitized Solar Cells. *Adv. Mater.* **2013,** *25* (13), 1881–1922. DOI: 10.1002/adma.201201372.

[269] Idígoras, J.; Burdziński, G.; Karolczak, J.; Kubicki, J.; Oskam, G.; Anta, J. A.; Ziółek, M. The Impact of the Electrical Nature of the Metal Oxide on the Performance in Dye-Sensitized Solar Cells: New Look at Old Paradigms. *J. Phys. Chem. C* **2015,** *119* (8), 3931–3944. DOI: 10.1021/jp512330f.

[270] O'Regan, B. C.; Durrant, J. R. Calculation of activation energies for transport and recombination in mesoporous TiO2/dye/electrolyte films--taking into account surface charge shifts with temperature. *The journal of physical chemistry. B* **2006,** *110* (17), 8544–8547. DOI: 10.1021/jp060979w.

[271] Strothkämper, C.; Bartelt, A.; Sippel, P.; Hannappel, T.; Schütz, R.; Eichberger, R. Delayed Electron Transfer through Interface States in Hybrid ZnO/Organic-Dye Nanostructures. *J. Phys. Chem. C* **2013,** *117* (35), 17901–17908. DOI: 10.1021/jp402042a.

[272] Koops, S. E.; O'Regan, B. C.; Barnes, Piers R F; Durrant, J. R. Parameters influencing the efficiency of electron injection in dye-sensitized solar cells. *Journal of the American Chemical Society* **2009,** *131* (13), 4808–4818. DOI: 10.1021/ja8091278.

[273] Yang, X.; Zhang, S.; Zhang, K.; Liu, J.; Qin, C.; Chen, H.; Islam, A.; Han, L. Coordinated shifts of interfacial energy levels: insight into electron injection in highly efficient dye-sensitized solar cells. *Energy Environ. Sci.* **2013,** *6* (12), 3637. DOI: 10.1039/c3ee42110d.

[274] Boschloo, G.; Hagfeldt, A. Characteristics of the Iodide/Triiodide Redox Mediator in Dye-Sensitized Solar Cells. *Acc. Chem. Res.* **2009,** *42* (11), 1819–1826. DOI: 10.1021/ar900138m.

[275] Nozik, A. J.; Memming, R. Physical Chemistry of Semiconductor−Liquid Interfaces. *J. Phys. Chem.* **1996,** *100* (31), 13061–13078. DOI: 10.1021/jp953720e.

[276] Peter, L. "Sticky electrons" transport and interfacial transfer of electrons in the dye-sensitized solar cell. *Accounts of chemical research* **2009,** *42* (11), 1839–1847. DOI: 10.1021/ar900143m.

[277] Wang, Q.; Ito, S.; Grätzel, M.; Fabregat-Santiago, F.; Mora-Seró, I.; Bisquert, J.; Bessho, T.; Imai, H. Characteristics of High Efficiency Dye-Sensitized Solar Cells †. *J. Phys. Chem. B* **2006,** *110* (50), 25210–25221. DOI: 10.1021/jp064256o.

[278] Smestad, G. P.; Krebs, F. C.; Lampert, C. M.; Granqvist, C. G.; Chopra, K. L.; Mathew, X.; Takakura, H. Reporting solar cell efficiencies in Solar Energy Materials and Solar Cells. *Solar Energy Materials and Solar Cells* **2008,** *92* (4), 371–373. DOI: 10.1016/j.solmat.2008.01.003.

[279] Volk, P. Zinkatbehandlung von Aluminium [Online] **2004**.

[280] Redmond, G.; Fitzmaurice, D. Spectroscopic Determination of Flatband Potentials for Polycrystalline Ti02 Electrodes in. *J. Phys. Chem.* **1993,** *97* (7), 1426–1430. DOI: 10.1021/j100109a029.

[281] Wang, W.; Zhao, Q.; Li, H.; Wu, H.; Zou, D.; Yu, D. Transparent, Double-Sided, ITO-Free, Flexible Dye-Sensitized Solar Cells Based on Metal Wire/ZnO Nanowire Arrays. *Adv. Funct. Mater.* **2012,** *22* (13), 2775–2782. DOI: 10.1002/adfm.201200168.

[282] Kerrec, O.; Devilliers, D.; Groult, H.; Chemla, M. Dielectric properties of anodic oxide films on tantalum. Electrochim. Acta 1995, 40 (6), 719–724. DOI: 10.1016/0013-4686(94)00330-4.

[283] Schultze, J. W.; Macagno, V. A. Electron transfer reaction on passive tantalum electrodes. *Electrochim. Acta* **1986,** *31* (3), 355–363. DOI: 10.1016/0013-4686(86)80090-1.

[284] Schultze, J. W.; Elfenthal, L. Electron-transfer reactions on pure and modified oxide films. *J. Electroanal. Chem. Interfacial Electrochem.* **1986,** *204* (1-2), 153–171. DOI: 10.1016/0022-0728(86)80515-0.

[285] Macagno, V.; Schultze, J. W. The growth and properties of thin oxide layers on tantalum electrodes. *J. Electroanal. Chem. Interfacial Electrochem.* **1984,** *180* (1-2), 157–170. DOI: 10.1016/0368-1874(84)83577-7.

[286] Mahé, E.; Devilliers, D.; Groult, H.; Pouilleau, J. Electrochemical behaviour of platinum-coated Ta/Ta2O5 electrodes. *Electrochim. Acta* **1999,** *44* (13), 2307–2315. DOI: 10.1016/S0013-4686(98)00352-1.